

N70-29956

**NASA CONTRACTOR
REPORT**



**NASA CR-1529
Part 2**

**NASA CR-1529
Part 2**

CASE FILE COPY

A STUDY OF 30 KM TO 200 KM METEOROLOGICAL ROCKET SOUNDING SYSTEMS

VOLUME I - LITERATURE AND DATA REVIEW

by Bruce Bollermann

*Prepared by
SPACE DATA CORPORATION
Phoenix, Ariz.
for George C. Marshall Space Flight Center*

1. Report No. NASA CR-1529 (Part 2)		2. Government Accession No.		3. Recipient's Catalog No.	
4. Title and Subtitle VOLUME I: A STUDY OF 30 KM TO 200 KM METEOROLOGICAL ROCKET SOUNDING SYSTEMS Part II. Literature and Data Review				5. Report Date May 1970	
				6. Performing Organization Code	
7. Author(s) Bruce Bollermann				8. Performing Organization Report No.	
9. Performing Organization Name and Address Space Data Corporation Phoenix, Arizona				10. Work Unit No.	
				11. Contract or Grant No. NAS8-20797	
12. Sponsoring Agency Name and Address NASA-George C. Marshall Space Flight Center Marshall Space Flight Center, Alabama 35812 Contract Monitor: Robert E. Turner				13. Type of Report and Period Covered CONTRACTOR REPORT	
				14. Sponsoring Agency Code	
15. Supplementary Notes Distribution of this report is provided in the interest of information exchange. Responsibility for the contents resides in the author or organization that prepared it.					
16. Abstract <p>This report reviews the contemporary literature on meteorological rockets and associated systems, to determine the accuracies and limitations of the current meteorological rocket systems from available data, and to determine the adaptability of the more complex geophysical rocket experiments to simplified, economical, routine meteorological rocket soundings. This literature review covers the various system requirements and techniques used in obtaining meteorological measurements of the 30 km to 200 km region of the atmosphere. In addition to the detailed descriptions of the various rocket vehicles, telemetry, sensors, decelerators and other related equipment, this review also includes a study of the gun probe systems.</p> <p>The study is presented in two books: Book 1 contains an introduction, a discussion of systems requirements and a description of the various sensing techniques; Book 2 contains details of the rocketsonde decelerator techniques, telemetry and tracking equipment, descriptions of the rocket vehicles, gun probe systems and a summary of the report. The two books are printed under separate cover, and are labeled Volume I.</p>					
17. Key Words (Suggested by Author(s))				18. Distribution Statement Unclassified - Unlimited	
19. Security Classif. (of this report) Unclassified		20. Security Classif. (of this page) Unclassified		21. No. of Pages 435	22. Price* \$3.00

FOREWORD

Most of the material in this report has been taken directly from the current literature; thus, to avoid frequent interruptions in the text, references have been omitted. Instead, acknowledgements are made preceding Book 1 for the primary investigators and authors whose works have been abstracted and whose data are presented. A bibliography of the digested literature follows the conclusion of Book 2.

This survey was made under Contract NAS8-20797 with the Aerospace Environment Division, Aero-Astrodynamic Laboratory, Marshall Space Flight Center. Mr. Robert E. Turner was the Contract Monitor.

ACKNOWLEDGEMENTS

Special recognition is expressed to the Meteorological Working Group of the Inter-Range Instrumentation Group, Range Commander's Conference, whose efforts brought about the formation of the Meteorological Rocket Network, and consequently the widespread distribution of its valuable data to the scientific community. The Network has grown worldwide, and has directly influenced developments in rocket meteorology.

Appreciation is expressed to Mr. Robert E. Turner and Mr. O. E. Smith of the Aerospace Environment Division, Aero-Astrodynamic Laboratory, NASA-Marshall Space Flight Center for their support and guidance in presenting this study, and to Mr. Edgar Schaefer for the many illustrations and Mr. David Gironde and staff of the Space Data Corporation for editorial assistance.

TABLE OF CONTENTS

VOLUME I

BOOK 2

<u>Chapter</u>		<u>Page</u>
	FOREWORD	iii
4	<u>ROCKETSONDE DECELERATORS</u>	
4.1	GENERAL	1
4.1.1	Ballistic Coefficient	1
4.1.2	Deployment Reliability	7
4.1.3	Stability	7
4.1.4	Radar Cross-Section	10
4.1.5	Constant Descent Rate	11
4.1.6	Cost	11
4.2	CONVENTIONAL PARACHUTES	
4.2.1	General	12
4.2.2	Design Parameters	12
4.2.3	Arcas 15' Gentex Parachute	23
4.2.4	Loki Dart 7.6' Parachute	44
4.2.5	NOL 6' Square Parachute	44
4.2.6	NOL Wind Sensor Parachute	53
4.3	PARACHUTES WITH GEOMETRY POROSITY	
4.3.1	General	55
4.3.2	Disk-Gap-Band Parachute	55
4.3.3	Cross Patch Parachute	62
4.3.4	Annular Ring Parachute	62
4.3.5	Miscellaneous Geometric Porosity Designs	66
4.4	STROKES FLOW RIBBON MESH PARACHUTE	
4.4.1	General	72
4.4.2	Theoretical	73
4.4.3	Proposed Parachute Design	74
4.4.4	Proposed Performance	78
4.4.5	Test Data	78
4.4.6	Summary	83

<u>Chapter</u>		<u>Page</u>
4.5	RAM-AIR DECELERATORS	
4.5.1	General	88
4.5.2	Ballute Principle	88
4.5.3	Arcasonde Ballute	89
4.5.4	Datasonde Starute	94
4.5.5	High Speed Ballutes	94
4.5.6	Biconical Decelerator	98
4.6	SUMMARY	100
5	<u>TELEMETRY AND TRACKING</u>	
5.1	GENERAL	101
5.2	RADAR	
5.2.1	General	103
5.2.2	Radar Descriptions	104
5.2.2.1	Radar Set AN/SPS-12	104
5.2.2.2	Radar Set AN/MPS-19	104
5.2.2.3	Mod II Radar	108
5.2.2.4	Radar Set AN/FPS-16	108
5.2.2.5	Radar Set AN/FPQ-11	112
5.2.2.6	Radar Set AN/MPS-504	112
5.2.2.7	NASA Long-Range S-Band (Spandar) . .	121
5.2.2.8	Radar Set AN/FPQ-6	121
5.2.2.9	Velocimeter, Model 10A, Doppler Radar .	125
5.2.3	Radar Application to Rocketsonde System .	129
5.3	TELEMETRY	
5.3.1	General	139
5.3.2	IRIG Telemetry Systems	140
5.3.3	DOVAP Telemetry Tracking System . . .	153
5.3.4	AN/GMD Telemetry and Tracking System .	159
5.3.4.1	General	159
5.3.4.2	Ground Station Equipment	160
5.3.4.2.1	Rawin Set AN/GMD-1	160
5.3.4.2.2	Rawin Set AN/GMD-2	165
5.3.4.2.3	Rawin Set AN/GMD-4	169
5.3.4.2.4	NASA Radiosonde ADP System	169

<u>Chapter</u>		<u>Page</u>
5.3.4.3	Rocketsonde Instrumentation	176
5.3.4.3.1	Stratospheric Temperature Sonde (STS-1) .	176
5.3.4.3.2	Arcasonde-1A	180
5.3.4.3.3	AN/DMQ-9	180
5.3.4.3.4	Datasonde	192
5.3.4.4	Miscellaneous Instruments	192
5.3.5	AN/SMQ-1 Telemetry Systems	199
5.3.5.1	General	199
5.3.5.2	Ground Station Equipment	199
5.3.5.3	Rocketsonde Instrumentation	202
5.3.6	Advanced Concept - Motorola Study . .	209
5.3.6.1	General	209
5.3.6.2	Ground Equipment	218
5.3.6.3	Radiosonde	223
6	<u>ROCKET VEHICLES</u>	
6.1	GENERAL	228
6.2	HISTORICAL REVIEW	233
6.3	CURRENT VEHICLE SYSTEMS	243
6.3.1	General	243
6.3.2	Arcas	248
6.3.3	Loki Dart	259
6.3.4	Skua	281
6.3.5	MT-135	282
6.3.6	Super Loki Chaff Dart	282
6.3.7	Viper Dart	298
6.3.8	Cajun Dart	303
6.3.9	Boosted Arcas	311
6.3.10	Nike Vehicles	321
6.4	DEVELOPMENT SYSTEMS	323
6.4.1	General	323
6.4.2	Improved Viper Dart	323
6.4.3	Super Loki Instrumented Dart	323
6.4.4	Destructable Arcas	324
6.4.5	Consumable Rocket	333
6.4.6	Army RDT&E Rocket	336

<u>Chapter</u>		<u>Page</u>
6.4.7	Kangaroo	337
6.4.8	Destructible Dart	339
6.5	DISCUSSION	346
6.5.1	General	346
6.5.2	Vehicle Performance	346
6.5.3	Vehicle Impact Dispersion	348
6.5.4	Vehicle Wind-Sensitivity	348
7	<u>GUN PROBES</u>	
7.1	GENERAL	351
7.2	5-INCH PROJECTILES	354
7.3	7-INCH PROJECTILES	358
7.4	16-INCH PROJECTILES	360
7.5	GUN-BOOSTED ROCKETS	362
7.6	METEOROLOGICAL ROCKET vs GUN PROBE COMPARISON	365
8	<u>SUMMARY</u>	369
	APPENDIX A	
	Corrections for Meteorological Rocket Temperature Soundings on an Individual Basis	379
	BIBLIOGRAPHY	381

LIST OF FIGURES

BOOK 2

<u>Figure</u>		<u>Page</u>
4.1 ROCKETSONDE DECELERATORS - GENERAL		
4.1-1	Velocity-Altitude Profile-Variou Ballistic Coefficients	3
4.1-2	Drop from 245,000 Ft to 200,000 Ft. W/C _D A-0.020	4
4.1-3	Altitude vs Decent Rate	5
4.1-4	Descent Curves from Various Release Altitude . .	6
4.1-5	Dynamic Pressure at Apogee	8
4.1-6	Critical Velocity for Parachute Self-Inflation . .	9
4.2 CONVENTIONAL PARACHUTES		
4.2-1	Hemispherical Parachute Gliding Mode	18
4.2-2	Arcas Gentex Parachute, 15 ^t Diameter	24
4.2-3	Cross-Sectional Diagram of the Arcas Parachute Assembly	26
4.2-4	Principle of Separation of the Arcas Payload Assembly	26
4.2-5	Arcas Parachute and Payload after Expulsion . . .	27
4.2-6	Arcas Parachute (Gentex Company) Descent Rate Average for Standard Payload Weight	29
4.2-7	Arcas Parachute Fall Rates	30
4.2-8	Arcas Parachute Descent Curve	31
4.2-9	FPS-16 Radar Tracks of Arcas Flights at Pacific Missile Range	34
4.2-10	Initial Wind Response Altitude vs Apogee Altitude .	35
4.2-11	Arcas Parachute Fall Rate Data-WSMR Flights #1 .	36
4.2-12	Arcas Parachute Fall Rate Data-WSMR Flight #2 .	37
4.2-13	Arcas Parachute Fall Rate Data-WSMR Flight #3 .	38
4.2-14	Arcas Parachute Fall Rate Data-WSMR Flight #4 .	39
4.2-15	Arcas Parachute Fall Rate Data-WSMR Flight #5 .	40
4.2-16	Arcas Parachute Fall Rate Data-WSMR Flight #6 .	41
4.2-17	Arcas Parachute Fall Rate Data-WSMR Flight #7 .	42
4.2-18	Arcas Parachute Fall Rate Data-WSMR Flight #8 .	43

<u>Figure</u>		<u>Page</u>
4.2-19	Dartsonde Instrument Package on 7.6' Chute . . .	45
4.2-20	Loki 7.6 Parachute-Sonde Descent Velocity . . .	47
4.2-21	Loki 7.6 Parachute-Sonde Descent Time	47
4.2-22	Loki #173 Launched 19 October 1967	48
4.2-23	Loki 7.6 Descent Rate Profiles - WSMR Flight Test Data, #1	49
4.2-24	Loki 7.6 Descent Rate Profiles - WSMR Flight Test Data, #2	50
4.2-25	Loki 7.6 Descent Rate Profiles - WSMR Flight Test Data, #3	51
4.2-26	Loki 7.6 Descent Rate Profiles - WSMR Flight Test Data, #4	52
4.2-27	NOL Wind Sensor Parachute	54

4.3 PARACHUTES WITH GEOMETRY POROSITY

4.3-1	Disk-Gap-Band Parachute Configuration	56
4.3-2	Modified Deployment Bag with Packed Parachute .	60
4.3-3	Sequence of DGB Deployment Events	61
4.3-4	Cross Patch Parachute	63
4.3-5	35' Cross Patch Parachute Fall Rate Results	65
4.3-6	Drag Coefficient of Annular Plates (Rings)	67
4.3-7	Annular Ring Parachute Design	68
4.3-8	Wagon Wheel Parachute	69
4.3-9	Ring Sail Parachute	70

4.4 STOKES FLOW RIBBON MESH PARACHUTE

4.4-1	Drag Coefficient of an Infinite Single Cylinder . .	75
4.4-2	Drag Coefficient for a Flat Disc with 20% Solidity in a Normal Flow	76
4.4-3	The Concept of the Stokes Flow Ribbon Mesh Parachute	77
4.4-4	Descent Trajectory of the Dartsonde Parachute . .	80
4.4-5	Descent Trajectory of the Dartdrifter Parachute . .	81
4.4-6	Descent Trajectory of the Arcas Parachute	82
4.4-7	Experimental Drag Coefficients for Models of 0.2, 0.1 and 0.05 Solidity as a function of Reynolds Numbers compared with Theory	85

4.5 RAM-AIR DECELERATORS

4.5-1	Ballute Configuration (Typical)	90
4.5-2	Ballute Drag Force Distribution	91
4.5-3	Typical Ballute	92
4.5-4	Loki Dart Starute Configuration Sketch	95
4.5-5	Typical Telemetry Records from Parachute Flight and a Loki Starute Flight	96
4.5-6	NOL Biconical Decelerator	99

5.2 RADAR

5.2-1	Radar Set AN/MPS-19, Block Diagram	107
5.2-2	Model 10A Velocimeter, Block Diagram	130
5.2-3	The Mean of 6 Cases from FPS-16 Tracks	133
5.2-4	S-Band Radar Track of 8-Foot Parachute	134
5.2-5	S-Band Radar Track of S-Band Chaff	136
5.2-6	X-Band Radar Track of X-Band Chaff	137
5.2-7	Signal Strength vs Time after Expulsion of Chaff . .	138

5.3 TELEMETRY

5.3-1	IRIG FM/FM Telemeter Subcarrier Bands	141
5.3-2	Pulse Duration Modulation	145
5.3-3	Missile Antenna Configurations	149
5.3-4	PDM/FM Telemetry System, Block Diagram	150
5.3-5	FM/FM Telemetry System, Block Diagram	151
5.3-6	FM/AM Telemetry System, Block Diagram	152
5.3-7	X-Band Telemetry Receiving System, Block Diagram .	154
5.3-8	Representative Dovap Telemetry Record	156
5.3-9	Shroud-Type Dovap Antenna Radiation Pattern #1 .	157
5.3-10	Shroud-Type Dovap Antenna Radiation Pattern #2 .	158
5.3-11	Rawin Set AN/GMD-1A, Systems	162
5.3-12	Rawin Set AN/GMD-1B, Functional Diagram . . .	163
5.3-13	Block Diagram of the TMQ-5 Recorder	166
5.3-14	Rawinsonde System AN/GMD-2, Block Diagram . .	168
5.3-15	Statistical AN/GMD-2 Wind Errors vs Slant Range for Averaging Times	170
5.3-16	Simplified Block Diagram of AN/GMD-4 System . .	171

<u>Figure</u>		<u>Page</u>
5.3-17	Radiosonde ADP System Simplified, Block Diagram .	174
5.3-18	Stratospheric Temperature Sonde, STS-1	178
5.3-19	STS-1 Electrical Circuit Diagram	179
5.3-20	Arcasonde-1A Instrument and Nose Cone	181
5.3-21	Arcasonde-1A Instrument Components	182
5.3-22	Arcasonde-1A, Block Diagram	183
5.3-23	AN/DMQ-9 Rocket Instrument Package	185
5.3-24	AN/DMQ-9 Block Diagram	187
5.3-25	AN/DMQ-9 Schematic Diagram	188
5.3-26	Datasonde Instrument Configuration	193
5.3-27	Arcasonde-3 Instrument	196
5.3-28	Arcasonde-3, Telemetry Block Diagram	197
5.3-29	AN/SMQ-1 Radiosonde Receptor, Block Diagram .	203
5.3-30	Radiosonde Set WOX-1A	205
5.3-31	WOX-1A, Block Diagram	206
5.3-32	Advanced Sounding System, Block Diagram	211
5.3-33	PN Range System	216
5.3-34	Telemetry Modulator, Block Diagram	217
5.3-35	Telemetry Extractor, Block Diagram	220
5.3-36	Range Signal Demodulator, Block Diagram	220
5.3-37	64 kHz Component vs Code Correlation-Zone Loop .	222
5.3-38	64 kHz Component vs Code Correlation-Code Loop .	222
5.3-39	AMSS Radiosonde, Block Diagram	225

6.3 CURRENT VEHICLE SYSTEMS

6.3-1	Meteorological Rocket Configurations	244
6.3-2	The Arcas Rocket	249
6.3-3	Arcas Nose Cone	251
6.3-4	Cross-Sectional Diagram of the Arcas Motor	253
6.3-5	The Major Components of the Arcas Vehicle	256
6.3-6	Major Components of the Closed-Breech Arcas Launcher	257
6.3-7	Principle of Operation of the Arcas Closed-Breech Launcher	258
6.3-8	The Loki Dart Meteorological Sounding Rocket . . .	261
6.3-9	Loki-Dart Vehicle Configuration	263
6.3-10	Cross Section of the Instrumented Dart	265
6.3-11	Photo of Instrumented Dart System	267
6.3-12	Meteorological Probe PWN-8B, Major Dimensions .	268

<u>Figure</u>		<u>Page</u>
6.3-13	PWN-8B System, Dart Cross Section	269
6.3-14	Payload Expulsion Sketch	271
6.3-15	Rocket Launcher LAU-66/A	278
6.3-16	Major Dimensions of Launcher LAU-66/A	279
6.3-17	Skua Performance Curves	283
6.3-18	Super Loki Vehicle Configuration	287
6.3-19	Super Loki Chaff Dart Vehicle Configuration	288
6.3-20	Super Loki Chaff Dart compared with Standard Loki Dart Vehicle	289
6.3-21	Cross-Section view of Super Loki Rocket Motor	291
6.3-22	Cross-Section view of Super Loki-Chaff Dart	292
6.3-23	Super Loki Launch Rail Assembly	294
6.3-24	Typical Base for Super Loki Launch Rail	295
6.3-25	Nominal Trajectory Summary - Super Loki Dart	296
6.3-26	Viper-Dart Vehicle Configuration	299
6.3-27	Viper-Dart (Dart) Cross Section View	300
6.3-28	Viper Motor and Components	302
6.3-29	Nominal Dart Trajectory, Viper Dart	306
6.3-30	Cajun Dart Vehicle Configuration	307
6.3-31	Cutaway View of the Cajun Dart	309
6.3-32	Cajun-Dart Altitude vs Range	310
6.3-33	Boosted Arcas Vehicle Configuration	312
6.3-34	Sidewinder Arcas Vehicle Configuration	315
6.3-35	Sparrow Arcas Vehicle Configuration	317
6.3-36	Boosted Arcas II Vehicle Configuration	319

6.4 DEVELOPMENT SYSTEMS

6.4-1	Super Loki Instrumented Dart Nominal Trajectory	325
6.4-2	Frangible Arcas Vehicle Configuration	328
6.4-3	Nominal Frangible Arcas Flight Events Sequence	331
6.4-4	Consumable Meteorological Rocket Operation Concept	334
6.4-5	Kangaroo Dart Vehicle Configuration	342

<u>Figure</u>		<u>Page</u>
	7.1 GUN PROBES - GENERAL	
7.1-1	Gun Probe Performance Summary	352
	7.2 5-INCH GUN PROJECTILES	
7.2-1	5-Inch Gun Projectile Configuration	355
7.2-2	5-Inch Projectile Nominal Trajectories	356
	7.3 7-INCH GUN PROJECTILES	
7.3-1	Gun Probe Loading Mechanism	359
	7.4 16-INCH GUN PROJECTILES	
7.4-1	Typical Martlet-2C Payload Configurations	363
	7.5 GUN-BOOSTED ROCKETS	
7.5-1	Gun Boosted Rocket Configurations	363
	8.1 SUMMARY	
8.1-1	ETR- APOLLO II Launch Support Density Profile 14 July 1969	371
8.1-2	ETR -APOLLO II Launch Support Density Profile 16 July 1969	372
8.1-3	ETR -APOLLO II Launch Support Wind Profile 14 July 1969	373
8.1-4	ETR -APOLLO II Launch Support Wind Profile 16 July 1969	374
8.1-5	ETR -APOLLO II Launch Support Temperature Profile - 14 July 1969	375
8.1-6	ETR -APOLLO II Launch Support Temperature Profile - 16 July 1969	376

LIST OF TABLES

BOOK 2

<u>Table</u>		<u>Page</u>
4. ROCKETSONDE DECELERATORS		
4-1	Fall Velocities at Various Altitudes	17
4-2	Arcas 15' Gentex Parachute	25
4-3	Fall Rate Study of Arcas Parachute and Sonde Payload	32
4-4	Initial Wind Response Lag Data	33
4-5	Loki 7.6 Irvin Parachute	46
4-6	Arcas Cross Patch Parachute Design Parameters . .	64
4-7	Proposed Parachute Design Parameters	79
4-8	Summary of Test Results and Model Weights for Models of Different Solidity	84
4-9	Comparison of Proposed Dartdrifter Model (Theoretical) with Chamber Tests Data	86
4-10	Arcasonde Ballute Specifications	93
4-11	Dartsonde Starute Specifications	97
5. TELEMETRY AND TRACKING		
5-1	Radar Set AN/SPS-12, Technical Characteristics . .	105
5-2	Radar Set AN/MPS-19, Technical Characteristics .	106
5-3	Mod II Radar, Technical Characteristics	109
5-4	Radar Set AN/FPS-16, Technical Characteristics . .	113
5-5	Radar Set AN/FPQ-11, Technical Characteristics .	117
5-6	Radar Set AN/MPS-504, Technical Characteristics .	120
5-7	SPANDAR, Technical Characteristics	122
5-8	Radar Set AN/FPQ-6, Technical Characteristics . .	126
5-9	Model 10A Velocimeter, Technical Characteristics .	131
5-10	Radar Characteristics	132
5-11	IRIG FM/FM Telemeter Subcarrier Bands	142
5-12	X-Band Telemetry System Characteristics	155
5-13	AN/GMD-1 Specifications	167
5-14	Rocketsonde Instruments	177
5-15	Arcasonde-1A Specifications	184

<u>Table</u>		<u>Page</u>
5-16	Arcasonde-2B Specifications	195
5-17	Arcasonde-3 Specifications	198
5-18	Advanced System Characteristics	212
5-19	AN/AMQ-9 vs AMSS Comparison	213
5-20	AMSS Radiosonde Characteristics	226

6. ROCKET VEHICLES

6-1	Meteorological Rockets	234
6-2	Summary of ARC Rocket Study	239
6-3	Summary of Current Meteorological Rocket Vehicles	245
6-4	Loki Dart Vehicles	246
6-5	Obsolete Vehicles	247
6-6	Arcas Rocket System Dimensions	252
6-7	Arcas Rocket Motor Performance Characteristics	255
6-8	Flight Performance Characteristics of the Arcas System	260
6-9	Principle Characteristics of the Loki Sounding Rocket	264
6-10	Rocket Motor Major Design Characteristics Summary	273
6-11	Hardware Design Characteristics Comparison	274
6-12	Rocket Motor Ballistic Performance Comparison	274
6-13	Skua - General Specifications	284
6-14	Japanese MT-135 vs Arcas	285
6-15	Super Loki Rocket Motor Design Characteristics Summary	290
6-16	Super Loki Chaff Dart Design Characteristics	290
6-17	Nominal Trajectory Summary, Super Loki Dart	297
6-18	Viper Dart Weight Table	304
6-19	Nominal Performance Summary	305
6-20	Summary of Boosted Arcas Vehicles	313
6-21	Summary of Nike-Boosted Vehicles	322
6-22	Comparison of the Super Loki with the Current Loki Dart System	326
6-23	Frangible Arcas Vehicle Dimension and Weight Comparisons	329
6-24	Detailed Weight Breakdown of the Frangible Arcas Vehicle	330

<u>Table</u>		<u>Page</u>
6-25	AMICOM RDT&E Rocket Design Characteristics . .	338
6-26	Kangaroo Weight Table	343
6-27	Corning Glass Works Pyro Ceram Physical Properties	344
6-28	Comparison of Wind Dispersion Effects for Various Vehicles	350

7. GUN PROBES

7-1	Meteorological Rocket vs Gun Probe Comparison . .	366
-----	---	-----

ROCKETSONDE DECELERATORS

4.1 General.

High altitude decelerators, such as parachutes or inflatable structures, have been used to conduct meteorological soundings to altitudes of at least 60 kilometers. Although many of these same data could have been obtained as direct probe measurements, it was found to be more economical to employ a descent vehicle and a rocketsonde payload. The instrumentation for these payloads has been a great deal less sophisticated and less costly than would be required for direct probing during rocket vehicle ascent. It is likely that rocketsonde techniques will be required for gathering data to the upper altitude limits of at least the simpler sensors to maintain a low system cost. Therefore, the need for improved decelerators in future systems is of paramount importance.

The requirements for a meteorological rocketsonde decelerator can be enumerated as follows:

1. Low ballistic coefficient
2. Deployment reliability
3. Acceptable stability
4. Adequate radar cross-section
5. Relatively constant descent rate
6. Low cost

Although the above factors are interdependent to some degree, each is discussed separately in the sections which follow for ease in presentation.

4.1.1 Ballistic Coefficient.

A low ballistic coefficient ($W/C_D A$) is the primary factor which governs the usefulness of a high altitude meteorological decelerator system. This characteristic determines the equilibrium or terminal fall rate of the rocketsonde

at the various altitudes as indicated in Figure 4.1-1. Also for a given apogee or deployment altitude, the ballistic coefficient determines the maximum dynamic overshoot velocity and the altitude at which the descending system reaches terminal velocity. Figure 4.1-2 presents initial trajectory data for a typical high-altitude deployment of a descent system with a given ballistic coefficient. The system accelerates downward past the zero g value (where drag equals weight) and then accelerates in the upward direction because the drag force at this point is greater than the weight. This upward acceleration continues until the vehicle slows down to terminal velocity for the particular altitude where the drag force equals the weight. In the meantime the descent velocity has significantly exceeded or overshoot the terminal velocity. At a lower altitude the descent velocity slows up to the terminal velocity value. After this the terminal velocity curve is followed during the remainder of the descent provided the system remains deployed and aerodynamically stable. The net result is that for a high altitude deployment, the descent systems fall faster than terminal velocity for a portion of the descent. The magnitude of this velocity overshoot is a function of ballistic coefficients as indicated in Figure 4.1-3. The overshoot velocity is also a function of deployment altitude as indicated in Figure 4.1-4.

For most meteorological measurements utilizing the rocketsonde technique, descent velocities must be maintained at subsonic levels. Aerodynamic heating of the sensor, stagnation pressure increase and wind shear measurement error are all a function of the square of the descent velocity and measurement errors increase drastically as fall velocity increases. In addition, faster fall rates present to the sensor instrumentation a greater timewise gradient of the parameter to be measured. Most of the inexpensive sensors and instrumentation are response time limited, and the measurement accuracy is thereby degraded by fast fall rates. Transonic and supersonic velocities render most of the meteorological measurements useless. Therefore, an adequately low ballistic coefficient for the descent system is necessary for accurate measurements. Once this ballistic coefficient is determined, then the optimum deployment altitude can be selected. To achieve a low ballistic coefficient the weights of the descent vehicle and payload instrumentation must be kept to as low a value as possible. Payload miniaturization must be carried to the extent which is economically feasible. In addition, the drag of the descent vehicle should be maximized based upon packaging volume requirements. Generally speaking, this means

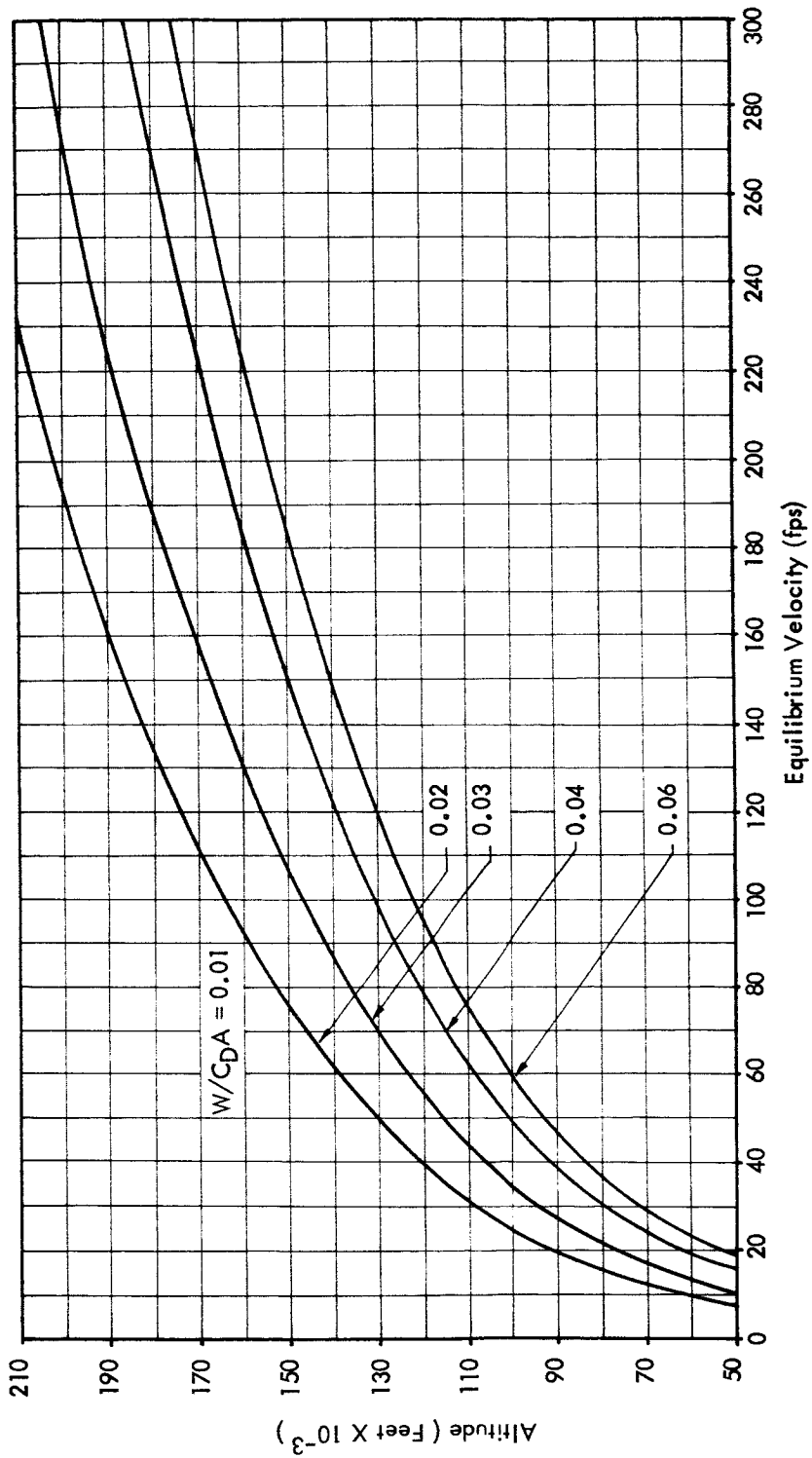


FIGURE 4.1-1 VELOCITY ALTITUDE PROFILE - VARIOUS BALLISTIC COEFFICIENTS

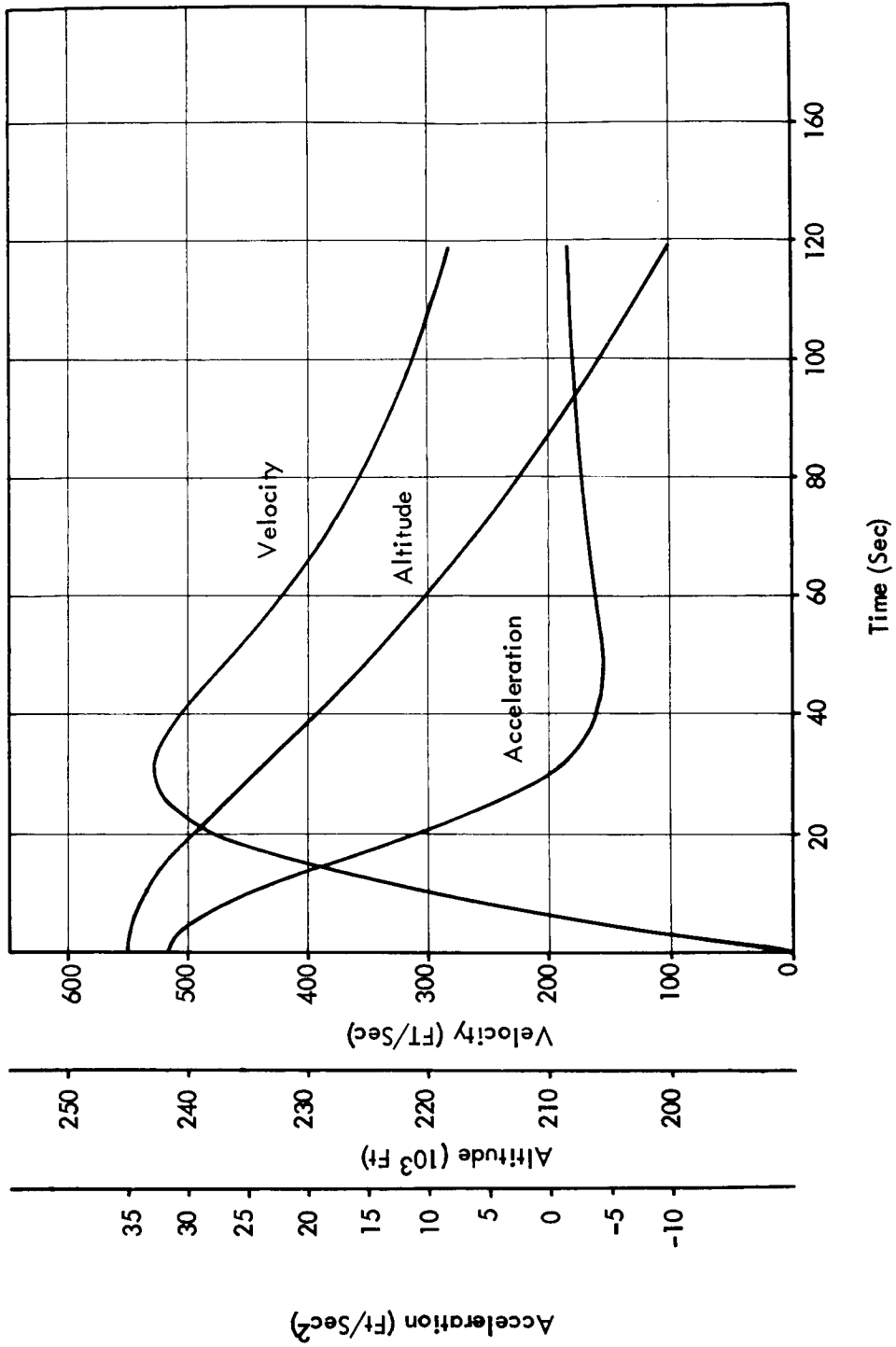


FIGURE 4.1-2 DROP FROM 245,000 FT. TO 200,000 FT. $W/C_{DA} = 0.020$

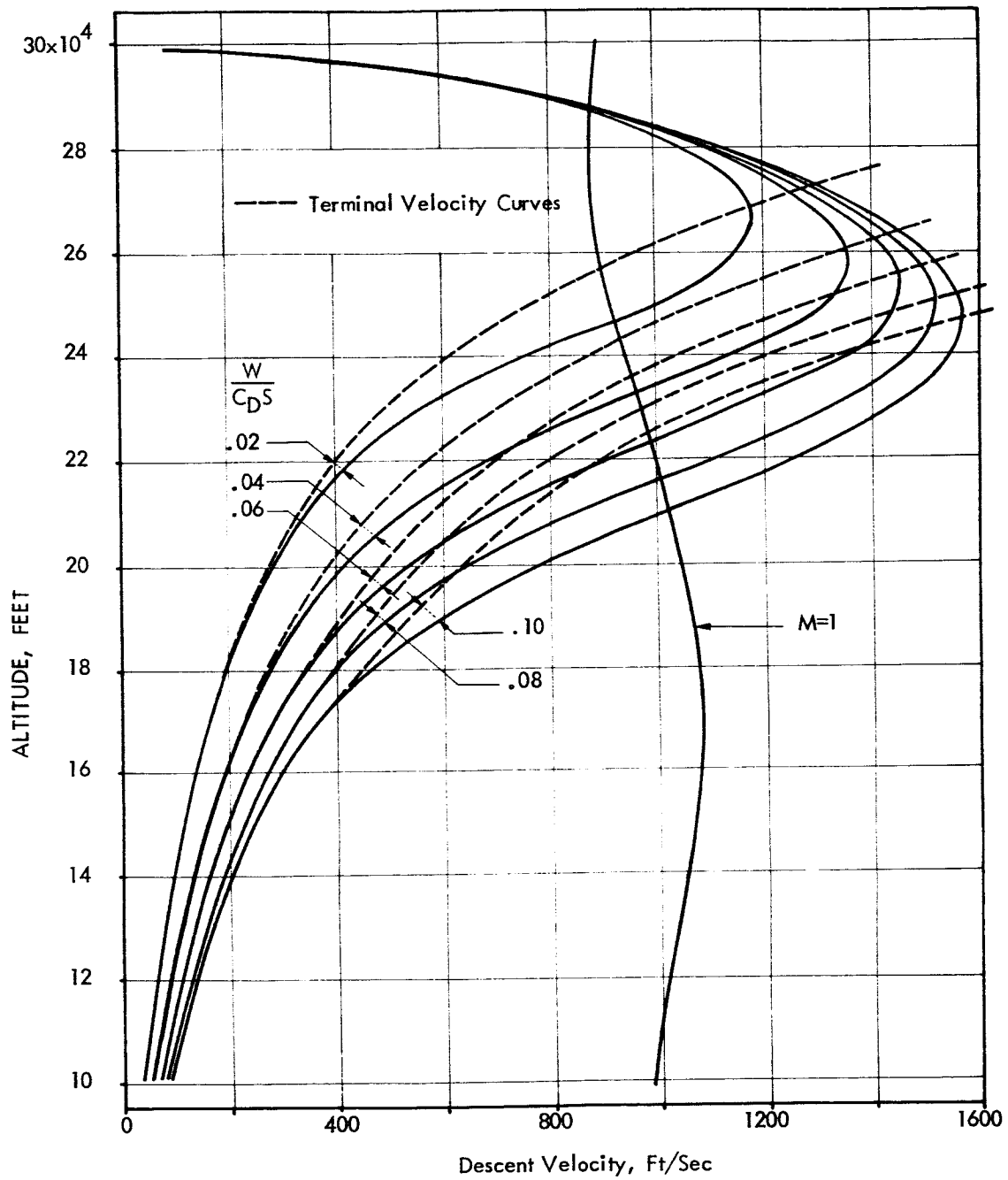


FIGURE 4.1-3 ALTITUDE VS. DESCENT RATE

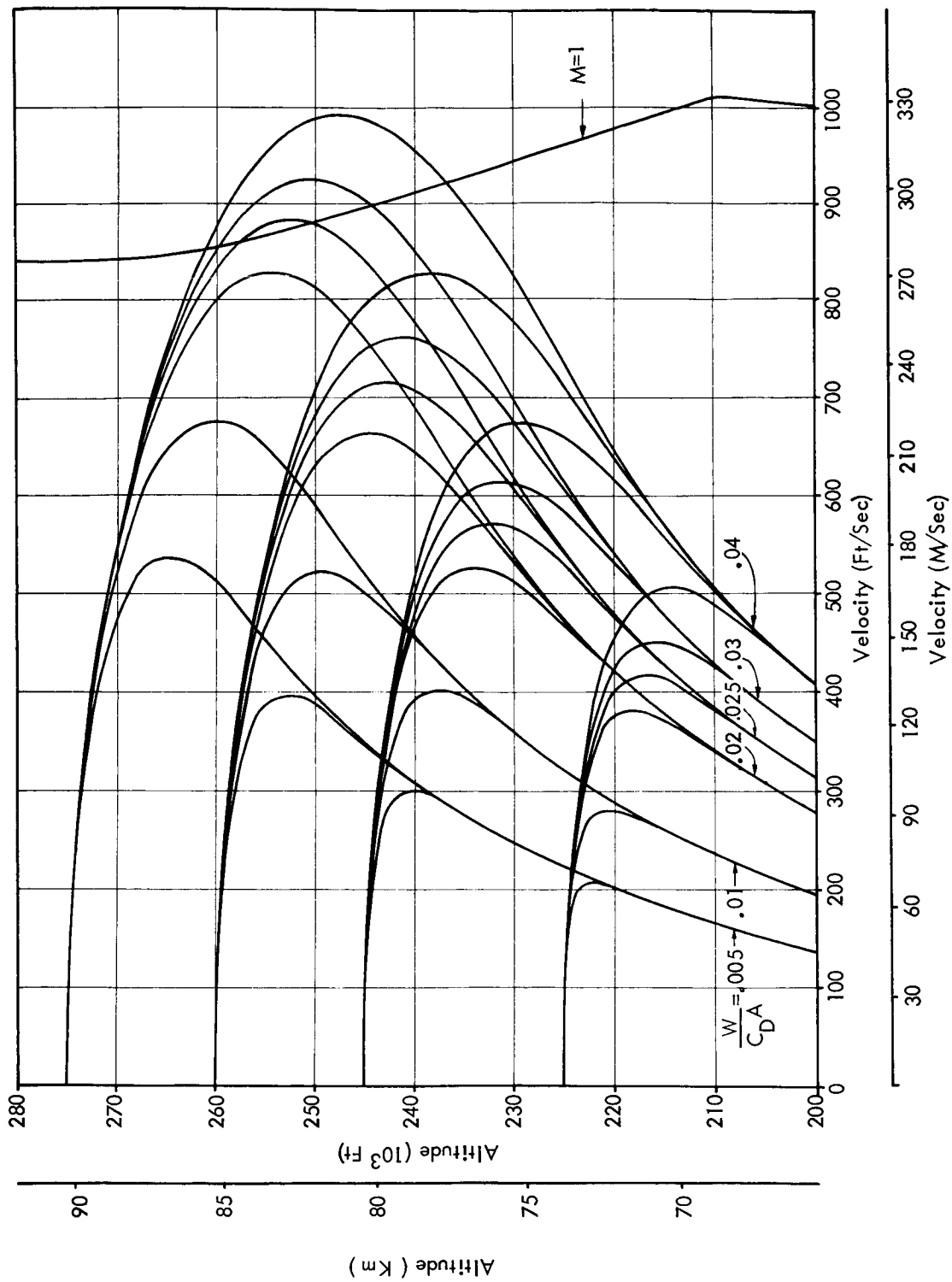


FIGURE 4.1-4 DESCENT CURVES FROM VARIOUS RELEASE ALTITUDES

that the drag coefficient per unit packaging volume should be maximized for the flow region being considered. This indicates the use of very thin and lightweight fabrics for canopy materials. The weight and packaging volume requirements for shroud lines and fittings should also be minimized.

4.1.2 Deployment Reliability.

To achieve the descent rates indicated by the respective ballistic coefficient, the decelerator must achieve full deployment upon ejection from the rocket vehicle. Conventional silk parachutes require a dynamic pressure of at least 0.03 to 0.07 lbs/ft², depending upon parachute design, in order to inflate reliably. The dynamic pressure is a function of deployment altitude and velocity. For a given rocket vehicle both of these factors are related to launch angle. Typical examples are presented in Figure 4.1-5 which indicated marginal inflation reliability for the Arcas parachute at launch angles above 86° and for the Loki Dart parachute at launch angles above 83°. Deployment velocity vs. deployment altitude for reliable inflation of conventionally shaped silk parachutes are presented in Figure 4.1-6. These data indicate that self inflation is not practical above an altitude of about 230,000 feet. Above this altitude the critical inflation velocity is in the transonic and supersonic flow regions.

In addition to the altitude and deployment velocity effects upon self inflation reliability, the deployment altitude wind velocity must be considered. High altitude winds can be as great as typical deployment velocities, and can either subtract from or add to the deployment velocity depending upon wind direction.

The above factors indicate the need for positive inflation techniques for decelerator deployment much above 180,000 feet.

4.1.3 Stability.

In order to take full advantage of the decelerator ballistic coefficient, a reasonable degree of stability must be achieved. The drag coefficient for many decelerators is slightly greater at a small angle of attack than at zero and does not fall off much until about 30 degrees is experienced. Therefore, from a fall rate standpoint oscillations as great as ± 30 degrees are not objectionable.

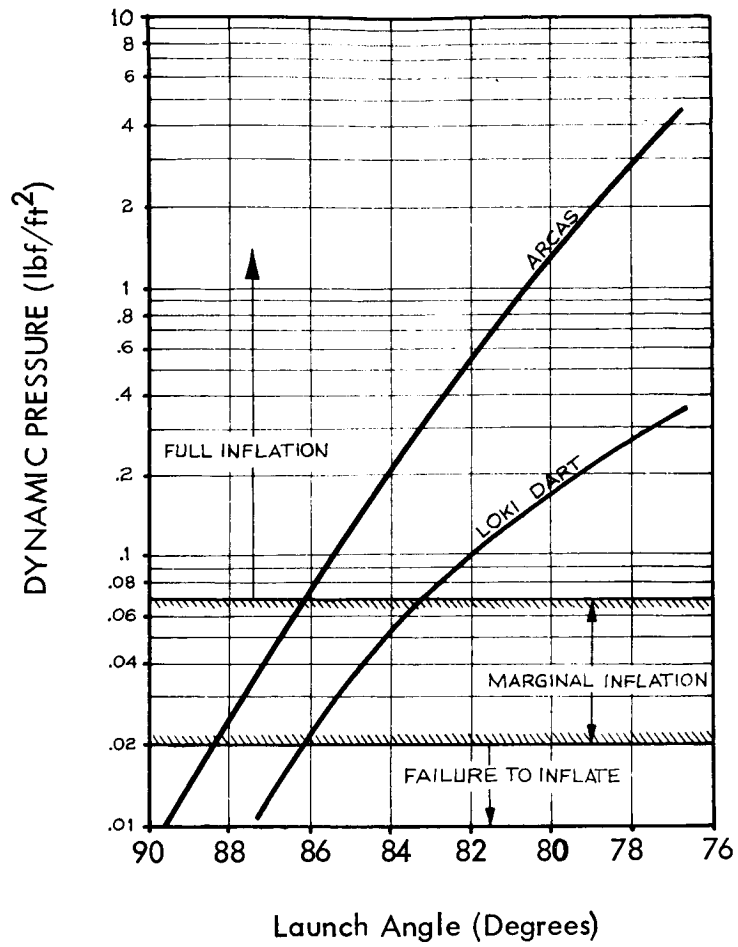
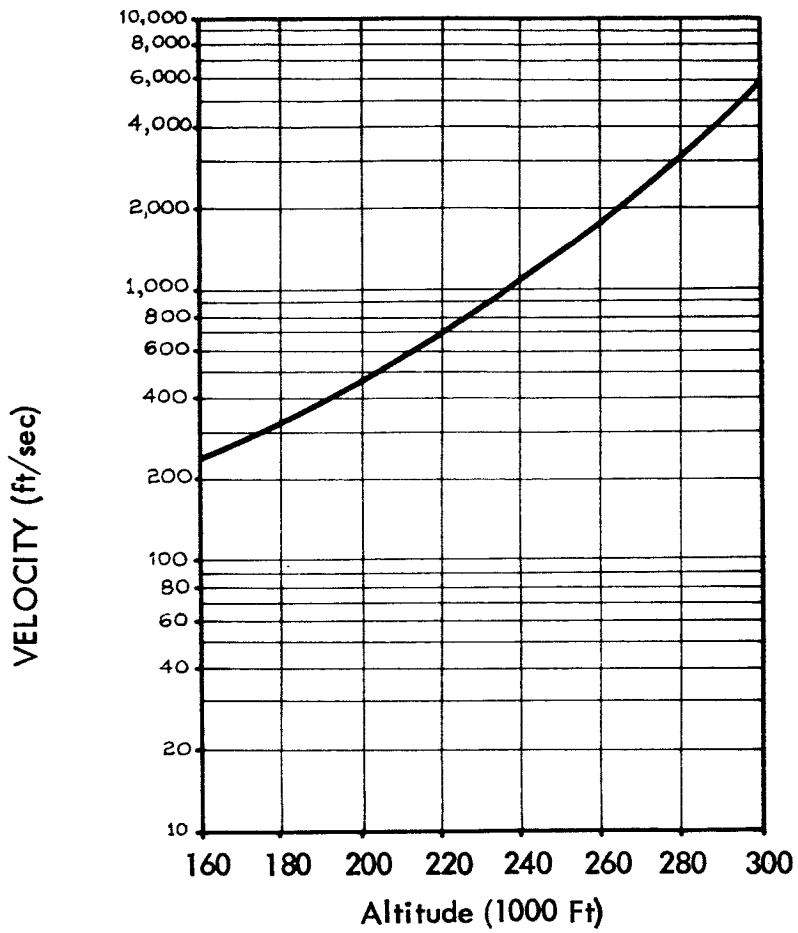


FIGURE 4.1-5 DYNAMIC PRESSURE AT APOGEE



Assuming Critical Inflation Dynamic Pressure = 0.07 lbf/ft^2

FIGURE 4.1-6 CRITICAL VELOCITY FOR PARACHUTE SELF-INFLATION

Some authors have implied that even a mildly oscillating system would result in wind measurement errors because of the instantaneous horizontal component of velocity established at an instantaneous angle of attack. However, when the period of the oscillation is taken into account, it has been found that the horizontal displacement due to the oscillation is negligible, i.e., within the random error (rms) of the typical tracking radars.

A major objection to instability of the decelerator is that relatively severe telemetry signal dropouts occur for severely oscillating decelerators. All of the sondes flown to date have nulls in the transmitted antenna patterns along the longitudinal axis of the sonde. At high elevation angles where the decelerators oscillate to the greatest extent, signal dropouts at the receiver are most troublesome. As the sonde descends to a lower altitude and the oscillations dampen, signal dropouts are virtually eliminated. Very often there is a severe loss of telemetered data in the high altitudes where it is most needed. Therefore, stability of the decelerator within reasonable bounds is important for high altitude data retrieval.

The effect of decelerator oscillations on the sensor instrumentation has been mentioned by some authors as an important factor, however, for the sensors flown to date the normal attitude variations of the sensors due to decelerator oscillations have not appeared to cause any significant error in the reduced data.

4.1.4 Radar Cross-Section.

A majority of the rocketsondes which have been flown in the past have required radar tracking of the decelerator. The current development trend is toward a telemetry instrument which incorporates slant range tracking in addition to azimuth and elevation angle determination. With such an instrument the requirement for radar tracking will be eliminated and the decelerator will not be required to present a radar target. However, if the cost of the transponder type instrument is significantly greater than the transmit-only type, the latter sonde will probably be used at launch sites where tracking radar is available. For these systems the decelerator will be required to incorporate a radar target with at least a 71m^2 radar cross-section. This is generally accomplished by coating the silk canopy material with either a silver or copper conductive finish. Canopies can also be formed with aluminized mylar for this purpose.

4.1.5 Constant Descent Rate.

Since the upper altitude densities are much less than those of the lower atmosphere, sensor response is generally a good deal slower at high altitudes. This is not only true of sensors such as the thermistor temperature measurement element but is also true of wind response of the decelerator. Most of the decelerators have a constant drag coefficient and fall fast at high altitudes and slow at the lower altitudes. This is indirect opposition to the sensor requirements. It would be advantageous to obtain as slow descent velocities as possible in the upper atmosphere and to increase the fall rates in the lower atmosphere. Although it is possible to employ reefing devices to achieve a more uniform fall rate, it is probably not worth the expense to speed up the fall rate in the lower atmosphere for the sake of saving a few moments of tracking time. Major efforts should be directed toward obtaining the slowest high altitude descent velocities possible.

4.1.6 Cost.

Since meteorological rocketsondes are being used on a routine basis, and a large number of them are being flown each year, the cost of the decelerator must be kept to a low value. One hundred dollars or so per unit seems to be a reasonable cost for such a device.

4.2 Conventional Parachutes.

4.2.1 General.

The meteorological rocketsonde parachute is used for wind measurement and to lower the temperature measuring sonde at a sufficiently slow velocity for adequate temperature measurements. The descent rate of the parachute is of prime importance since wind measurement errors and temperature measurement errors due to aerodynamic heating and sensor response lag are directly related to rate of fall of the parachute-sonde system. Of course, the parachute must deploy properly and fully inflate to take advantage of its shape and fabric area. Although the flat and hemispherical silk parachutes seem to inflate fairly reliably at altitudes as high as 180,000 feet, the mylar and specially shaped parachutes seem to require mechanical inflation aids, such as an inflatable torus ring. Although parachute stability is a desirable feature, oscillations as great as 30-degrees for most designs are probably not too harmful for descent rates, or telemetry signal drop outs. In general, the drag coefficient for most parachute designs increases with angle of attack up to about 15 to 20 degrees. For parachutes oscillating within this range, slower rather than more rapid descent rates, compared to a perfectly stable parachute, are to be expected. The period of oscillation has been found experimentally to agree with the law of the simple pendulum where the effective length of the pendulum is related to the shroud line length in the expression for the natural period, T , as in

$$T = 2 \pi \sqrt{L/2} \quad \text{where } L = \text{Length of shroud lines}$$

For the Arcas parachute the effective length, L , is 20-feet and the period, T , is 5-seconds. For the smaller dartsonde parachutes the effective lengths, about 10-feet, and the corresponding periods, about 3.5-seconds, are shorter than for the Arcas parachute. For both types of parachutes the oscillation periods are so short that displacements of the parachutes which might lead to wind determination error are negligible. The prime consideration for parachute design should, therefore, be to obtain as slow a descent rate as possible to minimize measurement errors.

4.2.2 Design Parameters.

To appreciate some of the problems of designing an effective parachute (or decelerator of any kind) imagine a stationary decelerator in a stream of moving air. Conservation of mass flow requires that the air must be deflected and caused to flow around the decelerator. The shadow area aft of the body experiences a low pressure and the diverted air tends to collapse into the shadow, usually in a highly turbulent manner.

Now, turbulence has both its good and its bad effects. It can be shown that those shapes that create the most turbulence also offer the highest amount of drag or resistive force. Because turbulence represents a consumption of energy, this correlation should not be surprising. Unfortunately, turbulence also produces undesirable instabilities.

Wind tunnel tests show that the shadow area behind the canopy tends to be filled from two sections at opposite points on the circumference in a seesaw manner. As the collapsing airstream oscillates, so does the local external pressure, and since the force on the canopy is governed by the difference between internal and external pressure, a cyclical rocking moment develops. The parachute oscillates at a rate and magnitude governed by a complex set of factors. In some cases the oscillation may cause the load to swing through an arc of 60-degrees or more.

None of the conventional parachute designs - and that includes the hemisphere, the flat-circular, and the conical - are particularly stable in flight. All of them allow the payload to swing beneath the canopy, particularly when the air itself is turbulent, gusty and unstable. Conventional parachutes do not open reliably at very low dynamic pressures and they exhibit poor stability with coning angles or oscillations of about $\pm 45^\circ$ or more at high altitudes. Experience with parachutes at dynamic pressures below 1 lb/ft^2 has shown that for repeatable and immediate canopy opening, an inflation aid must be provided.

Descent rates of current conventional parachutes are excessive for accurate meteorological measurements above an altitude of 180,000 feet. The ballistic coefficients of the current parachute - sonde systems are greater than 0.05 lb/ft^2 and larger parachutes are required for the given payload weight to reduce the fall rates. As long as metalization of the silk canopy fabric is required for radar tracking, it appears that the conventionally shaped parachute is limited to a ballistic coefficient of at least 0.01 lb/ft^2 by itself without any allowance for payload weight.

Fairly extensive investigations indicate that a major problem in parachute deployment is the tangling and twisting of the parachute shroud lines and their interference with the canopy. Photography has shown that shroud lines flung over the crown of the parachute have reduced the effective flying area and have caused the abnormal descent rates. There have also been discontinuities in the descent rates of recent conventional parachute systems. It appears that once the parachute has been sized properly for the

desired descent rate and the dynamic pressure is adequate for self-inflation, the major cause of failure to attain this rate is mechanical tangling of the shroud lines which causes a reduction in the effective canopy area. High rocket spin rates may certainly be a cause of such interference and twisting of the shroud lines, but it is probable that some degree of tangling will take place even with modest vehicle spin rates.

Although the high altitude parachutes are suspected of gliding to a certain degree, this has been difficult to detect since gliding would be interpreted as wind drift during data reduction of the tracking data. Solid mylar parachutes, without special apertures to create an artificial porosity, and even the fine mesh 3-momme silk parachutes most likely have very little effective permeability at high altitudes. These parachutes, therefore, must be susceptible to a degree of instability in gliding and/or oscillating. It is well known that the Arcas and Loki parachute oscillate to angles nearly horizontal with the horizon, and that these oscillations, although eventually damped out, will persist down to altitudes of 80,000 feet. Variations in the initial deployment or injection conditions will no doubt govern the magnitude of the high altitude oscillations from flight to flight. There is a great deal of flight data on received telemetry signal strength variations to indicate that large oscillations occur on every flight.

Although parachute stability is desired, payload packaging volume and fall rates are critical in the rocketsonde application; therefore, the parachute fabric area is critical.

A brief review of the factors which affect parachute performance is presented in the paragraphs as follows:

1. Basic Shape - The drag coefficient of a particular parachute design does not vary appreciably with flow speed at Reynolds numbers above $R_e = 1000$. For the high altitude applications it is certain that the descent conditions will maintain values well above this limit so that a constant drag coefficient can be used.

The Reynolds number data for typical conditions in the high altitude for parachutes is as follows:

Altitude	170,000 feet
Descent Velocity	225 ft/sec
$\rho = 1.6929 \times 10^{-6}$	lbf-sec ² - ft ⁻⁴
$\mu = 3.6816 \times 10^{-7}$	lbf-sec ft ²

<u>Parachute</u>	<u>Flying Diameter</u>	<u>Crown Height</u>	<u>Reynolds Number</u>
Arcas	15.0 ft	7.5 ft	8,800
Dartsonde	6.0 ft	3.0 ft	3,520

Experimental evidence indicates that a maximum drag coefficient, which is based on projected area, is obtained for a parachute with a crown height to inflated to flying diameter ratio of one-half (0.5); that is, for a parachute which is approximately hemispherical in shape. If designed and joined together as flat circles, parachute canopies have inflated diameters which are approximately two-thirds (0.66) of the laid-out fabric diameters and are essentially hemispherical in shape. The ratio of their inflated frontal area, S_{\square} , to that of the area of the fabric, S_{\circ} , is consequently on the order of $S_{\square} / S_{\circ} = 0.45$. The drag coefficient referred to canopy fabric area is then approximately $C_{D_{\circ}} = 0.45 C_{D_{\square}}$. The parachute descent velocity, U , can then be calculated as either,

$$U = \sqrt{\frac{2W}{\rho C_{D_{\square}} S_{\square}}} \quad \text{-- or --} \quad \sqrt{\frac{2W}{\rho C_{D_{\circ}} S_{\circ}}}$$

2. Equilibrium Descent Velocity - The descent velocity of a parachute system can be given by:

$$\dot{Z} = \sqrt{\frac{1}{K\rho} \left(1 + \frac{\ddot{Z}}{g} \right)}$$

where: $K = \frac{C_D S}{2 mg}$

$\rho =$ atmospheric density

$\ddot{Z} =$ altitude coordinate

$g =$ acceleration of gravity

If the second term, $\frac{\ddot{Z}}{g}$, is neglected, descent velocity can be predicted within 5-percent accuracy for $\dot{Z} \leq 140$ m/sec, and within a 1-percent accuracy for $\dot{Z} \leq 63$ m/sec. Table 4-1 can be used to predict descent velocities at various altitudes for given values of K.

3. Gliding - The stable equilibrium of a nonporous hemispherical parachute about a point 1.3 times the diameter below the canopy is at an angle of attack of approximately 45 degrees. A hemispherical parachute which does not oscillate may therefore maintain a steady gliding angle of 45 degrees in still air. The weight of the parachute and load is supported in this case by the resultant aerodynamic force, R, composed of both lift and drag as indicated in Figure 4.2-1. The effective vertical velocity or weight coefficient, $C_{W_{\square}}$, used to calculate descent velocity may be defined as

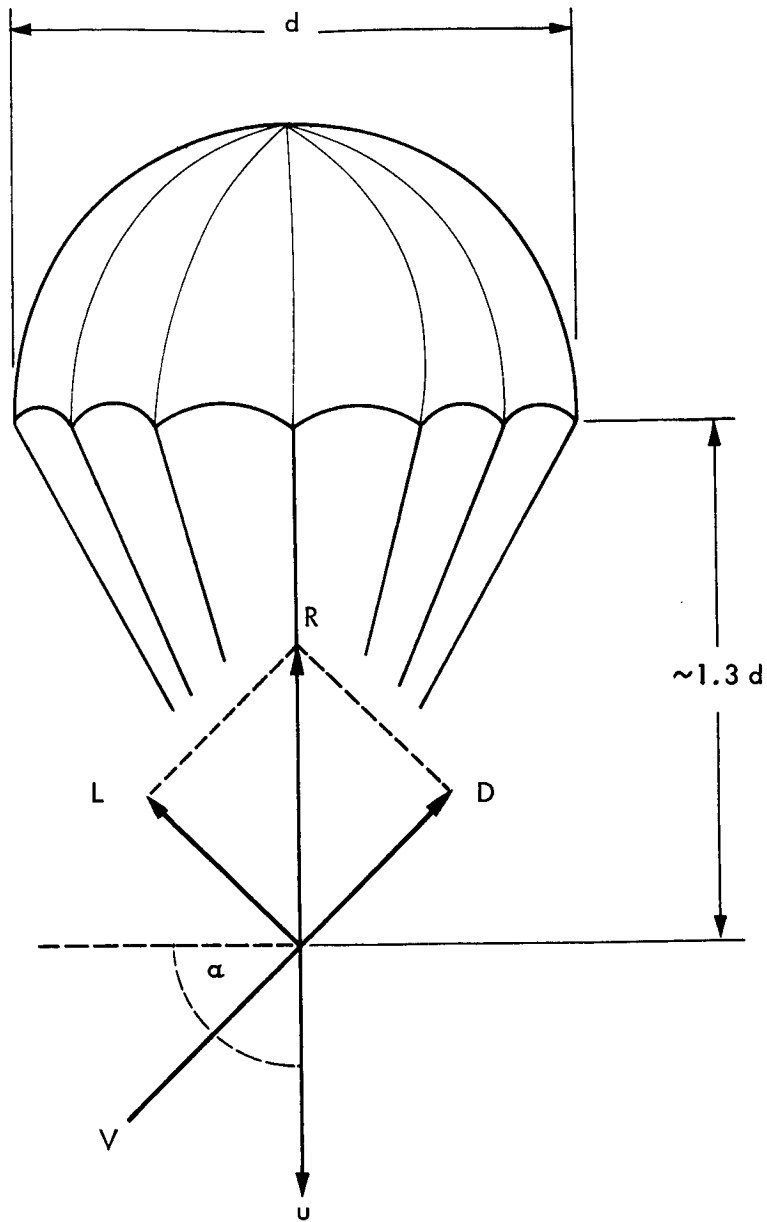
$$C_{W_{\square}} = \frac{W}{1/2 \rho U^2 S_{\square}} = \frac{C_{R_{\square}}}{\sin^2 \alpha}$$

where $C_{W_{\square}}$ may be as much as twice the value of $C_{R_{\square}}$. A gliding parachute has a slower rate of descent than a nongliding parachute by a factor of the square of the sine of the angle of attack. The angle of stable gliding is also affected by the shroud line length. For the rocketsonde application the gliding mode is to be avoided since the horizontal glide velocities will be interpreted as wind velocities in the data reduction and erroneous wind velocities will be reported. Gliding can be reduced by increasing the porosity or permeability of the parachute canopy.

TABLE 4-1 FALL VELOCITIES AT VARIOUS ALTITUDES (meters/sec)

$$\dot{z} = \sqrt{1/K\rho}$$

ALTITUDE		DENSITY	K VALUES																	
Km	Ft (App)	Kg/m ³	0.05	0.1	0.2	0.3	0.4	0.5	0.6	0.7	0.8	0.9	1.0	1.2	1.5	2.0	5.0	10.0	20.0	
20	65,600	8.8909x10 ⁻²	15	11	7	6	5	5	4	4	4	3	3	3	3	2	1	1	1	1
25	82,000	4.0639x10 ⁻²	22	16	11	9	8	7	6	6	6	5	5	5	4	3	2	2	2	1
30	98,400	1.7861x10 ⁻²	33	24	17	14	12	11	10	9	8	8	7	7	6	5	3	2	2	2
35	114,800	8.2619x10 ⁻³	49	35	25	20	17	16	14	13	12	12	11	10	9	8	5	3	2	2
40	131,200	4.0027x10 ⁻³	71	50	35	29	25	22	20	19	18	17	16	14	13	11	7	5	3	3
45	147,600	2.0206x10 ⁻³	99	70	50	41	35	31	29	27	25	23	22	20	18	16	10	7	5	5
50	164,000	1.0829x10 ⁻³	136	96	68	55	48	43	39	36	34	32	30	28	25	21	14	10	7	7
55	180,400	6.0924x10 ⁻⁴		128	91	74	64	57	52	48	45	43	41	37	33	29	18	13	9	9
60	196,800	3.4918x10 ⁻⁴			120	98	85	76	69	64	60	56	54	49	44	38	24	17	12	12
65	213,200	1.9189x10 ⁻⁴				132	114	102	93	86	81	76	72	66	59	51	32	23	16	16
70	229,600	1.0040x10 ⁻⁴						141	129	119	112	105	100	91	81	71	45	32	22	22
75	246,000	4.9582x10 ⁻⁵											142	130	116	100	64	45	32	32



d = Flying Diameter
 V = Total Velocity
 u = Descent Velocity
 D = Drag Force
 L = Lift Force

R = Resultant Aerodynamic Force
 $R = \sqrt{L^2 + D^2}$
 γ = Glide Angle
 α = Angle of Attack

FIGURE 4.2-1 HEMISPHERICAL PARACHUTE GLIDING MODE

4. Oscillating Parachutes - Stable gliding occurs only under certain favorable conditions. A more probable mode of motion for most parachutes is an oscillation which is produced through dynamic interaction between canopy forces and the suspended load. While gliding may prevail at slow rates of descent, oscillations are predominant at speeds anticipated for the rocketsonde application. The drag or weight coefficients are significantly reduced from stable conditions to the oscillating mode, and telemetry signal strength variations (i.e., signal dropouts) at the ground-based receiver are caused by the oscillating payload. In such a system, let α be the angle from the vertical through which the pendulum acts. From the previous discussion, it is seen that α could initially have almost any value from 0 to 180° depending upon the direction in which the nose cone is pointing during separation. The dynamic behavior is then subject to analysis as a circular pendulum for which the period, T, is defined in the following:

$$T = 4 \sqrt{\frac{L}{g}} \int_0^{\pi/2} \frac{d\phi}{\sqrt{1 - K^2 \sin^2 \phi}}$$

where, L, is the length of the pendulum, g is the acceleration due to gravity, and, K, is the $\sin(\alpha/2)$. ϕ is a function of α whose maximum value is $\pi/2$.

An evaluation of one of the probable limiting cases, where α approaches 180°, yields a period of approximately 8.0 seconds for a typical 15-foot diameter parachute for the initial condition immediately after deployment, neglecting drag and damping, and assuming a rigid pendulum. In the other limiting case, where α is a small angle, the period is approximately 5.5 seconds under the same assumptions.

5. Permeability - Permeability is a measure of the average speed of the flow of air passing through the parachute fabric. The effective permeability of parachute canopies can be expressed as:

$$W_{\text{eff}} = W_{\text{test}} \left(\frac{S_{\circ}}{S_{\square}} \right) \left(\frac{1/2 \rho V^2 C_{D_{\circ}}}{\Delta P_{\text{test}}} \right)^{0.6}$$

and the flow speed ratio as

$$W/V = W_{\text{test}} \left(\frac{S_{\circ}}{S_{\square}} \right)^{0.2} \left(\frac{1/2 \rho C_{D_{\square}}}{\Delta P_{\text{test}}} \right)^{0.6}$$

where W_{eff} = Effective permeability flow speed
 W_{test} = test permeability flow speed
 ΔP_{test} = test pressure differential

The drag or weight coefficients are reduced by permeability as indicated in the expression,

$$C_{D_{\square \text{ corr}}} = C_{D_{\square}} (1-W/V)$$

where $C_{D_{\square}}$ is the drag coefficient for a nonporous material and $C_{D_{\square \text{ corr}}}$ is

the corrected value which allows for flow through the canopy. The drag on a parachute is reduced as the permeability increases. Permeability tends to reduce the drag but also reduces the tendency for a parachute to oscillate and glide. Although the effect of permeability can be predicted for low altitude flight, there is some question as to the effect at high altitudes. The large mean-free-paths of air molecules at high altitudes significantly affect the permeability of small-sized pores such as are found in the 3-momme silk fabric being currently used in the fabrication of current high altitude meteorological rocket parachutes. There are indications that at the 200,000-foot levels these parachutes are essentially impervious to flow through the canopy fabric. A means of increasing the permeability of such parachutes would be by the cutting out of sufficiently large holes in the canopy material.

6. Critical Velocity - For every parachute there is a velocity, called the "critical velocity", above which it will not inflate but instead remain in a duffle bag or "squidged" configuration. The more porous the fabric, the lower the critical velocity and, of course, the less useful the parachute. Fortunately, the squidged parachute will generally introduce

sufficient drag to cause the velocity to drop below the critical velocity and to permit inflation to proceed - assuming, of course, that it does not strike the ground first.

The critical velocity depends upon the overall porosity of the canopy and the distribution of porosity. It also depends upon the shape of the canopy mouth opening. No precise analytical method exists for determining the critical opening velocity but it can be estimated from assumed values of the critical parameters.

7. Aeroelasticity - The permeability of textile fabrics is increased by applying tension and causing elastic deformation in the material. Inasmuch as tension in canopies is proportional to the dynamic pressure, in low altitudes the drag coefficient of a fabric parachute decreases as the speed is increased. This factor may not be significant in the high altitudes for the reasons mentioned in the previous section.

8. Parachute Size and Rigging Line Length - For a given speed of descent the drag coefficient decreases as parachute size is increased since rigging line tension increases as the diameter is made larger. The flying diameter can be increased slightly, however, by increasing the length of the rigging lines.

9. Breathing - This is a dynamic phenomenon resulting in an oscillation in the diameter of the parachute. Since the breathing involves changes in shape, it may be dependent to some extent upon the elasticity of the parachute system. Changes in parachute diameter are necessarily attended by changes in overall length which are communicated to the suspended load through the suspension lines, an efficient spring mass system in itself. The results in a spring mass system supported by an elastic envelope containing a considerable mass of circulating air, i.e., two free masses joined by an elastic link. The forces resisting deformations of shape are apparently negligible for the normal equilibrium condition of shape of the parachute so that a transient disturbance is easily translated into small periodic undamped oscillations in both the length and diameter of the system.

10. Deployment - The complete deployment of a conventional parachute consists of a number of steps as follows:

- a. Release or ejection from the vehicle
- b. Line and canopy stretch terminated by snatch force
- c. Inflation to opening shock, terminated by overinflation
- d. Rebound and recovery to "steady" drag condition
- e. Completion of deceleration to near equilibrium velocity
- f. Steady or controlled descent

11. Deployment into a Wind Field - High altitude winds have quite frequently been found to be as great as 100 meters per second which is similar in magnitude to the horizontal velocity of some rocket vehicles at apogee. Experience indicates that parachute deployment and streaming problems increase when the rocket horizontal velocity is in the same direction and of the same order of magnitude as the deployment altitude winds. Of course, the effect is a reduction in the relative wind velocity with respect to the parachute and a reduction in the available dynamic pressure. Since high altitude wind reversals and wind speeds are a seasonal and geographical phenomena, without a positive inflation aid, parachute deployment reliability can be quite variable.

12. Deployment from a Spinning Missile - Parachute deployment from a spinning missile is a fairly complex phenomena and defies a precise analytical treatment. The spin energy may help to open and spread out the parachute canopy to some extent and no doubt the spin rate of the deployed canopy is greatly reduced from its packaged condition. In general, the payload will not be despun during the opening process, therefore, a difference in spin rate between the canopy and the payload will be created. This factor no doubt tends to twist and tangle the shroud lines and prevent full inflation in many cases.

4.2.3 Arcas 15' Gentex Parachute.

The standard Arcas parachute as shown in Figure 4.2-2 is a pre-formed hemispherical-shaped silk parachute manufactured by the Gentex Company. Details of this parachute are presented in Table 4-2.

The parachute is generally supplied with alternate gores metalized for radar tracking. Twenty-two percent of the silk fabric is metalized for use with FPS-16 quality radar and fifty percent is metalized for use with the lower powered radars.

The Arcas parachute assembly consists of an instrument mounting base and a radar-reflective parachute (diameter 4.5 meters) packaged inside a cylindrical parachute container. A cross-sectional diagram of the parachute assembly is shown in Figure 4.2-3. The parachute container is a sealed unit which is attached to the forward retaining ring of the motor case. A lanyard connects the after-closure of the parachute container to the head-end closure of the rocket motor. The instrument package to be used is attached to the instrument base and inserted into the nose-cone. When the payload is assembled, the cone is secured to the instrument base by six steel balls that are held in place by the collar of the parachute container. The instrument base is attached to the forward closure of the parachute container by joining the stud of the parachute container closure with the stop nut mounted on the instrument base. A cork spacer is used between the parachute container and the instrument base to absorb some of the shock of separation. The process for the assembly of the payload is outlined in greater detail in the discussion of the rocket-launching procedure.

The principle of separation of the Arcas payload assembly is illustrated in Figure 4.2-4. Pressure generated by the separation charge acts on the afterclosure of the parachute container, and the pressure is transmitted through the inner cylinder of the container assembly. The shear pins which secure the forward closure of the parachute container break, thus allowing the nose-cone, instrument package and parachute pack to be ejected. The parachute and lanyard retain the after-closure assembly of the parachute contained. When the parachute is fully extended, the snap line attached to the crown of the parachute breaks and the steel ball joining the instrument base and nose-cone fall away thus allowing the nose-cone to separate from the instrument base and package. Figure 4.2-5 gives the dimensions of the parachute and the configuration of the parachute and payload after expulsion.

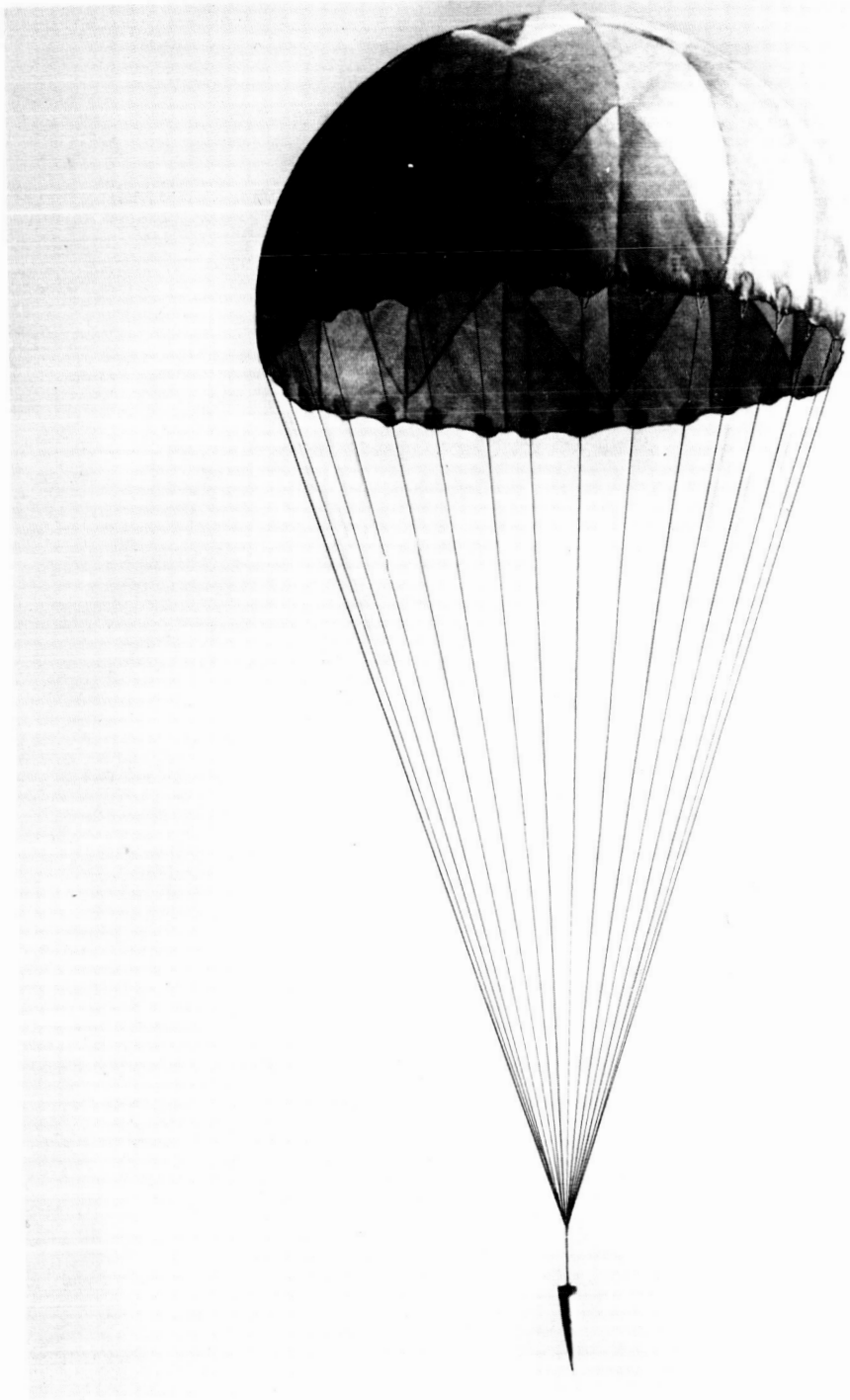


FIGURE 4.2-2 ARCAS GENTEX PARACHUTE, 15 FOOT DIAMETER

TABLE 4-2

ARCAS 15' GENTEX PARACHUTE

<u>Design</u>	<u>Preformed Hemispherical</u>
Flying Diameter	15.0 ft
Line Length	28.0 ft
Number of Lines	24
Parachute Weight	2.62 lbs
Canopy Material	3-Momme Silk
Canopy Weight	0.865 lbs
Canopy Weight Density	2.43×10^{-3} lb/ft ²
Weight of Shrouds and Fittings	1.75 lbs
Surface Area	354 ft ²
Flying Cross-Section Area	177 ft ²
Standard Payload Weight	4.65 lbs
C _D	0.624
C _D	0.335
Ballistic Coefficient W/C _D A	0.065 lb/ft ²

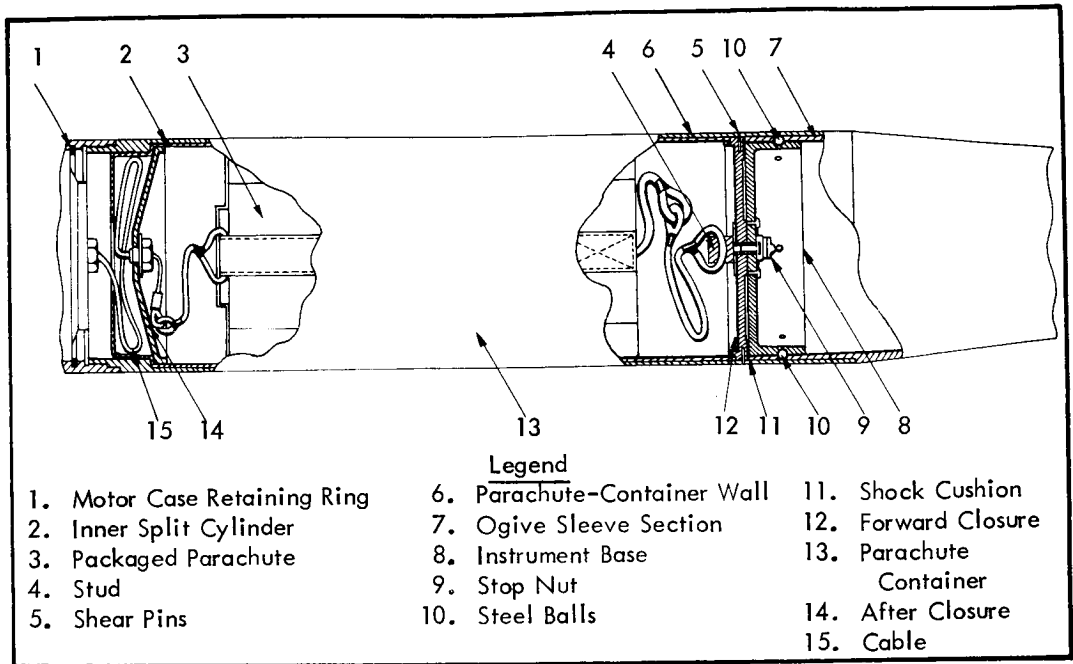


FIGURE 4.2-3 CROSS-SECTIONAL DIAGRAM OF THE ARCAS PARACHUTE ASSEMBLY

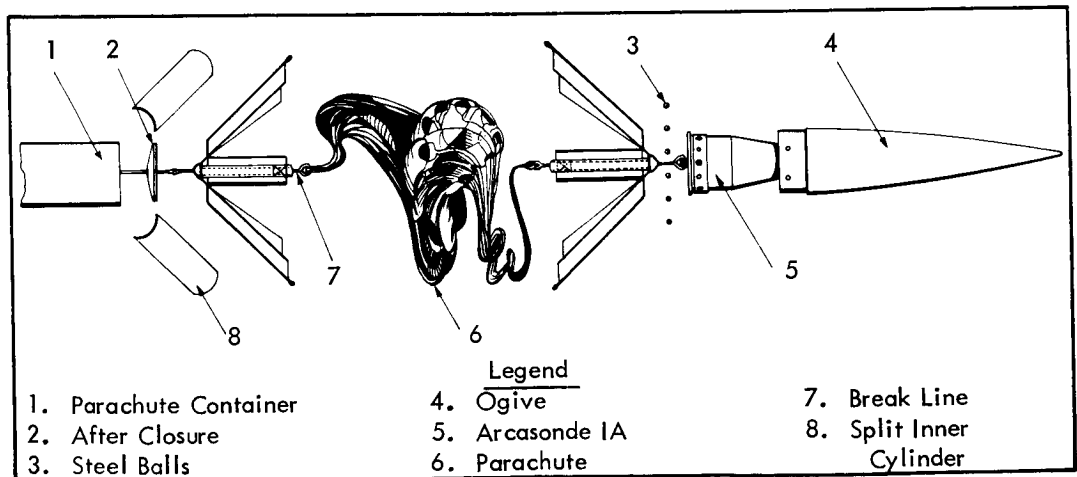


FIGURE 4.2-4 PRINCIPLE OF SEPARATION OF THE ARCAS PAYLOAD ASSEMBLY

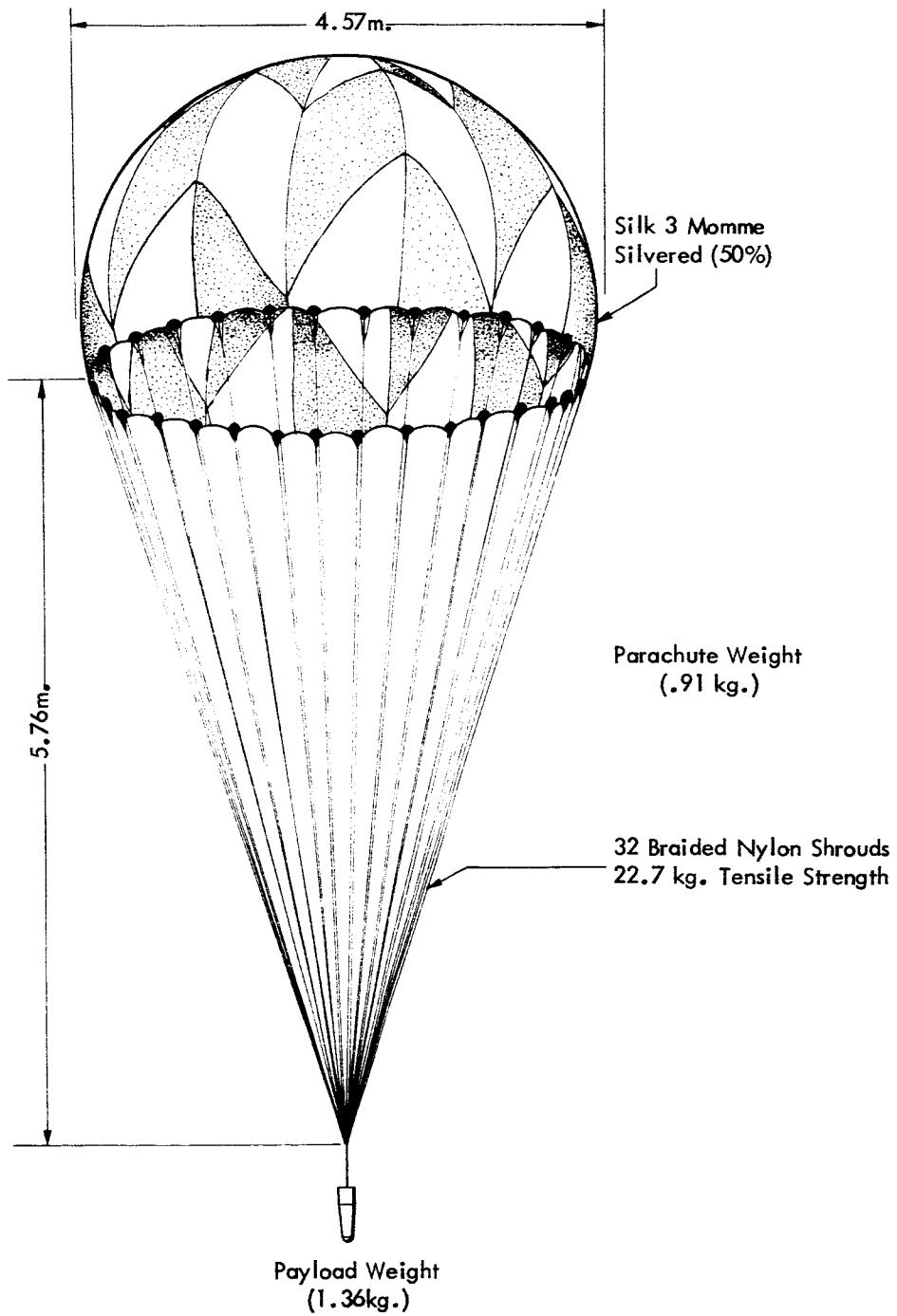


FIGURE 4.2-5 ARCAS PARACHUTE AND PAYLOAD AFTER EXPULSION

An analysis has been made of flight test data for the Arcas Gentex parachute. Figure 4.2-6 presents the descent rate average for hundreds of Arcas parachute flights with a standard payload of 4.65 pounds. The weight to effective or flying area ratio, W/S , for these flights was 0.0410 lb/ft^2 , and except for occasional erratic flights, the descent rate data agrees within ± 8 per cent of altitudes below 170,000 feet. Figure 4.2-7 presents descent rate data for heavier and lighter payload weights for the Arcas parachute with weight to effective area ratios of 0.0459 lb/ft^2 and 0.0334 lb/ft^2 . Descent times are presented in Figure 4.2-8 for various Arcas payload weights. A statistical analysis of Arcas parachute descent rates has been conducted by the Air Force at Cape Kennedy. The results are tabulated in Table 4-3.

WSMR reports that the Arcas parachute does not fully deploy for the first 25,000 ft. to 35,000 ft. or 80 seconds to 90 seconds after deployment at apogee. The fall rates are higher than expected right after apogee and the radar signal is weak. Oscillations of $\pm 45^\circ$ to $\pm 90^\circ$ with a 5-second period are experienced at the high altitudes, and these are damped out with a period of 8-seconds in about 23-minutes of descent. For systems ejected at 250,000 ft. velocities on the order of 800 to 900 ft/sec. are attained at 230,000 feet. The lag in initial wind response at 60 Km is about 20-seconds. The wind response lag after apogee which we have studied is presented in Table 4-4.

Figure 4.2-9 presents two typical radar plots from which these kind of data were derived. Figure 4.2-10 presents the initial wind response altitude against apogee altitude. Although the scatter of points on this plot indicate that a correlation does not exist between apogee and wind sensing altitude, the data are too few from which to draw any final conclusions. However, it appears that some chutes respond at 2,000 to 3,000 feet below apogee, while others lose 20,000 to 30,000 feet before responding to the wind.

A recent study of Arcas parachute descent rates has been conducted by the Army at WSMR. Descent velocities for the standard Arcas system have been plotted by the Army as shown in Figures 4.2-11 through 4.2-18. These data indicate that the parachute becomes fully deployed and descent rates are stabilized to the theoretical values by an altitude of 40 km. It appears that occasionally the parachute deploys very soon after ejection from the rocket vehicle and follows the theoretical descent ratio curve essentially

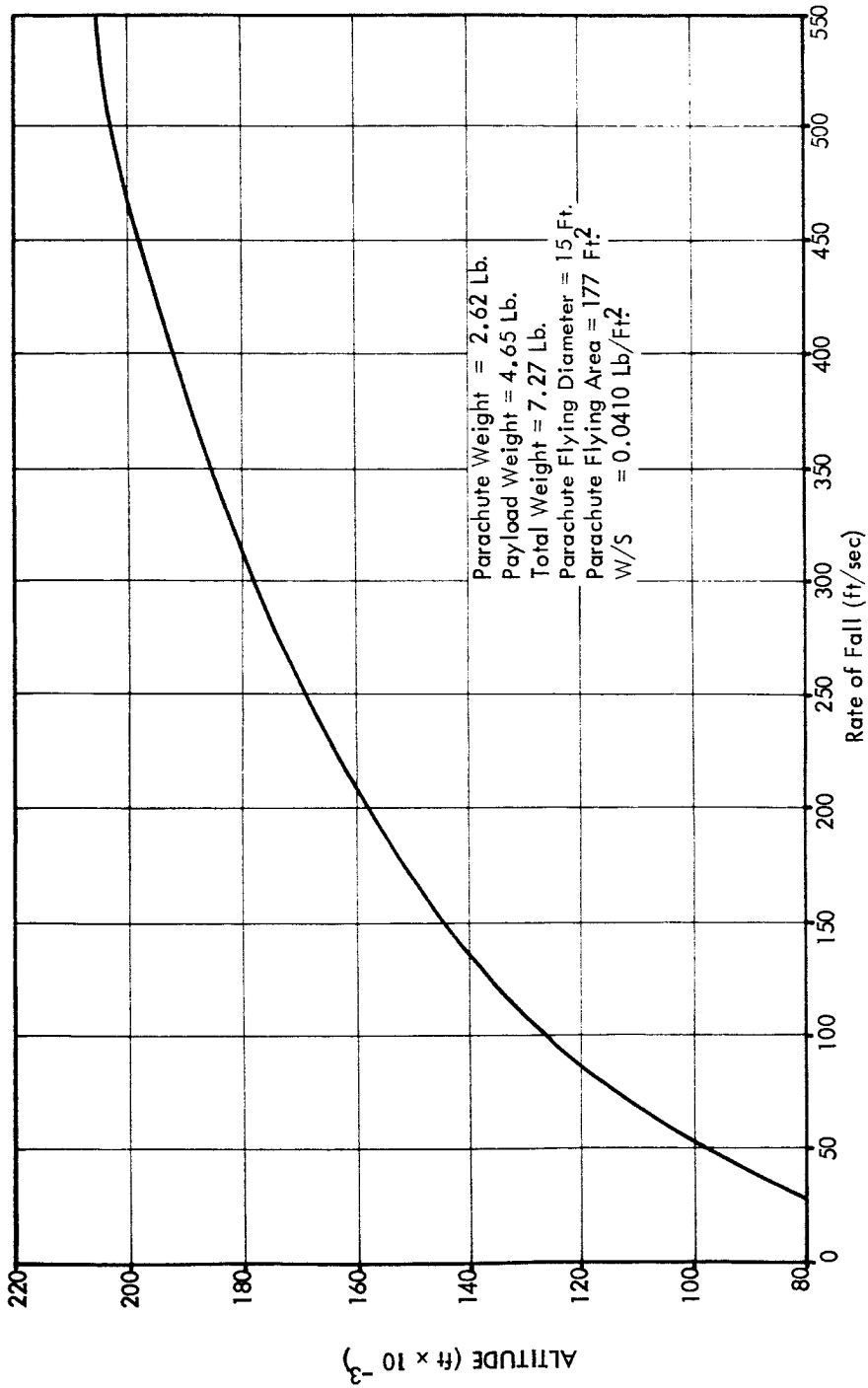


FIGURE 4.2-6 ARCAS PARACHUTE (GENTEX COMPANY) DESCENT RATE AVERAGE FOR STANDARD PAYLOAD WEIGHT

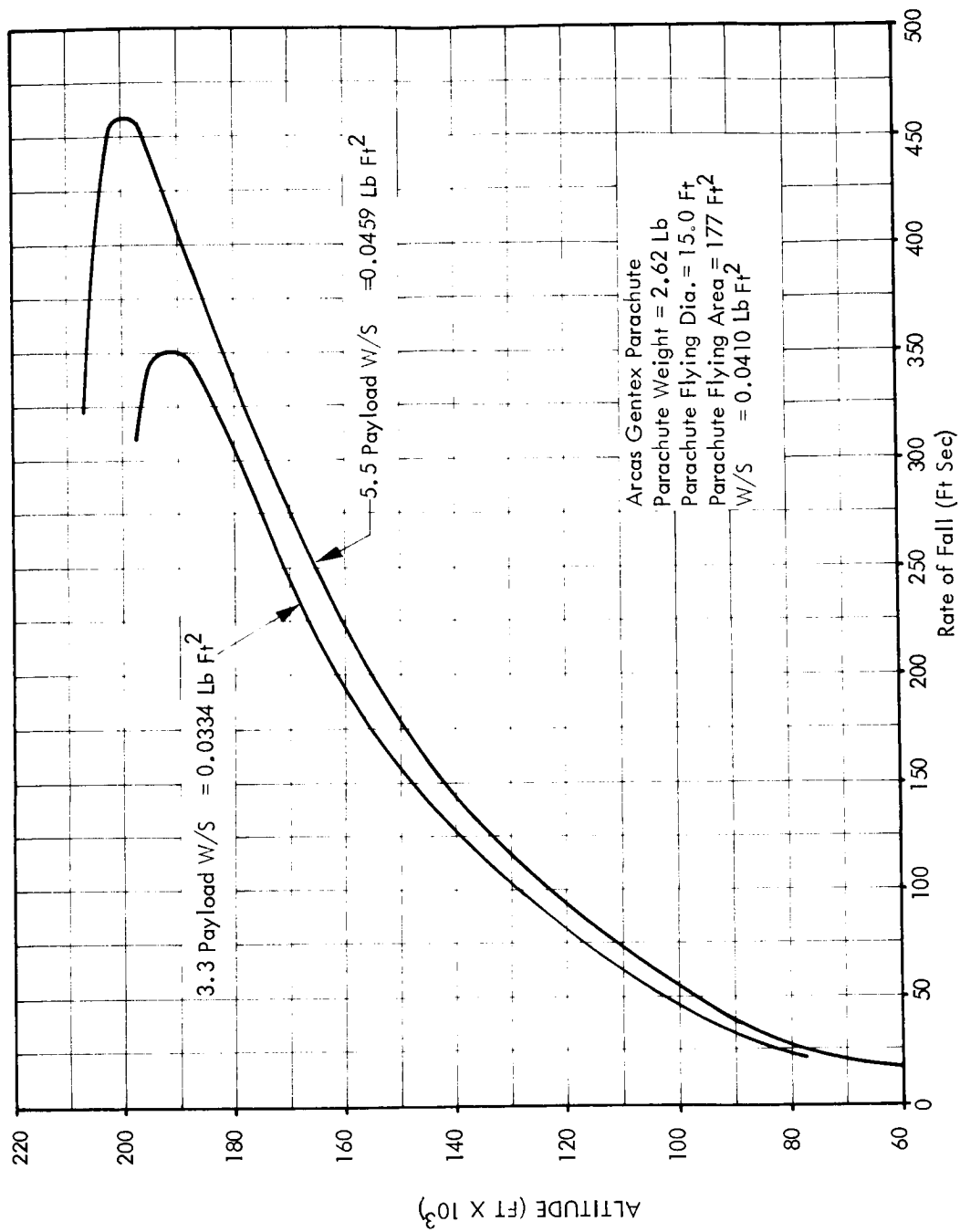


FIGURE 4.2-7 ARCAS PARACHUTE FALL RATES

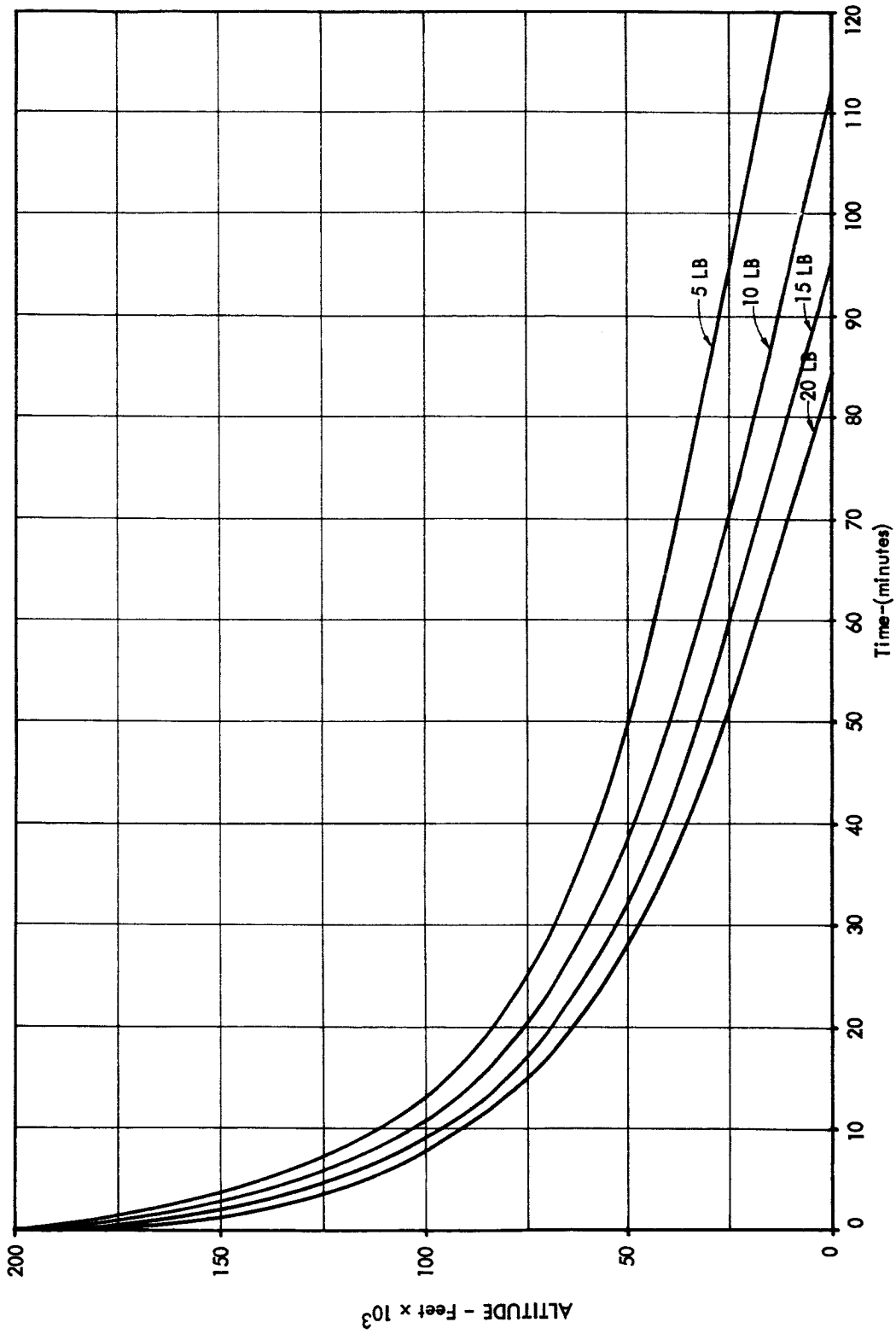


FIGURE 4.2-8 ARCAS PARACHUTE DESCENT CURVE

TABLE 4-3

FALL RATE STUDY OF
ARCAS PARACHUTE AND SONDE PAYLOAD

<u>Ht (K ft)</u>	<u>Avg Fall (FPM)</u>	<u>No. Samples</u>	<u>Standard Deviation</u>	<u>% 1 Dev</u>	<u>% 2 Dev</u>
81-85	1891	25	62.3 Ft.	68	92
86-90	2233	25	58.6	76	92
91-95	2674	25	72.4	64	100
96-100	3118	25	105.3	56	100
101-105	3568	25	119.8	72	92
106-110	4076	25	134.0	72	92
111-115	4579	25	122.0	64	96
116-120	5168	25	187.2	68	96
121-125	5855	24	228.9	71	92
126-130	6543	24	150.2	71	96
131-135	7275	25	228.9	72	96
136-140	8120	25	225.1	60	96
141-145	9118	25	316.4	68	96
146-150	10220	25	283.1	72	92
151-155	11387	25	314.9	52	100
156-160	12557	24	467.2	67	96
161-165	13816	24	340.8	75	92
166-170	15113	24	482.1	75	92
171-175	16677	23	468.8	61	100
176-180	18117	19	554.6	74	95
181-185	19857	16	430.3	62	100
186-190	21807	10	608.5	70	100
191-195	23611	6	394.2	67	100
196-200	25786	4			
201-205	27902	2			

Based on Arcasonde launches at Cape Kennedy Florida 1964-65

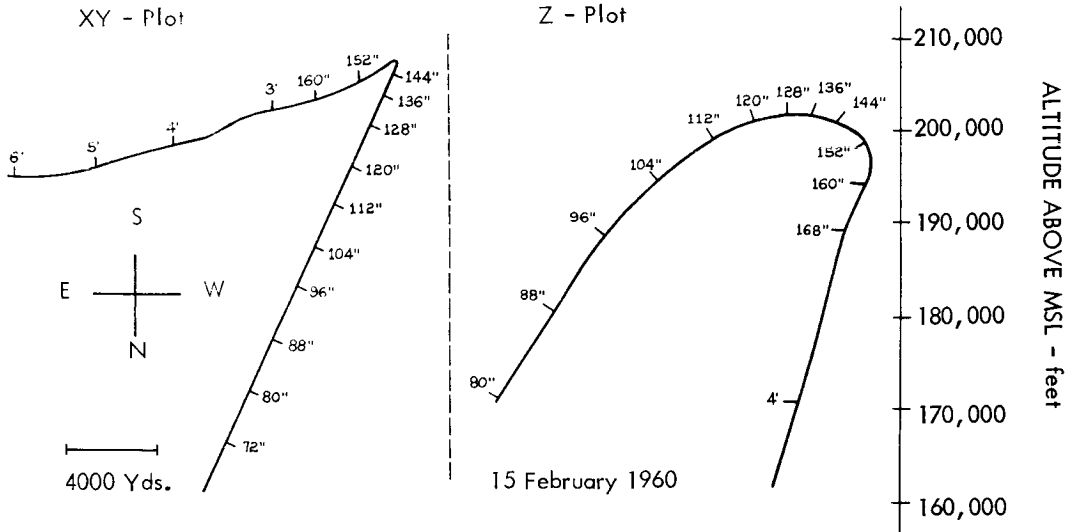
TABLE 4-4

INITIAL WIND RESPONSE LAG DATA

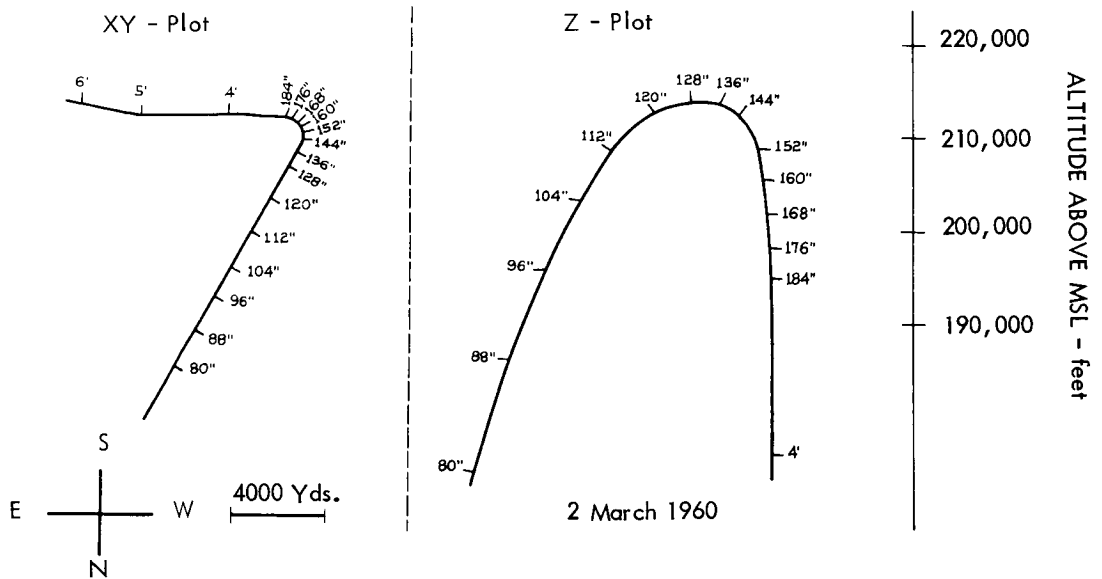
<u>Apogee</u>		<u>First Indication of Wind Response</u>	
<u>Altitudes</u>	<u>Time</u>	<u>Altitudes</u>	<u>Time</u>
220 K'	128 Sec	200 K'	240 Sec
212	128	180	176
182	128	177	145
188	128	186	136
201	133	196	150
213	128	171	192
203	128	200	148
213	128	205	160

FIGURE 4.2-9 FPS-16 RADAR TRACKS OF ARCAS FLIGHTS AT PACIFIC MISSILE RANGE

NOTE: Parachute Expulsion at 128 Seconds



NOTE: Parachute Expulsion at 128 Seconds



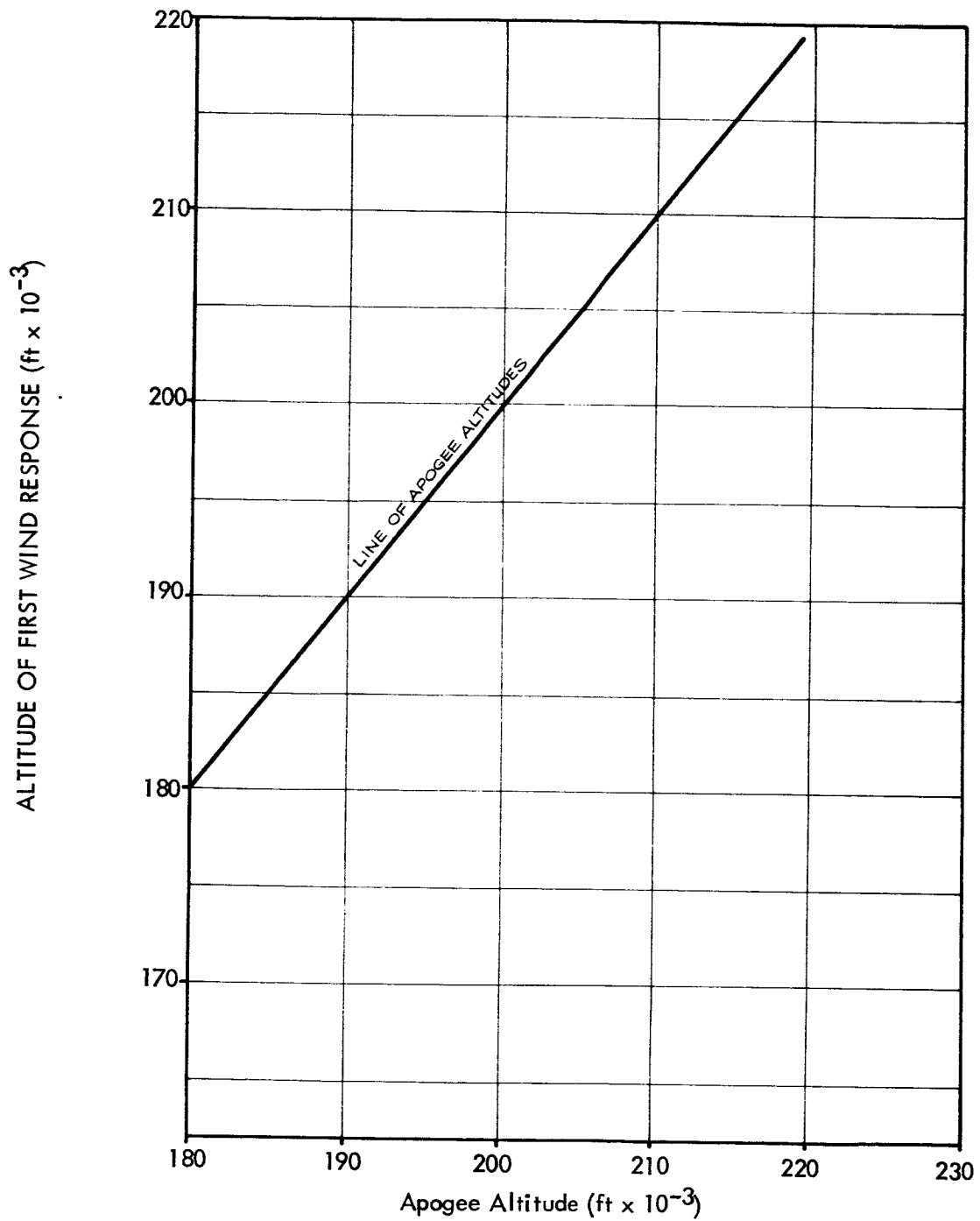


FIGURE 4.2-10 INITIAL WIND RESPONSE ALTITUDE VS. APOGEE ALTITUDE

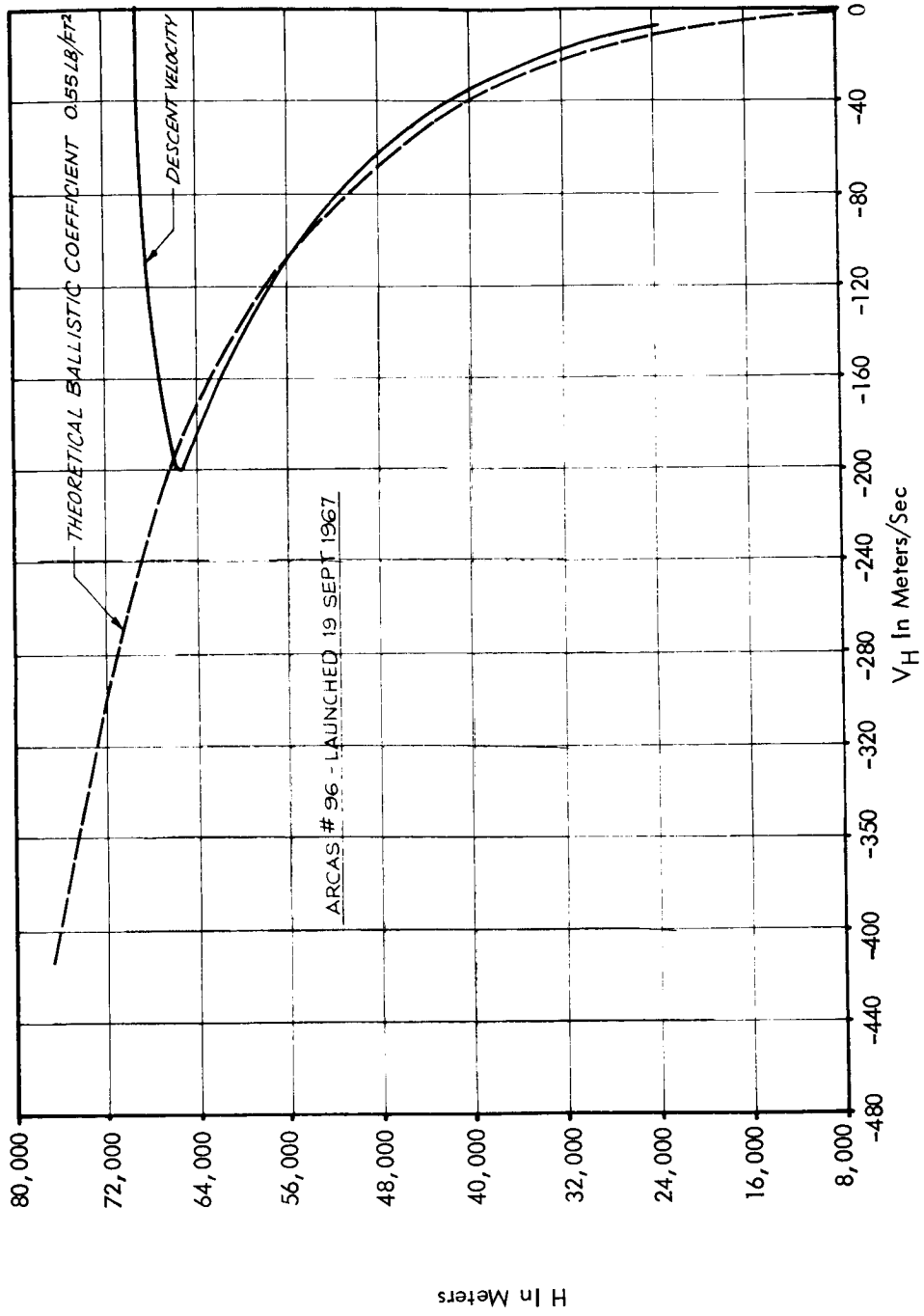


FIGURE 4.2-11 ARCAS PARACHUTE FALL RATE DATA WSMR FLIGHTS

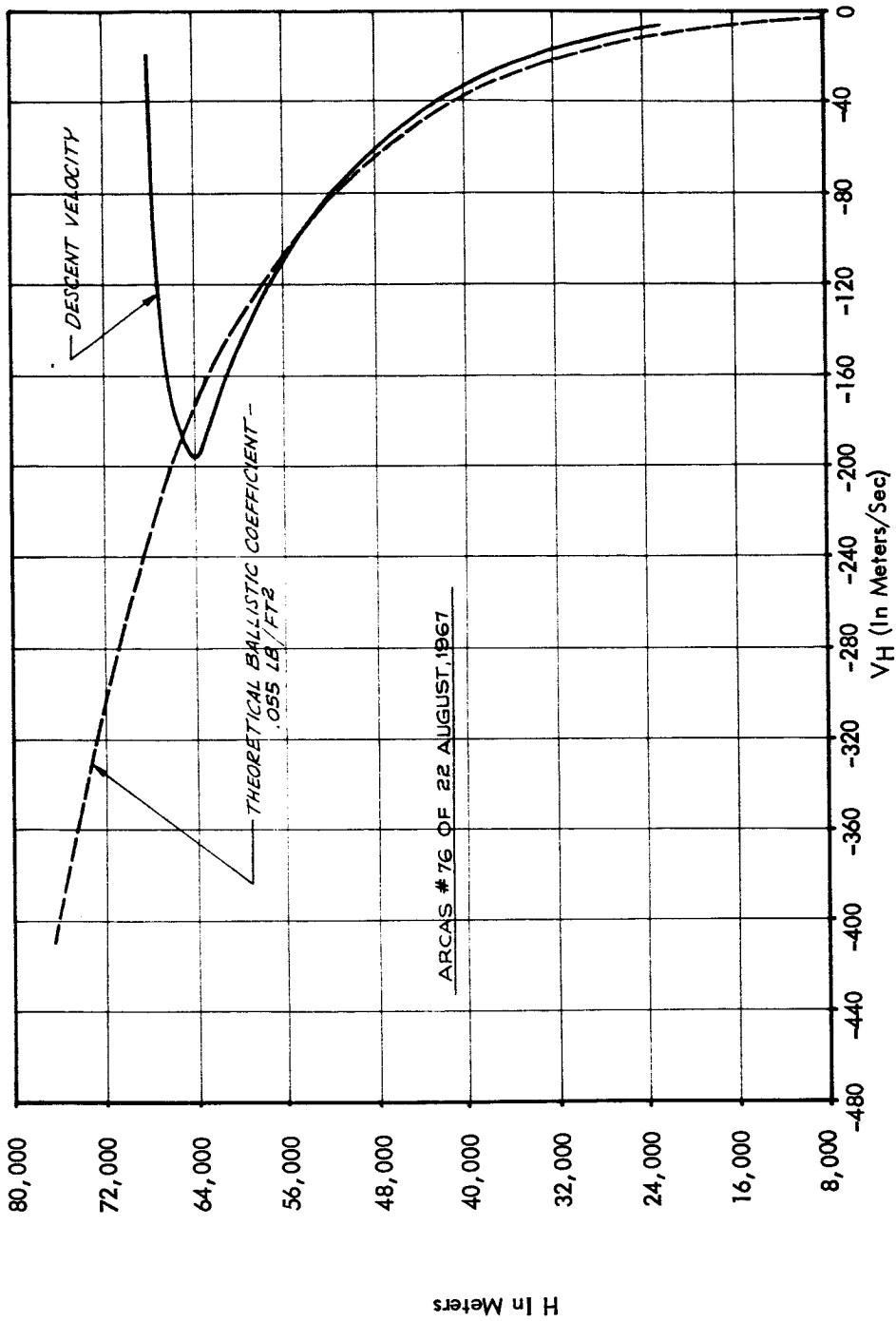


FIGURE 4.2-12 ARCAS PARACHUTE FALL RATE DATA WSMR FLIGHTS

H In Meters

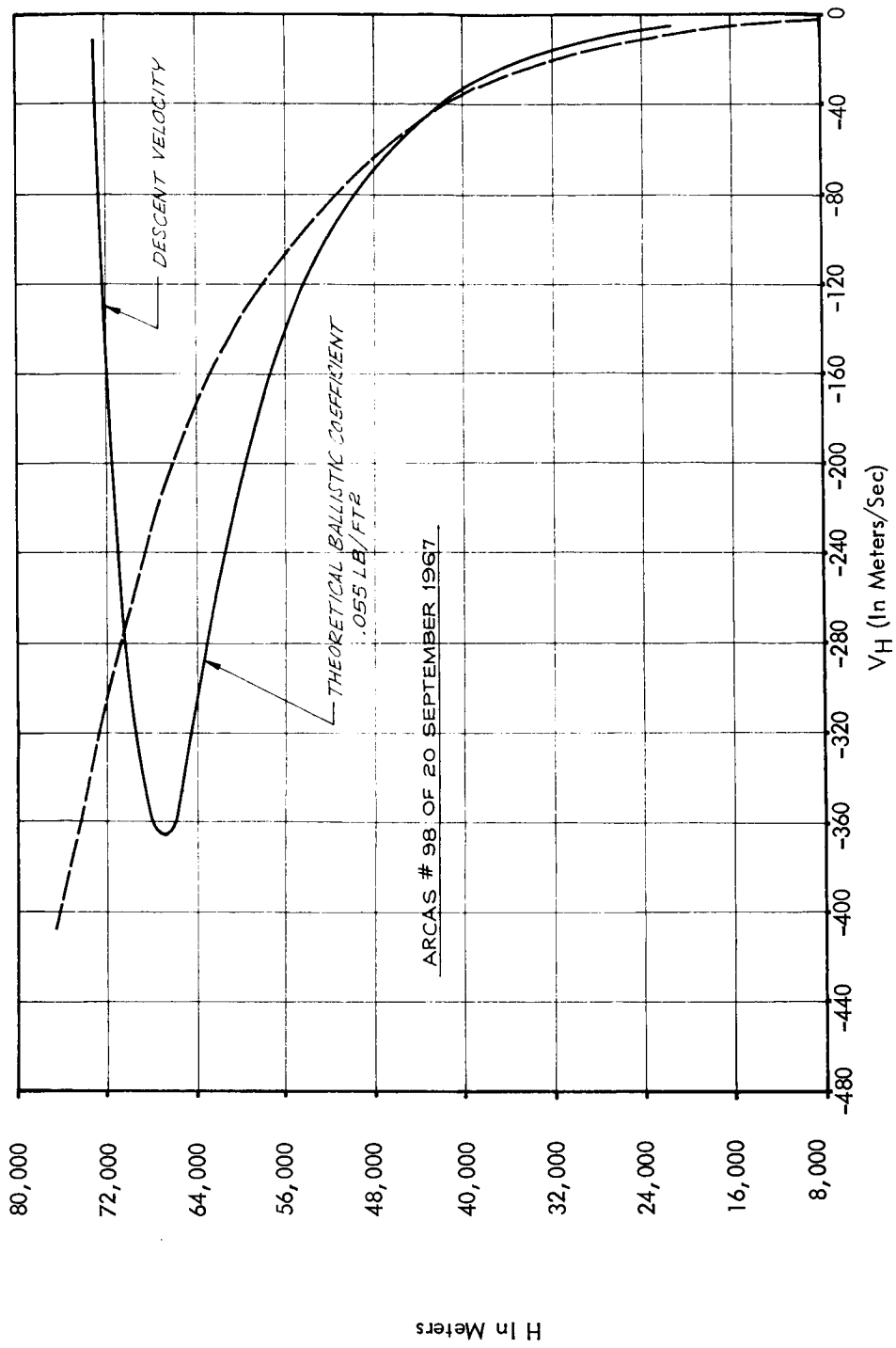


FIGURE 4.2-13 ARCAS PARACHUTE FALL RATE DATA WSMR FLIGHTS

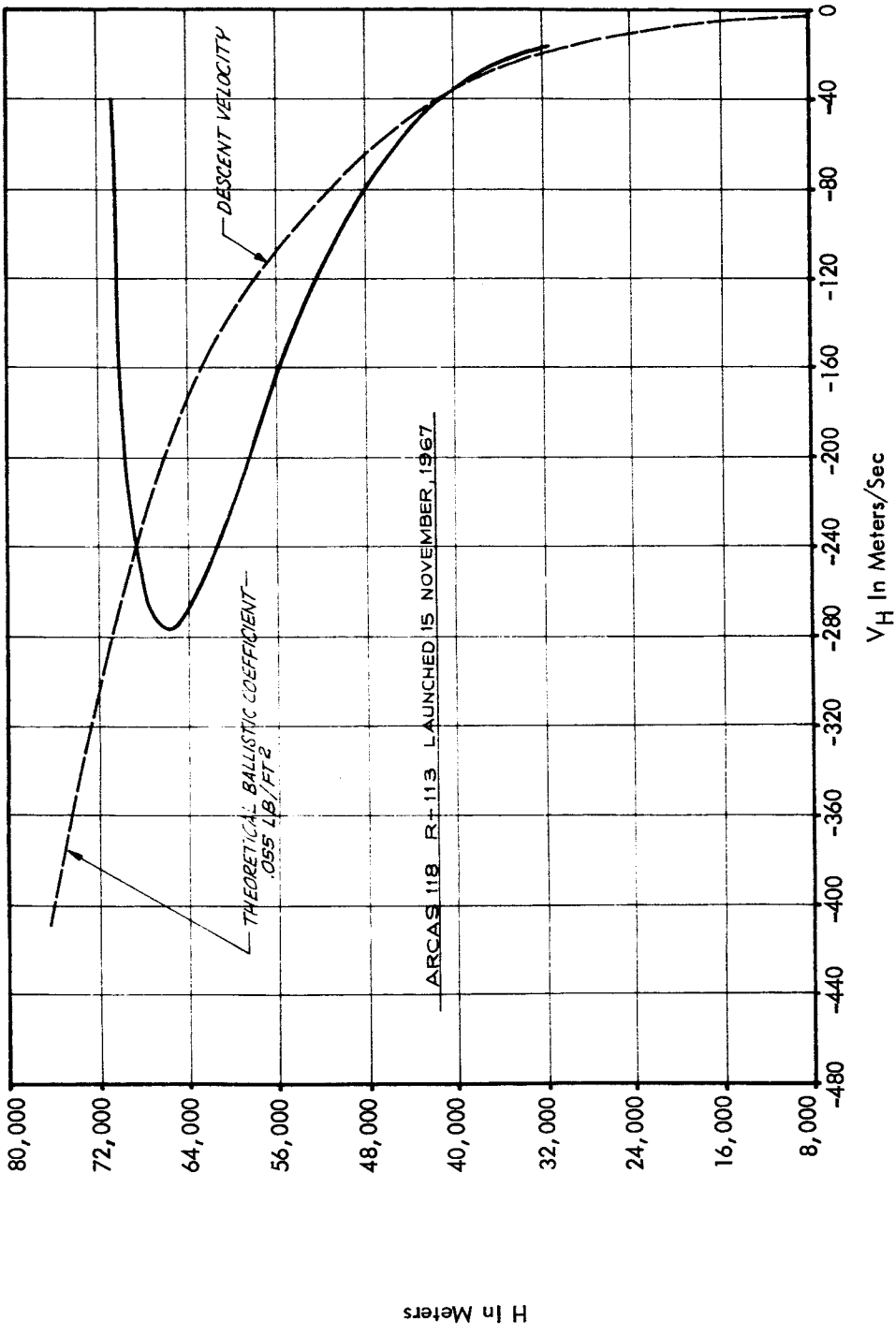


FIGURE 4.2-14 ARCAS PARACHUTE FALL RATE DATA WSMR FLIGHTS

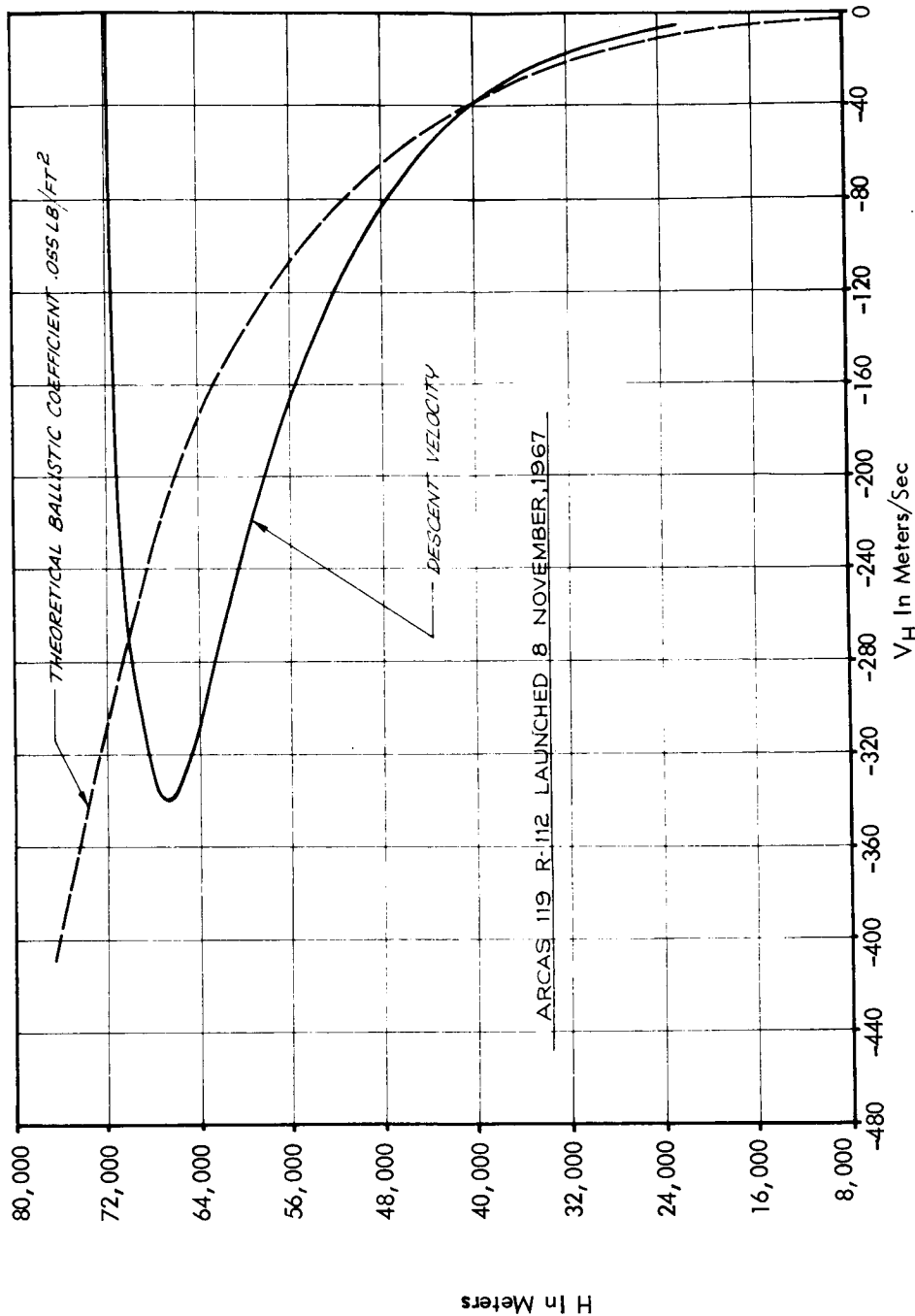


FIGURE 4.2-15 ARCAS PARACHUTE FALL RATE DATA WSMR FLIGHTS

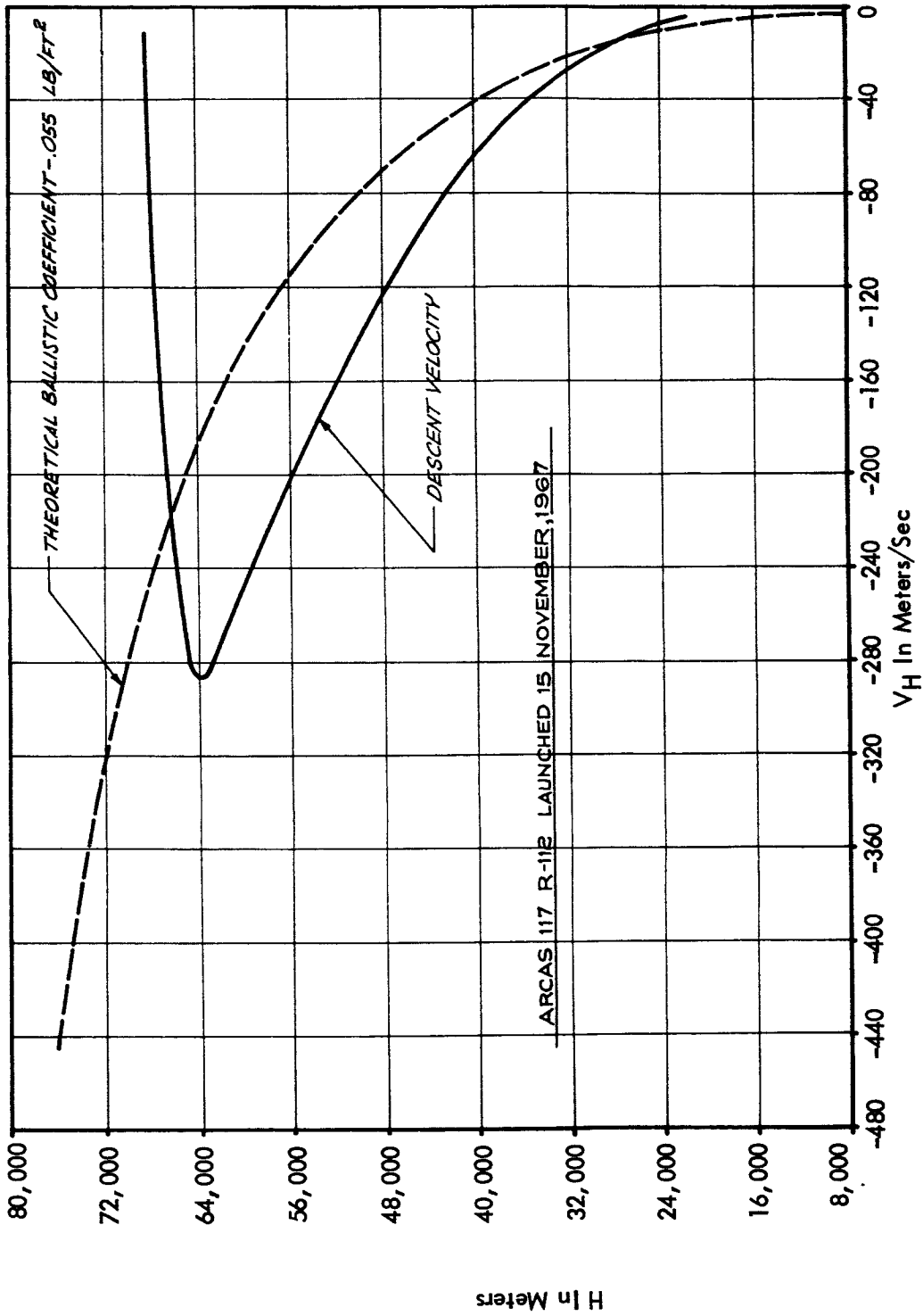


FIGURE 4.2-16 ARCAS PARACHUTE FALL RATE DATA WSMR FLIGHTS

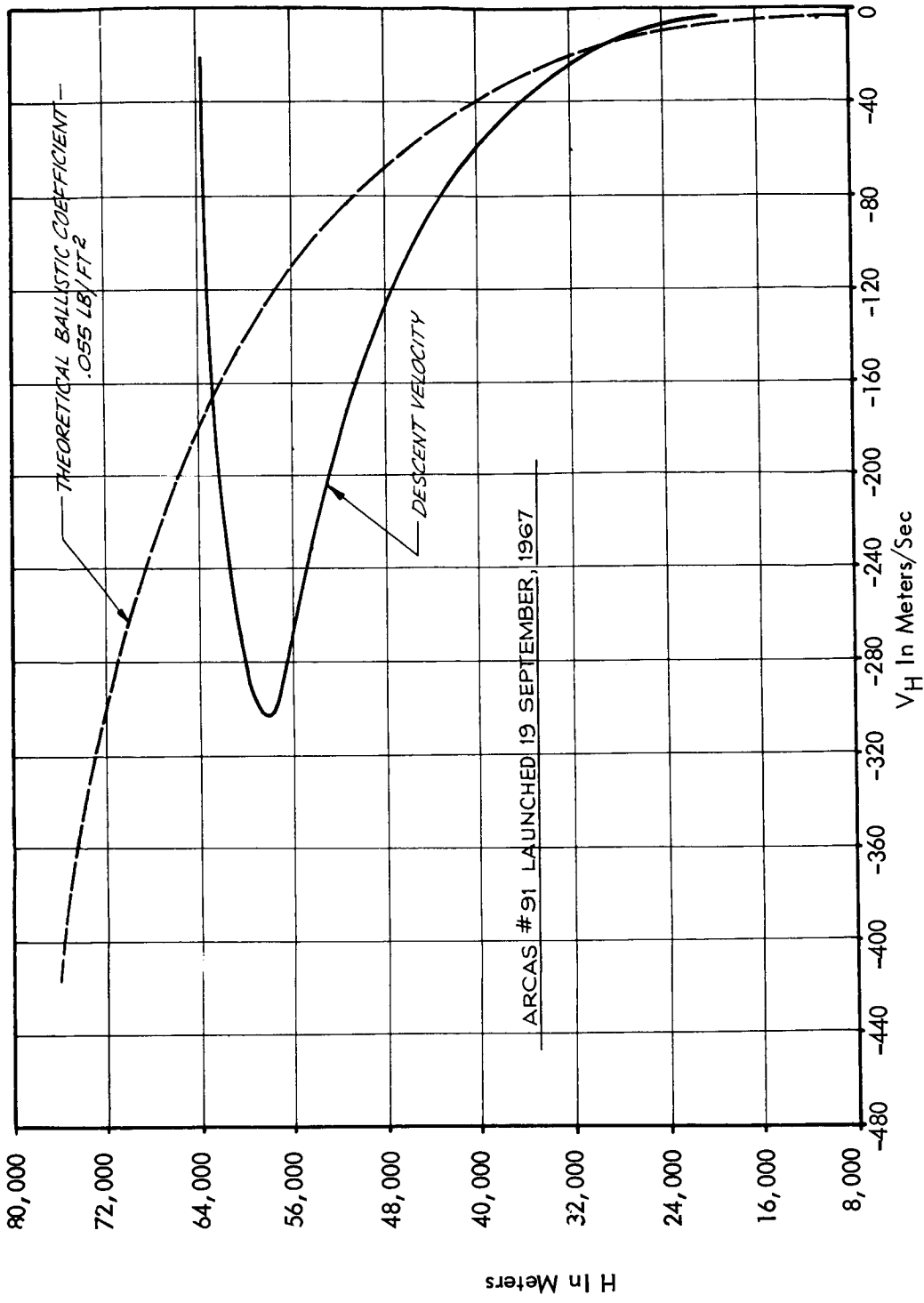


FIGURE 4.2-17 ARCAS PARACHUTE FALL RATE DATA WSMR FLIGHTS

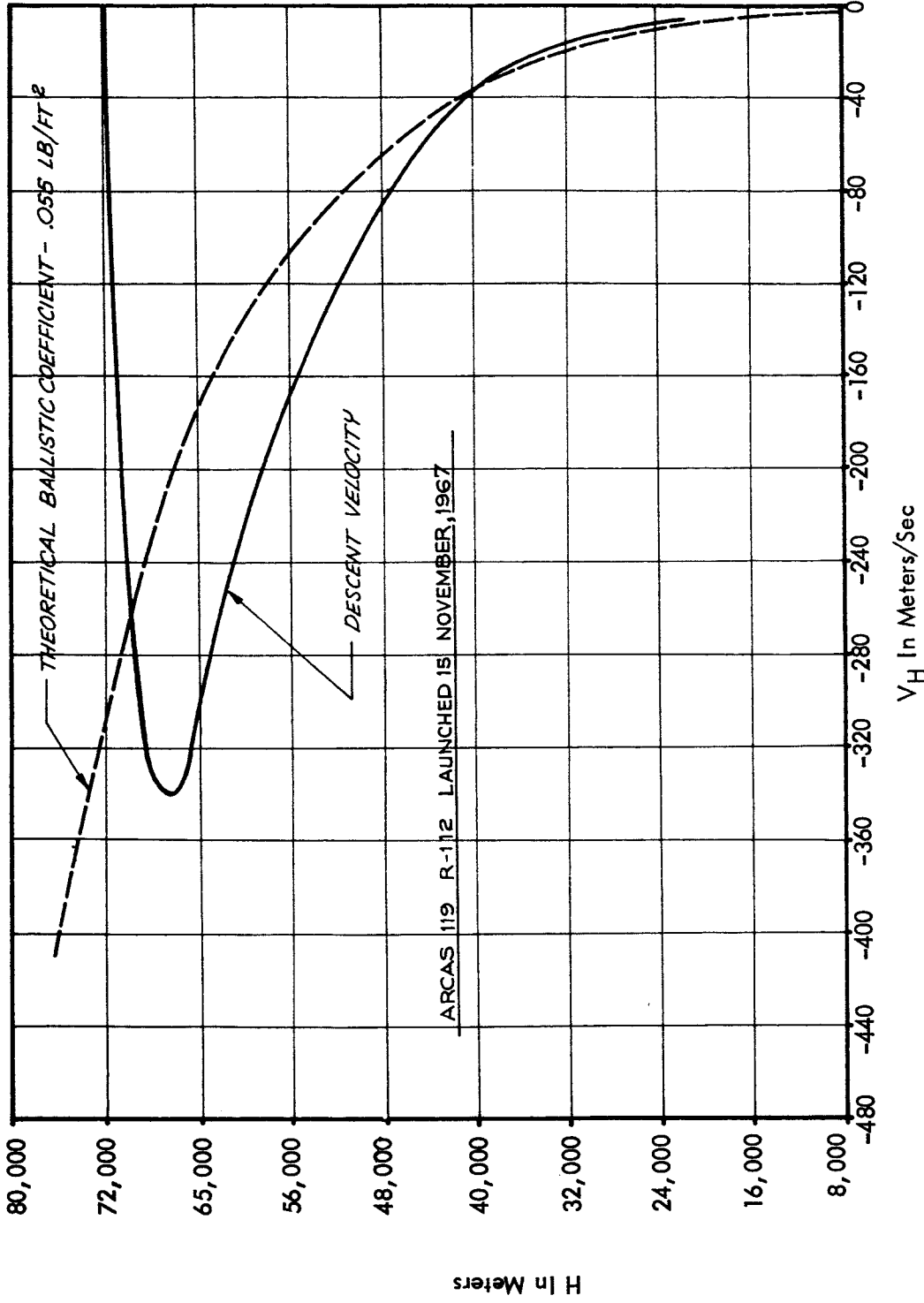


FIGURE 4.2-18 ARCAS PARACHUTE FALL RATE DATA WSMR FLIGHTS

from apogee. More often, however, the descent velocities exceed the theoretical values and show a rather erratic pattern above 40 Km.

4.2.4 Loki Dart 7.6' Parachute.

A standard Loki Dart parachute as shown in Figure 4.2-19 is a circular flat silk parachute which is manufactured by the Irvin Air Chute Company. Details of this parachute are presented in Table 4-5.

This parachute is made radar-reflective by metalizing alternate gores so that fifty percent of the area presents a target. A center or squib line is attached from the payload to the crown of the canopy, so that the crown is drawn somewhat from the hemispherical shape. This is done to increase the drag coefficient and to improve deployment reliability. However, a less stable descent results as compared with the hemispherical shape. Figure 4.2-20 presents typical descent rates for the 7.6' parachute and Figure 4.2-21 presents altitude vs. time profiles for various ejection altitudes.

A recent study of the 7.6' Loki Dart parachute descent rates has been conducted by the Army at WSMR. Flight test data from this study are plotted in Figures 4.2-22 through 4.2-26. These data indicate that this system is capable of achieving a ballistic coefficient better than 0.050 lb/ft^2 , but many of the flights possess excessive fall rates above an altitude of 40 kilometers. No doubt deployment problems are the cause of the rapid fall rates.

4.2.5 NOL 6' Square Parachute.

A standard NOL parachute is the 6-foot square silk parachute which has been used with the Loki Dart (Hasp) and the five-inch gun probe projectile. This parachute consists of 71" x 71" square of 3-Momme silk and eight shroud lines of 9-foot length. The silk canopy is metalized for radar reflection. Each of four shroud lines is attached to a corner of the canopy, and each of the remaining shroud lines is attached to a point slightly offset from the mid-point of each of the four sides. The purpose of the slight offset is to induce a slow spin rate to the descending parachute to prevent gliding which might lead to erroneous wind data. A weight breakdown for this parachute is as follows:

Canopy	0.088 lb.
Shroud and fittings	0.100
Payload	<u>0.750</u>
TOTAL	0.938 lb.

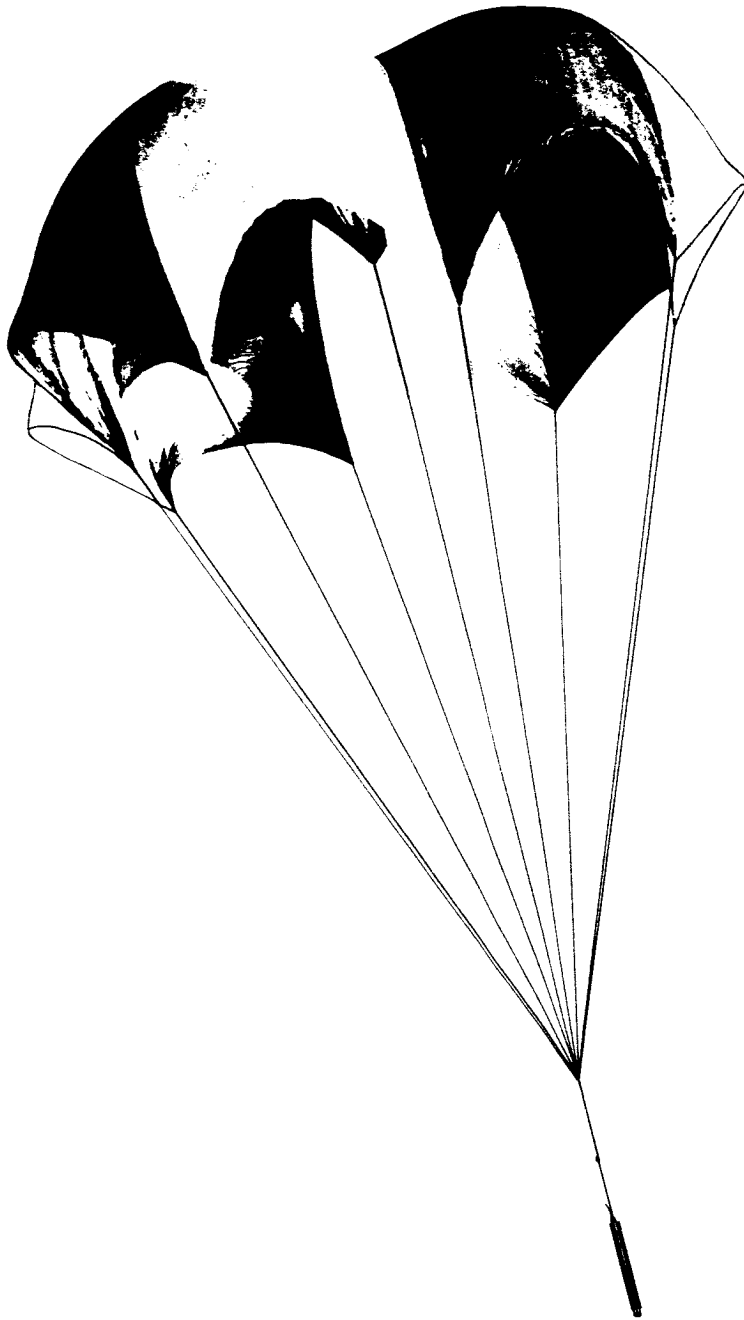


FIGURE 4.2-19 DARTSONDE INSTRUMENT PACKAGE ON 7.6 FOOT CHUTE

TABLE 4-5

LOKI 7.6' IRVIN PARACHUTE

<u>Design</u>	<u>Flat Circular</u>
Flying Diameter	5.7 Ft.
Line Length	7.6 Ft.
Number of Lines	9
Parachute Weight	0.225 lb.
Canopy Material	3-Momme Silk
Surface Area	45.5 Ft. ²
Flying Cross-Section Area	25.5 Ft. ²
Fabric Diameter	7.6 Ft.
Standard Payload Weight	0.788 lb.
$C_{D_{\square}}$	0.660
$C_{D_{\circ}}$	0.370
Ballistic Coefficient	0.060 lb/ft ²

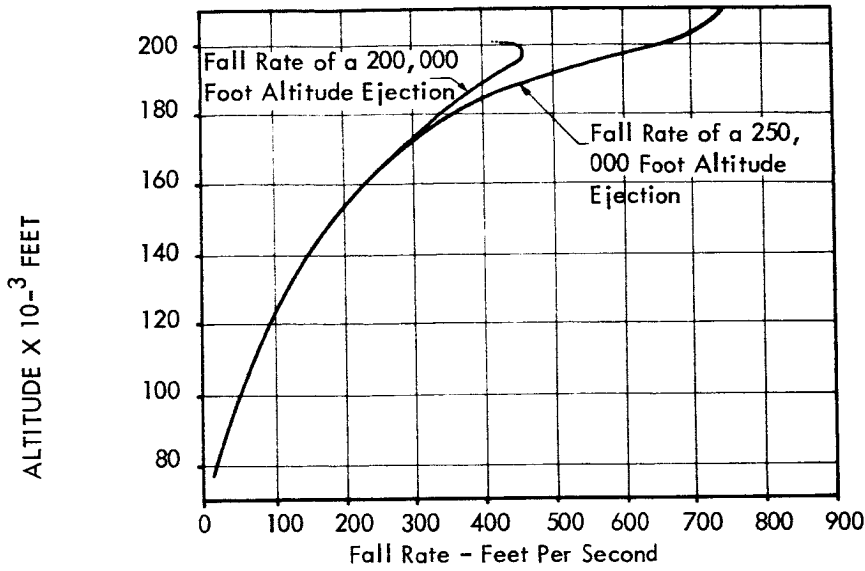


FIGURE 4.2-20 LOKI 7.6 PARACHUTE - SONDE DESCENT VELOCITY

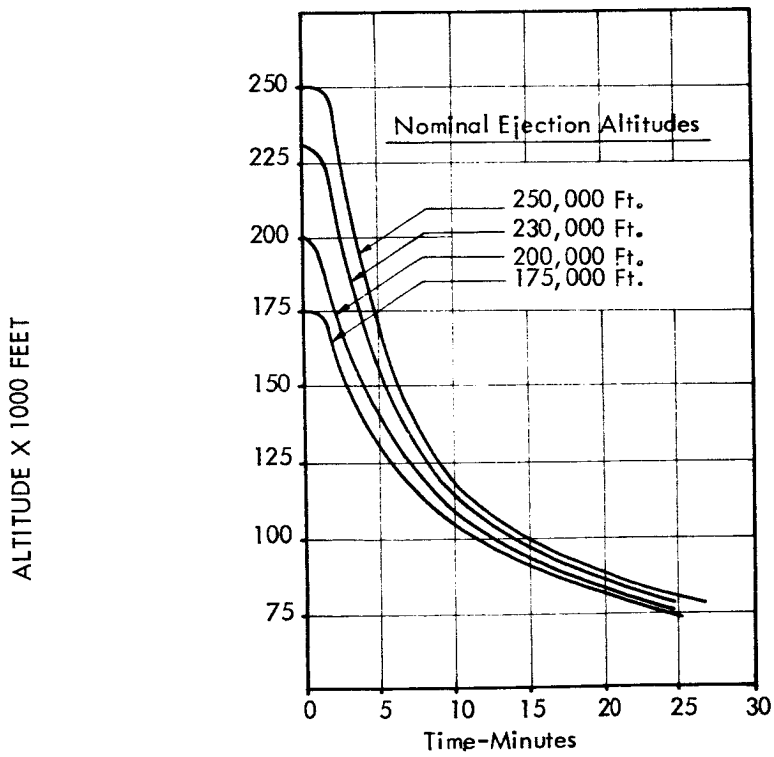


FIGURE 4.2-21 LOKI 7.6 PARACHUTE-SONDE DESCENT TIME

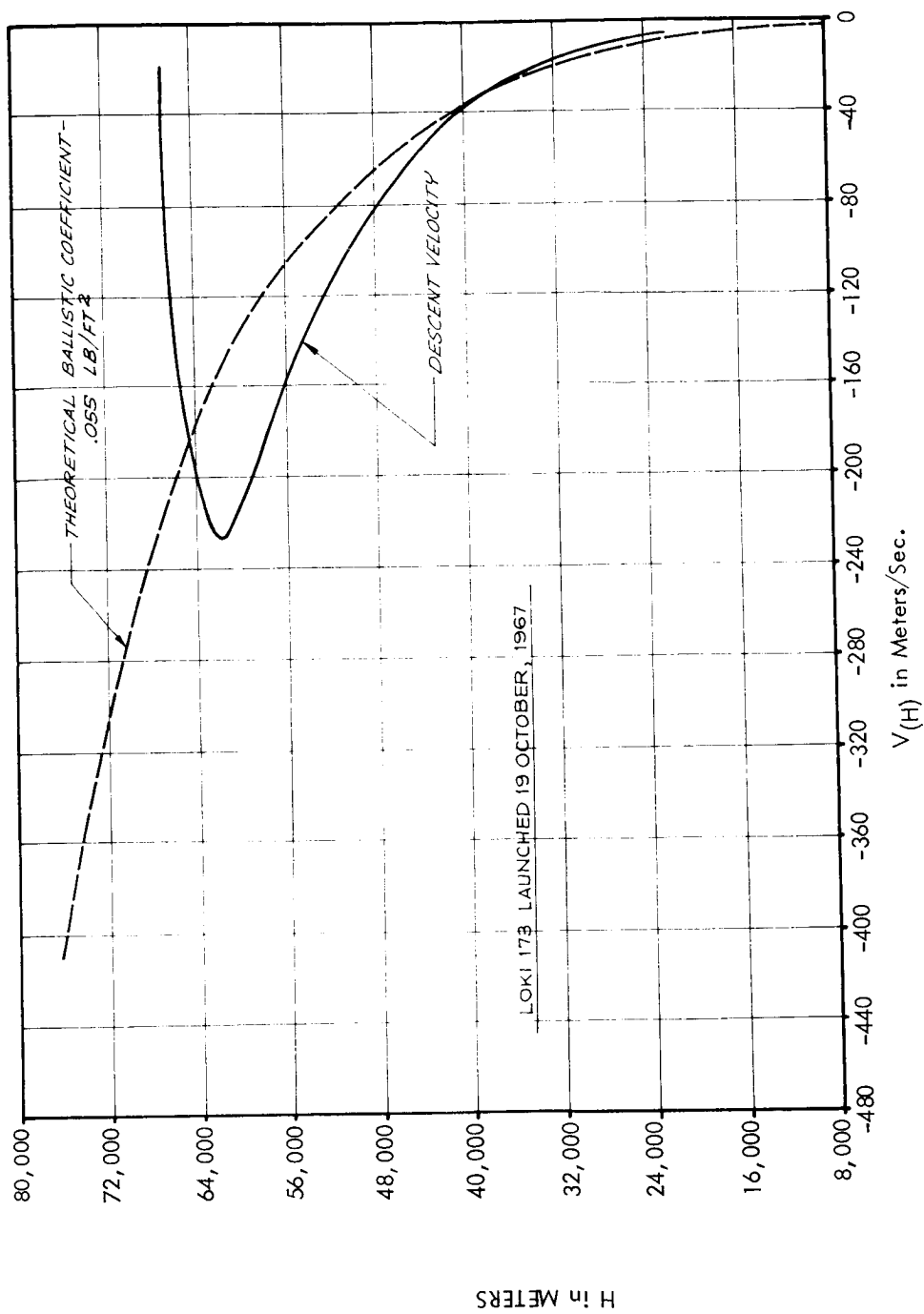


FIGURE 4.2-22 LOKI 173 LAUNCHED 19 OCTOBER 1967

H in METERS

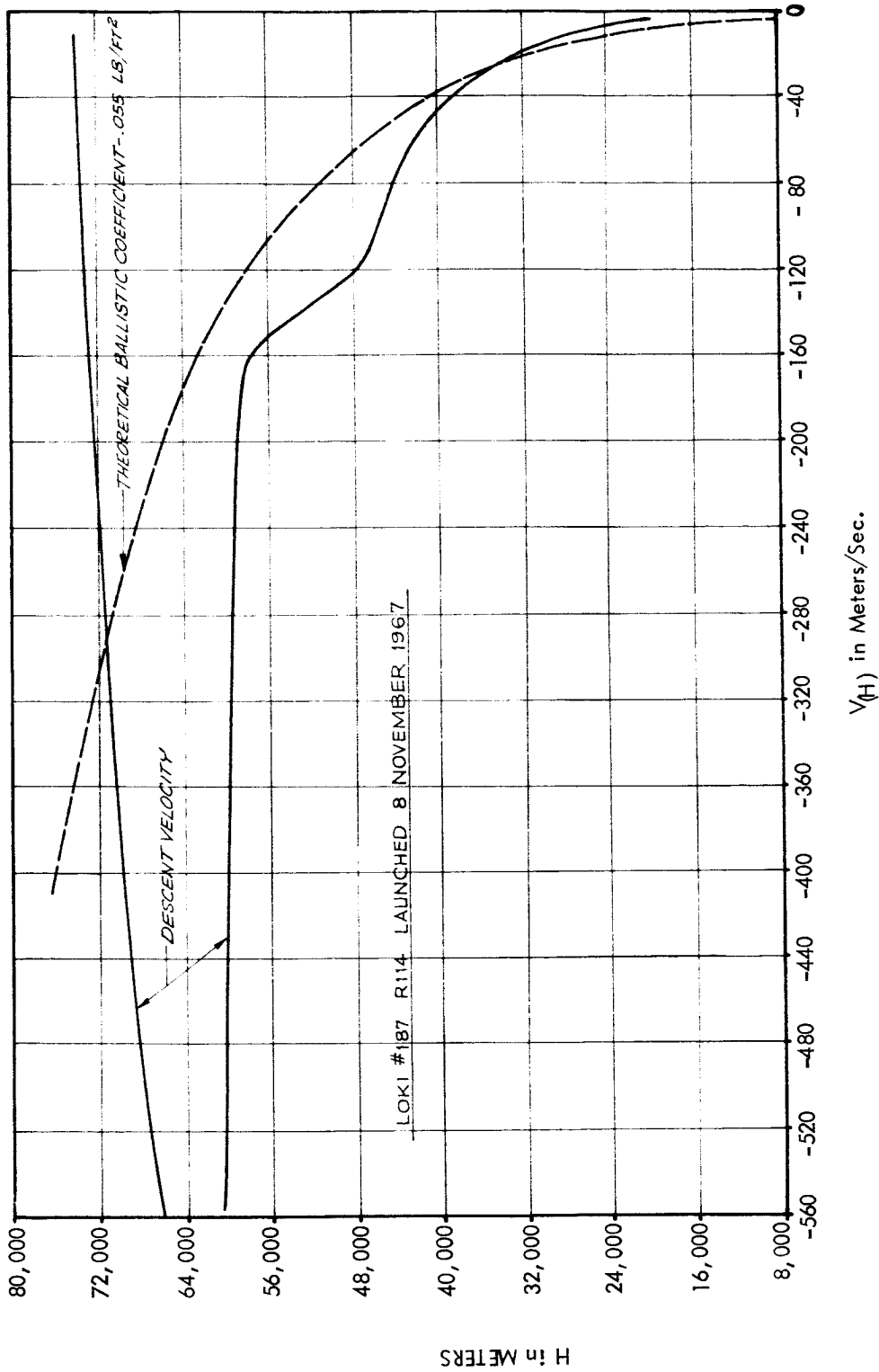


FIGURE 4.2-23 LOKI 7.6 DESCENT RATE PROFILES WSMR FLIGHT TEST DATA

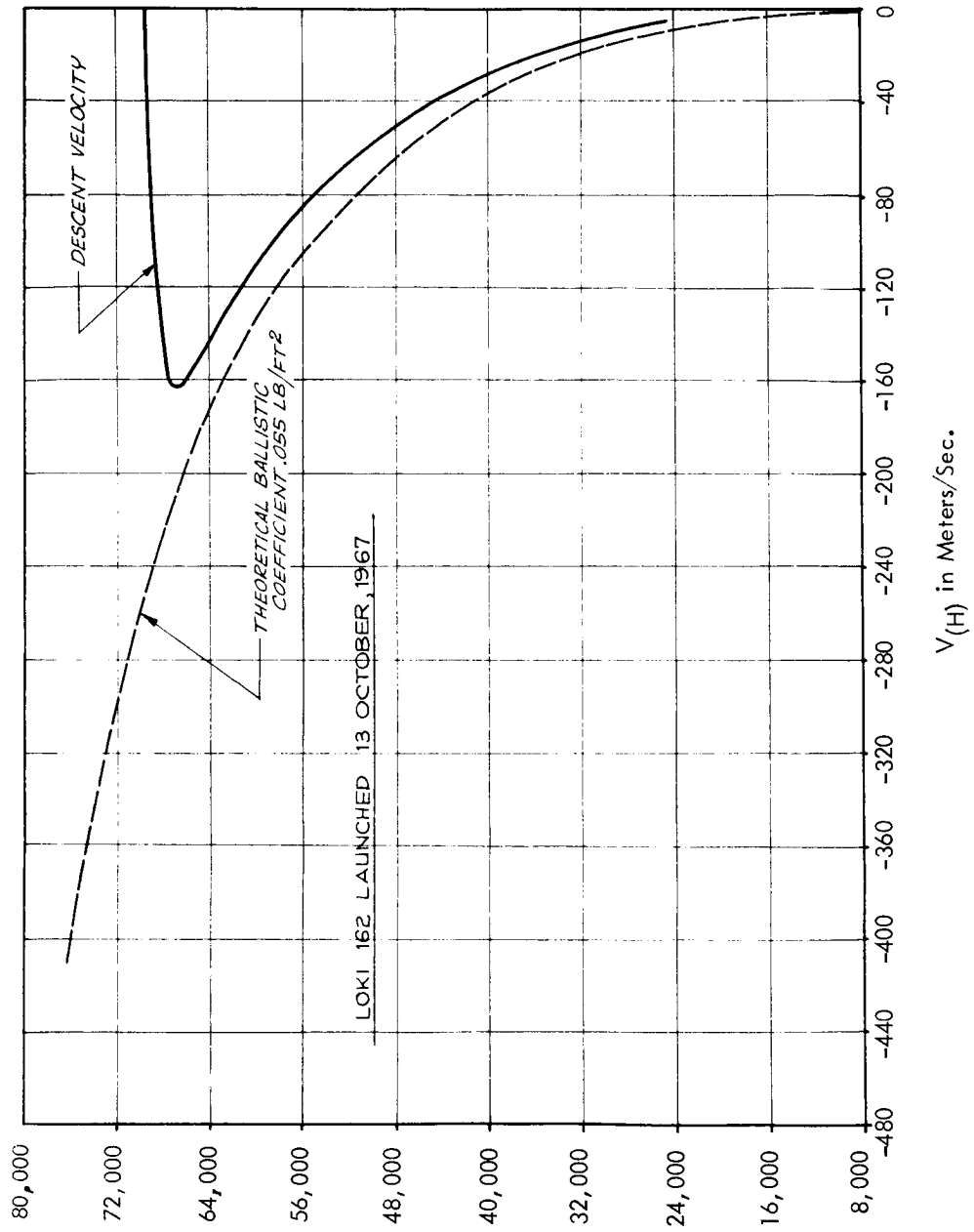


FIGURE 4.2-24 LOKI 7.6 DESCENT RATE PROFILES WSMR FLIGHT TEST DATA

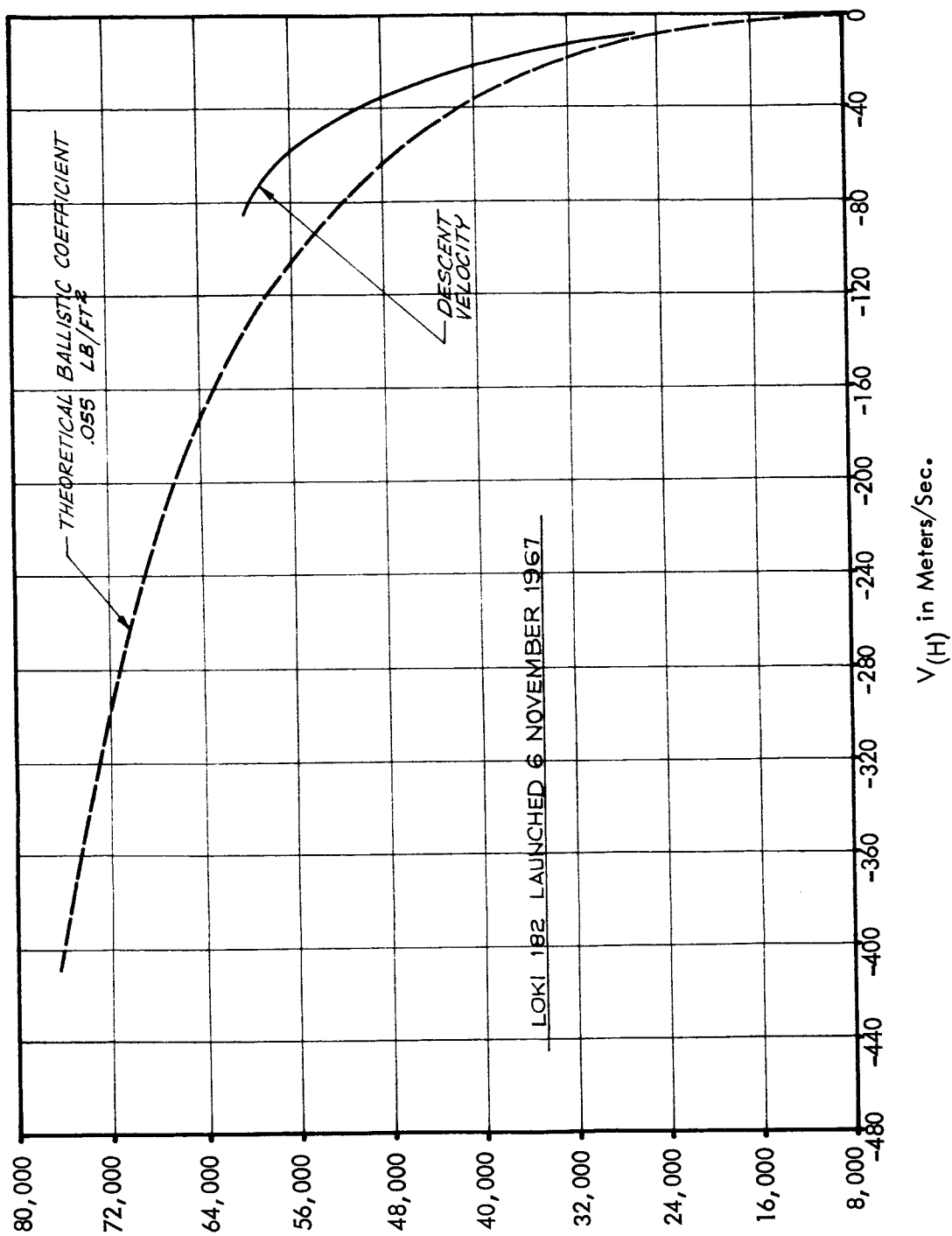


FIGURE 4.2-25 LOKI 7.6 DESCENT RATE PROFILES WSMR FLIGHT TEST DATA

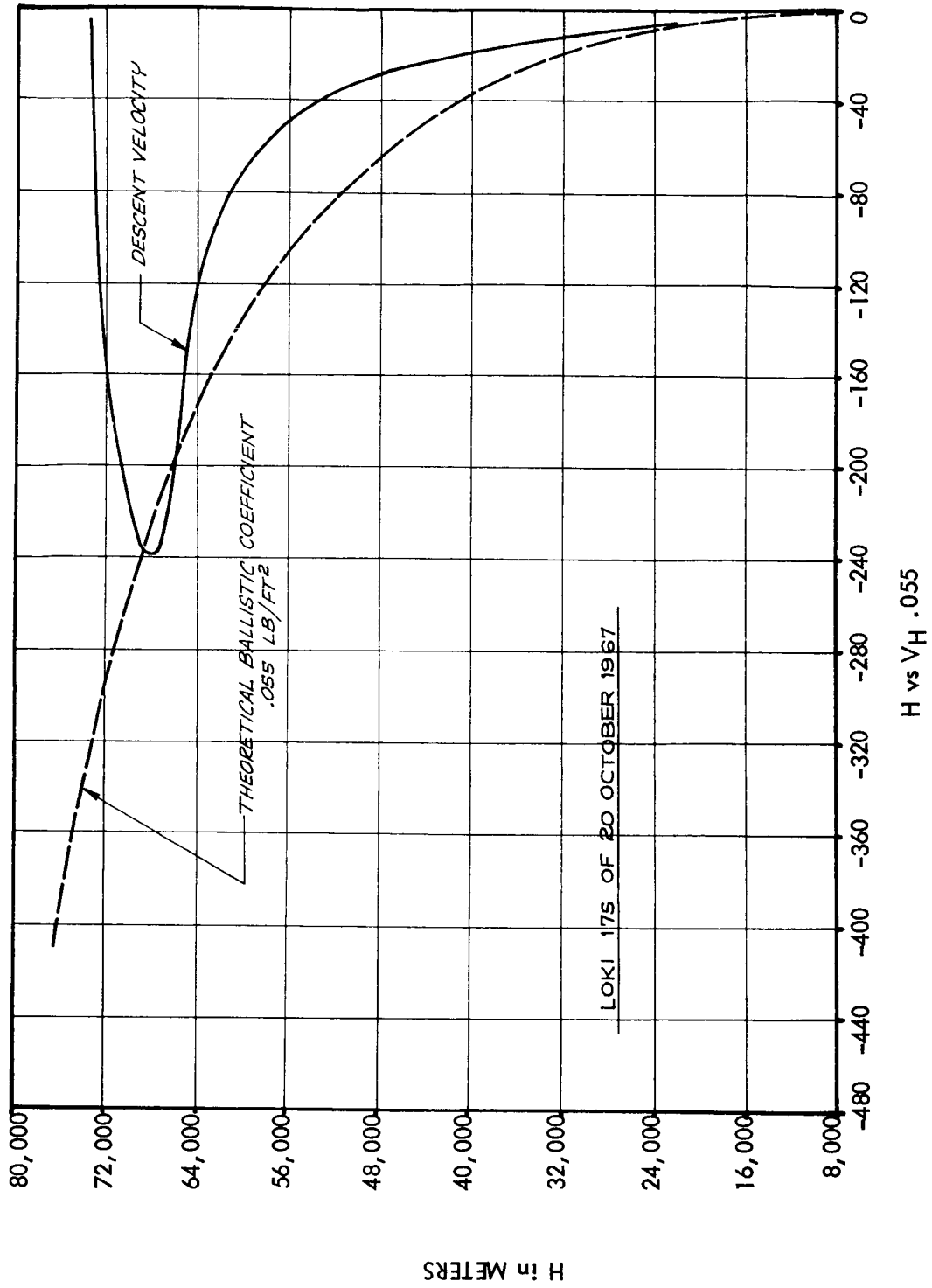


FIGURE 4.2-26 LOKI 7.6 DESCENT RATE PROFILES WSMR FLIGHT TEST DATA

The fabric area for this parachute is 35 ft² and NOL reports a drag coefficient of 0.714 and a ballistic coefficient of 0.040 lb/ft² with 0.750 payload. This parachute can be packaged into a 1.6 inch diameter cylinder with a length of 5.5 inches.

4.2.6 NOL Wind Sensor Parachute.

Most of the parachutes so far described as conventional parachutes have been used with sonde payloads, and ballistic coefficients have been about 0.050 lb/ft². In general, these systems have been adequate for obtaining wind data to altitudes of about 55 km. To obtain wind data at higher altitudes NOL has developed a parachute-sphere combination with a theoretical ballistic coefficient of about 0.010 lb/ft². The parachute has a 41 square canopy of unmetalized 2-3/4 momme silk. The sphere is a 16-inch diameter inflatable Mylar structure with internal radar corner reflectors. The sphere is supported by the parachute shroud lines as shown in Figure 4.2-27. Eight shroud lines of 27-pound test nylon cord are attached to the parachute similar to the shroud line attachment method used in the six-foot square chute. The inflatable sphere is constructed of two layers of 0.5-mil mylar, back-to-back. An aluminized mylar corner reflector is rigged inside the sphere. The sphere is self-inflated on ejection by two cubic inches of entrapped air. In addition, the chute carries inflation aids in the form of two self-inflated tubes formed from 0.5-mil mylar, 38 inches long by 1.5 inches in diameter. The tubes are attached to the chute across the diagonals with heat-sealing tape.

A considerable saving in weight (i.e. 50%) over the conventional metalized canopy is made by using the 16-inch inflatable sphere with corner reflector in lieu of silvering the canopy. The theoretical weight-to-drag/cross sectional area ratio of the balloon-chute is 0.01 lb/ft², compared with 0.04 lb/ft² for the 71-inch square chute and approximately 0.05 lb/ft² for the Arcas chute. Comparative descent rates at 60 kms are 61 m/sec (200 ft/sec) for the $\overline{CDA} = 0.01$ chute, 122 m/sec (400 ft/sec) for the 71-inch chute, and over 151 m/sec (460 ft/sec) for the Arcas chute. These descent rates are based on ejection from 69 kilometers (225,000 feet). It must be pointed out, however, that the flight test results for the balloon-parachute combination have averaged a ballistic coefficient of 0.020 lb/ft² instead of the theoretical value. It is expected that improper deployment, i.e., twisted shroud lines, is the problem.

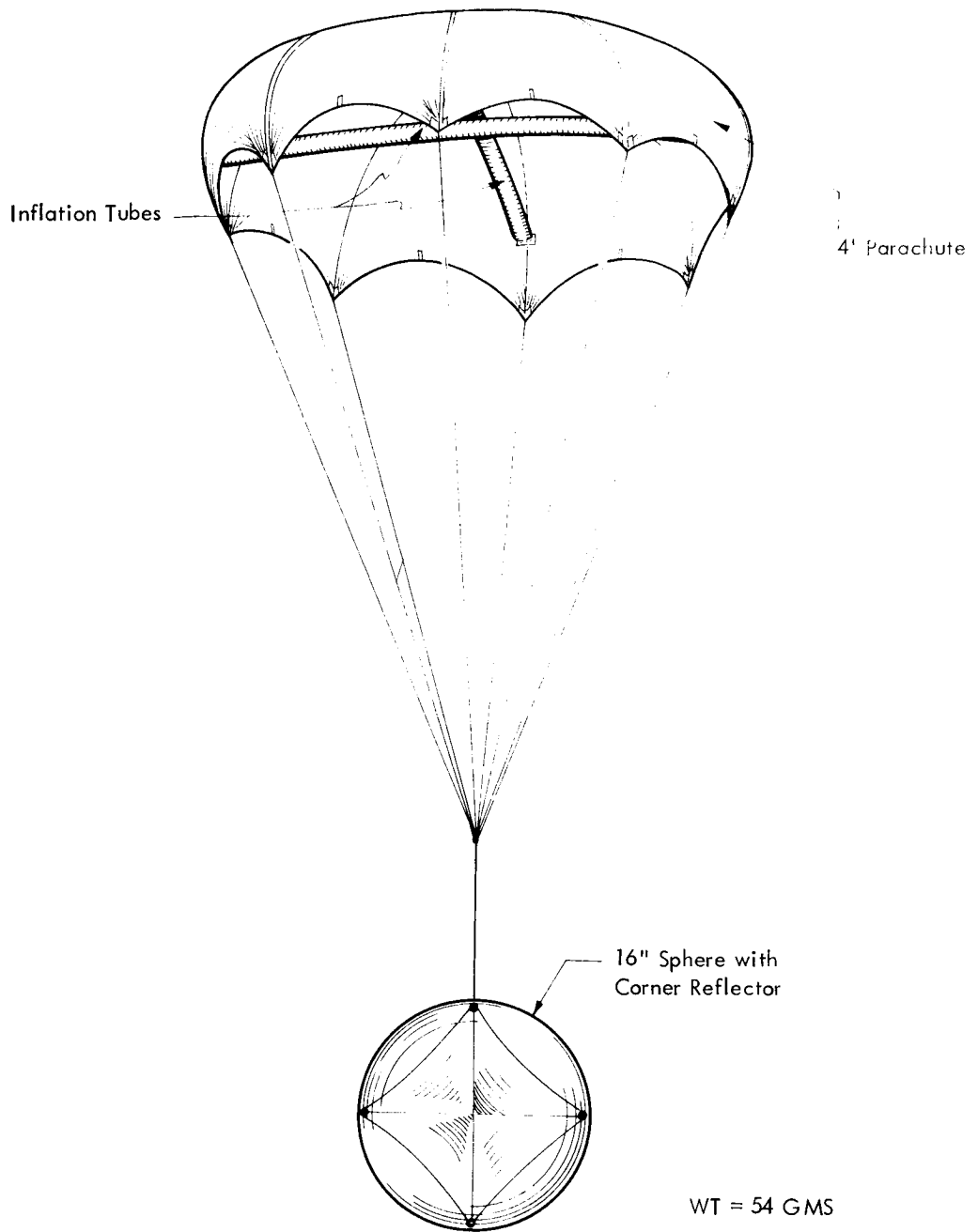


FIGURE 4.2-27 NOL WIND SENSOR PARACHUTE

4.3 Parachutes with Geometry Porosity.

4.3.1 General.

Most of the conventional parachutes utilize fabric canopies with the porosity of the canopy material permitting a stabilizing flow during descent. The pore size, however, is quite small and when it approaches the mean free path of the molecules of air in the high altitudes, the effective porosity of the fabric is reduced to a negligible value. Although this fabric has a large degree of porosity in the lower altitudes, it is essentially non-permeable at high altitudes. These parachutes oscillate rather severely from deployment down to about 80,000 feet where the fabric porosity and damping become effective. In an attempt to achieve more stability in the high altitudes, various experimenters have devised parachute shapes which offer air flow through sections of the canopy that have been cut out from the conventional shape. In general, an improvement in stability has resulted from these efforts, and in some cases reduced descent rates have been achieved. This is most likely due to more efficient use of the canopy surfaces. A review of the designs incorporating the canopy cut-out modifications on geometric porosity, as this is called, is presented in the next sections.

4.3.2 Disk-Gap-Band Parachute.

Various models and sizes of the Disk-Gap-Band parachute have been developed and tested by the G. T. Schjeldahl Company for NASA Langley Research Center. The configuration of this parachute design is shown in Figure 4.3-1. The geometric porosity of this design is in the formation of a gap between the top disk and the side band positions of the canopy. An inflatable torroidal ring is attached to the inner surface of the band for positive deployment.

A 16.6 foot diameter DGB parachute has been designed for use with the Arcas. This design has a total canopy area (S_c) of 216 ft² and a drag coefficient of 0.50 based upon total canopy area. Parachute weight is 1.7 pounds. With a payload weight of 3.30 lbs. the ballistic coefficient is 0.050 lb/ft². The parachute canopy is constructed of two major parts designated as the disk and the band. The disk, which is a flat circular sheet, forms the central part of the canopy; and the band, which is cylindrical in shape, extends down from the outer edge of the disk and forms the lower portion or skirt of the

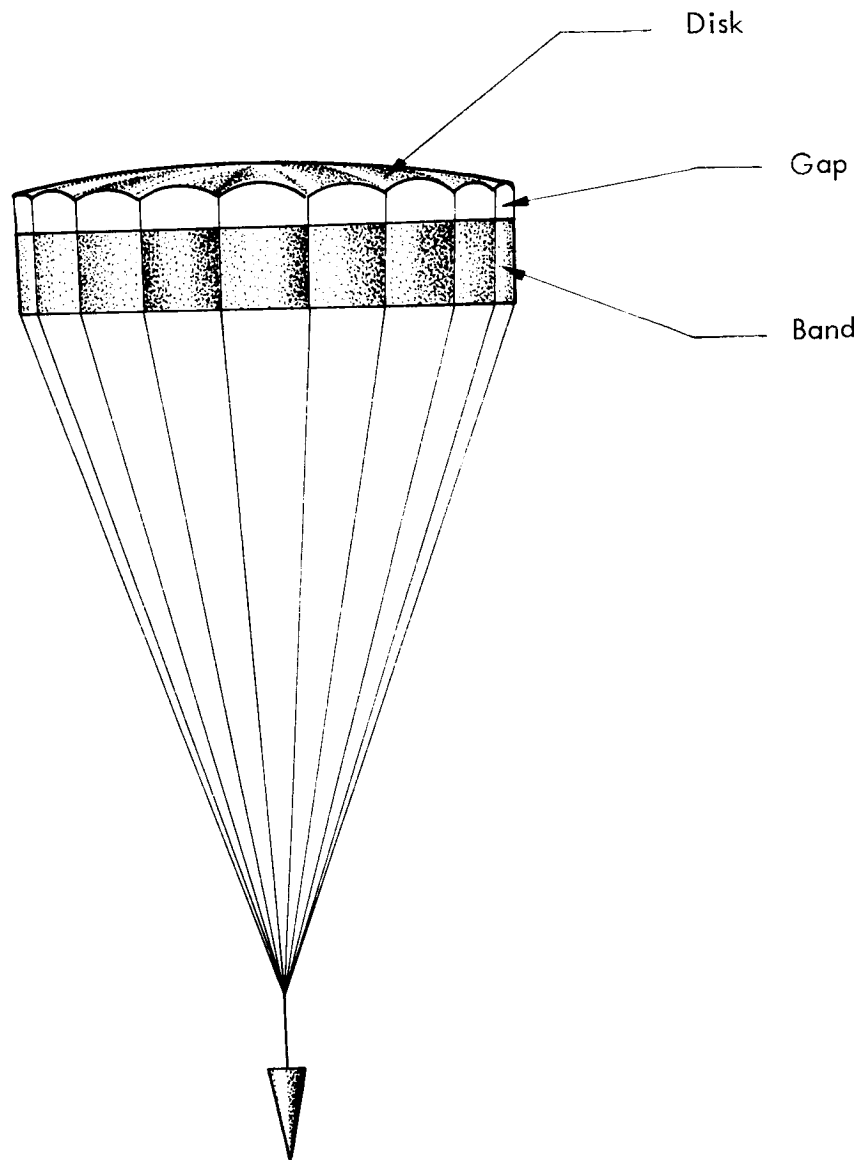


FIGURE 4.3-1 DISK-GAP-BAND PARACHUTE CONFIGURATION

canopy. The disk and the band are separated to provide a geometric opening designated as the gap. The area relationships of the canopy are as follows:

Disk Area	=	52.4% of total area
Gap Area	=	12.4% of total area
Band Area	=	35.2% of total area

The torus inflation aid is constructed of 4-inch diameter tubular sections. The torus has a major diameter of 11-feet and is attached to the inside surface of the band portion of the canopy at each of the twenty suspension line tapes. Three (3) Saran wrapped water soaked blotters are located equally spaced inside the torus and each has sufficient water to pressurize the torus. Each torus is pressure tested to assure leak-proof construction before installation into the parachute canopy.

The DGB parachute systems are equipped with a miniature ball bearing swivel located between the confluence point of the parachute suspension lines and the payload lanyard. This swivel allows for differential rotation rate decays. Clevis type hardware is provided for attachment of the suspension lines to the swivel and the swivel to the payload lanyard. The lanyard is 24-inches in length.

The parachutes are provided packed in deployment bags fabricated of cotton canvas and nylon webbings. The deployment bags are of such size as to fit firmly but easily into the standard Arcas rocket canister.

The deployment bag is provided with a permanently attached strip of material having elastic loops which hold the suspension lines in place and allows the suspension lines to deploy only from the payload end of the holding strip. This arrangement assures an orderly deployment of the suspension lines and assists in preventing problems of line entanglement. The parachute deployment bag is equipped with two (2) 1-3/4 inch wide nylon webbings which retain the parachute canopy in the deployment bag until the last loop of the suspension lines pull out and unlatches the restraint webbings. This system assures that the suspension lines are deployed full length before the canopy is released.

The deployment bag attachment lanyard is provided with five sewn-in loops to absorb the shock of stopping the bag and restrained canopy while

the suspension lines are deploying. The Arcas DGB parachute dimensions are as follows:

Nominal Diameter	16.6 ft.
Number of suspension lines	20
Length of suspension lines	18 ft.
Torus cross section diameter	4 in.
Torus major diameter	11 ft.
Attachment lanyard length	24 in.
Miniature swivel	1-1/2 in. long by 3/4 in. dia.

The disk and band portions of the canopy are fabricated of a dacron-thread reinforced metalized mylar film material designated as G. T. Schjeldahl material X-821. This mylar film is of 1/4 mil thickness and is 100 percent metalized for radar reflectivity. The dacron reinforcement threads carry the stress loads and provide ripstop characteristics. The X-821 material is joined by mylar tapes which are also reinforced by dacron threads. This same tape is used as suspension line tape to join the band to the disk portion of the canopy.

The suspension lines are 85 pound test coreless nylon line. Each suspension line is continuous through the confluence point and is tied off at each end to a suspension line tape at the edge of the canopy. The twenty 18-foot long suspension lines are actually formed from ten lines, each 36-feet long.

The torus is constructed of 1/2 mil clear mylar film and is joined to the canopy by dacron reinforced mylar tapes. The attachment tapes are sewn to the canopy in addition to being adhesive bonded.

The payload lanyard and the deployment bag, shock-attenuating lanyard are both constructed of 1500 lb. test nylon webbing.

The deployment bag is constructed of cotton canvas to reduce damage resulting from hot sparks emitting from the separation charge. Nylon webbings are used for the attachment loop and the canopy restraint straps. Nylon tape is used to edge cover flaps of the deployment bag. Rubber bands mounted in a dacron mylar tape are used to hold the folded suspension lines in place in the deployment bag.

A scaled-down version of the Arcas DGB parachute design has been flight tested with the Loki Dart system. The results have been poor because of deployment problems which are most likely spin rate related.

In the course of the development flight tests for the DGB parachute, it was found that the deployment from a spinning missile caused shroud line tangling and canopy entanglement. Therefore, the parachute was packed in a special deployment bag designed with canopy restraint straps, suspension line holders and a shock attenuating attachment lanyard. The most important factor to be considered for any parachute deployment method is assurance that suspension lines are kept in tension at all times during line and canopy deployment. To accomplish this, the deployment bag was redesigned by placing one and three-quarter inch wide canopy restraining straps inside the bag, and by attaching the suspension line holding strip to the deployment bag. This accomplished three things: 1) attaching the suspension line holding strip to the deployment bag assured that the lines deployed from the payload attachment end only; 2) use of the deployment of the last loop of the suspension lines as the activating mechanism for release of the canopy assured against premature release; and 3) restraint of the canopy until the suspension lines were fully deployed assured that the canopy did not eject from the deployment bag until the suspension lines were stretched full length and under tension. The modified deployment bag is shown in Figure 4.3-2 and the sequence of deployment events is presented in Figure 4.3-3. With this system, reliable deployment has been obtained as high as high as 232,000 feet.

The above deployment technique has certainly been an improvement in the state-of-the-art for deploying meteorological rocketsonde parachutes. Other significant improvements developed during the DGB development program have been the use of a positive inflation aid and an improvement in stability. The DGB parachute system is equipped with a water vapor pressurized torus inflation aid, to provide instantaneous and full opening of the parachute canopy immediately after deployment. The canopy design uses geometric porosity

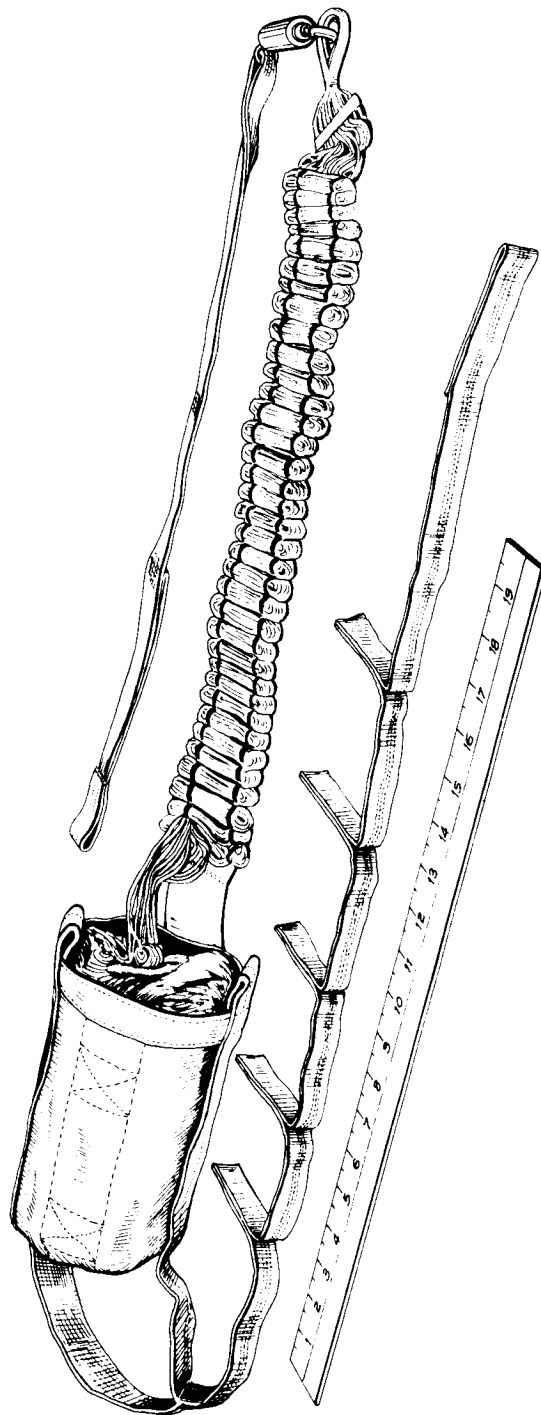


FIGURE 4.3-2 MODIFIED DEPLOYMENT BAG WITH PACKED PARACHUTE

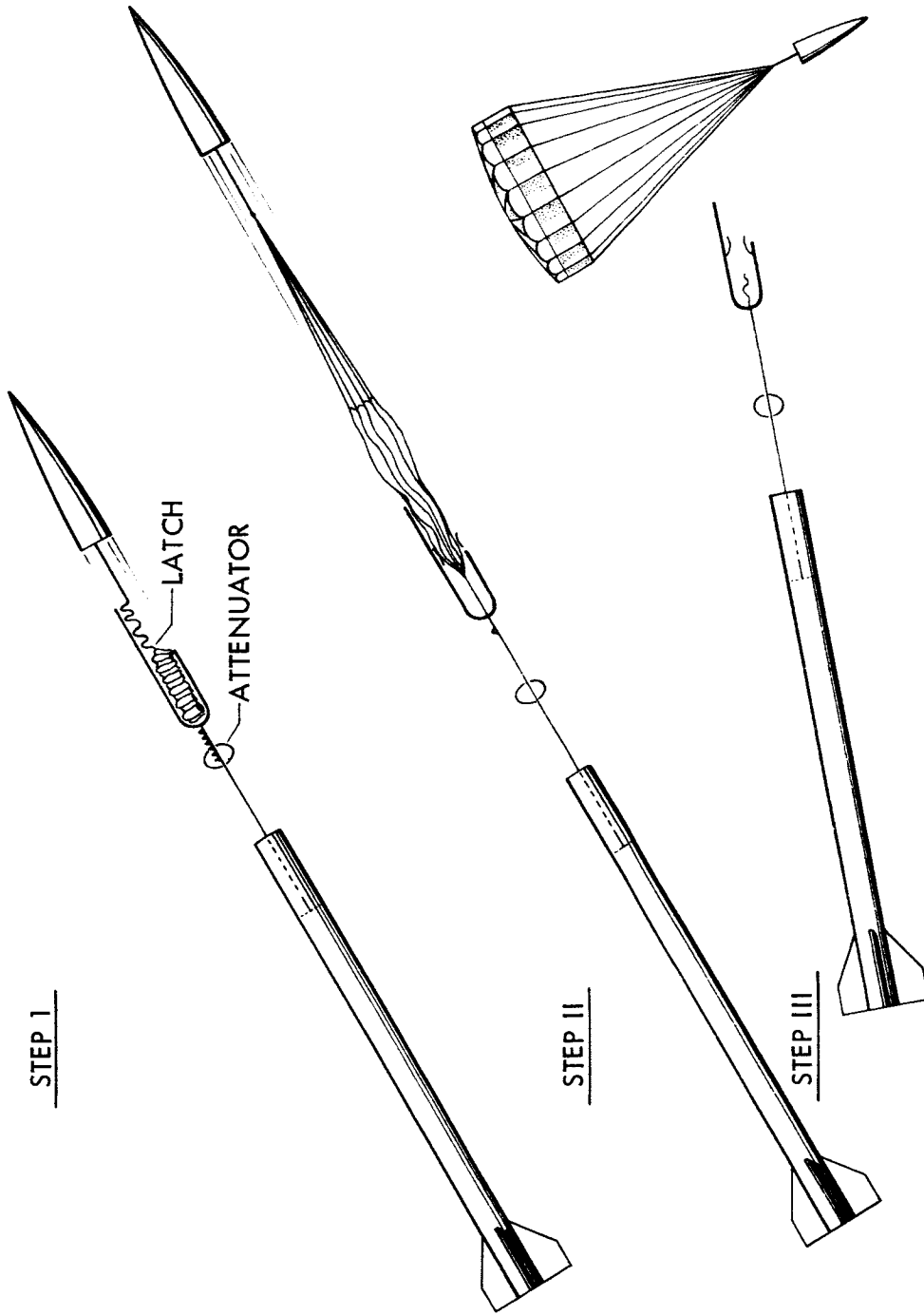


FIGURE 4.3-3 SEQUENCE OF EVENTS

as a means of achieving stability so that stability characteristics will not vary with the altitude of operation. Wind tunnel tests indicate that the DGB parachute is stable at approximately 6-degrees angle of attack. Several rocket flight tests have been conducted using on board camera and long range ground-based cameras to check stability in actual operation at high altitudes and indications are that inflight stability is as good or better than predicted by the wind tunnel tests. Absence of periodic oscillation in telemetry signal strength and radar return signal records is also an indication of in-flight stability.

4.3.3 Cross Patch Parachute.

The cross patch or plus parachute is formed by crossing two rectangular canopy sections in the shape of a cross and joining the intersecting areas. The shroud lines are attached to the ends of each cross member as shown in Figure 4.3-4. NOL has fabricated and flight tested a 35-foot cross patch parachute for use with the Arcas system. Design parameters for this parachute are presented in Table 4-6.

During flight tests, this parachute exhibited a much slower descent rate than the regular Arcas 15-foot Gentex parachute. At 200,000 feet the cross patch parachute descent velocity was 275 ft/sec. while the regular Arcas 15 foot parachute falls at 460 ft/sec. The cross patch, however, showed an oscillation in descent velocity with a 10,000 foot period and a 25 ft/sec amplitude at 200,000 feet. This pattern is a characteristic of breathing instability. Typical fall rate results are shown in Figure 4.3-5. It appears that an inflation aid, such as an inflatable torus would be required for high altitude opening and breathing stability. Although this would detract from the theoretical ballistic coefficient to some degree, the resulting fall rates should still be quite good. The simplicity of design and fabrication for the cross patch parachute should make it quite inexpensive.

4.3.4 Annular Ring Parachute.

For solid fabric parachute designs the hemispherical shape seems to create the greatest drag per unit of projected area. Since the drag coefficient of a circular disk, $C_D = 1.15$, is not significantly reduced by cutting a hole in its center up to a diameter ratio of twenty-five percent, it may be advisable to consider a hemispherical design with an aperture cut in the crown to reduce the magnitude of parachute gliding and oscillating. A vent hole in the center

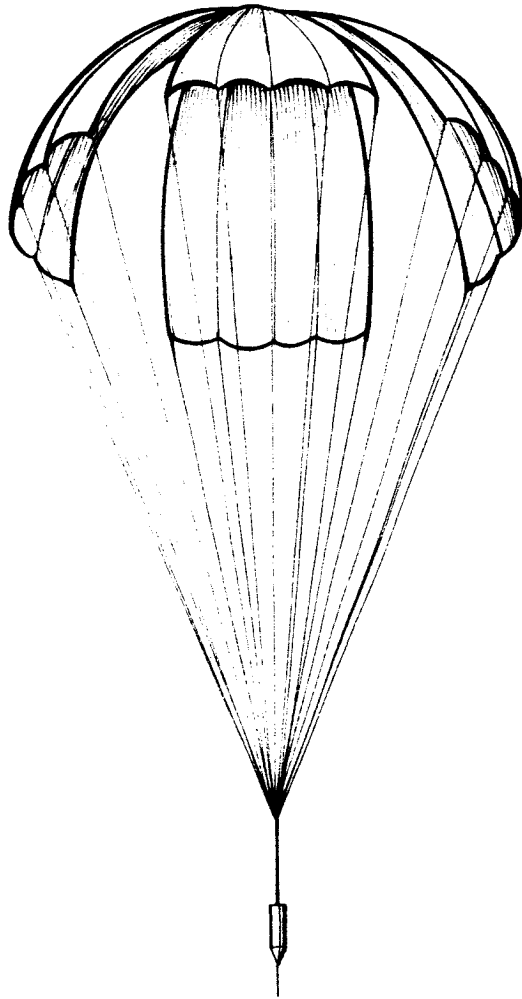


FIGURE 4.3-4 CROSS PATCH PARACHUTE

TABLE 4-6

ARCAS CROSS PATCH PARACHUTE DESIGN PARAMETERS

Canopy material 2-3/4 momme silk	
Panel Length	35 ft.
Panel Width	9 ft.
Fabric Area	549 ft. ²
Fabric Density	2.23×10^{-3} lb/ft ²
Fabric Weight	1.40 lb
Shroud Line and Fittings Weight	1.75 lb
Total Parachute Weight	3.15 lb.
Payload Weight	4.60 lb.
Total Weight	7.75 lb
C_D (210 ft/sec @ 180,000 ft)	0.464
C_D (180 ft/sec @ 170,000 ft)	0.447
Ballistic Coefficient	0.026 lb/ft ²

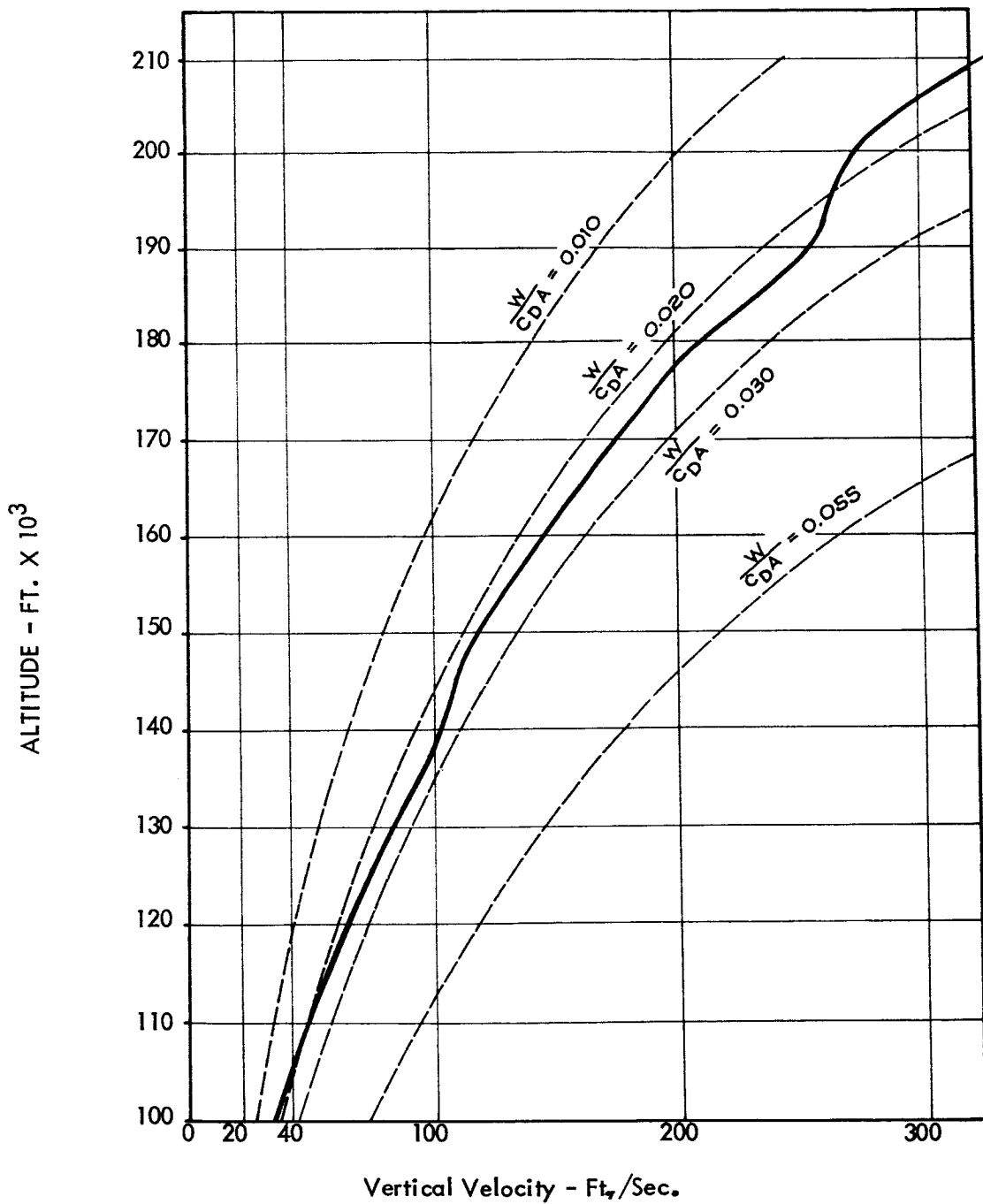


FIGURE 4.3-5 35' CROSS PATCH PARACHUTE FALL RATE RESULTS

of the canopy provides a flow of air into the normally turbulent flow above the crown. This short circuits the collapsing air stream and increases the parachute stability. As long as the aperture diameter is kept below 25 percent of the flying diameter, the stability of the parachute should be significantly improved with no reduction in the drag coefficient or drag based upon fabric area. Although the drag decreases as the diameter of the center hole increases beyond 25 percent, the drag coefficient based upon the area of the resulting ring, hence fabric area, increases and reaches a theoretical limiting value of 1.98 at a diameter ratio of 1.0. Figure 4.3-6 presents experimental data on the drag coefficients of annular flat plates for increasing center hole diameter ratios.

The theoretical drag coefficient data indicates a maximum drag coefficient based on fabric area occurs for an infinitely large inside and outside ring diameter, i.e., a hoop with an infinitely large diameter. This design is impractical since shroud line loads would increase severely as the diameter of the parachute increases and the chute would collapse. Although the center hole concept may not be considered as within the state-of-the-art for high altitude rocketsonde parachute designs at the present time, it might be considered for this application after suitable flight test results under a special parachute evaluation program.

Parachutes based upon this center hole concept as shown in Figure 4.3-7 are called annular ring parachutes. These designs are promising although they would require a positive inflation aid for the rocketsonde application. To our knowledge there has not been any meteorological flights conducted with this design.

4.3.5 Miscellaneous Geometric Porosity Designs.

There have been various other parachute designs with geometric porosity proposed for high altitude meteorological rockets which have not as yet been successfully flight tested. These designs include the wagon wheel and the ring-sail parachutes as shown in Figures 4.3-8 and 4.3-9. It is expected that most of these parachutes would require an inflation aid, and the advantages over the previously discussed designs is not obvious.

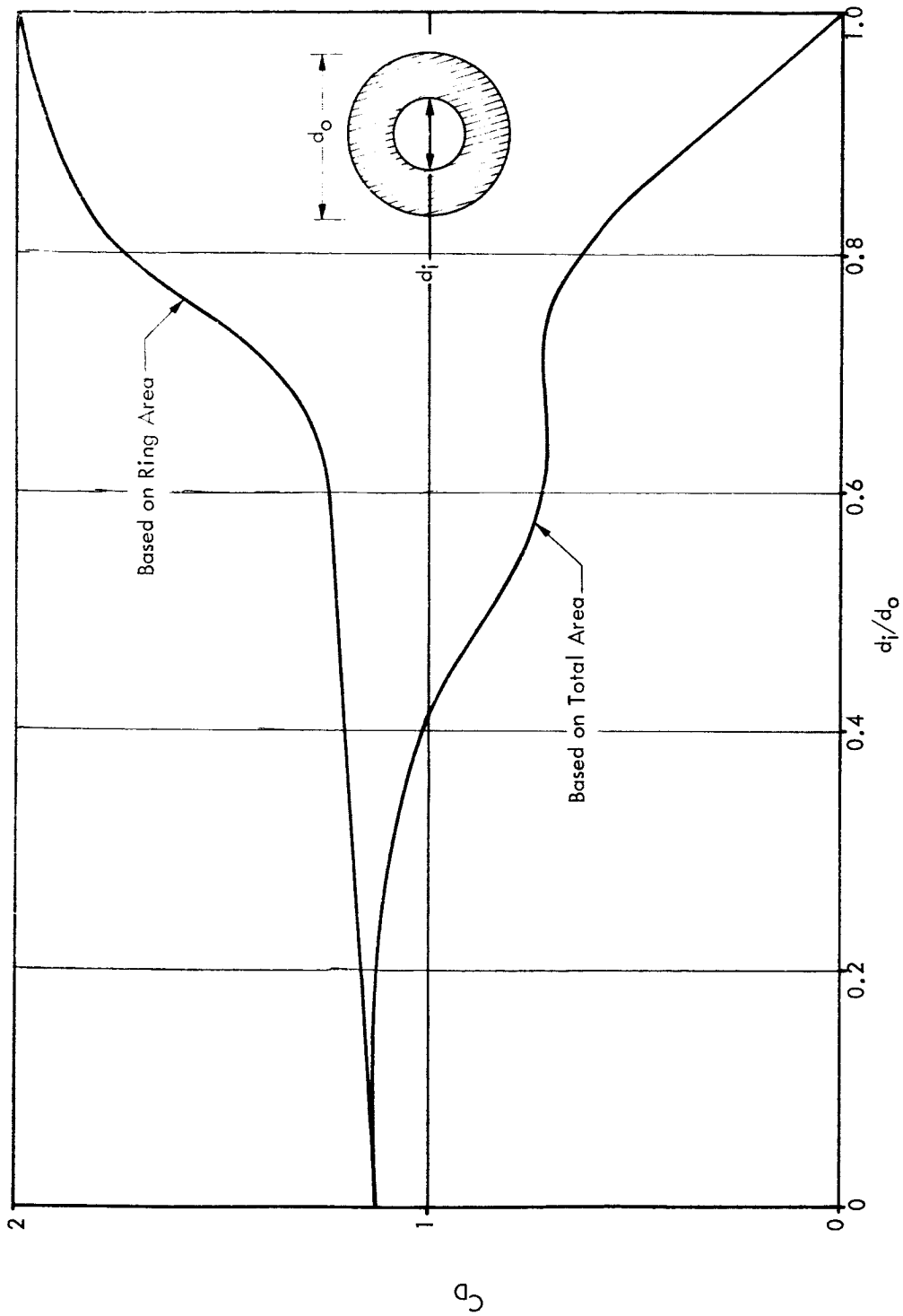


FIGURE 4.3-6 DRAG COEFFICIENT OF ANNULAR PLATES (RINGS)

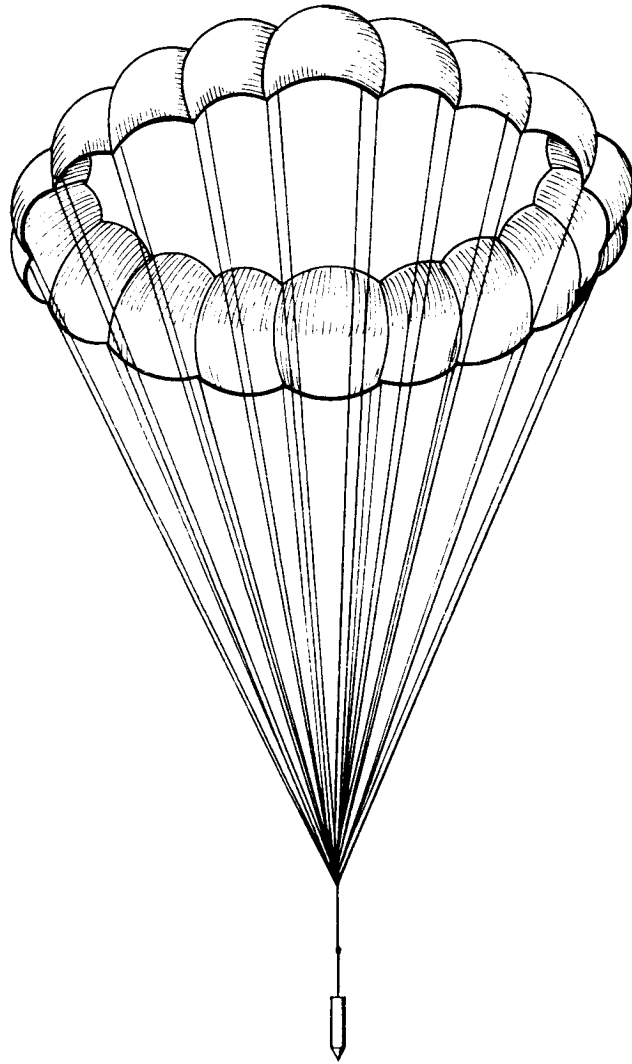


FIGURE 4.3-7 ANNULAR RING PARACHUTE DESIGN

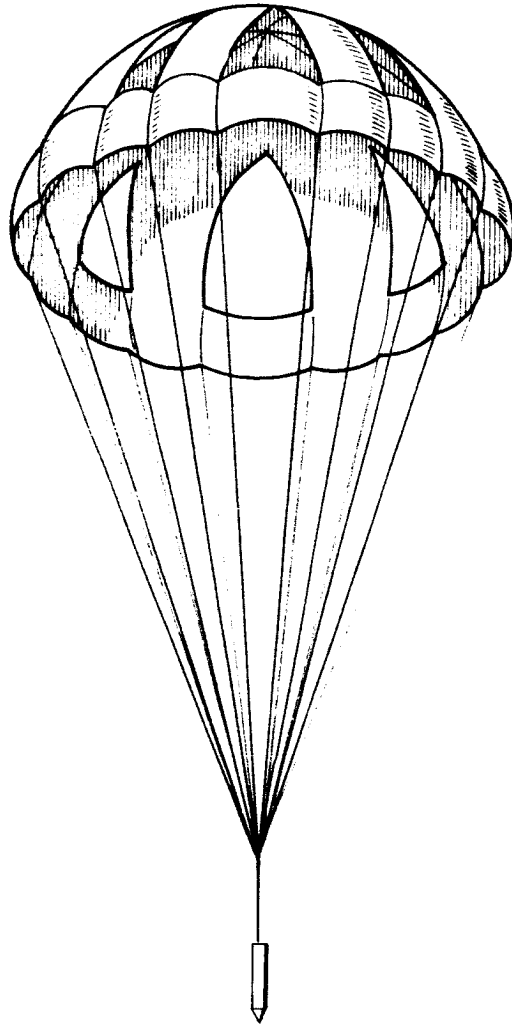


FIGURE 4.3-8 WAGON WHEEL PARACHUTE

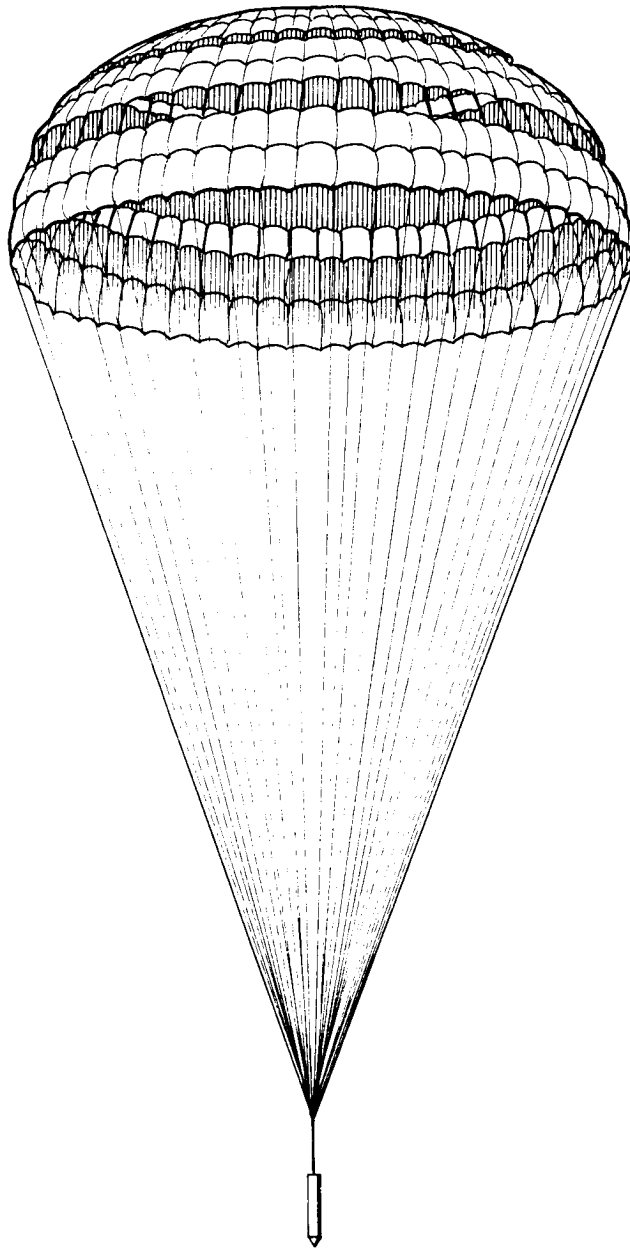


FIGURE 4.3-9 RING SAIL PARACHUTE

The vortex-ring parachute is based upon a rather unique concept. The drag coefficient of a conventional flat-circular parachute is about 0.75 while that of a ribbon parachute generally averages around 0.50 to 0.55. The parachute that holds the record so far as drag coefficient is concerned is the vortex-ring parachute. The canopy of the vortex-ring is divided into four separate panels which are tilted in flight in such a way that the parachute behaves like a four-bladed propeller -- the panels deflect the air-stream and cause the whole canopy to whirl. The turbulence that creates drag also creates instability unless it is controlled and balanced. The vortex-ring canopy takes advantage of this. The drag coefficient can be as high as 2.00, and the oscillations are usually below five degrees. It is necessary to have a precision swivel between the payload and the canopy. The swivel and the natural complexity of the canopy add to the cost and weight with the result that the vortex-ring chute is used only for specialized applications.

Early flight tests of the Arcas rocket included some flights of the vortex-ring parachute. In all cases, the vortex-ring parachute failed to deploy and streamed to impact. It will probably be necessary to construct the canopy panels so that they can be inflatable structures.

4.4 Stokes Flow Ribbon Mesh Parachute.

4.4.1 General.

The Stokes flow ribbon mesh parachute with inflatable struts appears to be a most promising subsonic decelerator to altitudes of 100 km. Wind measurement analysis of this system was described in Section 3.2.9. The canopy mesh is constructed from fine filaments or ribbons and the spaces between these elements creates geometric porosity which is conducive to stability. The small filament diameter or ribbon width takes advantage of the Stokes flow region of low Reynolds number, R_e , and creates high viscous drag. For R_e less than one, the drag coefficient is inversely proportional to R_e ; and hence, the smaller the filament diameter, the greater the drag coefficient. Both the theory developed by Astro Research Corporation and vacuum chamber tests conducted by NASA-Langley indicate that ballistic coefficients can be achieved which are much less than 0.010 lb/ft². Theory indicates that without a payload this design could descend as slowly as 400 meters per second at 100 km. Packaging techniques, inflatable braces, and radar cross-section are factors which require further investigation.

The Stokes flow parachute design offers the primary advantage of a reasonably slow descent rate for high altitudes. A secondary advantage is that the drag coefficient decreases during descent to the lower altitudes so that the terminal velocity does not slow down with decreasing altitude as much as for more conventional designs. Since there is a large amount of geometric porosity, even for high altitude operation, stability characteristics are significantly improved and severe oscillating and tumbling at high altitudes should be eliminated. Deployment of the Stokes flow design requires inflatable struts or braces which contain an inflation medium. Since parachute packaging volume is the primary limiting factor for small meteorological rockets, the drag coefficient per unit packaging volume becomes a most important factor. The Stokes flow parachute should be superior over all other descent devices considered in this respect. However, shroud line tangling may be a problem which must be solved since deployment will most likely be from a spinning missile.

4.4.2 Theoretical.

For very low Reynolds number, $Re = \frac{\rho u l}{\mu} < 1$, the drag on an object is approximately inversely proportional to the Reynolds number as indicated by

$$D = k_i \mu l u \quad \doteq \quad \left(\frac{k_2}{Re} \right) A \frac{\rho u^2}{2}$$

where $C_D \doteq \frac{k_2}{Re}$ for $Re < 1$

Symbols:

Re	Reynolds Number = $\frac{\rho u l}{\mu}$
ρ	Air density
μ	Air viscosity
u	Free stream velocity
l	Characteristic length, i.e., length of an object in the direction of flow
k_i	Constants related to object shape and size
$C_{D_{ij}}$	Drag coefficient referenced to object i and reference area j
A	Area projected normal to flow.

For small Reynolds numbers viscous effects predominate and the resulting drag is due to the fluid deformation and friction rather than pressure differentials. Experimental data have been taken and corrections have been made to Stokes law by Oseen, Wieselsberger and Prandtl for the viscous drag on an infinite single cylinder, and the resulting C_D vs R_e is plotted in Figure 4.4-1.

It can be seen that extremely high drag coefficients are obtained when Reynolds numbers become small, i.e., for small diameter fibers or thin ribbons.

When a series of single fibers or small elements are combined to form a fish-net or grid geometry, actuator disc theory of fluid dynamics can be used to estimate the overall drag coefficient of the network. The network drag coefficient varies with the Reynolds number and the solidity ratio, E , which is the ratio of the frontal area of the network, A , and the frontal area of all the fiber, a , as $E = a/A$. For a particular value of E , the network drag coefficient approaches that of a flat plat, i.e., $C_{DA} = 1$, as the solidity ratio is reduced. A typical plot of drag coefficient vs Reynolds number is presented in Figure 4.4-2. This figure indicates that a parachute can be constructed from small elements with an 80% porosity ($E = 0.20$), and the drag coefficient is the same as for a solid canopy for R_e below 0.8. Furthermore, as this system descends to lower altitudes, i.e., high R_e values, the drag coefficient decreases so fall rates do not decrease as much as for conventional parachutes with constant drag coefficients.

4.4.3 Proposed Parachute Designs.

The concept of the Stokes flow ribbon mesh parachute is shown in Figure 4.4-3. The parachute consists of a square canopy deployed and rigidized by an x-shaped bracing system fixed diagonally into the square net. There are two straight inflated thin walled brace tubes, each with the length of a full diagonal, one fixed above the network and one below it. The four sectional network sails between adjacent brace legs are designed such as to provide upward bent conical surface when in operation. The braces also provide the attachment point for the suspension lines for the payload. The network or canopy is composed of a square angled net made from aluminized mylar tapes approximately 0.100-inch wide and 0.00025-inch thick. The braces consist of 0.00025-inch thick mylar tubes,

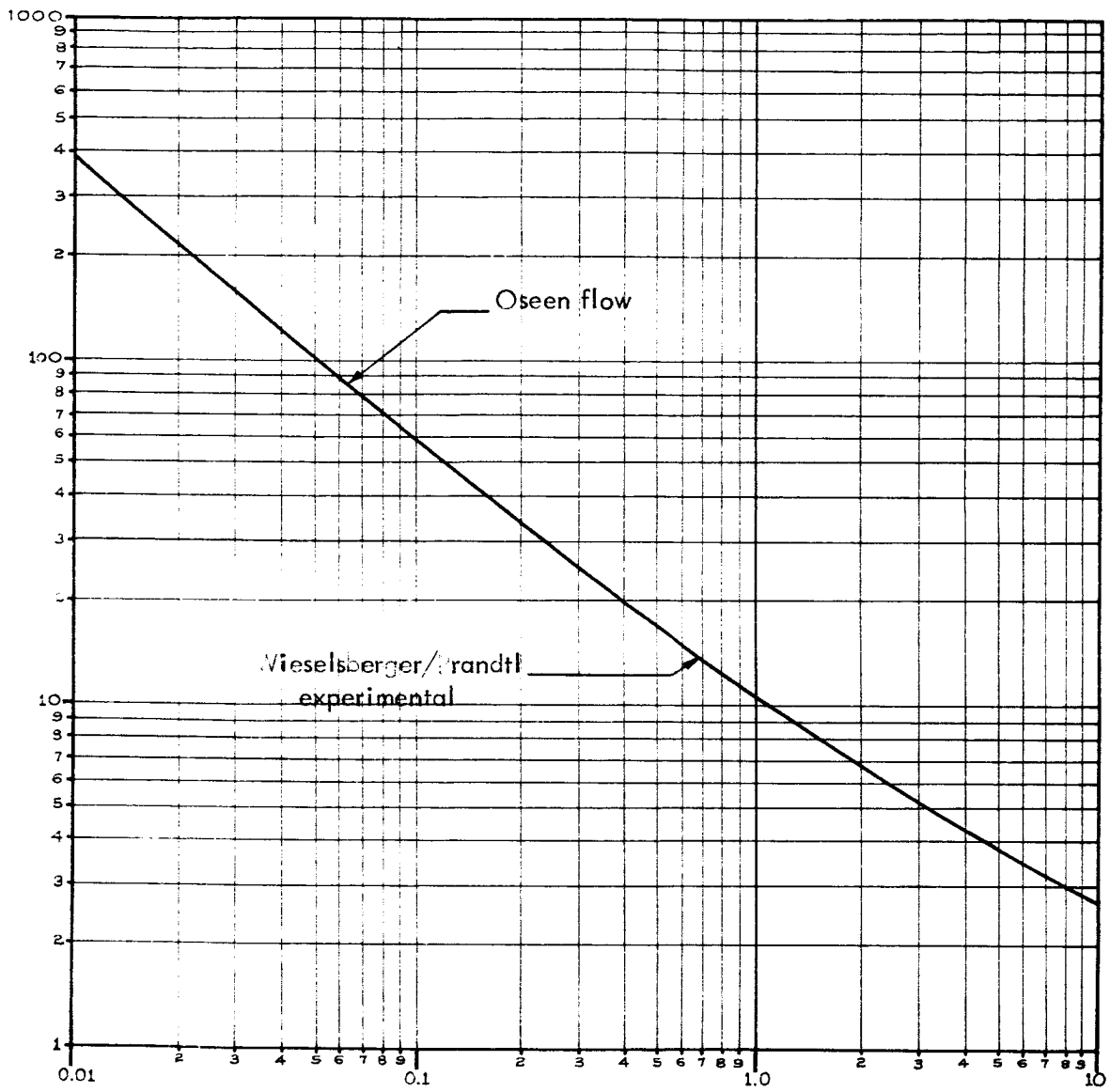


FIGURE 4.4-1 DRAG COEFFICIENT OF AN INFINITE SINGLE CYLINDER

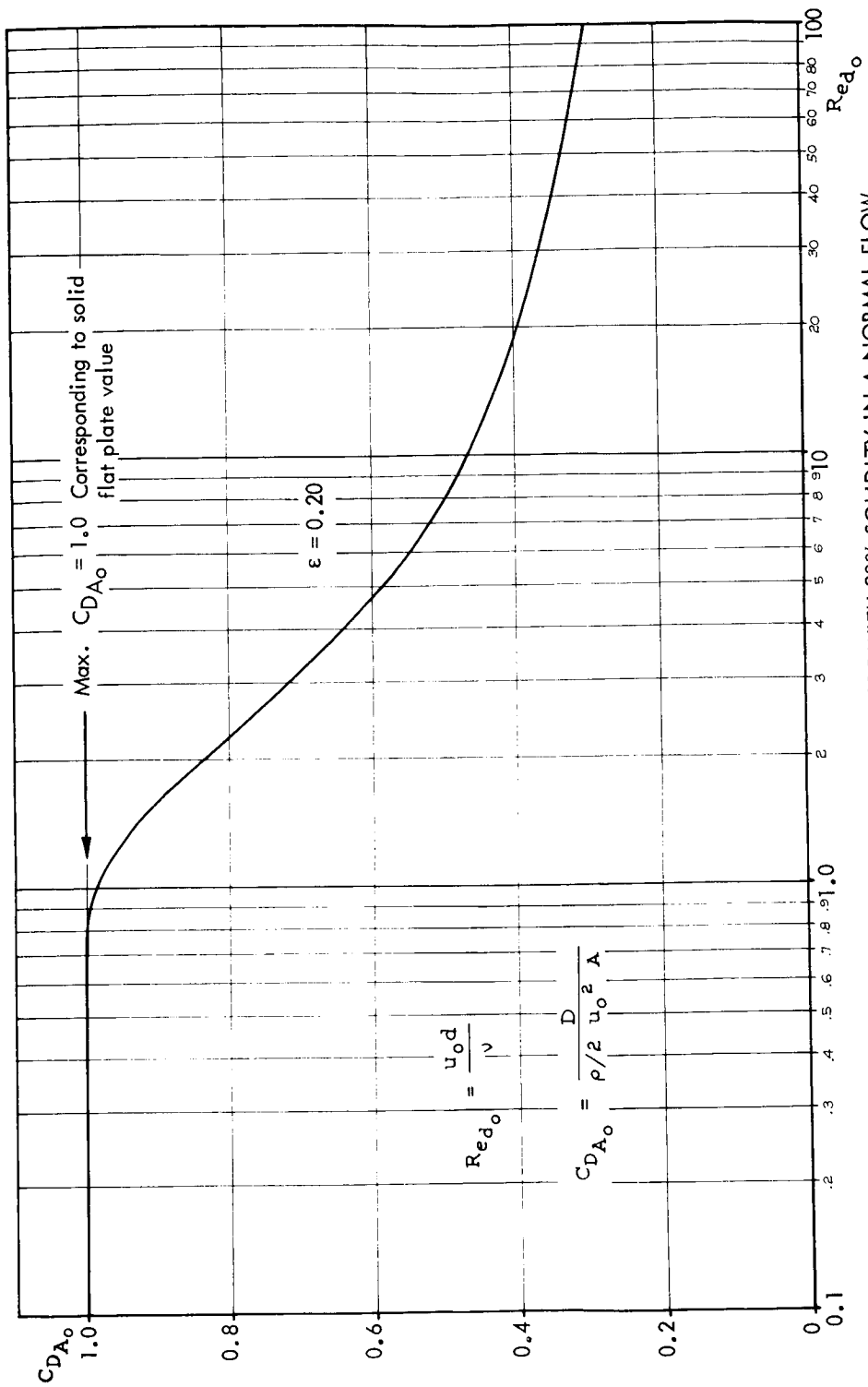


FIGURE 4.4-2 DRAG COEFFICIENT FOR A FLAT DISC WITH 20% SOLIDITY IN A NORMAL FLOW

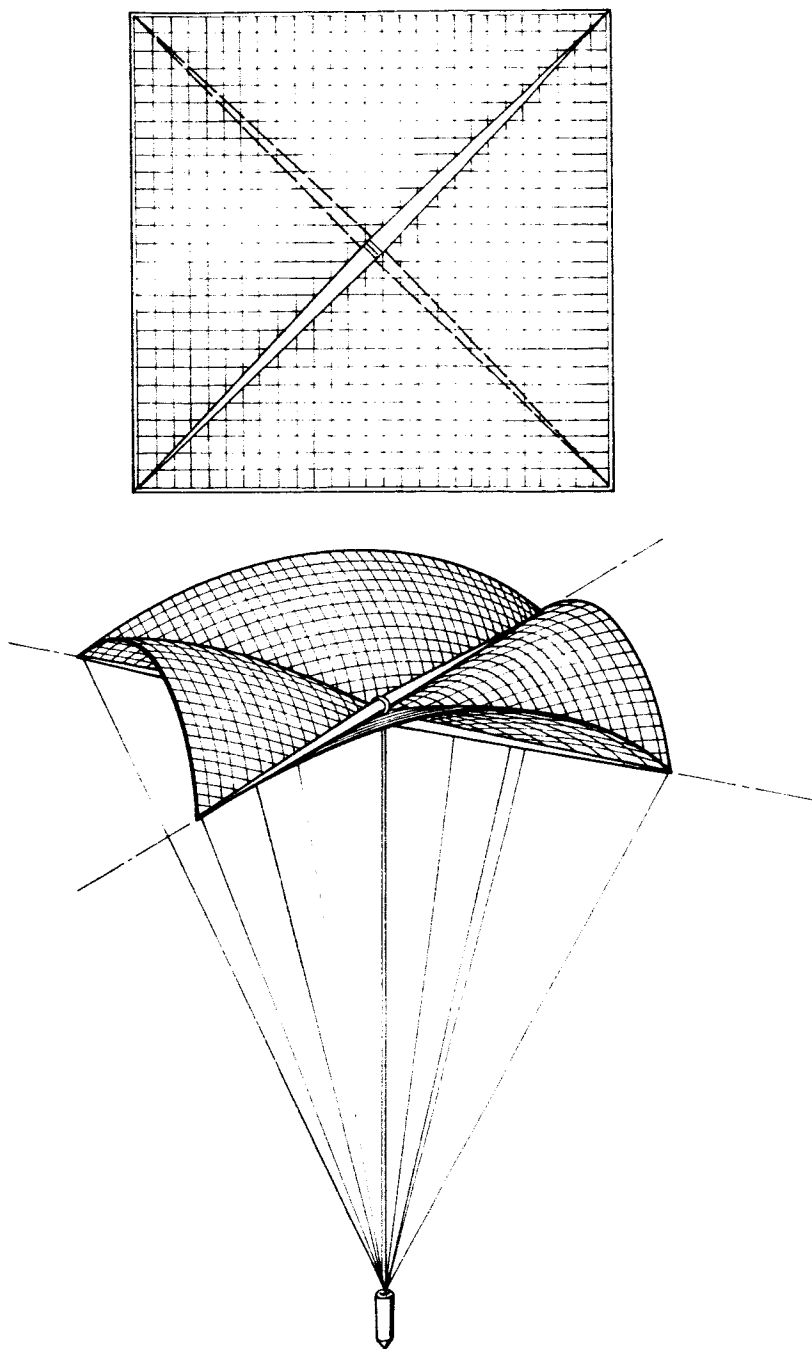


FIGURE 4.4-3 THE CONCEPT OF THE STOKES FLOW RIBBON MESH PARACHUTE

and the suspension lines are nylon monofilaments with an 0.005-inch diameter for the dart application and an 0.010-inch diameter for the Arcas application.

Three parachute designs have been proposed by Astro Research Corporation for application as follows:

1. Dartsonde Parachute
2. Dart Wind Drift Target
3. Arcasonde Parachute

The main design parameters are presented in Table 4-7.

Various methods have been proposed for pressurization of the braces such as pressurized gas containers and liquid freon. However, we would suggest the use of isopentane alcohol as used in the Robin inflatable sphere applications. This material is easy to seal in a closed container and has proven to be quite reliable in numerous flight tests. Inflatable structures with isopentane routinely collapse at about 120,000 feet altitudes. This self collapsing feature is desirable for this application to speed descent rates at the lower altitudes.

4.4.4 Proposed Performance.

The flight performances for the three proposed parachute designs are presented in Figures 4.4-4 through 4.4-6. The full lines represent the descents of the fully deployed canopies. The dotted lines are estimates of the descent rate after brace support tubes collapse. The dardrifter design remains subsonic almost up to 100 km (330,000 ft.). For higher altitude subsonic operation, thinner materials than the 0.00025-inch mylar are required. The total descent times for the three designs are as follows:

- | | | |
|----|------------|------------|
| 1. | Dartsonde | 34 minutes |
| 2. | Dardrifter | 93 minutes |
| 3. | Arcasonde | 25 minutes |

4.4.5 Test Data.

Chamber tests of the Stokes flow parachute concept have been conducted by NASA-Langley by dropping models of various solidity ratios in high altitude simulation environments. The major chamber test variables are listed as follows:

TABLE 4-7

PROPOSED PARACHUTE DESIGN PARAMETERS

<u>Application</u>	<u>Dartsonde Parachute</u>	<u>Dartdrifer Parachute</u>	<u>Arcasonde Parachute</u>
Canopy Side Length	3.58 m	3.58 m	10.4 m
Brace Tube Radius	$18 \cdot 10^{-3}$ m	$14 \cdot 10^{-3}$ m	$37 \cdot 10^{-3}$ m
Length of Suspension	7.6 m	-	22.1 m
Canopy Weight	0.318 N	0.318 N	2.35 N
Brades Weight	0.110 N	0.08 N	0.58 N
Suspension Weight	0.012 N	-	0.13 N
Payload Weight	3.330 N	-	31.10 N
TOTAL WEIGHT	3.770 N	0.398 N	34.16 N
Operating Altitudes	270 K' - 70K' 82.4 km - 21.3 km	-	200 K' to 0 61 km to 0
Design Point	80 fps @ 150 K' 24.4 m/s @ 45.8 km	-	200 fps @ 200 K' 61 mps @ 61 km
Packaging Volume	13.75 in^3 $2.25 \times 10^{-4} \text{ m}^3$	16.1 in^3 $2.64 \times 10^{-4} \text{ m}^3$	182.5 in^3 $29.8 \times 10^{-4} \text{ m}^3$

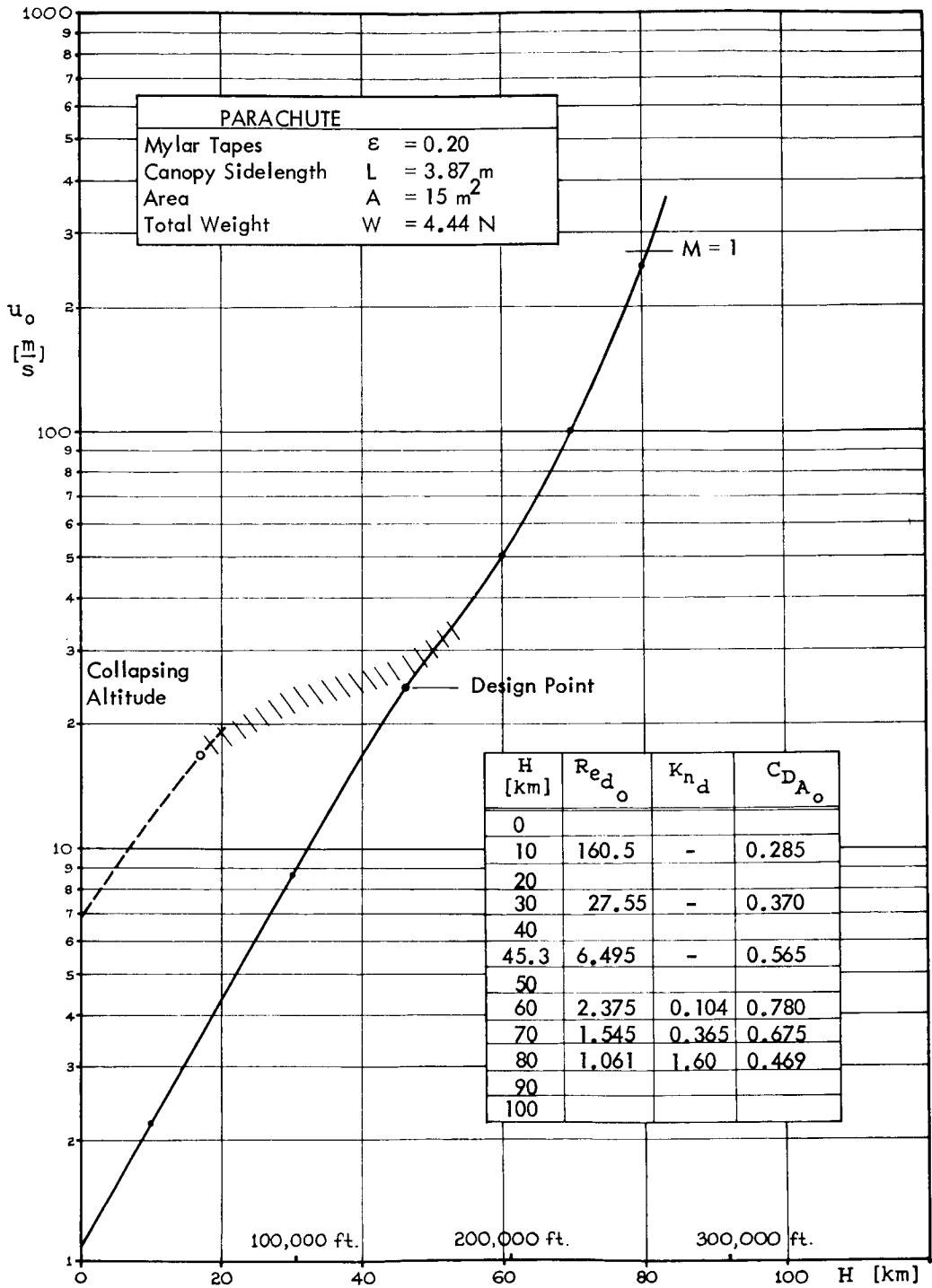


FIGURE 4.4-4 DESCENT TRAJECTORY OF THE DARTSONDE PARACHUTE

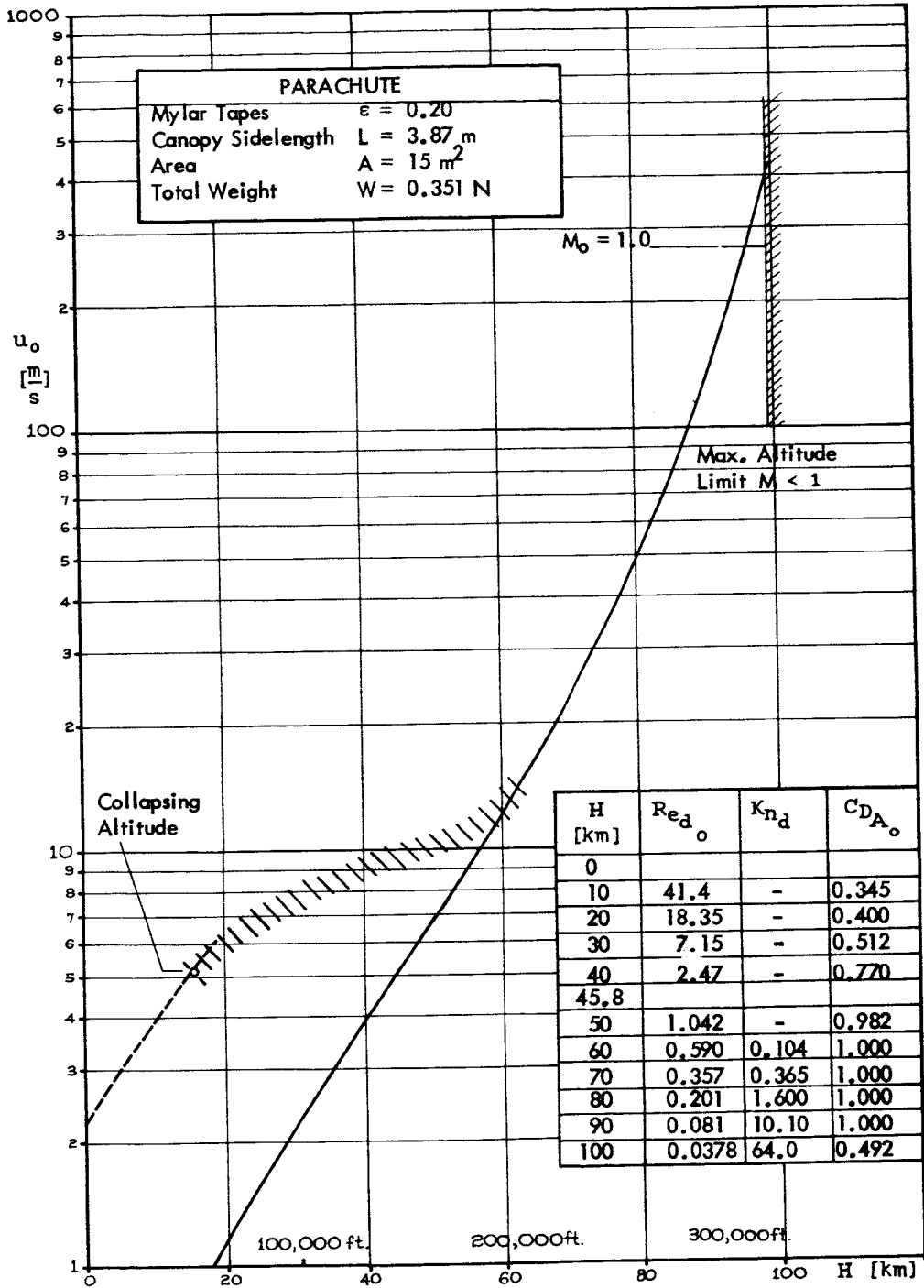


FIGURE 4.4-5 DESCENT TRAJECTORY OF THE "DARTDRIFTER" PARACHUTE

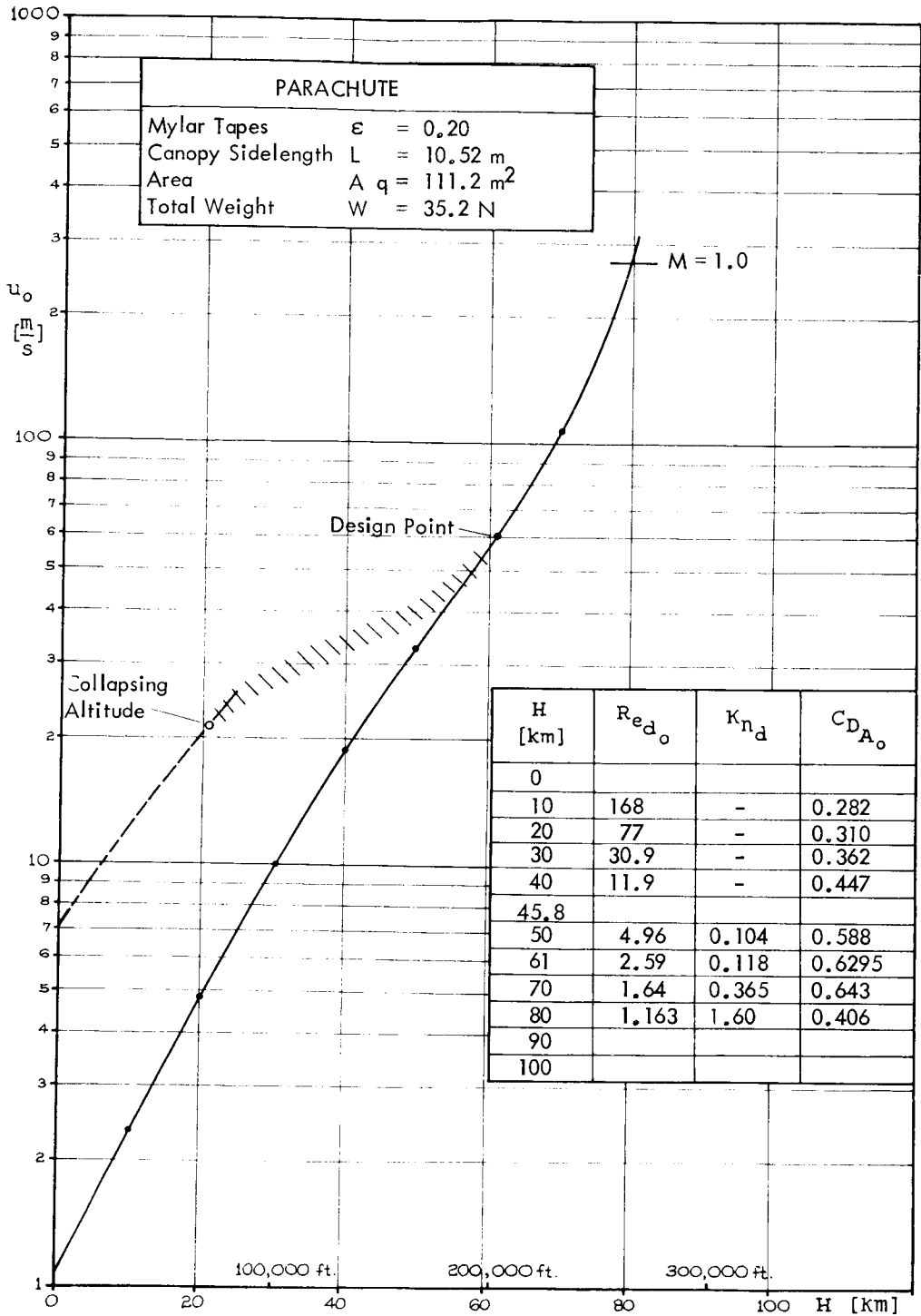


FIGURE 4.4-6 DESCENT TRAJECTORY OF THE "ARCAS" PARACHUTE

Simulated Altitudes	100-, 125-, 150-, 165- x 10 ³ ft.
Solidity Ratios, E	0.20, 0.10, 0.05
Reynolds Numbers, R _e	1.6 to 18.1
Mylar Ribbon Width	0.100 in
Mylar Ribbon Thickness	0.00025 in
Grid Spacing	1, 2, 4 in.

The canopy size was a 3-foot square, and the drag reference area was 9 square feet. However, the slack ribbon mesh balloons upward and inward between the braces during flight to reduce the projected flying area to 6.25 square feet. A summary of the test results is presented in Table 4-8. The resulting drag coefficient data is plotted against Reynolds number in Figure 4.4-7 and compared with the theoretical curves.

The experimental drag coefficients compare favorably with the theoretical values, and for the lower Reynolds numbers are considerably greater. This is most likely due to the added structural areas in the constructed models such as the bracing struts and taped edges of the canopies. The 0.20 solidity ratio design resulted in the greatest drag coefficient, since the other designs did not reach a Reynolds number low enough for them to approach the flat plate drag coefficient, $C_D = 1$. The ballistic coefficient data, $W/C_D A$, for these tests are presented along with the proposed Dardrifter theoretical values in Table 4-9 for a solidity ratio of $E = 0.20$. Although the experimental drag coefficient for $E = 0.20$ agrees extremely well with the theoretical, the ballistic coefficient is more than twice as great. This is caused by the fabricated model having a weight-to-area ratio of 2.4 times that estimated for the proposed model. No doubt the estimated weight is quite optimistic, but since the chamber model is a good deal smaller in size, it no doubt suffers a relative weight penalty.

4.4.6 Summary.

The Stokes flow ribbon mesh parachute appears to offer significant advantages over the more conventional designs, especially for high altitude (100 km) operation. The main advantage is a much greater drag per unit weight and per unit packaging volume. Other advantages are stability and

TABLE 4-8

SUMMARY OF TEST RESULTS AND MODEL WEIGHTS
FOR MODELS OF DIFFERENT SOLIDITY

<u>Drag Coefficient</u>	<u>Reynolds Number</u>	<u>Model Weight (lbs.)</u>	<u>Terminal Velocity (ft/sec)</u>	<u>Equivalent Altitude (ft)</u>
0.2 Solidity				
.370	10.41	.010715	13.65	99,100
.517	4.73	.010715	21.05	124,800
.722	2.58	.010715	28.00	145,400
.983	1.60	.011458	35.65	163,400
0.1 Solidity				
.200	11.68	.0095745	19.36	103,300
.306	5.83	.0095745	25.81	124,600
.305	5.83	.0095745	25.92	124,800
.534	2.83	.0095745	30.77	145,400
.736	1.69	.0095745	37.65	163,400
.733	1.68	.0095745	37.88	163,600
0.05 Solidity				
.0896	18.12	.0078540	23.76	99,100
.213	6.32	.0078540	28.00	124,600
.210	6.36	.0078540	28.29	124,800
.337	3.23	.0078540	35.12	145,400
.576	1.76	.0078540	38.70	163,600

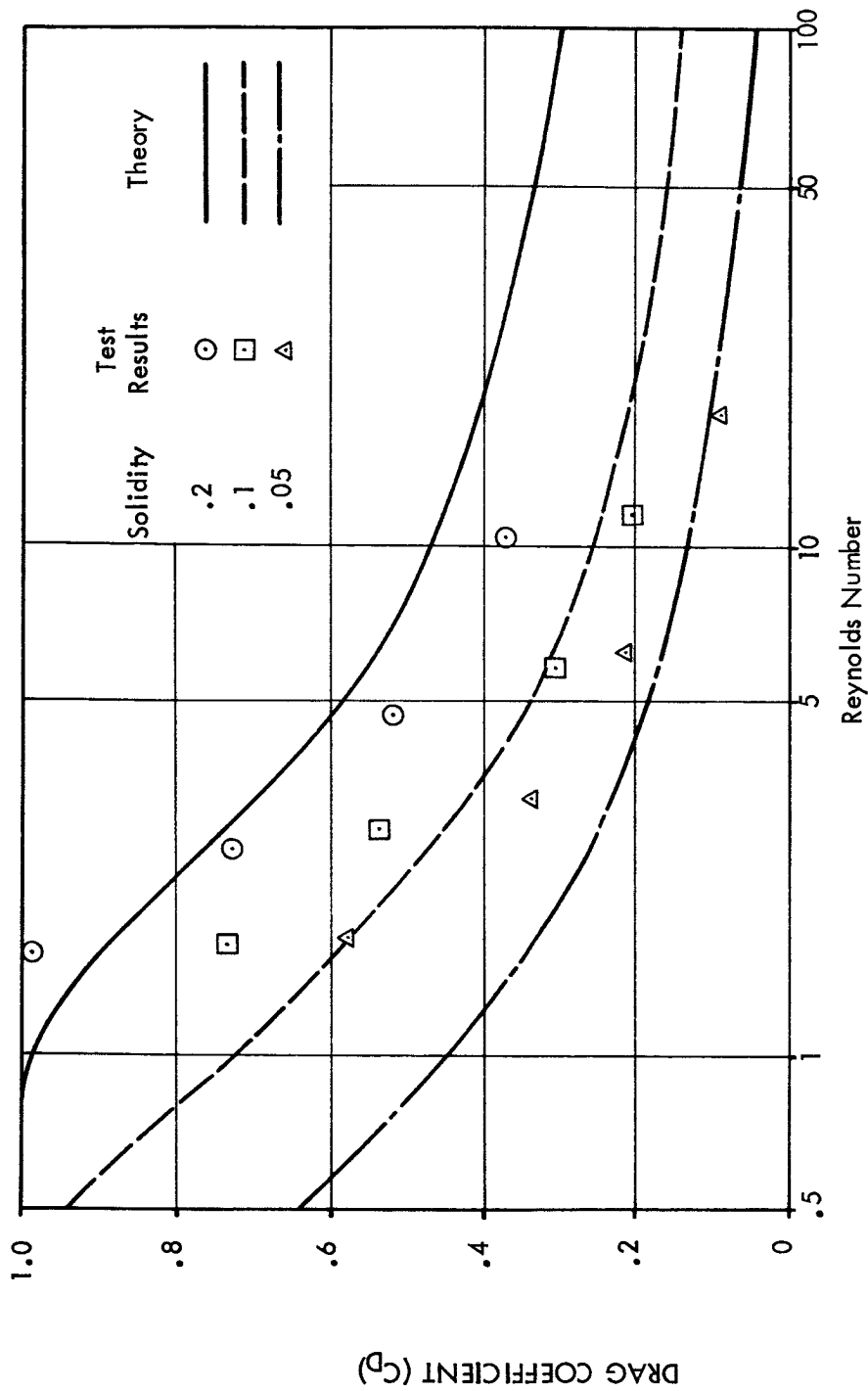


FIGURE 4.4-7 EXPERIMENTAL DRAG COEFFICIENTS FOR MODELS OF 0.2, 0.1, AND 0.05 SOLIDITY AS A FUNCTION OF REYNOLDS NUMBER COMPARED WITH THEORY

TABLE 4-9 COMPARISON OF PROPOSED DARTDRIFTER MODEL (THEORETICAL) WITH CHAMBER TEST DATA

	E	Spacing	Area	C _D (Max)	Weight	$\frac{W}{CDA}$	Altitude	W/A
Chamber Tests	0.05	4 In	9.0 ft ²	0.576	0.00785 lb	0.00152 lb/ft ²	163,000 ft	
	0.10	2	9.0	0.736	0.00957	0.00145	163,000	
	0.20	1	9.0	0.983	0.01072	0.00121	163,000	.001192
Dartdrifter	0.20	1	161.2	0.982	0.0790	0.00050	163,000	.000490
Theoretical								

a variable drag coefficient which permits more rapid descent rates at the lower altitudes than constant drag coefficient systems. Smaller ribbon widths might be utilized to obtain reduced Reynolds numbers so that flat plate drag values may be approached with the solidity ratios below 0.20. In this way even slower descents in the high altitudes may be possible.

4.5 Ram-Air Decelerators.

4.5.1 General.

The general principle of the ram-air decelerators is to capture an inflation pressure from the flowing air stream to positively and reliably inflate the structure. An inlet is employed to achieve stagnation or total pressure within the inflatable structure. This internal pressure is the sum of the ambient air pressure and the dynamic pressure and is directed normal to the inside surface of the structure. Although the external pressures tending to collapse the structure are also composed of both ambient and dynamic components, the dynamic component is generally applied obliquely over most of the external surface of the structure, hence the internal pressure forces will always be greater and inflation is assured. Two advantages of this technique are that a separate self-inflation system is not required and the ratio between internal and external pressure is more constant at the various altitudes during descent. This permits the use of a minimum thickness and weight canopy.

4.5.2 Ballute Principle.

The Goodyear Aerospace Corporation pioneered in the development of the Ballute in a series of steps which evolved as follows:

1. During experiments to decelerate, stabilize and recover payloads at high altitudes and supersonic velocities, drag was attained by towing a pressurized sphere behind the recoverable payload. Although drag was achieved, the sphere was violently unstable in the subsonic and transonic velocity regimes.
2. To stabilize the sphere an inflated torus called a burble fence was added to ensure flow separation at a constant station. The burble fence progressed from the original size of three percent of the sphere diameter to about 25 percent as is employed in some of the current Ballute designs.

3. Ram-air inflation was used instead of canned gas pressurization.
4. Isotensoid theory of pressure membrane design was employed to permit minimum thickness films to be used. This is made possible by designing the structure so that membrane stresses are nearly equal in all directions over the entire Ballute surface.

A significant advantage of the Ballute is that it has relatively small inflation inlets and takes a few seconds to inflate. Thus opening stresses for both the structure and the payload are minimized. A typical Ballute is shown in Figure 4.5-1. The major portion of the drag results from negative base pressure rather than from direct frontal loads. This is indicated in Figure 4.5-2. The center of pressure is, therefore, located quite a bit aft and stability is enhanced. Historically, the burble fence design has transitioned from a toroidal type, to a hexagonal and more recently to a square type to improve stability and fabrication simplicity. An improvement in descent rates has recently been achieved by increasing the included angle at the leading apex of the Ballute to increase pressure drag.

4.5.3 Arcasonde Ballute.

The most recent ballute configuration tested on the Arcasonde system has a 14-ft diameter with a 10-percent burble fence, as shown in Figure 4.5-3. The body of the ballute is constructed of 12 gores of 1/2-mil mylar. The seams are butt and tape construction. Six gores are aluminized to provide the necessary radar trackability. The burble fence also is made of 1/2-mil mylar and is attached by lap seams and tape. Meridian straps that transmit drag load to the instrument are flat woven nylon lacing stock attached to the center of each gore with 1/2-mil mylar tape. The inlet assembly consists of 12 beryllium-copper leaf springs mounted on a swivel plate. Specifications for the Arcasonde Ballute are shown in Table 4-10.

Unlike a parachute, the Ballute is an impermeable pressure vessel with the only opening a relatively small ram-air inlet. To prevent bursting at deployment from expansion of air trapped within the packaged unit, a perforated canister was developed for the Arcas to permit bleeding off this residual air prior to deployment. Early versions of the Arcasonde Ballute used 1/4-mil mylar but were found to be unreliable as a majority of

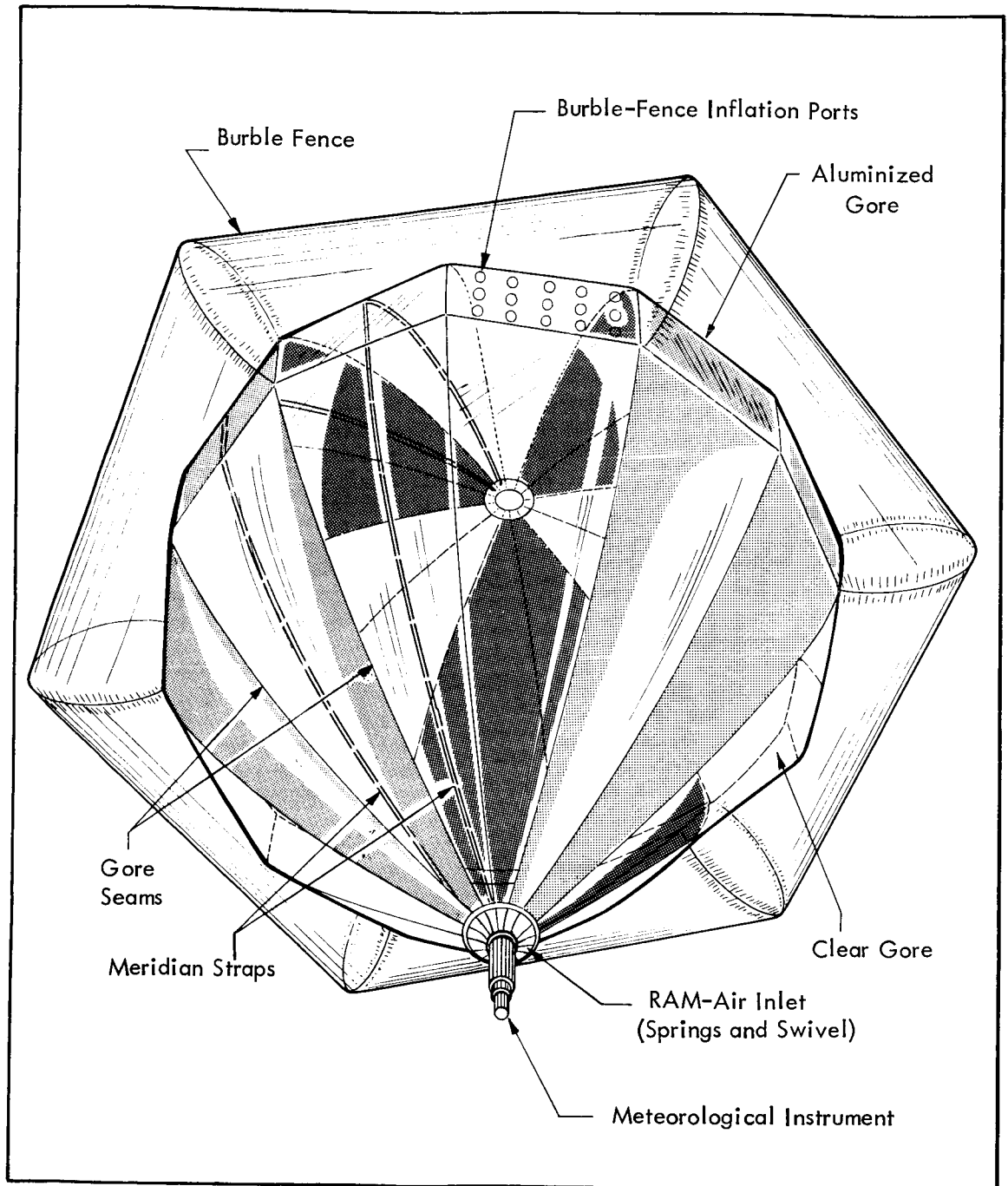


FIGURE 4.5-1 BALLUTE CONFIGURATION (TYPICAL)

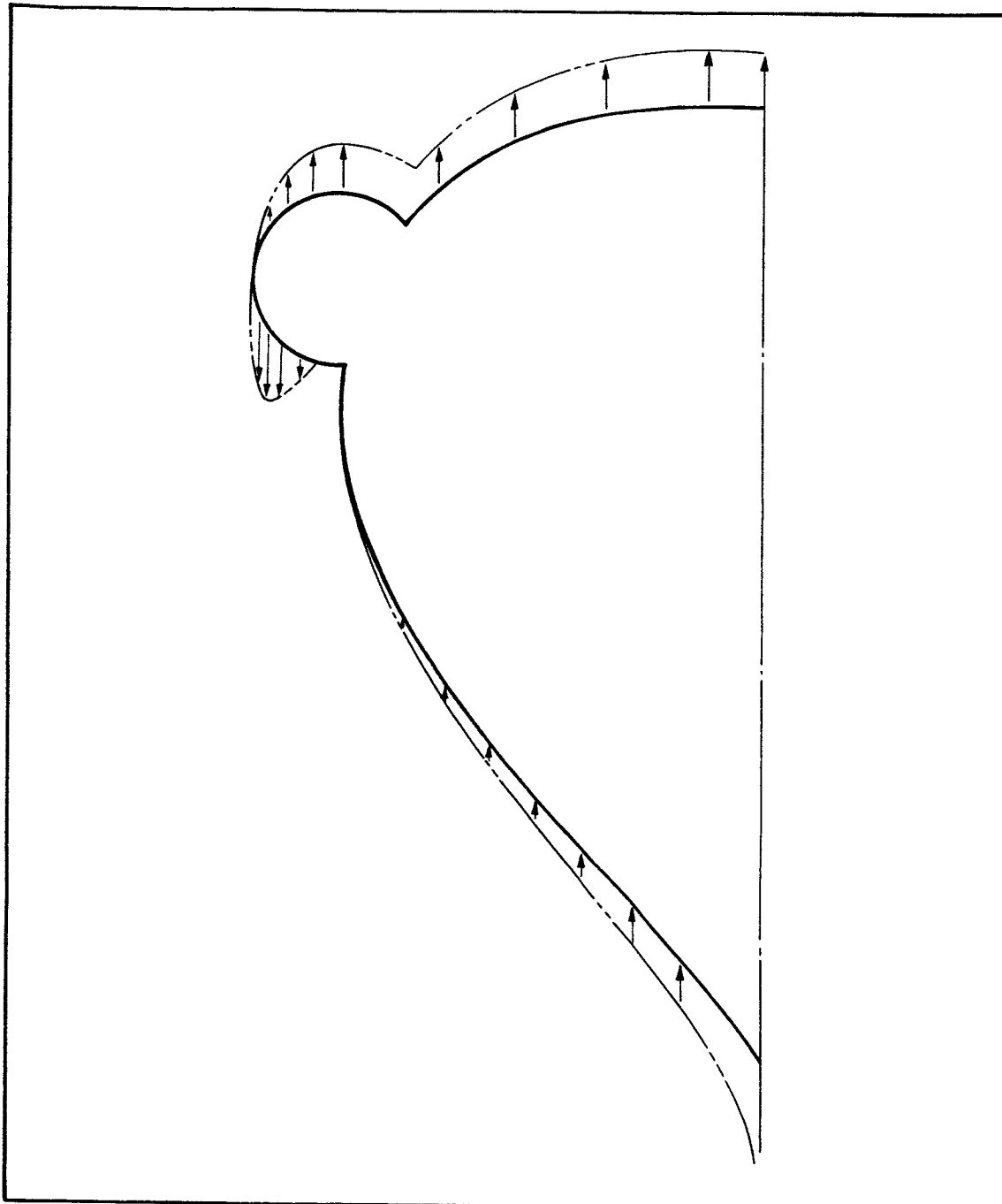


FIGURE 4.5-2 BALLUTE DRAG FORCE DISTRIBUTION

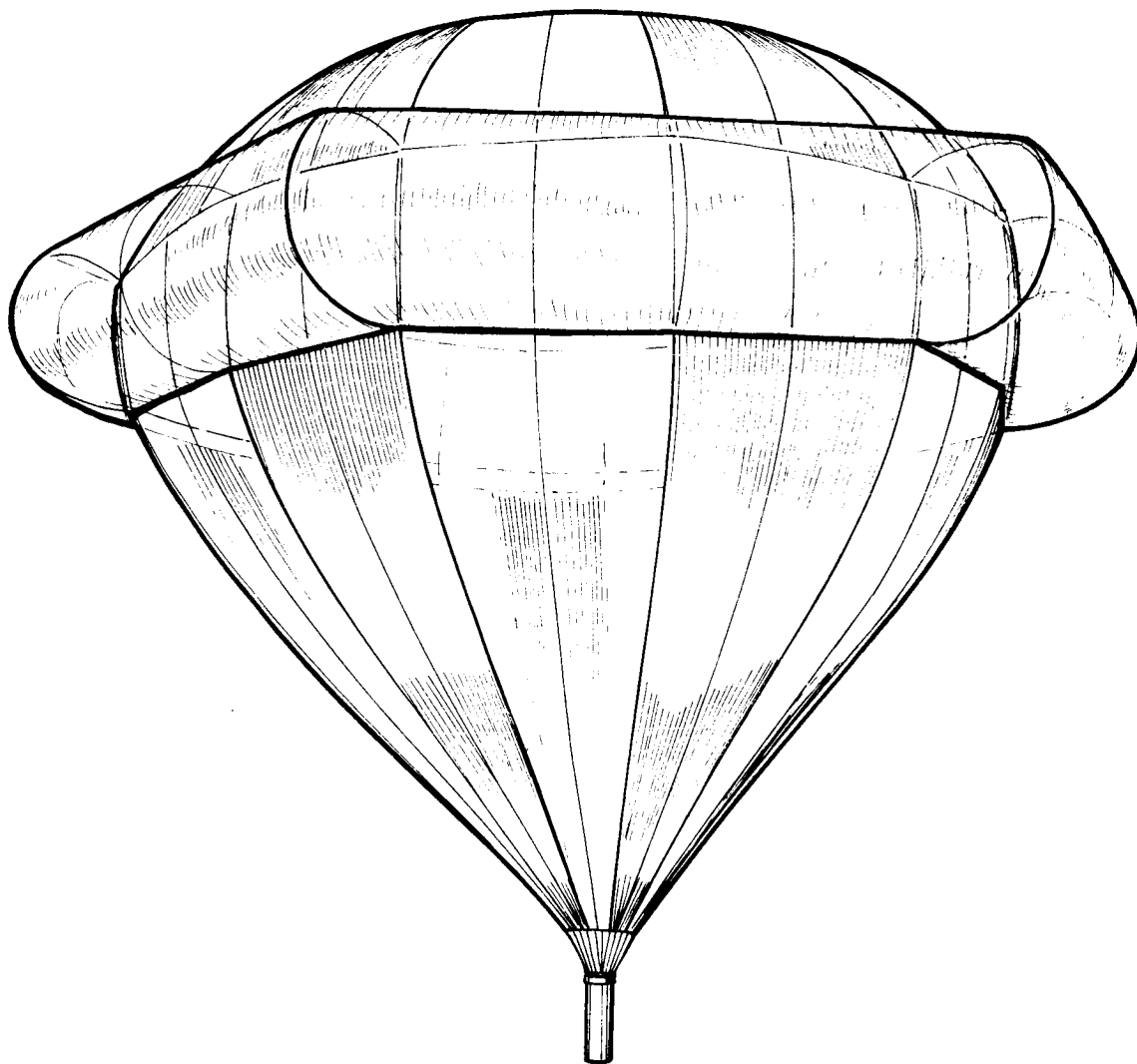


FIGURE 4.5-3 TYPICAL BALLUTE

TABLE 4-10

ARCASONDE BALLUTE SPECIFICATIONS

<u>Specification</u>	<u>Arcasonde</u>
Type BALLUTE	12 gores - 80 - degree angle
Fence Type	6 sides
Material type	Mylar-clear-alum
Material gage	0.00050 in.
Suspension system	(12) 50 in. straps
Inlet assembly	12 springs - 11.2 diameter
Swivel assembly	Mounted on needle bearings
Canister assembly	Perforated
BALLUTE weight	1.89 lb
Swivel assembly weight	0.84 lb
Total Weight	2.73 lb
BALLUTE diameter	14 ft
BALLUTE volume	878.03 cu ft
Inlet area	110 sq ft
Frontal area	169.7 sq ft
Packing density	25.7 pcf

these units failed structurally at deployment. Reliability was subsequently improved by the use of the heavier 1/2-mil mylar, but descent rates were slightly faster than the standard Arcas Gentex parachute. The current unit is 14-foot in diameter and has a ballistic coefficient of 0.060 lb/ft². However, telemetry signal dropouts have essentially been eliminated with this design, although descent rates are not satisfactorily slow.

4.5.4 Dartsonde Starute.

A small 7-foot Ballute-type decelerator has been developed for the Loki Dart system. This decelerator has been designated as the Starute by the U. S. Air Force and is essentially a scaled down version of the Arcas Ballute. However, with the lightweight Datasonde instrument as the payload, the Starute shows a significant improvement in descent velocity with a ballistic coefficient of 0.030 lb/ft². In addition the deployment reliability has been excellent, and the stability has essentially eliminated all of the telemetry signal dropouts. Figure 4.5-4 presents an illustration of the Loki Starute. A comparison of typical telemetry records from a regular parachute flight and a Loki Starute flight is presented in Figure 4.5-5. Loki Starute specifications are presented in Table 4-11. A larger 12-foot Starute is being developed under an AFCRL program to be used with the Instrumented Super Loki Dart system to obtain even slower descent rates in the higher altitudes to 75 km for improved rocketsonde wind and temperature measurements.

4.5.5 High Speed Ballutes.

Both the Arcasonde and Dartsonde Ballutes have been designed for medium to low speed subsonic descents from altitudes of about 200,000 feet down. The geometries of these designs will most likely have to be changed for higher altitude and higher speed operation to obtain optimum performance. The leading apex angle and the separation distance between payload and Ballute become important drag determining factors in the higher speed regimes. In subsonic flow the pressures and drag coefficients decrease slightly with increased separation distance. At supersonic speeds a discontinuous variation in pressure profile and drag coefficient is obtained by varying the separation distance. At close distances the Ballute causes divergence of the forebody (payload) wake, and the resulting pressures and drags are low. As the Ballute is moved aft, the forebody wake converges and pressures and drag increase. A separation distance of at least 4 forebody diameters is required to realize maximum drag in the low supersonic flow regimes. Wind tunnel measurements from Mach 1.57 to Mach 4.65 indicate that included apex angles should be

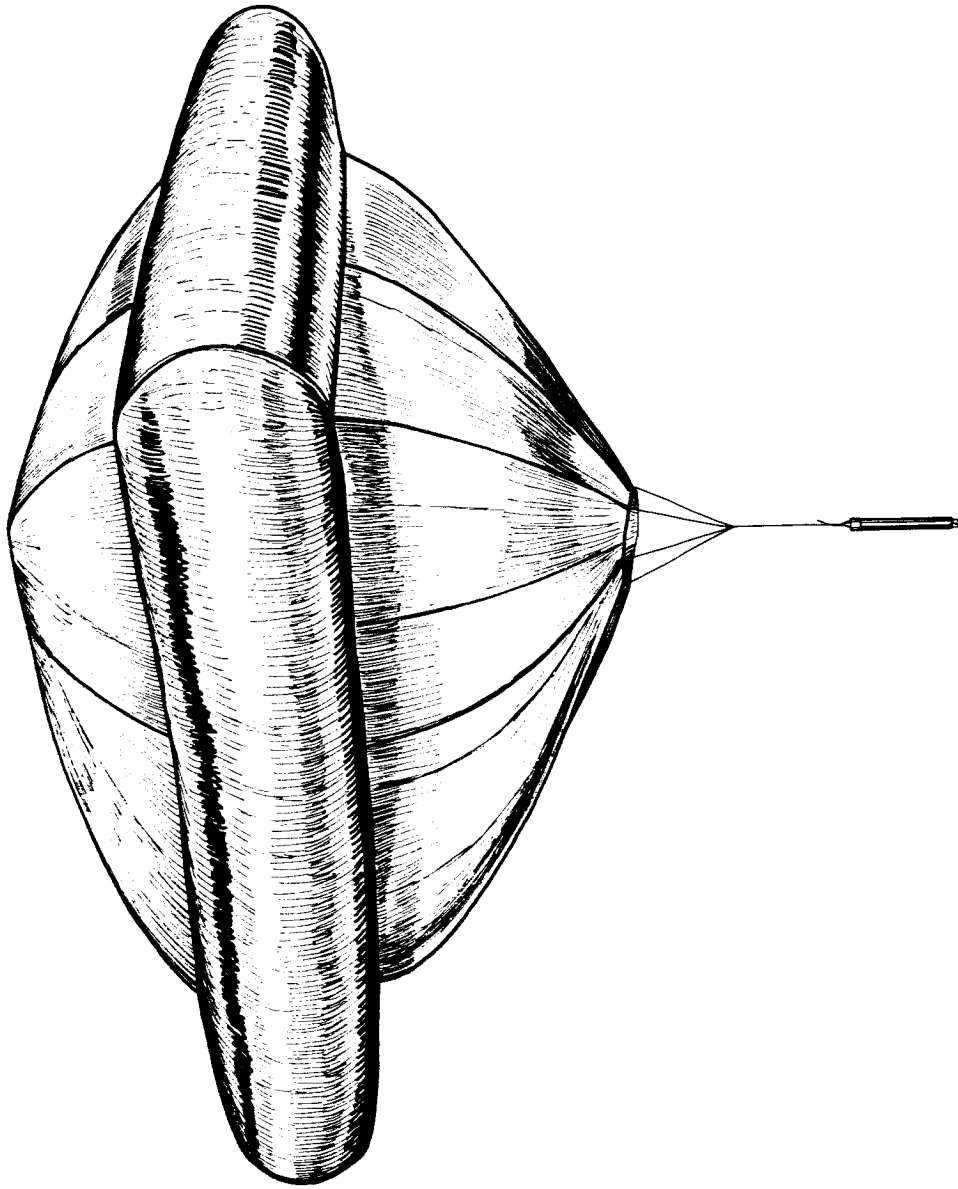
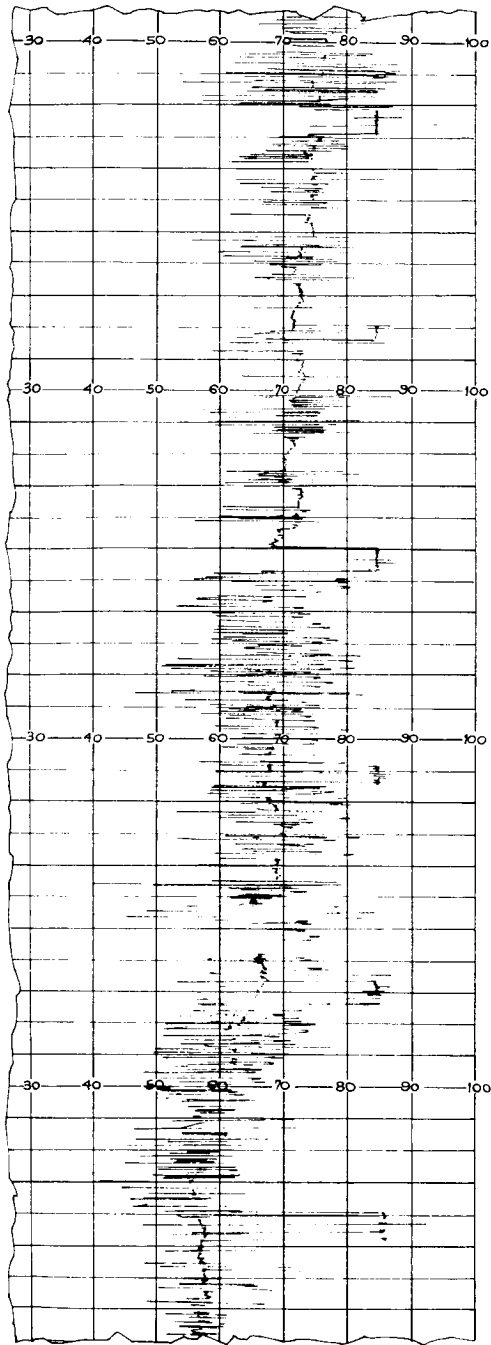


FIGURE 4.5-4 LOKI DART STARUTE CONFIGURATION SKETCH

LOKI PARACHUTE FLIGHT



LOKI STARUTE FLIGHT

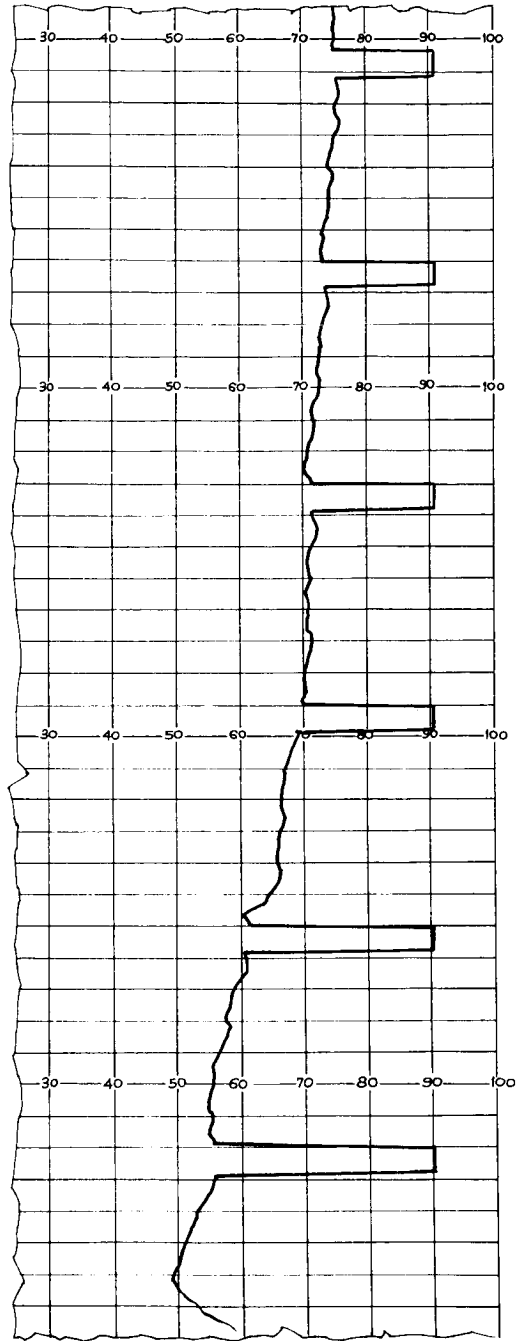


FIGURE 4.5-5 TYPICAL TELEMETRY RECORDS FROM PARACHUTE FLIGHT AND A LOKI STARUTE FLIGHT

TABLE 4-11
DARTSONDE STARUTE SPECIFICATIONS

<u>Specification</u>	<u>Dartsonde</u>
Type BALLUTE	8 gore
Fence type	4 sides
Material type	Mylar-clear-alum
Material gage	0.00025 in
BALLUTE weight	0.316 lbs
Swivel assembly weight	0.026 lbs
Total Weight	0.342 lbs
BALLUTE diameter	7 ft
Flying area	49 sq ft

80° to 90° to achieve maximum drag. The Ballute may be useful in meteorological rocket applications to altitudes significantly above 200,000 feet, but descent velocities will most likely be in the transonic and supersonic regimes at altitudes approaching 300,000 feet.

4.5.6 Biconical Decelerator.

The Naval Ordnance Laboratories are currently developing a ram-air inflated biconical decelerator for high altitude meteorological applications. This decelerator is in the form of two inverted truncated cones of differing apex angles as shown in Figure 4.5-6. This design increases the base area and hence the base drag for a given amount of canopy material as compared with the Ballute. Since in the subsonic flow regime a major portion of the Ballute drag is due to base pressure, the biconical geometry capitalizes on this fact and should be more efficient than the Ballute. The basic shape should be inherently stable, and the flow separation should be tripped consistently at the top edge.

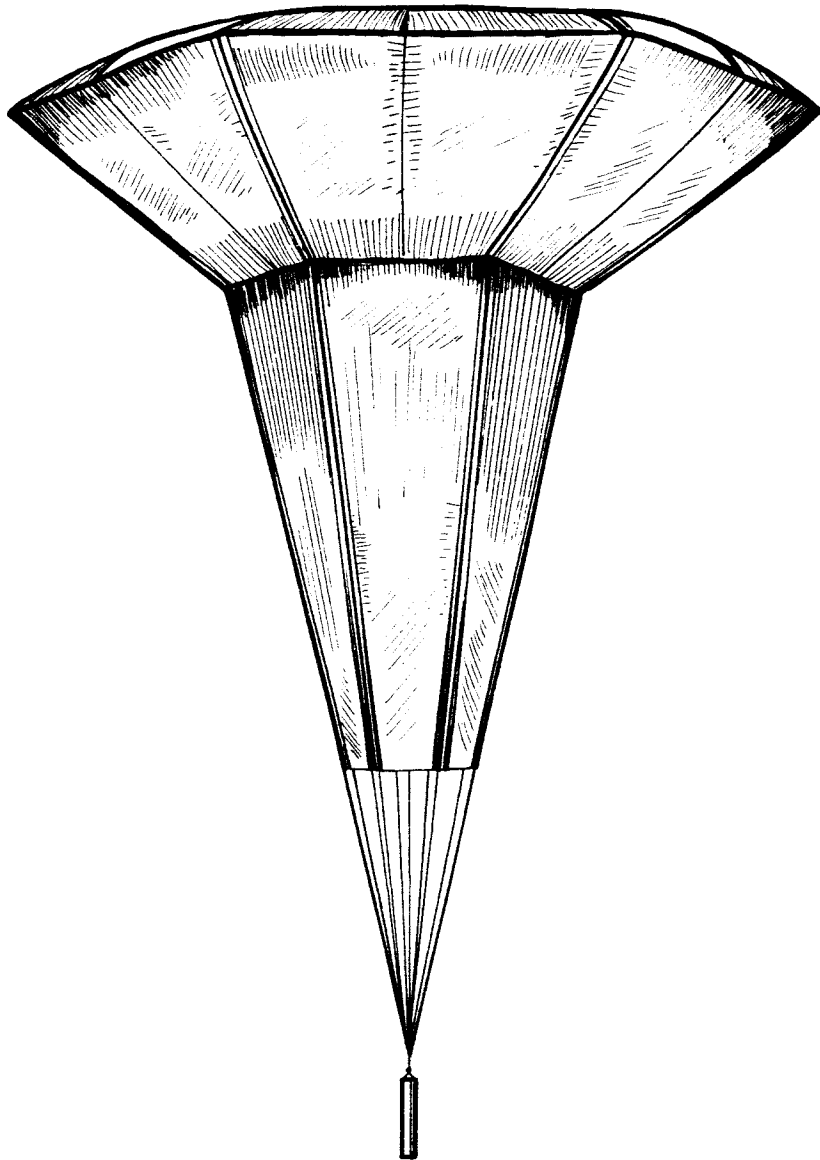


FIGURE 4.5-6 N.O.L. BICONICAL DECELERATOR

4.6 Summary.

A comparison of the drag efficiency of the various decelerators for which flight test data are available may be made by comparing the ballistic coefficients of the decelerators alone without payloads as follows:

<u>Decelerator</u>	<u>Ballistic Coefficient (lb/ft²)</u>
Arcas Gentex Parachute	0.024
Loki 7.6' Irvin Parachute	0.013
NOL 6' Square Parachute	0.008
Arcas D-G-B Parachute	0.016
Arcas Cross Patch Parachute	0.013
Dartsonde Starute	0.009
Stokes Flow Ribbon Mesh Parachute (Theoretical)	0.001

It appears that the only decelerator which has a chance of maintaining subsonic descent velocities to altitudes as high as 100 km is the Stokes flow ribbon mesh parachute. The ram-air inflated decelerators may prove useful to the high altitudes if transonic and supersonic velocities are permissible with the given sensor system.

5.

TELEMETRY AND TRACKING

5.1 General.

Telemetry and tracking have not proven to be a problem for the 60 km rocketsonde flights since the equipment in current use at almost all of the missile ranges has been sufficiently reliable and accurate for this application. The tracking accuracy requirements for wind and altitude determination and the telemetry accuracy requirements for the temperature data are not particularly stringent. The rocketsonde decelerators offer targets of high radar cross-section and are easy to track - once acquired. Chaff clouds offer large radar targets and are simple to acquire and track for at least 50,000 feet of descent before they disperse into clusters and the radar starts searching for the high spots within the cloud.

The only significant problem experienced with data acquisition from rocketsonde flights has been an occasional late acquisition of either radar track of the decelerator or telemetry reception of the temperature data. The dart vehicles offer a relatively small radar target going into apogee, and radar with less capability than the AN/FPS-16 will probably lose track until the payload deploys. Although the radar signal returns from the deployed decelerator is very good, acquisition may be a problem, due to the narrow beam width of tracking radars, unless an uptrack is maintained. With experienced operators this has not been a problem, and generally only a thousand or so feet of data are lost due to later radar acquisition. The 1680 MHz telemetry signal is generally weaker during the uptrack because of antenna pattern nulls toward the rear of the vehicle. Sometimes the signal is lost during uptrack, and a late acquisition of the temperature data after deployment occurs. Most of the experienced operators acquire the GMD track within a few seconds after deployment. This generally does not cause a loss of temperature data since the thermistor is still in the process of cooling to atmospheric temperature during this time period.

For the more specialized high altitude experiments data acquisition becomes a more significant problem. Passive falling sphere experiments require precision in the radar data - the equivalent of the FPS-16 quality. In fact,

if a more precise radar is used, the data accuracy would be better and the altitude of useful data could be extended upward. Also, without a radar uptrack of the vehicle, acquisition of the sphere could be a problem. Accelerometer falling spheres require rather precise telemetry accuracy, and so far have used IRIG channels. The pitot probe requires rather precise telemetry accuracy and tracking data. The vehicle velocity enters into the data reduction equations as does the telemetered ram pressure information. However, the Denpro system discussed in Section 3.5 used GMD-2 telemetry and tracking data with reasonably good results. In this application, telemetry modulation rates were increased to 1,000 pps and the GMD-2 velocity and altitude data compared favorably with FPS-16 radar data. The grenade experiments require quite specialized ground-base data acquisition equipment as described in Section 3.6. Many of the other high-altitude experiments require a greater frequency response in the telemetry modulation and the standard 20 to 200 rps AM of the GMD systems is not adequate. In these cases FM may be used with GMD system or pulse rates may be increased.

5.2 Radar.

5.2.1 General.

There are a number of radars which are currently in use at the various missile ranges for various specialized purposes such as surveillance and range safety, acquisition, beacon tracking, skin tracking and deep space probe tracking. These radars represent various stages in the state-of-the-art in radar development and operate in various frequency bands as shown below:

RADAR FREQUENCY BANDS

Band	Center Frequency (mHz)
L	1,300
S	2,700
C	5,500
X	9,000

The L-band systems are generally used for surveillance and have not been found adequate to track meteorological rockets. The X-, S- and C-band radars have been the most useful for meteorological rocket applications. The X-band M-33 modified (by WSMR) is a mobile unit which has been used to track meteorological payloads at remote sites, but is incapable of uptracking the vehicles. The S-band SCR-584 Mod 2 radar has been used extensively and is adequate to skin track the Arcas to about 130,000 ft but cannot track the Loki Dart. This radar is certainly adequate to track rocketsonde payloads. The C-band FPS-16 is the most used and most desirable of the commonly available radars. This radar is capable of tracking the Loki Dart thru apogee and the precision is good enough to reduce passive falling sphere density data to 2% accuracy at 90 km. The FPS-16 is also capable of tracking a 2-inch diameter 50-inch long dart (Viper Dart System) to an altitude of about 430,000 feet. More accurate and powerful radars than the FPS-16 exist, but they are located at a limited number of sites and are not generally available for meteorological

soundings. Doppler radars have been found useful in the development of meteorological rocket vehicles, but the range limitations of the common sets restrict their use from tracking the payloads.

5.2.2 Radar Descriptions.

A summary of the technical characteristics of typical radar systems is presented as follows:

5.2.2.1 Radar Set AN/SPS-12.

Radar Set AN/SPS-12 is a medium-range surveillance radar equipment designed to detect aircraft and surface vessels. Target range and bearing data are obtained for presentation on associated ppi units. Radar Set AN/SPS-12 transmits and receives pulses of r-f energy in the frequency range of 1250 to 1350 mc (L band).

Radar Set AN/SPS-12 requires three-phase, 60-cycle, 440 volt input power at approximately 6000 watts. The circuits in all units (except the radar modulator high-voltage-supply circuit) operate from single-phase, 60-cycle, 115-volt power supplied by the power distribution transformer, which is connected across two lines of the three-phase 440-volt input. The technical characteristics of Radar Set AN/SPS-12 are given in Table 5-1.

5.2.2.2 Radar Sets AN/MPS-19.

Radar Sets AN/MPS-19 are modified, mobile units used for acquisition and weather observation. Table 5-2 lists the characteristics of the unit used for acquisition and Figure 5.2-1 is a block diagram of the AN/MPS-19 equipment. The AN/MPS-19 provides data outputs in the following forms:

1. Synchro voltages representing slant range and azimuth and elevation angles.
2. Potentiometer voltages representing slant range and sine and cosine functions of azimuth and elevation angles.
3. Precision digital data representing slant range and azimuth and elevation angles.

Transmitting System	
Frequency	1250 to 1350 mc
Transmitter	Tunable magnetron
Peak r-f power	500 kw
Pulse rate	300 or 600 pps variable $\pm 5\%$
Pulse length	4 μ sec at 300 pps, 1 μ sec at 600 pps
Modulator type	Hydrogen-filled thyratron
R-f lines	Waveguide (3-1/4 by 6-1/2 inches)
Antenna System	
Type	Cosecant-squared reflector
Beam width	3° horizontal; 30° vertical
Polarization	Vertical
Azimuth slew rate	2-1/2 to 15 rpm, or manual
Range Data	
Maximum range	200 miles
Minimum range	400 yards
Range indicators	4, 20, 80 miles at $\pm 0.5\%$, 200
Receiving System	
Antenna coupling	TR & atr cavities, crystal mixer, etc
I-f frequency	30 mc
I-f bandwidth	0.5 mc at 300 pps, 2 mc at 600 pps
Local osc freq control	Afc
Receiver mds	-100 dbm
Sweep ranges	400 to 8000 yards, 1 to 20 miles, 4 to 80 miles, and 4 to 200 miles
Data Readout	
One A scope and up to six ppi	
Sweep expander	1000 yards per inch up to 80-mile range

TABLE 5-1 Radar Set AN/SPS-12, Technical Characteristics

Transmitting System Frequency range Peak power Average power Output power tube Pulse width Prf Receiving System I-f frequency Bandwidth Dynamic range Noise figure Sensitivity Antenna System Diameter Beam width R-f transmission line Power capability	2700 to 2900 mc 500 kw 164 w (single pulse), 492 w (triple pulse) Magnetron 0.8 μ sec 300 to 2000 cps; beacon 410 cps 30 mc 3 mc 80 db 4 db 108 db 8 ft (parabolic) 3° (half power) Rectangular waveguide 500 kw
Antenna System (Continued) Vswr Line loss, receiving Azimuth coverage Elevation coverage Ranging System Maximum range Minimum range Maximum tracking rate Maximum slew rate System Facts Accuracy System Power Load	2 db 3 db 360° -15° to 89.5° 360,000 yards 500-1000 yards 28,000 yards/second 25,000 yards/second Azimuth, 1 mil Elevation, 1 mil 3 phase, 110 volt, 12 kw (util) 3 phase, 208 volt, 10 kw (oper)

TABLE 5-2 RADAR SET AN/MPS-19, TECHNICAL CHARACTERISTICS

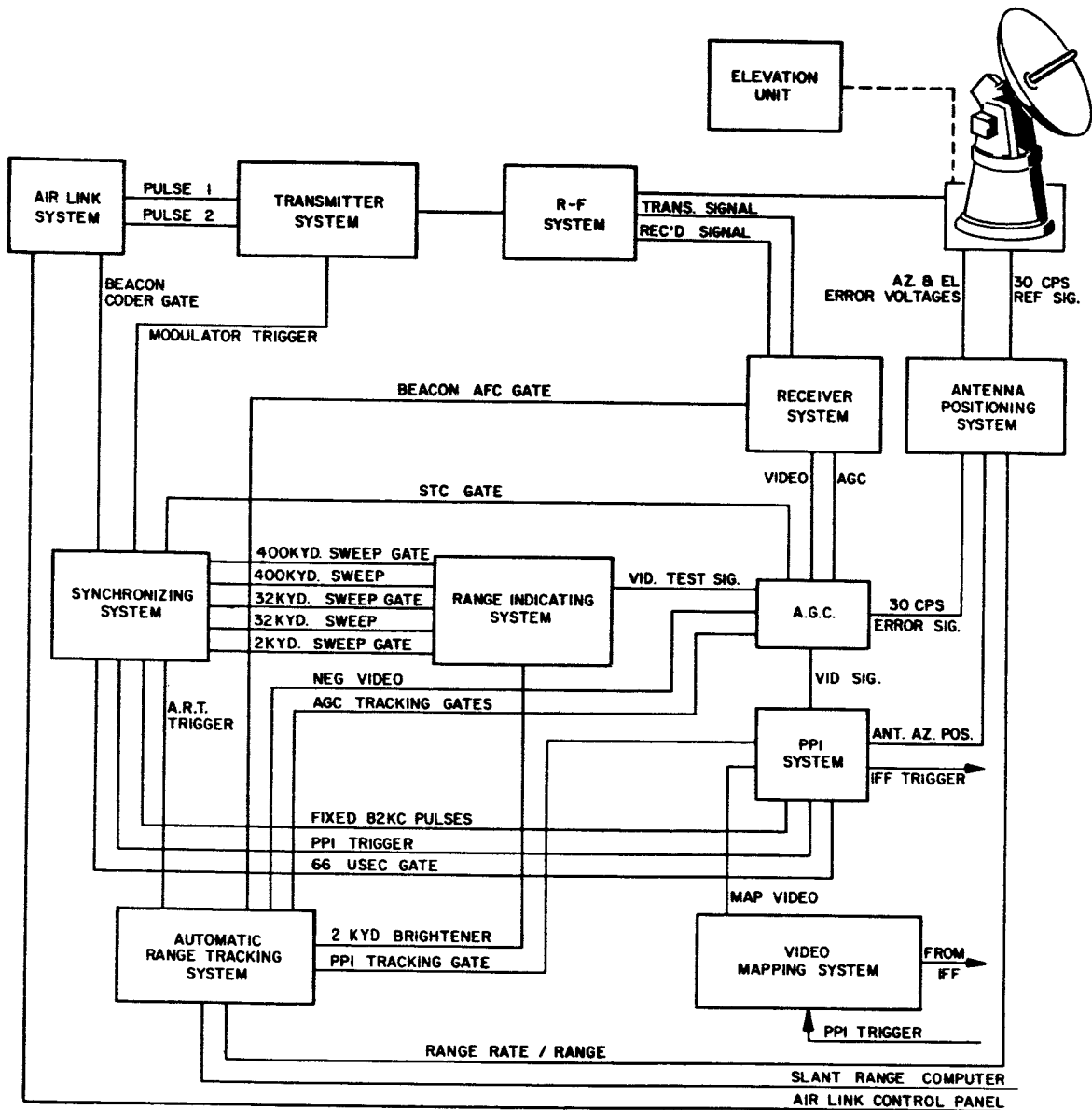


FIGURE 5.2-1 Radar Set AN/MPS-19, Block Diagram

5.2.2.3 Mod (II) Radar.

The Mod II Radar, is an extensively modified and rehabilitated SCR-584 Radar. Mod II is an automatic angle and range tracking radar designed to provide the following:

1. Synchro voltages representing slant range and azimuth and elevation angles.
2. Potentiometer voltages representing slant range and sine and cosine functions of azimuth and elevation angles.
3. Precision digital data representing slant range and azimuth and elevation angles.

Improvements over the SCR-584 radar include: dual local oscillators for skin and beacon tracking, A-scope range presentation, intermediate servo system for smoothing purposes, tunable S-band magnetron, output power attenuation, traveling wave tube r-f amplification in the receiving system, multipulse and coding capability, nutating antenna feed to allow vertical or horizontal polarization, waveguide transmission line, and pulse repetition frequency selection.

In general, the Mod II provides recorded metric data for range users, real-time position data for range safety or guidance, and target acquisition data for other ground instrumentation equipment.

Table 5-3 list the technical characteristics of the system.

5.2.2.4 Radar Set AN/FPS-16.

The AN/FPS-16, is a C-band, high precision, monopulse tracking radar. The accuracy of the AN/FPS-16 is such that the position data obtained from point-source targets has azimuth and elevation angular errors of less than 0.1 mil rms and range errors of less than 5 yards rms with a signal-to-noise ratio of 20 db or greater. The AN/FPS-16 provides data outputs in the following forms:

TABLE 5-3 MOD II Radar, Technical Characteristics

Transmitting System	
Frequency range	2650 - 2850 mc
Transmitter	Tunable magnetron
Peak r-f power	250 kw
Average power	0.5 kw
Pulse width	0.75 μ sec
Prf	205, 341, 366, 410, 467, 569, 682, 732, 852, 1024, 1280, and 1707 cps
Pulse shape	Square
Modulator type	High vacuum
Receiving System	
I-f frequency	30 mc
Sensitivity	-102 dbm
Noise figure	7.5 db
Bandwidth	2 mc
Type	Superheterodyne
Antenna coupling	R-f amplifier into single-ended crystal
Antenna System	
Type	10-foot parabolic
Focal length	35.6 inches
Beam crossover	80% or 50%
Gain	37 db
Beam width	2.5°
Drive	2/4 hp in each axis
Side lobe location	1st, 4.12°; 2nd, 6.22°

TABLE 5-3 MOD II Radar, Technical Characteristics (Continued)

Antenna System (Continued)	
R-f transmission line	Rectangular waveguide with transition to rigid 7/8-inch coaxial at azimuth rotary joint
Type of feed	Nutating
Type of scan	Conical
Scan frequency	30 cps
Polarization	Vertical-circular-horizontal
Ranging System	
Maximum range	768,000 yards, beacon track
Minimum range	500 yards
Maximum tracking rate	8000 yards/second (automatic)
Maximum slew rate	20,000 yards/second (manual)
Master oscillator frequency	82 kc
Range tracking	Manual, rate aided, and automatic
Skin track range	65 statute miles, 1-square-meter target
Tracking gates	12, 0.5 mil/second
System Facts	
Synchro inputs	Azimuth, 1:1; elevation, 1:1
Tracking rates	20°/second, azimuth; 8°/second, elevation
Slewing range	20°/second, azimuth; 20°/second, elevation
Range accuracy	20,000 yards/second, range
Range indicators	±10 yards
Other presentation	3 A-scopes; 2000 yards, 32,000 yards, full-tracked ranges
System Data Readout	
Timing Box	Ppi
Cursor scale camera	One 35-mm camera photographs the following: range timing, camera pulses from radar cameras, sync pulses from programmer, and signal tone from programmer
	Azimuth and elevation cursor scales on antenna mount photographed with 35-mm Mitchell camera similar to that on MPS-19; resolution ±0.2 mil

TABLE 5-3 MOD II Radar, Technical Characteristics (Continued)

System Data Readout (Continued)	
Scope camera	2000-yard J-scope photographed with 35-mm Mitchell camera
Boresight camera	40-inch focal length (35-mm Mitchell camera)
Digital readout	Azimuth, elevation, range, and timing recorded on 1/2-inch magnetic tape
System Power	
Load	3 phase, 110 volt, 12 kw
System Data Output	
Azimuth, potentiometer type	Sine-cosine
Number of turns	1
Wiper resistance	10 kilohms
Brush load required	0.25 m
Resistance/quadrant	15 kilohms
Elevation, potentiometer type	Sine-cosine
Number of turns	1
Wiper resistance	10 kilohms
Brush load required	0.25 m
Resistance/quadrant	15 kilohms
Range, potentiometer	192, 000 and 384, 000 yards
Number of turns	10
Linearity	0.02%
Brush load	0.25 kilohm
Resistance	20 kilohms
Wiper resistance	10 kilohms

1. Synchro voltages representing slant range and azimuth and elevation angles.
2. Potentiometer voltages representing slant range and sine and cosine functions of azimuth and elevation angles.
3. Precision digital data representing slant range and azimuth and elevation angles.

The AN/FPS-16 radar also provides real-time, present-position analog data for range safety use.

Table 5-4 lists the technical characteristics of the system. All random errors listed in the table are referenced to beacon operations. In skin tracking, increased angular dispersion will result from either target glint, when the angular physical dimensions of the target exceed the resolutions of the radar, or from thermal noise at small signal-to-noise ratios. According to the beam width of the radar, listed angle tracking performance is expected to be maintained down to elevation angles of approximately 0.5° . At smaller elevation angles, tracking errors of increasing magnitude will occur and can be corrected only by means of boresight camera data.

5.2.2.5 Radar Set AN/FPQ-11.

These radars, based on the MPS-19 design, have been reconfigured to improve and extend tracking capability by the addition of 14 ft. diameter parabolic antennas; precision torque drive pedestals; new receiving systems; wide range gate; a selectable 0.25 us pulse; auxiliary track system and digital data encoders and by complete replacement of the antenna positioning system.

The technical characteristics are presented in Table 5-5.

5.2.2.6 AN/MPS 504 Surveillance Radar.

This radar provides continuous surveillance to a maximum ground range of 200,000 yards. It is used for range safety and as an aid in recovery missions. The technical characteristics are presented in Table 5-6.

TABLE 5-4 Radar Set AN/FPS-16, Technical Characteristics

Transmitting System	
Frequency range	High power: 5480 \pm 30 mc Low power: 5480 to 5825 mc
Peak power	1 megw (fixed)
Average power	1.7 kw
Output power tube	Magnetron
Pulse widths	0.25, 0.5, and 1 μ sec
Prf	142, 341, 394, 366, 467, 569, 682, 732, 853, 1024, 1280, and 1364 cps
Frequency accuracy	\pm 1.5 mc
Pulse shape	Square
Modulator	High-vacuum type
Normal operating power	250 to 300 kw with tunable magnetron; 750 to 900 kw with fixed magnetron
Receiving System	
Type	Superheterodyne

TABLE 5-4 Radar Set AN/FPS-16, Technical Characteristics (Continued)

Receiving System (Continued)	
I-f frequency	30 mc
Sensitivity	-99 dbm
Noise figure	11 db
Bandwidth	1.8 and 8 mc (narrow-wide)
Dynamic range	-93 db with stc
I-f noise figure	6 db
Ranging System	
Maximum range	1, 000, 000 yards
Minimum range	500 yards
Maximum tracking rate	10, 000 yards/second
Maximum slew rate	40, 000 yards/second
Bandwidth (maximum)	10 cps
Acceleration	4000 yards/second ²
Master oscillator frequency	82 kc
Oscillator stability	1 in 10 ⁶
Range accuracy	±5 yards
Tracking gates	0.5, 1, 1.5 μsec
Target designation	Manual or automatic modes
Range tracking	Manual, rate aided, or automatic
Tracking noise	Angle std deviation, 0.1 mil
Dispersion	Range std deviation, 1.5 yards
Antenna System	
Type	12-foot parabolic reflector
Feed	4-horn monopulse
Focal length	48.4 inches
Beam crossover	0 db
Gain	43 db
Beam width	1.2°, r-f axis to 1/2 power point, horizontal and vertical
Polarization	Vertical, horizontal, circular
Tracking point	Center of main lobe (no crossover point)
Drive	Azimuth: two 2-hp motors Elevation: one 2-hp motor
Antenna temperature	40°K above 50° elevation (dark sky)
Side lobe location	1.72° (1st) 2.62° (2nd)
Capture area	7.88 square meters

TABLE 5-4 Radar Set AN/FPS-16, Technical Characteristics (Continued)

Antenna System (Continued)	
Type of scan	Monopulse
R-f transmission line	Rectangular waveguide
Line loss receiving	1.3 db
Line loss transmitting	2.3 db
System Facts	
Azimuth coverage	360°
Elevation coverage	-10° to 190° (tracking -10° to 85°)
Range accuracy	±5 yards
Serial readout rate	100 pps maximum
Granularity	±1 yard
Pulse duration	0.2 μsec minimum 1.0 μsec maximum
Rise time	0.1 μsec
Tracking rates	Azimuth: 42°/second Elevation: 22.5°/second Range: 10,000 yards/second
Slewing rates	Azimuth: 45°/second Elevation: 22.5°/second
Accelerations	Azimuth: 45°/second Elevation: 24°/second Range: 40,000 yards/second
Bearing accuracy	Azimuth: 0.1 mil Elevation: 0.1 mil
Range on 1 square meter	272,000 yards
Random noise errors in output data	Slant range: σ_R 1.5 yards Azimuth and elevation: σ_A, σ_E 0.1 mil
Systematic errors	Zero setting errors: ±0.7 to 2.0 yards Drift errors due to external beacon delay variations estimated to be less than 100 feet Total mechanical errors: 0.04 mil rms
System Data Readout	
Data box	35-mm Mitchell camera for the following: azimuth and elevation synchro dials, timing lights, sync pulses, and signal tone
Range scope	35-mm Mitchell camera photographs

TABLE 5-4 Radar Set AN/FPS-16, Technical Characteristics (Continued)

<p>System Data Readout (Continued) Range scope (Continued)</p> <p>Nixie readout</p> <p>Pedestal cursor dial</p> <p>Ungated video</p> <p>Consolidated recorder</p> <p>Sanborn recorder</p> <p>Magnetic tape system</p> <p>System Power Load</p>	<p>2000-yard segment of range and 72,000 yards synchro</p> <p>35-mm pulse-operated flight research camera: azimuth, elevation, and range; timing; model number; and radar mode of operation</p> <p>Azimuth: 35-mm flight research camera Elevation: 35-mm flight research camera</p> <p>Boresight: 80-inch EFL lens with 35-mm research camera</p> <p>Tektronix scope, 2000-yard segment of range, 35-mm flight research camera</p> <p>Agc, WWV, range timing, radar timing, radar camera shutter pulse, CHU</p> <p>Four channels; can record any four of the following: agc, 2000-yard range synchro output, timing, sync pulse, WWV, CHU, azimuth and elevation error, and range error signals</p> <p>Records binary output of range, azimuth, timing, azimuth error, and elevation error</p> <p>3 phase, 120/208 volt, 100 kva</p>
--	--

Table 5-5 Radar Set AN/FPQ-11, Technical Characteristics

Transmitting System

Frequency	2,700 - 2,900 MHz tunable
Peak Power	500 kW minimum
Normal operating power	550 - 850 kW
Pulse repetition frequency	Both Radar & Beacon 410, 512, 585 pps
Pulse width	0.25 μ s, 0.8 μ s, selectable
Pulse shape	Square
Coding capability	1 to 3 pulses
Modulator	Soft tube
RF lines	Rectangular waveguide
Line loss	Less than 1 dB

Antenna System

Type	Parabolic 14 ft diameter
Drive	dc torque motors
Feed	Conical scan, (30 Hz)
Gain	39 dB
Polarization	Vertical or horizontal, or RH circular or LH circular (remotely selectable)
Beam width	1.8° axis to half power points
Tracking point	50% or 80% (manually selected prior to test)
Sidelobes	At least 20 dB down from Main lobe
Azimuth coverage	Plus or minus 360°
Elevation coverage	-1.5 to 181.5°
Angular tracking accuracy	0.15 mils
Slew rates	Greater than 40°/sec in both axis

Range System

Maximum range	1,999,500 yards, Verlor system
Minimum range	300 yards in narrow pulse
Skin Track range	50 nmi on 6" sphere
Range accuracy	0.01% (same as the MPS-19 accuracy)
Master oscillator frequency	81,946,427 kHz
Oscillator stability	2.5 x 10 ³
Tracking gate	0.3 μ s
Maximum range track rate	16,000 yd/s

Table 5-5 Radar Set AN/FPQ-11, Technical Characteristics (continued)

Range System (continued)

Range slew rate	40,000 yd/s/s
Range tracking	Manual, automatic, rate aided
Target acquisition	MPS-19 radar, MK-51 optical tracker, infrared tracker, CCTV and other FPQ-11 radar.

Receiving System

Frequency	2,650 - 2,950 MHz
Type	Superheterodyne
Antenna coupling	Parametric amplifier (15 MHz bandwidth)
Noise figure	Better than 2 dB
Minimum discernible signal (MDS)	With parametric amplifier - 115 dBm Without parametric amplifier - 102 dBm
Bandwidth	5.6 MHz, 2.6 MHz (selectable with pulse width)
IF	25 MHz
Image rejection	20 dB down or greater by SSB mixer
Range indicators	Three 5 in A-scopes, single sweep, as follows: Total range according to PRF approximately 365,000 yards, 32,000 yards sweep centered around target presentation, triple sweep, 2,000 yd segment of range including target presentation, the three sweeps displaying beacon video, radar video and summed video.

Transmitter

Frequency	2700 - 2950 MHz
Power	150 W (minimum)
Pulse width	0.5 plus or minus 0.1 μ s
Repetition rate	1-2000 pps
Type output tube	Triode cavity
Type modulator	Solid State
Recovery time	Less than 50 μ s
Delay	2 μ s nominal

Table 5-5 Radar Set AN/FPQ-11, Technical Characteristics (continued)

Power Supply

Primary power source	6.9 Vdc plus or minus 10%
Primary power input	Approximately 9 W
Internal power source	5 HR-1 Yardney Silvercels, life approximately 60 min.

Mechanical

Size	25.5 in ³
Form	3 & 3/4 x 3 x 2 & 1/4 in excluding mounting flange
Weight	Less than 2 lb
Pressurization	15 psi

Environmental

Temperature	-20 to 70° C
Vibration	5-2000 c/s at 10g, 3 min sweep
Shock	100g all planes
Acceleration	80g all planes

Table 5-6 Radar Set AN/MPS-504, Technical Characteristics

Transmitting System

Frequency	2700 - 2900 MHz
Peak Power	500 kW minimum
Normal operating power	600 kW
Pulse repetition frequency	410 pps
Pulse width	2 μ s
Pulse shape	Square
Modulator	Soft tube
RF lines	Rectangular waveguide and rigid coaxial cable

Antenna System

Type	Half parabolic cylindrical reflector
Beam width azimuth	2°
Beam width elevation	15°

Range System

Maximum range	200,000 yds
Minimum range	2,000 yds
Range accuracy	plus or minus 1,000 yds

Receiver System

Type	Superheterodyne
Minimum discernible signal	-97 dB
Bandwidth	1.2 MHz
Range indicator	PPI scope, provided with 3 sweep ranges, 50,000, 100,000 and 200,000 yds.
Azimuth coverage	360°
Elevation coverage	-3 to 45° dependent of the mechanical tilt of the antenna

5.2.2.7 NASA Long-Range, S-Band (SPANDAR).

The NASA Long-Range, S-Band, located on the Wallops Mainland area directly opposite Wallops Island, is a high-powered, conical-scan, tracking radar. The radar employs a 60-foot parabolic reflector on a 95-foot mount. Features of the radar include: at least 5 megawatts peak power, parametric amplifier in the receiving system, a digital data system, a doppler system, and a 5000-mile range for beacon tracking. The estimated skin-tracking range for a 1-square-meter target is approximately 600 statute miles. Table 5-7 lists the technical characteristics of the radar.

The NASA Long-Range SPANDAR provides data outputs in the following forms:

1. Synchro voltages representing slant range and azimuth and elevation angles.
2. Potentiometer voltages representing slant range and sine and cosine functions of azimuth and elevation angles.
3. Precision digital data representing slant range and azimuth and elevation angles.

5.2.2.8 Radar Set AN/FPQ-6.

The AN/FPQ-6 is a pulse radar capable of nonambiguous range measurements of targets at ranges up to 32,000 nautical miles.

Features of the AN/FPQ-6 system include: built-in acquisition features in the ranging equipment; an auxiliary nonreferenced range system (AUXTRACK); a C-scope with video integrator to enhance long-range target acquisition; rapid slewing circuits with added tracking features; and four A-scopes displaying range increments.

The transmitter is convertible to doppler measurements, pulse compression, and other more elaborate coherent transmitter-receiver techniques. The transmitter frequency synthesizer and multiplier may be used with minor variations to drive r-f output stages covering other r-f frequency bands, such as L, S or X bands.

Transmitting System	
Frequency	2700 to 2900 mc
Transmitter	High-power klystron
Peak r-f power	5 megawatts
Average power	10 kw
Pulse rate	256 to 390 pps (in 4 steps)
Pulse length	1, 2, and 5 μ sec
Prf	256, 303, 328, and 390 cps
Frequency stability	1 part in 10^6 per month 5 parts in 10^9 per day
Frequency resolution	1 mc
Pulse shape	Square
Antenna System	
Type of reflector	60-foot parabolic reflector
Focal length	25 feet 1/2 inch
Beam crossover	1.5 db
Gain	52.8 db
Beam width	0.39°
Weight	84 tons (antenna & tower top)
Drive	Two 32 hp in each axis

TABLE 5-7 SPANDAR, Technical Characteristics

TABLE 5-7 SPANDAR, Technical Characteristics (Continued)

Antenna System	
Antenna temperature	30°K (dark sky)
Side lobe location	1st 0.68°; 2nd 1.04°
Side lobe height	13 db down
Null depth	16.8 db
Type of feed	Rotating circular horn
Type of scan	Conical
Scan frequency	30 cps
Polarization	Circular, vertical, horizontal
R-f transmission line	Rectangular waveguide
Vswr	1.18
Line loss receiving	0.8 db
Line loss transmitting	2 db
Receiving System	
Frequency range	2600 to 2900 mc
Receiver type	GE FPS-6B
I-f frequency	30 mc
Image rejection	18 db down PAR
Sensitivity	-116 dbm
Noise figure	3 db
Bandwidth	1.3 mc - 650 kc
Low-noise device	Parametric
Dynamic range	-117 db
Ranging System	
Maximum range	10,000,000 yards
Minimum range	1000 yards
Maximum tracking rate	10,000 yards/second
Maximum slew rate	40,000 to 500,000 yards/second
Master oscillator frequency	82 kc
Range accuracy	±25 yards
Tracking gates	6 & 18 μsec
Data bits	20
Serial readout rate	50 pulses/second
Granularity	±10 yards
Digital "1"	-3 vdc
Digital "0"	-11 vdc

TABLE 5-7 SPANDAR, Technical Characteristics (Continued)

System Facts	
Tracking rates	Azimuth: 6°/second Elevation: 6°/second Range: 10,000 yards/second
Slewing rates	Azimuth: 15°/second Elevation: 15°/second Range: 500,000 to 40,000 yards/second
Accelerations	Azimuth: 7°/second ² Elevation: 9°/second ²
Accuracy	Azimuth: ±1 mil Elevation: ±1 mil Range: ±25 yards
Azimuth coverage	360°
Elevation coverage	0° to 90°
Elevation travel	-15° to 90°
Capture area	1261.78 square feet
System Power	
Load	3 phase, 208/440 vac, 500 amp

The antenna mount has the following capabilities: precise data takeoffs; high and low servo response bandwidth capability with high gain across the variable range; high torques to counteract wind forces and achieve high accelerations; hydrostatic bearing in azimuth and phased ball bearings in elevation to provide tracking smoothness at extremely low and high angular velocities; and stability with thermal changes. Table 5-8 lists the technical characteristics of this radar system.

The AN/FPQ-6 provides data outputs in the following forms:

1. Synchro voltages representing slant range and azimuth and elevation angles.
2. Potentiometer voltages representing slant range and sine and cosine functions of azimuth and elevation angles.
3. Precision digital data representing slant range and azimuth and elevation angles.

5.2.2.9 Velocimeter, Model 10A, Doppler Radar.

The Velocimeter, Model 10A, is a mobile doppler radar which generates a continuous-wave radio-frequency signal that is radiated from a directional transmitting antenna. The part of this transmitted signal that strikes a target is reflected back to a directional receiving antenna. If the target is stationary, the frequency to the reflected signal is identical with that of the transmitted signal. If the object is moving toward or away from the antenna, the frequency of the reflected signal is increased or decreased, respectively. The amount of the frequency shift, which is proportional to the radial speed (V) of the moving target, is known as the doppler frequency. This mobile doppler radar has an output power of 125 watts.

The Model 10A Velocimeter uses an audio beat frequency to determine test vehicle velocity. Its average useful range is about 50 to 100 thousand feet. The audio output is recorded on magnetic tape along with the timing and control signals. Each cycle of the audio frequency represents 0.1864 feet/second; readings are to the nearest one-fourth cycle in the data reduction process. The radar operates at about 2640 mc and requires two operators: one for azimuth and one for elevation control. After visual sighting is no longer possible, the operators use tracking radar data in a "bug-matching" process to follow the desired target.

TABLE 5-8 Radar Set AN/FPQ-6, Technical Characteristics

Transmitting System	
Frequency range	5400 to 5900 mc
Frequency stability	1 in 10 ⁸ /hr
Peak power	2.5 to 3 megw
Average power	4.8 kw
Output power tube	Klystron
Power programming	-30 db
Pulse widths	0.25, 0.5, 1, and 2.5 μ sec
Prf	160, 640, 341, 1280, 1707, 142, 233, 285, and 366 cps
Coding capability	Yes
Frequency resolution	243 kc in steps
Receiver System	
Tuning range	5370 to 5930 mc
I-f frequency	30 mc
Image rejection	40 db
Sensitivity	-110 dbm
Noise figure	8 db
Bandwidth	$\frac{1.2}{PW} < B < \frac{1.6}{PW}$
Dynamic range	-110 db with programming
Antenna System	
Type	29-ft Cassegrainian parabola
Focal length	8 ft
Beam crossover	0 db
Gain	51 db
Beam width	0.4°
Drive	Hydraulic motors (two - 37.5 hp)
Antenna temperature	26°K, dark sky
Side lobe height	20 db down
Null depth	35 db (minimum)
Capture area	14.88 square meters
Elevation coverage	-2° to 182°
Gear ratio	720:1
Backlash	0.005 mil
Linearity	0.09 mil (rms)

TABLE 5-8 Radar Set AN/FPQ-6, Technical Characteristics (Continued)

Antenna System (Continued)	
Azimuth coverage	360° continuous
Gear ratio	650:1
Backlash	0.005 mil
Slip rings	Video: 16 to 60 cps to 50 mc If: 6 to 25 mc to 50 mc
Angle noise	0.03 mil (rms) servo
Feed system:	
Type of feed	5-horn
Type of scan	Monopulse
Polarization	Vertical or circular
R-f transmission line	Rectangular waveguide
Line loss receiving	2.3 db
Line loss transmitting	3.5 db
Ranging System	
Maximum range	32,000 nautical miles (nonambiguous)
Maximum tracking rate	20,000 yards/second
Maximum slew rate	240,000 yards/second
Velocity memory	99%/5 seconds
Velocity lag	0.555 cps/nmi/second
Bandwidth (maximum)	19 cps
Acceleration	100,000 yards/second ² (10,000 g's)
Master oscillator frequency	5 mc
Oscillator stability	1 in 10 ⁷
Acquisition data accuracy	±5 nautical miles
Range accuracy	±5 yards
Tracking gates	0.25, 0.5, 1, and 2.4 μsec
Data bits	25 binary
Serial readout rate	50 kc/second
Granularity	2 yards
Digital "1"	8 ±2 volts
Digital "0"	0 volt
Pulse duration	1 ±0.15 μsec
Rise time	0.3 μsec
System Facts	
Tracking rates	Azimuth: 28°/second Elevation: 28°/second

TABLE 5-8 Radar Set AN/FPQ-6, Technical Characteristics (Continued)

<p>Ranging System (Continued) System Facts (Continued) Slewing rates</p> <p>Accelerations</p> <p>Accuracy</p> <p>Range on 1 square meter, corner reflector, 1 meter side length</p> <p>Scan modes</p> <p>System Data Analog outputs Digital outputs: Bits</p> <p>Granularity</p> <p>System Power Load</p>	<p>Range: 20,000 yards/second Azimuth: 28°/second Elevation: 28°/second</p> <p>Range: 240,000 yards/second Azimuth: 20°/second² Elevation: 20°/second²</p> <p>Range: 10,000 g's Azimuth: ±0.05 mil Elevation: ±0.05 mil</p> <p>Range: ±5 yards 800 nautical miles</p> <p>Circle, spiral, raster, rectangular</p> <p>Same as AN/FPS-16</p> <p>Azimuth: 20 Elevation: 20 Range: 25 Azimuth: 0.0122 mil Elevation: 0.0122 mil Range: 2 yards</p> <p>208 volts, industrial, 239.1 kva 208 volts, critical, 107.6 kva 480 volts, industrial, 98.8 kva 480 volts, critical, 50 kva</p>
---	---

Figure 5.2-2 is a block diagram of the Model 10A Velocimeter. Table 5-9 lists the technical characteristics of the radar.

5.2.3 Radar Application to Rocketsonde Systems.

Several types of radars are used extensively for tracking meteorological rocket systems. They are the mobile systems M-33 (X-band), AN/MPA-12 (X-band), and AN/MPQ-18 (S-band), and the stationary system AN/FPS-16 (C-band). The major characteristics of these radar systems are given in Table 5-10. Currently the FPS-16 radar system is the one most suitable for tracking meteorological rockets, in that it can skin-track the rocket during its flight and then immediately track the payload at the time of its expulsion from the rocket.

Most of the high-performance range radars are fixed emplacements and are too expensive (\$1-3 million) to establish at remote meteorological rocket sites. To make available a low-cost mobile tracking radar for remote sites, the Army personnel at WSMR have developed modifications to surplus M-33 mobile gun-laying radars for tracking meteorological rocket payloads. As the slew rate and sensitivity of this radar do not permit skin tracking of the rocket during ascent, these radars have been slaved to the GMD telemetry tracking systems to aid in acquisition. Other modifications to make the M-33 more suited to meteorological rocket work include the extension of the effective plotting board range to 100,000 yards, and the installation of a 10-foot parabolic reflector antenna to increase radar sensitivity over that available with the original lens system.

A usable passive wind sensor or rocketsonde deflector must provide adequate radar signal return to be tracked with the available radar to a slant range of at least 100,000 yards. Consequently, the parachutes are coated with a metallic substance for radar reflectivity. As a measure of the radar efficiency of the sensors, AGC voltages are recorded against slant ranges. The voltages are calibrated to decibels above the minimum discernable signal (MDS). The results from the FPS-16 tracks of Arcas 15-foot parachutes is presented in Figure 5.2-3. The efficiency of the 8-foot Loki parachute is illustrated in Figure 5.2-4. The radars used with the Loki parachute were MPQ-12 and MPQ-18 units from White Sands Missile Range. For comparative purposes, the results of an S-band corner reflector track are included. The corner reflector track was a standard ML 307/ ap aluminum foil reflector carried aloft by a 1200 gram balloon. It is apparent that both

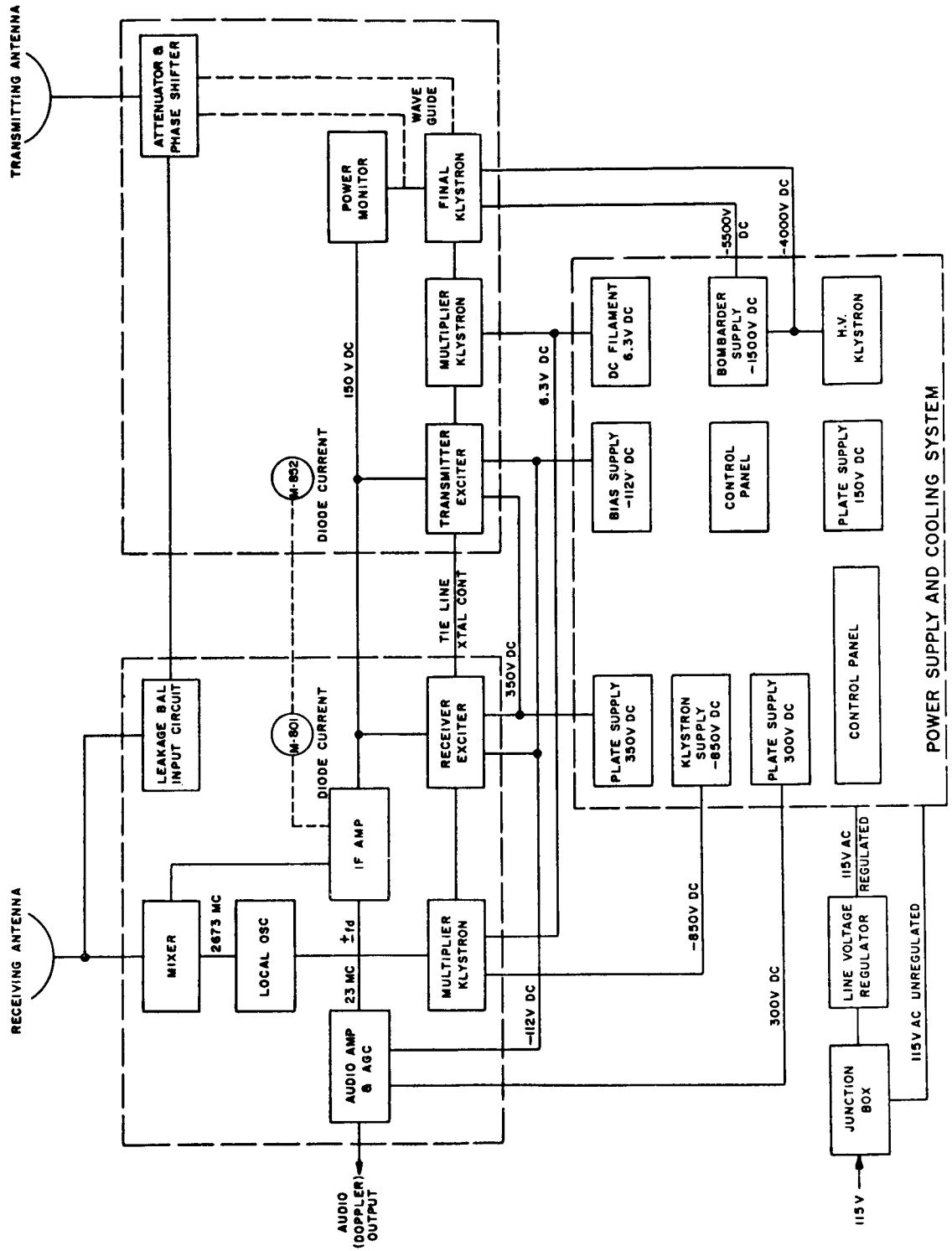


FIGURE 5.2-2 Model 10A Velocimeter, Block Diagram

TABLE 5-9 Model 10A Velocimeter, Technical Characteristics

Frequency	2640 mc
Range	50,000 to 100,000 feet
Antenna beamwidth	4.5° between half-power points
Flat response	Up to 11,000 feet/second (8000 mph)
Power output	200 watts peak, 125 nominal
Noise figure	12 db
I-f bandwidth	200 kc
Doppler output	3 watts into 500-ohm load
	Lowest frequency, 1000 cps; velocity = 186 feet/second
	Highest frequency, 60,000 cps; velocity = 11,160 feet/second

TABLE 5-10 RADAR CHARACTERISTICS

	X-BAND SYSTEM (9000 Mc)	X-BAND SYSTEM (9000 Mc)	S-BAND SYSTEM (2700 Mc)	C-BAND SYSTEM (5500 Mc)
TYPE	M-33 modified	AN/MPQ-12	AN/MPQ-12 & 18	AN/FPS-16
ANTENNA	3.0 meter parabolic	2.5 meter parabolic	3.0 meter parabolic	3.7 meter parabolic
BEAM WIDTH	1.3×10^{-2} radians	1.6×10^{-2} radians	5.1×10^{-2} radians	1.9×10^{-2} radians
POLARIZATION	Vertical	Vertical, horizontal and circular	Linear, rotating and circular	Vertical, horizontal and circular
PEAK POWER	225 KW	200 KW	250-300 KW	1,000 KW
MAXIMUM RANGE	91,500 meters	365,800 meters	365,800 meters	365,800 meters
TRACKING PRECISION	Approx $\pm 2 \times 10^{-3}$ radians and ± 23 meters	Approx $\pm 2 \times 10^{-3}$ radians and ± 37 meters	Approx $\pm 2 \times 10^{-3}$ radians and ± 37 meters	$\pm 0.14 \times 10^{-3}$ radians and ± 14 meters
PRF	1,000 pps	Variable	Variable	Variable
OVERALL SENSITIVITY (Including Antenna Gain)	-145 dbm	-140 dbm	-140 dbm	-158 dbm

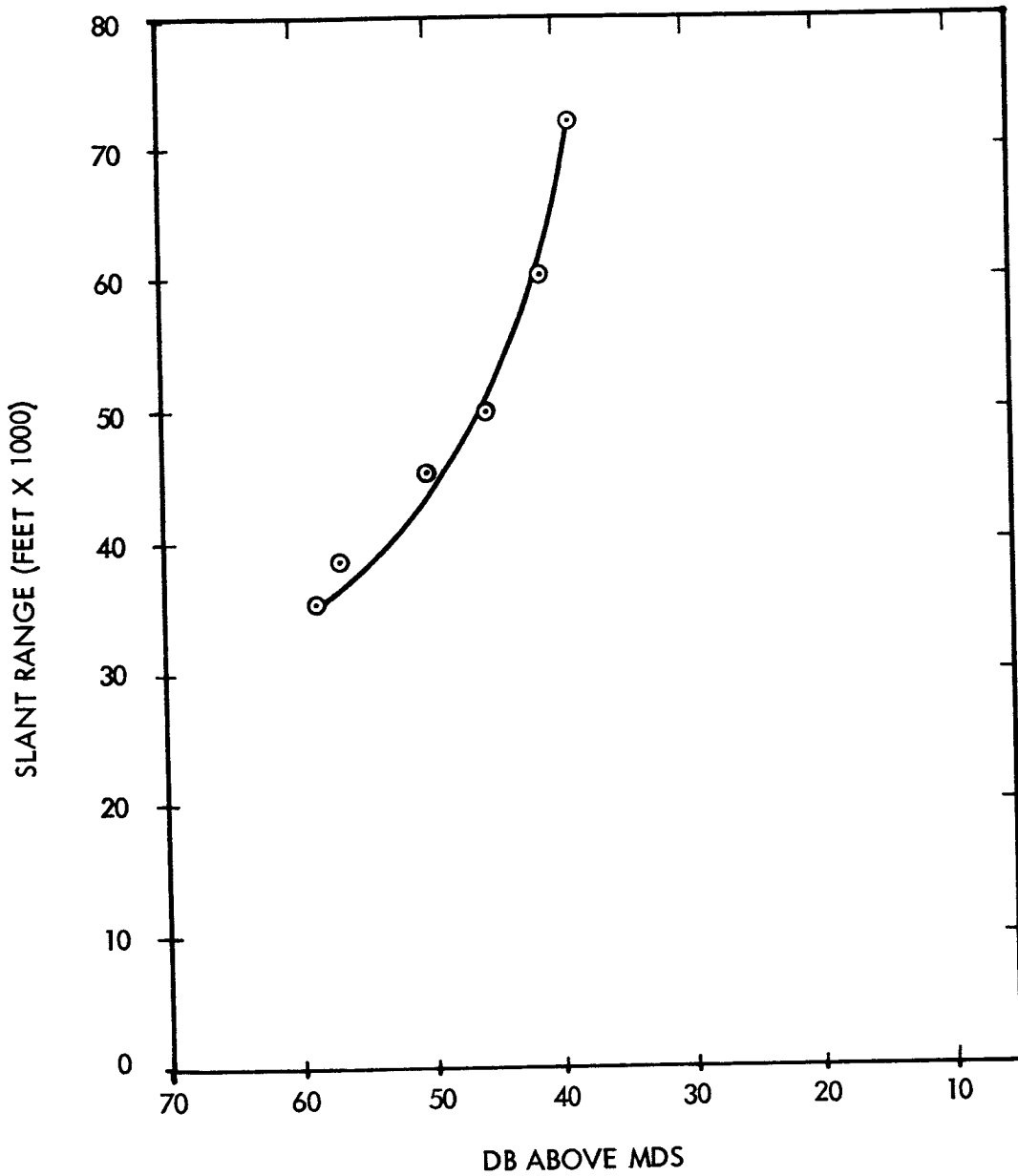


FIGURE 5.2-3 The mean of 6 Cases from the FPS-16 Tracks of Arcas 15-foot Parachutes at Pacific Missile Range, California

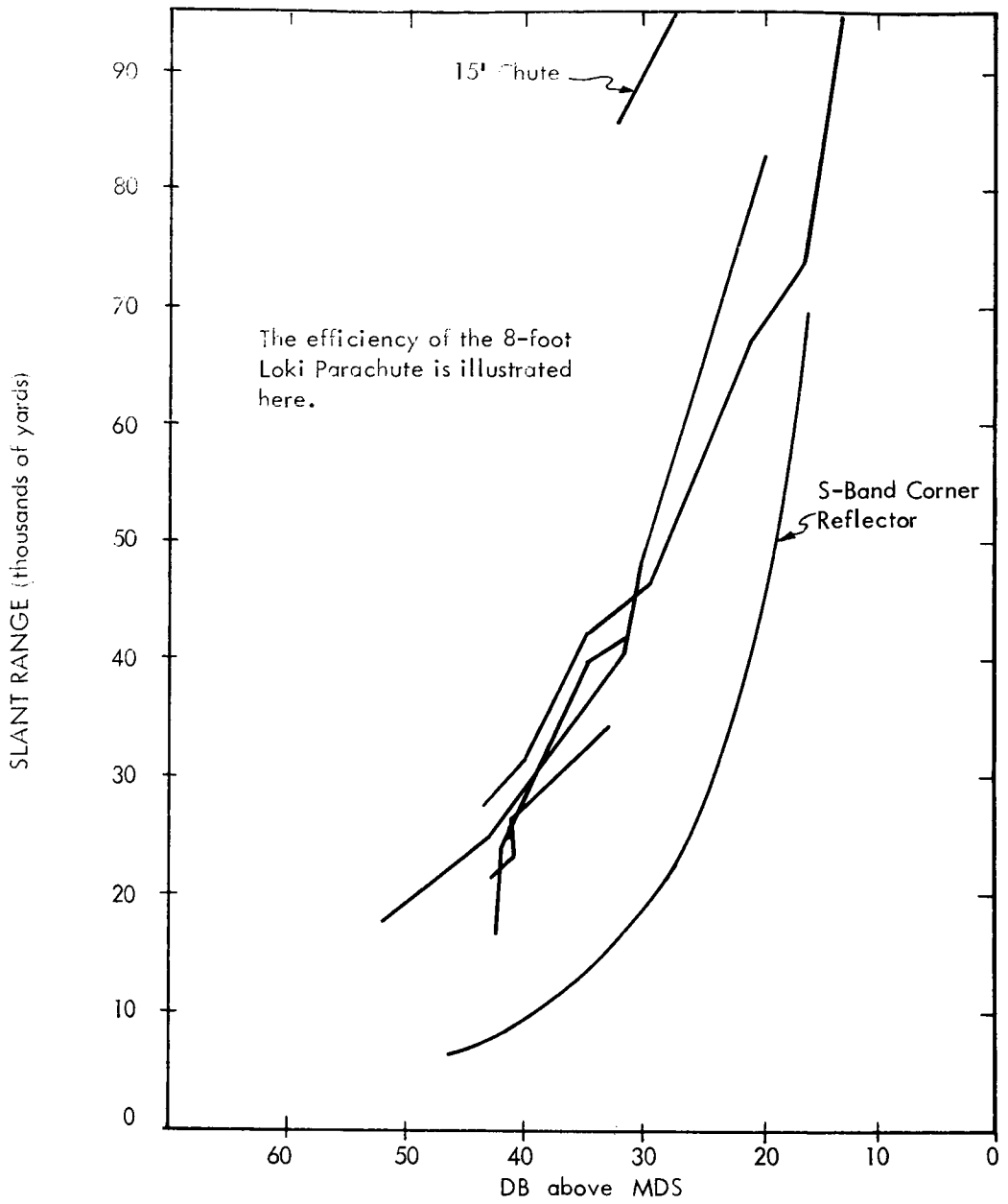


FIGURE 5.2-4 S-BAND RADAR TRACE OF 8 FOOT PARACHUTE

parachutes can be tracked to 100,000 yards slant range and are adequate reflectors for the available radar. Using the above recordings and the radar range equation it appears that the 15-foot and 8-foot parachutes provide effective targets of 45 meters² and 9 meters², respectively.

Signal strength recordings made during chaff tracks at WSMR are presented in Figures 5.2-5 and 5.2-6. Signal return is undoubtedly a function of dispersion due to the additional parameters, time and wind structure, as well as slant range. To approximate the effects of time and wind structure, the variation with slant range was removed. This was accomplished by treating the target as a solid sphere. Although it would be supposed that the signal level would always decrease with time, plots of signal strength vs time contain instances of the reverse (Figure 5.2-7). This is attributed to a probable shift of the radar to a different "patch" of chaff in the target area, that is, one with a stronger return. Another possible explanation is a redistribution of chaff so that a greater signal return was evidenced for a time. However, both of these mechanisms which serve to enhance signal return should provide only temporary stimulus. Generally, the signal should and does deteriorate with time (range being constant). It has been the experience at WSMR that most chaff tracks were terminated within 30 minutes after deployment due to signal deterioration resulting from chaff dispersion.

There has been some question regarding the effect of chaff wave length and radar polarization on signal return. No presentable recordings were made during these tests but there is definite evidence from observed signal return at the radar that it is not necessary to match chaff dipole and radar wave length exactly. X-band chaff can be tracked with S-band radar with only an approximate 10-percent loss in signal return compared with S-band chaff signal return. Similar results were obtained when X and C-band radar were used with S-band chaff. Polarization appears interchangeable since similar signal levels were observed on a single parcel of chaff whether circular, horizontal, or vertical polarization was applied. It might be inferred then, that as the chaff falls, it is randomly oriented with respect to the radar.

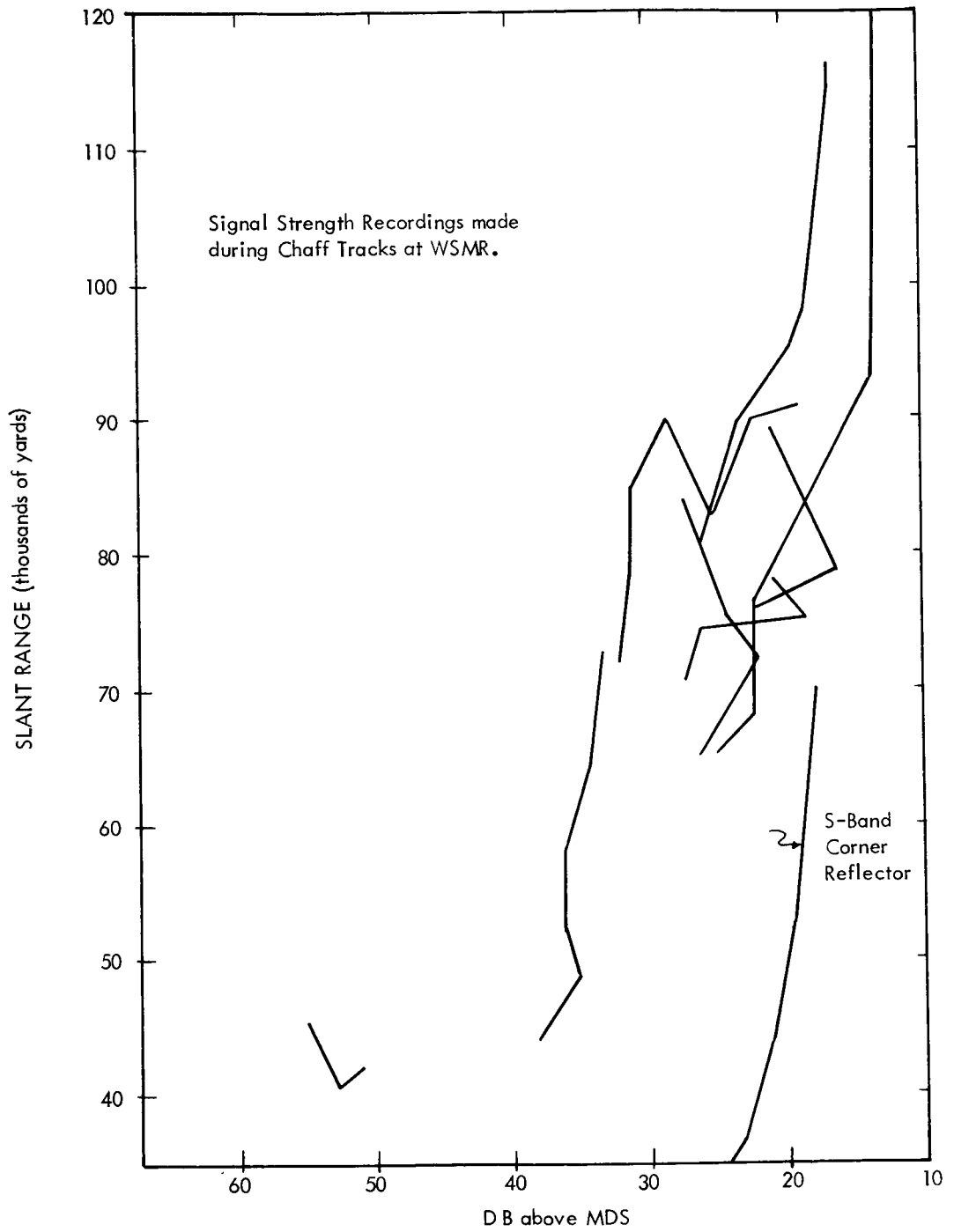


FIGURE 5.2-5 S-BAND RADAR TRACK OF S-BAND CHAFF

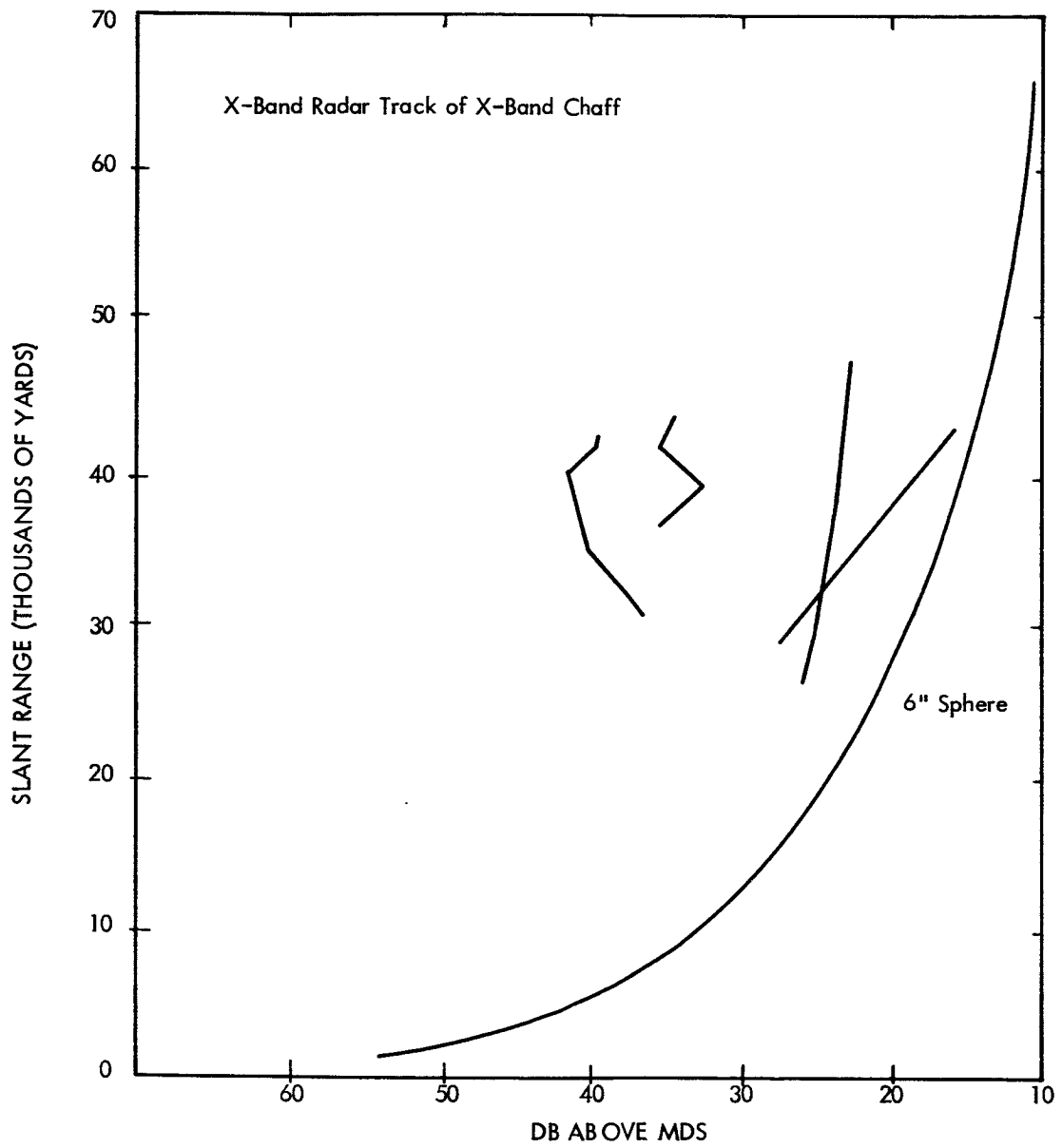


FIGURE 5.2-6 X-BAND RADAR TRACK OF X-BAND CHAFF

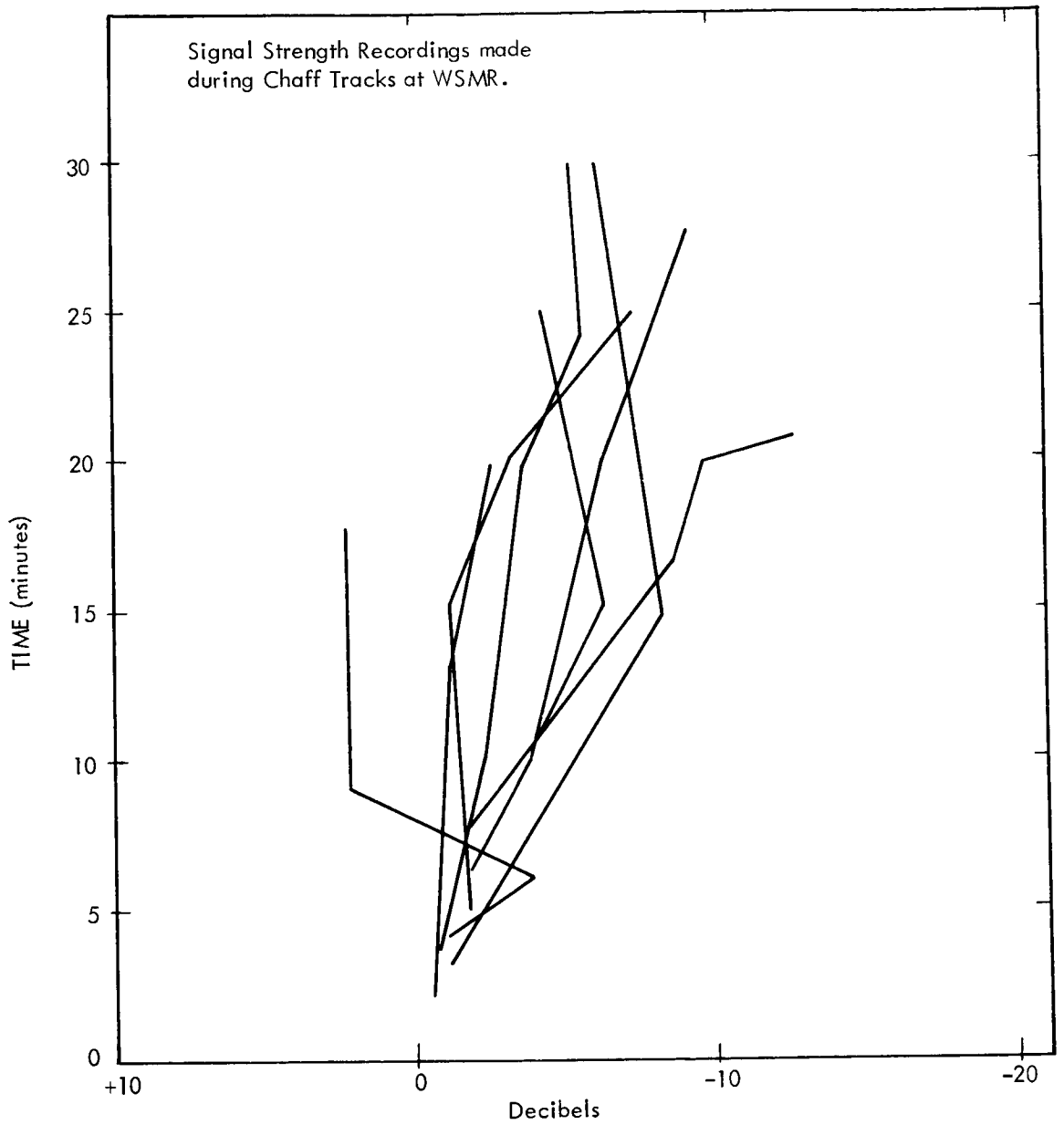


FIGURE 5.2-7 SIGNAL STRENGTH VS. TIME AFTER EXPULSION OF CHAFF

5.3 Telemetry.

5.3.1 General.

The four basic kinds of telemetry which have been used with meteorological rocket systems have been the 216 mHz to 235 mHz standard IRIG telemetry, the 1680 mHz AN/GMD-(x), the 403 mHz AN/SMQ - (x) and the specialized 38 mHz DOVAP tracking telemetry. Considering present equipment, the advantages of the IRIG telemetry over the GMD and SMQ types is a better modulation frequency response, multichannel potential, and an inherently stable crystal-controlled transmitter frequency. The disadvantages, however, far outweigh the above advantages. Current IRIG telemetry payloads are too costly (\$1,000 for a one channel sonde) for routine use. Although the components could be miniaturized, current components are too large for the small dart diameters. The antenna lengths for the 200 mHz range of transmitter frequencies are too long for small rocket systems, and the systems are not set up for tracking the vehicle, i.e., radar is required. Perhaps the greatest disadvantage is that the IRIG systems do not operate at the assigned meteorological frequencies of 403 mHz and 1680 mHz. The DOVAP system offers the advantage of obtaining tracking data, but has all of the other disadvantages discussed above.

The SMQ system offers the advantages of a small lighter weight instrument for the rocketsonde application because the modulation duty cycle is more efficient than for the GMD types. Also, an omnidirectional ground-based receiver is used so that a vehicle track does not have to be maintained. The SMQ receiver is smaller, less complex and lower in cost (\$3500) than the GMD receiving system. It also requires less maintenance. However, radar is required with the SMQ system to obtain tracking data.

The GMD system is currently the most appealing among the various telemetry systems because the instruments can be made small enough for even the small darts, and tracking data can be obtained with the AN/GMD- (2-4) systems. Since the GMD operates at the meteorological frequency bands, meteorological rocket operations can be conducted as a complete weather station function. Since radar is not required with the GMD - (2-4) systems, remote sites can be established with minimum cost and complexity. The cost of the ground equipment is not prohibitive (\$35,000 for GMD-1, \$65,000 for GMD-2), and the complete payload instruments should be from \$200 to \$400. A GMD-2 system has been used to successfully track a pitot probe experiment (Denpro) during vehicle ascent, and the tracking data compared favorably with

the FPS-16 radar results. For probe applications the modulation pulse rate will probably have to be increased as it was for the above pitot probe (from 200 pps to 1000 pps) for better data accuracy and frequency response or FM modulation can be used.

5.3.2 IRIG Telemetry Systems.

IRIG telemetry systems currently operate at carrier frequencies between 216 MHz and 235 MHz with the newer systems to operate in the 2200 MHz to 2300 MHz band. In the FM-FM or FM-PM system, various methods are used to enable the r-f carrier to carry more than one signal. Eighteen different channel frequencies can be applied to modulate the r-f carrier; they may be applied either one at a time or, under the proper circumstances, all at once. These 18 frequencies are subordinate carrier frequencies, called subcarrier frequencies. Subcarrier frequencies are in turn frequency-modulated by a source of information. The width of Channel 1 as set by the standards is 30 cycles above or below the center frequency of 400 cycles. The value of 30 cycles is determined by the standards, which call for a deviation of $\pm 7.5\%$ of the center frequency.

To keep the lowest signal-to-noise ratio, a modulation index (deviation ratio) of five was chosen. This is shown in Channel 1 by dividing the 30-cycle deviation by 5 and finding 6, which represents the frequency, in cycles per second, at which applied information can modulate Subcarrier Channel 1. A modulation index lower than five may be used at the expense of the signal-to-noise ratio. A modulation index of unity (1) would permit all 30 cycles of information to be passed. However, the signal-to-noise ratio would be low, severely handicapping the resultant output signal. In addition to possible distortion, another difficulty with a modulation index of unity, where the full deviation would be used, is the probability of the information of each channel overlapping, producing "cross talk". Figure 5.3-1 shows how the bandwidths increase with increasing channel frequency. For full details of the complete channel frequencies, deviation limits, and standard information-carrying capabilities of all channels, see Table 5-11. As the frequency of each succeeding channel increases, the frequency by which the channel may be modulated increases. The modulating frequency of Channel 1 is six cycles, that of Channel 18 is 1050 cycles. Thus Channel 18 may be used to convey information changing at a maximum rate of 1050 cycles. Slow variations in information are applied to the lower-frequency channels. To allow the subcarrier channel

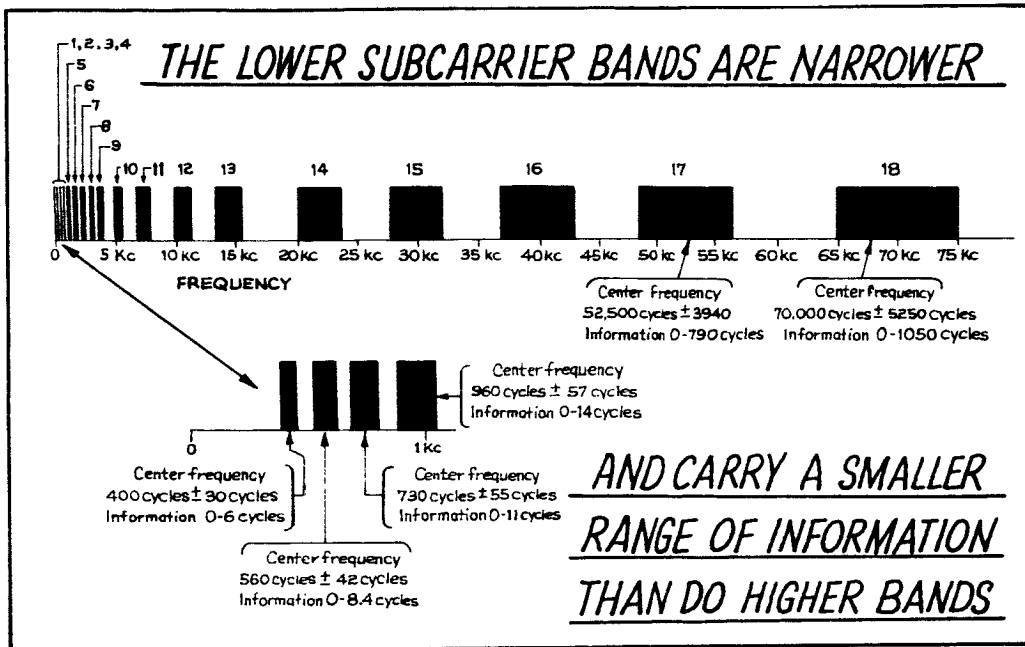


FIGURE 5.3-1 IRIG FM/FM Telemeter Subcarrier Bands

TABLE 5-11

IRIG FM/FM TELEMETER SUBCARRIER BANDS

Band	-7.5%	Center Freq.	+7.5%	Intelligence, cps	
				MI=1	MI=5
1	370	400	430	30	6
2	518	560	602	40	8
3	675	730	785	55	11
4	888	960	1,032	70	14
5*	1,202	1,300	1,398	100	20
6*	1,572	1,700	1,828	125	25
7*	2,127	2,300	2,473	175	35
8*	2,775	3,000	3,225	255	45
9*	3,607	3,900	4,193	300	60
10 *	4,995	5,400	5,805	400	80
11 *	6,799	7,350	7,901	550	110
12 *	9,712	10,500	11,288	800	160
13 *	13,412	14,500	15,588	1,100	220
14	20,350	22,000	23,650	1,650	330
15	27,750	30,000	32,250	2,250	450
16	37,000	40,000	43,000	3,000	600
17	48,562	52,500	56,438	3,950	790
18	64,750	70,000	75,250	5,250	1,050
19	86,025	93,000	99,975	6,975	1,395
20	114,700	124,000	133,300	9,300	1,960
21	156,625	165,000	177,375	12,375	2,475
	-15%	Center Freq.	+15%		
A*	18,700	22,000	25,300	3,300	660
B	25,500	30,000	34,500	4,500	900
C*	34,000	40,000	46,000	6,000	1,200
D	44,620	52,500	60,380	8,000	1,600
E*	59,500	70,000	80,500	10,500	2,100
F	79,050	93,000	106,950	13,950	2,790
G	105,400	124,000	142,600	18,600	3,720
H	140,250	165,000	189,750	24,750	4,950

USE OF OPTIONAL BANDS

Band A may be employed by omitting Band 13, 15 and B.
 Band B may be employed by omitting Band 14, 15, A and C.
 Band C may be employed by omitting Band 15, 17, B and D.
 Band D may be employed by omitting Band 16, 18, C and E.
 Band E may be employed by omitting Band 17, 19, D and F.
 Band F may be employed by omitting Band 18, 20, E and G.
 Band G may be employed by omitting Band 19, 21 F and H.
 Band H may be employed by omitting Band 20 and G.

NOTE: Bands 20, 21, G and H are to be used on 1435-1535 & 2200-2300 megacycle systems only.

to carry higher information frequencies, the deviation limits of a subcarrier channel may be increased. Doubling the deviation doubles the frequency of information that can be handled by a channel. As a result, the last five channels, 14 through 18, may be used with an increased value of 15% deviation limits. For identification, these channels are labeled A through E.

The synchronizing information is detected on the ground and assures that the information is recovered in the proper sequence. This means that the pulse representing information channel No. 1 always follows the synchronizing pulse and the pulse preceding the synchronizing information is the last information channel.

The subcarrier oscillator is a low-frequency oscillator that conveys the information gathered by the transducer. The frequencies vary from an audio frequency of 400 cycles to as high as 70,000 cycles. The subcarrier frequency is then applied to modulate a high-frequency R-F transmitter. The IRIG subcarrier frequencies can carry varying degrees of intelligence, depending upon the frequency of the channel selected. The higher the channel frequency the higher the frequency of the information it can carry. The information reproduced by the transducer at the point being measured may vary from zero to a maximum of 2100 cycles. This varying information is used to modulate the subcarrier oscillator. The type of modulation used may be Amplitude Modulation (AM), Phase Modulation (PM), or Frequency Modulation (FM). Frequency modulation of the subcarrier oscillator is most frequently used at present.

A subcarrier oscillator requires that the modulations vary the frequency linearly. It must have high stability, low drift, and low distortion. Since space and weight are important considerations, simple basic circuits are often used. To aid in achieving these goals, high-grade, close-tolerance components are used throughout the equipment. Various methods may be used to check frequency drift. The simplest is to remove, for an instant, the input to the subcarrier oscillator. It then oscillates at a known specific frequency. Another method is to apply a calibrating voltage to the subcarrier oscillator to produce a known specific frequency. There are three types of oscillator circuits in general use as subcarrier oscillators:

1. Inductance-capacitance
2. Resistance-capacitance phase - shift
3. Multivibrator

The inductance of an L-C tank circuit is often the coil winding of an inductive-type transducer. An R-C phase-shift oscillator may use the varying resistance-type transducer part of the phase-shifting network. Multivibrator oscillators are generally free-running, with their frequency varied by variations in their bias caused by the output of a resistive-type transducer.

The output frequency of a voltage-controlled subcarrier oscillator may be varied so that an increase in the applied signal either causes an increase or a decrease in the output frequency. The value of input voltage required to achieve $\pm 7.5\%$ frequency swing, or $\pm 15\%$ frequency swing, varies with each manufacturer. An average value is from 3 to 5 volts. The input voltage may be unipolar, such as zero to + 5 volts, or zero to -5 volts. Or it may be bipolar, such as zero to ± 2.5 volts.

In summary, the subcarrier oscillator is a self-contained oscillator that has as its center frequency any one of the 18 IRIG standard values. The subcarrier oscillator is modulated by the varying output of a transducer, most often by FM.

The output of the subcarrier oscillators is used to modulate the r-f transmitter. The form of modulation used for the r-f transmitter is usually frequency modulation or phase modulation. Crystal-controlled phase modulation is more prominent. The r-f carrier frequency used is in the 216 to 235 megacycle band assigned for telemetry use.

The PDM-FM or PDM-PM system enables the r-f signal carrier to carry more than one information channel. This is accomplished by dividing the time the carrier is on the air into known amounts, each amount representing a different channel of information. The information is converted to a value of time, then the r-f carrier is turned on to transmit a pulse of energy for the length of time representing the value of the information. As shown in Figure 5.3-2, a pulse duration of 90 microseconds (μ sec) represents a minimum-information reading; a pulse duration of 700 (μ sec) represents a

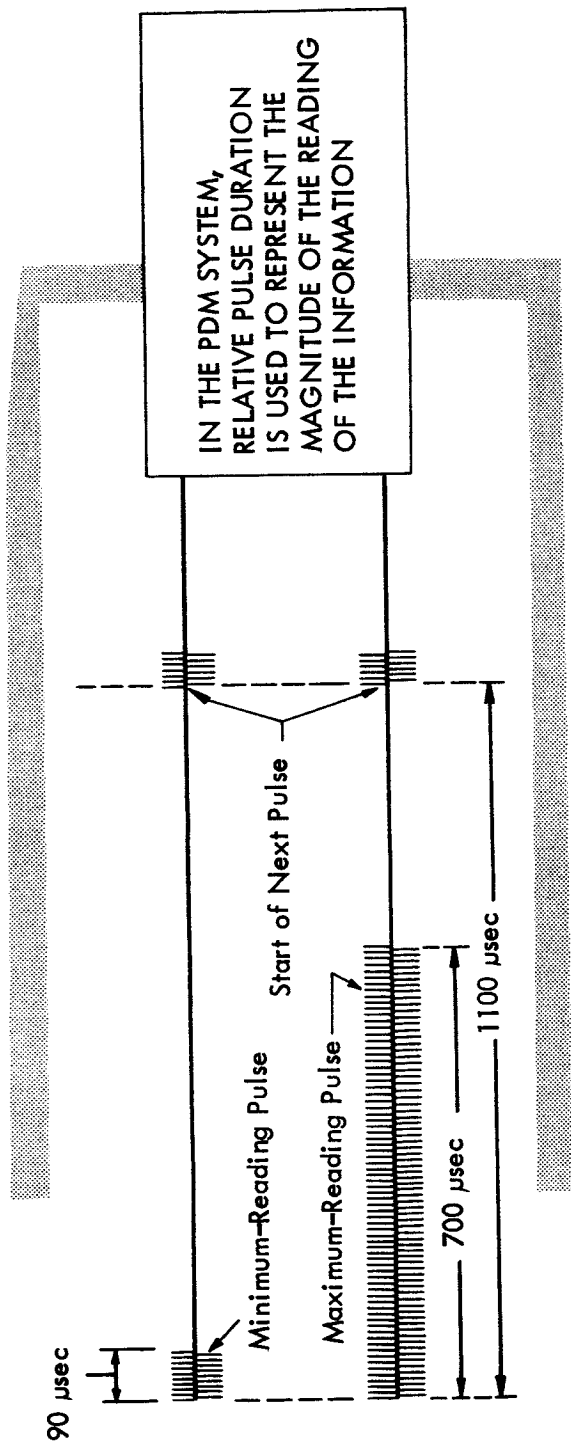


FIGURE 5.3-2 Pulse Duration Modulation

maximum-information reading. For example, 90μ sec might represent a minimum-information level of the output of an instrument. The 700μ sec might represent a maximum-information level.

These pulses of information are sent in specific numbers, 900 per second. This could represent 43 information channels sampled 20 times per second. Two additional channels are transmitted with no information to identify the beginning and end of each group of information.

One problem in having the output of two or more subcarrier oscillators simultaneously modulating the r-f transmitter is cross modulation, or cross talk. This results essentially from harmonics of some of the lower-frequency subcarrier oscillators missing with the primary frequencies of the high frequency subcarrier oscillators. Harmonics are generated in nonlinear circuits, or circuits in which overloading causes operation in a nonlinear region. To prevent formation of harmonic frequencies, linear mixing networks are used at the output of the subcarrier oscillators. These are sometimes called harmonic suppression filters.

To keep an equal signal-to-noise ratio output for all subcarrier oscillators, the high-frequency subcarrier oscillators must deviate the transmitter more than the lower-frequency subcarrier oscillators. The transmitter frequency deviation of the lower-frequency subcarrier oscillators is kept to a minimum to reduce the effects of cross talk and other problems.

The operating range of the transmitter is to a large degree determined by three factors:

1. Transmitter power
2. Receiving and transmitting antenna gain
3. Receiver sensitivity

The power output of a transmitter averages 3 watts, giving an approximate range of 50 miles under line-of-sight conditions. To obtain higher power, the transmitter is used to drive a high-power r-f amplifier. R-f amplifiers average 40 to 50 watts of output, increasing the range of transmission.

The problems encountered in constructing r-f transmitters are the same as those found in constructing all previously discussed telemetering equipment; compactness, ruggedness and dependability. R-f transmitters pose the additional problem of heat generated in the transmitters. Forced-air cooling has been used from some circuits, other immerse the entire unit in oil for better heat dissipation. Shock is an especially serious threat of the r-f transmitter because a slight movement of some of the tuned-circuit elements causes undesired modulation of the output, producing an erroneous signal. Frequency drift is held to a minimum by the use of high-quality components and other techniques, especially crystal control.

The transmit r-f power requires an antenna, which must be efficient to make the most of the small power output of the transmitter. An efficient antenna is not difficult to produce under ordinary circumstances. However, on a missile moving at supersonic speed, it is quite a problem. Since the missile may be spinning about its longitudinal axis, the antenna must radiate in all directions. This may also be accomplished by having more than one antenna. In addition, the sudden acceleration and high temperatures involved require that the antenna be of sturdy construction and correct materials. To keep the missile as streamlined as possible, the antenna cannot be a bulky unit that would alter the missile's shape.

These problems often result in a compromise in the type of antenna used. The most popular types are:

1. The airframe is the radiator.
2. Carefully located stubs or wires are used as the radiator.
3. A projecting portion of the vehicle, such as a fin, is electrically isolated by a notch and used as a radiator.
4. Slot antennas, mounted flush with the skin of the vehicle, are used as a radiator.
5. A resonant cavity is used to isolate a portion of the vehicles for excitation as a radiator.

Use of the entire airframe as the radiator is shown in Figure 5.3-3A. A spike placed in the nose cone of the vehicle is a simple form of stub antenna, Figure 5.3-3B. The length of the spike and its use are largely determined by the length of the vehicle. A notch cut through a projecting part of the vehicle, such as a fin, produces a surface suitable for radiation (Figure 5.3-3C). (When necessary, the notch is filled with a solid dielectric material). A slot antenna (Figure 5.3-3D) may be mounted flush with the skin of the vehicle. The radiation pattern of this type of antenna is quite similar to that of a dipole and reflector. A fifth method, shown in Figure 5.3-3E, utilizes a resonant cavity to isolate the outer skin surface of the forward section from the rest of the rocket. The outer skin surface of the isolated portion is utilized as a radiator.

Typical PDM/FM Telemetry:

PDM (Pulse Duration Modulation) telemetry systems are used when a strictly time division multiplex system is capable of meeting the bulk of telemetering requirements. Compared to the subcarrier channels system, the PDM/FM facilities permit the use of a relatively large number of channels, but only at lower frequencies. Figure 5.3-4 is a block diagram of the PDM/FM system.

Typical FM/FM Telemetry:

The FM/FM telemetry system is a frequency division, multiplex type device. Subcarriers of different frequencies modulate an r-f carrier and the subcarriers are frequency modulated by the intelligence. The channel capabilities of the system can be increased by using the commutation method to modulate the carrier frequency with combinations of the sub-carrier frequencies. Subcarrier frequencies for FM/FM telemetry are selected from a chart compiled by the Inter-Range Instrumentation Group (IRIG). Figure 5.3-5 is a block diagram of the FM/FM telemetry system.

Typical FM/AM Telemetry:

The FM/AM telemetry system is a frequency-modulated-subcarrier, amplitude-modulated-carrier type facility. Sixteen converters, each of a specified frequency, receive and convert data for the individual channels of the tape recorder. Channels 1 through 14 are converted to 5 kc; channels 15 and 16 are converted to 10 kc. The converted channels are then recorded on separate tracks of tape recorder. Figure 5.3-6 is a block diagram that is representative of FM/AM systems.

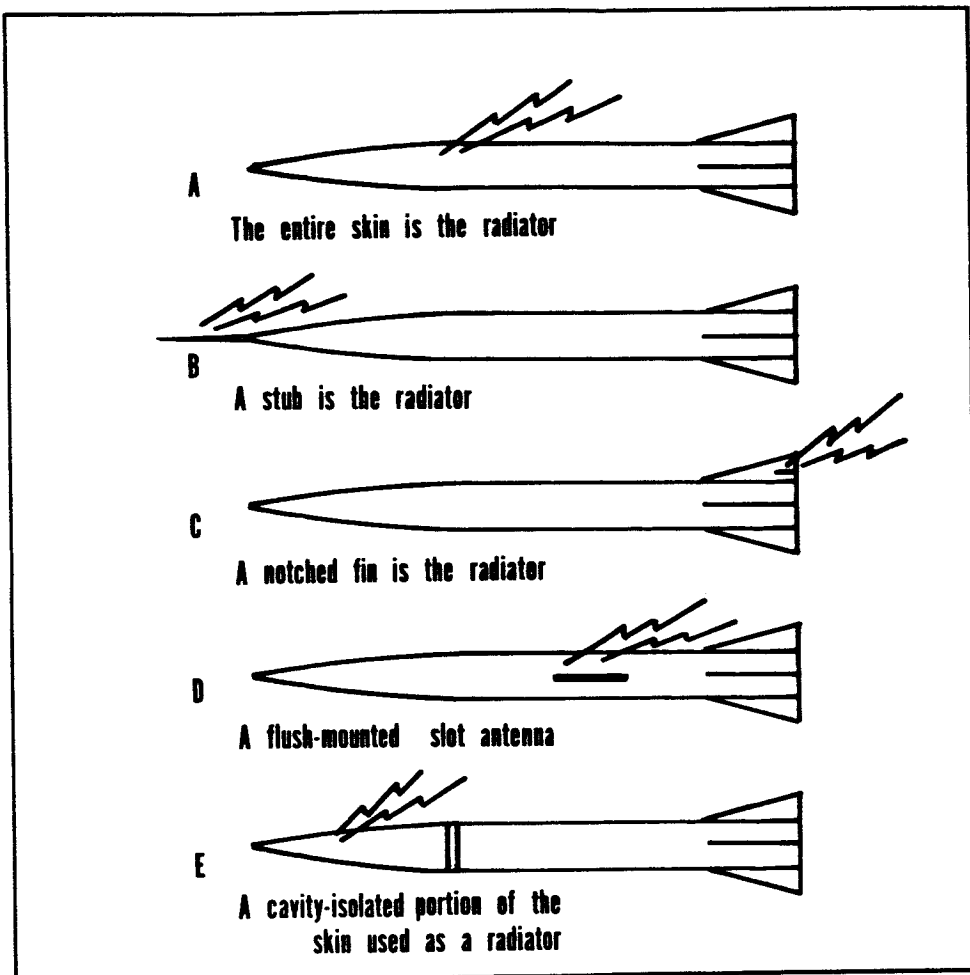


FIGURE 5.3-3 Missile Antenna Configurations

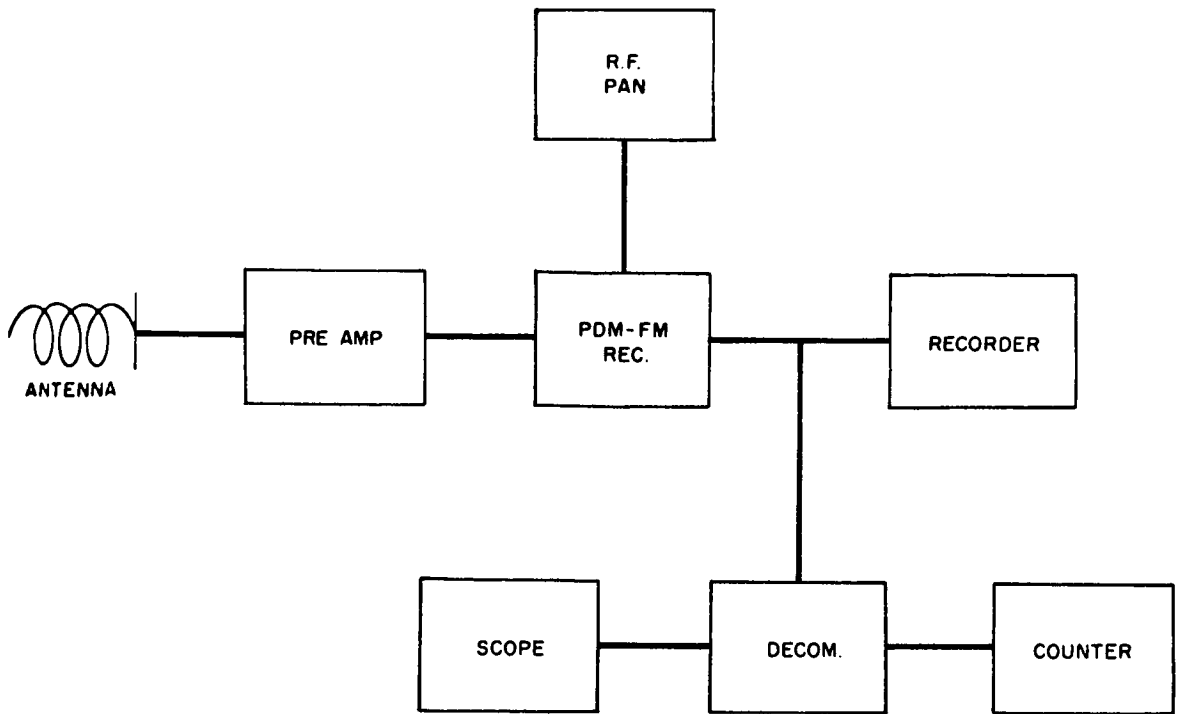


FIGURE 5.3-4 PDM/FM Telemetry System, Block Diagram

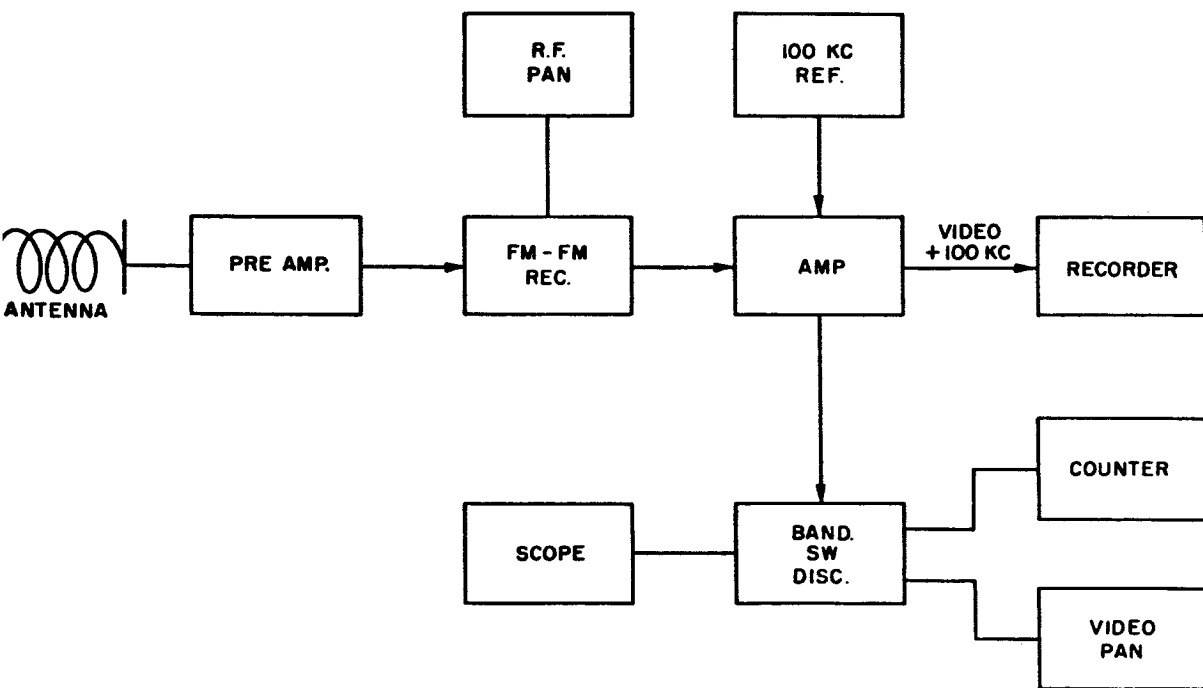


FIGURE 5.3-5 FM/FM Telemetry System, Block Diagram

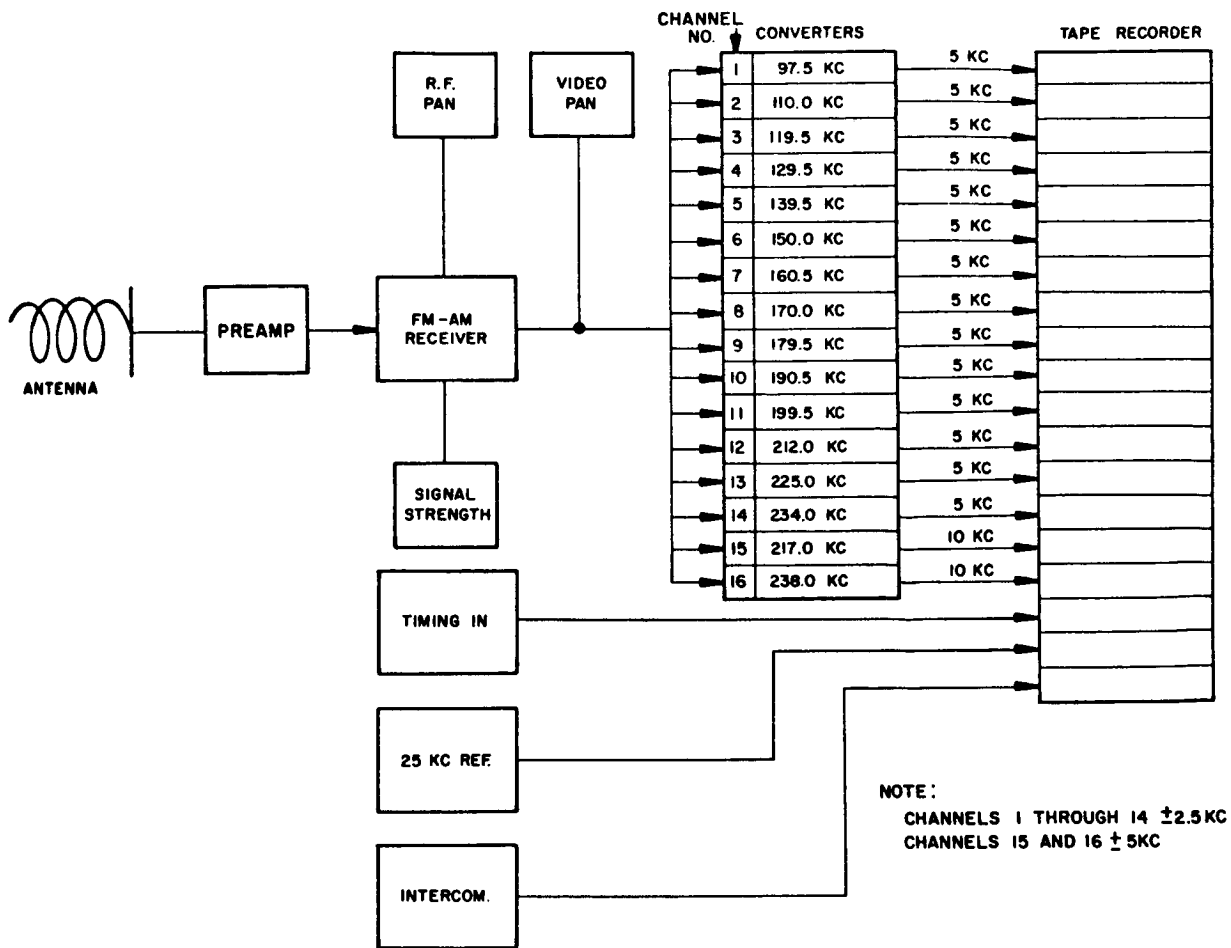


FIGURE 5.3-6 FM/AM Telemetry System, Block Diagram

Typical X-Band Telemetry:

Figure 5.3-7 illustrates the X-band telemetry receiving system in simplified block diagram form. Table 5-12 list the characteristics of this system.

5.3.3 DOVAP Telemetry Tracking System.

The DOVAP system functions as a combined telemetry and tracking system. A 38.031-mc transmitter located at the launch site emits a CW signal that is received by the rocket, and by each of four widely spread DOVAP stations. A DOVAP transponder in the rocket doubles the frequency of the received signal and retransmits to the DOVAP stations. At each DOVAP station the 38.031-mc signal from the launch site transmitter is received, doubled in frequency, and mixed with the signal from the rocket. The frequency difference between the two signals results in an audio frequency doppler signal whose frequency is proportional to the time rate of change of the transmitter-rocket-receiver path-length. Tape recordings of the doppler signal, along with precision timing are made at each DOVAP station. At the DOVAP Master Station, simultaneous recordings of the doppler signals from each DOVAP station are made, along with recordings of DOVAP telemetry. Accurate trajectories can be obtained from the doppler data.

The telemetry receiving stations consist of amplitude modulated receivers, discriminators, multichannel magnetic oscillographs, and magnetic tape recorders. Circularly polarized helical antennas, fixed in both elevation and azimuth are used with the receivers.

The rocket-borne DOVAP telemetry subcarrier oscillator consists of a single channel frequency modulated positive grid balanced multivibrator having a center frequency of 30 kc/s, and a frequency deviation of plus or minus 40% of center frequency for an input signal level of from zero to plus five volts. Negative voltage excursions of the subcarrier oscillator key the transponder radio frequency carrier off for one half the period of the subcarrier frequency. The telemeter is an integral component of the DOVAP transponder.

A representative DOVAP telemetry record is shown in Figure 5.3-8. Typical shroud-type DOVAP antenna radiation patterns, are shown in Figures 5.3-9 and 5.3-10. The nearly omni-directional pattern in the plane of the loop is an important feature of these antennas.

FIGURE 5.3-7 X-Band Telemetry Receiving System, Block Diagram

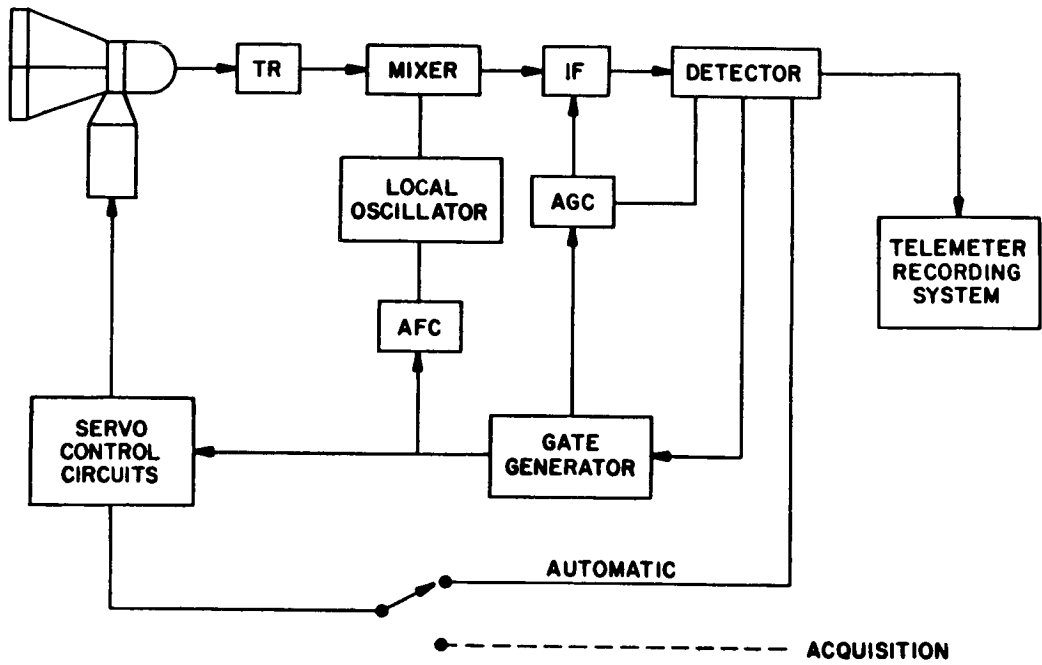


TABLE 5-12 \ X-Band Telemetry System Characteristics

Receiver	
Frequency range	8500 to 9600 mc
Sensitivity	-95 dbm
Noise figure	Approximately 9 db
I-f bandwidth	10 mc
Modulation	PDM/AM
Recording System	
Tape recorder	100-kc response
Recorder channels	PPM, PDM, azimuth angle error, elevation angle error, AGC voltage, timing and voice
Display	
Detected video	Oscilloscope
PDM raster	Oscilloscope
Single PDM channel	Pulse-duration (interval counter)
Antenna	
Type	Metal plate lens
Radiating element	Monopulse type, four feedhorns
Beamwidth	Approximately 1.2° (6-db points)
Gain	40 db
Polarization	Horizontal, vertical linear, or circular
Azimuth scan	360° continuous
Elevation scan	-10° to +180°
Maximum tracking rate	40° per second (azimuth and elevation)

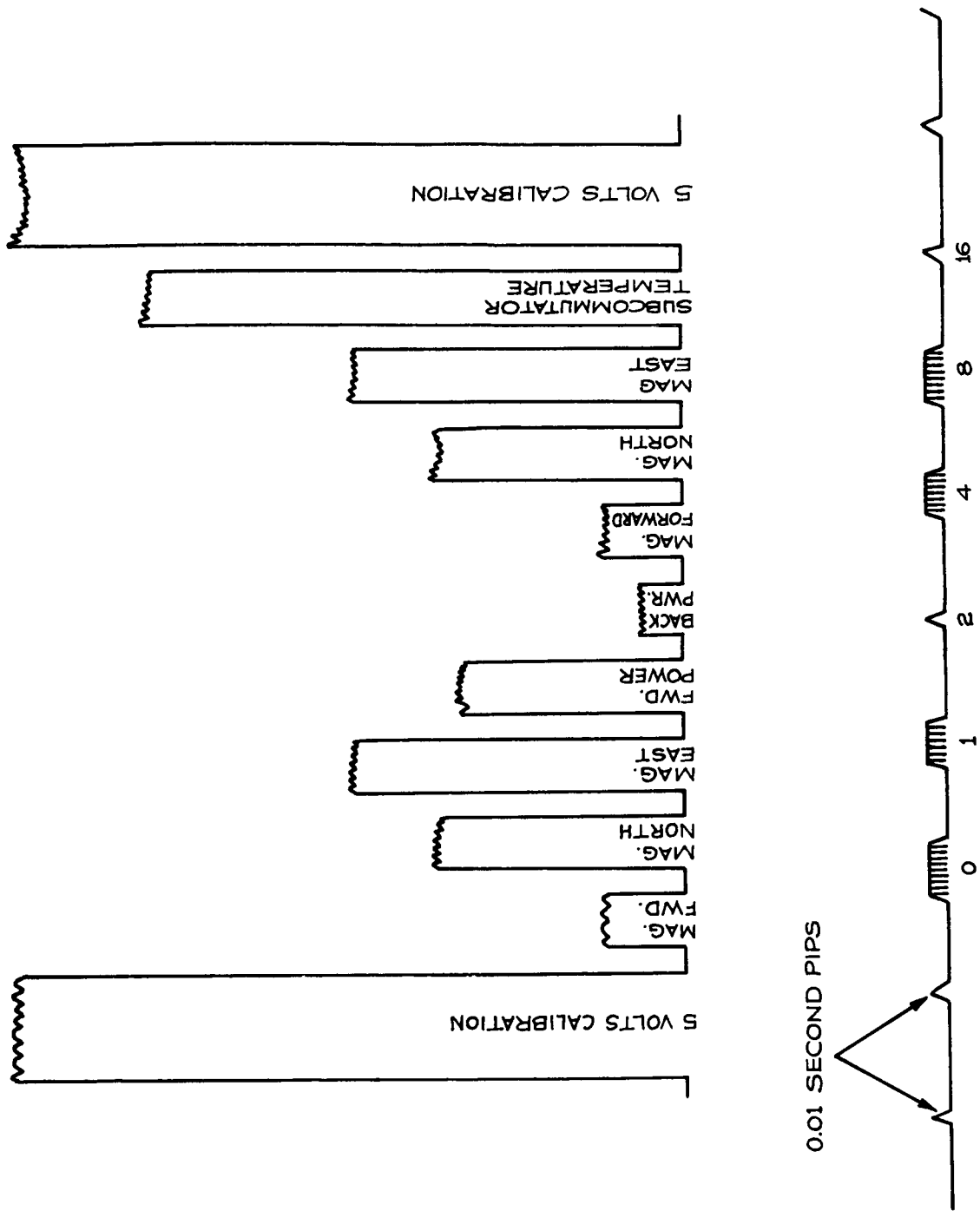
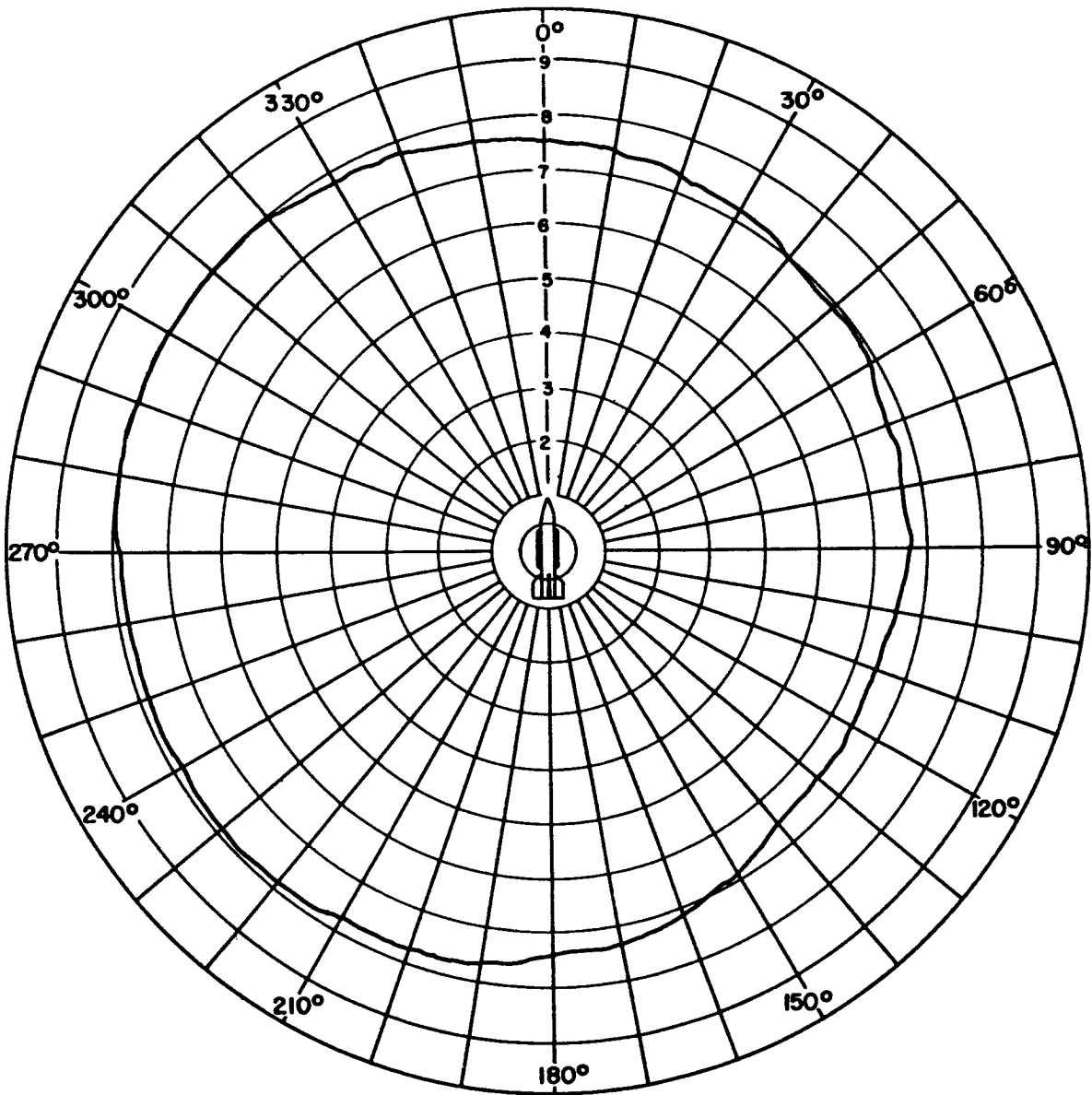
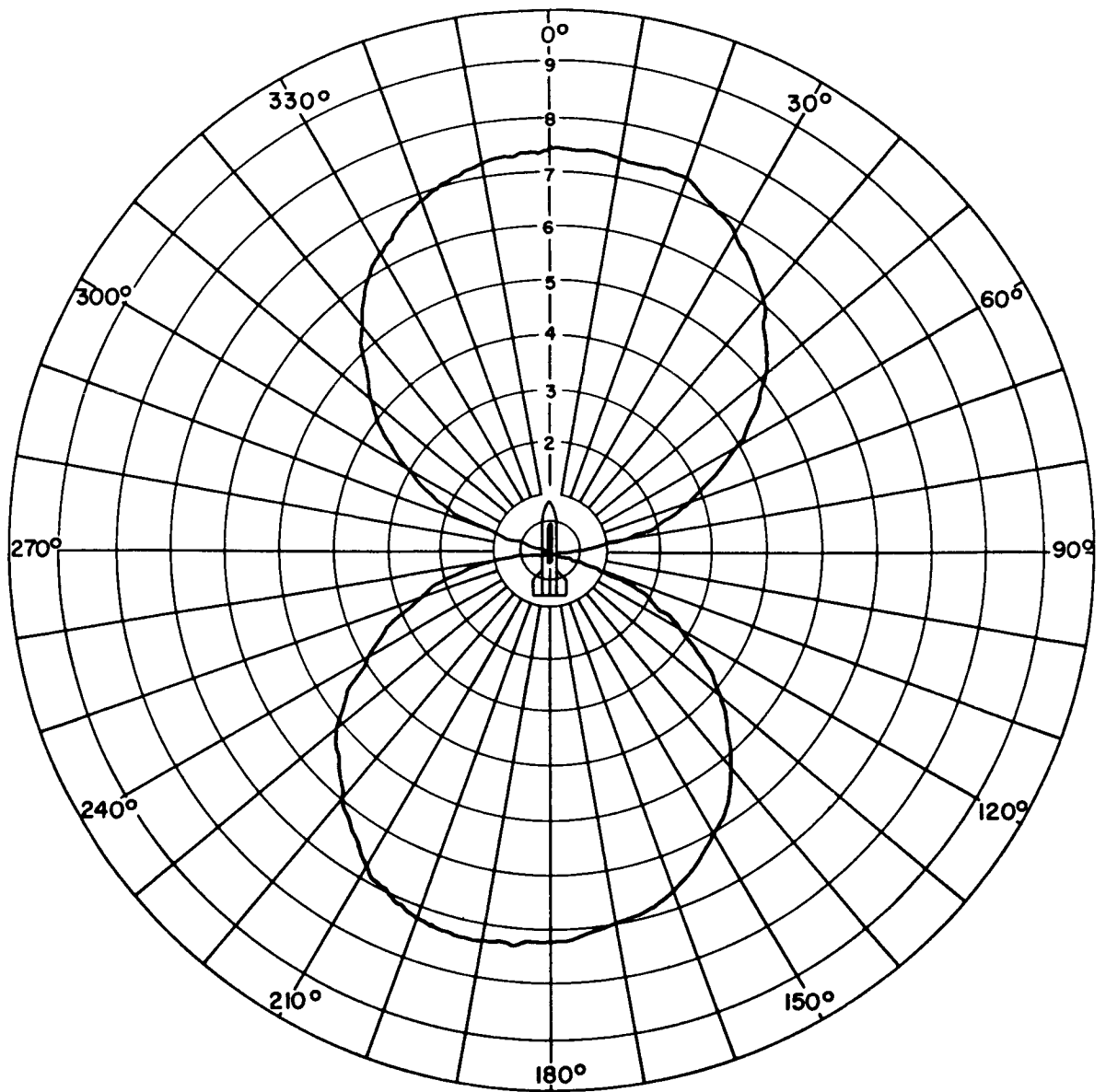


FIGURE 5.3-8 Representative Dovap Telemetry Record



Pattern and Polarization in Plane of Loop

FIGURE 5.3-9 SHROUD - TYPE DOVAP ANTENNA RADIATION PATTERN



Pattern in Plane Perpendicular to Plane of Loop Polarization in Plane of Loop

FIGURE 5.3-10 SHROUD - TYPE DOVAP ANTENNA RADIATION PATTERN

5.3.4 AN/GMD - (x) Telemetry and Tracking Systems.

5.3.4.1 General.

The AN/GMD - (x) ground-station equipment has been developed and standardized for radiosonde data acquisition. The AN/GMD-1, which is common at many of the military weather stations, not only receives the meteorological data but tracks the airborne transmitter in azimuth and elevation angles. For radiosonde measurements altitude is determined from the pressure measurement with this equipment. This technique is not accurate enough at rocketsonde altitudes and radar must be used. The AN/GMD-2 performs the same functions as the GMD-1 with the addition of the capability of measuring slant range. The feature is quite important for the rocket use since it eliminates the need for radar tracking. The azimuth and elevation slewing rates of these equipments are not fast enough to uptrack the rocket systems from lift off with most of the existing missile range site geometries. However, intercept methods of acquisition soon after lift off have been routinely employed with a large degree of success. The AN/GMD-4 has been developed to upgrade the GMD-2 system by employing coarse ranging to eliminate the slant range ambiguity problem and to provide automatic data processing of the received meteorological data. The GMD systems appear to be adequate for meteorological rocket work. If a faster data transmission response is required for advanced probe applications, the modulation rates can be increased or FM may be employed. Both of these techniques have been used. The tracking accuracies appear to be adequate for most meteorological rocket applications as a rather good agreement has been obtained with AN/FPS-16 radar tracking data.

The design philosophy of the GMD equipment has been to minimize the cost of the airborne instrumentation. Since approximately 400,000 radiosondes are flown each year, it has been quite important to keep as much of the required complexity and cost of the telemetry systems as possible in the ground station equipment. Therefore, the airborne instruments or sondes are fairly simple to design and minimal cost. This advantage has to some degree been passed on to the current rocketsonde instruments for they basically are copies of the equivalent radiosondes as far as the electronic circuitry is concerned.

For the next few years at least the GMD system appears to offer the greatest advantages in routine meteorological rocket applications because the ground equipment is standard weather station equipment, telemetry is accomplished at the assigned meteorological frequencies, the payload instrumentation is simple and low in cost and tracking data can be obtained so that the requirement for radar tracking can be eliminated.

5.3.4.2 Ground-Station Equipment.

The GMD ground-station equipment consists of either the AN/GMD-1, the AN/GMD-2 or the AN/GMD-4 as described in the following sections.

5.3.4.2.1 Rawin Set AN/GMD-1.

The Rawin Set AN/GMD-1, together with its associated equipment, has been the standard ground equipment for tracking of balloon-borne atmospheric probes since 1949. This transportable radio direction finder was designed to track automatically a balloon-borne radio-sonde transmitter (frequency range 1660-1700 mc). Its major units include a parabolic antenna with a pylon scanner assembly, a pedestal which supplies support and rotation machinery for the antenna in elevation and azimuth, an antenna control which energizes and controls the tracking machinery, and a receiver which detects and amplifies both the data signal and the tracking error signal from the scanner.

No modifications of the basic AN/GMD-1 are necessary to permit its use in tracking the Arcas-borne meteorological instruments in current use. At several sites receiver sensitivity has been increased 15 decibels through the use of a tunnel diode or parametric pre-amplifier to permit tracking of the dart instruments. The elevation slew rate is sufficient to follow the Arcas sounding rocket from launch to apogee when the tracking site is located approximately one-half mile from the launching pad. The dart instruments can likewise be tracked shortly after launch since their velocity in the first 15,000 feet is too great for tracking from the launch site.

The Recorder AN/TMQ-5 is the standard data recording device supplied with the AN/GMD-1 system and is used for the recording of temperature information from the rocket-borne transmitter. The

demodulator stage converts the data pulse frequency (0-200 pps) to a DC level which is recorded on 10-inch chart paper usually at a rate of one inch per minute with an accuracy of $\pm .5$ cycles per second.

The GMD-1 ground equipment consists of a tracking dish antenna and receiver unit, a control recorder unit and a TMQ-5 chart recorder as shown in Figures 5.3-11 and 5.3-12. Other versions of the system contain various auxiliary equipment such as ranging transmitter and various automatic data equipment.

The antenna and receiver unit consists of a seven foot diameter dish, mounted on a pedestal which contains the receiver and antenna motor controls. The dish may be operated in either automatic or manual track mode locally at the pedestal or from controls on the recorder, which is usually remote from the pedestal. The antenna system consists of a parabolic reflector, an eccentric cup which is rotated by a drive motor and hollow drive shaft, a dipole antenna, and a transmission line. The rocketsonde transmitter transmits a pulse-modulated radio-frequency signal (1680 Mc). The antenna lobe (received signal intensity pattern) rotates slowly. When the rocketsonde is in line with the electrical axis of the antenna reflector, the signal intensity of the dipole has a constant value; when the rocketsonde drifts to a point off the electrical axis of the antenna reflector, the intensity of the signal at the dipole varies with the rotation of the eccentric cup. Some of the radio-frequency energy from the transmitter is received by the parabolic reflector and reflected to the dipole antenna. As a result, the amplitude of the radio-frequency signal at the dipole takes the shape of a modulated sinusoidal wave. The relative phase and amplitude of the sinusoidal modulation is indicative of the angular distance of the rocketsonde transmitter from the axis of the antenna.

In the receiving system, the modulated wave is beat against the output of the local oscillator to produce a 30 Mc intermediate frequency which retains the pulse modulation and amplitude variations. The intermediate-frequency signal is then amplified and detected and the demodulated signal (30 cycles/sec sine wave and pulses) is passed to the antenna positioning system and to the meteorological data transmission system. The receiving system also contains an automatic frequency control (AFC) circuit to maintain a constant 30 Mc intermediate frequency and a service meter for checking various currents and voltages present in the Rawin set.

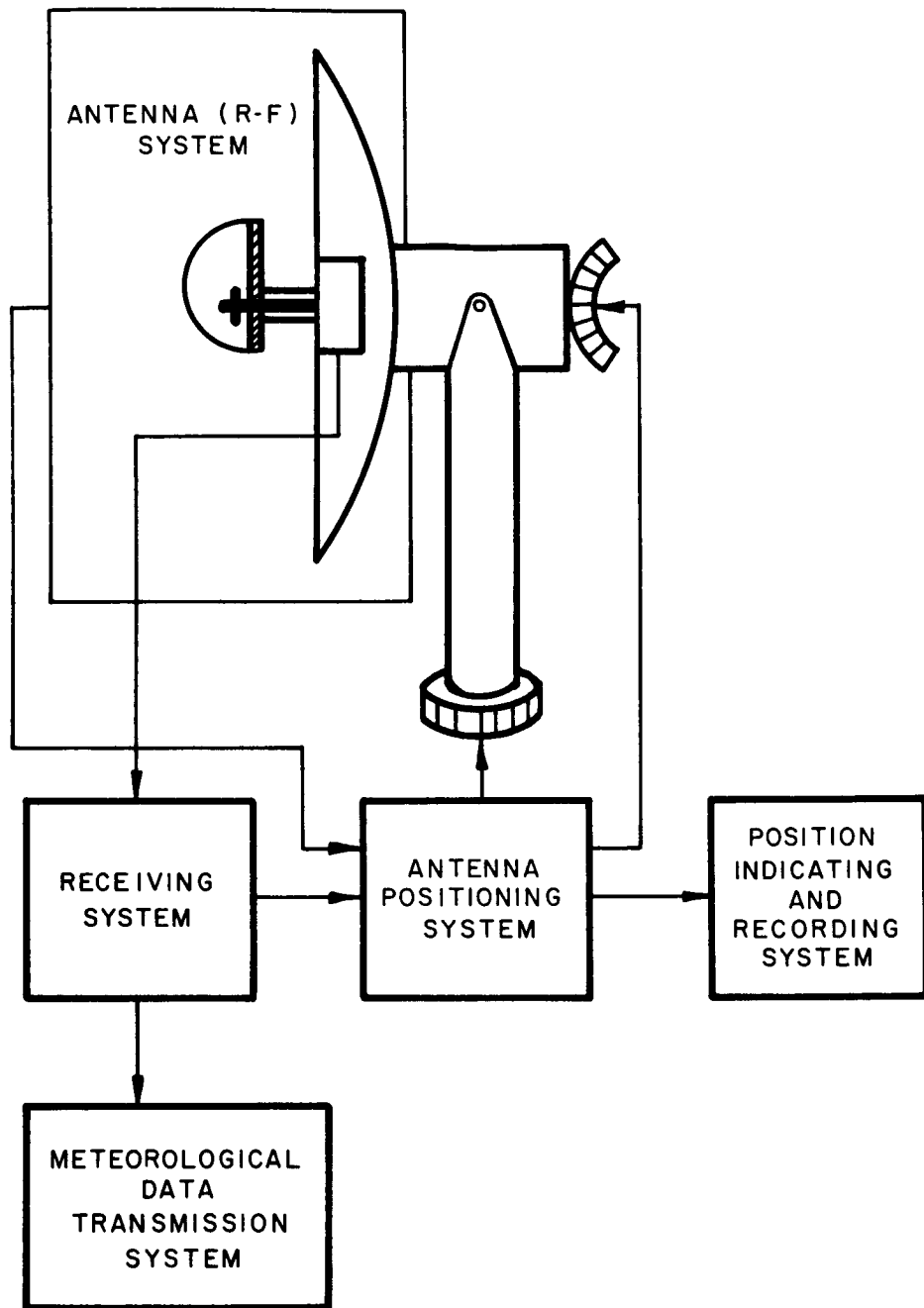


FIGURE 5.3-11 Rawin Set AN/GMD-1A, Systems

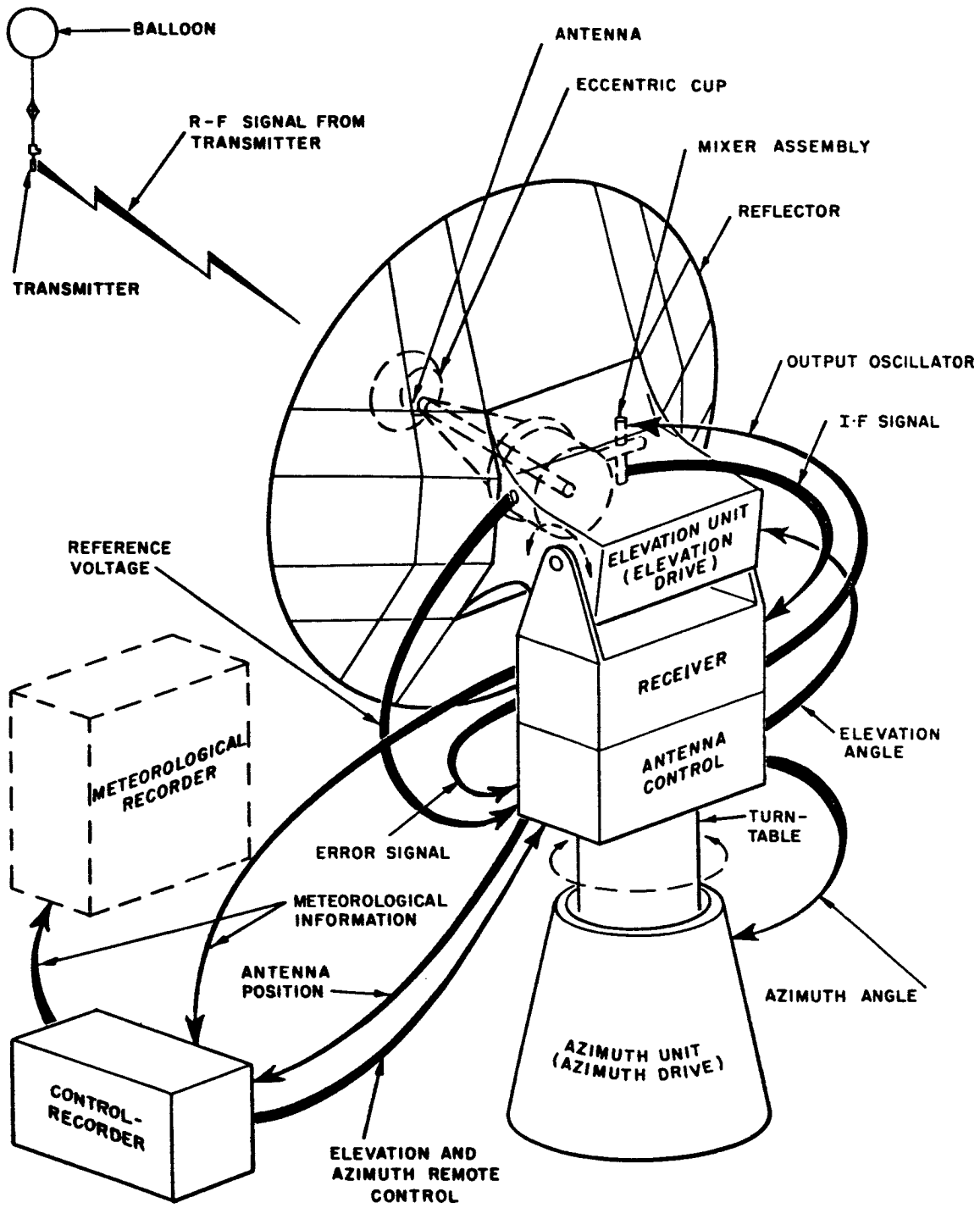


FIGURE 5.3-12 Rawin Set AN/GMD-1B, Functional Diagram

The antenna positioning system receives the detected sinusoidal signal from the receiving system. It rejects the pulse modulation and then amplifies and compares the sinusoidal content with two reference voltages from the reference voltage generators. These reference voltages correspond to the elevation and azimuth components of the position of the antenna axis. This results in two dc voltages, one for elevation and one for azimuth. The magnitude and polarities of these voltages are indicative of the magnitude and direction of the angular difference of the radiosonde with respect to the electrical axis of the antenna. The azimuth error voltage is applied to the azimuth drive to position the antenna reflector in azimuth. The elevation error voltage is applied to the elevation drive to position the antenna reflector in elevation. Since the position of the rocketsonde is constantly changing, the azimuth and elevation drives are constantly positioning the antenna reflector to track the rocketsonde. Error voltages can also be introduced so as to track the rocketsonde manually.

The elevation and azimuth angles of the antenna are indicated and recorded by the Rawin set and are recorded at successive instants of time.

The receiver covers a band from 1655 mc to 1705 mc and will operate in either AM or FM mode. AM mode is utilized by the current dart system. The modulation type, when viewed from the carrier, is PDM-AM in that the intelligence is impressed upon the carrier in the form of negative pulses of sufficient magnitude to exceed 100% AM and hence terminate the carrier for the duration of each pulse. The repetition of the carrier terminating pulses contains the data. This technique results in pulses of carrier frequency energy of varying duration as a function of the data transmitted. The incoming signal is mixed with the local oscillation frequency in a wave guide, and a 30 mc IF is detected in the receiver which reconstructs the chain of pulses originally impressed upon the carrier. These pulses are then differentiated, and the resulting positive pulse from the trailing edge is used to trigger a multivibrator which results in a train of pulses of very constant amplitude and duration. These pulses are fed into a self-balancing servosystem which positions a pen on a strip chart recorder. The recorder pen is displaced as a function of pulse repetition frequency and can accommodate rates up to 200 pps. Various auxiliary amplifier systems have been used to enhance the incoming signal and, of these, the parametric amplifier seems to be the most satisfactory.

The meteorological data transmission system receives the detected signal from the receiving system. It then rejects the sinusoidal modulation for antenna positioning, shapes and amplifies the meteorological pulses and passes them to the meteorological recorder. The meteorological recorder (which is not an integral part of the Rawin set) converts the pulses, whose rate is determined by the sensor resistance, into a graphical representation of sensor resistance as a function of time. More detailed information concerning this receiving system can be found in the technical manual concerning the receiver (Rawin Set AN/GMD/1A).

The meteorological recorder AN/TMQ-5 is used in conjunction with the AN/GMD-1 and AN/GMD-2 receivers. A block diagram of the recorder is shown in Figure 5.3-13. The variable-rate pulses from the receiver are fed to the frequency converter of the recorder which converts them to a dc voltage. The value of the dc voltage at any instant is proportional to the pulse frequency which created it. This dc voltage excites a servo system that positions a pen whose displacement from its zero position on a calibrated chart is again proportional to the pulse frequency which in turn was determined by the value of the temperature sensor resistance in the rocketsonde.

Detailed information concerning the meteorological recorder can be found in the technical manual (Radiosonde Recorder AN/TMQ-5) concerning the recorder. Specifications for the AN/GMD-1 are presented in Table 5-13.

5.3.4.2.2 Rawin Set AN/GMD-2.

The GMD-2 is essentially the same as the GMD-1 with the addition of a slant range determination system. In fact a number of GMD-1 sets have been converted to GMD-2 sets by adding a 403 mHz transmitter and a ranging modulation discriminator. A block diagram of the AN/GMD-2 is presented in Figure 5.3-14. The essential difference between this and the GMD-1 system is the addition of 403 mHz transmitted signal containing an 81.94 kHz sine-wave modulation to the airborne instrument. The airborne instrument contains a 403 mHz receiver which accepts the ground-station transmitted ranging signal, detects the 81.94 kHz modulation and frequency modulates the airborne 1680 mHz transmitter at the 81.94 kHz rate. Thus the airborne instrument operates as a transponder in addition to a data telemetry transmitter. The meteorological data is AM pulse modulated as in the case of the GMD-1 system.

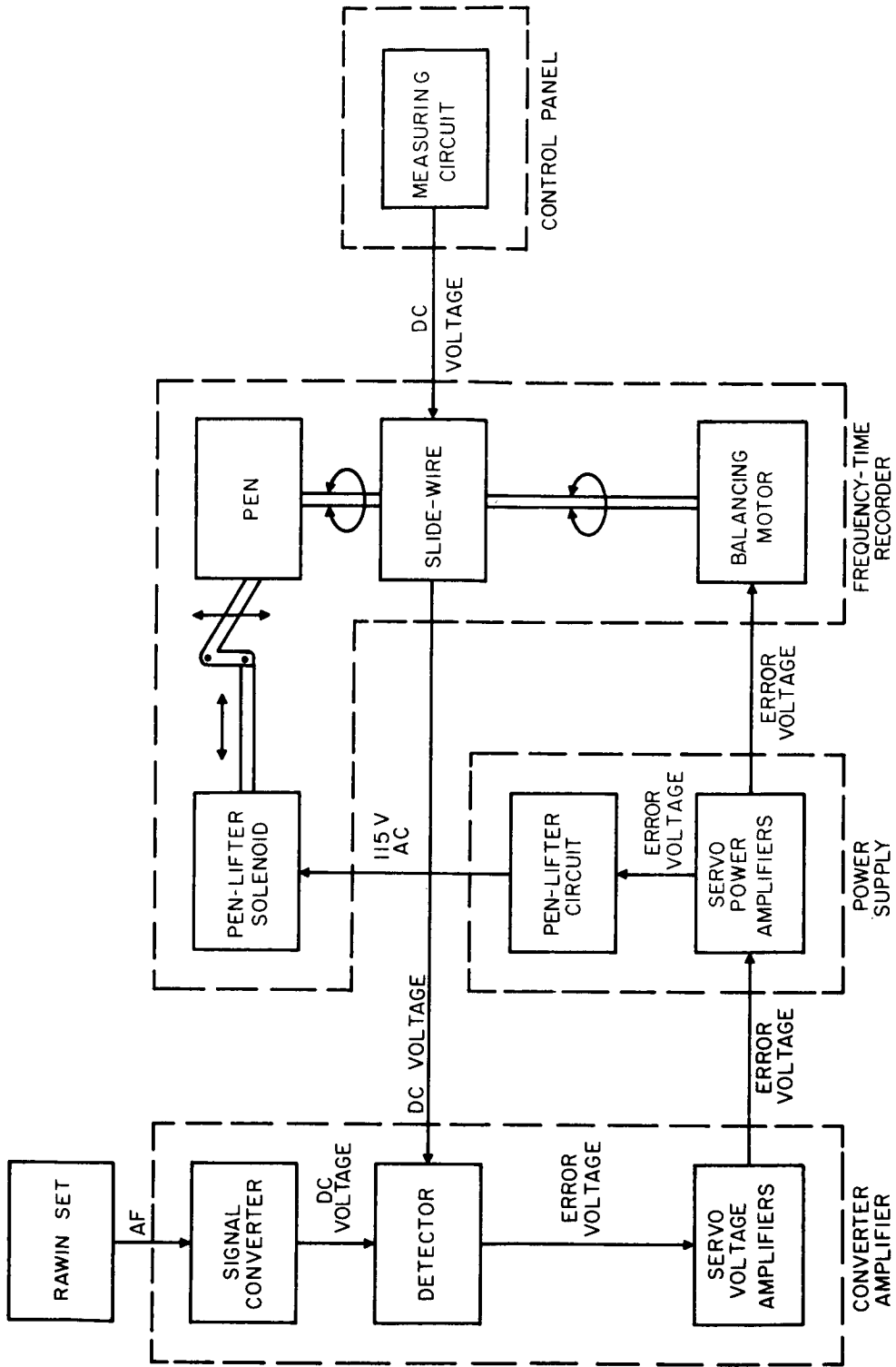


FIGURE 5.3-13 Block Diagram of the TMQ-5 Recorder

TABLE 5-13

AN/GMD - 1 SPECIFICATIONS

R-F System

Scanning	Conical
Antenna	Dipole
Reflector	Parabolic
Spinner motor	Induction
Spinner generator	2 phase, self-excited; 15 volts, 30 cps

Receiving System

Type	Superheterodyne
Normal frequency	1680 mc
Intermediate frequency	30 mc
Frequency control	AFC or manual
Local oscillator	Tube type
Local oscillator frequency	1650 mc
Input impedance	50 ohms
Data	Error signal
Modulation	FM or PM
Bandwidth	0.8 mc or 2.5 mc

Antenna Positioning System

Tracking	Automatic, local manual, remote manual
Drive motors	60 volts dc, 1.4 amperes, 1/20 hp at 500 rpm
Tachometer generators	2.1 volts dc at 100 rpm

Position Indicating and recording System

Synchro transmitters	Type IV, single phase, self-synchronous; 115 volts, 60 cps
Synchro receivers	Type V, single phase, self-synchronous; 115 volts, 60 cps
Recording	Tape (digital imprint)
Printer motor	Synchronous type; 115 volts, 60 cps

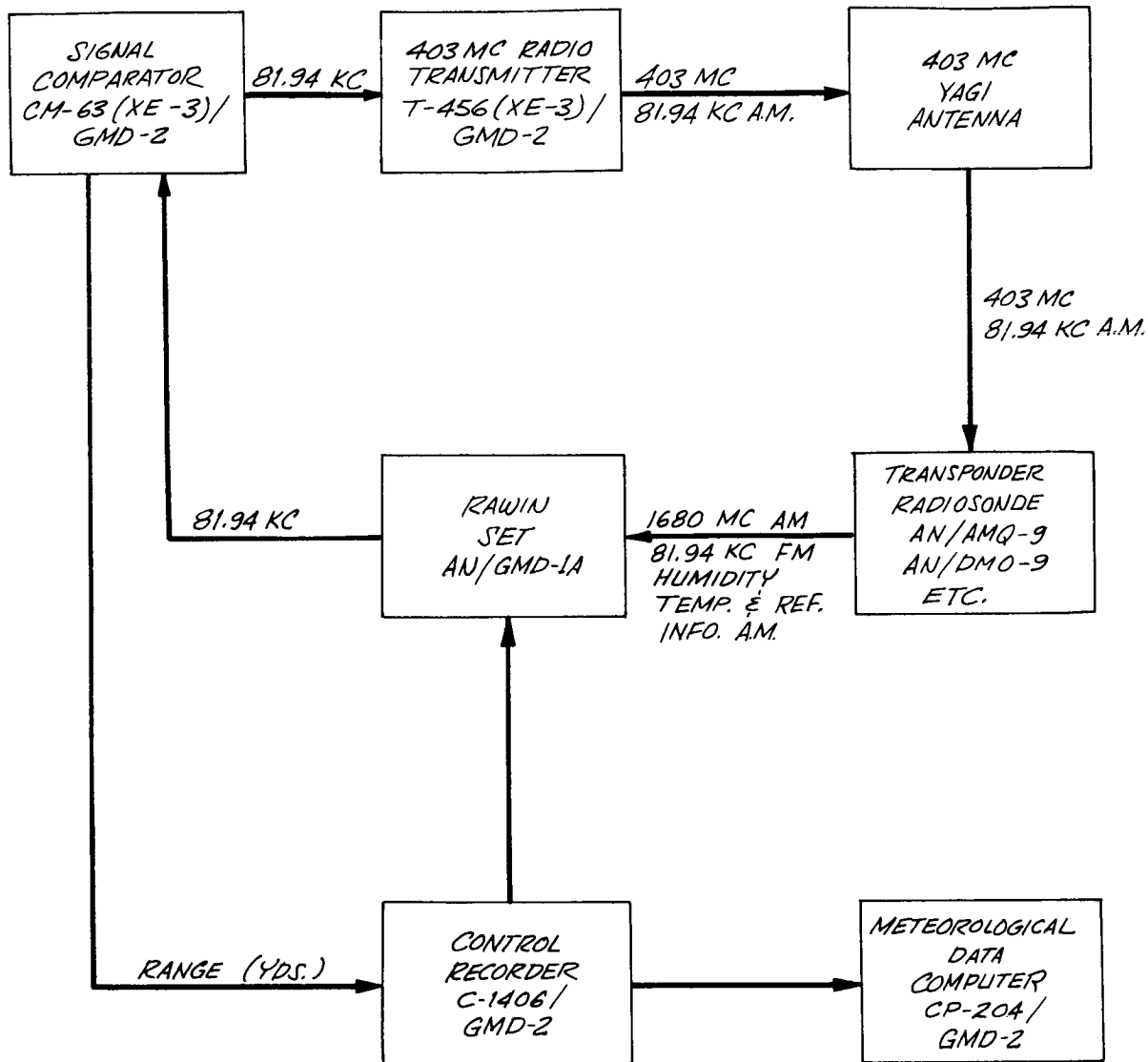


FIGURE 5.3-14 Rawinsonde System AN/GMD-2, Block Diagram

When the ranging signal is received at the ground-equipment, the 81.94 kHz modulation is detected and its phase is compared with the transmitted signal to determine the time for a round trip, i.e., from the ground station to the sonde and back to the ground station. One complete phase shift of the ranging modulation is equivalent to 4,000 yards, therefore, a slant range of 2,000 yards.

The GMD-2 system is currently in operation at a limited number of locations with both balloon sondes and rocket sondes. The main disadvantage with the system is that the range data can be ambiguous if the signal is lost for an appreciable period of time. The ranging modulation places the sonde range within a range of 2,000 yards but does not indicate which 2,000 yard increment it is unless an accurate count of completed phase shifts is made from a known point in space or launch. A coarse ranging provision can be added to the GMD-2 as a modification. This coarse ranging modulation determines the slant range with an accuracy sufficient to determine the 2,000 yard increment. The regular ranging modulation is then used to determine the accurate slant range.

The wind error from GMD-2 data is a function of the slant range and averaging period. Typical wind errors are presented in Figure 5.3-15.

5.3.4.2.3 Rawin Set AN/GMD-4.

The GMD-4 is essentially the same as the GMD-2 with the addition of a coarse ranging facility and automatic data processing for both the tracking data and the meteorological data. A simplified block diagram is presented in Figure 5.3-16. When signal dropouts or temporary loss of signal from the airborne instrument occur, the ranging modulation is momentarily interrupted and then started again. The time of arrival of the reinstated signal places the slant range data into the proper 2,000 yard increment and the normal 81.94 kHz modulation is used for the required accurate determination. Range rate data recording is also improved over the original GMD-2.

5.3.4.2.4 NASA Radiosonde ADP System.

A number of schemes for automatic and semi-automatic processing of radiosonde data have been devised with varying degrees of success. An operational automatic data processing system was developed for use with the AN/GMD-2 Rawin Set. This system was supplied by the Bendix

STATISTICAL AN/GMD-2 WIND ERRORS VS SLANT RANGE
 FOR AVERAGING TIMES OF 12, 24 AND 120 SECONDS (REF. 1)

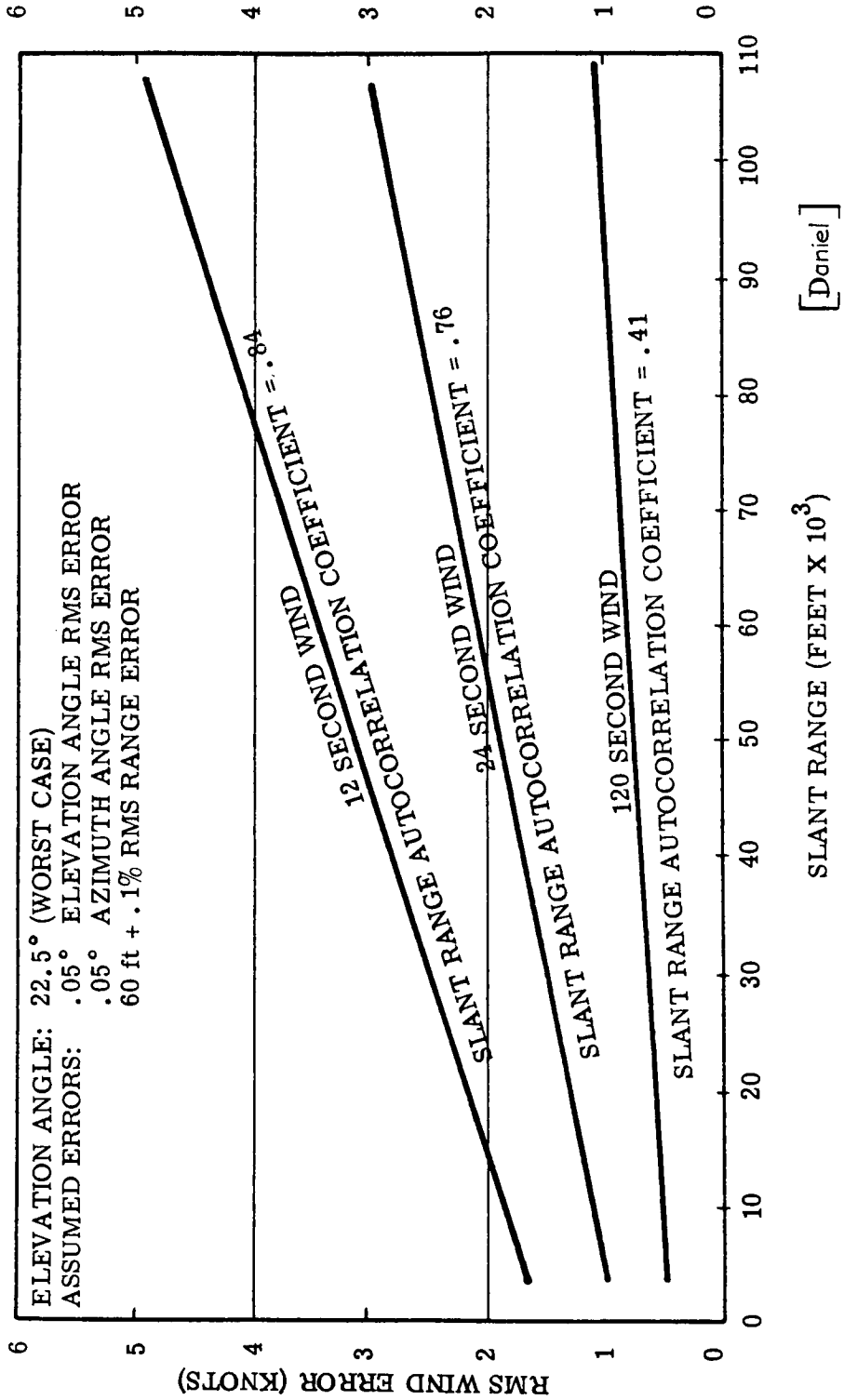


FIGURE 5.3-15 Statistical AN/GMD-2 Wind Errors Vs Slant Range for Averaging Times of 12, 24 and 120 Seconds

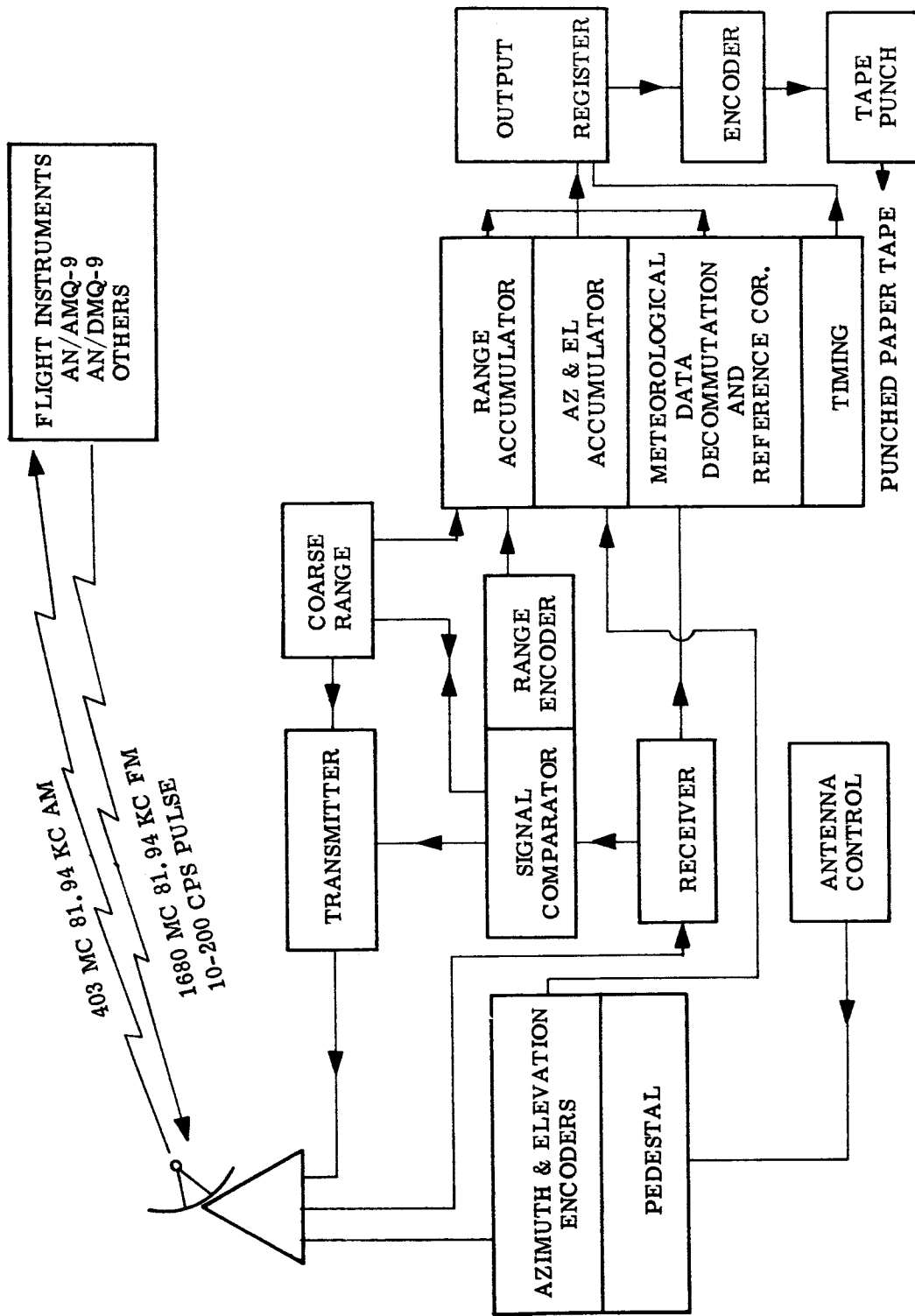


FIGURE 5.3-16 SIMPLIFIED BLOCK DIAGRAM OF AN/GMD-4 SYSTEM

Friez Instrument Division to NASA/MSFC and installed at the Huntsville facility in September 1963. The system was designed with a number of functional systems utilizing standard "off-the-shelf" meteorological equipment. These items required only minor modifications, in some cases, to provide system interface. The remaining units which were wholly designed and fabricated at Bendix Friez include the tracking data Digitizer, the Converter-Detector and the Control-Decommutator. The later two units contain the logic and control circuits essential for automation of the met data. A data processor commands a printing summary punch to produce punch cards as desired.

The AN/AMQ-9 radiosonde unit is utilized with the following telemetry modifications:

1. A special commutator designed to include 1/2-second reference segment preceding each temperature and each humidity segment. These reference identifiers clearly indicate a change from one sensor to the next, so that close or equal signal ratios are not confused, and that noise or signal dropouts are not mistaken for frequency changes.

2. Since the slant range is desired in meters, the ranging modulation frequency of the sonde is changed from 81.94 kHz. Modifications of the Rawin set transmitter and comparator are necessary to be compatible with the frequency change, and the data processor is used to handle the printout, the visual indication and the monitoring of slant range data obtained from the Rawin set.

The difficulty in recognizing the reference frequency is the spread of 40 pulses per second allowed by the specification and the fact that zero humidity can produce a pulse rate just 15 pulses per second below the actual reference frequency. To attempt to recognize reference as any frequency above 170 pulses per second would erroneously detect a zero percent humidity frequency (175 pps) of a radiosonde having a reference frequency of 190 pulses per second. To eliminate this difficulty, the automatic data processor stores and updates the reference frequency continuously during the flight. The reference frequency can then be automatically detected as that frequency within 10 cycles per second of the stored reference. This scheme will be workable for all normal shifts in the radiosonde blocking oscillator.

The measurement of the temperature and humidity data is made in the voltage realm with 0.905 volts corresponding to 190 cycles per second. The linear conversion to voltage is accomplished in the Converter-Detector unit. Referring to the block diagram in Figure 5.3-17, the output of the frequency to DC voltage converter is connected to the signal loss detector, the "reference detector," and the A to D Converter. The A to D Converter is a digital voltmeter-ratiometer with front panel decimal display. This unit measures the reference frequency (voltage), the temperature ratio, and the humidity ratio. The "signal loss detector" will actuate if the frequency falls below 10 cps (0.047 VDC) for more than one half second. The "reference detector" will actuate if the incoming frequency is within 10 cps of the stored reference frequency.

The tracking of the radiosonde commutator is accomplished by a stepping switch. Each time the "reference detector" is actuated, the stepping switch is advanced. The stepping switch "home" position corresponds to the reference segment of the commutator with the remaining five positions corresponding to the temperature and humidity segments. The stepping switch therefore keeps the synchronism with the radiosonde commutator. When the "reference detector" is actuated longer than 1.5 second (as it is during the 3.9 second reference frequency transmission) the stepping switch will "home" unless it is already in the "home" position. A word description of the sequence of events, starting with the reference frequency, will show the signal flow through the simplified block diagram. The reference detector actuates for 3.9 seconds and immediately advances the stepping switch to "home" from the last temperature position. After 1.5 seconds, the "home detector" generates a home command which will reestablish synchronism if the stepping switch had fallen out of step. After 2.2 seconds total delay, a measure command is sent to the A to D Converter. The mode command of the A to D Converter is connected through the stepping switch to the VOLTS mode. The DC input (reference frequency) is measured; the decimal output is converted to binary coded decimal (BCD), and appears at the BCD-to-Analog Converter input. Within 0.33 second after the A to D Converter receives its measure command, it generates an end-of-measure command which goes through the "signal loss detector," the stepping switch, the "reference quality" circuit, and the "reference detector". The command then causes the BCD-to-Analog Converter to store the data appearing at its input. The "reference quality" circuit will inhibit storage of the reference frequency if it is more than 5 cps below the previously stored reference. This guards against storing the reference frequency during even a slight signal dropout.

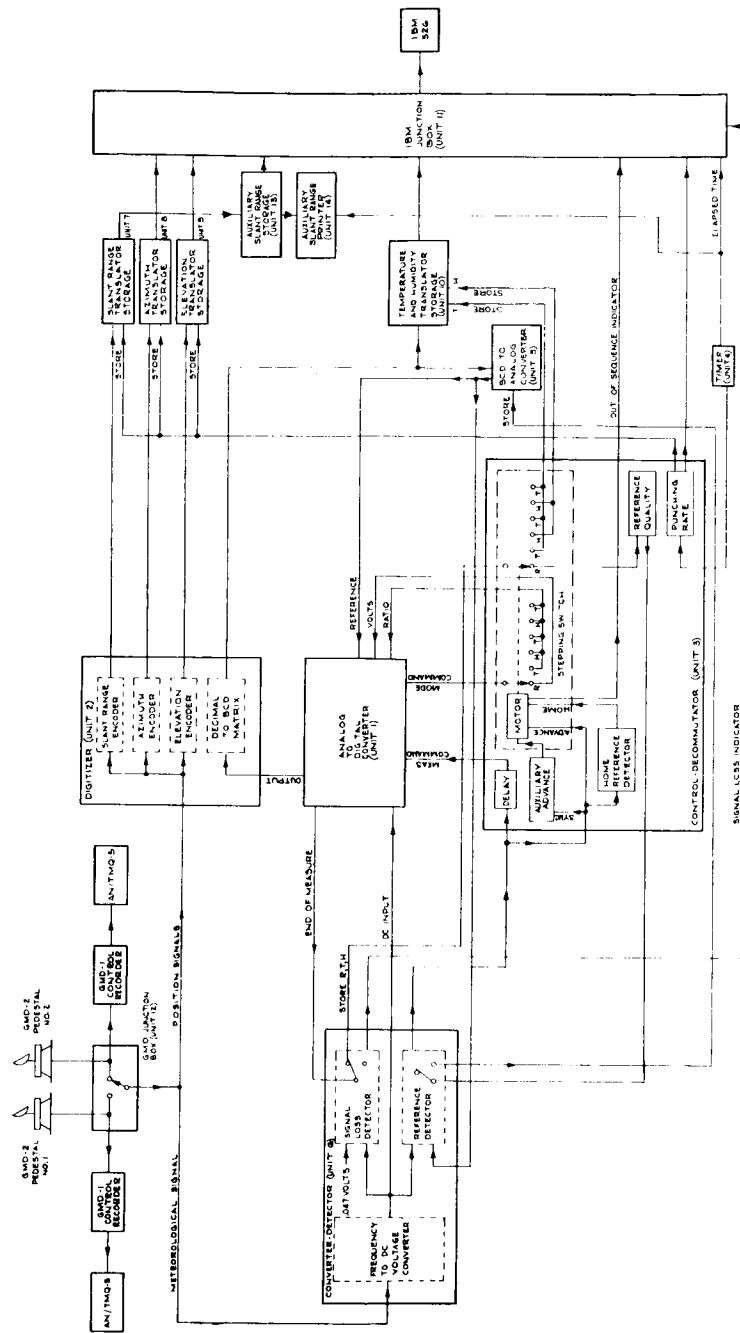


FIGURE 5.3-17 RADIOSONDE ADP SYSTEM, SIMPLIFIED BLOCK DIAGRAM

There is no reference identifier preceding or following the reference data transmission. The stepping switch advances to the first temperature position after 3.2 seconds total delay (by means of a circuit not shown on the simplified block diagram). At 2.2 seconds later than the advance of the stepping switch, a measure command is sent to the A to D Converter to measure the incoming temperature frequency (voltage). Now the A to D Converter mode command is switched to "ratio" to measure the DC input as a ratio of the reference voltage from the BCD to analog converter. Within 0.33 seconds after the A to D Converter receives its measure command it generates an end of measure command which goes through the "signal loss detector", and the stepping switch to the Temperature and Humidity Translator Storage. The command causes the output of the A to D Converter to be stored in the temperature section of the Temperature and Humidity Translator Storage.

The stepping switch is advanced to the next, or humidity, position when the first reference identifier actuates the "reference detector". At 2.2 seconds after the stepping switch is advanced a measure command is sent to the A to D Converter. This time the store command appears on the "store H" line of the Temperature and Humidity Translator Storage unit. The stepping switch is advanced each time a reference identifier is received until the long reference frequency is received when the entire sequence described above is repeated.

In case one reference identifier is not received due to a signal dropout the Control-Decummutator contains an auxiliary advance circuit which will advance the stepping switch. No measure command will be generated since the "reference detector" will not have actuated. Synchronization of the stepping switch with the radiosonde commutator is maintained, and the temperature or humidity information punched out on the IBM card is the previously stored data.

The azimuth, elevation, and slant range data from the pedestal are in the form of synchro-signals. By means of a selector switch on the Control Decummutator front panel, the operator switches to the desired pedestal and control recorder. Reed relays within the GMD Junction box connect the Data Processor to the synchro-signals. In the Digitizer, the synchro signals position digital encoders and frontal panel indicators by means of servo-motor drives. The digital outputs are stored in their respective Translator Storage units on command from the Timer. Azimuth, elevation and slant range data are stored simultaneously to be punched out on the card identified with the proper elapsed time.

The ADP system is designed to give the operator the ability to observe the output in printed form on the IBM cards, to observe the meteorological data on the A to D Converter, and to observe the azimuth, elevation and slant range data. The printed card can be compared with AN/TMQ-5 record to ensure that the meteorological data are being processed properly. In the event that the IBM 526 printing summary punch would hang up due to a damaged card or some other reason, the raw data will be available from three paper records. The azimuth and elevation angles are printed (with time) by the C-577 Control Recorder. The slant range and elapsed time are printed by the Auxiliary Slant Range Printer, and the meteorological data are recorded by the AN/TMQ-5 Meteorological Recorder.

5.3.4.3 Rocketsonde Instrumentation.

Although twenty-three rocketsonde instruments are listed in the "Data Report, Meteorological Rocket Network Firings, World Data Center A", (see Table 5-14), only five of these instruments are currently used on an operational basis. Four of these five instruments are used with GMD equipment and are described in the following section.

5.3.4.3.1 Stratospheric Temperature Sonde (STS-1)

The STS-1 instrument in Figure 5.3-18 has been developed for the Arcas by Ballard, et. al., at WSMR as an improved version of the Delta I for operation with the AN/GMD-1 ground-station. The improvements have included the reduction of power in the measuring circuit, the use of a thin-film Mylar thermistor mount and a better matching of the sensor input resistance calibration of the sonde with the thermistor calibration to achieve better accuracy over the full temperature range. A circuit diagram of the STS-1 is presented in Figure 5.3-19. The temperature data measurement circuit consists of a current amplifier transistor which feeds the amplified thermistor current into a unijunction relaxation oscillator to form data or reference pulses at a rate depending upon sensor or reference resistance. The pulses are fed to a buffer amplified transistor which AM modulates to cut off a standard pencil triode 1680 MHz cavity-oscillator radiosonde transmitter tube. A solid-state switching circuit and a relay are employed to switch to and from the temperature sensor and reference resistor.

TABLE 5-14

ROCKETSONDE INSTRUMENTS

<u>INSTRUMENT</u>	<u>STATUS</u>
Delta	Obsolete
DMQ-6	Obsolete
Gamma	Obsolete
Borg-Warner	Obsolete
Gamma II	Obsolete
Arcasonde	Obsolete
PMR II	Obsolete
Arcasonde 1A *	Operational in Arcas (USAF)
Resistance Wire	British Skua
Metrosonde	Obsolete
Servo-mech Sonde (SMI)	Obsolete
Arcasonde II-A	Experimental
DMQ-9 *	Operational in Arcas (USAF)
Arcasonde II	Obsolete
Datasonde *	Operational in Loki Dart (USAF, USA, USN)
Delta (T.F.)	Obsolete
Stratospheric Temp. Sonde (STS)*	Operational in Arcas (WSMR)
Mini Loki (S.T.S.M.L.)	Obsolete
Echasonde	Obsolete
Solid State Arcasonde	Developmental
Hasp WOX I-A *	Operational (USN)
Hasp WOX 3-A	Obsolete

Note: * Operational Instruments

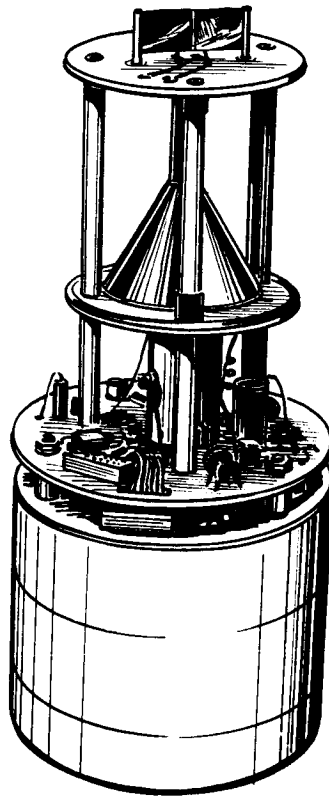


FIGURE 5.3-18 Stratospheric Temperature Sonde STS-1

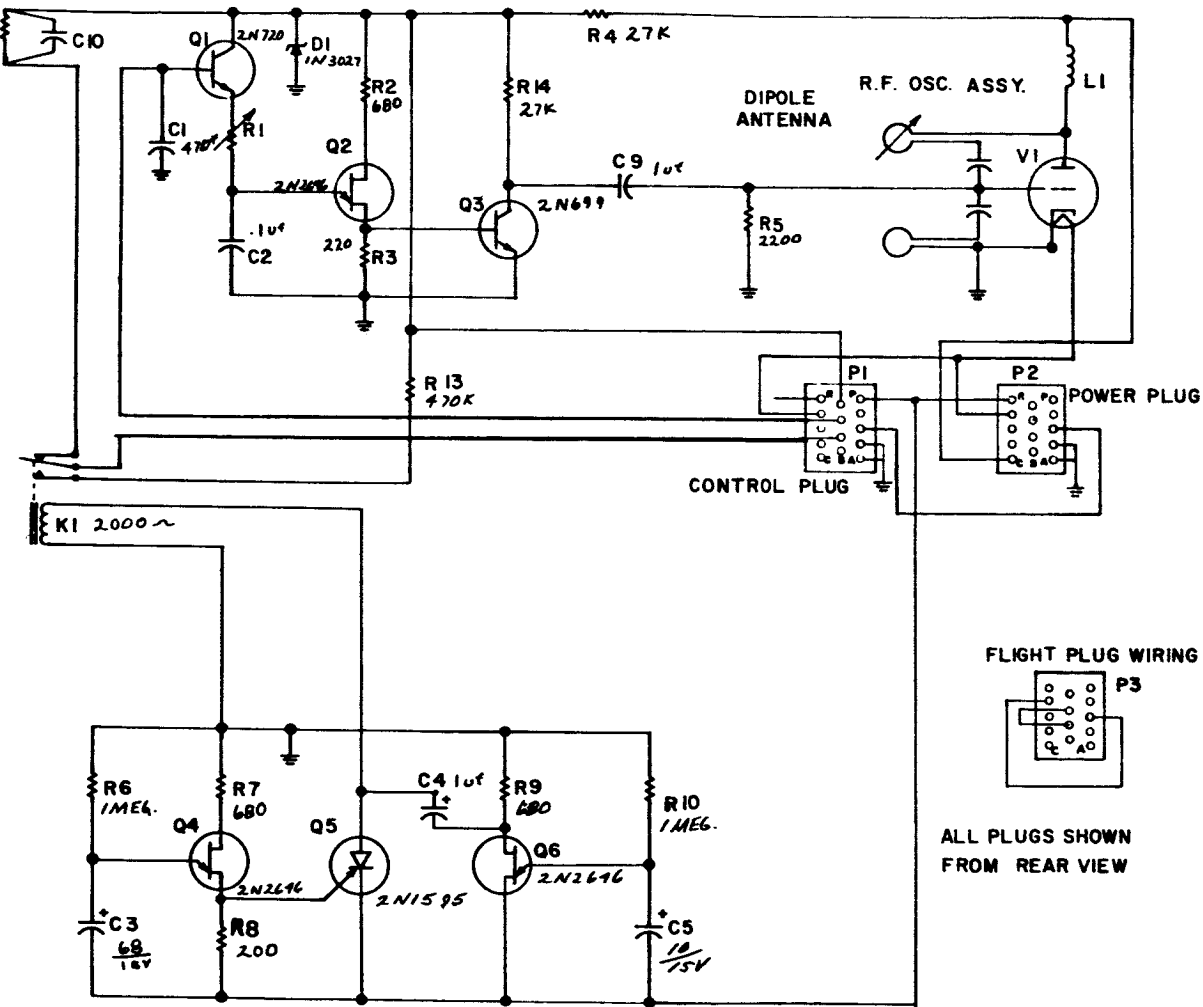


FIGURE 5.3-19 Stratospheric Temperature Sonde STS-1 Electrical Circuit Diagram

The transmitter oscillates at a nominal frequency of 1680 megacycles and generates approximately 500 milliwatts of power at a plate voltage of 120 volts. This gives an extreme range of approximately 160 km for small quadrant elevation angles when the transmitter is used in conjunction with the Rawin receivers AN/GMD-1 and AN/GMD-2. The antenna is a brass dipole above a copper, conically shaped ground plane and serves to match the tube impedance to that of the antenna.

5.3.4.3.2 Arcasonde - 1A.

The Arcasonde-1A as shown in Figure 5.3-20 has been developed by Atlantic Research Corporation for use with the Arcas rocket as an AN/GMD-1 type instrument. This instrument includes a thin-film Mylar thermistor mount, a replaceable dry-cell power pack, a blocking oscillator data circuit and an electronic commutator. The Arcasonde-1A telemetry package consists of an integral-cavity-oscillator transmitter, operating in the 1660-1700 mHz band, modulated by a blocking-oscillator-type pulse generator at rates between 10 and 205 pulses per second. An electronic commutator provides a reference pulse rate of six seconds duration after each 20 seconds of thermistor dwell. The instrument is modular in designing; complete functional units can be interchanged or replaced in the field.

The instrument components are shown in Figure 5.3-21 and a simplified block diagram is presented in Figure 5.3-22. Arcasonde 1A specifications are presented in Table 5-15.

5.3.4.3.3. AN/DMQ-9.

The DMQ-9 instrument, as shown in Figure 5.3-23, has been developed by USAF-CRL for use with the Arcas rocket as a GMD-2 type transponder instrument.

The basic instrument package is a 3.3 lb instrument which consists of a 403 megacycle self-quenching super-regenerative receiver, a 1680 megacycle radiosonde transmitter, receiving and transmitting antenna assemblies, motor actuated sensor switches, electronic circuitry to properly modulate the transmitted carrier and a battery power supply.

The 403 megacycle receiving antenna system is located directly above the power supply module. Four 1/2 inch wide steel strips making up the receiving elements are eyeleted to a glass epoxy disc and retained in a folded position by the nose cone. After the nose cone is

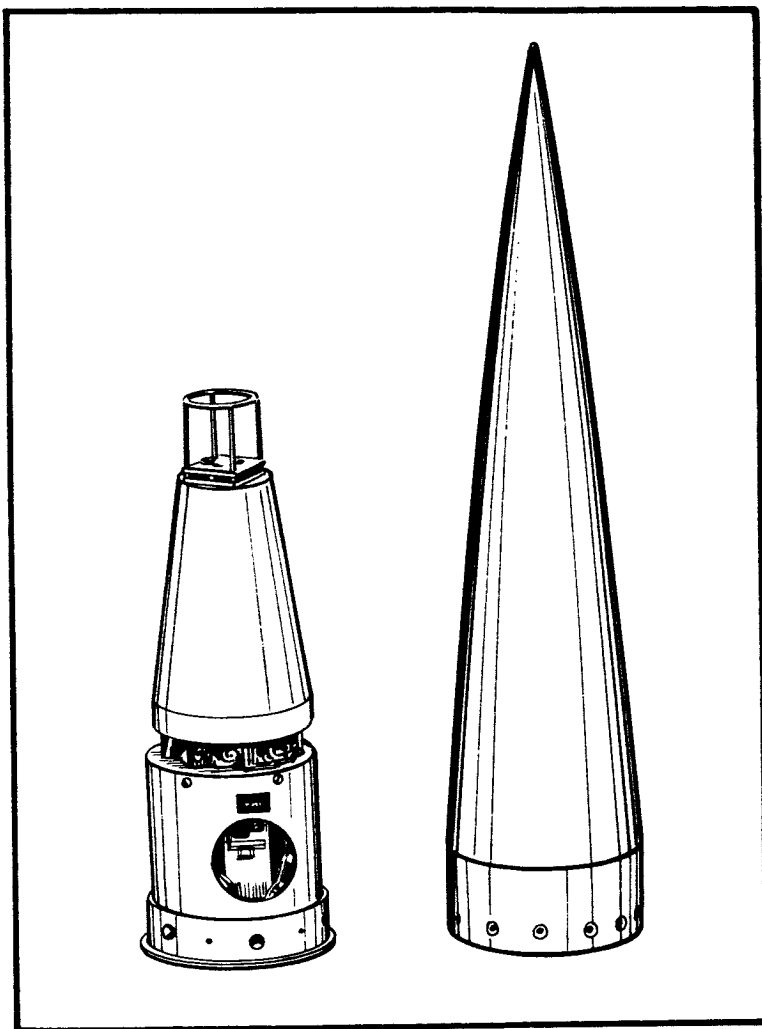


FIGURE 5.3-20 ARCASONDE 1A Instrument & Nose Cone

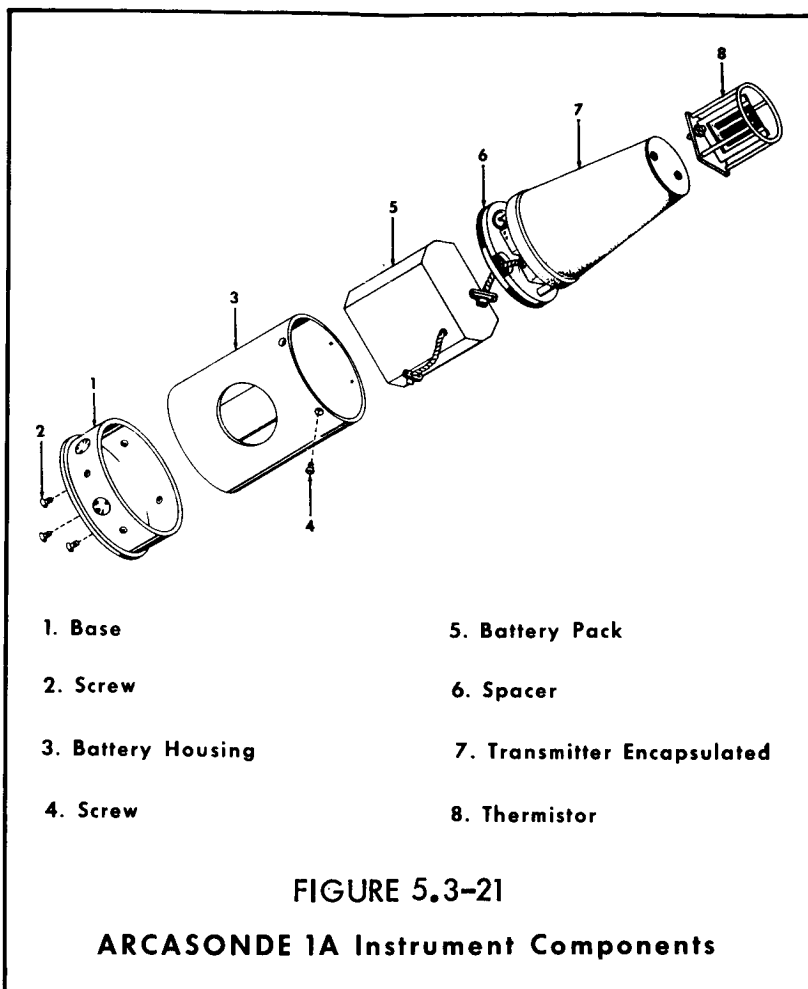


FIGURE 5.3-21

ARCASONDE 1A Instrument Components

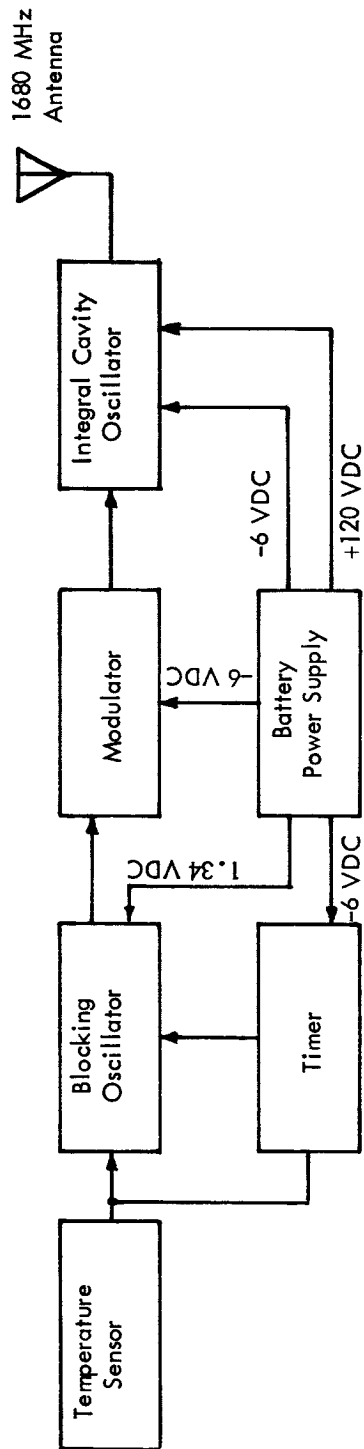


FIGURE 5.3-22 ARCASONDE 1A BLOCK DIAGRAM

TABLE 5-15

ARCASONDE - 1A SPECIFICATIONS

Height	29.6 cm (11.66 in)
Maximum Diameter	11.1 cm (4.38 in)
Weight	2.04 kg (4.5 lb)
Transmitter Type	Pulse-modulated cavity oscillator
Frequency	1660-1700 MHz
Modulation	10 - 205 pps
Power Output	300 mW
Antenna	Helical Slot
Temperature Sensor	10-mil coated bead thermistor
Power Supply	Dry battery pack
Battery Life	3 Hours (at 20° C)

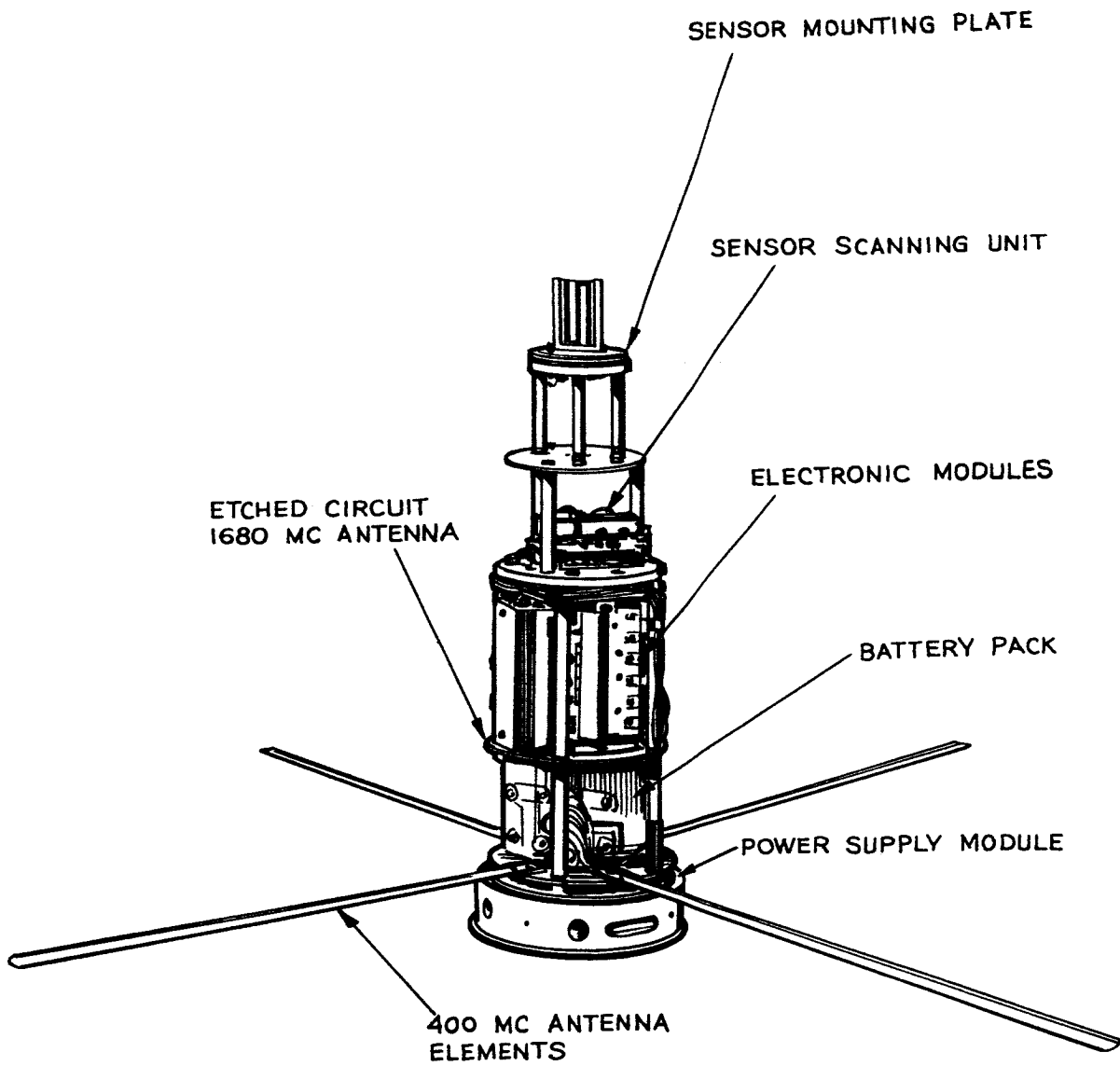


FIGURE 5.3-23 AN/DMQ-9 Rocket Instrument Package

discarded at apogee, these elements open to a position normal to the longitudinal axis of the package. The battery pack is clamped against the receiving antenna deck. Access is provided to the battery area by removing the two screws by which the battery holder is attached to and forms an integral part of the structure.

The next section of the package consists of three modules: the 1680 megacycle cavity oscillator (encapsulated in foam plastic), the self-quenching super-regenerative receiver, and the blocking oscillator and 81.94 kc slant ranging signal amplifiers. The last two modules are shielded against r.f. interference. The lower disc to which these modules are attached comprises the etched circuit 1680 megacycle dipole antenna.

A scanning switch subassembly, consisting of a motor driven cam that actuates two snap-action switches, is located immediately above the electronic modules. The motor shaft rotates at 3 rpm and the four lobe cam is of such design as to alternately switch between reference and temperature with a dwell of approximately 4.5 seconds on either, plus and "off" time of approximately 0.5 second preceding each switching operation.

A sensor mounting plate is located at the forward end of the instrument package to accommodate a plug-in type sensor assembly.

The electronic circuitry consists of a 403 mHz self-quenching super-regenerative receiver which receives and detects the 81.94 kHz amplitude modulated carrier from the Rawin Set AN/GMD-2 transmitter. The 81.94 kHz signal is in turn retransmitted on a 1680 mHz carrier (FM) to the Rawin Set where phase comparison of the outboard and incoming modulation permits direct measurement of slant range. Switching between the meteorological sensor and reference resistor is accomplished with cam actuated snap-action switches and the signals derived therefrom are used to frequency modulate the 1680 mHz transmitter at a rate of approximately 20 to 200 cycles per second. Power for the sonde is obtained from a silver oxide-zinc battery pack in conjunction with a DC to DC converter.

A block diagram of the circuit shown in Figure 5.3-24. Figure 5.3-25 is a schematic diagram of all the components indicated in the following detailed description.

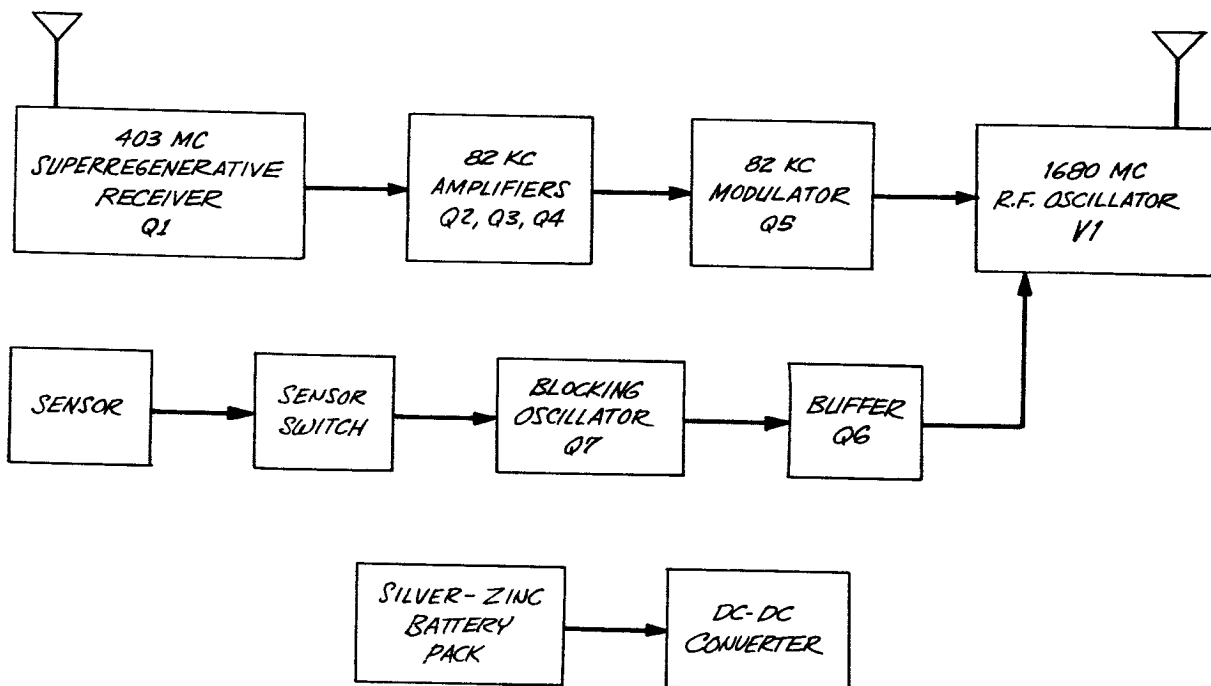
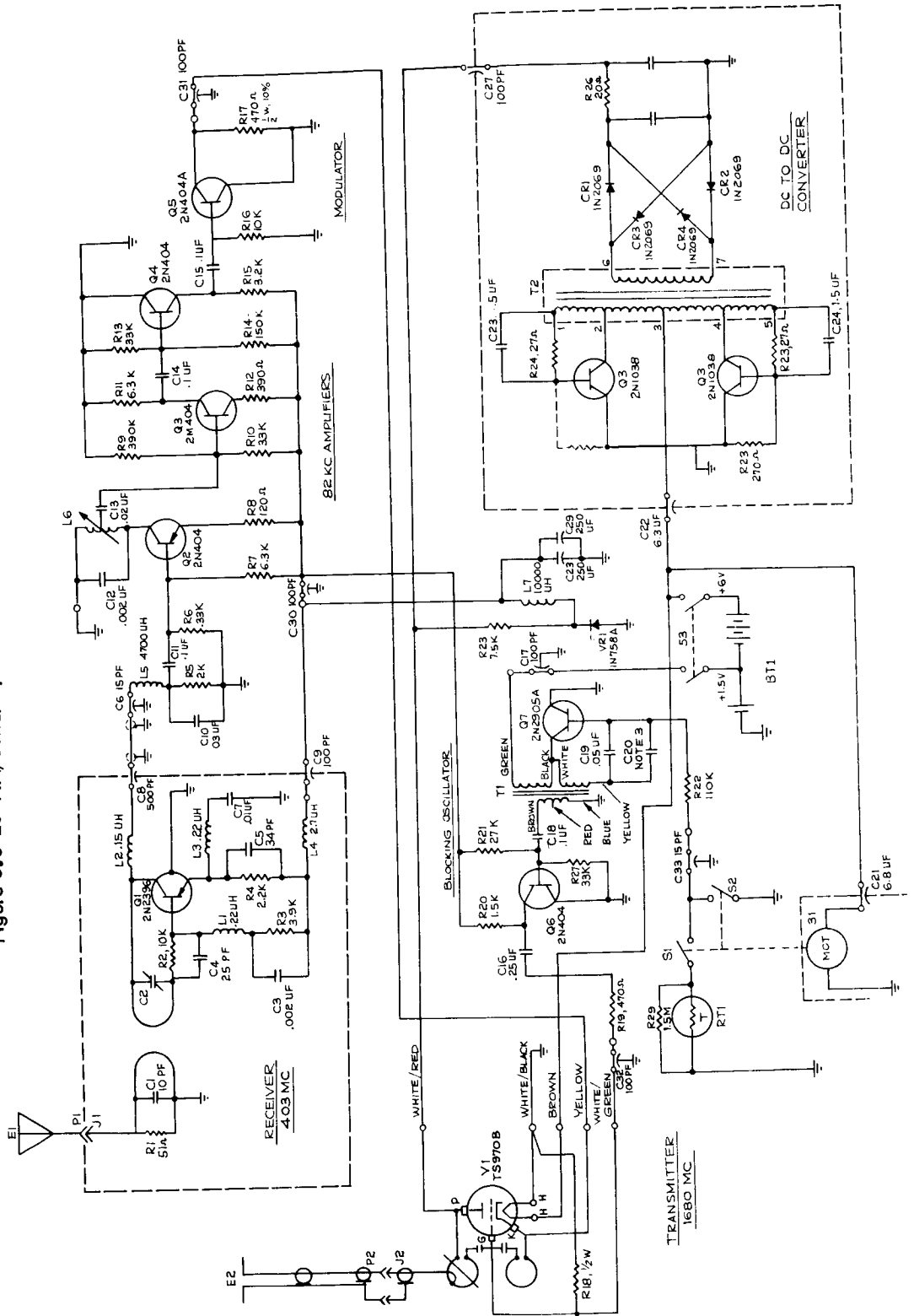


Figure 5.3-24 AN/DMQ-9, Block Diagram

Figure 5.3-25 AN/DMQ-9, Schematic Diagram



Self-Quenching Super-regenerative Receiver.

The 403 mHz signal received by the sonde is inductively coupled from the antenna to the input tank of the super-regenerative detector Q1. Trimmer capacitor C2 is the only adjustment necessary to tune the receiver to the specific operating frequency of the Rawin Set transmitter. The quench voltage, a saw-tooth signal approximately two to three volts in amplitude at the collector of Q1 and having a frequency of approximately 400 kHz, is generated within the detector stage itself. This frequency is determined principally by C5 and the distributed parameters of the circuit. The effect of the quench signal is to alternately drive the detector into and out of self-oscillation.

The initial portion of the self-oscillating condition may be considered a sampling period at which time the amplitude of the 81.94 kHz modulation on the 403 mHz carrier influences the performance of the stage during the remainder of that particular quench cycle. Thus, over a number of quench cycles the collector current of the super-regenerative detector consists of components at the modulation frequency (81.94 kHz), the quench frequency (400 kHz) and the carrier frequency (403 mHz). These latter two frequencies are appreciably attenuated from the desired 81.94 kHz signal by means of components L2 and C8, and L5 and C10 respectively.

81.94 kHz Amplifiers and Modulator.

The super-regenerative detector is followed with an amplifier, Q2, having an output tank, C12 and L6, tuned to resonance at 81.94 kHz. The overall gain of this stage is approximately 15. A portion of the 81.94 kHz signal appearing across the tank is tapped off and further amplified by a factor of approximately 10 in Q3. No further amplification takes place through Q4 which serves as an impedance matching element between Q3 and the transmitter modulator Q5.

The modulator, an emitter follower is parallel with cathode resistor R17 of the 1680 mHz cavity oscillator, changes the effective cathode bias of the r.f. oscillator as a function of the 81.94 kHz signal. As a result, the oscillator produces a frequency modulated carrier having a deviation of approximately 175 kHz for the 81.94 kHz ranging signal at threshold 403 mHz input to the sonde receiver.

Blocking Oscillator.

The blocking oscillator, Q7, is a transistorized (2N2905A PNP silicon epitaxial), relaxation oscillator which utilized half of the primary windings of transformer T1 for feedback. The other half of the primary is connected to the 1.5 volt supply. The combination of low supply voltage and high reference resistance, R22, in the sensor loop, results in a maximum power dissipation in the temperature measuring thermistor of approximately 6 microwatts. Reference frequency is a function of the inductance of the transformer, the reference resistor, and capacitor C19. If required, padding capacitor C20 is added to give a reference frequency of approximately 190 cycles per second.

Buffer stage Q6, connected as an emitter follower isolates the blocking oscillator from 1680 mHz oscillator. The output of this stage, approximately 0.75 volts peak negative pulses about 85 microseconds wide, is applied to the grid of the transmitter to shift the carrier frequency at the repetition rate generated by the blocking oscillator.

1680 mHz Transmitter.

The 1680 mHz transmitter V1 is, with the exception of a sub-miniature coax cable fitting for the antenna output jack a standard 6562 single tuned cavity oscillator as used in other radiosonde applications. Grid resistor R18 is selected to give a plate current of approximately 30 ma. The transmitter is frequency modulated by both the 81.94 kHz ranging signal and meteorological intelligence as described above. To prevent environmental factors from affecting the transmitter, such as severe frequency shifts or complete failure, the tube is potted in a foam-in-place resin.

Power Supply.

The primary power source for the instrument consists of four Eagle-Picher type 1515 silver oxide-zinc cells that will provide approximately three hours of operation. A freshly activated battery pack has an initial output voltage of about 7 volts which decreases to 6 volts after the first few minutes of use. The full 6 volts potential is used for the transmitter filament, the switching motor and as the input to a DC-DC converter. A 1.5 volt connection feeds the blocking oscillator. A two-pole, double-throw power switch is provided.

The DC-DC converter supplies the operating voltages for the remainder of circuitry. Oscillation of the transistorized converter is initiated by starting resistor R23 in the otherwise symmetrical configuration. The frequency of oscillation is approximately 1 kHz as transistors Q8 and Q9 alternate operation in an on-off condition. Feedback is provided by the base to emitter transformer windings. The square wave voltage produced by this circuit is stepped up by the transformer and the output is rectified by the full wave bridge consisting of CR1, CR2, CR3 and CR4. Final filtering by C25, R26 and C26 provides a substantially ripple-free plate supply of approximately 118 volts which is used for the transmitter directly and also as the source from which zener diode VR 1 provides a nominal 10 volt supply for the receiver, 81.94 kHz amplifiers and buffer stages. Filter components L7, C28 and C29, mounted on the rear of the receiver case, attenuate DC-DC converter noise on the 10 volt line.

To improve the stability of the receiver and to assure satisfactory operation of the super-regenerative detector stage with normal variations in circuit parameters, the supply voltage to the receiver was increased from 6 volts to approximately 10 volts prior to the final series of flight tests. The higher voltage was obtained with a zener diode voltage regulator circuit operating from the nominal 115 volt B+ generated by the DC-DC converter.

Antennas.

The receiving antenna is a configuration of four, half wavelength elements spaced 90 degrees apart on the mounting board. These elements feed half wavelength segments of sub-miniature coaxial cable in such a manner as to produce the equivalent effect of two mutually perpendicular dipole antennas.

The transmitting antenna is an etched circuit, centerfed dipole made up of two 152° segments of copper - one on each side of the base material. A length of sub-miniature coaxial cable connects the radiating elements to the 1680 mHz oscillator.

5.3.4.3.4 Datasonde.

The Datasonde as shown in Figure 5.3-26 is a miniature 1680 mHz instrument which has been designed for the Loki Dart and is operationally used with the GMD-1.

The instrument is 13 ounces in weight, 11.1 inches in length and 1.1 inch in diameter, with the antenna at the forward end and the sensor at the aft end. The electronic system and batteries are enclosed in a thin phenolic-fiberglass tube, and all voids are filled with an encapsulation compound. The electronics are solid-state except for the standard pencil tube triode cavity oscillator transmitter tube used for 1680 mHz radiosondes. The data modulation circuit consists of a unijunction relaxation oscillator. The power supply consists of a rechargeable nickel-cadmium battery and a DC-DC converter. Solid-state switching circuits are employed for switching between data and reference channels.

The Datasonde employs the thin film mylar loop thermistor mount which has been developed by Space Data Corporation specifically for this instrument. A rather unique feature of the Datasonde design is that the antenna of the instrument energizes the nose tip of the dart to obtain an uptrack signal during vehicle ascent.

Flight tests of the Datasonde instrument have been conducted by USAF-CRL to determine the telemetry accuracy. Precision resistors were flown instead of the thermistor. The telemetered resistance values were compared with the laboratory values to determine that the telemetered accuracy was within the equivalent of $\pm 0.5^\circ \text{K}$ over approximately ten flight test units. This error estimate includes errors in the ground-equipment and in the reading of the AN/TMQ-5 recorder chart.

5.3.4.4 Miscellaneous Instruments.

The Arcasonde-2B transponder instrument has been developed by Atlantic Research Corporation for use with the Arcas rocket and the GMD-2. It is essentially similar to the AN/DMQ-9 which the Air Force has standardized.

The Arcasonde-2B telemetry package consists of a 403 mHz receiver to detect the AN/GMD-2 range signal and an integral-cavity-oscillator transmitter operating in the 1660-1700 mHz band. The transmitter is modulated by a blocking-oscillator-type pulse generator at rates from 10 to 205 pulses per second. An electronic timer alternately samples a stable reference resistor and the thermistor, with dwell times of six seconds on each. A blanking circuit prevents pulsed data from modulating the



FIGURE 5.3-26 DATASONDE INSTRUMENT CONFIGURATION

transmitter for 0.5 seconds after each reference or data sample, permitting use of the instrument with automatic data-handling equipment. The instrument is modular in design; complete functional units can be interchanged or replaced in the field. The specifications are presented in Table 5-16.

To the best of our knowledge the Arcasonde-2B is not being used operationally since the Air Force has standardized and is using the AN/DMQ-9.

The Arcasonde 3 transponder instrument is shown in Figure 5.3-27. It was incorporated with the Denpro system to telemeter sensor information from the ascending probe and to obtain a track without the need for radar support. The Arcasonde 3 telemetry package is designed to function during the ascent of the Arcas sounding rocket vehicle. Transmitting in the 1660-1700 mHz band of the standard meteorological telemetry receivers, the package can process input from both variable voltage and variable resistance sensing elements. Pulse repetition rates from 100 to 1000 pps provide higher resolution than the standard GMD sondes in telemetered data. Optional features include a 403 mHz receiver for slant range measurement with the AN/GMD-2 Rawin set and a timing unit to allow sequential sampling of several sensors. The Arcasonde 3 package was designed to fit into the parachute canister of the standard ARCAS rocket vehicle. Receiver antennas are stowed flush with the rocket's external surface during the high-draw portion of the flight and extended at a 45° angle in the upper atmosphere. The package is modular in design with printed circuit intermodular connection. Complete functional units can be interchanged or added in the field. External jacks allow use of a ground power supply for prelaunch testing and standby. A block diagram is presented in Figure 5.3-28 and specifications in Table 5-17.

Resistance wire sondes have been flown by the British on the Skua rocket and by the Japanese (Echo-sonde) on the MT-135 rocket. Very little information is available on these sondes except that they telemeter at the 1680 mHz carrier frequency and are about the size of the Arcasonde-1A. These sondes employ resistance wire instead of a thermistor as the temperature sensor. Since the change in resistance of the wire with temperature is very small, rather expensive preamplifiers (by American standards) must be employed to boost the sensor signals from the microvolt region to volts in order to modulate the telemetry transmitter.

TABLE 5-16

ARCASONDE - 2B SPECIFICATIONS

Height	29.6 cm (11.66 in)
Maximum Diameter	11.1 cm (4.38 in)
Weight	2.04 kg (4.5 lb)
Transmitter Type	Frequency - modulated cavity oscillator
Frequency	1660 - 1700 mHz
Modulation	10 - 205 pps
Power Output	300 mW
Antenna	Helical slot
Receiver Type	Super-regenerative detector, self quenched
Frequency	400 - 406 mHz
RF Sensitivity	50 mV
Antenna	Dipole
Temperature Sensor	10-mil coated bead thermistor
Power Supply	Dry battery pack
Battery Life	2 Hours (at 20° C)

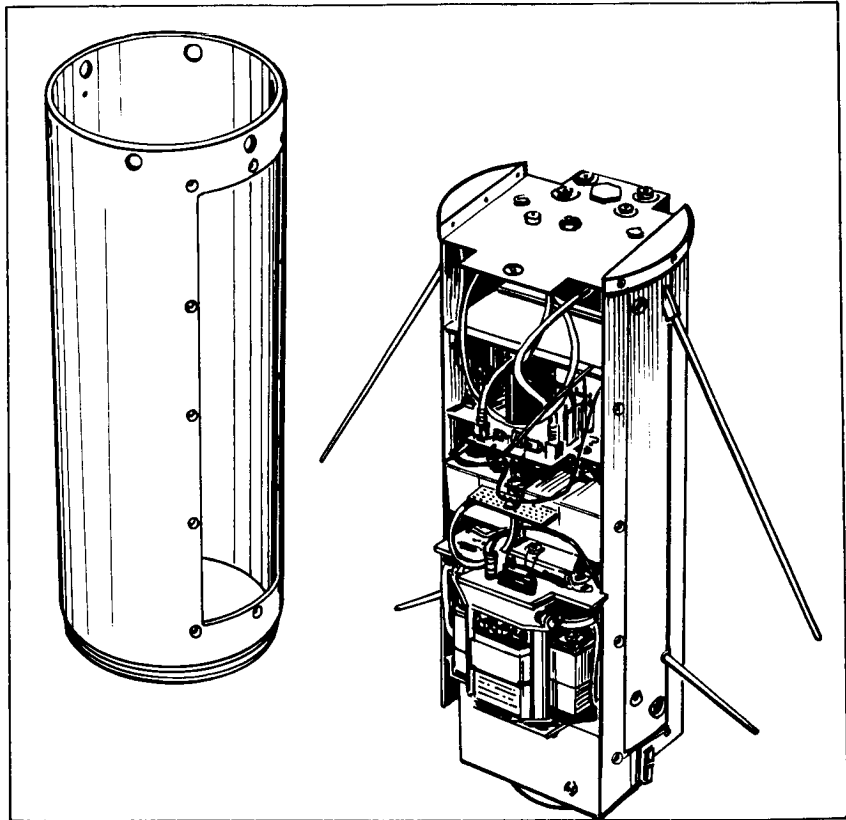


FIGURE 5.3-27 Arcasonde 3

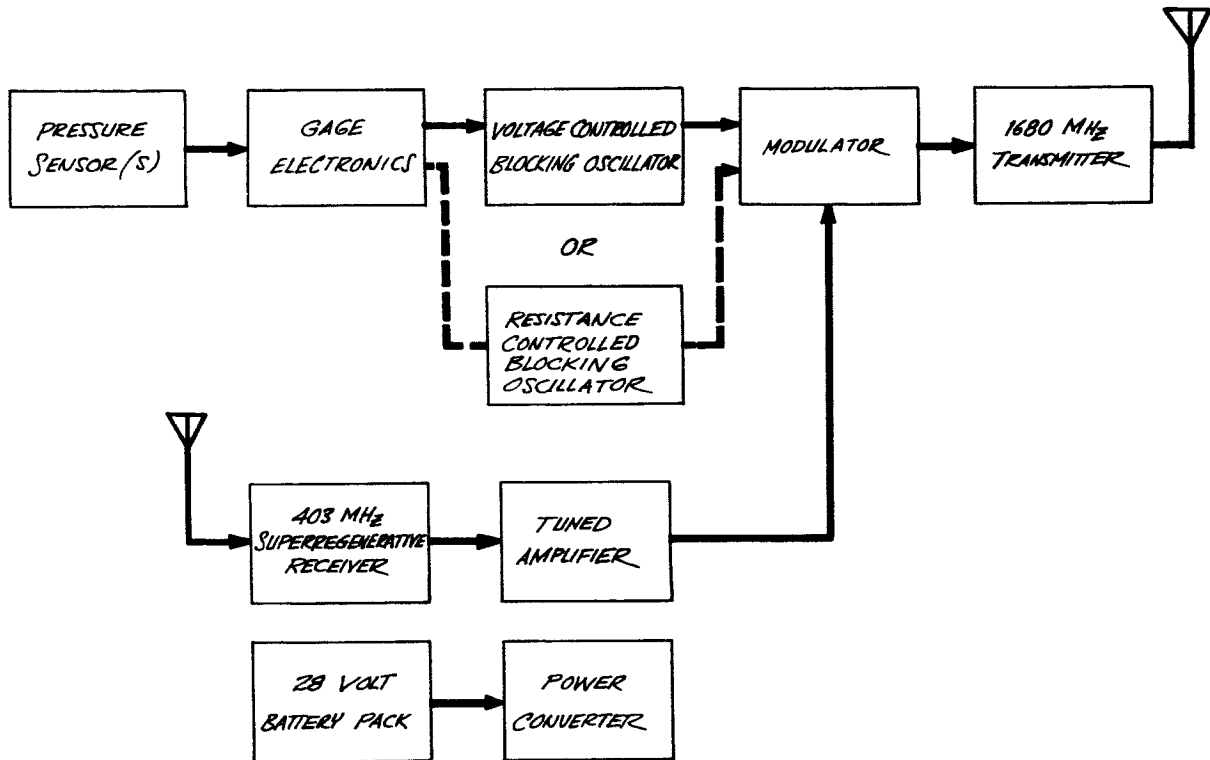


FIGURE 5.3-28 Arcasonde 3 Telemetry Block Diagram

TABLE 5-17

ARCASONDE 3 SPECIFICATIONS

Height	31.1 cm (12.25 in)
Diameter	11.4 cm (4.5 in)
Weight (including optional receiver)	2.95 kg (6.5 lb)
Transmitter Type	Frequency - modulated cavity oscillator
Frequency	1660-1700 mHz
Modulation	100 - 1000 pps
Power Output	300 mW
Antenna	Two quarter-wave dipoles
Receiver (Optional) Type	Super-regenerative detector, separately quenched
Frequency	400 - 406 mHz
RF Sensitivity	50 mV
Power Supply	20 silver-zinc cells, 28 VDC

5.3.5 AN/SMQ-1 Telemetry Systems.

5.3.5.1 General.

The AN/SMQ-1 systems operate at a carrier frequency of 403 mHz and employ pulse rate modulation as do the GMD systems. However, instead of pulsing the transmitter off as in the GMD systems, the modulation pulses the transmitter on through a pulse transformer thereby eliminating the DC-DC converter of the GMD sonde systems. More important, however, is the fact that the typical duty cycle of the pulses is from about 0.2 to 2.0%. Therefore, the SMQ airborne systems are turned on and radiating only 0.2 to 2.0% of the time while the GMD systems are turned on and radiating about 99.8 to 98.0% of the time during the relatively long dwells between pulses. This means that the SMQ sondes can be made smaller and lighter than the GMD sondes. This is a distinct advantage for improving the ballistic coefficient of the rocketsonde decelerator systems, since in addition to a decrease in weight more payload volume is made available to the decelerator. Another advantage is that for a given signal strength at the receiver site and a given slant range, the required power radiated from the sonde is considerably less for the 403 mHz carrier than for the 1680 mHz carrier. Also the SMQ ground-based receiver system does not require a tracking antenna and is much simpler to maintain and is considerably lower in cost. The only disadvantage of the SMQ systems is that they do not track and require radar support for altitude and wind data.

5.3.5.2 Ground-Station Equipment.

The ground-station equipment consists of the Navy developed AN/SMQ-1 Radiosonde Receptor or the smaller transistorized version of this set developed by the U. S. Weather Bureau.

Radiosonde Receptor AN/SMQ-1 is a receiving and recording device operating in the frequency range of 390 to 410 mHz. The receptor is employed in a HASP III system to receive and record upper atmospheric temperature data from the HASP Radiosonde Set WOX-1A. The components of the receptor are the antenna, receiver, recorder, power supply, electrical cabinet and a paper table.

The antenna is approximately 1-1/2 feet high and is designed to operate effeciently over a frequency range of 390 to 410 mHz. One hundred

feet of coaxial cable is supplied with each antenna. One end of the cable is fitted with a male plug for connection to the antenna input jacks; the other end is connected to the top rear corner of the electrical cabinet by four type N connectors on the cabinet. PMR has developed a helical antenna for use with rocket system for a higher antenna gain.

The receiver is designed for receiving the radiosonde pulse modulated radio frequency signals on a continuously variable tuning range of 390 to 410 mHz. The receiver amplifies, demodulates and converts the signals to d.c. voltage. The magnitude of the d.c. voltage appearing at the receiver output is directly proportional to, and varies in exact accordance with, the received signal pulse repetition rate. A loudspeaker for aural monitoring and an oscilloscope for visual monitoring are included in the receiver circuitry. All operating controls, the loudspeaker, and the oscilloscope are located on the receiver front panel. A coaxial type antenna switch is located on the back of the receiver front panel. The control for this switch is on the front panel. It permits selection of four antenna inputs and provides means for grounding the receiver antenna input. The d.c. output of the receiver is fed to the recorder.

The recorder displays the data from the receiver on roll chart paper. The voltage output from the receiver is applied to a servo-drive motor, which actuates an ink pen through a system of shafts, gears and a pulley wire. The ink pen records data on moving chart paper which is driven over three paper rolls by a chart drive motor. The chart paper is graduated in 100 divisions across the paper. Readings on the chart usually correspond to half the pulse rate of the RF signals in pulses per second (pps) from the radiosonde.

The power supply operates from a 115-volt, 60-cycle, a.c. source and supplies all of the voltage requirements for the receiver and recorder. Power and heater on-off switches and associated pilot temperature indicators and blown fuze indicators are recessed in the upper center of the front panel.

The electrical cabinet is a shock mounted, drip proof, metal structure provided with space heaters and sliding drawers. The top drawer contains the receiver; the middle drawer contains the recorder, and the bottom drawer contains the power supply.

The radiosonde signal received by the receptor consists of pulses of 403 MHz radio frequency energy. The frequency of repetition of these pulses is dependent on meteorological conditions. Each pulse is approximately 250 to 275 microseconds in duration and the pulse repetition frequency may vary from 10 to 200 pulses per second. The received signal pulses will generally be a series of pulses at one audio rate followed by a series at a different audio rate. Each series of pulses will cause the receptor to print on the chart in a position determined by the audio rate of that particular series of pulses.

The received pulsed signals are fed from an antenna through the signal selector switch to the R.F. section which contains an R.F. amplifier, mixer and local oscillator. The output of the R.F. Section is fed to the I.F. strip which consists of five stages of I.F. amplification. The second and third stages of amplification are available to adjust receiver gain while the fifth stage acts as a first limiter. The I. F. output is fed to the detector section consisting of a limiter and a discriminator. The discriminator is used as a slope detector and its output in the form of negative d-c pulses is fed into the audio section.

The audio section contains a pulse amplifier, clipper and a pulse shaper. This section amplifies and shapes the input signal and eliminates noise to form a strong consistent trigger pulse to the frequency meter section which follows. In addition, the output of the pulse amplifier is fed as the observed signal to the vertical amplifier in the video monitor circuit.

The frequency meter section converts the pulsed signals into varying d.c. voltages to control the servo system in the recorder. It also provides signals for the audio and video monitors. This section consists of a trigger gate, a multivibrator, a ringing and damping circuit, a pulse generator, filter and attenuator in the order mentioned. As the signal progresses through the trigger gate and multivibrator, it is further stabilized. The multivibrator output energizes a ringing circuit which is damped after each first half cycle providing strong trigger pulses to the pulse generator. The pulses are accurately formed by the pulse generator and its associated delay line and fed into a lowpass filter which converts them into a positive d.c. voltage proportional to the repetition rate. The d.c. output is fed

into an attenuator which provides a means of accurately calibrating the signal to the recorder.

Video and audio monitoring are provided as a means of tuning and maintaining proper receiver gain. The audio signal is picked up from the multivibrator output, while video signals are obtained from the multivibrator in the frequency meter section, and from the pulse amplifier in the audio section.

The recorder section consists of comparator circuits, a 60 cycle servo amplifier and a pen drive servo system to which a potentiometer is connected, feeding back a reference signal to the comparator. The varying d-e output from the receiver is combined with the reference signal from the potentiometer. The resultant is amplified and fed to the servo motor as a directional signal moving the pen to a position proportional to the pulse rate of the received signal. Limit stops prevent over-travel of the pen. A two-speed chart drive system allows a selection of chartpaper feed.

The power supply provides the necessary voltages for all signal and control circuits. This unit provides regulated and unregulated 6.3v a-c for filaments, +400 volt unregulated, regulated and unregulated 270v d-e, regulated +150 v d-e and -430 v. d-c unregulated supplies. In addition, all 115 v. a-c supplies are controlled by the main power switch in the power supply. A block diagram of the AN/SMQ-1 is presented in Figure 5.3-29.

5.3.5.3 Rocketsonde Instrumentation.

The WOX-1A has been developed and standardized by the U. S. Navy for use with the HASP III (Loki Dart type) rocket and the AN/SMQ-1 ground-based receiver.

The radiosonde, externally is cylindrically shaped, approximately 11 inches long, 1.4 inches in diameter and weighs 22 ounces. In ejection, as the payload package leave the body, a spring-loaded button on the radiosonde body is released to start the radiosonde operation. After ejection, the payload package opens to release the parachute by the action of two flat springs placed between the staves and insulation strips inside the staves. The staves, piston and closure plug separate from one another and from the parachute-radiosonde payload, leaving the parachute free to open with the aid of the radiosonde's weight.

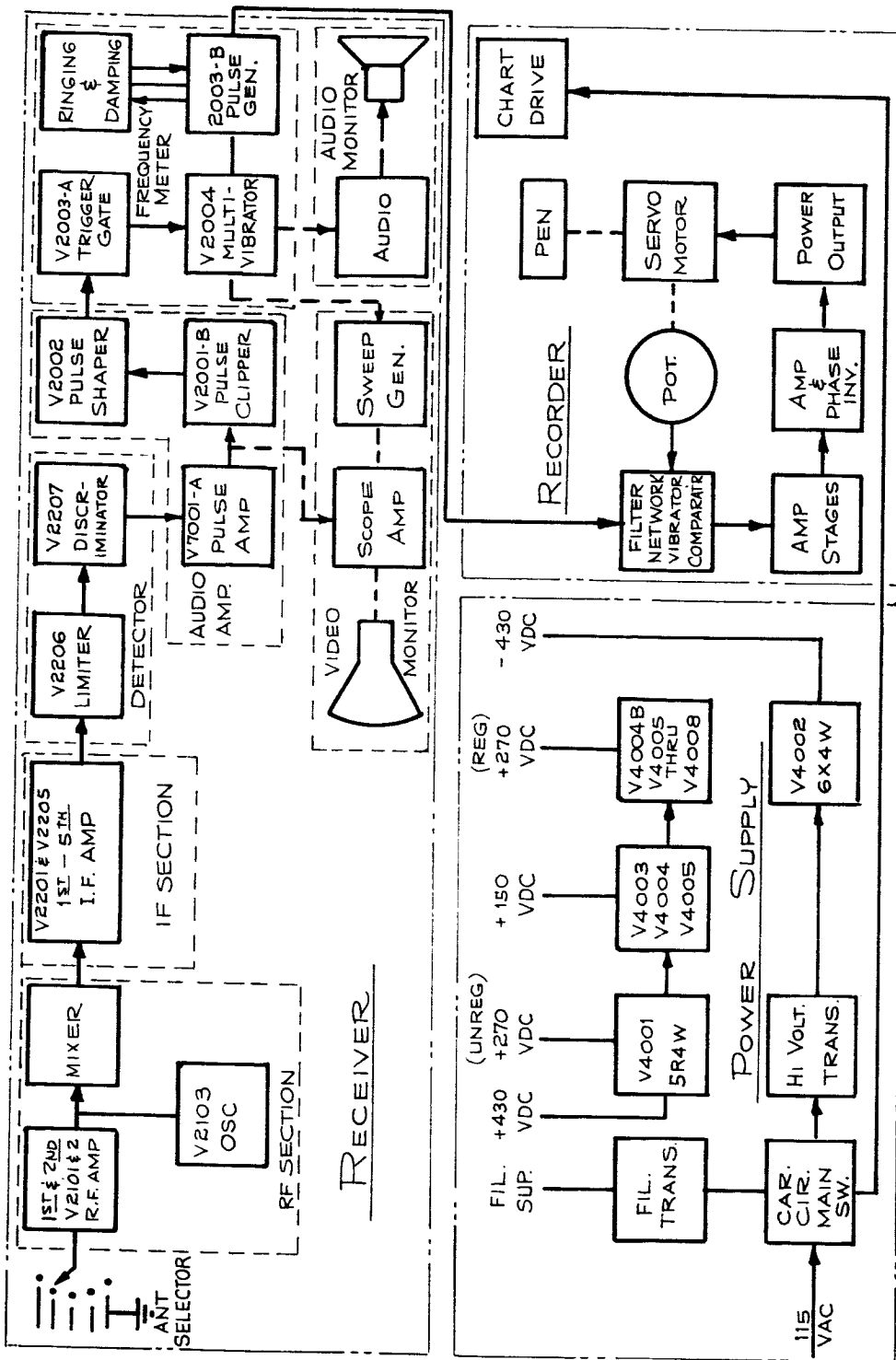


FIGURE 5.3-29 Block Diagram Radiosonde Receiver AN/SMQ-1 Principles of Operation

The radiosonde collects and transmits temperature data to a ground or shipboard Radiosonde Receptor AN/SMQ-1. The major components of the radiosonde, shown diagrammatically in Figure 5.3-30 are a 6 volt nickel-cadmium battery, a temperature sensor, a transistorized modulating circuit and a transmitter which telemeters on a 403 MHz frequency. The transmitter is coupled to an antenna wire which is also a connecting line from the radiosonde to the non-radiating riser of the parachute. In addition to the antenna wire itself, the steel case of the radiosonde is used as a part of the antenna.

The battery of the radiosonde powers the radiosonde operation. Prior to launching, the battery is slow-charged for a six-hour period. A closure plug in the forward end of the body is fitted with a removable screw to provide access to the connector for battery charging.

The temperature sensor of the radiosonde is a bead thermistor, through which a current is passed. The transmitter transmits a pulse modulated radio frequency signal whose pulse rate is dependent on the resistance of the thermistor and, therefore, the atmospheric temperature.

The pulse rate transmitted depends not only on resistance of the thermistor, but also on changes in the operation of the radiosonde components due to atmospheric temperature and a depletion in battery voltage. To correct for the irregularities, a reference resistor of accurately known resistance is put in the radiosonde on a circuit separate from the thermistor circuit. Signals, called reference signals, from the known resistor circuit are transmitted for two-second intervals alternately with temperature data signals from the thermistor circuit, which are transmitted for four-second intervals. These alternating signals are received and recorded on rolled chart paper by a radiosonde receptor. Combining the two signals eliminates consideration of the adverse effects of temperature and voltage loss.

The Radiosonde Set WOX-1A is comprised of essentially four electronic functioning blocks; namely, a commutator, an analog to frequency converter, a driver-modulator stage and a UHF transmitter-antenna section. Due to the severe environments encountered during flight and also the limited volume available for both the electronic circuitry and the power supply, semiconductors were used for all the active circuit components except for the transmitter. A schematic is presented in Figure 5.3-31.

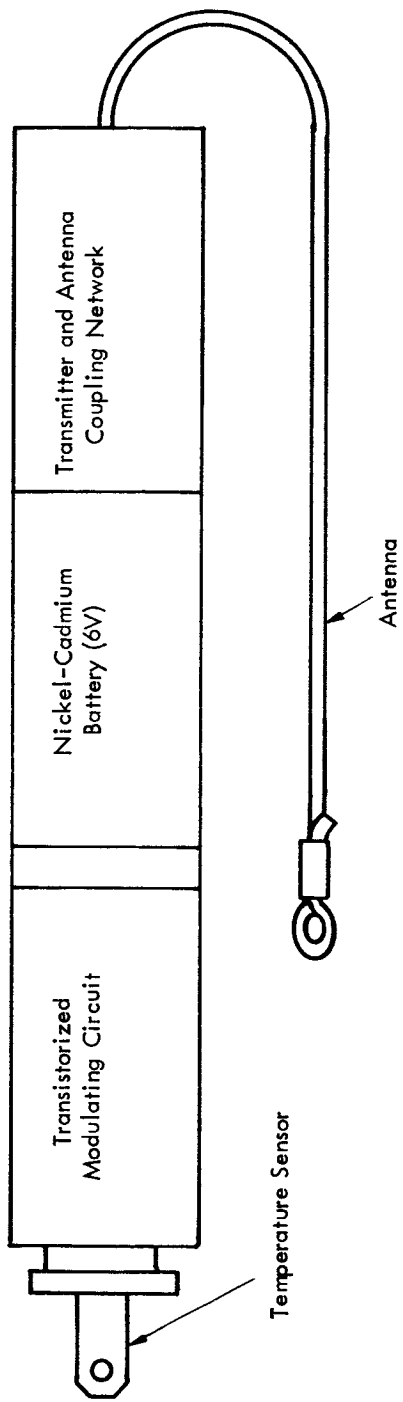


FIGURE 5.3-30 RADIOSONDE SET WOX-1A

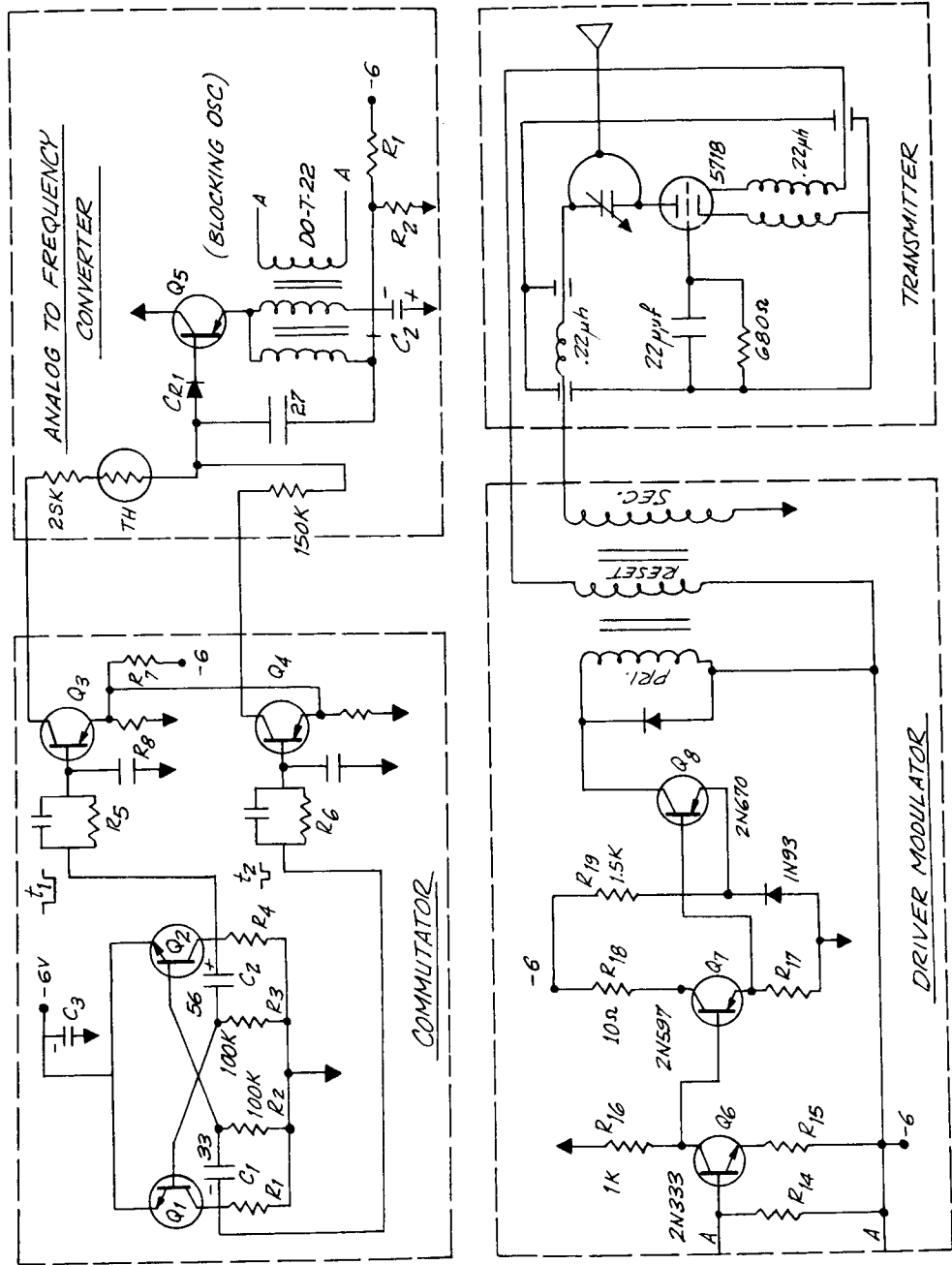


Figure 5.3-31 Radio Set WOX-1A, Block Diagram

The two channel commutator circuit in the WOX-1A system is an asymmetrical free-running multivibrator that samples the air temperature sensor for a period of four seconds, then subsequently samples a fixed precision reference resistor for a period of two seconds. The time sharing sequence was selected to obtain a maximum sampling of the temperature altitude profile with a minimum loss due to sampling the reference.

The subsequent functioning block consists of the amplifying stages and transmitter modulator. The modulator is designed to deliver 3.0 ampere pulses at 5.0 volts which represents 15.0 watts of pulsed power. This capability required an amplifier section with a power gain of approximately 35 db. The blocking oscillator was designed to delivery 3.0 volts into a 2000 ohm load. The value of 2000 ohms was sufficiently high so that its reflected impedance into the blocking oscillator circuit during the pulse did not affect the repetition rate. The first stage, Q6, is essentially an emitter follower having a minimum current gain of approximately 10. An output current of the order of 15 ma is realized from an input current of 1.5 ma. The collector voltage remains constant at 1.5 volts during the pulse. The second amplification stage, Q7, provides a minimum gain of 10 resulting in a base drive to the modulator, Q8 of 150 ma. The 10 ohm resistor, R18, in the collector of the second stage limits the current below the maximum dissipation of the 2N597. The 100-ohm resistor, R17, in the base circuit of the modulator and diode 1N93, CR4, in the emitter leg provides DC stabilization and prevents thermal runaway. The 1N93 was selected on the basis of its current carrying capacity of 3.0 amps during the pulse. With 150 ma into the base of the modulator and a minimum beta of 20 the collector current is of the order of 3.0 amps. During saturation the maximum voltage across the pulse transformer is approximately five volts; the remaining voltage is distributed across diode CR4 and the collector to emitter junction of 2N670. The diode in the emitter circuit of the modulator insures cutoff at high temperatures thereby preventing thermal runaway. The 2N670 also has a specially designed heat sink, which is also an aid to prevent thermal instability.

The pulse modulating transformer, which was designed at the Naval Ordnance Laboratory, has special characteristics that were not available in commercial types. The magnetic core is grain oriented silicon steel with a relatively high maximum flux density. The primary and secondary are wound on the magnetic toroid such that the leakage inductance is extremely small. The wire size was selected so that the resistance losses

are equal in each winding. The core size and the wire stacking make maximum utilization of the geometric volume available in the package. The inner diameter of the complete wound toroid was required to accept the 2N670 transistor and heat sink. The tertiary winding is used to reset the core so that the entire change in flux can be realized. This results in a more efficient and smaller size transformer. The current use for resetting the core is the filament current for the transmitter tube. The modulator stage is capable of delivering 3.0 ampere pulses of current at 5.0 volts. The B+ pulses appearing at the plate of the transmitter are in the order of 240 volts at 40 ma.

The transmitter uses a Colpitts type oscillator capable of delivering 3.0 watts of peak power at 403 mHz. The oscillation tube is a UHF triode, type 5718. The oscillator circuit utilizes the inter-electrode capacity for positive feedback from plate to grid. The oscillator frequency is adjusted by a vernier capacitor across the printed circuit coil. The tuned inductance is a printed copper coil on Rexolite dielectric. This material is superior for low loss qualities and is ideal as a dielectric for high frequency-circuits. The oscillator is completely shielded in a copper case which minimizes radiation other than via the antenna. The shield also serves to "fix" the stray distributed capacitance and inductance parameters for better frequency predictability.

The R.F. power for the triode is directly coupled to a center-fed fullwave antenna. The antenna is asymmetrical; one-half is a stainless steel cylinder which houses the transmitter and telemetry circuit, while the other is a thin stranded copper wire of one-half wavelength. The thin wire also acts as a supporting cable attached at the upper end to the parachute. This asymmetrical antenna itself is not a simple geometric configuration, consequently the impedances and current distributions are difficult to solve analytically. Approximations to the exact impedance equations were made in order to obtain results that could be used in resolving the antenna parameters and matching network. The final antenna parameters were adjusted empirically to yield optimum R. F. power radiation in free space.

Although initial procurement quantities of the WOX-1A were unreliable in flight performance, a change from germanium to silicon transistors improved the conditioning temperature capability of the instrument. Recent production units have demonstrated sufficient reliability to consider the system as operational.

Design limitations of the WOX-1A have led to funding by NOL for the development of an advanced version which is called the WOX-4A. Design goals for this new instrument are for a smaller diameter (1.1 inches), a shorter instrument length (6 inches), a lighter weight (6 ounces) and a thin-film mylar thermistor mount. The original WOX-1A must be flown in a 1-5/8 inch diameter dart which does not achieve adequate altitude. The new instrument will fit into the 1-3/8 inch diameter Navy chaff darts. The shorter length of the new unit will permit more space for the rocketsonde decelerator, and the lighter weight will improve the ballistic coefficient of the descent system for slower fall rates. The older WOX-1A uses a rather heavy thermistor fiber mounting structure which voids the temperature measurements above 150,000 feet. The new thin-film mounts should upgrade the temperature measurements to the current state-of-the-art.

5.3.6 Advanced Concept-Motorola Study.

5.3.6.1 General.

Motorola Inc., has been funded by AFCRL to conduct a design study for an advanced meteorological telemetry and tracking system for both radiosondes and rocketsondes. The purpose of developing an Advanced Meteorological Sounding System (AMSS) is to update the present system with particular emphasis on improved reliability, decreased operating costs and increased accuracies. As opposed to the present ground based meteorological tracking system, the AMSS provides a smaller and lighter radiosonde, improved ranging and telemetry accuracies, higher data rates including a continuous data channel, unambiguous ranging to 580 kilometers, digitized output data and a solid state design throughout.

The objective of the AMSS was to develop a ground based meteorological sounding system which would effectively use modern design techniques in the gathering of accurate meteorological data. The system evaluation did not include any study of the meteorological sensors, airborne vehicles (balloons or rockets) or final data processing equipment. In selecting a system configuration the following guidelines were used:

1. The system design should favor techniques which reduce operating complexity and minimize maintenance and technical obsolescence. Design mechanization should include maximum utilization of solid state and integrated circuits.

2. The design should emphasize simplification of the flight expendable radiosonde and make use of techniques which would reduce cost, weight and power consumption.
3. The ground equipment should be designed with adequate performance margins to achieve long life and maximum reliability.
4. The system performance should exceed that presently available from the existing AN/GMD-2 system.

In keeping with the program objectives a study was conducted to develop a system which would reflect as many of the current design capabilities as possible. During the initial stages of the program a number of trade studies were made in an attempt to arrive at the optimum system configuration. At the conclusion of this synthesis and analysis period certain portions of the system were implemented. This included both the radiosonde and ground equipment, and after a laboratory evaluation a number of balloon borne flight tests were made. These tests were primarily concerned with the range and telemetry functions in which overall system performance was demonstrated. Although a number of configurations are possible, that which was selected is shown in a simplified block diagram in Figure 5.3-32. Some of the more significant system characteristics are shown in Table 5-18 and although this table may briefly describe the proposed system, it is of interest to compare this with the systems that are currently operating in the field. This is done in Table 5-19 in which the AMSS is compared to the present AN/AMQ-9. These two systems differ in a number of areas but probably the most noticeable is in the radiosonde configuration and ranging system.

The primary measurement parameters are slant range, antenna angle data, time and four telemetry channels. The telemetry data may consist of temperature, humidity, pressure or whatever is desired. From the above raw data suitable processing will allow computation of such meteorological information as winds aloft, altitude, temperature and humidity profiles, air densities, refraction indices and so forth.

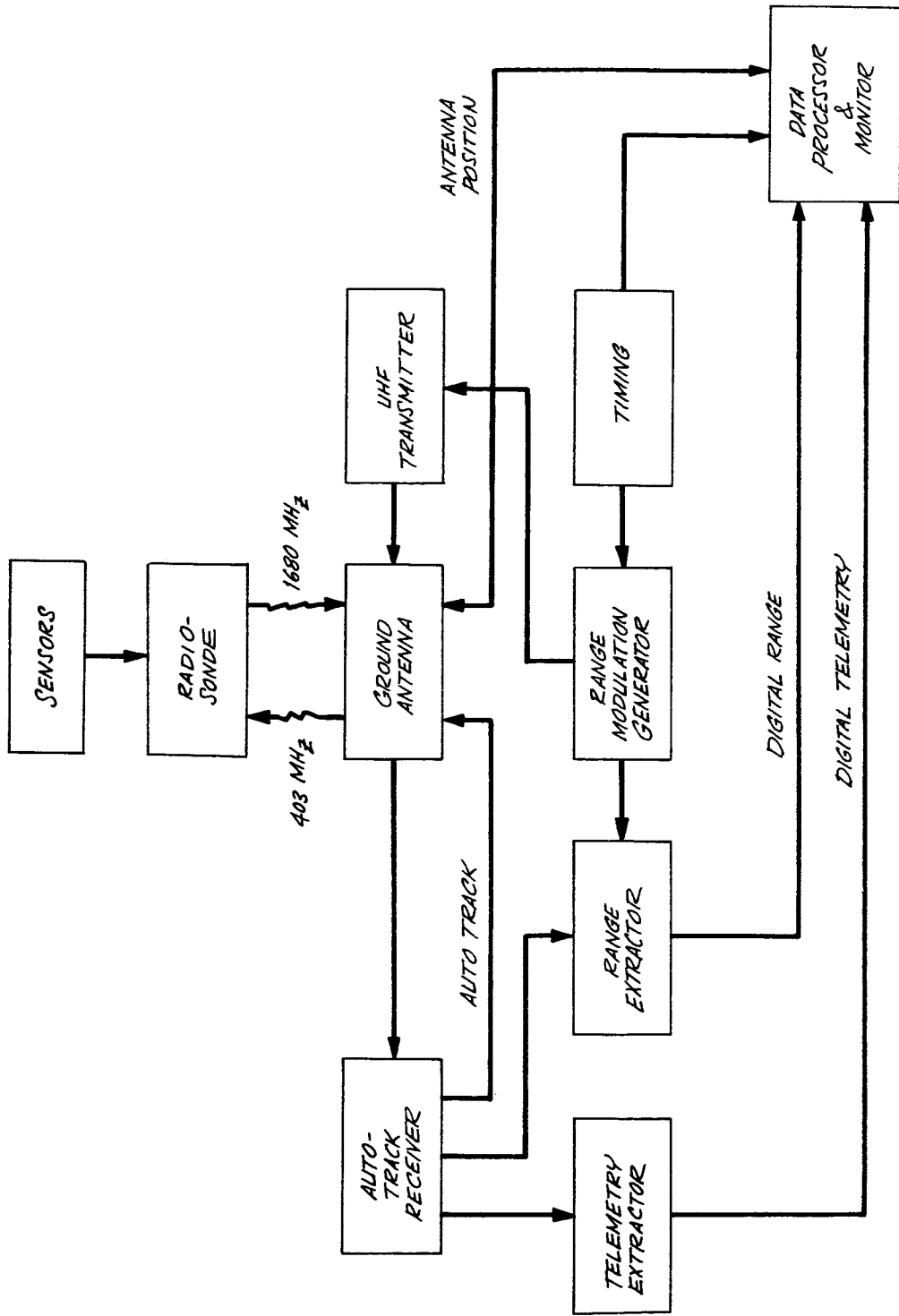


FIGURE 5.3-32 Advanced Sounding System, Block Diagram

TABLE 5-18

ADVANCED SYSTEM CHARACTERISTICS

Maximum Slant Range	300 km
Uplink Frequency	400 - 406 mHz
Uplink Power	30 Watts
Uplink Data	Range
Uplink Modulation Form	FM at Index of 0.7
Radiosonde Receiver Type	Superheterodyne
Radiosonde Output Power	35 Milliwatts
Radiosonde Transmitter Type	Crystal Multiplier
Downlink Data	Range and Telemetry
Downlink Modulation Form	PM
Ground Receiver Type	Phase Locked
System Acquisition Time	10 sec
Information	Time Antenna Pointing Angles Slant Range Telemetry - 3 Time Shared Chan 1 Continuous Chan
Range Resolution	5 Ft. Unambiguous to 580 km
Ranging System	BI-Phase PRN
Telemetry Resolution	0.02% of Full Scale
Output Data Form	Punched Tape

TABLE 5-19

AN/AMQ-9 VS. AMSS COMPARISON

<u>Item</u>	<u>AN/AMQ-9</u>	<u>AMSS</u>
Sonde Receiver Sensitivity	50 μ V or -73 DBM @ 50 ohms	96 DBM
Sonde Receiver Type	Super-regenerative	Superheterodyne
Sonde Receiver Selectivity	3 DB Bandwidth: 60 mHz	IF Bandwidth: 300 kHz
Sonde Transmit Power	300 Milliwatts	35 Milliwatts
Sonde Transmit Frequency	Tunable 1660-1700 mHz	Crystal Selection From 1668-1693 mHz
Sonde Frequency Stability	\pm 4 mHz	\pm 75 kHz
Downlink Modulation Form	FM	PM
Ranging System	81.94 kHz Tone	64 kHz \oplus PN
Allowable Range Error (sonde)	560 feet	\pm 100 feet
Unambiguous Range	115 Miles	365 Miles
Range Resolution	3 feet	5 feet
Range Extr Construction	Electro-Mechanical	Electronic
Telemetry Form	Blocking Oscillator	Two Subcarriers
Telemetry Channels	Two Time Shared	One Continuous Three Time Shared
Frame Rate	One per 20 seconds	One per second
Commutator Construction	Mechanical	Solid State
Sonde Weight	925 grams less Battery	705 grams less Battery
Sonde Power Requirements	7.58 Watts	3.4 Watts

The uplink signal consists of a 403 mHz carrier which is frequency modulated with a PRN ranging signal. The maximum transmit power is 30 watts in which the actual level is controlled by the receiver AGC. Such a coarse control limits the signal range over which the transponder must operate and this in turn aids in decreasing the group delay variations within the radiosonde. The transmitter output is fed to the antenna system, which radiates the signal to the radiosonde. The transponder, operating as a superheterodyne receiver, converts the 403 mHz received carrier to a 17 mHz IF. This is then applied to a standard discriminator which detects the range signals and PM modulates the down-link carrier. In addition to the ranging signal, two telemetry subcarriers are also modulated on the down link carrier. One of these subcarriers is used to transmit continuous telemetry channel data while the other subcarrier contains time shared telemetry information. The down link carrier operates at a nominal 1680 mHz and 35 milliwatts.

At the ground terminal this signal is received and auto-tracked by the antenna system. The sum channel signal is fed to the Phase Locked Receiver which is a double conversion, superheterodyne receiver with intermediate frequencies of 50 mHz and 10 mHz. The receiver then demodulates the input signal and provides baseband range information to the Range Extractor and subcarrier telemetry information to the Telemetry Extractor. The slant range is obtained by measuring the time delay between the transmission of the range code and reception of this same code signal. The elapsed time is computed in a Timer Interval Counter which allows range resolution measurements of 4.9 feet. The output range data is then digitally recorded and transferred to the data processor. The telemetry information is generated in the transponder through appropriate sensors and is received at the ground station in the same manner as the range signal. However, in the Telemetry Extractor the process is somewhat different in that the detector is an FM discriminator in which the output amplitude is a measure of the sensor condition. The analog output data is then applied to a digital voltmeter which converts the analog information to a digital format and transfers this data to the Data Processor. The Data Processor then accepts, converts and stores tracking data, meteorological data and time data obtained during the flight of a radiosonde and produces a punched paper tape output suitable for transmission over standard teletype lines.

In measuring slant range there are a number of methods which will accomplish this purpose. The three outstanding systems are a radar range measuring system, a PN (pseudo noise) ranging system and a tone ranging system. All three systems have been used extensively in various

phases of the space program. The advantage of the radar system is the simplicity of the radiosonde since a passive corner reflector may be substituted for the receiver in the radiosonde. The principal disadvantage of such a system is the high transmit power required at the ground stations. If radar systems are available for such use then it is desirable to take advantage of this condition. However, where such is not the case a range system using tones or PN is more desirable. For the AMSS system a PN ranging system was selected. As opposed to the tone system an PN ranging provides considerable jamming immunity, and for distant ranging, extremely low frequencies are not required. In reality the system selected is a hybrid PN ranging system which utilizes a resolution range tone and a short PN sequence for ambiguity resolution. Although the code used here is much simpler than that used in many space programs, the operation is much the same. For example, referring to Figure 5.3-33 a 64 kHz sine wave is bi-phase modulated at an 8 kilobit rate. That is, after each eight (8) cycles of the 64 kHz range tone a decision is made as to whether to change the phase by 180° or leave the sinewave undisturbed. The code format which makes such a decision is commonly a PN sequence. That is, its spectrum resembles noise to the extent that the code length will allow such a representation. Then by measuring the time delay between the transmission and reception of the code sequence a measure of range may be obtained. The AMSS code length is 31 bits which corresponds to an unambiguous range of 580 kilometers and a further description of the range extraction process is described in the subsystem section.

The telemetry requirements are to provide four channels of data with one channel being continuous and the other three time shared. The maximum data rate on each time shared channel is one reading per channel per second. The modulation technique is shown in Figure 5.3-34 where the reference channel width is three times that of any information channel and the measurement data is contained in the amplitude of the information channel relative to the reference channel. Requirements on the subcarrier VCO's are those of extreme linearity (better than 0.1%), good stability (both long and short term) and the units must be economical throw-away components. Such units are now practical and played a key role in establishing this method as the telemetry format.

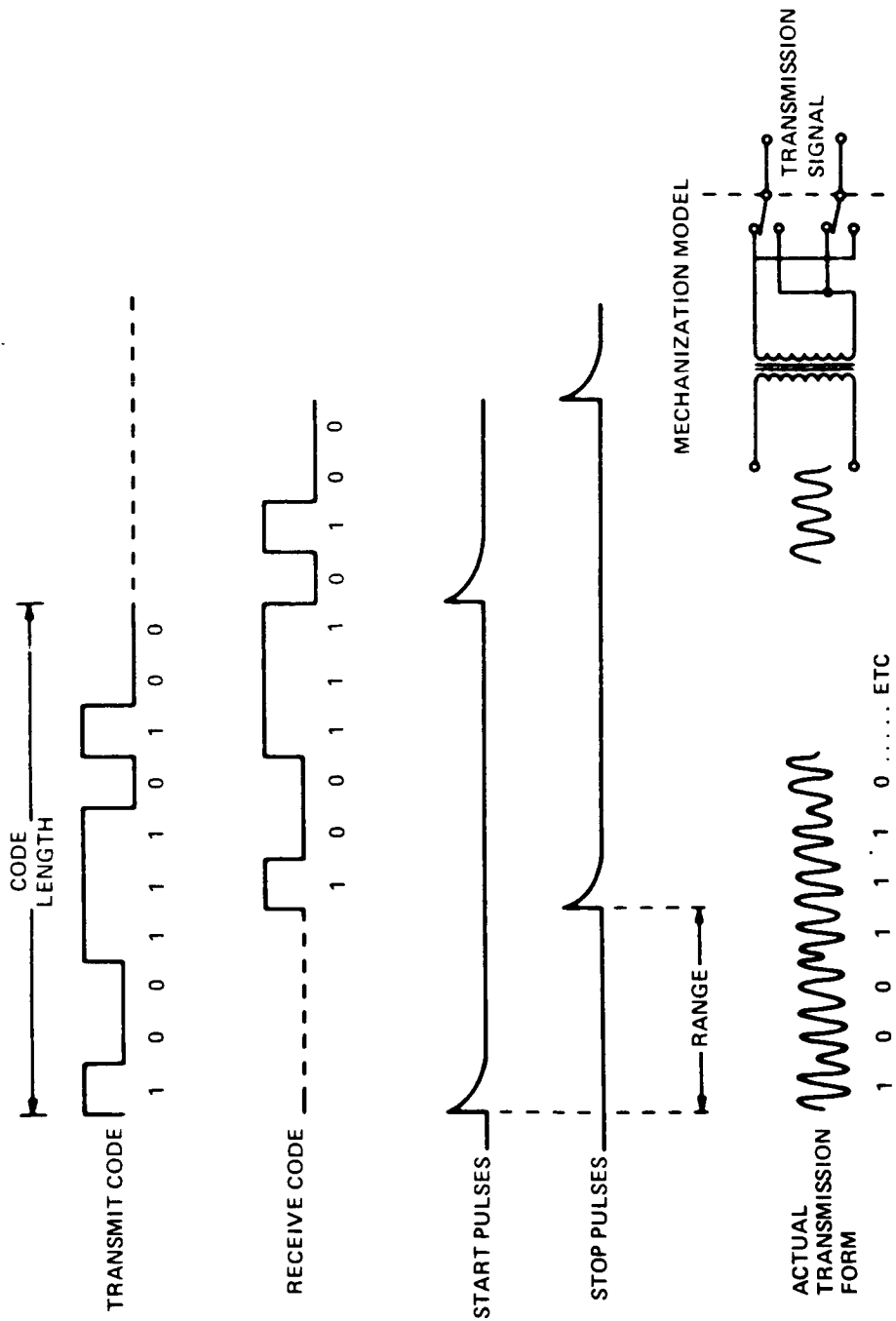


FIGURE 5.3-33 PN RANGE SYSTEM

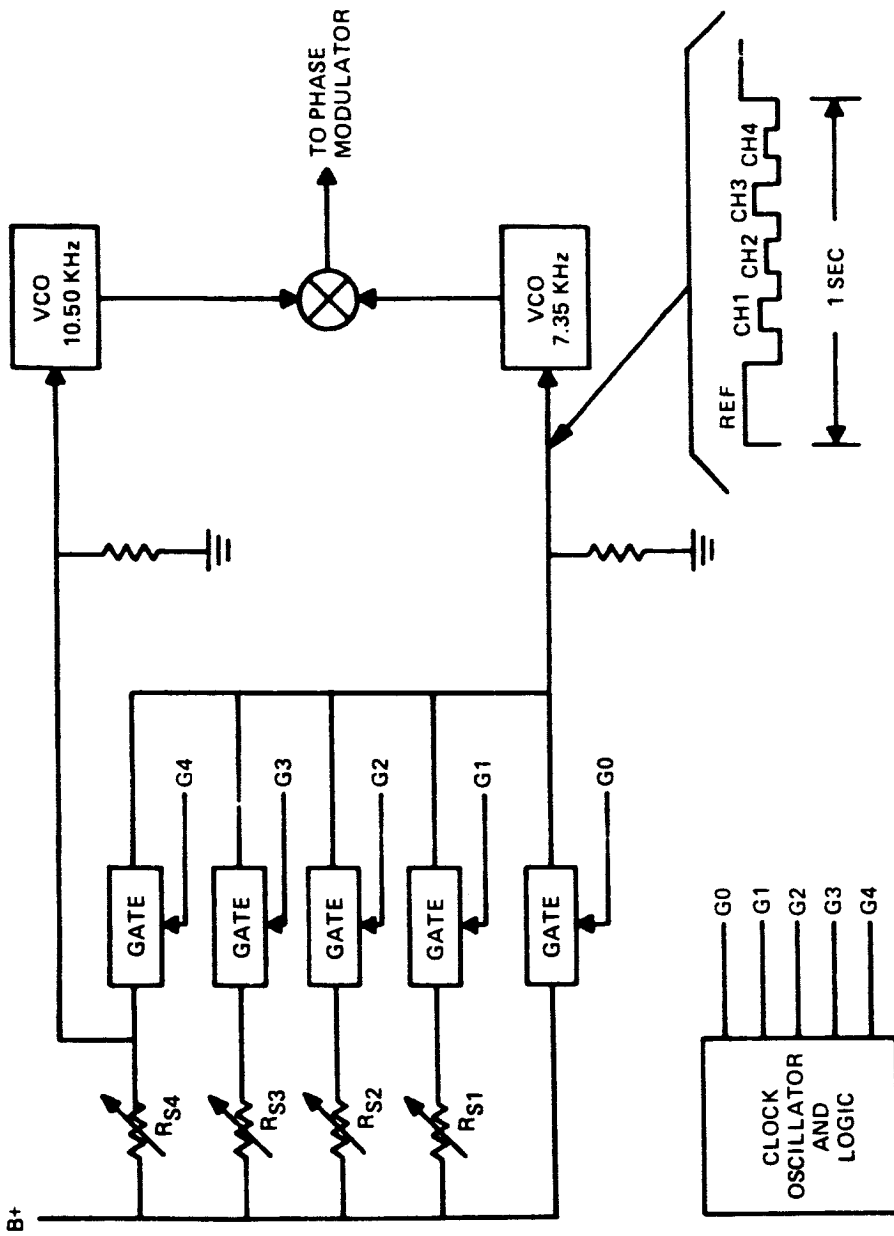


FIGURE 5.3-34 TELEMETRY MODULATOR, BLOCK DIAGRAM

5.3.6.2 Ground Equipment.

The block diagram of the proposed advanced sounding system, as shown in Figure 3.5-32, consists of several major elements described as follows:

1. VHF Transmitter.

The ground transmitter is a solid state unit operating at a crystal controlled nominal frequency of 403 MHz. The output power level varies between 5 milliwatts and 30 watts and is controlled by the receiver AGC. Over this output level the transmitter must demonstrate less than ± 10 nanoseconds group delay variation and for overall operating conditions, the group delay stability should be better than ± 20 nanoseconds. The transmitter is FM modulated with the 64 kHz \oplus PN ranging data and the output is supplied to the ground antenna system.

2. Ground Antenna.

The ground antenna system consists of a transmit antenna operation at 403 MHz and a receive antenna operating at 1680 MHz. The transmit function associated with the ground antenna does not pose any significant design problems as the required gain is only 3 db. This is not true in the case of the receive function where there are a number of conflicting requirements.

3. Auto-Track Receiver.

The ground receiver is a phase lock tracking receiver which is used to track the downlink RF carrier and to convert the range and telemetry data to baseband. In addition to the above, the receiver must also provide signals proportional to the antenna pointing error which are in turn used to drive the antenna servo system. The receiver design to perform these functions is a double conversion superheterodyne receiver with 50 MHz and 10 MHz IF frequencies. The receiver will automatically acquire the carrier signal and the acquisition will not be affected by the presence of the telemetry sidebands. Coherent AGC is used to maintain the IF signal to the phase detector constant so that loop bandwidth is not affected by signal level.

4. Telemetry Extractor.

The purpose of the telemetry extractor is to develop output signals which are proportional to the sensor resistance values in the radiosonde. A block diagram of such a circuit is shown in Figure 5.3-35.

The baseband input consists of two subcarriers which have been frequency modulated with the telemetry data. The extraction system consists basically of a low frequency FM receiver which detects the sub-carrier and provides a multiplexed output signal (a cw signal in the case of the continuous channel). This signal is applied to a phase locked loop which serves to detect the bit sync of the multiplexed signal. This bit sync drives logic circuitry to derive frame sync as well as gate signals to properly decommutate the multiplexed input and derive correction signals to calibrate the telemetry data.

The band pass filters have a bandwidth of 520 Hz ($2\beta L$) such that the signal-to-noise input into the discriminator will be above threshold under all expected condition and the phase lock loop bandwidth used for sync purposes is 2.0 Hz ($2\beta L$).

The telemetry extractor is completely automatic and does not require prior calibration of manual checks throughout a radiosonde flight. The circuitry has been designed such that the digital circuits and operational amplifiers are utilized wherever possible. In this way the telemetry extractor is readily adapted to present day integrated circuits.

5. Range Extractor.

The purpose of the range extractor is to develop an output signal which is a measure of the slant range to the transponder. The range extractor will measure relative phase shifts between the transmitter and received range signals with the total range being displayed as the timer interval between a start and stop pulse. The ranging system selected was a PN ranging system in which the Range Extractor is shown in Figure 5.3-36. The input signal is a 64 kHz sine wave which has been bi-phase modulated with a 31 bit PN code. The bit rate is 8 kbits/sec. Operation of the range extractor is such that after acquisition the Word Detector provides an output pulse at some pre-set code condition. This

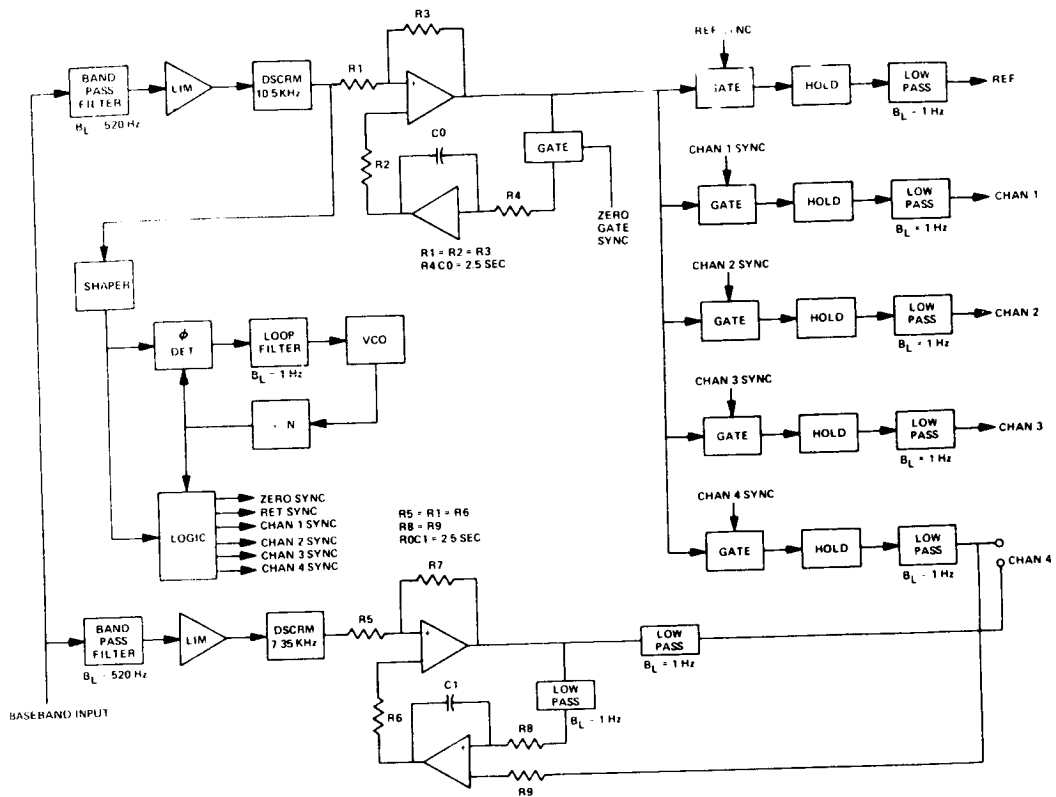


FIGURE 5.3-35 TELEMETRY EXTRACTOR, BLOCK DIAGRAM

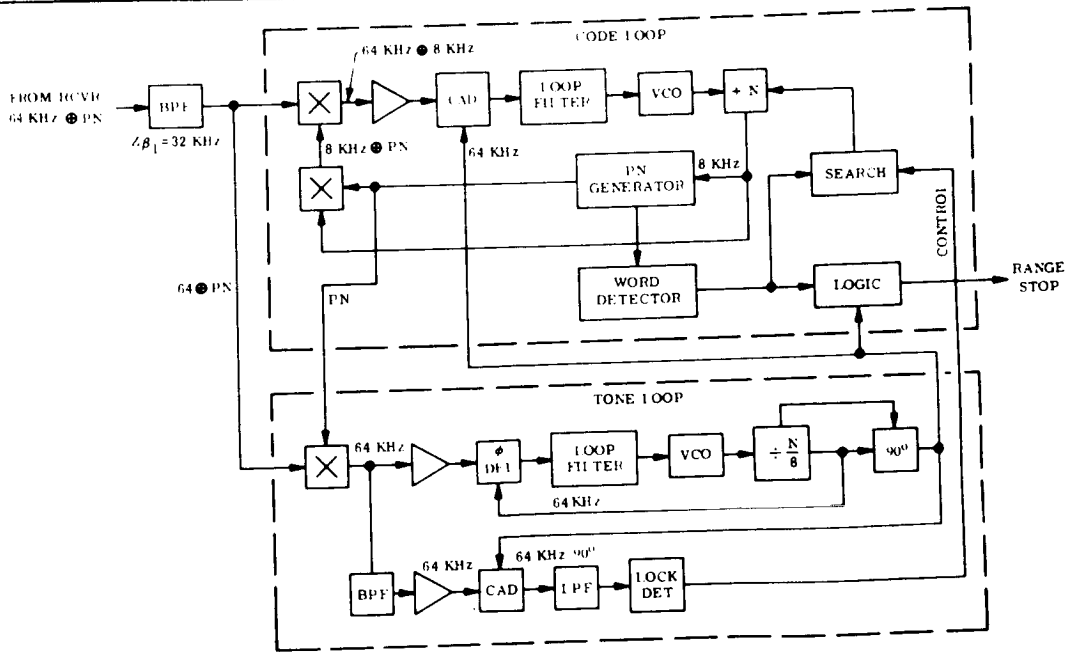


FIGURE 5.3-36 RANGE SIGNAL DEMODULATOR, BLOCK DIAGRAM

is then fed to a logic function which simply creates an output pulse at the first 64 kHz zero crossing after reception of an input from the Word Detector. This output is termed the stop pulse which terminates the count in a time interval counter. Initiation of the counter is done by means of the start pulse which is generated in an identical manner to the stop pulse except the acquisition and tracking functions are not required. As can be seen the demodulator consists of a code loop and a tone loop. Operation of these two loops is as follows:

1. The ground tracking receiver locks to the input RF carrier after which
2. The PN generator in the code loop is precessed in time at a rate of about 10 PN bits per second.
3. When the PN sequence of the demodulator approaches that in the modulator a coherent 64 kHz signal appears at the input to the phase detector in the tone loop. This is shown in the correlation function of Figure 5.3-37. When the tone loop locks to the 64 kHz signal the lock indicator stops the PN precessing and indicates lock.
4. The code loops which has a correlation function as shown in Figure 5.3-38 will then drive itself so as to null out the 64 kHz component. Thus when the code loop has driven the PN generator to this state the 64 kHz signal to the tone loop will be maximum.

As can be seen, once the acquisition process has been completed the operation of the system is identical to a tone ranging system except that ambiguities have been resolved by means of a PN code instead of the addition of tones. The tone loop bandwidth ($2\beta L$) is 2 Hz and acquisition time of the system is based on the code search time. Since the code is precessed at a rate of 10 bits/sec. and the code length is 31 bits, the maximum acquisition time is 3.1 seconds. Zero setting of the range is straight-forward. Coarse range is set in by merely establishing the word detector input state which will allow resolution to within one bit. The fine resolution is obtained by increasing or decreasing the delay in the stop pulse output.

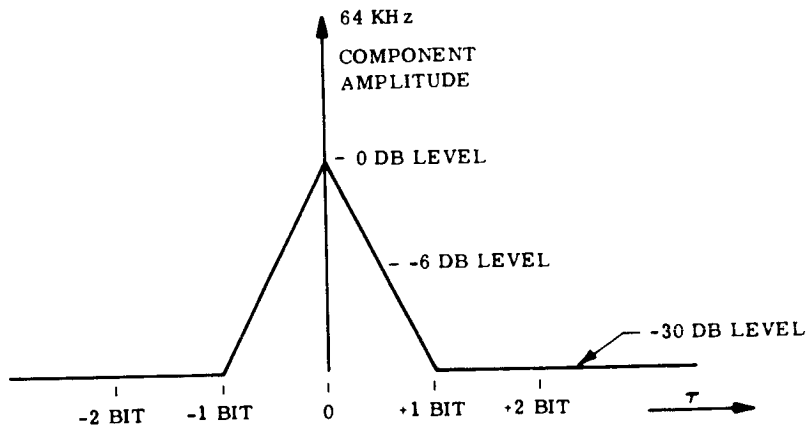


FIGURE 5.3-37 64KHz COMPONENT VS CODE CORRELATION - TONE LOOP

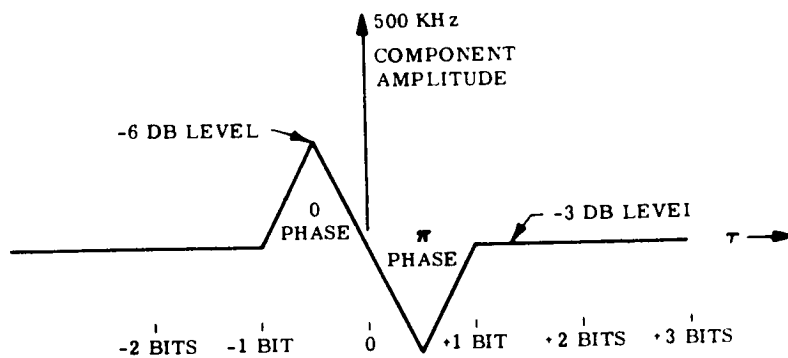


FIGURE 5.3-38 64KHz COMPONENT VS CODE CORRELATION - CODE LOOP

6. Range Modulation Generator.

The purpose of the range modulation generator is to generate the ranging signals which are furnished to the ground transmitter and the range extractor. The ranging signal consists of a 64 kHz resolution tone and ambiguity tones of 8 kHz, 1 kHz and 250 kHz which are coherent with the resolution tone or else the PN signal to resolve the ambiguities of the 64 kHz resolution tone.

7. Timing.

The time is provided by a digital clock in the Time Interval Counter and may be designed to furnish local or elapsed time in digital form for use by the Range Modulation Generator. This time data is also applied to the Data Processor for analysis and recording purposes.

8. Data Processor and Monitor.

This contains all ground equipment controls for acquisition, tracking, monitoring and recording the performance of the system. The data processor provides a display of time, slant range, azimuth and elevation angles and telemetry. It also provides a punched paper tape on which all pertinent data is recorded in teletype code format.

5.3.6.3 Radiosonde.

The radiosonde is designed to perform two functions. As a transponder, it must receive the up-link range signals, demodulate them, and retransmit them to enable the determination of slant range. As a telemetry transmitter, it must accept the outputs of the meteorological sensors, condition them and transmit them along with calibration information to the ground station.

It would be desirable to have a single transponder design for both balloon and rocket launch applications, but the comparatively high packaging costs which are inherent in the rocket environment are an unnecessary restriction on the balloon sonde and, therefore, in order to

reduce per unit costs of the high volume balloon application, a less rigorous mechanical design is used for the balloon.

A block diagram of the radiosonde is shown in Figure 5.3-39 and a list of performance characteristics is shown in Table 5-20. The transponder uses a narrow band FM superheterodyne receiver and a phase modulated transmitter in which the received frequency modulated ranging information is translated to the downlink transmitted signal. The transponder signal levels, gains and bandwidths are based on the use of an inexpensive quartz crystal in the transponder. This quartz crystal, located in the transmitter voltage controlled oscillator, is the source of the receiver local oscillator signal and the transmitter downlink signal. The quartz crystal pays its way by permitting a reduction in the downlink transmitter output power to only 35 milliwatts while operating at slant ranges up to 300 kilometers. This power level allows a substantial savings in battery cost, weight and packaging costs. As can be seen the functional block diagram of the radiosonde does not present any startling or new innovations and the real significance of the design is the development of a radiosonde unit which will economically provide the required outputs. Some of the more important features of the low cost design are:

1. Use of crystal oscillator as described above
2. Use of highly accurate and economical VCO's for the telemetry subcarriers. See Figure 5.3-34.
3. Design of a transponder with low group delay variations over the operating environment.
4. Use of transistorized front end to provide system noise figures less than 7.5 db.
5. Use of a stripline filter in the final X4 output stage to improve reproducibility and eliminate tuning controls.
6. Use of low cost switching gates to provide the necessary channel isolation in an accurate PAM telemetry system.
7. Use of foam packaging to provide a shock resistant, thermally insulated, lightweight design.
8. Design which will allow modular addition or elimination of functions within the radiosonde.

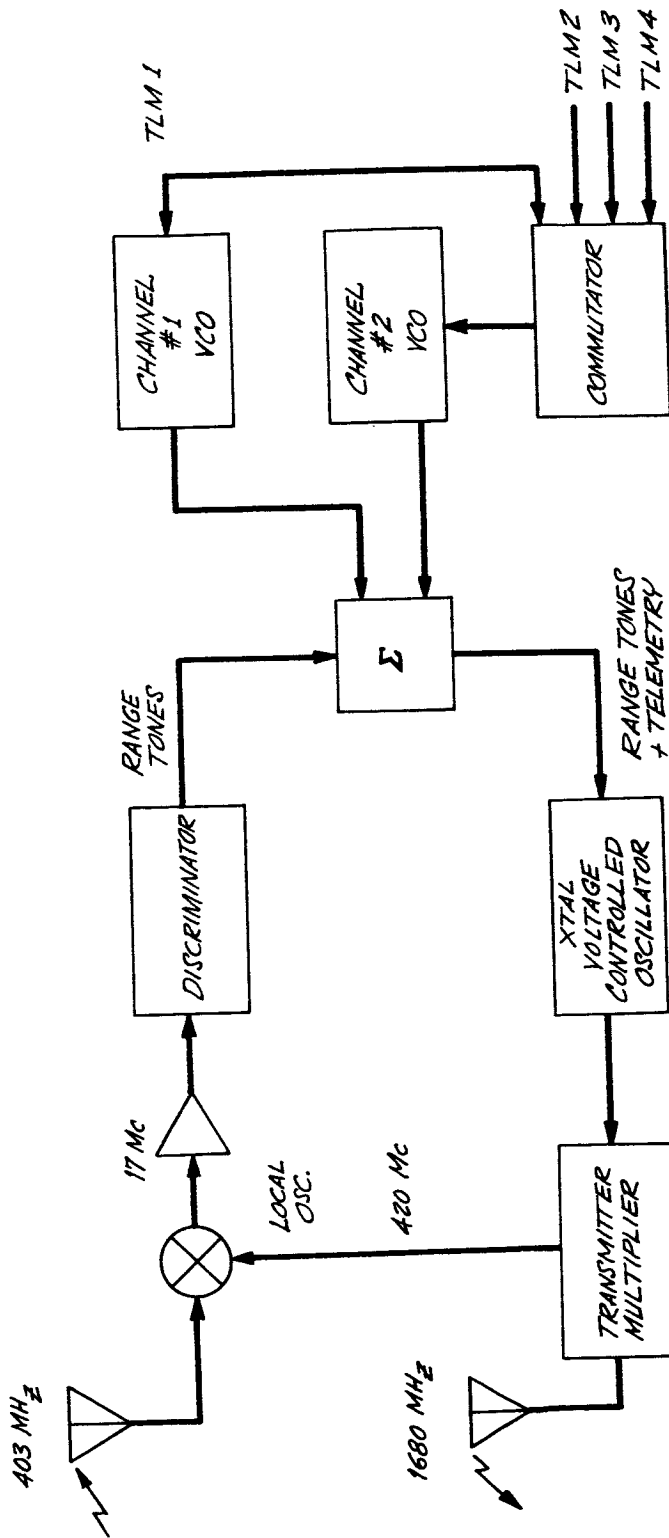


Figure 5.3-39 AMSS Radiosonde, Block Diagram

TABLE 5-20

AMSS RADIOSONDE CHARACTERISTICS

RECEIVER

Input Frequency	400-406 mHz
Type	Superheterodyne FM Receiver
Input Signal Level	-96 to -56 DBM
Input Signal Level w/o Damage	-6 DBM
Noise Figure	8 DB Maximum
IF Bandwidth ($2\beta_{LO}$)	470 kHz
Video Bandwidth (β_{LO})	125 kHz

TRANSMITTER

Output Frequency	1680 mHz Nominal 1660-1700 mHz Band
Output Power	35 Milliwatts
Local Oscillator Output	0 DBM
Subcarrier Deviation Linearity	0.1% of Best Straight Line
Gate Switch Impedances	On - Less than 500 ohms Off - Greater than 500 megohms
Gate Oscillator Frequency	12 Hz
Gate Oscillator Stability	\pm 10%

GROUP DELAY VARIATION

For a 64 kHz Tone the Maximum Group Delay Variation within the Radiosonde over the Operating Temperature, Signal Level and Time	\pm 270 Nanoseconds
---	-----------------------

WEIGHT

Electronics	Less than 2 lbs.
Total Package including Battery	Less than 4 lbs.
Modulation Type	PM
Deviation Linearity	\pm 20% of Best Straight Time

TABLE 5-20 AMSS RADIOSONDE CHARACTERISTICS - continued -

FREQUENCY STABILITY

Short Term	1 Part in 10^9
Long Term (8 Hours)	6 Parts in 10^5

TELEMETRY

Channels	1 Continuous and 3 Time Shared
Frame Rate	One (1) per second
Subcarrier Frequencies	
Continuous Channel	10.5 kHz
Multiplexed Channel	7.35 kHz
Subcarrier Deviation	± 125 Hz Maximum

LIFE

Operating	4 Hours
Storage	1 Year

OPERATING ENVIRONMENT

Temperature	-70° C to $+70^{\circ}$ C
Humidity	To 100% with Condensation
Altitude	To 200 Kilometers
Shock (Rocket Launch)	100 G's of 11 Milliseconds
Acceleration	Duration in each Major Axis 200 G's

ROCKET VEHICLES

6.1 General.

Of the various kinds of launch vehicles and modes of propulsion, so far the only type which has proven to be practical for routine meteorological soundings is the solid-propellant sounding rocket. Gun-launched projectiles have successfully carried chemical trail and chaff payloads to the higher altitudes, but their payload diameter and acceleration loads have restricted their use to these payloads. Also the overall cost of the gun-launched projectile firings appears not to be competitive with the booster dart rocket vehicles. Gun-launched telemetry systems have not been used for meteorological applications, and in fact, their feasibility in general has not been proven. Other methods of propulsion such as liquid-propellant rockets, hybrid solids, ramjets and ducted rockets appear to be too costly and complex without any significant advantage over the solid-propellant rockets.

The solid-propellant sounding rockets for meteorological applications can be categorized as either single stage, booster dart or two stage vehicles. Each of these types has its own advantages and disadvantages. A selection among the various vehicle types for a particular mission can only be made after the sensor instrumentation, telemetry and measurement altitude region have been determined.

For the larger sounding rockets which carry all kinds of large and heavy scientific equipment payloads, some using agencies rate the vehicles on a cost and performance index, such as vehicle cost per pound of net payload per mile of altitude. Some have tried to apply such an index to the meteorological rockets, where it would have no significance at all. When considering a meteorological rocket system, the important parameters are the meteorological measurements to be made, their range of altitude and their cost. Thus, the first consideration should be selection of the sensor, its accuracy and the altitude range of the measurements. Next, one must decide upon the telemetry instrumentation to be used and whether or not to employ a rocketsonde decelerator. Only after the payload and

desired altitude range have been determined, can a reasonable choice of vehicle be made. The efficiency of the vehicle in carrying arbitrary pounds of weight to arbitrary altitudes is not important. The important factor is the ability of the vehicle to carry the required payload to the required altitude at the minimum cost. In addition, there are a number of secondary factors in the choice of a vehicle for the meteorological rocket application. A listing of factors which might be considered in the choice of a rocket vehicle for a typical meteorological rocket system is as follows:

1. Performance.

The vehicle must be able to carry the required measurement payload to the required altitude or it is worthless for the application.

2. Cost.

Since meteorological rockets are used for routine soundings, cost is perhaps the most important factor.

3. Wind Sensitivity and Dispersion.

Since meteorological rockets are used on an operational basis, essentially all over the world, they must be capable of being launched under the most severe wind conditions. Wind sensitivity and the resulting impact dispersion must be kept to a reasonable minimum so that launches will not have to be cancelled due to weather conditions. Dispersion factors other than wind sensitivity are about the same for the various rocket designs, and the resulting impact dispersions (minus wind effects) are primarily a function of apogee altitude.

4. Reliability.

Reliability is a term often used to rate potential vehicles, but is meaningless without a great deal of flight data. What designer does not design for 100% reliability? For vehicles which have not been

thoroughly flight-tested, estimates of reliability are fictions. Many people like to assign a higher reliability to single-stage vehicles than to two-stage vehicles on a statistical basis, yet there are technical factors, such as aerodynamic heating, dynamic pressure and pitch-roll resonance problems, which may more severely affect the single-stage vehicle. There have been many two-stage vehicles which have flown more reliably in a two-stage configuration, i.e., Nike-Cajun, Nike-Apache, Nike-Hydrac, Nike-Tomahawk. Even with a great deal of flight testing and operational usage, reliability can be a variable parameter. It took the Arcas system about four years and three-thousand flights to achieve a 90% reliability. Then after two years of continued success, the reliability fell to a fairly low level. Reliability is difficult, or impossible, to assess with sufficient accuracy for a new design and has been quite variable for the designs in use.

5. Operational Capability.

A meteorological rocket should be capable of being handled and launched by a crew of two people without the necessity for elaborate handling equipment. The system should be relatively simple to operate under adverse weather conditions, for world-wide launchings may be required for remote sites by relatively inexperienced personnel. Conditioning temperature limits should be as wide as possible for compatibility with extreme geographic regions from the tropics to the Arctic.

6. Flight Characteristics.

Flight characteristics such as aerodynamic heating, vibration, acceleration, attitude stability and roll rate have occasionally been used to rate vehicles. However, if the intended payload will adequately function under the given level of each of these factors, what further consideration is required?

7. Safety Characteristics.

Most of the solid propellants used in current motors (except double base propellants) are quite safe to handle and ship so there is little choice among them. Payload separation device initiators are perhaps a greater safety hazard, depending upon their design.

8. Telemetry and Tracking Potential.

Rocketborne telemetry instrumentation is considered as part of the payload for meteorological rockets and, therefore, is included in Item 1. However, if tracking telemetry is employed, a fast moving vehicle may be more difficult to acquire and track than a slow one. This is also true for radar tracking and here a small vehicle may be more difficult to radar track than a large one. These factors should be considered in evaluating a new design.

9. Versatility.

Vehicle or rocket motor versatility has occasionally been used as a rating factor for meteorological rockets in the past. Thus, people have sought a rocket which would perform for a 100 km requirement as well as a 60 km requirement or for a temperature measurement and as well as an ozone measurement. In many cases this versatility criteria is self-defeating from an economic standpoint because it implies that the vehicle system or the rocket motor is overdesigned for one of the mission requirements. Generally this is the requirement for the greater number of flights. For instance, an Arcas-type vehicle might be chosen because it is capable of carrying a fairly bulky ozonesonde instrument and can also be used for routine temperature and wind measurements. However, the requirements for wind and temperature measurements might be for three thousand flights per

year. The Arcas-type vehicle might cost three times as much as a dart vehicle which can only carry the wind and temperature measuring payloads. The obvious economic choice would be to use the larger more costly rocket for the one hundred ozone flights and the smaller lower cost rocket for the three-thousand wind and temperature flights. The same argument holds for altitude versatility consideration. A much greater quantity of 60 km flights are required than 100 km flights. Therefore, why pay a great deal more for the 60 km data by using the 100 km vehicle to obtain it, when the data could be obtained with a smaller lower cost vehicle?

Before a vehicle can be chosen for a meteorological rocket system application, the payload requirements of weight, diameter and length must be determined. Also, payload interfacing requirements, such as the need for telemetry antennas, should be studied.

A fairly wide variety of sounding rocket vehicles are currently available for the meteorological rocket applications. In fact, additional vehicles are being developed each year. The adaptation of these vehicles, or at least the design concepts, to a given payload - altitude requirement can now be a straight-forward engineering development. The development of frangible, consumable or destructable vehicles to eliminate or reduce the falling mass hazard will at the current time require a state-of-the-art advancement.

6.2 Historical Review.

Over the past eight years there have been many studies and attempts to produce a meteorological rocket which could be used for routine soundings to 65 km altitudes. A review of the meteorological rocket vehicle development attempts is presented in Table 6-1. It is interesting to note that only the Arcas and Loki-type systems are currently being used for routine soundings to 65 km.

The Loki type vehicles employ a high-thrust short-duration booster rocket with a non-propulsive dart payload stage. These vehicles offer considerable advantage in operational simplicity, low wind sensitivity and dispersion and low production cost. A disadvantage, however, has been a restriction for some instrumented payloads because of the relatively high boost accelerations and limited payload diameter and volume.

The Arcas vehicle was designed to accommodate a relatively large payload diameter, weight and volume in a low acceleration environment. However, because of its long burning time, the Arcas has proven to be quite wind-sensitive. Wind-sensitivity and dispersion in combination with a relatively high cost for Arcas have been major disadvantages for its use in routine operations.

The past several years have seen a number of attempts to develop more suitable meteorological vehicles, but to date, none have yielded operational systems. The Army Ballistic Research Laboratory and the Canadian Armament Research and Development Establishment have experimented with atmospheric probes launched from 5-inch, 7-inch and 16-inch guns. The acceleration of 16,000 g and upwards associated with this technique make difficult their use with state-of-the-art type meteorological instruments - especially the sensors. Two Navy sponsored programs were directed toward development of single-stage vehicles with substantial payload capacity which would be less wind-sensitive and less expensive than the Arcas. Both used relatively long burning time (9 to 12 seconds) internal burning solid-propellant grains in an attempt to compromise between high accelerations and low-launching velocity. One of these vehicles, the Aeolus, has severe reliability problems and was canceled. The Raven proved to be unstable with payloads of less than 20 pounds. This vehicle will reach only about 160,000 feet from sea level with this minimum payload weight. Both of these vehicles appear to be a move in the proper

TABLE 6-1 Meteorological Rockets

VEHICLE	TYPE OF PAYLOAD	MAXIMUM ALTITUDE FEET FROM SEA LEVEL	PAYLOAD CAPACITY		APPROXIMATE COST		MAXIMUM ACCELERATION g's	STATUS
			WEIGHT (LBS)	VOL (CU ³)	MOTOR(S)	COMPLETE SYSTEM		
Arcas	Robin	230K	8	170	\$1500	\$1800	80	Developed
	Arcasonde	200K	11.0	310	\$1500	\$1950	60	Operational
	AN/DMQ-9	190K	12.0	310	\$1500	\$2300	60	Developed
Loki I (Hasp I)	Chaff	120K	----	24	\$ 300	\$ 450	200	Operational
Loki II (Hasp II)	Chaff	220K	----	28	\$ 300	\$ 450	250	Operational
Hasp III	Wox-1A	160K	----	47	\$ 300	\$ 900	200	Operational
Deacon-Arrow	Chaff	320K	15	120	\$2500	\$3050	40	Operational
	Telemetry	320K	15	120	\$2500	\$ --	40	Operational
Boosted Arcas	Chaff	410K	9	170	\$1800	\$2125	25	Developed
	Telemetry	350K	11	310	\$1800	\$ --	25	Developed
Metroc	Telemetry	100K	2	40	\$ 400	\$ 550	128	Failed
Aeolus	---	200K	6	---	\$ --	\$ --	30	Failed
AG-32	---	200K	1.5	9	\$ --	\$ --	---	Failed
Atmos	---	200K	10.5	47	\$ --	\$ --	30	Failed
Judi Dart	Chaff	240K	----	28	\$ 300	\$ 450	200	Operational

TABLE 6-1 Meteorological Rockets (Continued)

VEHICLE	TYPE OF PAYLOAD	MAXIMUM ALTITUDE FEET FROM SEA LEVEL	PAYLOAD CAPACITY		APPROXIMATE COST		MAXIMUM ACCELERATION g's	STATUS
			WEIGHT (LBS)	VOL (CU ³)	MOTOR(S)	COMPLETE SYSTEM		
SDC Laki Dart	Telemetry	220K	----	35	\$ 300	\$ 500	160	Operational
	Chaff	250K	----	28	\$ 300	\$ 450		
Sidewinder Arcas	---	400K	15.0	310	\$2500	\$ --	28	Developed
Arcas II Arcas	---	450K	15.0	310	\$3300	\$ 00	20	Developed
Sparrow-Arcas	---	500K	15.0	310	\$3800	\$ --	39	Developed
Boosted Metroc	---	200K	2	40	\$ --	\$ --	30	Failed
Raven	---	200K	10	300	\$ --	\$ --	30	Failed
Sirroco	---	220K	20	400	\$ --	\$ --	30	Developed
Hopi-Dart	Chaff	300K	12	20	\$2000	\$1000	150	Developed
Skua	Telemetry	200K	12	300	\$ --	\$ --	30	Operational

direction, but it seems that the developers underestimated the aerodynamic design requirements. The Atmos is a third Arcas-type vehicle which has proved to be unreliable. Two other efforts, the AG-32 ramjet and the Stratos solid-propellant steam-powered system, both directed toward a low-cost vehicle, have not proven practical.

The British, Canadians, Germans and French have all been active in the meteorological rocket area, but the only operating vehicle designed for the 65 kilometer range to come from these efforts to date is the British Skua. This Arcas-type vehicle is slightly larger in diameter and length than Arcas and uses a recoverable booster to increase launching velocity. Cost data is not available to us, but it appears to be a very expensive system. The Japanese have developed an Arcas-type vehicle, the MT-135 which is about twice the size of Arcas and reaches the same altitude.

From a survey of current vehicle programs, it appears that efforts to compromise between Arcas and booster-dart type vehicles have not met with significant success. In most instances, the developers appear to have underestimated the aerodynamic propulsion and structural design requirements for these vehicles.

In 1965 NASA-LRC awarded a contract to North American Aviation, Inc. to conduct a study to define a state-of-the-art rocket vehicle which is suitable for synoptic meteorological soundings. The apogee altitude chosen for this study was 65 km, and the various rocket vehicle design studied were a single stage, a booster dart, a dual-thrust single stage, and a two stage configuration. All designs employed solid-propellant rocket motors. An Arcas-type 4.5 inch diameter single stage vehicle was found to be optimum after consideration of a number of factors such as reliability, versatility and cost. The burning time was reduced from the Arcas value of 29 seconds to 19 seconds to reduce the wind sensitivity. However, the propellant grain weight was even less than that of the Arcas and so was the total impulse even though quite a high value of specific impulse (248.5 seconds) was used in the calculations. The trajectory calculations appear to be quite optimistic in view of the increased drag losses due to the reduction in burning time, and the specific impulse value appears to be higher than obtainable with current state-of-the-art low cost rocket motors.

A major factor in the choice of the single-stage vehicle was versatility in the payload-carrying capacity. Measurements of wind, temperature, pressure, density and ozone concentration were cited as being desirable on a single

flight. This led to the assumption that it would be desirable to retain a significant amount of instrument package installation flexibility in the design of the payload compartment to incorporate future sensors. Models of existing Arcas telemetry packages, i.e., AN/DMQ-9, were also used for payload size requirements. Aside from the problem of over-estimating the performance of this vehicle, it now appears that the requirement for versatility in payload volume is a false requirement for the routine meteorological rocket.

In 1965 the Atlantic Research Corporation completed a study for USAF-CRL to investigate the optimum meteorological sounding rocket configurations from among off-the-shelf rocket motors for missions to 100 km, 150 km and 200 km. Single stage, booster dart and two-stage vehicles were synthesised from among sixty-five available solid-propellant rocket motors to determine the optimum vehicles for the missions as defined below:

<u>Mission</u>	<u>Weight (lbs)</u>	<u>Diameter (in)</u>	<u>Apogee Altitude (km)</u>
A	15	2-5	100
B	15	2-5	150
C	10	4.5-6	200
D	20	6	200

Although 225 vehicle combinations were found which would meet the specific performances, these systems were further evaluated by consideration of the factors as follows:

- Reliability
- Payload Diameter Versatility
- All-Weather Launch Capability
- Handling Requirements
- Safety
- Acceleration Loads
- Aerodynamic Heating
- Temperature Limitations
- Cost

The results of the study indicated that single stage vehicles are not useful for light weight meteorological payloads such as specified for the study. This is because fairly large motors must be used for the high altitude performance and these large motors would require ballast in the payload section for adequate stability. Oversize payloads or ballast weight were not allowed under the ground rules of the study. These restrictions have had a significant effect on the study results. Booster dart vehicles did not rate high in the study because of the payload diameter limitations imposed by the study and the value rating scheme which was used. Although twenty-one booster dart vehicles qualified on performance basis, they were severely down-rated on grounds of having small available payload diameters, large motor sizes and handling. The two-stage vehicles were scored as the first twenty desirable vehicles for each of the four-performance classes. Thus, the study results would indicate that for the meteorological rocket requirements above 100 km, two-stage vehicles are probably the best overall choice. The proposed best choices are tabulated in Table 6-2.

It is interesting to note that the Arcas appears as the second stage for the first four vehicles of categories A and B, and for the first nine vehicles of category C. Loki second stages rate almost equal to Arcas for category A and appear to also be desirable for category B requirements. The larger diameter requirement of category C dictates the use of the Hopi IV in place of the Loki. Very few successful candidates were found for category D (6-inch diameter minimum payload to 200 km) and even those few had low value scores. These vehicles were all quite a bit large and more expensive than the current concept of a meteorological rocket would allow.

As with previous studies of optimum meteorological rockets, this ARC study has suffered from too generalized payload requirements, rather arbitrary ground-rules, and a quite subjective value judgement scoring system. A meteorological rocket which is to be used frequently should be designed for the exact measurement instrumentation to obtain the required data throughout the required altitude region at the lowest possible cost. There is much too great a difference between a two-inch and five-inch diameter payload for them to be considered in the same category. The study ground-rules of not permitting ballast or over-sized payloads (larger diameter payload than the final stage rocket motor) are unrealistic limitations which arbitrarily restrict the number of possible vehicle combinations.

TABLE 6-2

SUMMARY OF ARC ROCKET STUDY

CLASS	(A)	(B)
Payload	15 lbs.	15 lbs.
P/L Dia.	2 to 5 in.	2 to 5 in.
Altitude	100 km	M=3.5 at 100 (150) km

RANK	ROCKETS	SCORE	ROCKETS	SCORE
1	Judi-Arcas	83.9	Spar.Sust-Arcas	78.6
2	Hasp II - Arcas	81.8	Side 1-A Arcas	76.3
3	Falcon-M58-Arcas	81.4	Aeroj.Sled-Arcas	75.4
4	Zuni-Arcas	76.2	Mauler-Arcas	72.4
5	Judi-Judi	73.5	Spar III-6B-Side 1-C	72.1
6	NPP Boost-Arcas	72.8	Falcon Gar II-Arcas	71.4
7	Judi-Hasp	72.4	Side 1-C-Side 1-C	69.0
8	Falcon-M58-Judi	72.4	Arcas Boost-Hopi IV	68.4
9	Hasp-Hasp	72.2	Cherokee-Side 1-C	67.9
10	Sup. Falcon-Arcas	71.8	Spar. Sust-Judi	66.8
11	Falcon M58-Hasp	71.2	Hopi III-Side. 1-C	66.4
12	Hasp-Judi	71.0	Aeron.Sled-Side 1-C	66.3
13	Spar. III-6B Side 1-A	70.4	Spar.Sust-Hasp	66.3
14	Spar. Sus-Side 1-C	68.5	Side. 1A-Judi	66.0
15	Falcon M58-Side 1-C	68.2	Hopi II-Side 1-C	65.7
16	Spar III-6B-Zuni	67.2	Hopi IV-Side 1-C	65.4
17	Zuni-Judi	67.1	Side 1A-Hasp	65.1
18	Deacon-Side 1-A	66.7	Yuma 1 - Side 1-C	64.1
19	Hopi III-Side 1-A	Aero	Aeroj. Sled-Judi	63.8
20	Falcon-Gar II-SI-C	66.0	NPP Boost-Hopi IV	63.0
25	Zuni-Side 1-C	64.6	AeroB. Boost-Side 1-C	61.9
30	Judi-Hopi II	63.7	Deacon-Side 1-C	60.0
40	NOTS-Boost-Arcas	62.0	Upstart-Side 1A (Bo)	58.0
First Dart	#42 Hawk-Dualt.	61.8	#62 Black Brant 10"	49.4
Sec. Dart	#48 Hopi IV	60.5	#67 Recruit	43.6
Third Dart	#58 Gar 9	58.0	#68 Lance	40.3
Last Rated Vehicle	#104 Terrier-Arcas Boost Boost	40.2	#69 Terrier-Dart MK-12 Boost	34.7

TABLE 6-2

SUMMARY OF ARC ROCKET STUDY - continued -

CLASS		SCORE		SCORE
Payload	Ⓒ		Ⓓ	
P/L Dia.	10 lbs.		20 lbs.	
Altitude	4.5 to 6.0 in.		6.0 to 12 in.	
	200 km		200 km	
RANK	ROCKETS	SCORE	ROCKETS	SCORE
1	Spar. Sust-Arcas	71.5	Javel. III-Viper 2B	51.4
2	Spar. III-68-Arcas	70.9	Recruit-Viper 1B	48.8
3	Aeroj-Sled-Arcas	68.2	Yardbird-Kiva 1	48.2
4	Cherokee-Arcas	68.1	Genie MD-1-Kiva 1	47.4
5	Mauler-Arcas	68.0	Hawk Dual-Deacon	47.0
6	Yuma 1-Arcas	66.9	Javel. III-Deacon	45.0
7	Hopi II-Arcas	66.8	Lacrosse-Kiva 1	44.7
8	Side, 1C-Arcas	65.5		
9	Hopi 1-C Arcas	64.8		
10	Spar. Sust.-Hopi IV	63.2		
11	Aerob Boost-Arcas	62.2		
12	Deacon-Arcas	61.0		
13	Falcon M58-Hopi IV	61.0		
14	Mauler-Hopi IV	59.8		
15	Genie MD-1-Arcas	59.5		
16	Cherokee-Hopi II	59.1		
17	Mauler-Hopi II	58.2		
18	Bullpup-Arcas	57.8		
19	Lacrosse-Side IIC	57.6		
20	Apache-Side 1-C	57.4		
25	Spar.Sust-Hopi II	59.7		
30	Gar 9-Side 1-C	55.5		
40	Bullpop-Hopi III	48.6		
First				
Dart	#37 Tomahawk 406	50.2		
Sec.				
Dart	#43 Black Brant (17")	43.0		
Last				
Rated Vehicle	#45 Black/Brant (10") (HVAR)	31.8	#7 Lacrosse-Kiva 1	44.7

Value judgements concerning the tradeoff of merit points for such factors as aerodynamic heating, maximum dynamic pressure, propellant safety, vehicle reliability and maximum acceleration are almost completely subjective. These factors may not be at all pertinent depending in many cases upon the specific payload. In general, vehicle reliability estimates are worthless for vehicles yet to be developed. If a particular vehicle and payload can withstand a certain dynamic pressure and aerodynamic heating, there is no value advantage in reducing these factors. Either the system performs or it does not. The validity of the final results of this study can be questioned on the basis for determining the relative importances among the various rating factors.

In spite of the shortcomings of the study, there is presented a good deal of detailed information which is quite useful for future planning of rocket vehicles. Some of the performance data, however, are not very accurate and should not be considered as valid without some further checking. For instance, the Viper 2B-Dart (2.0 inch diameter) is shown as achieving an apogee of only 350,000 feet, while subsequent flight tests of this same vehicle resulted in apogees as high as 435,000 feet.

The Arcas has been the primary meteorological rocket network and 60 km support vehicle for the last six years. Although the systems reliability started out at a relatively low level, it gradually improved over the years to a level of about ninety percent. However, over the past year or so this reliability level has suffered somewhat.

At the current time, it appears that the Arcas is being phased out as the primary 60 km meteorological rocket in favor of the instrumented Loki Dart vehicle. This Loki Dart system has been qualified and standardized by the Air Force as the Meteorological Probe PWN-8B. The Loki Dart system with a ram-air decelerator (Starute) and a 1680 mHz temperature measuring payload (Datasonde) currently is 42 percent of the Arcas-Arcasonde cost and this figure has been obtained at fairly modest production rates. Increased production requirements should reduce this cost ratio to approximately one-third. An additional advantage of the Loki system is a reduction of the wind sensitivity from a value of 1.20 nm/knot for the Arcas to a value of 0.32 nm/knot for the dart.

Loki Dart vehicles have been used for years to dispense chaff for routine wind data. Current Loki Dart chaff systems are routinely dispensing chaff to altitudes of 250,000 feet from sea level launch sites and 280,000 feet from WSMR. A high energy Loki motor was developed two years ago by

Space Data for the Army to obtain chaff winds to 280,000 feet from sea level sites. The Hopi Dart and Cajun Dart vehicles were developed for NASA-MSFC to obtain winds to 90 km with chaff payloads from Cape Kennedy in support of the Saturn. Just this year the Super Loki vehicle has been developed to obtain winds to 90 km with chaff payloads from Cape Kennedy in support of the Saturn. The Super Loki vehicle has been developed for NASA-MSFC to replace the Hopi Dart and Cajun Dart with a lower cost system for the high altitude chaff winds requirement. An instrumented dart for the Super Loki is currently being developed to obtain winds and temperatures to a higher altitude than the capability of the current PWN-8B system.

Instrumented payloads for the higher altitude measurements have historically been flown with the larger geophysical rockets such as the Aerobee-150, the Nike Cajun, the Nike Apache and others. A significant break-through a few years ago was the development of the Sparrow Arcas for soundings to about 475,000 feet with moderate size (4.5-inch diameter) and moderate weight (16-lb) payloads. Other versions of the boosted Arcas have been developed for altitudes between 200,000 feet and 475,000 feet.

The Viper Dart has just recently been developed for carrying the Robin passive inflatable sphere to an altitude of 125 km. Further development efforts are currently being expended to increase the Viper Dart altitude to 140 km. The dart has a 2-inch diameter, weighs 29.5 pounds and has a payload volume of 46 cubic inches.

6.3 Current Vehicle Systems.

6.3.1 General.

Although there have been a number of attempts to develop optimized meteorological rockets over the past few years, the only ones currently being used on a routine, synoptic basis are the Arcas and the Loki Dart. Since reliable instrumentation has been developed for the Loki vehicle, it is currently replacing the more expensive and wind-sensitive Arcas for the majority of the Meteorological Rocket Network and routine support launchings. Thus, the Arcas is gradually being relegated to the less frequent research soundings where the versatility in payload diameter is required. Until a GMD-2 transponder-type telemetry instrument is developed for the Loki system, however, the Arcas will still be used routinely with the AN/DMQ-9 transponder sonde at the few locations requiring a GMD-2 track. For routine measurements above 65 km the Super Loki and the Viper Dart are currently being employed to measure chaff winds and falling sphere densities and winds respectively. The various boosted Arcas vehicles available have had limited use, generally for special research payloads. The various Nike boosted vehicles have been used for large research payloads, and are too large and costly to be considered seriously for routine meteorological sounds. The two foreign meteorological rockets, Skua I, (British) and MT-135 (Japanese), are basically Arcas-type vehicles which appear to have no particular advantage over the Arcas. A summary of the current meteorological rocket vehicles is presented in Figure 6.3-1 and Table 6-3.

Although the monthly Data Report on Meteorological Rocket Network Firings lists twenty-six meteorological rocket types, most of these vehicles are either obsolete or redundant. All of the Loki type vehicles of Table 6-4 are essentially the same, and the only operational version of the instrumented Loki is the PWN-8B. The obsolete vehicles from the Data Report are listed in Table 6-5. More detailed information on the currently active vehicles are presented in the sections which follow.

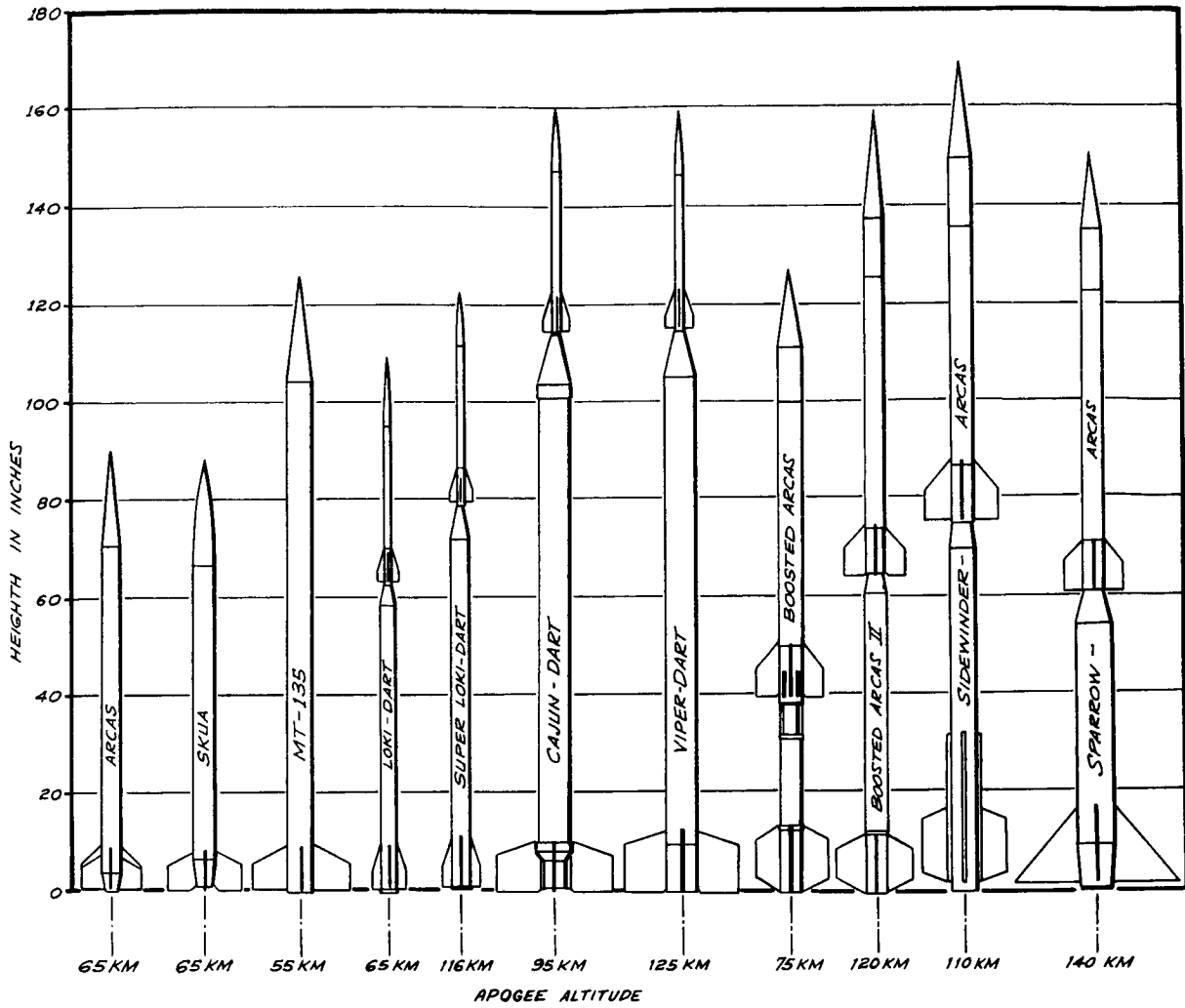


FIGURE 6.3-1 METEOROLOGICAL ROCKET CONFIGURATIONS

TABLE 6-3

SUMMARY OF CURRENT METEOROLOGICAL ROCKET VEHICLES

VEHICLE	ALTITUDE	PAYLOAD TYPE	PAYLOAD Dia. / Wt.	ANNUAL USAGE	BASE COST	REMARKS
Arcas	65 km	Temp. Sonde	4.5" / 5 kg	2,000	\$ 2,000	Medium price, being replaced by Loki Dart.
Skua I	65 km	Temp. Sonde	4.5" / 5 kg	100	Unknown	Appears to be expensive.
MT-135	60 km	Temp. Sonde	4.5" / 5 kg	Few	Unknown	Limited use so far.
Loki Dart	65 km	Temp. Sonde	1.462" / 1 kg	1,000	\$ 700	Inexpensive, replacing Arcas for routine soundings.
	75 km	Chaff or Robin	1.375" / 1 kg	500	\$ 500	
Super Loki	116 km	Chaff	1.625" / 1 kg	25	\$ 700	Introduced at Cape Kennedy late 68.
Cajun Dart	90 km	Chaff	1.750" / 1.5 kg	50	\$ 2,500	Used at Cape Kennedy for routine winds.
Viper Dart	125 km	Robin	2.000" / 2 kg	25	\$ 2,500	Introduced at Cape Kennedy late 68.
Boosted Arcas	75 km	Any	4.5" / 5 kg	Few	\$ 3,500	Limited Use.
Boosted Arcas II	120 km	Any	4.5" / 5 kg	Few	\$ 3,000	Just Developed.
Sidewinder						
Arcas	110 km	Any	4.5" / 5 kg	Few	\$ 3,500	Limited Use.
Sparrow Arcas	140 km	Any	4.5" / 5 kg	Few	\$ 4,500	Limited Use.
Nike Cajun	120 km	Any	6.5" / 25 kg	150	\$ 6,000	Large and Expensive.
Nike Apache	160 km	Any	6.5" / 25 kg	150	\$ 6,000	Large and Expensive.
Nike Iriquois	220 km	Any	7.8" / 20 kg	20	\$10,000	Large and Expensive.
Nike Tomahawk	300 km	Any	9.0" / 30 kg	40	\$15,000	Large and Expensive.
Nike Hydac	300 km	Any	9.0" / 30 kg	40	\$13,000	Large and Expensive.

TABLE 6-4

LOKI DART VEHICLES

JUDI

LOKI I

ROCKSONDE 200 (Obsolete)

HASP I

HASP II

HASP III

TALLY HI (Obsolete)

LOKI DART

PWN-8B

TABLE 6-5

OBSOLETE VEHICLES

LOKI I

JUDI

ROCKSONDE 200

HASP I

METROC

BOOSTED METROC

DEACON ARROW

ARCHER

RAVEN

HOPI DART

TALLY HI

HASP III

SIROCCO

CAJUN

6.3.2 Arcas.

Such a great deal of information has been published concerning the Arcas, that to include a detailed description here would be painfully redundant. Therefore, only a brief description will be given.

The Arcas sounding rocket is an unguided vehicle with a diameter of 4.5 inches and is designed to carry payloads of 12 pounds or less to heights in excess of 200,000 feet when launched from sea level. Four fixed fins stabilize the vehicle during flight. A pyrotechnic separation device is included to separate the payload from the missile at peak altitude. The rocket is designed for launching from a specifically designed closed-breech launcher to reduce its inherent wind-sensitivity to a somewhat tolerable level.

A cross-section of the Arcas rocket vehicle is shown in Figure 6.3-2. The rocket is 4.5 inches in diameter, 90.9 inches long and weighs 77 pounds when provided with a nominal 12-pound payload. The high performance rocket motor is powered by an end-burning solid-propellant grain, generating a 336-pound thrust for approximately 30 seconds. The application of long-burning propellants is advantageous because acceleration is experienced over a long period of time, peak g-loading is minimized and more efficient conversion of thrust to vehicle velocity is realized based on the greater percentage of thrust time in a more rarefield region of the atmosphere.

The Arcas has a cylindrical parachute container threaded to the head cap of the motor case. The parachute is packaged in to this section and the forward head closure of the parachute compartment is secured with three shear pins. The barrel section of the plastic nose cone slides inside the forward end of the parachute container. The active payload is secured to a metal instrumentation base plate which is secured, in turn, to a center stud bolt by means of a lock-nut. The nose cone may be secured to the instrumentation base plate by set screws, or, if nose cone jettison is desired, by six steel balls which fall away upon expulsion of the parachute-payload combination. The steel-ball separation device permits exposure of sensing elements to the atmosphere during descent of the payload.

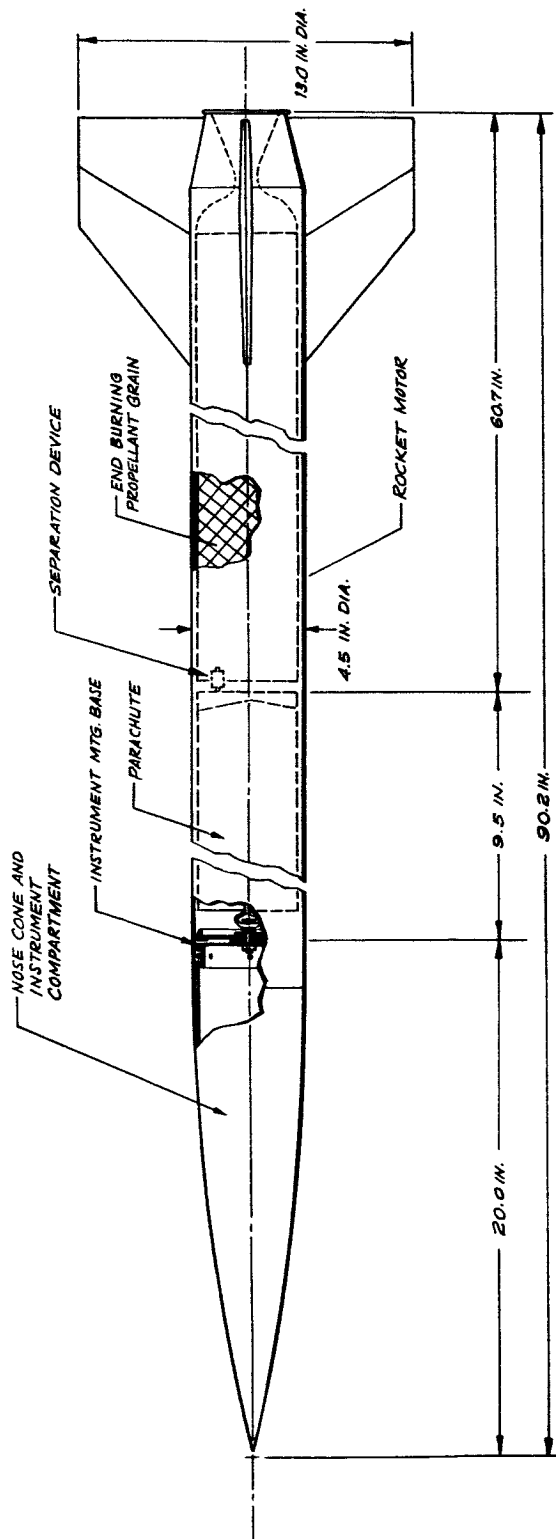


FIGURE 6.3-2 THE ARCAS ROCKET

A gas-generator separation device mounted in the head cap of the rocket motor functions at apogee, separating the parachute and instrumentation section from the rocket motor. This separation device incorporates a pyrotechnic delay column which is activated at termination of the propellant burn phase, providing a 130-second function period from rocket lift-off to payload separation. The gas-generator, acting on the after closure of the parachute container, expels the parachute, instrumentation and nose cone from the burned-out motor by piston-type action.

The Arcas nose cone (Figure 6.3-3) provides a volume of 140 cubic inches for instrumentation. An additional 150 cubic inches of volume can be utilized if the parachute is not required, or, for every large payloads, as many as 127 cubic inches can be obtained by extending the parachute cylinder or cylindrical section of the nose cone. In the nominal active payload configuration section, the nose cone, instrumentation, base plate, parachute container, and associated components weigh four pounds. The parachute weighs an additional 2.3 pounds, making the gross component weight 6.3 pounds and permitting up to 5.7 pounds active payload weight for the nominal configuration. By use of an extended payload section and parachute container, payloads up to 20 pounds can be accommodated.

The Arcas Robin balloon is a variation of the basic Arcas rocket system design. The payload consists of a 1-meter-diameter mylar balloon bearing an internal corner reflector for passive radar tracking purposes. The balloon weighs 0.3 pound and is inflated by chemical action upon expulsion from the rocket at apogee. In the Robin configuration, the parachute container is eliminated, and the nose cone is attached directly to the motor case by means of a threaded adaptor sleeve. The Robin rocket vehicle is 80.8 inches long and the total weight is 72.5 pounds, including ballast required to maintain vehicle stability brought about by the extremely light balloon payload. Separation of the Robin balloon is accomplished by means of the standard Arcas separation device.

Major Arcas parameters are listed in Table 6-6.

The rocket motor (Figure 6.3-4) contains an end-burning charge of plastisol type solid propellant. The motor case consists of a one-piece steel outer casing with an insulator liner. The nozzle structure is a tapered graphite insert supported by the tapered after-end of the case. A steel retaining ring, welded to the head end of the case, is used to secure the

Six steel balls, to be used when the nose cone is to separate from instrument base. Flat head screws are used when separation is not required.

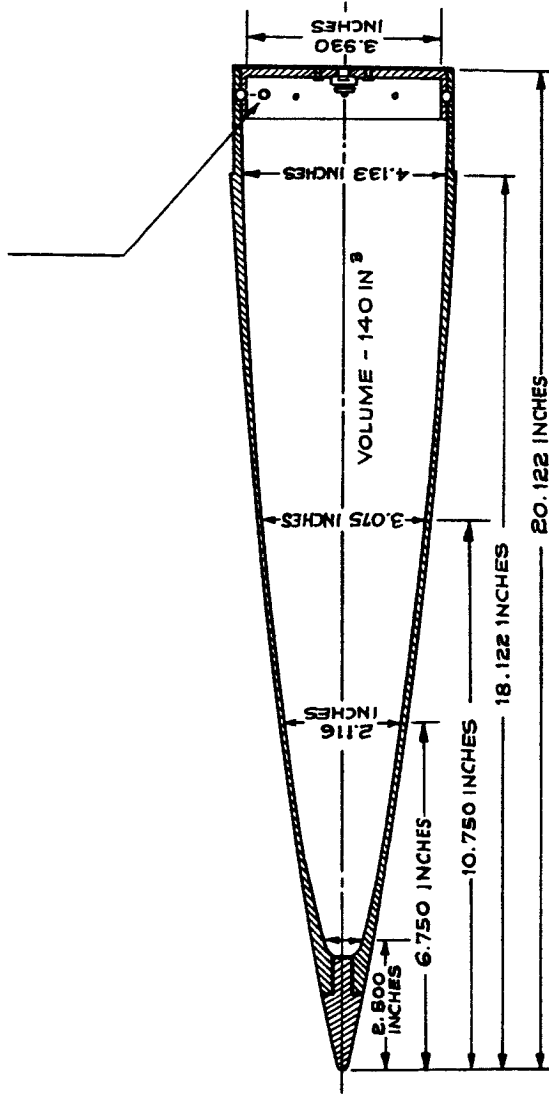


FIGURE 6.3-3 ARCAS NOSE CONE

TABLE 6-6

ARCAS
ROCKET SYSTEM DIMENSIONS

PARAMETER

Length (in.)	90.9
Overall	60.8
Rocket motor	12.0
Parachute container	18.1
Nose cone	
Diameter (in.)	4.5
Fin span (in.)	13.0
Fin area (4 fins) (in. ²)	94
Interval volume (in. ³)	140
Parachute container	170
Nose cone	
Nominal weight (lbs.)	
Total vehicle	70.5 *
Motor burnout	29.5 *
Nose cone	1.5 *
Parachute container (loaded)	4.0
Rocket motor	65.0

* Does not include instrument package and instrument base, which total 4 to 6.5 lbs. depending on the type of rocketsonde payload.

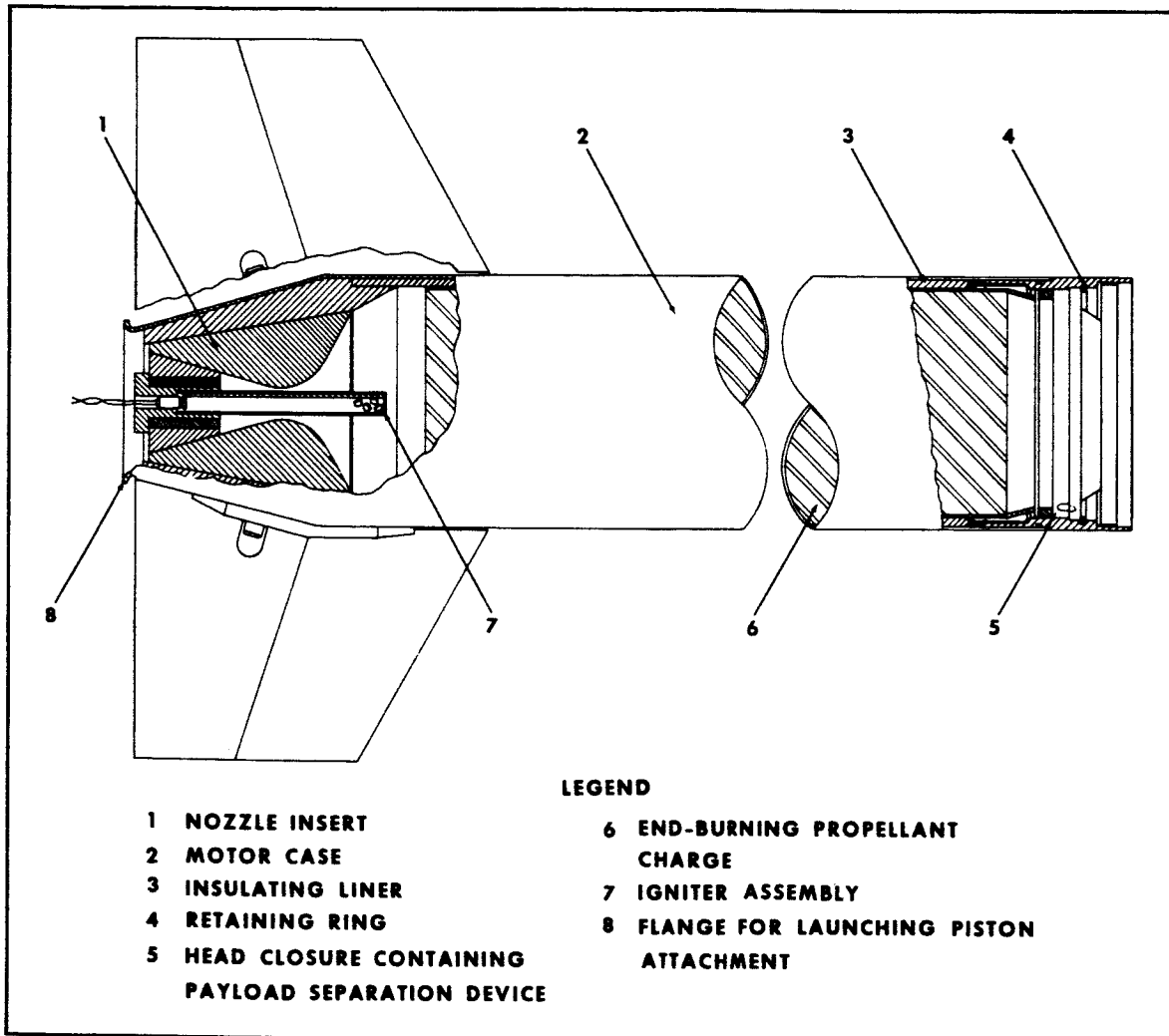


FIGURE 6.3-4 CROSS-SECTIONAL DIAGRAM OF THE ARCAS MOTOR

motor head closure and also provided a threaded joint for attachment of the payload sections. The motor is delivered completely assembled and cannot be disassembled in the field. Nominal performance characteristics of the motor are shown in Table 6-7.

A pyrotechnic device is used for payload separation and is an integral part of the motor head closure. This device contains a delay column of pyrotechnic material that burns for 100 seconds. It is ignited as combustion of the propellant nears completion after approximately 28 seconds. This delay column in turn ignites a gas-generating charge, which separates the payload from the expended rocket motor at a relative velocity of 50 feet per second with a maximum acceleration of less than 50 g's.

The igniter is packaged separately for shipment and is installed through the nozzle of the rocket just prior to firing. It employs an electrically activated squib and five grams of pyrotechnic booster compound. The parachute container assembly, including parachute, is provided as a sealed unit and cannot be disassembled in the field. It is coupled to the motor case by connecting a lanyard to an attachment hole in the case head closure.

The major components of the Arcas are shown in Figure 6.3-5.

A closed breech launcher is normally used for launching the Arcas rocket. The major components of the launcher as shown in Figure 6.3-6 are a 20-foot tube to guide the vehicle during initial acceleration, a free-volume cylinder to retain the exhaust gases, and a base assembly constructed to permit azimuth and elevation angle settings. Access to the launcher for loading is provided by a hinged breech plate on the bottom of the free-volume cylinder. The breech plate is equipped with a connector for the firing line and the igniter leads.

In operation as indicated in Figure 6.3-7 the free-volume cylinder entraps the exhaust gases of the burning rocket motor. These gases exert pressure on a piston attached to the nozzle end of the rocket vehicle, accelerating the vehicle up the launching tube. The rocket is centered and supported in the tube during launching by four plastic spacers that fall away from the rocket along with the piston as the rocket leaves the tube.

TABLE 6-7

ARCAS ROCKET MOTOR PERFORMANCE CHARACTERISTICS

<u>CHARACTERISTICS</u>	<u>TEMPERATURE (° F)</u>	<u>NORMAL VALUE</u>
Average thrust (lbs)	- 10	268
	+ 70	336
	+110	385
Burning time (sec)	- 10	35.4
	+ 70	29.0
	+110	24.8
Average pressure (psi)	- 10	805
	+ 70	1020
	+110	1150
TOTAL IMPULSE (lb - sec)	----	9089

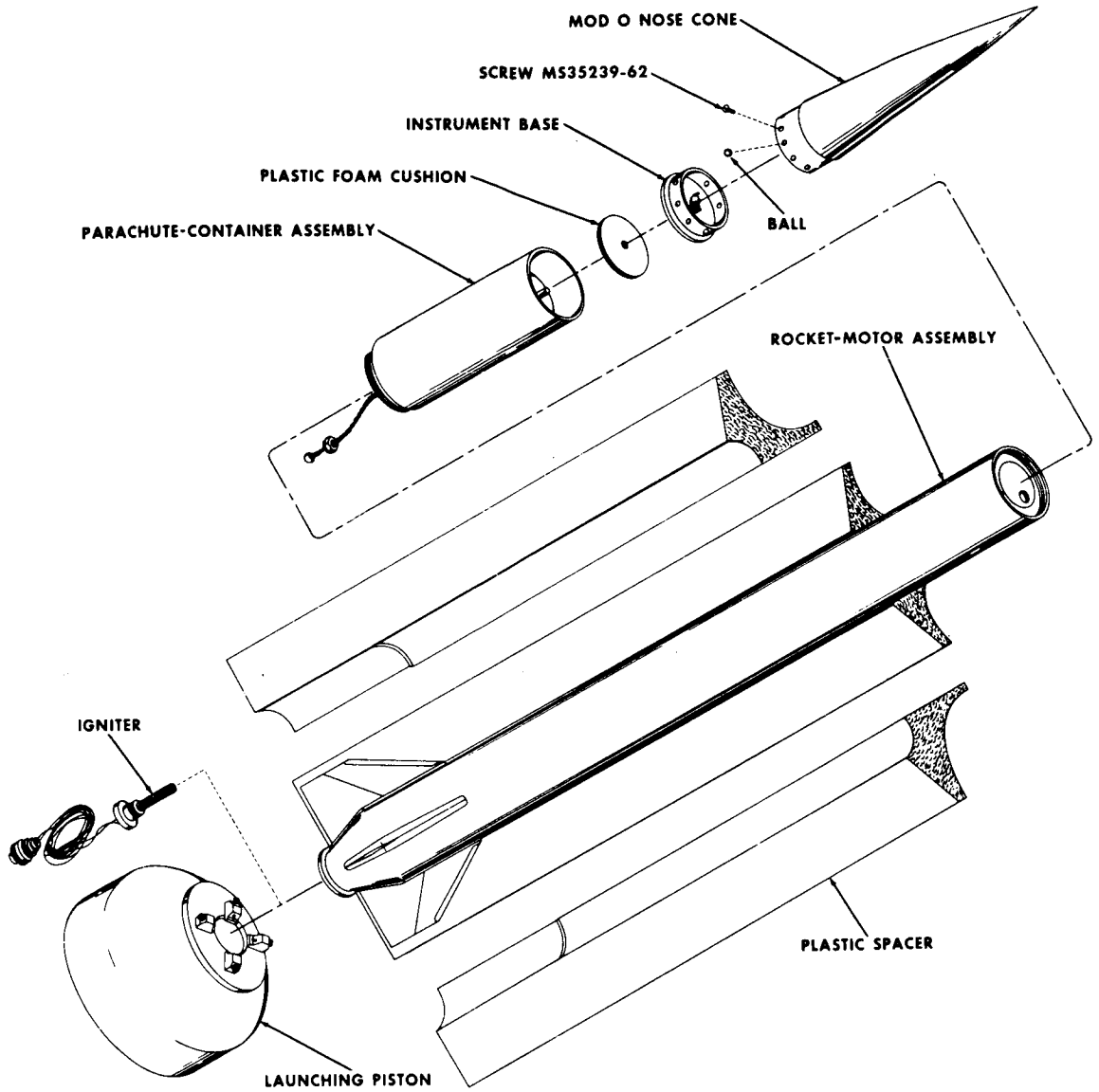


FIGURE 6.3-5 THE MAJOR COMPONENTS OF THE ARCAS VEHICLE

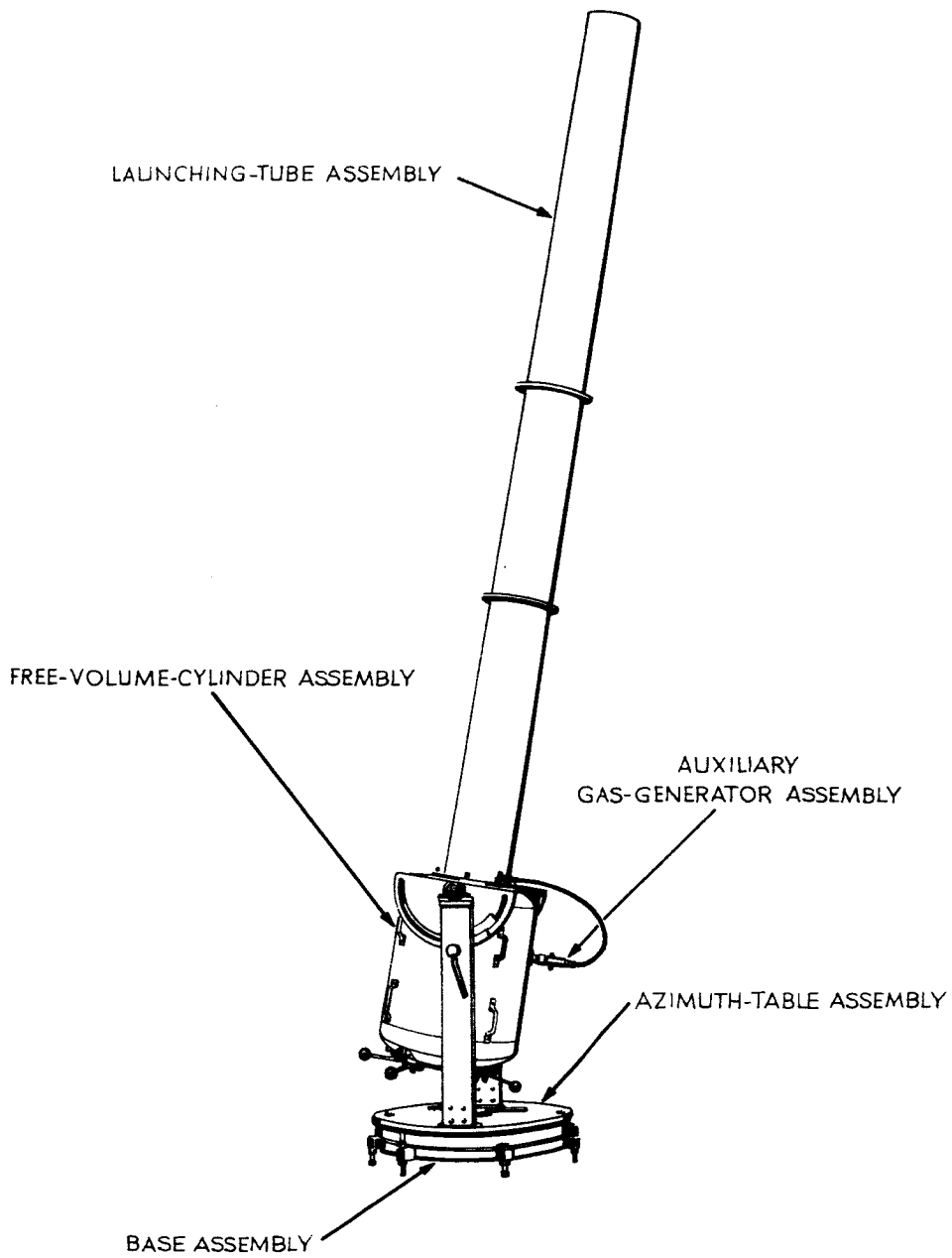


FIGURE 6.3-6 MAJOR COMPONENTS OF THE CLOSED-BREECH ARCAS LAUNCHER

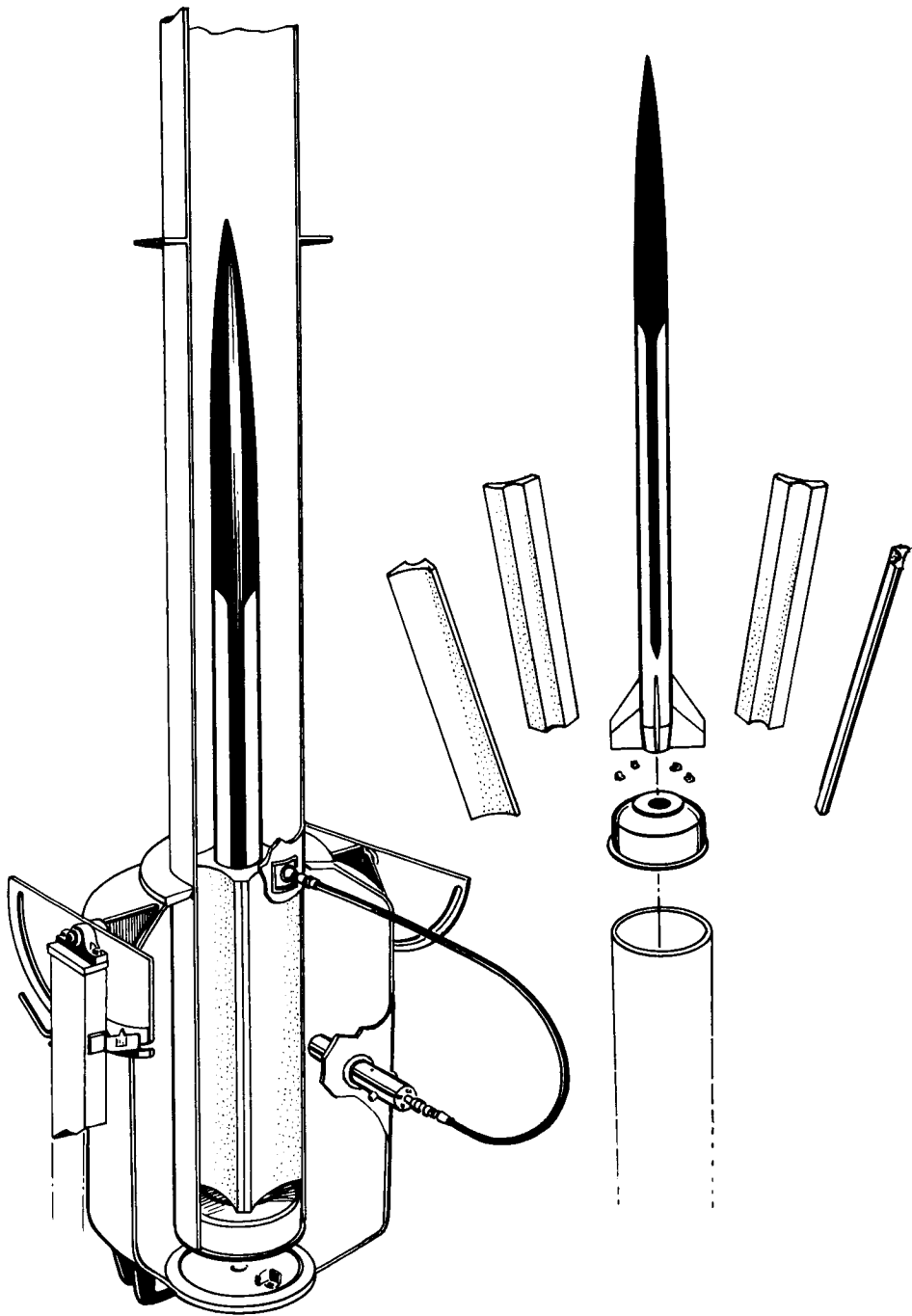


FIGURE 6.3-7 Principle of Operation of the Arcas Closed-Breech Launcher

If desired, an auxiliary gas generator which is incorporated into the free-volume cylinder may be used. This will increase the launching velocity over that obtainable with the basic launching system. The gas generator contains a propellant charge that generates additional gas pressure into the cylinder. The generator is fired mechanically by gas pressure from the launcher transmitted through a high temperature, high pressure hose. The U. S. Navy at PMR has recently developed a compressed air system to be used in conjunction with the Arcas launcher to accomplish the same objective.

Utilization of the gas generator technique results in an increase of the Arcas rocket launch velocity. In the case of the rocket-sonde system the increase is from 150 feet per second to 230 feet per second. This has the effect of reducing the Arcas wind sensitivity slightly.

Typical Arcas flight performance values are shown in Table 6-8 for 88° and 84° launch elevations for both the Robin and Arcasonde configurations, with and without the launcher gas generator.

6.3.3 Loki.

The Loki meteorological rocket sounding system is designed to measure temperature and wind velocity as functions of altitude to a height of 65 km. A sketch of the Loki rocket system is shown in Figure 6.3-8.

The rocket is launched from a helical-railed launcher. The vehicle, consisting of a rocket motor and payload-bearing dart, is propelled to a motor burnout height of 5,000 feet where the dart is separated from the rocket motor. The dart then follows a ballistic trajectory to a peak height where the payload is expelled from the dart. The payload consisting of the temperature sensing device and small radio-frequency transmitter then descends on a radar-reflective parachute or other decelerator.

Other payloads commonly employed in the Loki system are radar-reflective chaff dipoles and radar-reflective parachutes for the determination of wind velocity while radar-reflective inflatable spheres have been utilized for the determination of stratospheric air density and winds.

The rocket vehicle is comprised of two stages, the booster motor and the unpowered dart which contains the payload. The Loki motor is an internal-burning type which provides an average thrust of 890 kilograms for a period of

TABLE 6-8

FLIGHT PERFORMANCE CHARACTERISTICS OF THE ARCAS SYSTEMS
FOR 88° AND 84° LAUNCH ANGLES

<u>STANDARD LAUNCH</u>	<u>ROCKETSONDE (12 lbs)</u>		<u>ROBIN (8 lbs)</u>	
	<u>88°</u>	<u>QE</u>	<u>84°</u>	<u>QE</u>
Max. altitude (ft)	197,000		181,000	
Time to max. altitude (sec)	124		120	
Max velocity (fps)	3,440		3,420	
Altitude at burnout (ft)	51,000		50,000	
Launch velocity (fps)	150		150	
Acceleration at launch (g)	33		33	
<u>GAS GENERATOR LAUNCH</u>	<u>ROCKETSONDE (12 lbs)</u>		<u>ROBIN (8 lbs)</u>	
	<u>88°</u>	<u>QE</u>	<u>84°</u>	<u>QE</u>
Max. altitude (ft)	210,000		198,000	
Time to max. altitude (sec)	128		125	
Max. velocity (fps)	3520		3510	
Altitude at burnout (ft)	53,000		52,000	
Launch velocity (fps)	230		230	
Acceleration at launch (g)	90		90	

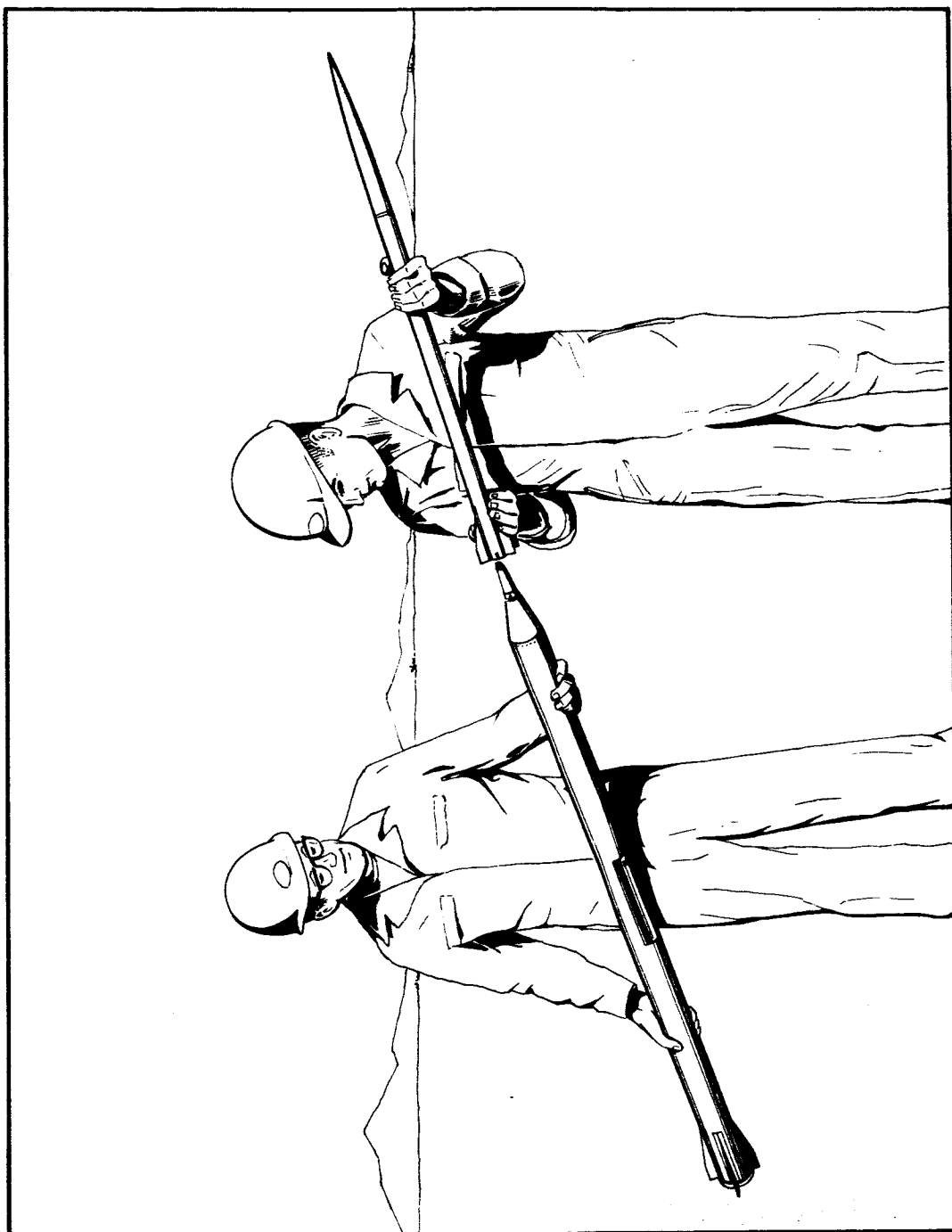


FIGURE 6.3-8 THE LOKI-DART METEOROLOGICAL SOUNDING ROCKET

2 seconds thus producing a rocket velocity of 1500 meters/sec at an altitude of 1500 meters. At this point the motor is separated from the dart which then follows a ballistic trajectory to an altitude of 65 km. At this altitude, and approximately 110 seconds after launch time, the payload is ejected by an explosive charge, the ejection time being determined by means of a pyro-delay fuze which is activated at the time of rocket launch.

The dimensions of the Loki rocket system are shown in Figure 6.3-9 while Table 6-9 lists the principal physical characteristics of the rocket and Figure 6.3-10 shows a cross-sectional view of the various components which comprise the dart payload for the determination of temperature and wind velocity in the stratosphere.

The balloon dart carries an inflatable plastic balloon as the sensing device. The balloon contains a corner-reflector radar target and is ejected from the dart at an altitude of 65 km to form a sphere one meter in diameter. The sphere is tracked by radar as it descends through the atmosphere. From the radar determination of balloon position as a function of time, air density and wind velocity are determined as functions of altitude. The data reduction techniques utilized for the determination of these parameters are contained in the bibliography of this manual.

The chaff dart carries radar-reflective dipoles as the sensing elements. The dipoles are ejected from the chart in the neighborhood of 65 km. The tracking of the chaff cloud by a ground-based radar system serves to determine the position of the chaff at successive time intervals. From the radar determination of the cloud position as a function of time, stratospheric wind velocity is determined as a function of altitude.

Two types of chaff are commonly utilized. Copper chaff 1.27×10^{-2} cm in diameter is used for the determination of wind velocity at altitudes between 65 and 15 km. At 15 km the copper chaff fails to provide an adequate target for the tracking radar because of the excessive dispersion of the chaff dipoles forming the chaff cloud. Nylon chaff 8.8×10^{-3} cm in diameter has been used to determine wind velocities at altitudes from 85 to 60 km.

The Meteorological Probe PWN-8B (Instrumented Loki Dart) has been developed, qualified and successfully flight tested for final standardization by the U. S. Air Force to make available a low cost meteorological sounding rocket system for operational use. The major components of the probe

ASSEMBLED WEIGHT: 15.41 KILOGRAMS

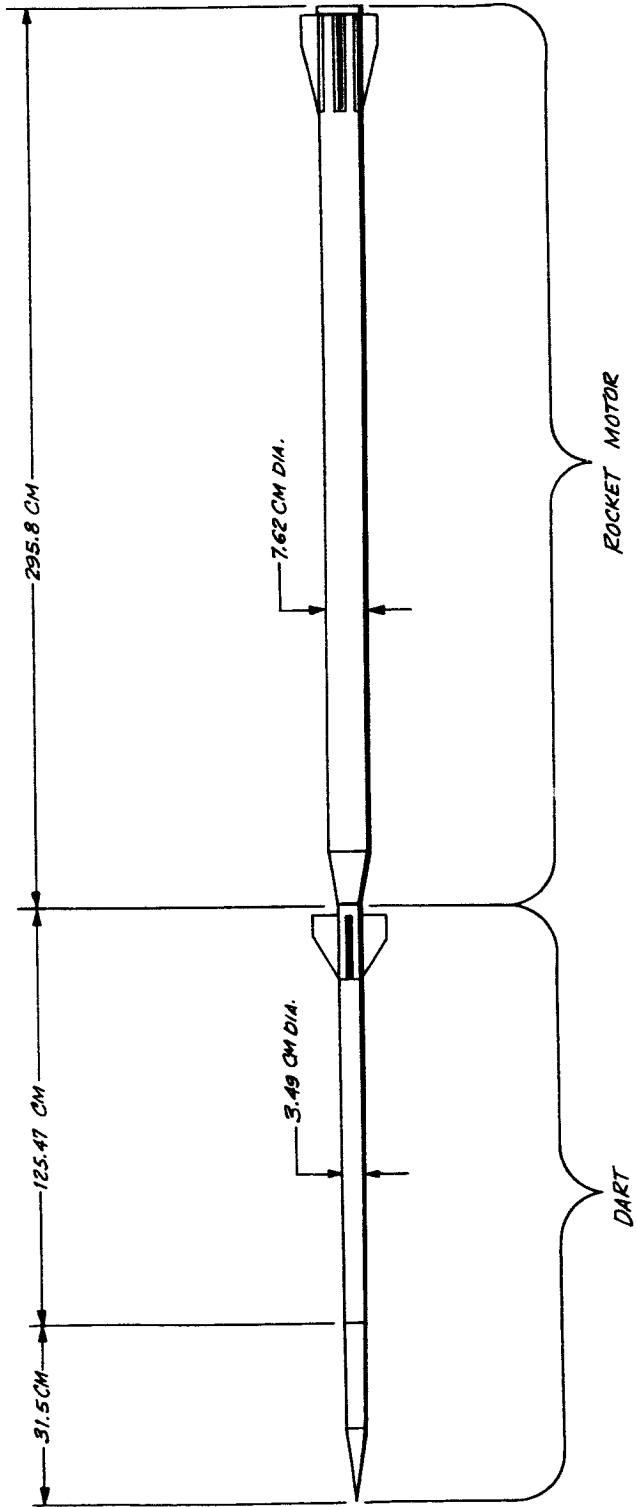


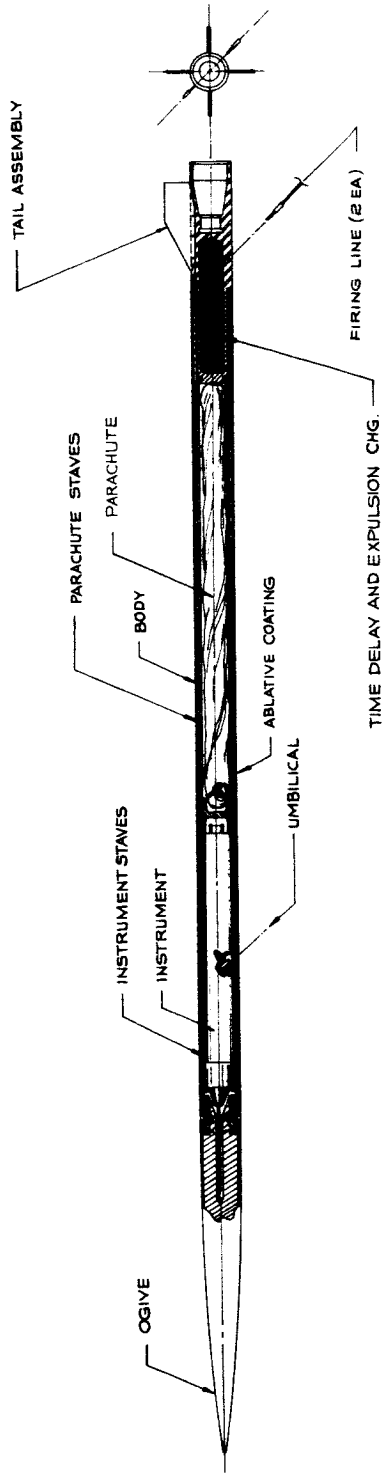
FIGURE 6.3-9 LOKI-DART VEHICLE CONFIGURATION

TABLE 6-9

PRINCIPAL CHARACTERISTICS OF THE LOKI SOUNDING ROCKET

<u>CHARACTERISTICS</u>	<u>NUMERICAL VALUE</u>
Length (meters)	
Overall	2.62
Rocket motor	1.53
Dart (Temperature - wind)	1.09
Diameter (cm)	
Rocket motor	7.60
Dart (Temperature-Wind)	3.80
Fin Span (cm)	
Rocket motor	13.00
Dart	7.60
Fin Area (cm ²)	
Rocket motor	
Dart	54.4
Nominal Weight (kg)	
Total vehicle (launch)	15.0
Motor case	2.6
Dart	4.1
Propellant	8.3
Total vehicle (burnout)	6.7
Average thrust (kg)	890
Burning time (sec)	1.8
Total impulse (kg-sec)	1550

FIGURE 6.3-10 CROSS SECTION OF THE INSTRUMENTED DART



system include a small solid-propellant rocket motor, a non-propulsive dart which contains the payload, a launcher and a ground-based test set. The system has been designed for launches at remote sites as well as at established missile ranges. Atmospheric temperature and wind data are obtained with this probe to an altitude of 200,000 feet.

The major components of the Meteorological Probe PWN-8B consist of the following:

Rocket Motor SR 71-AD-1	Rocket Motor Igniter Assembly
Ogive, Instrumentation Group A/A 37U-26	Dart Body Dart Tail
Launcher, Meteorological Probe LAU-66/A	Launcher
Test Set, Ogive Instrumentation Group TTU-273/E	Test Set

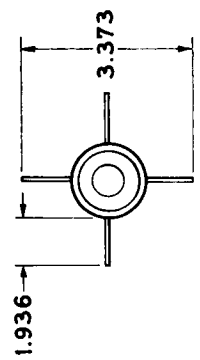
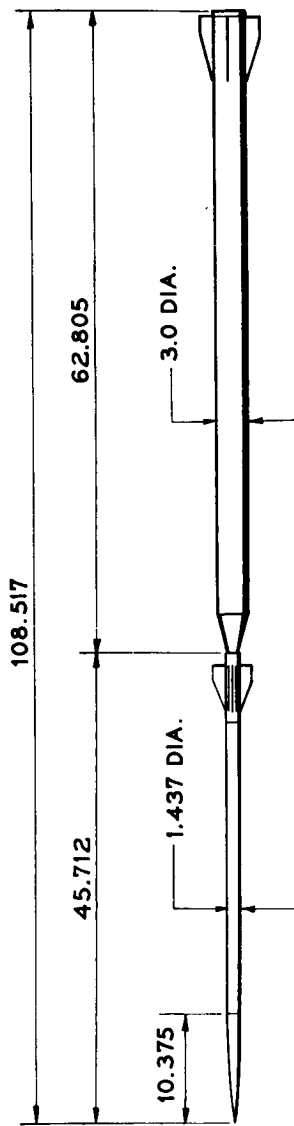
Each of these components has undergone environmental and performance testing, and each component was used in the qualification flight tests. All of these components have been designed to withstand both storage and operation temperature extremes from -40° F to $+140^{\circ}$ F. The rocket motor has been qualified to MIL-R-MIL-STD-810. The test set has been designed and qualified in accordance with MIL-21200, Class 2 and MIL-STD-108.

The design of the vehicle system incorporates an improved Loki rocket motor and a 1.437 inch diameter dart. The dart design is similar to that which was developed under the CRL Contract No. AF 19(628)-4164 for a Loki Instrumented Dart System. Figure 6.3-11 presents a photograph of the vehicle system. Figure 6.3-12 is a dimensioned sketch of the vehicle configuration.

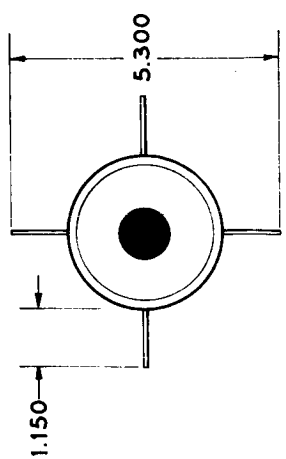
The dart system design is indicated in Figure 6.3-13. The tail assembly consists of the booster coupling receiver, tail fins, firing line umbilical receptors, pyrotechnic time delay and expulsion charge. The



FIGURE 6.3-11 PHOTO OF INSTRUMENTED DART SYSTEM



OGIVE, INSTRUMENTATION GROUP



ROCKET MOTOR, SR 71-AD1

FIGURE 6.3-12 METEOROLOGICAL PROBE PWN-8B, MAJOR DIMENSIONS

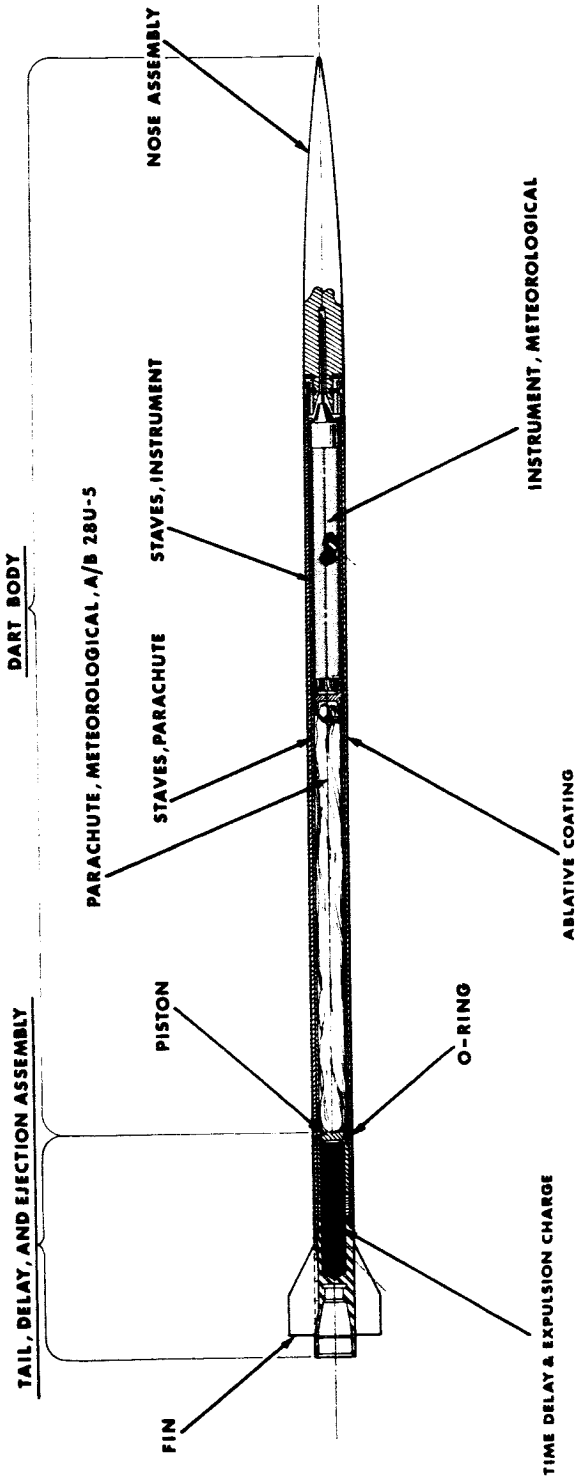


FIGURE 6.3-13 PWN-8B SYSTEM, DART CROSS-SECTION

parachute-sonde payload resides inside two sets of split staves which transmit the ejection piston load directly to the nose cone or ogive during expulsion. The staves are also used the sliding the payload into the dart body during assembly and out from the dart body during ejection. Both the dart body and the staves contain a payload umbilical hole for external power and calibration. The staves are lined with an asbestos paper to reduce the heat transfer from the dart body into the payload. The staves are split to permit deployment of the parachute and instrument with minimum interference. The nose cone or ogive is shear-pinned to the dart body so that during expulsion, the ogive separates from the dart, leaving the front end of the dart body open for payload ejection. The ogive has a drilled hole down the center for the sonde antenna to make contact. The ogive is isolated from the dart body by means of an electrical insulator. Thus, the ogive acts as an active antenna while the dart body forms the ground plane.

The operation sequence of the proposed booster-dart vehicle system is as follows:

1. Rocket motor and dart time delay ignition.
2. Initial vehicle motion disengages dart umbilicals.
3. Vehicle travels up through helical rail launcher which imparts spin or roll to the vehicle.
4. Vehicle exits the launcher at 180 ft./sec. with a spin rate of 13 rps. Spin rate at launch is necessary to reduce effects of thrust misalignment on vehicle dispersion.
5. Booster rocket burns out at 1.91 sec. at 4,750 ft. and 5,120 ft./sec. Spin rate has decreased to 10 rps.
6. Dart separates, spins up to 50 rps and coasts to apogee.
7. Pyrotechnic delay train ignites expulsion charge.
8. Ejection piston transmits load through packaging staves to ogive where retaining pins are sheared.
9. Ejection piston expels payload, staves and ogive as indicated in Figure 6.3-14.

The rocket motor design is specified by USAF Drawing Number 67D57300 and is an improved version of the Loki motor. The total impulse of the present design is increased by 316 pounds-seconds by

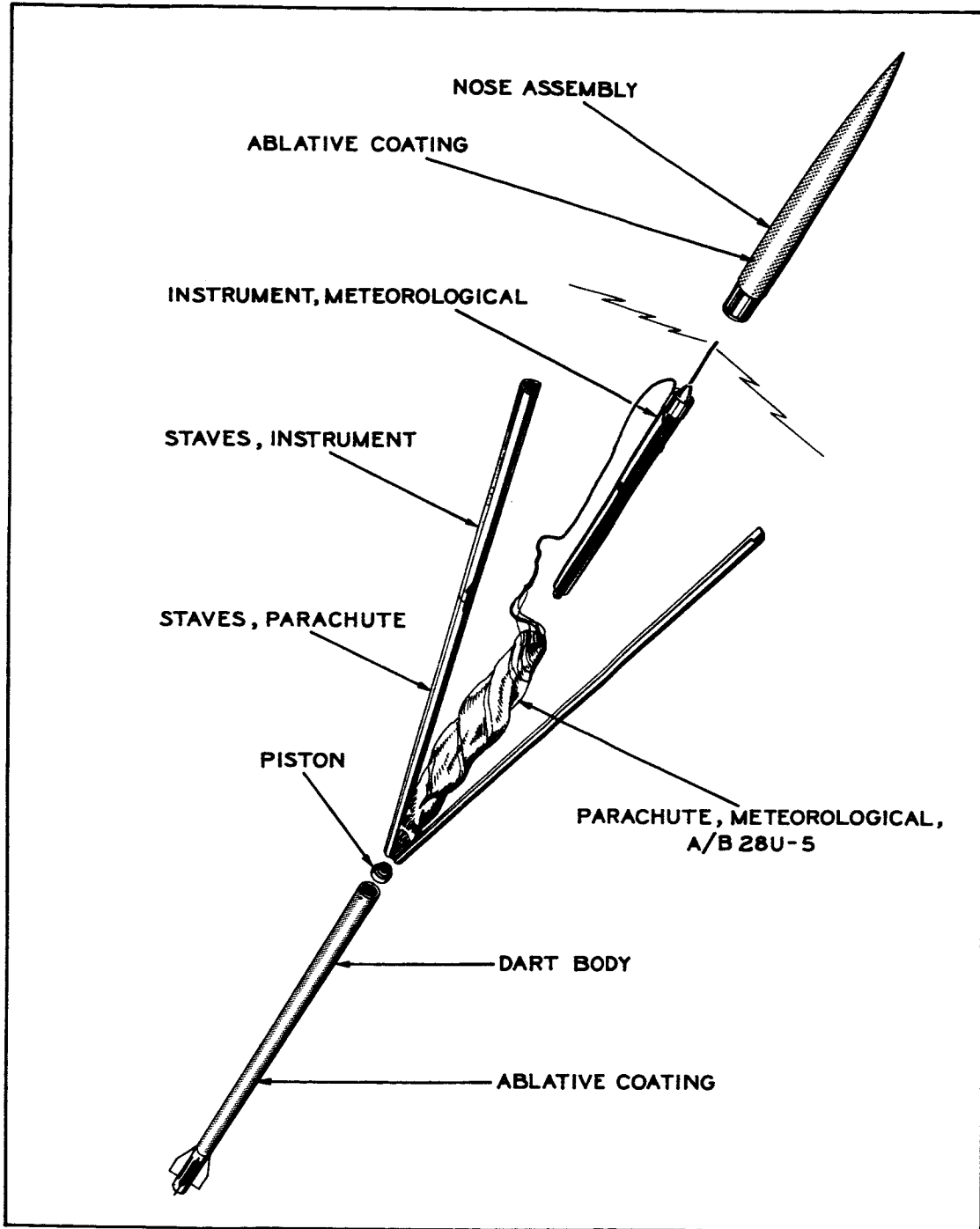


FIGURE 6.3-14 PAYLOAD EXPULSION SKETCH

increasing the specific impulse and weight of propellant. This has been done to assure that the minimum apogee altitude specification at an effective launch angle of 80° of 200,000 feet will be satisfied.

A summary of the major design characteristics of the SR 71-AD-1 rocket motor is presented in Table 6-10 along with similar data for the Loki II and HASP type motors. The differences in hardware design between the SR 71-AD-1 and these motors is summarized in Table 6-11. These improvements in the design and performance of the rocket motor have significantly improved both altitude performance and flight reliability of the system. The rocket motor is specified by MIL-R-83064 (USAF) Model Specification, Rocket Motor SR 71-AD-1.

The total impulse of the SR 71-AD-1 rocket motor is 4076 pound-seconds, which is significantly higher than the Loki II and HASP Mark 32 Mod O motor impulses of 3,760 pound-seconds. This has been accomplished by increasing the propellant specific impulse from 223 seconds to 231 seconds and the propellant weight from 16.88 lb to 18.25 lb. The increase in propellant weight is due to a high volumetric loading rather than the use of a higher density propellant. The port volume of the SR 71-AD-1 motor is reduced from the Mark 32 Mod O design, and the nose piece is not loaded with propellant. The nozzle throat area is also increased to give a higher thrust at a lower chamber pressure than the Mark 32 Mod O design. The steel ring at the nozzle end of the Mark 32 Mod O is replaced with a rubber boot to reduce the problem of motor wall-burn throughs at the junction of the forward end of the nozzle and the motor wall.

A comparison of the ballistic performance between the SR 71-AD-1 motor and the Loki II or HASP motors is presented in Table 6-12.

Rocket Motor Hardware Design.

The SR 71-AD-1 rocket motor major hardware components consist of the forward closure, the motor tube, the nozzle assembly, the fins, the forward boot and the aft boot.

TABLE 6-10

ROCKET MOTOR MAJOR DESIGN CHARACTERISTICS SUMMARY

<u>Design Characteristics</u>	<u>SR 71-AD-1</u>	<u>Loki II & Mark 32 Mod 0 HASP Types</u>
Length (in)	66.06	66.06
Diameter (in)	3.126	3.126
Wall Thickness (in)	0.061	0.061
Weights:		
Case (lb)	4.39	4.39
Nozzle (lb)	0.81	1.52
Liner (lb)	0.60	0.50
Propellant (lb)	18.25	16.88
Total (lb)	24.05	23.29
Motor Mass Fraction	0.76	0.73
Burning Time (Sec.)	1.86	1.86
Action Time (Sec.)	2.04	1.97
Chamber Pressure:		
Maximum (psi)	1,447	1,500
Average (psi)	979	1,340
Total Impulse at Sea Level (lb.-sec)	4,076	3,760
Propellant Specific Impulse (sec)	231	223
Throat Area (in ²)	1.41	0.983
Expansion Ratio	5.44	6.05
Grain Port Diameter (Tapered) (in)	1.30-1.00	1.58-1.00

TABLE 6-11

HARDWARE DESIGN
CHARACTERISTICS COMPARISON

<u>Hardware Design</u>	<u>SR 71-AD-1</u>	<u>Loki II & Mark 32 Mod 0</u>
Motor Case	Same	Same
Nozzle	Recessed 0.81 lb. "O" Ring Seal	Not Recessed Steel Sleeve
Nozzle - Motor Case Junction Protector	Rubber Boot	Steel Sleeve
Nose Piece Loading	None	Propellant
Forward End Seal	Rubber Boot	Rubber

TABLE 6-12

ROCKET MOTOR BALLISTIC PERFORMANCE COMPARISON NOMINAL
80° F CONDITIONS

	<u>SR 71-AD-1</u>	<u>Loki II & Mark 32 Mod 0 HASP Types</u>
Total Impulse (lb.sec)	4,076	3,760
Action Time (sec)	2.04	1.97
Maximum Thrust (lb-ft)	2,902	2,380
Average Thrust (lb-ft)	2,033	2,020
Specific Impulse (sec)	231	223

LOKI LAUNCHER

General.

Loki type vehicles have been launched utilizing several different types of launchers such as the standard helical-rail tube, a zero-length launcher, a rail launcher with no spin and a five-inch gun launcher. Of these techniques, the most successful has been the helical-rail tube because of its inherent capabilities to induce the spin rate to the vehicle prior to the time it is released for free flight. The helical-rail launch tube was developed for the original Loki anti-aircraft dart system to reduce dispersion for greater aiming accuracy. This launch technique has been used for the Loki-Dart meteorological rockets for a number of years up to the present time with excellent success in restricting dart impacts to relatively small regions - a significant advantage of the Loki-Dart system. The LAU-66/A launcher has been designed to a helical-rail identical in function to the original Loki helical-rail launch tube.

Vehicle Dispersion Considerations.

During the original Loki I system development program at JPL, firings were made using both spiral-rail launch tubes and straight rails. Also, long (14 feet) and a short (7 feet) spiral-rail launch tubes were compared. The results of a number of firings with each launch system are summarized below:

<u>Launcher Type</u>	<u>Helical Rails</u>	<u>Straight Rails</u>	<u>Helical Rails</u>
Launcher Length (ft.)	14	14	7
Launch Velocity (ft/sec)	359	362	244
Launch Spin Rate (rps)	18.1	0	12.7
Average Wind Effect (mil/mph)	1.3	1.3	1.0
Dispersion w/wind (5 mph)	6.6	22.8	7.2
Dispersion w/wind (5 mph)	7.3	--	7.4

For a high-acceleration, high-velocity system such as the PWN-8B

Probe vehicle the effect of wind at launch and during flight upon impact dispersion is relatively insignificant. This fact leaves the vehicle airframe and, especially, thrust misalignment as the next major sources of impact dispersion. The dispersion resulting from these misalignment factors can be significantly reduced by imparting spin to the vehicle, before they can alter the course of the rocket vehicle. A critical period for a vehicle with no spin at launch is just as the vehicle leaves the constraints of the launcher. The thrust misalignment vector operates immediately upon launch to turn the vehicle into a new heading without the benefits of any appreciable aerodynamic restoring forces to resist the moment generated by the thrust misalignment. Hence, a new heading is taken before the vehicle has a chance to build up sufficient spin, by means of canted fins, to vector out the misalignment effects.

Firings using the conventional helical-rails had less than one-third of the dispersion experienced with the straight no-spin rail. It was concluded by JPL that the initial spin imparted to the vehicle by the helical-rail launchers strongly reduces the dispersion. The average wind effect does not seem to be influenced significantly by either straight or spiral rail designs or launcher length changes, at least from 7 feet to 14 feet. Dispersion does not seem to be particularly influenced by launcher rail length for variations of the above magnitude.

Launcher Design.

General.

The LAU-66/A Launcher has been designed as a helical-rail launcher of moderate length, i.e., 10 feet long, to maintain trajectory and impact dispersion at a low value. Increasing launcher length beyond 10 feet does not significantly reduce either the average wind effect or dispersion, but makes a more cumbersome and costly launcher. Since the basic vehicle dispersion for the probe system is so small, i.e., 7.0 mils, accuracy in launcher settings, launcher rigidity and launcher straightness (lack of bowing) become limiting factors in making possible a minimum trajectory and impact dispersion. These factors, in addition to the practical aspects of cost, mobility and environmental fidelity, have been the main design goals for the LAU-66/A launcher.

Requirements.

As discussed above, it is necessary to provide a rigid structure to support the launch tube to limit the dispersion. In addition to providing

the rigid structure for the launch tube, the other design goals for the launcher has been:

1. Adjustable in elevation to $\pm 1/4$ degree.
2. Adjustable in azimuth to $\pm 1/2$ degree.
3. Allow the launch rails to be supported in such a way that one man can easily elevate the rails into the launch position or move the rails into the horizontal position.
4. Provide elevation and azimuth locking mechanisms which are easily locked and unlocked.
5. Provide a motor retainer stop which is easy to actuate and will withstand the rocket blast of the motor at launch.
6. Provide access for the umbilical connector to the instrument.
7. Provide junction boxes for the firing lines.
8. The basic design shall be such that it can be assembled in the field with two people without auxiliary lifting equipment. This has been accomplished by using a component type construction and limiting the weight of each component to not more than 240 pounds.
9. Azimuth and elevation indicators are an inherent part of the launcher.

Description.

The Launcher, Meteorological Probe LAU-66/A (Figure 6.3-15) consists of four major components: base, pedestal assembly, support assembly, and the rail assembly. The launcher base supports the pedestal assembly, which in turn supports the support assembly to which the rail assembly is secured. The rail assembly supports the Meteorological Probe PWN-8B during launch operations and imparts a stabilizing spin of approximately 10 revolutions per second to the probe as it travels out of the launcher into free flight. Launch elevation angles are set with the support assembly. Launch azimuth angles are set with the pedestal assembly. Electrical firing circuitry for the PWN-8B and the appropriate connectors are provided as part of the support assembly and pedestal assembly. Major dimensions of the launcher are presented in Figure 6.3-16.

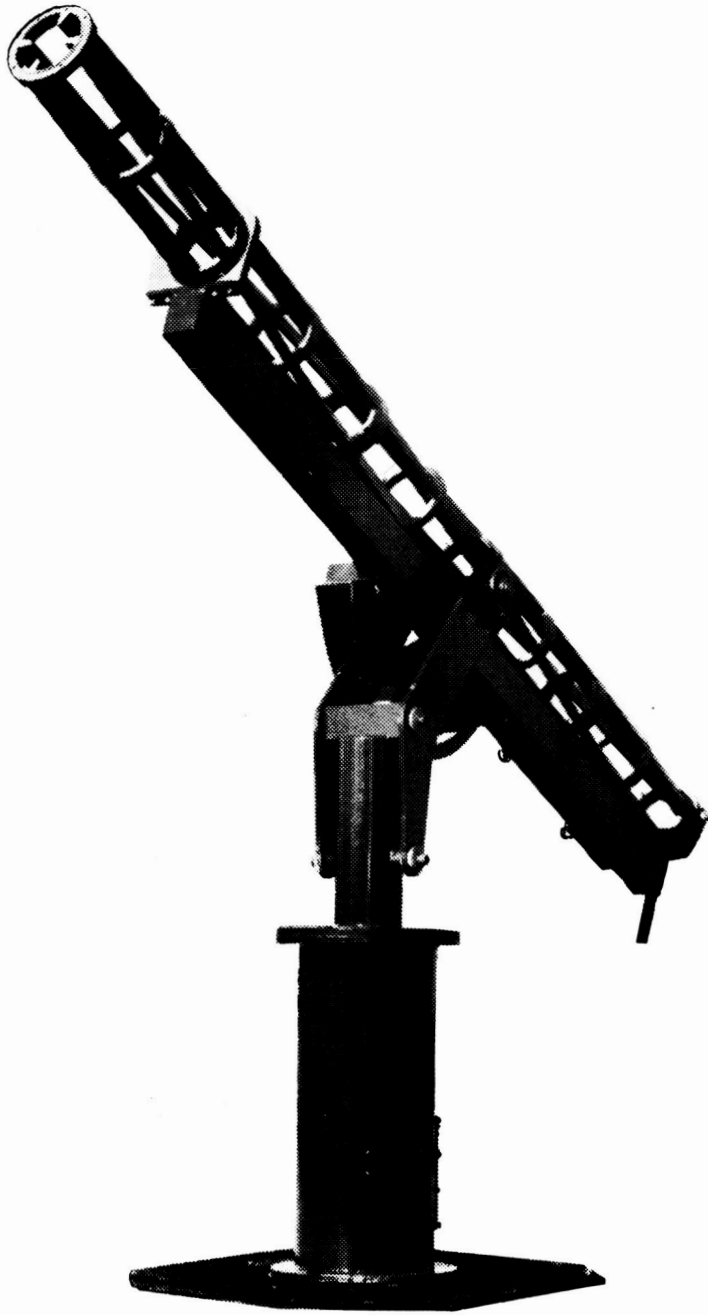
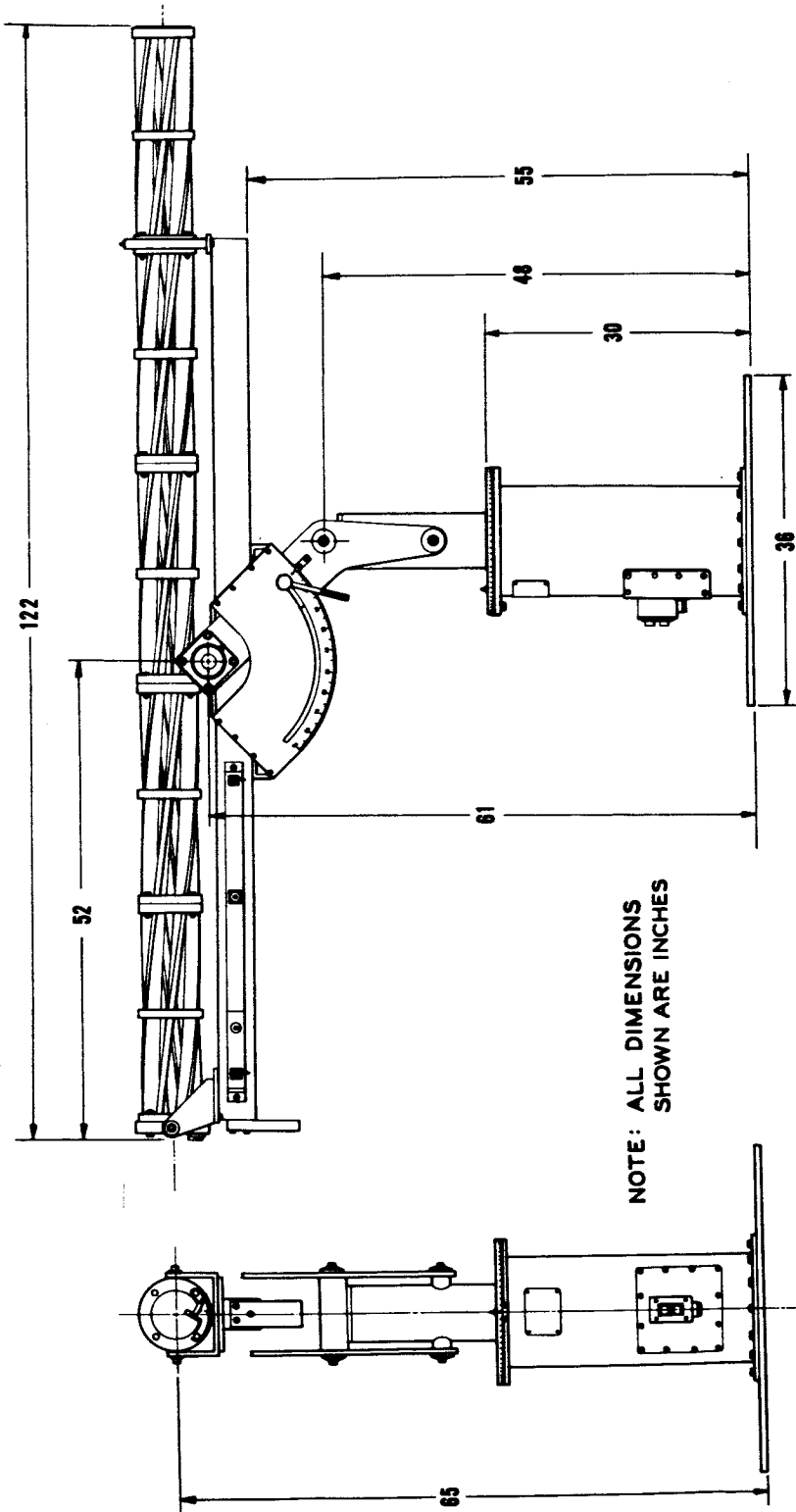


FIGURE 6.3-15 ROCKET LAUNCHER LAU-66/A



NOTE: ALL DIMENSIONS SHOWN ARE INCHES

FIGURE 6.3-16 MAJOR DIMENSIONS OF LAUNCHER LAU-66/A

Launcher Base.

The launcher base is a heavy steel plate which anchors the pedestal assembly to the concrete launch pad.

Pedestal Assembly.

The pedestal assembly consists of a fixed outer cylinder with an azimuth angle setting plate. The fixed cylinder and a rotating inner cylinder with an azimuth angle setting plate. The fixed cylinder consists of a heavy-wall aluminum cylinder with flanges at both ends. The bottom flange is bolted to the launcher base in a fixed position. The upper flange supports the rotating azimuth plate which is welded to the inner rotating cylinder. A junction box is supplied as part of the fixed cylinder to accept the blockhouse firing line connector and also the wiring harness connector from the support assembly. The inner rotating cylinder consists of a heavy-wall aluminum cylinder, welded to the azimuth angle setting plate. The top end of the inner cylinder is fitted with a yoke for attachment of the support assembly.

Support Assembly.

The support assembly consists of an aluminum "I" - beam for the launch rail support, two elevation bearings, and side-plate aluminum bracketry for attachment of the support assembly to the pedestal assembly elevation angle setting lock. Attachment fixtures for the rail assembly are located fore and aft on the aluminum "I" -beam. The two bearing subassemblies are included for the primary attachment to the pedestal assembly. Firing line wiring harness, associated junction boxes and electrical connectors are included as part of the support assembly.

Rail Assembly.

The rail assembly consists of five identical aluminum cast rail sections which have been bolted together to form a ten foot long 4-rail assembly. The four rails are equally spaced and form a continuous helix throughout the length of the launch rail assembly. Approximately one-third of a revolution is completed by the rails from the breech end to the muzzle end. The edges of the rails are stepped to support the probe by the dart fins and the rocket motor bourrelet.

6.3.4 Skua.

The Skua is 226 cm (89 in) long, 13.1 cm (5.15 in) diameter and weighs 37.5 kg (82 1/2 lb). The rocket motor case is manufactured from 100 t/in² steel and is filled with a moderate specific impulse end burning case-bonded solid propellant. The rocket is fitted with four fins and, in the parachute role, the nose cone is made of glass fibre. Separation of the payload compartment is obtained by means of a thermal switch which operates at the end of motor burning and a time switch which may be pre-set to achieve the required separation height. These switches close the firing circuit to another small solid propellant motor which ejects the payload compartment clear of the rocket with a relative velocity of 14 m/sec (45 ft/sec).

The boost arrangement is recoverable. It separates from the main rocket at an altitude of 15 m (50 ft) and descends by parachute. The boost motor can then be returned for refilling and the boost support structure can be cleaned, inspected and re-assembled for the next firing. It has been found that 85% of the boost and boost support structure can be re-used after each firing.

A payload space of 8,200 cu cm (500 cu in) is available and payloads of up to 6 kg (13 lb) may be accommodated. The standard equipment is a British (Irving) radar reflecting parachute of 4.6 m (15 ft) diameter and a sonde transmitter capable of transmitting at 28 m/cs.

Skua has operated successfully from a launch site at South Uist in the Hebrides, and it is in service with the British Meteorological Office.

Performance.

The Skua can reach an altitude of 90 km (295,000 ft) with a payload of 1.8 kg (4 lb) using a 85° launch. This performance is attained using a 0.2 second boost system giving a launch velocity of 100 m/sec (328 ft/sec). Without the boost the altitude is approximately 64 km (210,000 ft) for the same payload.

Using the standard boost and launching techniques i.e., correction for the ballistic winds, the dispersion of impact points due to wind lies within a circle of 5.3 kilometers radius for 1 m/sec (3.3 miles for 3 ft/sec) error in ballistic wind for a 72 km (236,000 ft) altitude.

The curves of Figure 6.3-17 illustrate the rocket altitude capabilities against payload, time and range. The Skua major characteristics are presented in Table 6-13.

Launch System.

The high speed launch system consists basically of a 3-part 54 cm (21 in) diameter tube mounted on an ordinary commercial vehicle for maximum mobility. The tube is elevated hydraulically and accurate adjustment is carried out by a manual screw acting on the diagonal stays. Azimuth adjustments are obtained by altering the direction in which the vehicle is pointing and a sighting bar is placed below the driver's position. It has been found that azimuth accuracies of $1/2^\circ$ can be obtained and elevation accuracies of $1/10^\circ$.

Loading is carried out by lowering the tube to an angle of 15° and inserting the complete rocket and boost assembly with the aid of special loading rods.

6.3.5 MT-135.

The MT-135 is the Japanese version of the Arcas. The MT-135 is longer, larger in diameter and weighs almost twice as much as Arcas. The burning time is appreciably shorter, the thrust level is greater and the altitude performance is slightly less than that of the Arcas. A comparison of the major characteristics is presented in Table 6-14.

6.3.6 Super Loki-Chaff Dart.

The Super Loki Dart meteorological rocket system has been developed for NASA - Marshall Space Flight Center to obtain high-altitude (85 km) wind data with a low cost rocket vehicle and a radar-reflective chaff payload. The Super Loki Dart consists of a scale-up of the older Loki Dart system, which has been in use for many years to gather wind data to altitudes up to 65 km. The Super Loki Dart two-stage vehicle consists of a high-impulse solid-propellant rocket motor as the first stage, and a non-propulsive dart which contains the chaff payload as the second stage.

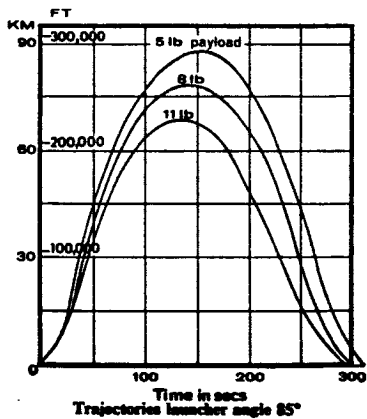
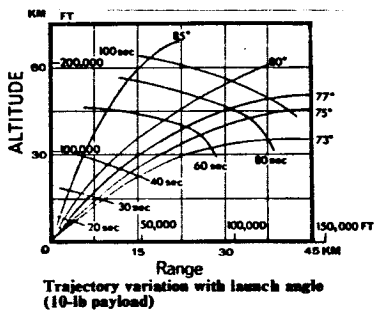
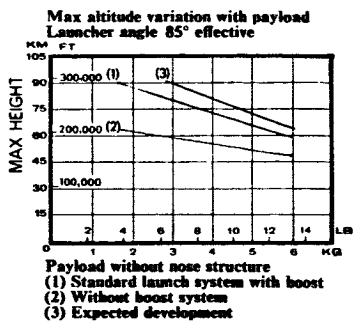


FIGURE 6.3-17 SKUA PERFORMANCE CURVES

TABLE 6-13

SKUA - GENERAL SPECIFICATIONS

ROCKET (with parachute and sonde)

Overall length with motor	226 cm (89 in)
Diameter	13.1 cm (5.15 in)
Weight including filled motor	37.5 kg (82 1/2 lb)
All burnt weight	14.3 kg (31 1/2 lb)
Payload weight	4.5 kg (10 lb)
Payload volume	8,200 cu cm (500 cu in)
Peak Altitude (for 10 lb payload)	70 km (230,000 feet)
Burn-out altitude (approximately)	15 km (48,000 feet)
Launch velocity	100 m/sec (328 ft/sec)
Initial acceleration (max)	57 g
Flight acceleration (max)	12 g
Boost breakaway altitude	15 m (50 ft)

PAYLOAD

Parachute (Irving Type)	4.6 m (15 ft) dia
Transmitter	Met Office Rocket Sonde Mk 1
Type	Met 56,000
Frequency	28 m/cs

LAUNCHER

Length	6.5 m (21 ft)
Vehicle Type	Bedford RL
Weight (vehicle and launcher)	5,084 kg (5 ton)
Launch tube length	9.8 m (32 ft)
Max launch angle range	Unrestricted

TABLE 6-14

JAPANESE MT-135 VS ARCAS

	<u>MT-135</u>	<u>ARCAS</u>
Total Length	3.2 m	2.3 m
Diameter	13.9 cm	11.4 cm
Total Weight	68 kg	35 kg
Payload Weight	10 kg	5.4 kg
Burn Time	10.5 sec	29 sec
Average Thrust	825 kg	155 kg
Max Velocity	1370 m/sec	1050 m/sec
Apogee (80° launch angle)	55 km	61 km

Altitudes as high as 125 km have been obtained with this vehicle system during the development flight tests at White Sands Missile Range. Altitudes to 110 km were achieved for flights from sea level launch sites. A helical-rail launcher has been developed to impart spin or roll to the vehicle prior to release in order to minimize impact dispersion and associated range safety problems.

The basic Super Loki rocket motor can be used to propel larger diameter instrumented dart systems to altitudes on the order of 85 km to upgrade the atmospheric temperature profile measurements currently being conducted by the standard-size Loki.

The Super Loki Dart as shown in Figure 6.3-18 is a two-stage sounding vehicle consisting of a solid-propellant Super Loki rocket motor as the first stage and a non-propulsive dart containing the payload as the second stage. A dimensional sketch of the vehicle is shown in Figure 6.3-19. This vehicle is essentially a scaled-up version of the standard Loki Dart vehicle as indicated in Figure 6.3-20.

The Super Loki rocket motor consists of an aluminum case with an internal burning cast-in-the-case solid propellant. Major design characteristics of the rocket motor are presented in Table 6-15. An aluminum inter-stage coupling structure is located at the head end of the rocket motor. The propellant fuel is a polysulfide polymer and the oxidizer is ammonium perchlorate. The igniter consists of two parallel 1 watt/1 ampere no-fire squibs and an appropriate ignition charge. The igniter is separable from the motor and is installed at the launch site. A cross-section view of the Super Loki rocket motor with the igniter installed is shown in Figure 6.3-21.

The high altitude chaff dart for the Super Loki system consists of a steel cylindrical body with a steel ogive and an aluminum tail piece. The cylindrical body contains the chaff payload which is packaged into split steel staves. The ogive is retained at the forward end of body with shear-screws which are sheared during payload expulsion out from the forward end of the dart. The tail piece contains an electrically-actuated 145-second pyrotechnic time delay and a small payload ejection charge. Four steel fins are roll-pinned into the dart tail for flight stability. The aft end of the dart tail is boattailed to reduce aerodynamic drag and to be used to mate the dart to the booster. A cross-section view of the chaff dart is shown in Figure 6.3-22. Major chaff dart characteristics are presented in Table 6-16.

The payload consists of 0.0127 mm (0.5 mil) "S"-band aluminumized-mylar chaff.

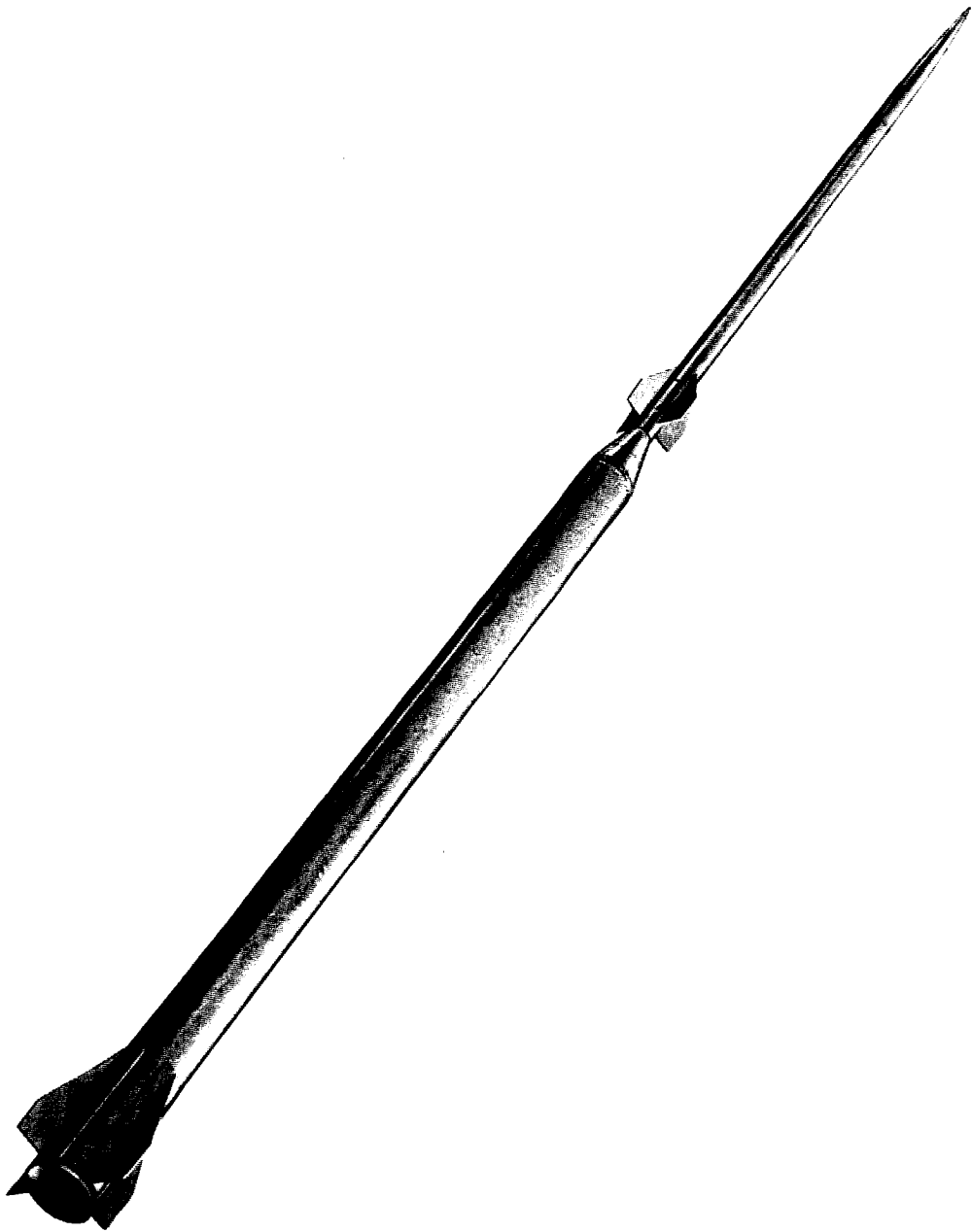


FIGURE 6.3-18 SUPER LOKI VEHICLE CONFIGURATION

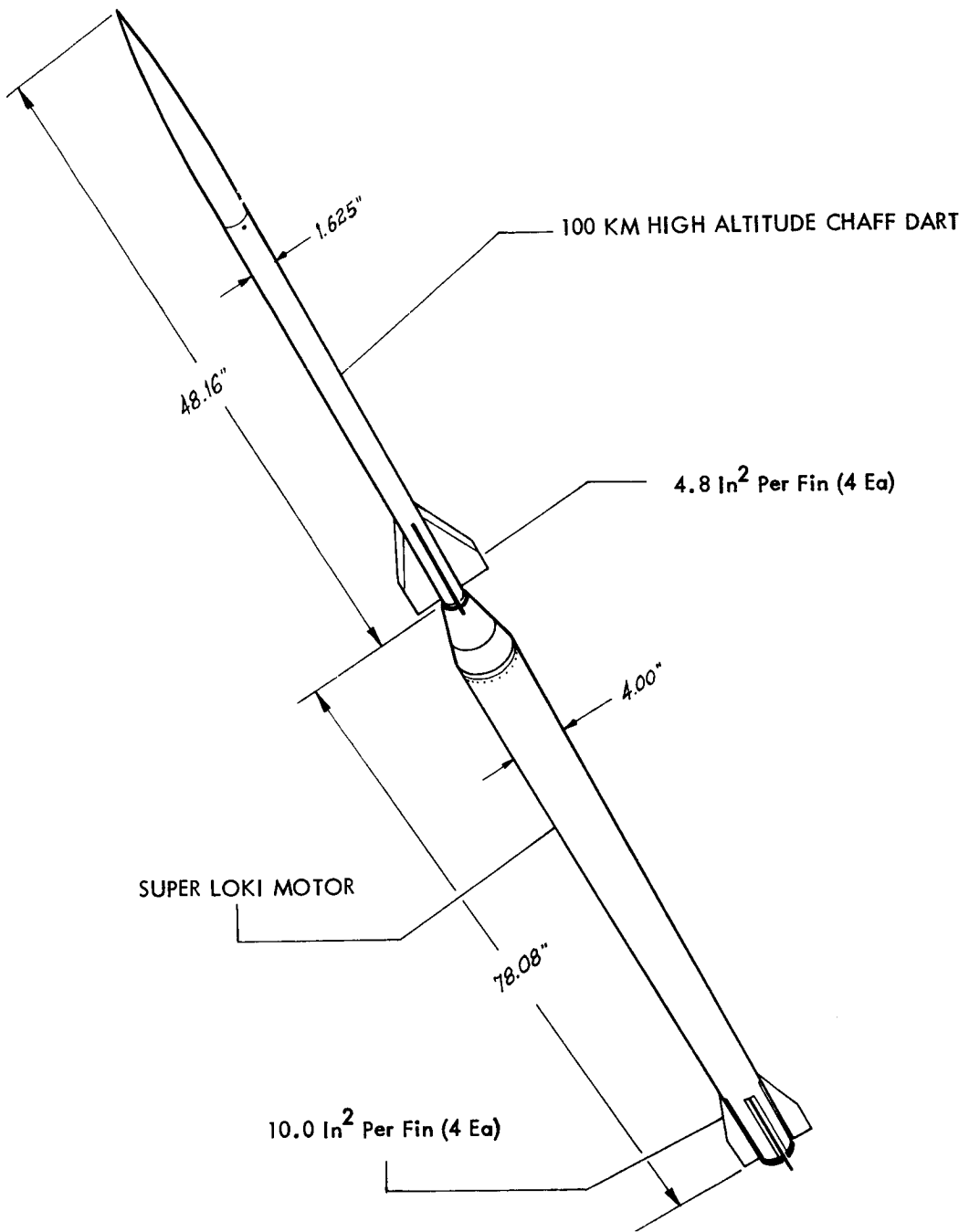


FIGURE 6.3-19 SUPER LOKI CHAFF DART VEHICLE CONFIGURATION

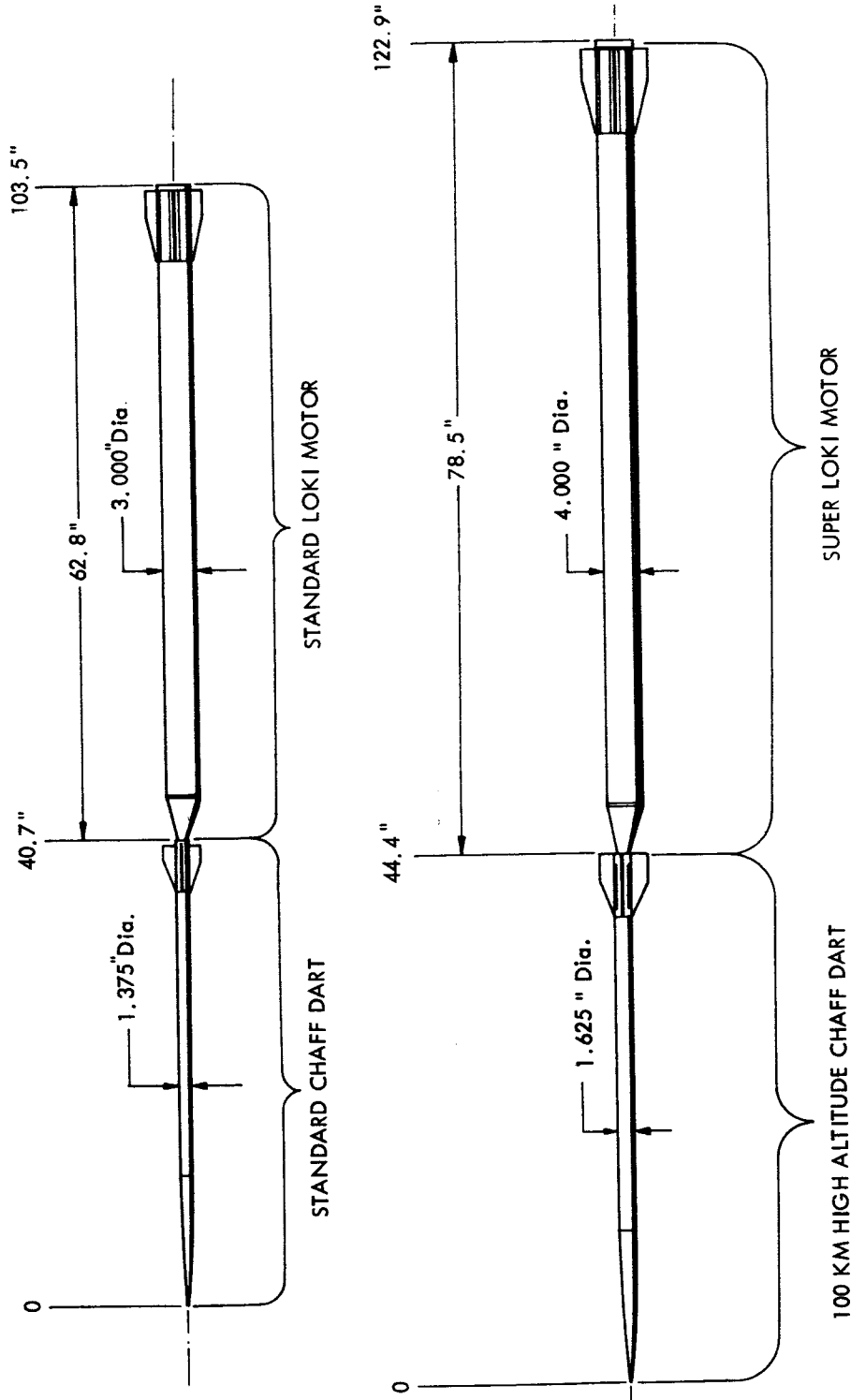


FIGURE 6.3-20 HIGH-ALTITUDE SUPER LOKI CHAFF DART (100 KM)
VEHICLE CONFIGURATION COMPARED WITH
STANDARD LOKI-DART VEHICLE

TABLE 6-15

SUPER LOKI ROCKET MOTOR
DESIGN CHARACTERISTICS SUMMARY

Length (inches)	78
Diameter (inches)	4
Weights:	
Inert Motor With Interstage (kg)	5.26 (11.6 lb)
Propellant (kg)	16.87 (37.2 lb)
Total (kg)	22.14 (48.8 lb)
Motor Mass Fraction	0.76
Burning Time (seconds)	2.0
Chamber Pressure:	
Maximum (Atmospheres)	100.02 (1470 PSig)
Average (Atmospheres)	83.69 (1230 PSig)
Thrust at Sea Level:	
Maximum (kg)	2608.20 (5750 lb)
Average (kg)	2018.52 (4450 lb)
Total Impulse at Sea Level (nt-sec)	3.96 (8900 lb-sec)
Specific Impulse at Sea Level	239

TABLE 6-16

SUPER LOKI CHAFF DART DESIGN CHARACTERISTICS

Length	122.33 cm (48.16 inches)
Diameter	4.13 cm (1.625 inches)
Weight	6.12 kg (13.5 pounds)
Payload Volume	491.61 cm ³ (30 inches ³)

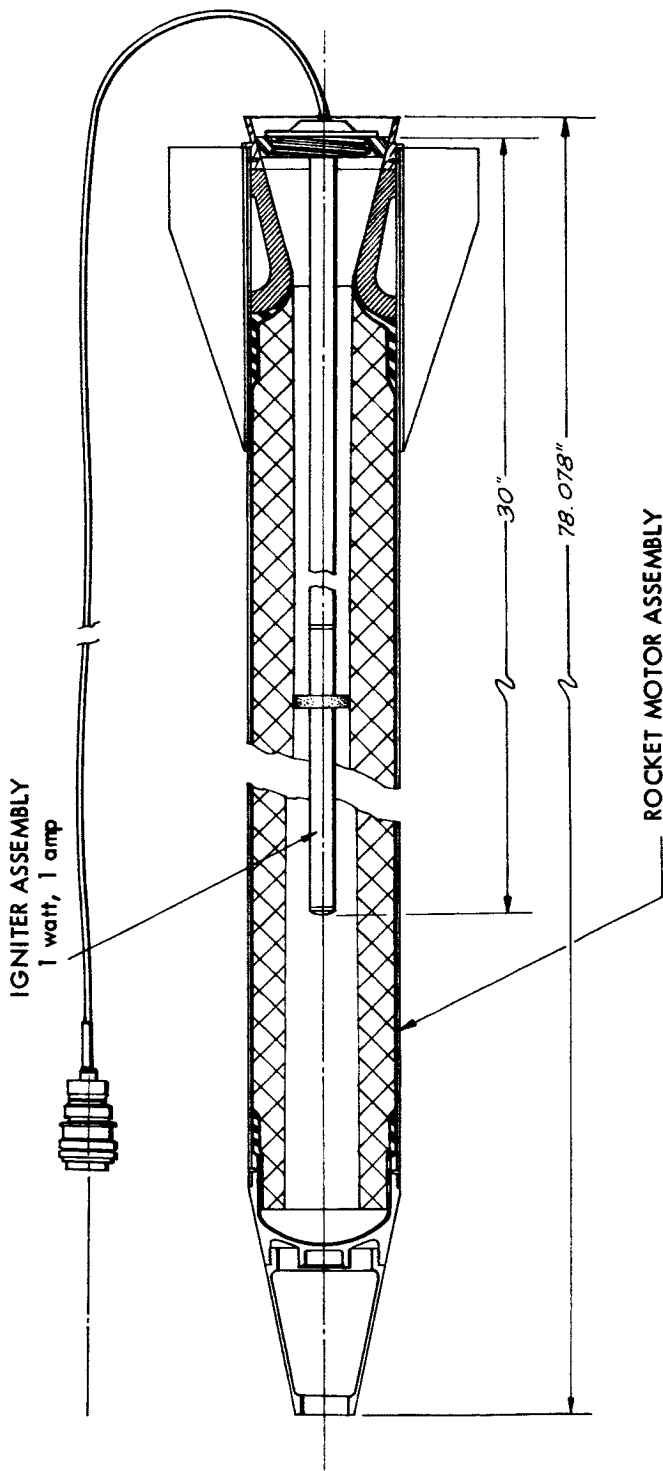
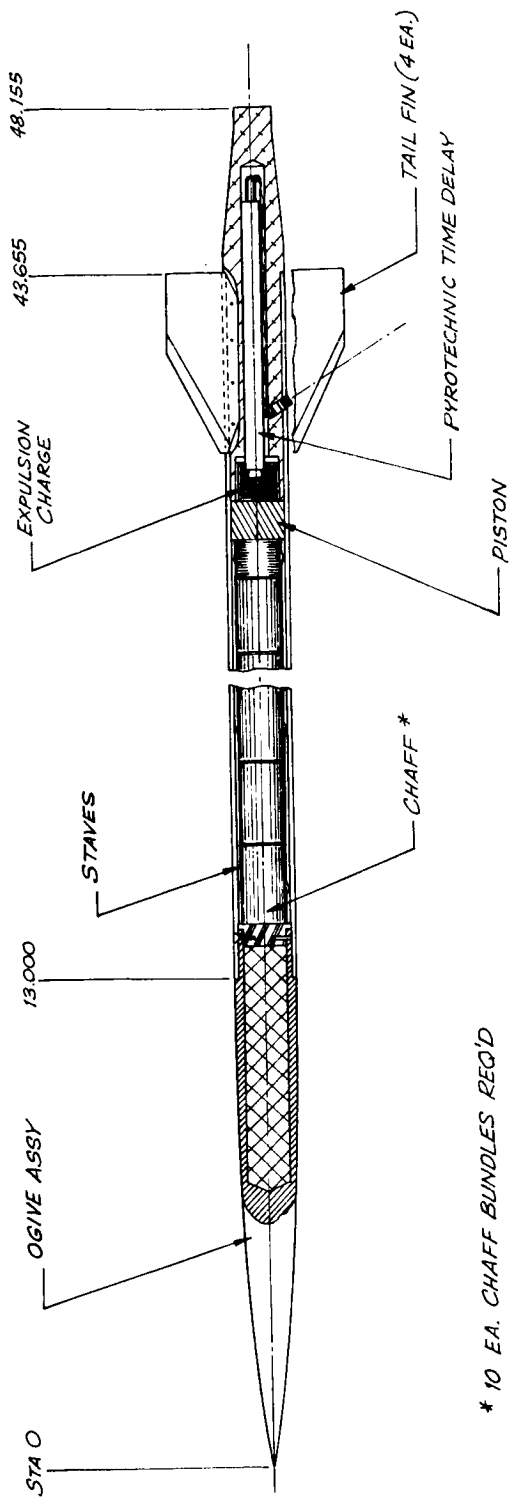


FIGURE 6.3-21 CROSS-SECTION VIEW OF SUPER LOKI ROCKET MOTOR



* 10 EA. CHAFF BUNDLES REQ'D

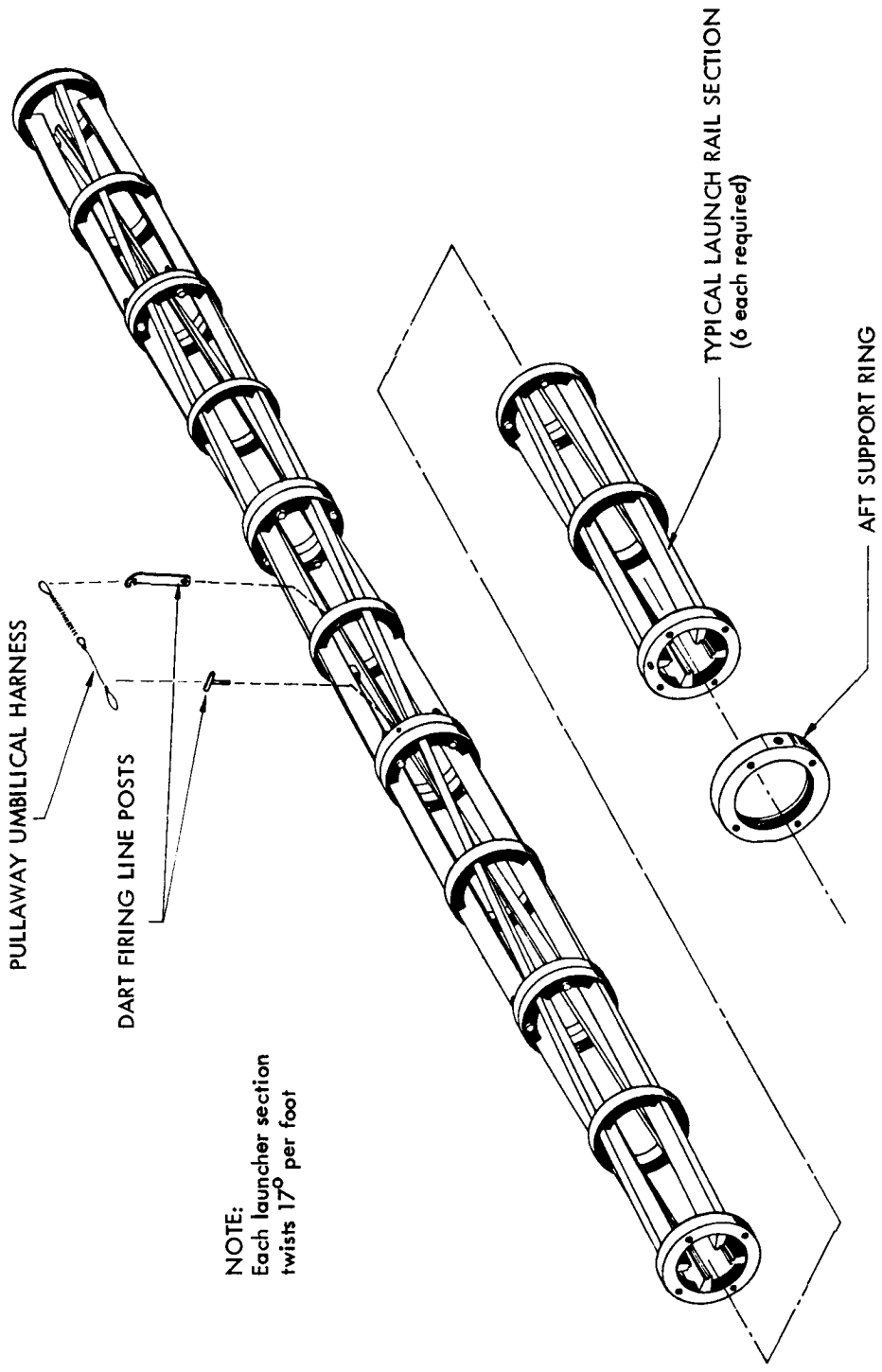
FIGURE 6.3-22 CROSS SECTION VIEW OF SUPER LOKI CHAFF DART

The Super Loki Launcher consists of four helical rails which complete approximately one-third of a revolution throughout the launch rail length. The launch rail assembly as shown in Figure 6.3-23 consists of six cast aluminum sections which are bolted together to form a continuous 4.39 m (12 feet) length. The edges of the rails are stepped to support the vehicle by the dart fins and the rocket motor nozzle ring. The outside diameter of the launch rail assembly is 26.04 cm (10-1/4 inches).

The purpose of the launch rail is to impart an 8.5 rps spin to the vehicle by constraining the dart fins to a helical path during their travel along the launch rails. The aft end of the motor travels for 4.39 meter (12 feet) prior to its release from the launcher.

The Super Loki Launch Rail Assembly can be mounted to any suitable launcher base by means of forward and aft mounting brackets. A launcher base specifically designed for this rail is shown in Figure 6.3-24.

Trajectories for the Super Loki are presented in Figure 6.3-25 for various launch angles from sea level. A nominal trajectory summary is presented in Table 6-17.



NOTE:
 Each launcher section
 twists 17° per foot

FIGURE 6.3-23 SUPER LOKI LAUNCH RAIL ASSEMBLY

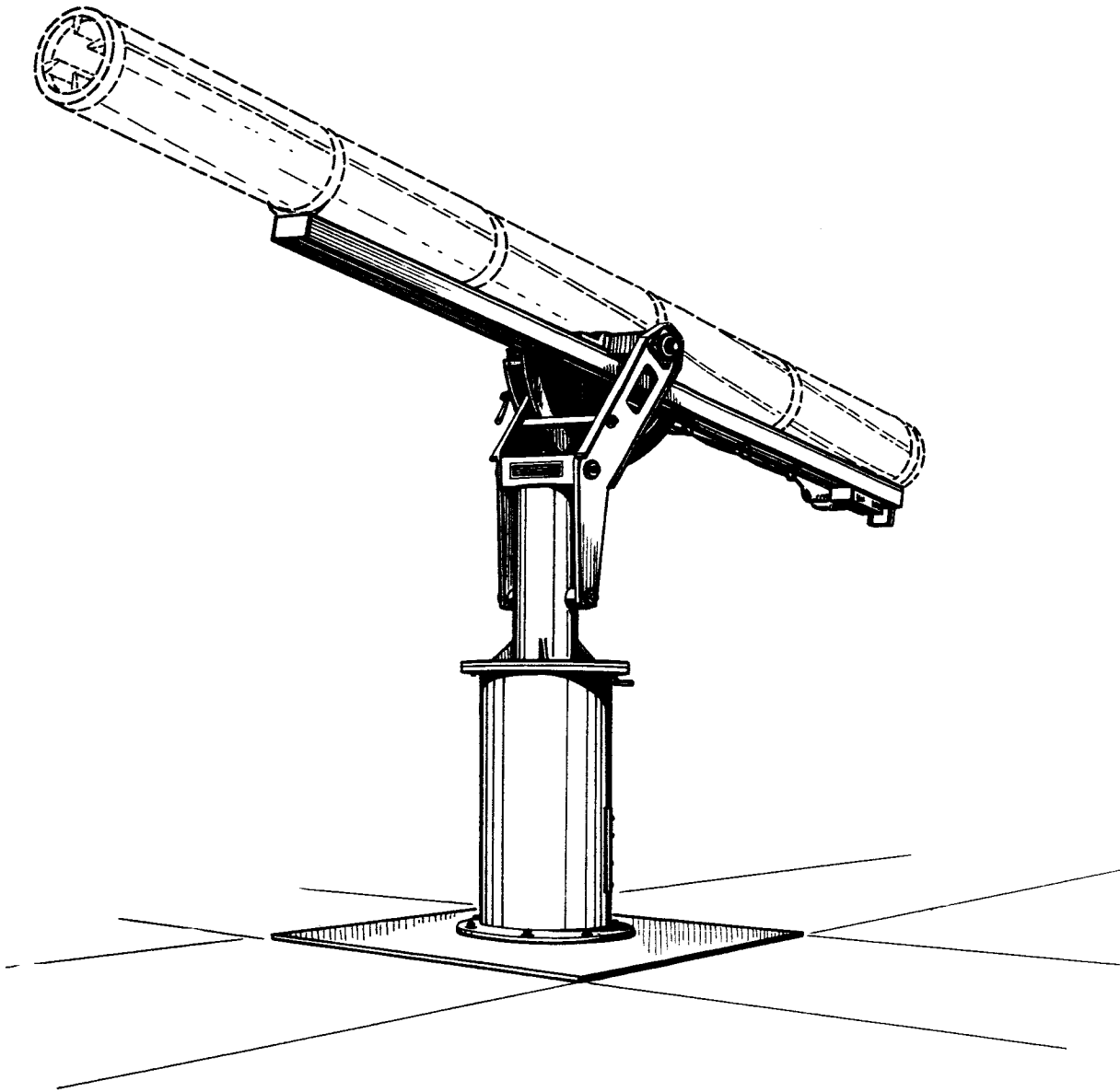


FIGURE 6.3-24 TYPICAL BASE FOR SUPER LOKI LAUNCH RAIL

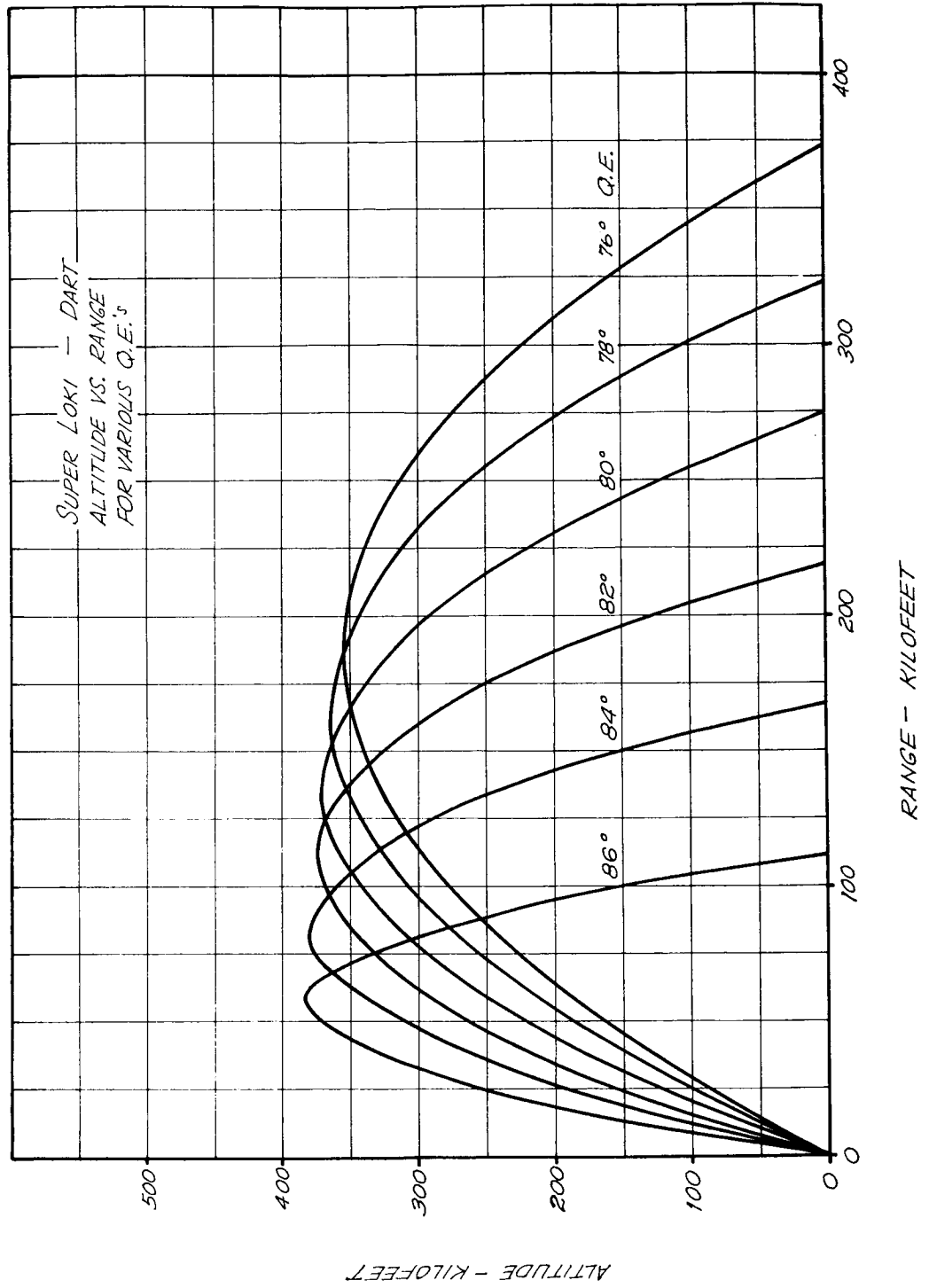


FIGURE 6.3-25 NOMINAL TRAJECTORY SUMMARY-SUPER LOKI DART

TABLE 6-17

NOMINAL TRAJECTORY SUMMARY
 SUPER LOKI DART, 80° Q.E. SEA LEVEL LAUNCH

	<u>BOOSTER</u>	<u>DART</u>
Burnout Altitude (m)	1577.6 m (5,176 ft)	1577.6 m (5,176 ft)
Burnout Range (m)	298.1 m (978 ft)	298.1 m (978 ft)
Burnout Time (sec)	2.1	2.1
Apogee Altitude (m)	2318.9 m (7,608 ft)	113.4 km (372,000 ft)
Apogee Range (m)	446.2 m (1,464 ft)	41.8 km (137,000 ft)
Apogee Time (sec)	6.1	6.1
Impact Range (m)	462.4 m (1,517 ft)	83.8 km (275,000 ft)
Impact Time (sec)	108	309

6.3.7 Viper Dart.

The Viper Dart Robin Meteorological Rocket System has been developed to obtain high altitude density and wind data by utilizing the Robin inflatable sphere as a sensing device. The system consists of a rocket motor, an unpowered dart and the Robin inflatable sphere. Flight tests of the system provided density, temperature, pressure and wind data from an altitude of about 90 kilometers to an altitude of approximately 40 kilometers or less.

During the flight test phases of the initial development program, reliable performance was obtained to 125 km with a slightly longer and heavier dart than originally contemplated. This was due to the added requirement for extra volume for a tracking aid. Although higher altitudes were obtained for smaller and lighter weight darts, the larger dart design was chosen as final for the initial development program.

The 125 km Viper-Dart vehicle consists of a Viper solid-propellant rocket motor as the first stage and an inert dart as the second stage. Figure 6.3-26 presents the vehicle configuration. The dart weight has been optimized to produce a high ballistic coefficient for efficient coasting to the desired apogee altitude. The dart diameter of 2.00-inches has been chosen as a tradeoff among factors of altitude performance, flight stability, payload packaging and thermal protection for the payload. The dart employs an aft-end boattail for interstage coupling, for housing the dart igniter leads and to reduce base drag during coasting-dart flight. The interstage has been designed as a tradeoff between shallow angles to reduce drag and larger angles which reduce weight. Launch lugs are located on fore and aft regions of the booster to mate the vehicle with the launch rail.

The dart design is shown in Figure 6.3-27. The dart has a relatively long length-to-diameter ratio with a high fineness-ratio ogive. A boat-tail structure aft of the fins is employed to reduce base drag and provide a convenient means of interstaging. The dart is designed to have a gross weight of 29.5 lbs. which gives reliable performance when used with the Viper Rocket motor. The basic dart diameter is 2.000-inches and the length is 58.0 inches.

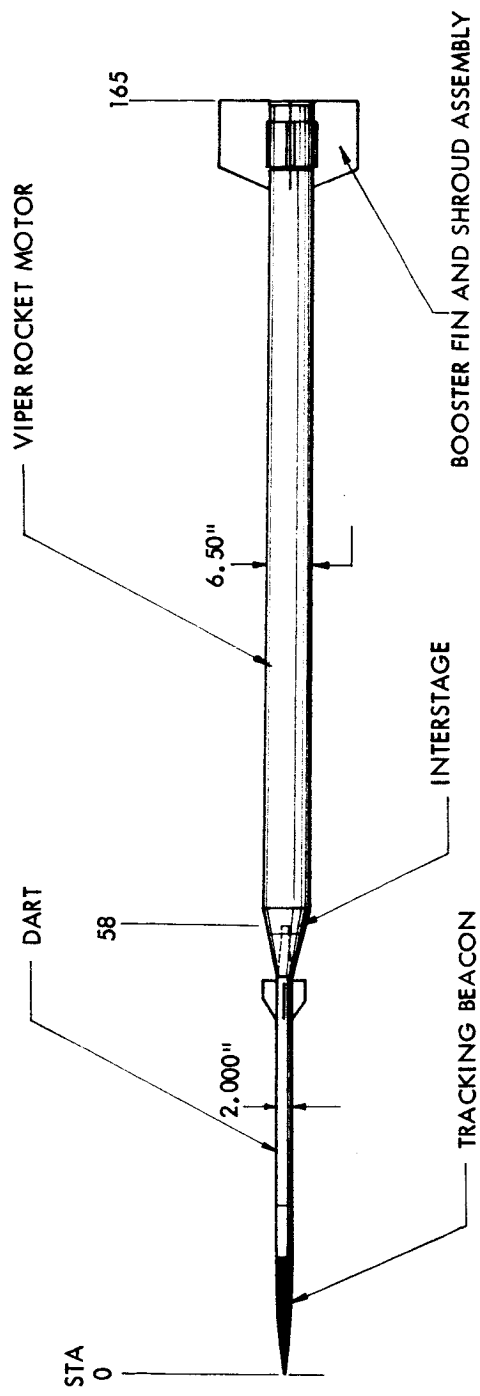


FIGURE 6.3-26 VIPER-DART VEHICLE CONFIGURATION

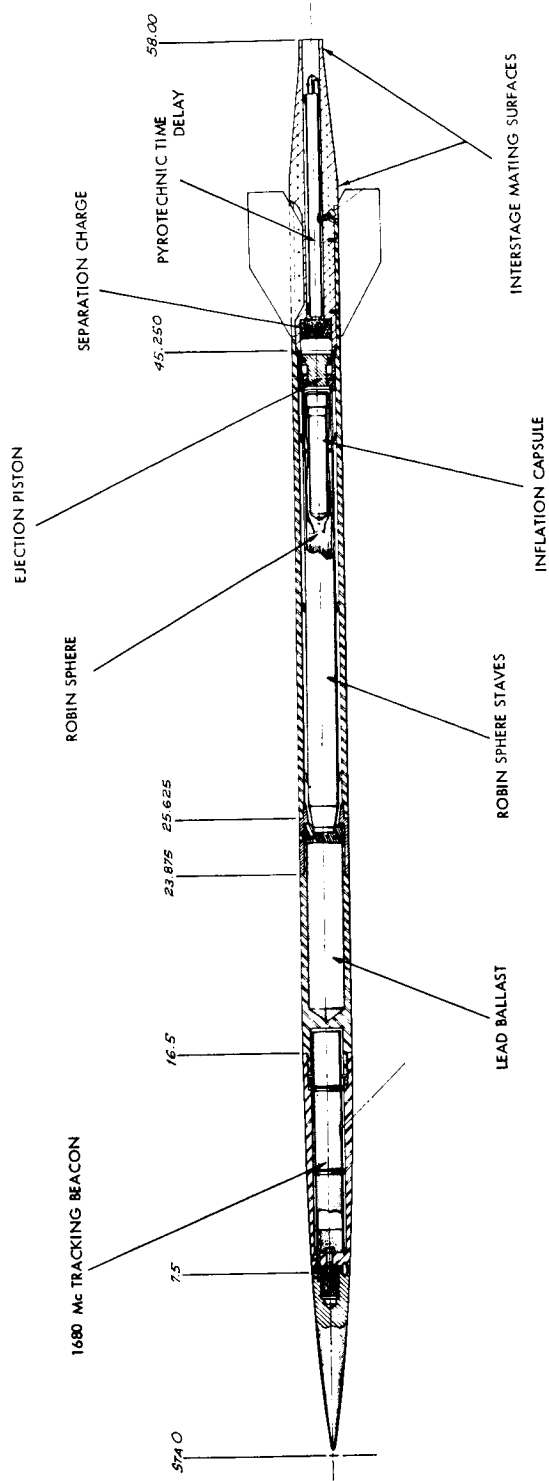


FIGURE 6.3-27 VIPER DART (DART) CROSS SECTION VIEW

The payload ejection system is made up of two components, i.e., the pyrotechnic time delay and the expulsion charge. The pyrotechnic time delay is ignited at launch at the same time the booster motor is ignited. After the time delay has burned for a specified time, ignition from the time delay is provided to the expulsion charge. The expulsion charge consists of 5 grams of boron potassium nitrate pellets. Upon ignition these pellets generate a high pressure behind the piston which forces the ejection piston forward. The first motion of the ejection piston forces a hollow metering pin into the Robin sphere inflatable capsule. Further forward motion picks up the outer piston, which transmits a force to the ogive to shear the shear-screws which hold the ogive in place. In this way, the sphere package and the ogive are ejected. At this point in the ejection sequence, the piston is stopped at the forward end of the dart by a swagging which prevents any of the burning boron potassium nitrate pellets or hot exhaust gases from contacting the sphere. The staves around the sphere are allowed to separate after ejection; thus allowing the sphere to expand and inflate. The dart ogive contains the tracking beacon.

The interstage is an aluminum coupling structure between the booster and the dart, which also forms an aerodynamic fairing from the dart diameter to the booster diameter. The interstage is connected to the booster through a threaded connection at the forward end of the booster. The interstage structure is thereby attached to the booster for the entire flight duration. Internal surfaces of the interstage are machined to accept the boat-tail of the dart at a point close to the motor and at another point at the forward end of the interstage. Longitudinal force, exerted from the dart when the system is accelerating, is absorbed at the end of the boat-tail and at the forward end of the booster. Because of the severe aerodynamic heating environment during boost, the interstage is coated with a 0.030-inch thickness of an ablative coating for thermal protection. The rocket motor and flight hardware are shown in Figure 6.3-28.

The Viper is a 3.52 KS 8500 solid-propellant rocket motor adaptable for sounding vehicle propulsion, sled propulsion and other uses. The motor case is a cylindrical rolled and welded tube with hemispherical ends of heat-treated chrome molybdenum steel, with a minimum yield point of 165,000 psi, and with nominal dimensions of 6.5 inches outside diameter and 107-inches in length. The nozzle is an assembly of carbon steel with a graphite insert. The propellant is polysulphide/ammonium perchlorate,

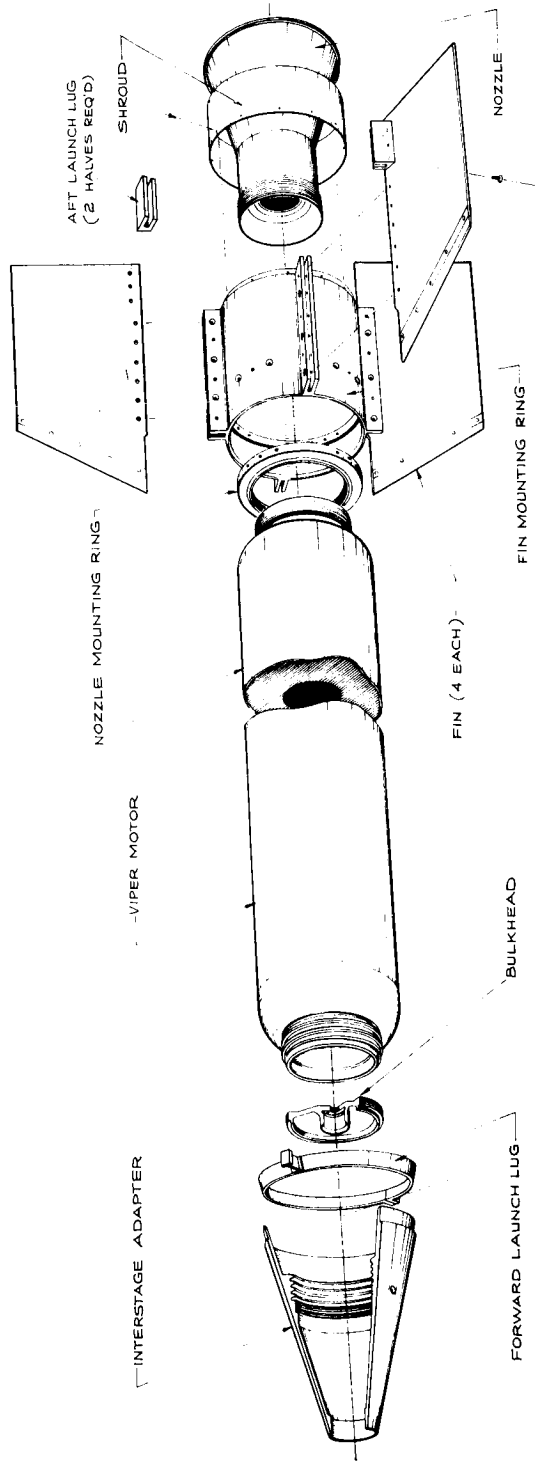


FIGURE 6.3-28 VIPER MOTOR AND COMPONENTS

case-bonded type.

The nominal weight of the complete rocket motor is 191.68 pounds. The nominal weight of the rocket motor components are as follows:

Metal Case	31.00 lbs
Head Cap	2.13
Nozzle	7.25
Liner	2.05
Insulation	0.50
Propellant	<u>148.75</u>
Total	191.68 lbs.

The nominal total impulse at sea level is 31,830.3 lb/sec for a nominal total time of 3.52 seconds. The vehicle component weights are presented in Table 6-18. A nominal performance summary is presented in Table 6-19 with a typical trajectory in Figure 6.3-29.

The Viper Dart Robin is currently being used for routine wind and density measurements at Cape Kennedy, WSMR and PMR in its present 125 km version. At the same time a further development program is being pursued by AFCRL to increase the altitude of this system to 140 km.

6.3.8 Cajun Dart.

The Cajun Dart vehicle was developed by Space Data Corporation for the Aero-Astrodynamics Laboratory of George C. Marshall Space Flight Center to measure winds in the altitude range from 70 to 90 kilometers.

The Cajun Dart chaff rocket is a two stage dart type sounding rocket vehicle. In the launch configuration the vehicle has a gross weight of about 200 pounds and an overall length of 13 feet. Figure 6.3-30 shows the vehicle with the basic dimensions and weights. The first stage of the Cajun Dart is the Cajun rocket motor, Mod III, manufactured by Thiokol Chemical Corporation, Elkton, Maryland. The Cajun motor is 102 inches long and has a principle diameter of 6.5 inches. The motor less flight hardware weighs 168 pounds with 118.5 pounds of propellant. The nominal burning time of 2.8 seconds, yields total impulse of 25,250 pounds seconds, yields a burnout velocity of slightly over 5000 feet per second at an altitude of 7,000 feet. At Cajun burnout, separation of the Dart from the Cajun booster is accomplished by allowing the aerodynamic drag differential between the booster and Dart to physically separate the two (2) stages.

TABLE 6-18

VIPER-DART WEIGHT TABLE

Vehicle Launch Weight	234.18 lb.
Vehicle Burnout Weight	85.33 lb.
Dart Coast Weight	29.50 lb.
Component Weight Breakdown:	
Dart	29.50 lbs.
Interstage	3.50
Booster Fins	9.50
Booster Motor	191.68
Case	31.00
Head	2.13
Nozzle	7.25
Miscellaneous	2.55
Propellant	148.75

TABLE 6-19

NOMINAL PERFORMANCE SUMMARY

Vehicle Name				Viper Dart
Booster - Stage I				Viper
Dart Weight/Diameter				29.5 lbs/2.00 in
Launcher Setting (Nominal)				80.0° Q.E.
Event	Time (Sec)	Altitude (feet)	Range (feet)	Velocity (Ft/Second)
<u>Stage 1</u>				
Ignition	0	0	0	0
Burnout (Separation)	3.10	8,500	1553	5934
Booster Apogee	10.9	18,000	3,500	22
Booster Impact	178.5	0	3620	97
<u>Stage 2</u>				
Dart Apogee	162	405,179	152,547	950
Dart Impact	323	0	305,140	4,600

The payload is deployed at dart apogee (162 seconds).

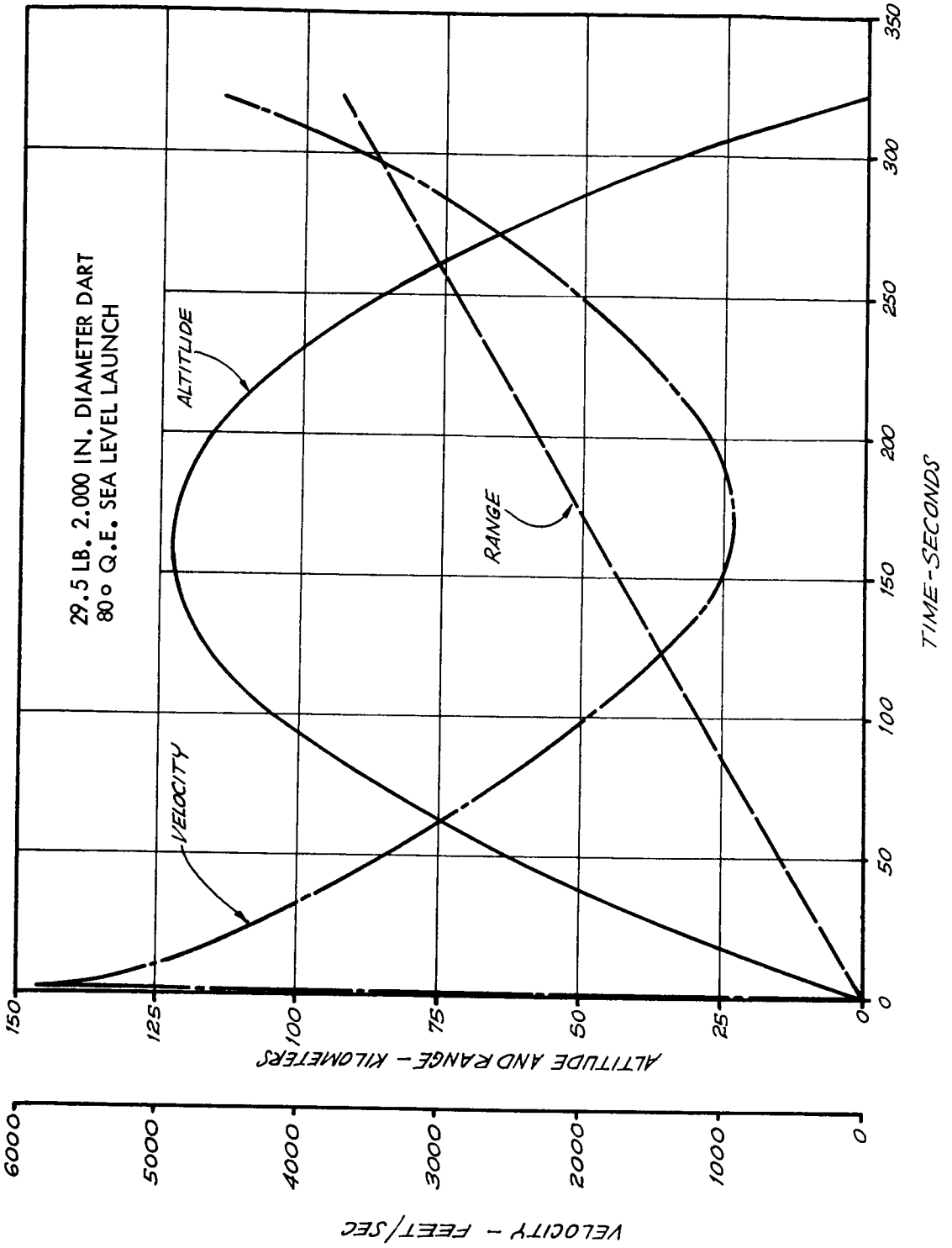
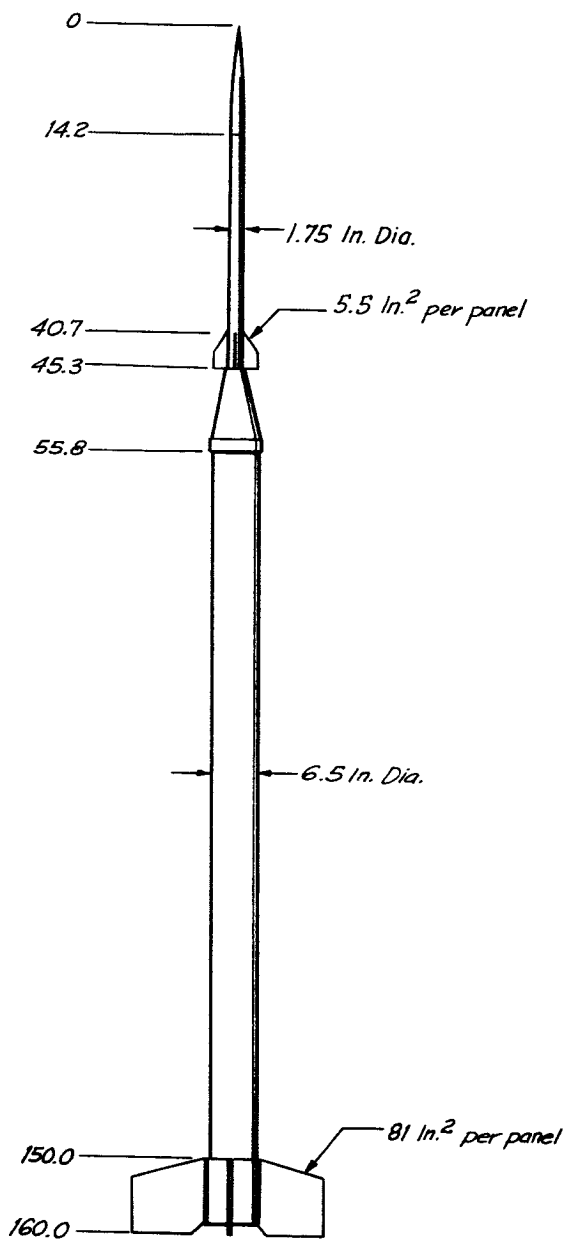


FIGURE 6.3-29 NOMINAL DART TRAJECTORY, VIPER DART



Weight Information

DART

Case	4.95
Ogive	7.00
Tail Ass'y	2.56
Chaff, Staves, etc.	2.77

TOTAL.....17.28 Lbs.

CAJUN

Interstage	4.00
Fins	7.32
Motor Hardware	49.30

Total @ Burnout.....76.90

Propellant.....118.5 Lbs.

Total Vehicle Wt.
at Launch.....196.40 Lbs.

FIGURE 6.3-30 CAJUN DART VEHICLE CONFIGURATION

After separation the Dart continues to coast to payload ejection.

The Dart 1-3/4 inches in diameter, weighs 17 pounds and is 51.7 inches long. The dart is a non-thrusting stage functioning only as a low drag payload housing. The nose of the Dart is designed to have a hypersonic optimum shape, keeping the aerodynamic drag to a minimum. The aft end of the Dart has been boat-tailed, forming the interstaging surfaces as well as reducing the base drag. These two (2) factors along with the otherwise sleek shape of the Dart combine to produce a very low drag rocket configuration. The payload housed inside the Dart is 30 cubic inches of 0.5 mil, aluminized mylar, foil chaff cut to S-band length.

Figure 6.3.31 is a cutaway drawing of the dart showing the external dimensions as well as the internal configuration.

In order to make a system reliably measure winds from 90 kilometers down, the nominal vehicle apogee must be above this altitude. As shown in Figure 6.3.32, the nominal apogee point for the Cajun Dart is 93 kilometers altitude, 37 kilometers range at a time of 140 seconds, when fired at an 80 degree elevation angle. This will keep the apogee of all flights above 90 kilometers even with the normal vehicle dispersion.

When the Dart has reached its apogee, the payload is ejected. This expulsion is accomplished by the use of 145 second pyrotechnic time delay housed in the Dart tail and initiated at launch. At 145 seconds the time delay ignites a 5 gram expulsion charge which ejects the Dart nose cone and the chaff payload by forcing a piston the full length of the Dart. The chaff is then free to drift with the winds as it falls.

The Cajun Dart has been used by NASA at Cape Kennedy for routine measurement of high altitude winds but is currently being replaced by the lower cost Super Loki.

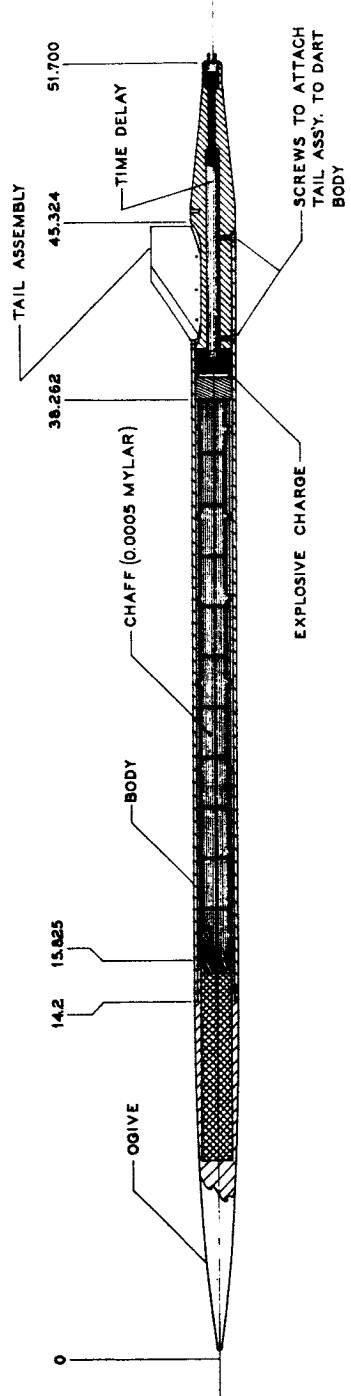
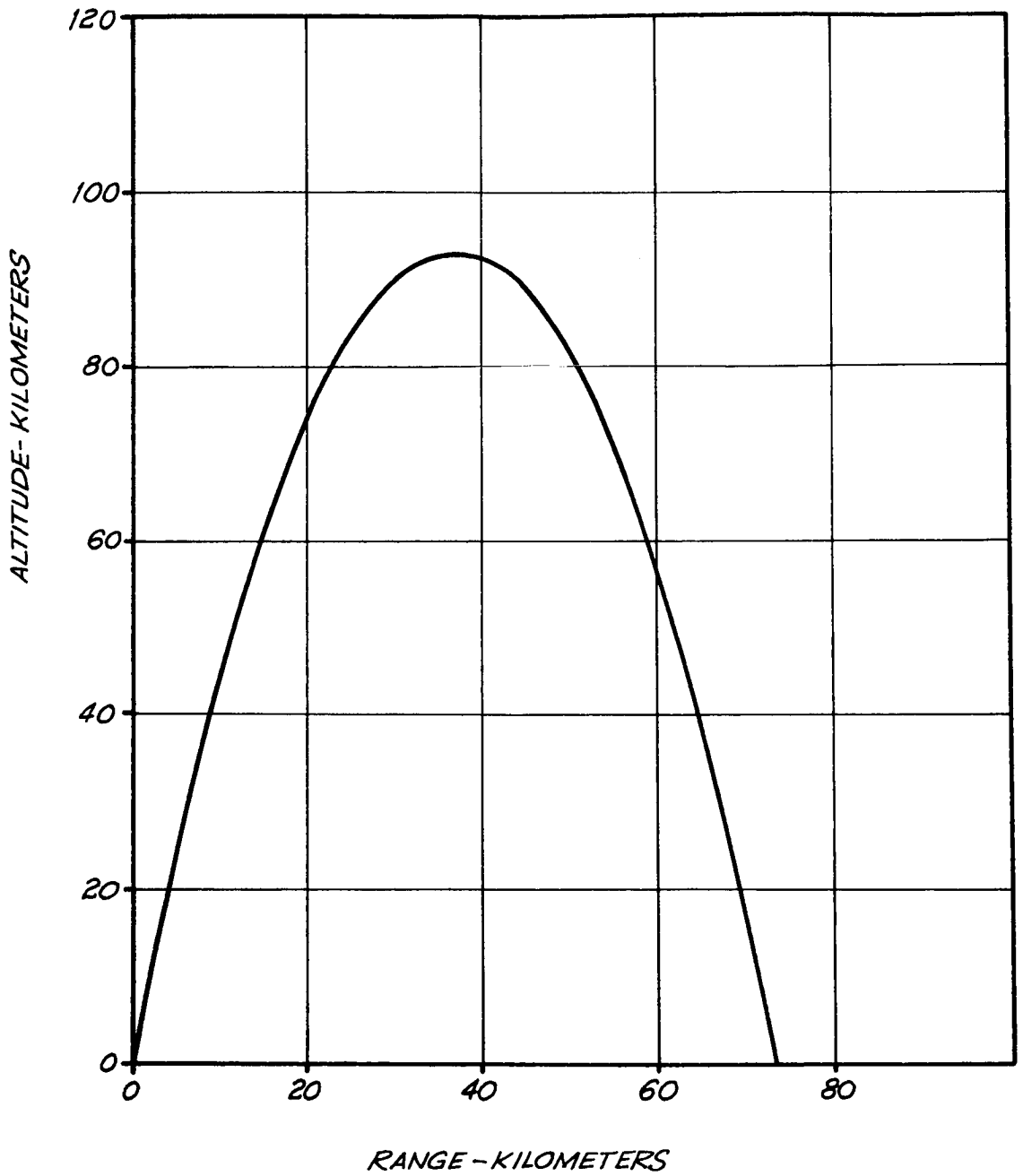


FIGURE 6.3-31 CUTAWAY VIEW OF THE DART

FIGURE 6.3-32 CAJUN-DART ALTITUDE VS. RANGE, 80° Q.E.



6.3.9 Boosted Arcas . (See Figure 6.3-33)

There are various versions of the boosted Arcas in limited use today as indicated in Table 6-20. The Arcas is used as a second stage in these configurations and the payload capacity is as follows.

Payload Weight	10-30 lb
Payload Diameter	4.25 in
Payload Length, Nominal	26 in.
Payload Volume, Nominal	305 in.

The performance of the boosted Arcas vehicles depends upon the booster used. A brief description of each of the boosted Arcas configurations is presented in paragraphs which follow.

The booster is an Atlantic Research 0.8-KS-2700 rocket motor. Power for ignition of both stages is provided by a ground source, a motion switch firing the sustainer igniter after positive ignition. An optional sustainer igniter incorporating a 2-second delay is also available. Fin assemblies are preset to provide a roll rate of approximately 25 rps at burnout.

The vehicle is launched from the standard ARCAS rocket launcher with the breech door open. Assembly and launch preparation requires no special handling equipment and can be accomplished by a two-man crew.

VEHICLE DATA

First-State Motor

MARC 14A1	
Nominal performance rating	0.8-KS-2700
Principal diameter	10.2 cm (4.0 in)
Overall length	71.6 cm (28.2 in)
Igniter: Type	Pyrotechnic
Recommended firing current	3.5-5 amp

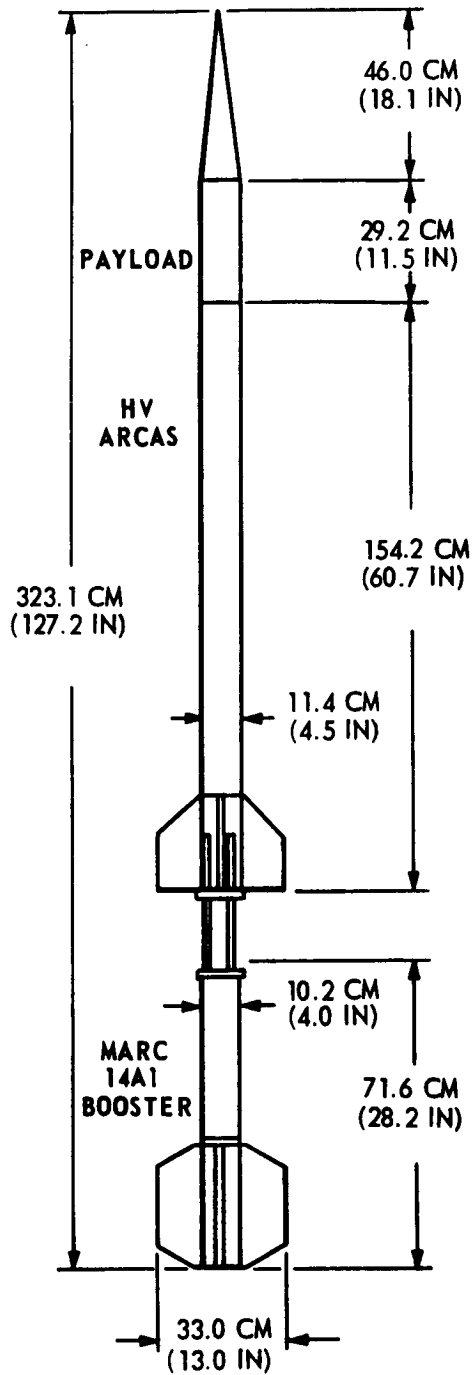


FIGURE 6.3-33 BOOSTED ARCAS VEHICLE CONFIGURATION

TABLE 6-20

SUMMARY OF BOOSTED ARCAS VEHICLES

	<u>BOOSTED ARCAS</u>	<u>SIDEWINDER ARCAS</u>	<u>SPARROW ARCAS</u>	<u>BOOSTED ARCAS II</u>
PEAK ALTITUDE (K FT) (85° Seal Level Launch)	250	360	460	400
PAYLOAD WEIGHTS (LB)	12	12	12	12
MAXIMUM VELOCITY (FT/SEC)	3450	4500	5500	4825
MAXIMUM ACCELERATION (G)	22	28	39	20
TIME TO PEAK ALTITUDE (SEC)	152	171	203	185
NOSE CONE VOLUME (CU IN)	370	370	370	370
OVERALL LENGTH (FT)	10.6	14.1	12.6	13.2
MAXIMUM DIAMETER (IN)	4.5	5.2	8.0	4.5
MAXIMUM FIN SPAN (IN)	13.0	15.0	30.5	13.0
TOTAL WEIGHT (LBS)	102	166	206	135
BOOSTER BURNING TIME (SEC)	1.0	2.4	2.0	3.0
BOOSTER BURNOUT ALTITUDE (FT)	336	2100	2076	
BOOSTER BURNOUT VELOCITY (FT/SEC)	690	1575	2161	

Second-Stage Motor

MARC 2B1 ARCAS	
Nominal performance rating	29-KS-324
Principal diameter	11.4 cm (4.5 in)
Overall length	154.2 cm (60.7 in)
Igniter: Type-Pyrotechnic (optional 2-second delay squib)	
Recommended firing current	5 amp

Weights (less payload)

Gross launch weight	46.3 kg (102.0 lb)
First-stage burnout	41.3 kg (91.0 lb)
Second-stage ignition	30.1 kg (66.4 lb)
Second-stage burnout	10.6 kg (23.3 lb)

Sidewinder Arcas. (See Figure 6.3-34)

Originally developed by the Naval Missile Center, under the sponsorship of Air Force Cambridge Research Laboratories, the Sidewinder-ARCAS vehicle used propulsive stages which are proven, qualified rocket motors. Staging is accomplished by a bayonet-type interstage adapter that provides structural rigidity during boost, but permits drag-induced stage separation. Fin assemblies are preset to provide approximate spin rates of 7 to 20 rps at second stage burnout.

The launch system is a 15 foot long rail assembly designed for mounting on an adjustable-boom launcher of the type available at most launch sites. Assembly and launch preparation require no special handling equipment and can be accomplished by a two-man crew.

Power for ignition of both stages is provided by a ground source, a motion switch completing the second-stage firing circuit only after positive booster ignition. A delay squib in the second stage igniter allows 2 seconds of coasting flight between booster burnout and second stage ignition.

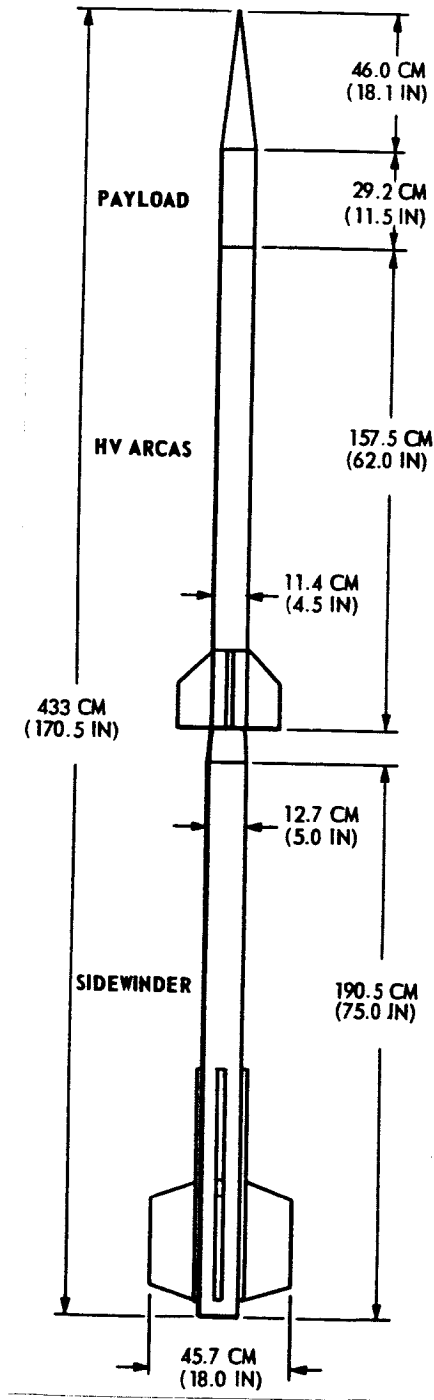


FIGURE 6.3-34 SIDEWINDER ARCAS VEHICLE CONFIGURATION

SIDEWINDER ARCAS VEHICLE DATA

First-Stage Motor

MK 17 Sidewinder 1A	2.14-ES-3972
Nominal performance rating	12.7 cm (5.0 in)
Principal diameter	190.5 cm (75.0 in)
Overall length	Pyrotechnic
Igniter: Type	3 amp
Recommended firing current	

Second-Stage Motor

MARC 2C1 HV ARCAS	29-KS-324
Nominal performance rating	11.4 cm (4.5 in)
Principal diameter	157.5 cm (62.0 in)
Overall length	
Igniter: Type - Pyrotechnic (with 4-second delay squib)	
Recommended firing current	7 amp

Weights (less payload)

Gross launch weight	75.5 kg (166.3 lb)
First-stage burnout	55.6 kg (122.5 lb)
Second-stage ignition	30.6 kg (67.5 lb)
Second-stage burnout	11.1 kg (24.4 lb)

Sparrow Arcas. (See Figure 6.3-35)

Developed originally for the Pacific Missile Range Density Probe (DENPRO) program, the Sparrow-HV ARCAS uses propulsive stages which are proven, qualified rocket motors. Staging is accomplished by a bayonet-type interstage adapter that provides structural rigidity during boost, but permits drag-induced stage separation. Fin assemblies are preset to provide approximate spin rate of 8 to 20 rps at second-stage burnout.

The launch system is a 15-foot long rail assembly designed for mounting on an adjustable-boom launcher of the type available at most launch sites. Assembly and launch preparation require no special handling equipment and can be accomplished by a two-man crew.

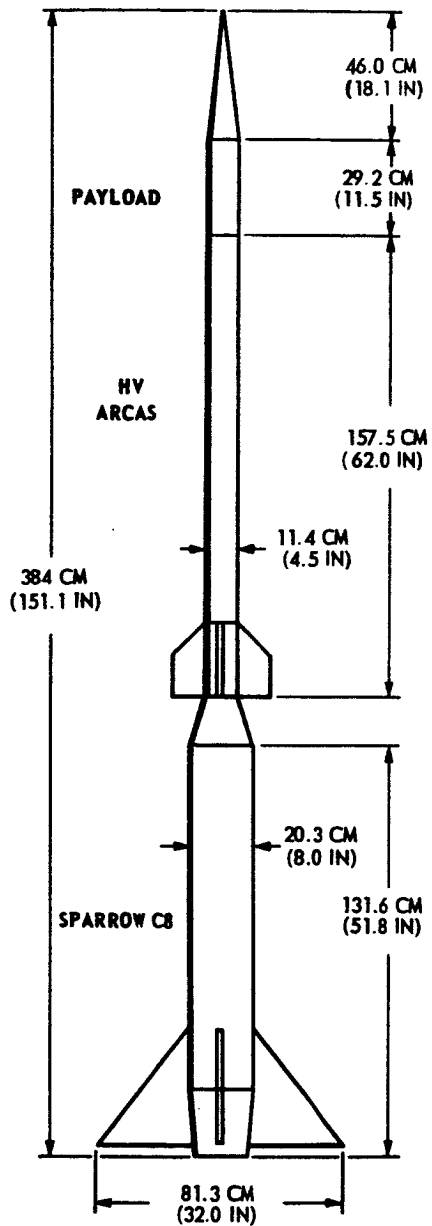


FIGURE 6.3-35 SPARROW ARCAS VEHICLE CONFIGURATION

Power for ignition of both stages is provided by a ground source, a motion switch completing the second-stage firing circuit only after positive booster ignition. A delay squib in the second-stage igniter allows 6 seconds of coasting flight between booster burnout and second stage ignition.

VEHICLE DATA

First-Stage Motor

MK 6 Mod 3 Sparrow C-8	
Principal diameter	20.3 cm (8.0 in)
Overall length	131.6 cm (51.8 in)
Igniter: Type	Glow plug
Recommended firing current	30 amp

Second-Stage Motor

MARC 2C1 HV ARCAS	
Nominal performance rating	29-KS-324
Principal diameter	11.4 cm (4.5 in)
Overall length	157.5 cm (62.0 in)
Igniter: Type - Pyrotechnic (with 8-second delay squib)	
Recommended firing current	7 amp

Weights (less payload)

Gross launch weight	93.5 kg (206.0 lb)
Second-stage ignition	30.6 kg (67.5 lb)
Second-stage burnout	11.1 kg (24.4 lb)

Boosted Arcas II. (See Figure 6.3-36)

The Boosted Arcas II uses a booster employing an internal burning propellant grain and an Arcas motor case. This booster was developed by Atlantic Research Corporation specifically for this vehicle and has had a limited flight test history.

Staging is accomplished by a bayonet-type interstage adapter that provides a rigid structure during boost, but permits drag-induced stage separation.

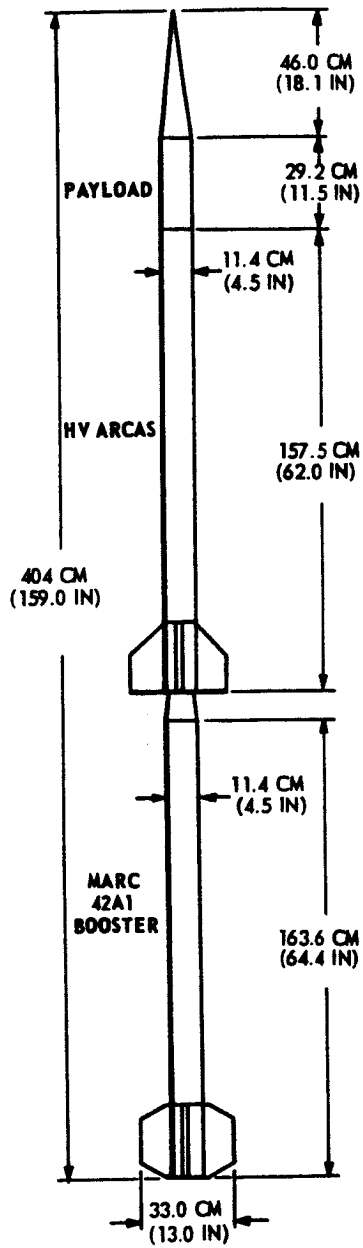


FIGURE 6.3-36 BOOSTED ARCAS II VEHICLE CONFIGURATION

Power for ignition of both stages is provided by a ground source, a position switch completing the second-stage ignition circuit only after positive booster ignition. A delay squib in the second-stage igniter allows 4.5 seconds of coasting flight between booster burnout and second stage ignition.

The vehicle is designed for launching from the standard ARCAS rocket launcher with open breech door or from a 15 foot long rail. Assembly and launch preparation can be accomplished by a two-man crew.

VEHICLE DATA

First-Stage Motor

MARC 42A1 Booster	
Nominal performance rating	3.0-KS-2740
Principal diameter	11.4 cm (4.5 in)
Overall length	163.6 cm (64.4 in)
Igniter: Type - Pyrogen, 1-watt, 1-amp squib	
Recommended firing current	7 amp

Second-Stage Motor

MARC 2C1 HV ARCAS	
Nominal performance rating	29-KS-324
Principal diameter	11.4 cm (4.5 in)
Overall length	157.5 cm (62.0 in)
Igniter: Type - Pyrotechnic (with 8.0 second delay squib)	
Recommended firing current	7 amp

Weights (less payload)

Gross launch weight	61.4 kg (135.3 lb)
First-stage burnout	45.4 kg (100.0 lb)
Second-Stage ignition	30.6 kg (67.5 lb)
Second-Stage burnout	11.1 kg (24.4 lb)

6.3.10 Nike Vehicles.

There are a number of Nike-boosted sounding rockets which are used for geophysical research. Although these vehicles are too large and too expensive for serious consideration as routine meteorological rockets, they are briefly described here for sake of completeness. A summary of the Nike-boosted vehicles is presented in Table 6-21. These vehicles are designed to carry large payloads (greater than 50 lbs) to altitudes between 100 km and 300 km. Each uses the Nike M5 rocket motor as the first-stage. This motor has a diameter of 16.5 inches, a length of 135.5 inches and weighs 1342 lbs. This motor alone requires significant handling equipment and could hardly be considered for routine meteorological operations.

TABLE 6-21

SUMMARY OF NIKE-BOOSTED VEHICLES

<u>NAME</u>	<u>NIKE CAJUN</u>	<u>NIKE APACHE</u>	<u>NIKE IRIQUOIS</u>	<u>NIKE TOMMAHAWK</u>	<u>NIKE HYDAC</u>
Payload Weight (lb)	60	60	80	120	120
Payload Diameter (in)	6.5	6.5	7.8	9.0	9.0
Apogee Altitude (km)	160	220	205	300	300
Second Stage Length (ft)	9.0	9.0	8.6	11.8	11.8
Second Stage Weight (lb)	172	216	279	530	610
Overall length (ft)	25	25	28	30	30
Overall Weight (lb)	1574	1618	1700	1992	2072
Second Stage Motor Designation	TE-82	TE-307	TE-M-388	TE-416	H-26A
Approximate Vehicle Cost	\$6,000	\$6,000	\$10,000	\$15,000	\$ 13,000

6.4 Development Systems.

6.4.1 General.

There are a number of meteorological rocket vehicle development programs which are currently being pursued. These programs range from rather modest efforts such as improving the Viper Dart performance to the state-of-the-art development of fragile boosters. A brief description of the current meteorological rocket vehicle development programs is presented in the sections which follow.

6.4.2 Improved Viper Dart.

The Viper Dart is currently being modified to improve the apogee altitude performance from 125 km to 140 km. This is being accomplished under an AFCRL program by using a propellant with a higher specific impulse than the standard Viper. Techniques of stabilizing the booster after burnout are also being investigated to reduce the problem of booster impact dispersion.

6.4.3 Super Loki Instrumented Dart.

The Super Loki vehicle is being modified by incorporating a large diameter (2.1 inch) dart to extend the standard rocketsonde temperature and wind measurements upward as high as 75 km. This program is sponsored jointly by AFCRL and NASA-MSFC. The large diameter dart will permit the incorporation of a large Starute decelerator, a GMD-2 transponder instrument and more room for advanced sensors. The cost of this vehicle should not be significantly greater than for the standard Loki vehicle.

The development of a 2.1 inch diameter instrument dart for the Super Loki system is a follow-on to the chaff dart system development to improve the altitude and measurement capability of current instrumented systems. An 85 km apogee is achievable with the proposed instrumented dart system, and the payload volume is more than double that of the current instrumented dart systems. This increased volume can be used for additional sensors, a transponder/telemetry sonde, and most important, an increased-size parachute to obtain significantly slower descent rates of the sonde during the measurement period. Temperature and wind measurement errors of current systems are functions of the square of the descent velocity,

and a significant improvement in measurement accuracy can accrue by reducing the parachute descent rate. The cost of this instrument dart system should not be significantly greater than the current instrumented dart systems.

The proposed Super Loki Instrumented Dart system consists of the Super Loki rocket motor and a 2.1 inch diameter dart. The dart is designed to contain a maximum diameter parachute to extend the altitude and improve the accuracy of wind and temperature measurements. Performance of this system is as follows:

Launch Angle	85°
Dart Weight	14 lb (6.35 kg)
Apogee Altitude	85 km
Apogee Range	15 km
Apogee Time	132 sec
Burnout Velocity	Mach 5.4
Maximum Acceleration	102 g

A nominal trajectory is plotted in Figure 6.4-1.

The 2.1 inch diameter instrumented dart contains a payload volume of 55 cubic inches. This is more than twice the payload volume of the 1.437 inch diameter (3.65 cm) instrumented dart which is currently being used. Either a 1680 mc/GMD-(x) or a 403 mc/SMQ-1 sonde can be used with the proposed dart depending upon ground-station equipment. Descent rates of the sonde system can be slowed to 230 fps (70.1 m/sec) at 61 km with a Super Loki system ($W/C_{DA} = 0.015 \text{ lb/ft}^2$ or 0.073 kg/m^2). Advantages of the Super Loki Instrumented Dart over the current Loki Instrumented Dart are presented in Table 6-22.

An inflatable falling sphere payload has been procured by the Army personnel at White Sands Missile Range for use with the existing chaff dart design. Since altitudes of 125 km were obtained at White Sands, reasonably good density data may be derived with the Robin falling sphere payload to altitudes below 90 km with the Super Loki. Since the apogee altitude for a sea level launch will only be about 113 km, the falling sphere density data may be restricted to a maximum altitude of 85 km for sea level sites.

6.4.4 Destructible Arcas.

A destructible or fragmentible Arcas has been developed under a previous AFCRL contract by incorporating explosive charges with a fiber-

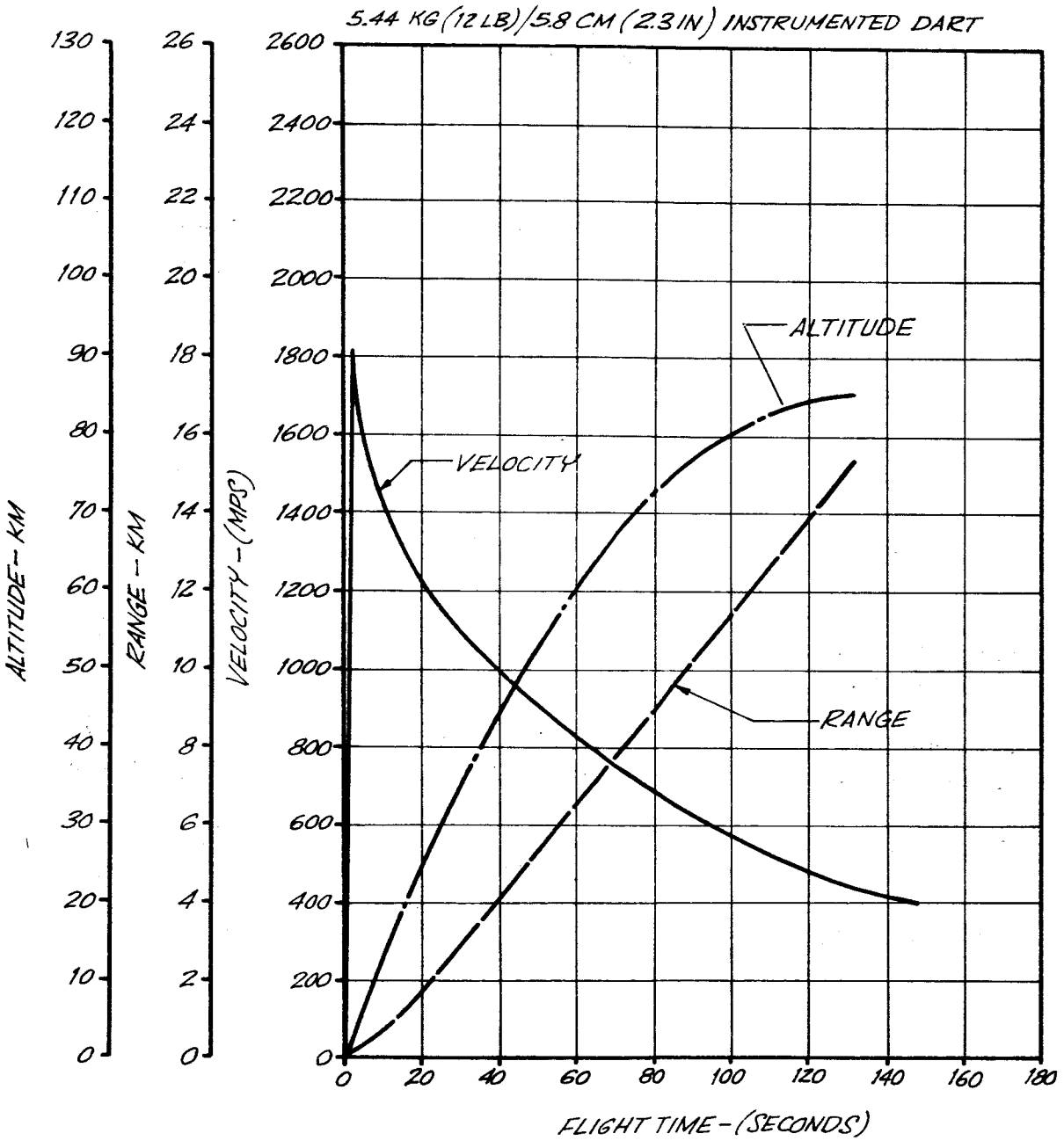


FIGURE 6.4-1 SUPER LOKI INSTRUMENTED DART NOMINAL TRAJECTORY
85° SEA LEVEL LAUNCH

TABLE 6-22

COMPARISON OF THE SUPER LOKI
INSTRUMENTED DART SYSTEM
WITH THE CURRENT
INSTRUMENTED DART SYSTEM

	<u>Super Loki System</u>	<u>Standard Loki System</u>
80°Q.E. Apogee Altitude	85 km (278.9 k ft)	63 km (206.7 k ft)
Dart Diameter	5.398 cm (2.125 in)	3.65 cm (1.437 in)
Payload Volume	901.3 cm ³ (55 cu in)	491.6 cm ³ (30 cu in)
Payload Volume Available for Parachute	612.87 cm ³ (37.4 cu in)	262.19 cm ³ (16.0 cu in)
Parachute-Sonde Ballistic Coefficient, W/C_dA	0.073 kg/m ² (0.015 lb/ft ²)	0.146 kg/m ² (0.030 lb/ft ²)
Descent Rate at 61 km	70.1 m/sec (230 ft/sec)	100.6 m/sec ² (330 ft/sec)
Dart Ablative Coating	Not Required	Required

glass plastic rocket motor design. Sheet explosive 0.042-inches thick was placed around the fiber-glass motor throughout its length in addition to an explosive charge located behind the payload section at the forward end of the rocket motor. After vehicle apogee and payload separation, the explosive charges were initiated and the remaining rocket was fragmented into rather small pieces which had a sea level impact energies on the order of 2.4 ft-lb (3.25 joules) maximum.

The vehicle contains an additional explosive charge between the rocket motor head closure and payload which is initiated by a mechanical timer unit at a timer predetermined and set prior to launch. Initiation of this primary explosive charge subsequent to payload ejection results in fragmentation of the forward section of the spent rocket motor assembly and induces sympathetic detonation of the sheet explosive material on the exterior of the motor case. Detonation energy of the sheet explosive produces fragmentation of the motor case and fin assembly.

A description of the vehicle, is presented in Figure 6.4-2. Comparison of dimensional and weight data between the Frangible Arcas and Arcas vehicles is presented in Table 6-23. A detailed weights breakdown of the frangible vehicle, less payload, is shown in Table 6-24.

The primary mission of the frangible vehicle is deployment of a payload at apogee, and subsequent self-induced fragmentation of the vehicle to particle sizes of very low impact kinetic energies. In order to ensure reliable fragmentation, the vehicle incorporates two independent initiation systems. The primary initiator is a mechanical timer unit which is armed at lift-off and started at rocket motor burnout. This unit is designed to initiate fragmentation twenty seconds after payload ejection. This time interval was selected to provide adequate clearance between the payload and the spent rocket vehicle.

A redundant, pressure sensing unit is incorporated as an independent unit. This secondary initiator is armed at a nominal altitude of 24.4 km (80,000 ft) during vehicle ascent and initiates fragmentation at a nominal altitude of 18.3 km (60,000 ft) during vehicle descent in the event of a failure of the primary system. The overall mission profile is illustrated in Figure 6.4-3.

A major objective and requirement of the program was the development of an integral explosive fragmentation system. Initial fragmentation

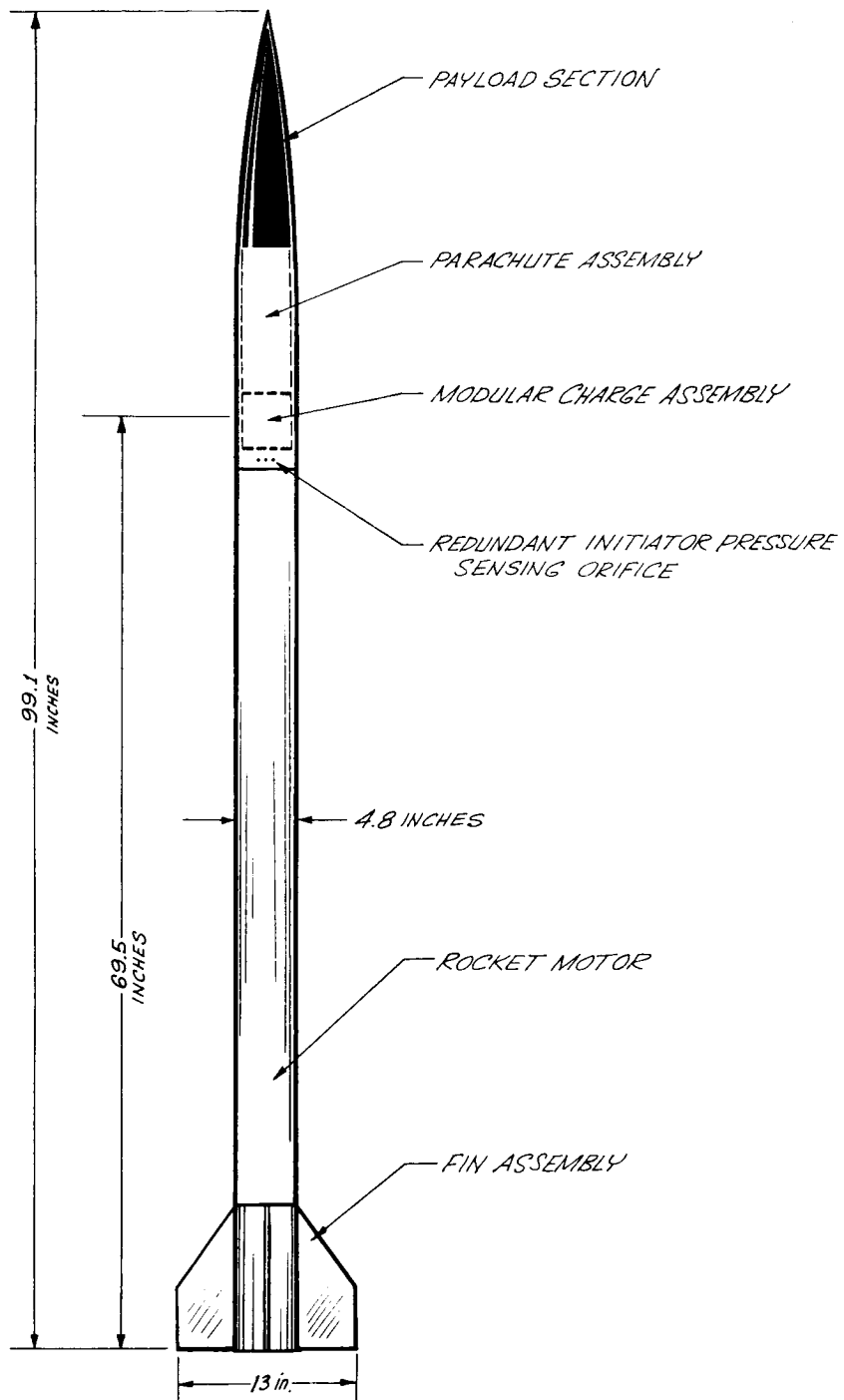


FIGURE 6.4-2 FRANGIBLE ARCAS VEHICLE CONFIGURATION

TABLE 6-23

FRANGIBLE ARCAS VEHICLE DIMENSION AND WEIGHT COMPARISONS

	Standard Arcas		Frangible Arcas w/o Fragmenta- tion System		Frangible Arcas with Fragmenta- tion System	
	Mod 0		Mod 3		Mod 3	
	cm	in	cm	in	cm	in
A. <u>Dimensions</u>						
Nose Cone	45.9	18.1	45.9	18.1	45.9	18.1
Parachute Container	29.2	11.5	29.2	11.5	29.2	11.5
Rocket Mtr. Assy	<u>154.0</u>	<u>60.7</u>	<u>164.0</u>	<u>64.5</u>	<u>176.5</u>	<u>69.5</u>
Over-all Length	229.1	90.3	239.1	94.1	251.6	99.1
Max. Body Diameter	11.4	4.5	11.9	4.7	12.2	4.8
Min. Body Diameter	11.4	4.5	11.2	4.4	11.4	4.5
Fin Span	33.0	13.0	33.0	13.0	33.0	13.0
B. <u>Weights</u>						
	kg	lb	kg	lb	kg	lb
Loaded Motor Assy	30.0	66.4	28.4	62.7	31.0	68.4
Payload ^a	<u>4.9</u>	<u>10.7</u>	<u>4.7</u>	<u>10.4</u>	<u>4.7</u>	<u>10.4</u>
Total Launch Wt. (Nom).	34.9	77.1	33.1	73.1	35.7	78.8
Vehicle Wt. at Mtr. Burnout (Less Payload Weight)	10.6	23.3	8.9	19.7	11.5	25.4

Note: ^a Includes parachute assembly, Arcasonde Instrument, nose cone and ballast.

TABLE 6-24

DETAILED WEIGHT BREAKDOWN OF THE FRANGIBLE ARCAS VEHICLE (LESS PAYLOAD)

Component	Nominal Weight at Lift Off		Nominal Weight at Burnout	
	kg	lb	kg	lb
Motor Case Assembly	7.48	16.50	6.89	15.20
Fin Assembly	0.76	1.69	0.76	1.69
Fin Screws	0.01	0.03	0.01	0.03
Propellant Assembly ^a	19.40	42.70	0.45	1.00
Retaining Sleeve	0.68	1.49	0.68	1.49
Explosive Module Fwd Plate	0.14	0.32	0.14	0.32
Explosive Module Aft Plate	0.13	0.29	0.13	0.29
Push Rod	0.01	0.02	0.01	0.02
Mechanical Timer Assembly	0.32	0.70	0.32	0.70
Redundant Initiator	0.14	0.30	0.14	0.30
Primary Explosive Charge	0.94	2.06	0.94	2.06
Sheet Explosive Charge & Overwrap	<u>1.04</u>	<u>2.30</u>	<u>1.04</u>	<u>2.30</u>
	31.05	68.40	11.51	25.40

Note: ^a Includes propellant, headplate, O-ring, dimple motor and inhibitor.

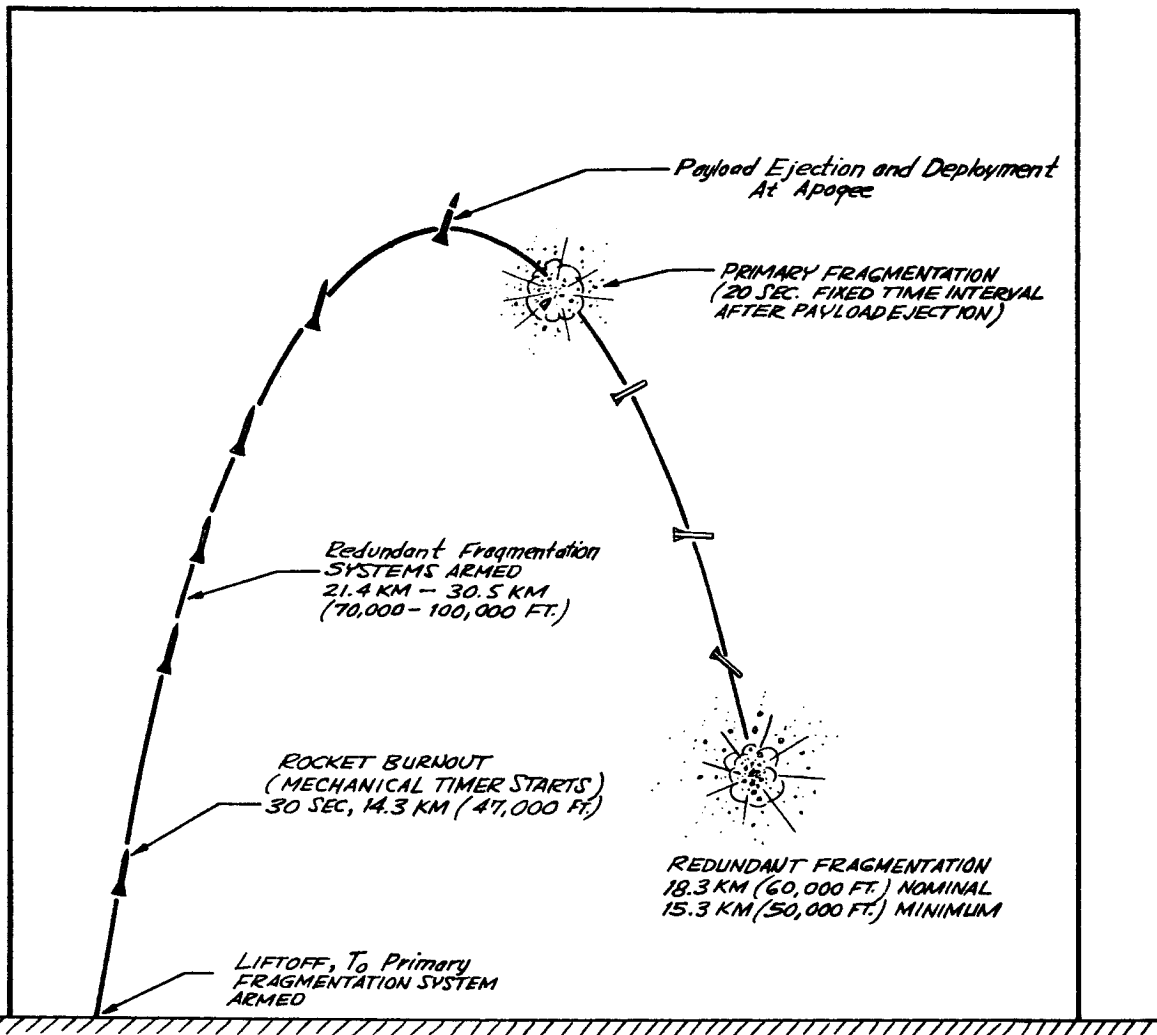


FIGURE 6.4-3 NOMINAL FRANGIBLE ARCAS FLIGHT EVENTS SEQUENCE PHASE III VEHICLE CONFIGURATION

tests incorporated a single modular shaped explosive charge in the forward end of the rocket motor. These initial tests showed adequate fragmentation of the forward and aft motor sections, but the center portion was left intact. It was interesting to note how the spent motor case acted as a shock tube and provided fragmentation of the nozzle/fin section while leaving most of the tube intact. Additional tests showed that the shape given the single explosive charge had no appreciable effect on the fragmentation results. Hence, it was evident that additional explosive material applied directly to the motor case was needed to achieve the required degree of fragmentation.

Tests utilizing linear shaped charges also proved unsuccessful. Although the motor case was sectioned at each location of the charge, the resulting fragments were unacceptable with regard to the maximum impact kinetic energy requirement. This could have been overcome by increasing the number of linear shaped charge strips, but the resulting vehicle weight would have been prohibitive.

Subsequent tests incorporating a primary explosive charge in the forward section of the vehicle, in combination with 1.07 mm- (0.042 in) thick sheet explosive material on the exterior of the motor case, were successful. Fragmentation to particle sizes yielding impact kinetic energies of 3.25 joules (2.4 ft/lb) or less were achieved.

Only one flight test of the complete system was conducted, and it was apparent that the destruct charges performed as a cloud of debris was tracked by radar. The apogee altitude for this test was only about 128,000 feet and a considerably larger vehicle would be required to make up for the addition weight and drag penalties created by the explosives system. In spite of the low performance, the principle of the destructible motor case was demonstrated with this program. However, the other problem areas were brought to light.

The major objections to the fragmentation technique are the safety aspects of ground-handling a live rocket motor which is surrounded by Class A explosives. The danger of such a device is considerably greater than for a rocket motor alone. In addition, if the explosives initiation system ever failed to function, then the subsequent ground-impact would surely cause a high-order explosion. Further, even if the system functioned satisfactorily, the nose cone itself presents a considerable falling mass hazard.

In addition, a tremendous number of full system flight tests would be required, without a single failure, to adequately demonstrate an order of reliability high enough for use over populated areas. For these reasons, further efforts on this program have been terminated.

6.4.5 Consumable Rocket.

The U. S. Army Missile Command supported jointly by NASA-LRC has been investigating the development feasibility of a consumable rocket. The falling mass hazard safety criteria of a maximum particle kinetic energy of 1 foot-pound (1.35 joules) and a particle size limitation of 0.1 pound (45.3 grams) were adopted for this program. The proposed concept of the consumable rocket is shown in Figure 6.4-4. After payload separation at apogee, the motor case material is to be ignited so that it completely burns to ashes before reaching the ground.

In the fall of 1965, on the basis of prior feasibility studies, a decision was made to proceed with further development of the consumable technique. Effort was directed toward improving the characteristics of combustible case wall composites, based upon the following general parameters in decreasing order of priority:

- (1) Completeness of neutralization
- (2) Safety in manufacturing and use
- (3) High strength
- (4) High autoignition temperature
- (5) Low environmental degradation
- (6) Least cost

Results of this study indicated two promising approaches to fabrication of consumable rocket cases -- use of a homogeneous composite, and use of a sandwich composite. These composites were investigated at Picatinny Arsenal beginning February 1966. Material composites were fabricated in 2.54 by 7.62 cm plates, 15.24 cm diameter standard test rings, 2.54 cm diameter by 10.16 cm cylinders, 7.62 diameter by 22.86 cm cylinders and 7.62 cm diameter by 45.72 cm pressure bottles.

The homogeneous composite structure was a filament-wound type, consisting of nitrocellulose fiber wound together with reinforcing fiber in

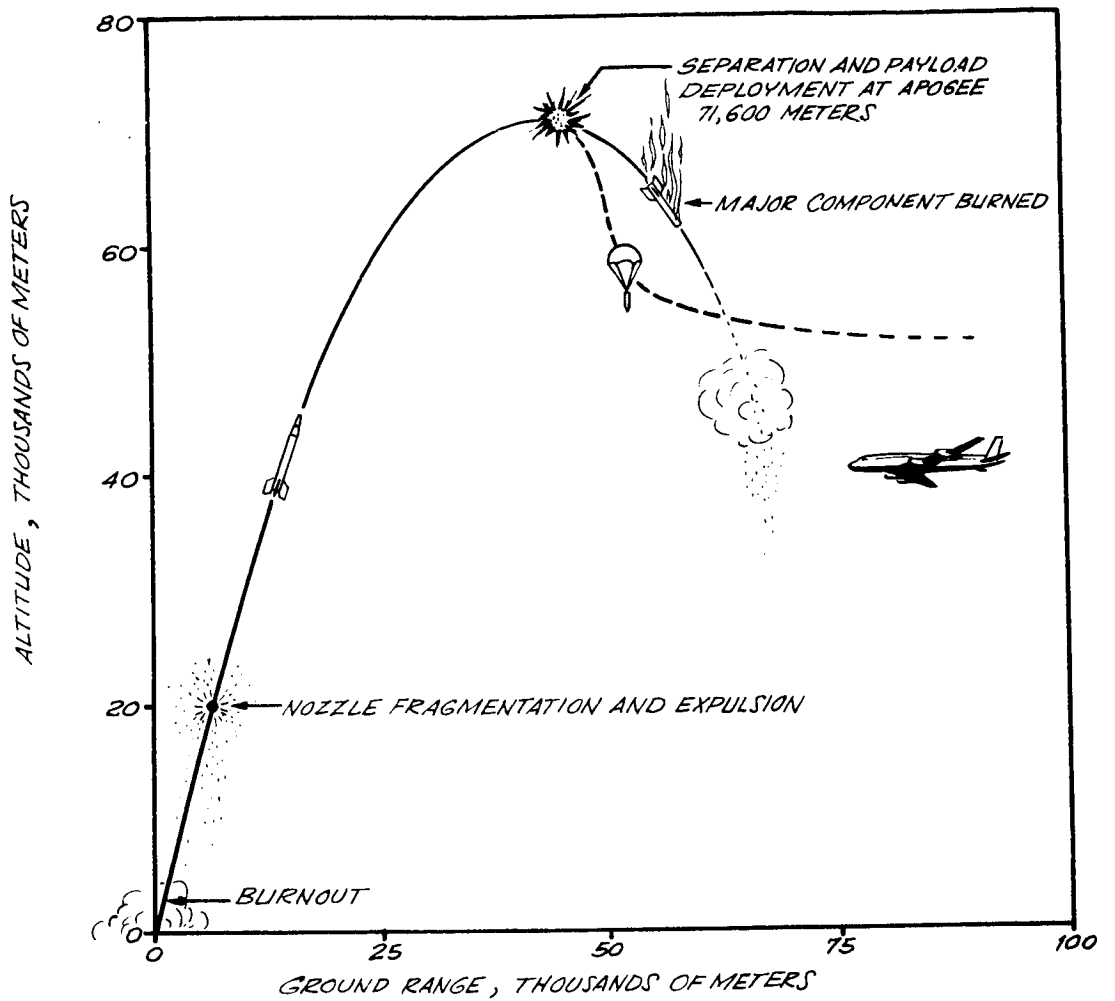


FIGURE 6.4-4 CONSUMABLE METEOROLOGICAL ROCKET OPERATION CONCEPT

in an epoxy binder. Reinforcing fibers considered for use were E-glass, Fortisan, HM-2 rayon, nylon and polypropylene. Samples of the homogeneous composite using from 50 to 100% nitrocellulose fiber were prepared and ignited at a simulated 61,000 meter altitude. The only structure of this type which was adequately destroyed was the 100% nitrocellulose/epoxy (6% of original weight). Other samples 2.54 cm diameter by 7.62 cm long) were burned with the following percentages of residue:

<u>SAMPLE</u>	<u>RESIDUE (Wt. %)</u>
73% NC/27% Fortisan	27
52% NC/48% Fortisan	49
77% NC/23% Fiberglass	39
63% NC/37% Fiberglass	60
73% NC/27% Nylon	32
40% NC/60% Nylon	56

The homogeneous composite remains a promising technique, whose major improvement potential lies in improved tensile strength of the nitrocellulose fiber.

The sandwich composite structure utilizes a pyrotechnic core "sandwiched" between alternate layers of filament-wound fiberglass or an organic fiber in an epoxy binder. These composites were prepared in flat specimens 2.54 cm by 10.16 cm, utilizing nitrocellulose paper, PETN paper, double base propellants and pyrotechnics as core materials laminated between 0.05 cm thick pieces of fiberglass-epoxy. Combustion tests at 61,000 meter simulated altitude showed the following results:

Nitrocellulose would ignite but would not propagate.

PETN paper would not ignite.

Propellants lacked sufficient energy to destroy the samples.

Pyrotechnics showed promise but needed further development.

A pyrotechnic core material was then developed by Picatinny Arsenal especially for use in the sandwich composite. This core develops about 1600 calories per gram with 5000° F flame temperature, burns at 0.5 cm per second at 60,000 meters altitude, autoignites about 860°F, is insensitive to shock, and will not detonate explosively. Pressure vessels, 7.62 cm diameter by 22.8 cm long, were fabricated in the sandwich construction utilizing a filament wound 0.05 cm inner layer of S-glass/epoxy, a 0.152 cm pyrotechnic core, and a 0.05 cm S-glass/epoxy outer layer. These vessels, with burst pressures of 280 kg/cm², were essentially reduced to small pieces of weak fibers when burned at a simulated 36.6 km altitude. A similar configuration of Fortisan rayon with a room temperature burst pressure of 176 kg/cm² was reduced to ash when burned at 36.6 km simulated altitude.

The new pyrotechnic core in a sandwich construction surpasses all other concepts studied to date for neutralization of the falling mass hazards. A continuation of the program is aimed at optimizing the sandwich construction, and designing a rocket motor case and fins for static and flight demonstration tests.

The nozzle construction presents a special problem which must also be included in the investigation. Data obtained in prior studies of consumable rockets revealed that dispersion of the heat absorbed in the nozzle section during the rocket motor thrust phase constitutes a threat to the surrounding consumable components. Any addition of insulation, however, is detrimental to efficient neutralization. A possible solution to this problem is the disposal of the nozzle section shortly after motor burnout. Means of accomplishing this includes (1) the use of a consumable nozzle section which is protected from erosion and heat for the duration of thrust, but which autoignites shortly thereafter; or (2) the use of a small detonable charge which breaks up the nozzle section without damaging the motor case. Early investigation of these and possibly other techniques is planned. Concepts will be developed and tested in rocket exhaust environment.

6.4.6 Army RDT and E Rocket.

Development efforts are currently under way on a new RDT and E rocket by the U. S. Army Missile Command. This rocket is a single-stage vehicle of about the same size and shape as the Arcas. Burning time is reduced, however, to about ten seconds, and it is doubtful that the desired

apogee altitude of 72 km will be achieved with the current design. Design characteristics are listed in Table 6-25.

The rocket motor consists of a resistance welded stainless steel tube, ARMCO 21-6-9, with a 0.055-inch \pm 0.004-inch wall and a yield stress of 150 ksi. The head closure consists of stainless steel 301 1/4 H SS and is 0.109-inches thick. The nozzle retaining ring is 321 stainless steel. There is a graphite throat insert and a threaded aluminum retaining ring. The motor insulation consists of 0.070-inch thick RFB. The design chamber pressure of the motor is 3750 psi. The propellant is acrylonitrile-butadiene-styrene.

The vehicle fins are made from 0.063-inch thick stainless steel and are resistance-welded to the motor case. A split parachute canister of PUC plastic is used. This is interesting since a split parachute canister was originally used with the Arcas. Lack of structural rigidity caused vehicle breakup with the Arcas.

The design goal is for a production cost of \$350 for the vehicle.

6.4.7 Kangaroo.

The Kangaroo Dart is a solid-propellant sounding rocket vehicle which was developed by the Aeromechanics Branch of the Pacific Missile Range. The Kangaroo concept consists of retaining a non-propulsive dart containing the payload in an insulated canister inside the rocket motor port during the boost phase of flight. This dart is expelled from the rocket motor at burnout by a combination of motor chamber pressure and drag deceleration of the booster. The dart then coasts to apogee, and the booster remains stable throughout its low altitude trajectory to impact.

The Kangaroo Dart two-stage vehicle employed a dart payload housing which was submerged in the rocket motor to contain the dart during propulsive flight. At motor burnout the dart is ejected by tail-off chamber pressure and booster deceleration. The ejecting dart causes the shear-pinned nose cone tip to be separated from the vehicle, and the dart continues to eject through the aperture thus formed. The aft end of the dart is tapered in order to receive a pick-up fins canister during dart

TABLE 6-25

AMICOM RDT & E ROCKET DESIGN CHARACTERISTICS (MK 4 Mod II)

Vehicle Performance

Altitude at apogee, 80° QE (ft)	246,760
Time to apogee (sec)	126
Velocity at burnout (ft/sec)	4700
Mach No. at burnout	4.67
Maximum Dynamic Pressure lb/ft ²	13,789

Vehicle Physical Characteristics

Diameter (in)	4.875
Weight	
Total (lb)	97.83
Burned (lb)	43.05
Discharge (lb)	54.78
Static Stability calibers	1.6
Nosecone	4-caliber tangent ogive (0.250" thick plastic)
Fins	
Number	4
Span (in)	12.83
Root	5.00
Sweep Angle (deg)	60

Dimensions and Performance Characteristics for Rocket Motor (MK 4 Mod II)

Diameter (in)	4.875
Propellant weight (lb)	54.00
Motor weight (lb)	79.69
Action time (sec)	10.33
Specific Impulse (sec)	231.6
Maximum pressure (psig)	2500
Grain length (in)	62.5

Table 6-25 AMICOM RDT & E Rocket Design Characteristics - continued -

Rocket Motor Weight Breakdown (lb)

Motor Chamber	18.28
Nozzle End Restrictor	0.13
Insulation	4.46
Nozzle	2.82
Propellant	<u>54.00</u>
Motor Weight	79.69
Consumables	<u>54.78</u>
Burnout Weight	24.91

Vehicle Weight Breakdown (lb)

Ogive	2.48
Sleeve (Steel)	0.36
Pedestal (Steel)	3.44
Separation Device	1.00
Parachute and Canister	4.55
Payload	3.00
Fins (Steel)	3.31
Motor	<u>76.69</u>
Vehicle launch	97.832
Discharge	54.780
Vehicle Burnout	43.052

Table 6-25 AMICOM RDT & E Rocket Design Characteristics - continued -

Drag Coefficient Data

<u>Mach No.</u>	<u>C_D</u>
0	0
0.5	0
1.0	.250
1.5	.290
2.0	.275
2.5	.250
3.0	.230
4.0	.200

Flight Velocity Profile

<u>Flight Time (sec)</u>	<u>Velocity (ft/sec)</u>
2.5	2250
5.0	3900
7.5	4600
9.0	4700
20.0	3550
30.0	3100

ejection. A propellant delay charge is used at the aft end of the dart canister housing to prevent initial motor chamber pressure from ejecting the dart at lift-off before vehicle acceleration becomes large enough to retain the dart. A scale drawing of the vehicle assembly is shown in Figure 6.4-5 and a vehicle weight breakdown is presented in Table 6-26 for the Viper rocket motor configuration.

The advantages of the Kangaroo concept are the elimination of the aerodynamic heating of the dart and payload during the early boost phase and a shorter vehicle length than for the more standard two-stage booster-dart configuration. Some of the dart payloads require an ablative coating on the dart surface to reduce the aerodynamic heating input. Dart separation problems have occasionally occurred and have caused low flights. These problems have been traced to large bending moments at the interstage coupling. The Kangaroo concept is an attempt to avoid these problem areas.

The disadvantages of the Kangaroo concept are a severe performance penalty and high cost. The canister housing must be machined and insulated to protect it from the motor chamber gases. In addition, a nose cone assembly, a delay charge, a forward bulkhead and a pick-up fin canister must be fabricated. All of these items add significant cost and weight to the regular booster dart system.

6.4.8 Destructible Dart.

A proposed solution to the falling mass hazard problem has been the use of a destructible dart constructed with Pyro Ceram - a Corning Glass Works product. The proposal has been to fabricate the dart structures with this material, use powdered lead as ballast and destruct the entire assembly at apogee to release the payload. It is reported that a concentrated point load will cause the Pyro Ceram material to fracture into small granular particles no larger than 0.250-inch in diameter. Table 6-27 presents a list of the physical properties of this material in fabricated form.

Although the Pyro Ceram material appears to be reasonably strong, fabrication into a dart structure and the mechanical fidelity during sharp-edged booster shocks may become significant problems. The material does not appear to be inexpensive.

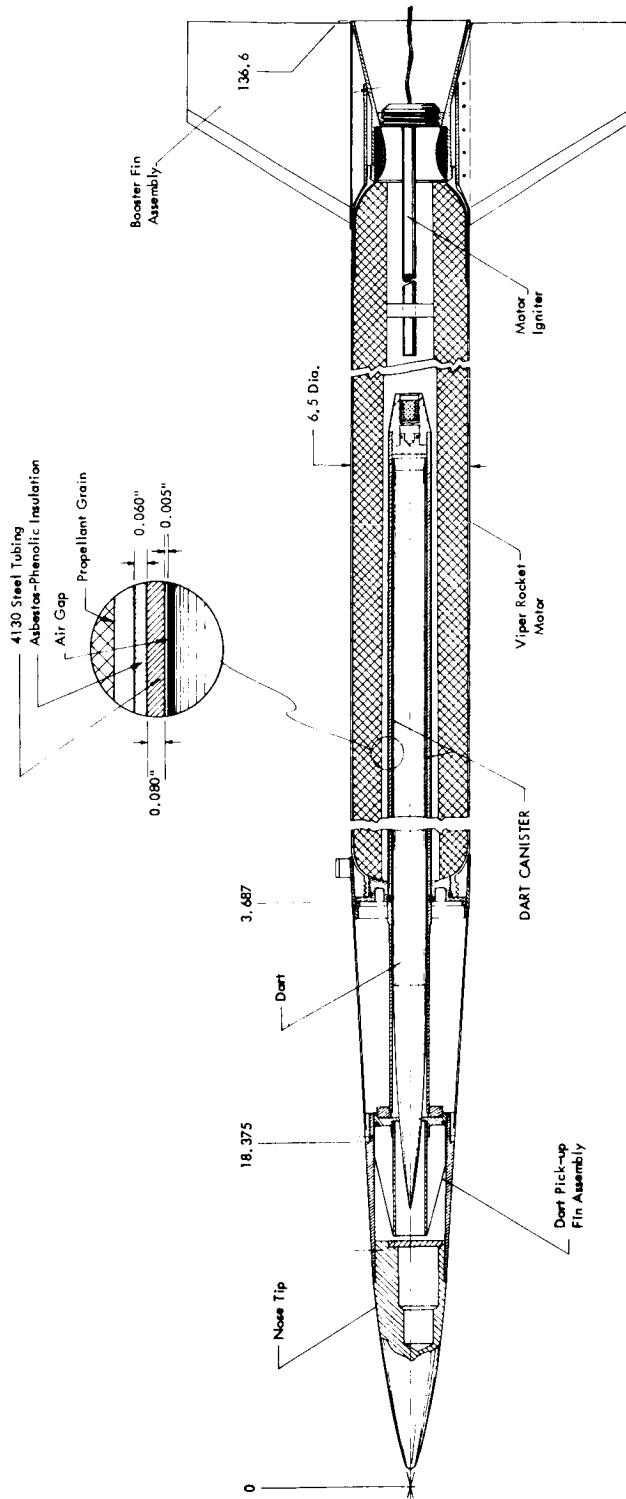


FIGURE 6.4-5 KANGAROO DART VEHICLE CONFIGURATION

TABLE 6-26

KANGAROO WEIGHT TABLE

Vehicle Launch Weight	243.75 lb.
Vehicle Burnout Weight	95.00
Dart Coast Weight	18.00

Component Weight Breakdown:

Dart	18.00 lb.
Head Adapter	
Nose Cone	24.07
Dart Retaining Tube	
Booster Fins	10.00
Booster Motor	
Case	31.00
Head	2.13
Nozzle	7.25
Miscellaneous	2.55
Propellant	<u>48.75</u>
	243.75 lb.

TABLE 6-27

CORNING GLASS WORKS PYRO CERAM PHYSICAL PROPERTIES

Density	2.93 gm/cm ³
Water Absorption	0.00%
Porosity	0.00% Void Volume
Ave. Coeff. of Expansion (0-300°C)	90x10 ⁻⁷ /°C
Thermal Diffusivity (at 25°C)	8.0x10 ⁻³ cm ² /sec.
Youngs Modulus	17.0x10 ⁶ psi
Compressive Strength	350x10 ³ psi
Poisson's Ratio	0.22
Shear Modulus	7.0x10 ⁶ psi
Bulk Modulus	10.1x10 ⁶ psi
Modulus of Rupture (Tumbler-Abraded)	100x10 ³ psi
Knoop Hardness (100 gm)	640
Loss Tangent (at 8.6 GHz)	7x10 ³
Dielectric Constant (at 8.6 GHz)	7
Volume Resistivity (at 250° C)	1x10 ⁸ ohm-cm

The proposed system includes a booster rocket which would impact within a 1-mile radius of the launch site. This is a serious limitation for launchings near populated areas, since 2,000 acres of land would be required to be cleared. Also to prove the reliability of the system would take thousands of flight tests without a single failure. This appears to be an expensive program.

6.5 Discussion.

6.5.1 General.

Several topics dealing with meteorological rocket vehicles are worthy of a brief discussion. These topics which concern vehicle performance, wind-sensitivity and impact dispersion are presented in the following sections.

6.5.2 Vehicle Performance.

The performance of single stage vehicles is particularly sensitive to burning time. For 65 km rockets a burning time of about 30 seconds results in maximum altitude. For longer burning times, the vehicle gravity turn causes the velocity vector to flatten out to a low flight path angle and apogee altitude is reduced. For shorter burning times, higher velocities are experienced in the lower high density regions of the atmosphere, and the resulting drag losses degrade the altitude performance. Thus, attempts to duplicate Arcas performance with short burning time internal-knowing rocket motor designs resulted in significantly larger and heavier rockets than the Arcas. Since the wind-sensitivity of a vehicle is a function of the burning time, a compromise should be made between maximum performance and wind-sensitivity. A single stage burning time between 10 and 20 seconds appears to be reasonable. This range of burning time is not easy to obtain in a small diameter rocket motor with a total impulse sufficient for the 65 km performance range. Motor designs are quite restrictive and critical for the single stage application.

The basic concept in the design of the booster dart vehicle is to utilize a high performance rocket motor for the first stage and a non-propulsive dart for the second stage to carry the meteorological payload to apogee altitude. To take full advantage of this basic concept, it is necessary to use a rocket motor with a relatively short burning time and high mass ratio. The basic technical advantage of this system occurs by obtaining a high velocity in a short period of time and separating the dart as early in the flight as possible. Since the dart has a comparatively high weight-to-drag ratio as compared to the booster, this early separation minimizes the energy lost to aerodynamic drag.

The velocity at the end of booster burnout is dependent upon the rocket motor mass fraction and specific impulse. However, when allowance is made for both the dart and associated flight weight hardware, the overall burnout weight of the system becomes of paramount importance. If booster burnout time is kept to a short duration, i.e., one or two seconds, then the accumulated velocity of impulse lost to drag during the boost phase will be relatively small. Booster diameter and the resulting interstage design, i.e., cone angle and weight, also have a relatively important influence on booster drag performance, especially which rocket motor burning times are appreciably longer than two seconds. In a similar manner, booster fin size is relatively important for relatively long burning time rocket motors. A careful trade-off should be made between dart weight and booster fin size in order to maintain an adequate static stability margin for the vehicle during boost phase, and yet not penalized the booster burnout performance with an excessively heavy dart.

Rocket motor design is not so critical for two-stage vehicles as it is for either the single stage or booster dart vehicles. The booster or first-stage need not have a particularly high value for mass fraction for it is weighted down with the second-stage and payload anyhow. The thrust level should be relatively high to provide an appreciable lift-off acceleration. This is to reduce wind effects. Since the interstage coast period can be selected by the vehicle designer, the burning time of the second stage is not critical. Short burning time second stages can be ignited at a higher altitude to reduce drag losses. Thus, there is a great deal of latitude in rocket motor design for the two-stage vehicles. Since short burning time rocket motors are generally less expensive to fabricate than the long burning time motors, and have higher mass fractions (less inert weight and insulation required) the obvious choice for a two stage meteorological rocket would be a minimum cost short burning time boiler plate booster and an improved mass fraction short burning time second stage motor.

Although it is expected that the booster dart vehicles will dominate the routine meteorological rocket applications to 140 km over the next few years (because of low cost and low wind dispersion), there probably will be a modest requirement for a single stage vehicle to replace the Arcas for semi-routine ozone soundings. Such a vehicle should have an

improved performance (carry a slightly larger diameter payload than 4.5 inches to about 75 km) and should be less expensive than the Arcas. For payloads diameters larger than about 2 inches and altitudes above 140 km the obvious choice is a two-stage vehicle. The 140 km Viper Dart application is probably as far as the booster dart concept can reasonably be used.

6.5.3 Vehicle Impact Dispersion.

Vehicle impact dispersion factors can be divided into wind effects and non-wind effect factors. The wind effects can further be sub-divided into random error and bias components. The wind effect bias can be significantly reduced by current wind-weighting techniques which permit off-setting the launch angles to correct for the wind. Since this procedure is not perfect, there is a wind measurement error, and the wind velocity changes with time there is a random wind effect which directly causes dispersion. The greater the wind sensitivity for a vehicle, the greater is the random wind effect error and resulting impact dispersion.

For most vehicles random wind effects and thrust misalignment cause a majority of the vehicle dispersion. By reducing or eliminating these two causes of vehicle dispersion, quite small impact patterns can be accomplished. Essentially all sounding rockets are caused to roll or spin about their longitudinal axis by employing fin incidence or cant. This is done to cancel or vector out vehicle misalignment dispersions. However, vehicle spin rates do not build up until an appreciable distance is achieved from the launcher, and vehicle velocity has become appreciable. In these cases the thrust misalignment, just as the non-spinning vehicle leaves the constraints of the launcher, diverts the course of the missile and a significant dispersion occurs. If the missile were pre-spun before leaving the launcher, this element of dispersion could be eliminated. The Loki systems accomplished this by using helical rails. This is one reason that the Loki dispersions are minimal. To reduce the random wind effects dispersion, the overall missile wind sensitivity must be reduced.

6.5.4 Vehicle Wind-Sensitivity.

Wind-sensitivity performance of the vehicle is a function of the boost acceleration, which is related to rocket motor burning time, and the relative magnitudes of the vehicle static stability margin and transverse moment of inertia. Wind effects are slight for a very fast acceleration and short burning time rocket motor. If the vehicle static margin at lift-off,

and during the boost phase, is maintained at an adequately small value, and the moment of inertia about the pitch axis is large, wind effects are slight. Although by increasing the launch velocity of a given vehicle a reduction in wind sensitivity can be made, such a reduction may not be great. The total time the vehicle is under propulsion is the main factor contributing to the wind sensitivity of a vehicle in spite of the launch velocity. Thus, Arcas wind sensitivity is not greatly reduced by employing the gas generator charge during the launch stroke or even by employing a booster rocket. Dual thrust vehicles will also be wind sensitive as long as relatively long burning times are employed for sustained thrust phase in spite of the increase in launch velocity. The only really effective answer to reduce wind sensitivity is short burning times.

A comparison of the wind dispersion of short and long burning time vehicles is presented in Table 6-28. It should be noted that the wind-sensitive altitude ceiling is considerably higher for the long burning time vehicles. Since the higher altitude winds are generally much stronger than the low altitude winds, the resultant ballistic wind will be greater. Thus, the wind displacement differences between the short and long burning are even greater than indicated.

TABLE 6-28

COMPARISON OF WIND DISPERSION EFFECTS FOR VARIOUS VEHICLES

	UNIT WIND EFFECT (Feet/Knot)	LAUNCHER TILT CORRECTION (Degree/Knot)	BURNING TIME (Seconds)	WIND-SENSITIVE ALTITUDE CEIL- ING (Feet)	APOGEE ALTITUDE (Feet)
ARCAS	7,720	0.525	28	50,000	210,000
LOKI DART	1,260	0.101	2	5,000	215,000
SPARROW ARCAS	11,400	0.268	30	100,000	460,000
VIPER DART	6,150	0.173	3	8,000	460,000

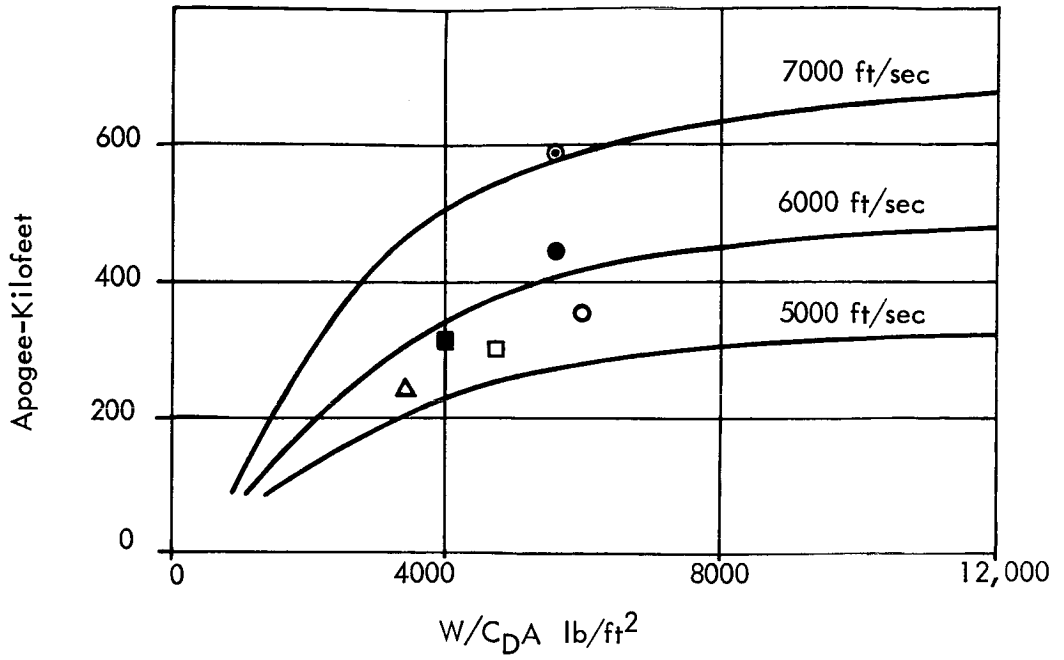
GUN PROBES

7.1 General.

Since 1961, high-performance, conventional guns have been used to launch atmospheric probes. This development has been undertaken by the U. S. Army Ballistic Research Laboratory (BRL) working closely with McGill University Research Institute of Montreal, Canada and NASA - Wallops Island, Virginia, under Project HARP (High Altitude Research Project). Project HARP is devoted to the development of high altitude gun launched rockets and projectiles, the acquisition of engineering and scientific data on the upper atmosphere and the critical vehicle-environment interactions. As part of this effort, 5-inch guns have placed 25-pound projectiles at 250,000 feet, 7-inch guns have placed 60-pound projectiles at 330,000 feet and 16-inch guns have reached 590,000 feet with 185-pound projectiles as indicated in Figure 7.1-1. Chaff, balloon, aluminized parachute and chemical payloads have been successfully used while on-board telemetry units are in an advanced state of development.

Although the major structural problems of high-'g' telemetry have been solved for the most part, the reactions to high velocities encountered in the lower realm of the atmosphere have hindered development of instrumented payloads. This has included the more slowly accelerated gun-boosted rocket vehicles of the 7-inch and 16-inch guns, developed to carry payloads to extreme altitudes and possibly orbital missions.

Initial tests of a gun probe system began on the 5-inch gun at BRL Aberdeen Proving Ground, Maryland, during June 1961. These tests, conducted at the Edgewood Peninsula launch site were followed by the installation of a 16-inch gun at Barbabos, W. I., and testing of the larger gun probes began in January 1963. Since these original tests, installation of the 5-inch gun as spread to sites at Wallops Island, Virginia; White Sands, New Mexico; Barbabos; Fort Greely, Alaska; Highwater, Quebec; and Yuma, Arizona. Additional 16-inch gun installation have included



<u>Gun</u>	<u>Velocity</u>	<u>Apogee</u>	<u>Weight</u>
5" Δ	5400 ft/sec	250 kft	23 lb
7" \square	5400 ft/sec	300 kft	59 lb
7" \blacksquare	5900 ft/sec	330 kft	27 lb
16" \circ	5600 ft/sec	350 kft	185 lb
16" \bullet	6300 ft/sec	465 kft	185 lb
16" \odot	7100 ft/sec	590 kft	185 lb

FIGURE 7.1-1 GUN PROBE PERFORMANCE SUMMARY

facilities at Yuma and Highwater, the latter being a horizontal test fire installation. Testing of the 7-inch gun probe was not initiated until May of 1964, since surplus or worn out hardware of this new gun were not available up to that time. The initial Wallops Island Tests were followed by installation of the gun at White Sands with additional facilities planned for other sites as the modern hardware becomes available.

Most of the test previously conducted have developed ballistic and design techniques for this entirely new field of technology so that reliable, optimum performance could be substantiated. The many problems encountered during the early phases of development showed that it was a more complex undertaking than had previously been anticipated. Significant engineering efforts solved many of the inherent problems in gun launched probes and some scientific data have been gathered. These successful probes are primarily wind profiles measured by chaff, aluminized balloons and parachutes and by tri-methyl-aluminum trials. A number of successful 250 MHz and 1750 MHz telemetry flights have been made primarily with the slower, larger 16-inch projectiles which carried various types of instrumented payloads. However, the greatest success of gun launched projectiles has been TMA chemical trial studies of the Sporadic E layer variations.

Generally, the gun probe may be considered in terms of two basic vehicle classifications: the ballistic glide vehicle which receives its thrust solely from the gun launch, and the rocket-assisted vehicle (described in Section 7.5). In the case of ballistic glide projectiles, the flight trajectory is controlled by launch vector velocity and ballistic coefficient. To obtain a high ballistic coefficient, high fineness ratio missiles are utilized having large vehicle mass densities. To obtain a high launch velocity, sabot launched sub-caliber vehicles are used, retaining a high ballistic coefficient after sabot separation. By an increase in barrel length equal to 75 calibers, muzzle velocity is also increased so that maximum gun performance and propellant efficiency is achieved. A further increase in muzzle velocity is realized when the muzzle end is sealed with a thin plastic sheet and the barrel evacuated of air. Larger bore diameter guns would increase the weight-to-drag ratio and decrease acceleration load, but development of a larger gun does not seem practical at the present state of gun probe development.

7.2 5-Inch Gun Projectiles.

Initial development of a 5-inch HARP probe system utilized a 120 mm, T-123 high performance tank gun, smooth-bored to 5.1 inches, muzzle extended to 33 feet and mounted on a 155 mm towed vehicle carriage. The entire system is mounted on a 30-degree inclined ramp to allow for near vertical firing. The missile and charge are loaded into the tube separately. To achieve proper seating and placement of the missile in the tube, the sabot quarters are backed with plastic and are made slightly oversize, so that a special loading fixture and hydraulic ram force loads the projectile at a peak force of 10 tons.

The flight vehicle is a subcaliber, fin-stabilized projectile, 45-inches long, weighing 20-pounds and has a maximum body diameter of 2.6 inches as indicated in Figure 7.2-1. The fins are slightly smaller than the gun barrel and are canted to induce a small spin rate. The payload cavity, 1.8-inches in diameter by 7-inches deep, is located in the forward body of the vehicle. Muzzle velocities in excess of 5,400 feet/sec and a load equivalent of 55,000 'g' occur at launch, producing a ballistic glide to a maximum altitude of 250,000 feet. Figure 7.2-2 illustrates the altitude vs range profile for various launch angles at 4,000 feet launch elevation.

Payloads originally consisted of chaff or meteor projectiles followed by testing of a 1750 mHz telemetry package with nose antenna. These tests were unsuccessful and provided evidence of poor design, which resulted in redesign of the entire system. This improved second generation gun probe had increased performance and reduced aerodynamic instability as well as incorporated an advanced telemetry and antenna system. Refinements of the Solistron(SOLId state klySTRON) transmitter were made to eliminate the change in frequency due to excessive launch temperatures. This included a reduction in size to 1-inch long by 1.125-inches in diameter, permitting the use of ample thermal insulation and heat sinking. However, temperature data showed that the package experiences temperatures during the glide portion of the flight in the order of 300°C, high enough to alter the electronic and mechanical characteristics of the antenna, RF circuit and telemetry instrumentation. Changes in load impedance due to excessive temperature caused deviations in frequency and power output. This results in weakened signal strength, high frequency drift, additional RF noise and eventual signal dropout. Efforts are underway to overcome

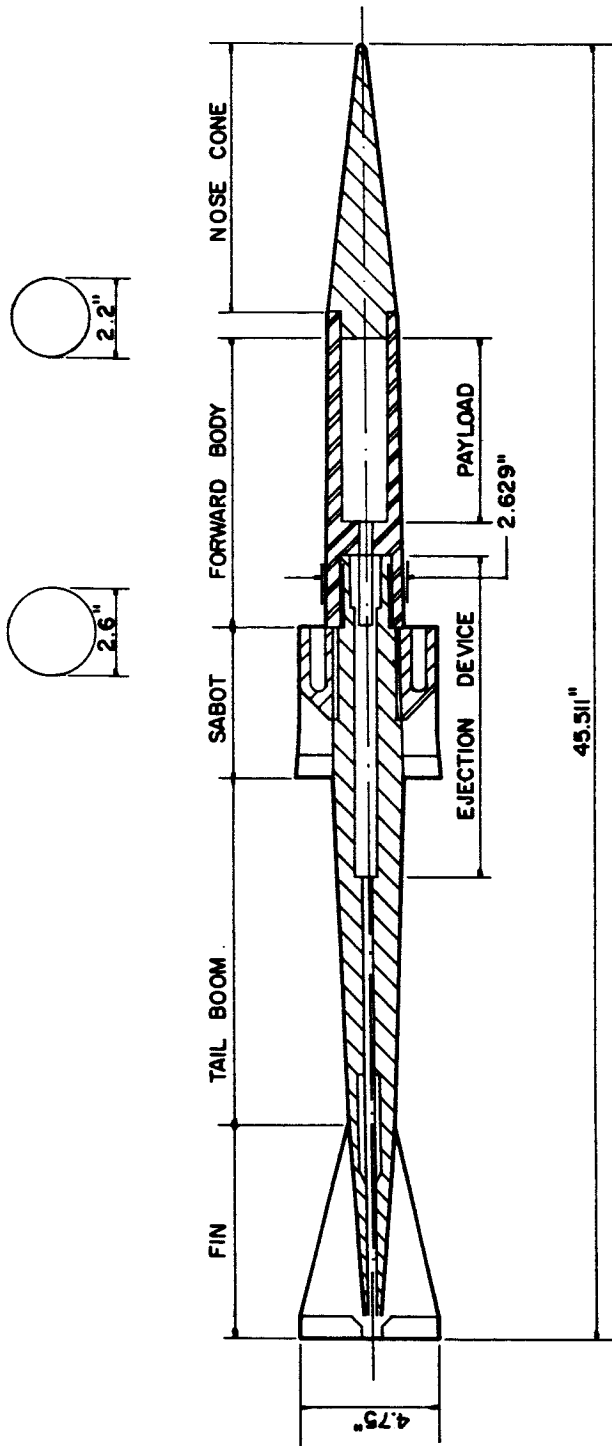


FIGURE 7.2-1 5-INCH GUN PROJECTILE CONFIGURATION

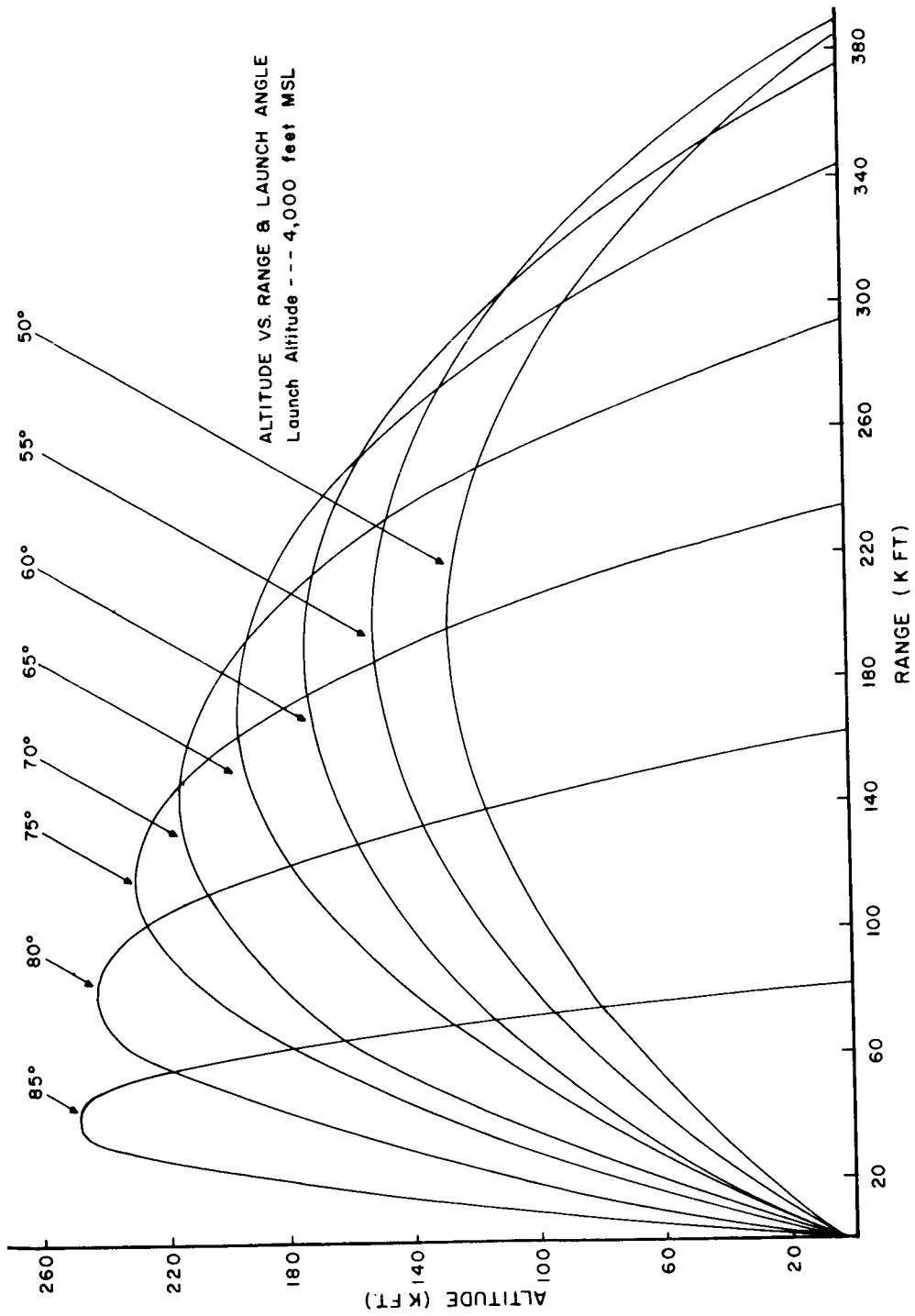


FIGURE 7.2-2 5-INCH PROJECTILE NOMINAL TRAJECTORIES

the problems of excessive aerodynamic heat transfer and temperature effects.

In order to readily provide wind sensing probes for the 5-inch gun, means to prevent tearing or burning of a parachute payload were developed. These aluminized parachute vehicles have been providing wind data to as high as 70 kilometers on an operational basis. Several attempts have been made to reduce production costs, amend the current payload volume restrictions and at the same time optimize vehicle performance. However, a practical, improved probe system is under the same basic physical restrictions inherent with the gun probe technique, and therefore confined to limited design innovations.

7.3 7-Inch Gun Projectiles.

The 7-inch system is essentially a scaled up version of the 5-inch system with three times the payload capacity and with an altitude performance of 350,000 feet. The modern 175-mm M-113 gun is smooth-bored, extended to 50-feet and placed in a highly modified T-76 double recoil field mount. Interior ballistics have been a major problem with this gun. Desired velocities are not always achieved at computed pressures and erratic pressure variations occurred with larger charges.

The basic flight vehicle is 64-inches long, 3.6-inches in diameter and weighs 60-pounds. The 7-inch diameter plastic sabot is again made oversize and force loaded at 10 to 30 tons using a hydraulic jack as shown in Figure 7.3-1. The vehicle achieves a muzzle velocity of 5400-feet/sec at 35,000 'g'. A smaller, high performance missile has been developed to reach 400,000 feet with a much smaller payload. This missile is 55-inches long having a 3-inch diameter and weighs 40-pounds. Metal parts behavior of this highly accelerated system have caused problems during development.

Payloads have utilized the usual chaff and aluminized parachutes to measure winds above 210,000 feet. Available payload volume is 125-cubic inches. Chemical payloads have been successfully used, including a package of cesium nitrate with high explosives to generate an observable cloud of electrons at 330,000 feet. Also a Langmuir probe instrumented payload has been tested. A full bore 7-inch rocket vehicle has also been developed consisting of a 125 pound projectile with a fiberglass case and solid propellant rocket having pop-out fins. Launched at muzzle velocities exceeding 4,000 feet/sec it should place a 20 pound payload at 500,000 feet.

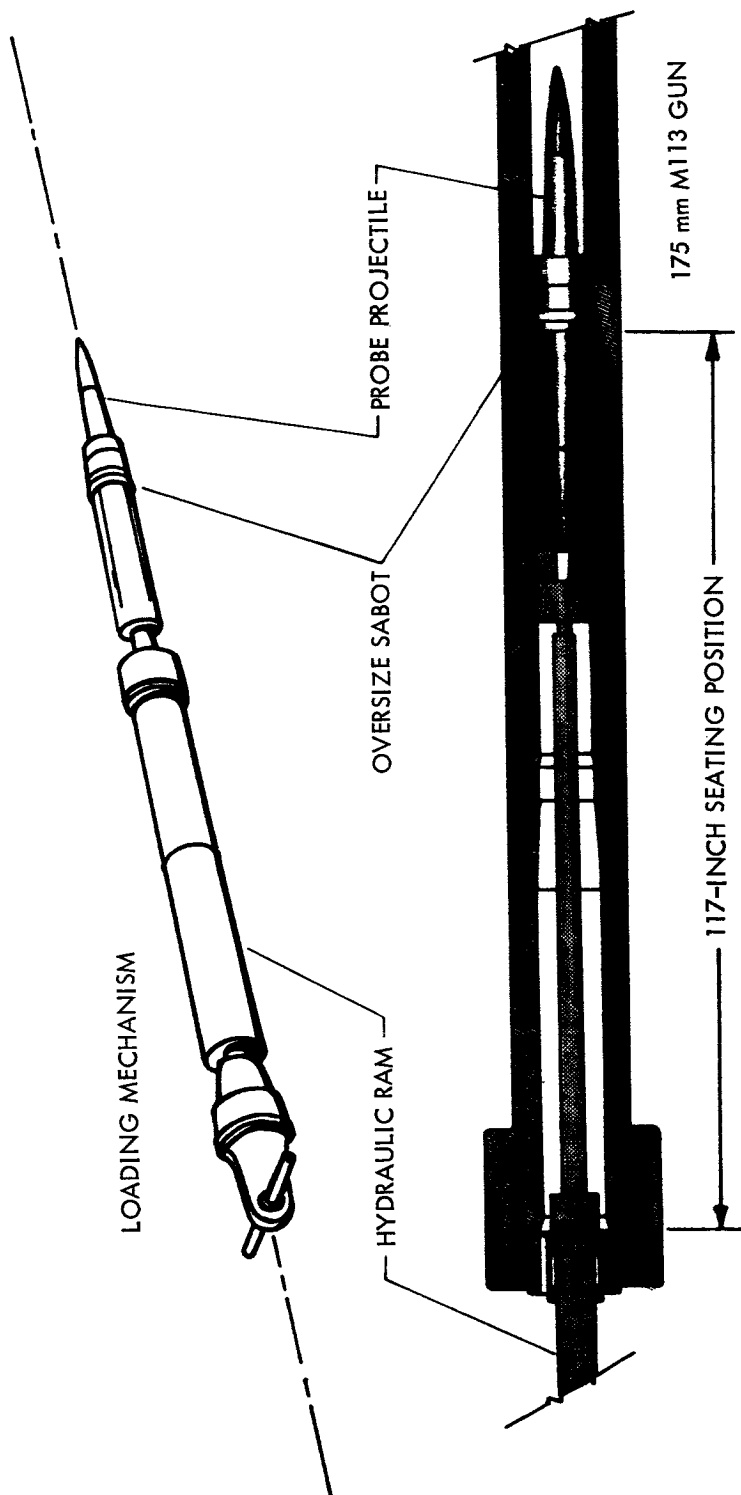


FIGURE 7.3-1 GUN PROBE LOADING MECHANISM

7.4 16-Inch Gun Projectiles.

The 16-inch gun incorporates the use of a Mark D barrel, smooth-bored to 16.4 inches and elaborately modified to support a barrel extension to 119-feet, 5-inches. Weighing approximately 200-tons, it can be elevated to 85 degrees in less than 8 minutes. Subcaliber, oversized sabot launched vehicles are rammed into seating position with a maximum force of 50 tons. The necessity for a fast burning, high pressure yield propellant charge lead to the development of a spaced charge, multi-point ignition technique which provides optimum efficiencies of the propellant charge, and is used in conjunction with the evacuated barrel technique.

Various types of vehicles and payloads have been used from Martlet 1 smoke and flash vehicles to Martlet 4 orbit potential rockets. The Martlet 2C, TMA loaded vehicle has been the system most utilized because of its simplicity and high performance. Details of its wind measurement technique were discussed in Section 3.2.7.3. Weighing 185-pounds carrying a 25-pound payload, it can achieve apogees in excess of 180 km. It is 55-inches long by 5.4 inches in diameter and is accelerated to 15,000 'g' at a launch velocity of 7,100 ft/sec. Typical payload configurations are illustrated in Figure 7.4-1. Other vehicles have been used to test various systems designs and payload configurations with the more recent efforts projected toward gun-boosted rockets. Active payloads using both 250 MHz and 1750 MHz telemetry have been carried on a number of flights. Onboard sensors have included magnetometers, sun-seekers, pressure gages and Langmuir electron density probes. However, difficulties in telemetry and antenna functions have again been a problem, and these devices must still be considered under development.

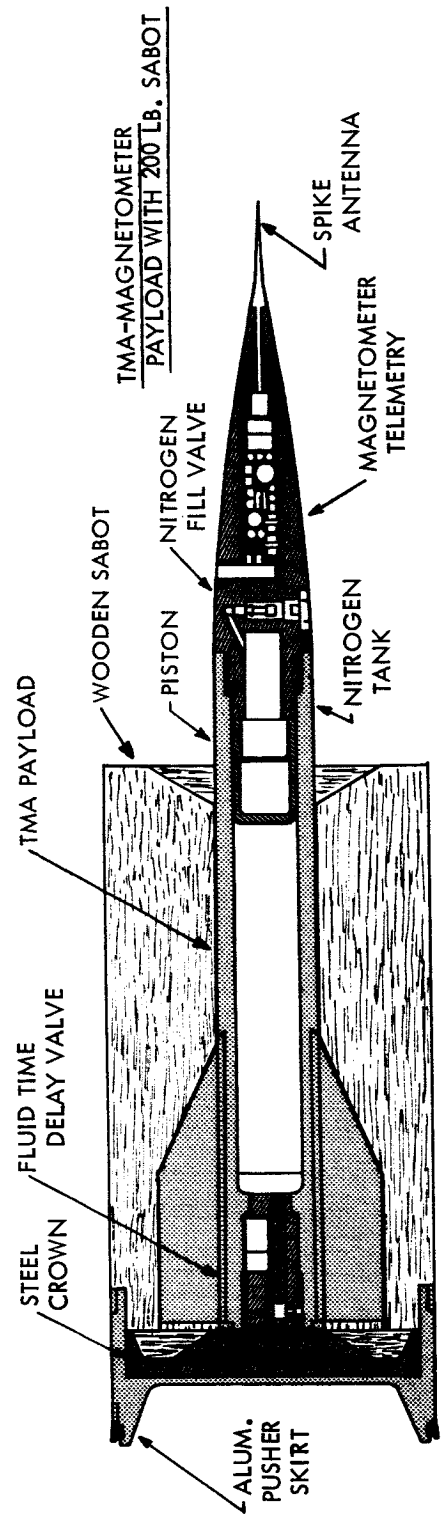
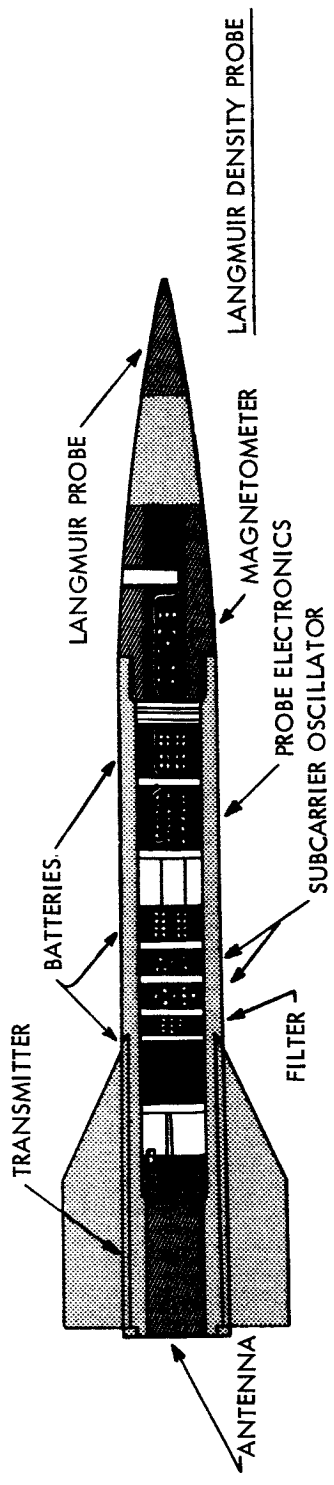


FIGURE 7.4-1 TYPICAL MARTLET - 2C PAYLOAD CONFIGURATIONS

7.5 Gun-Boosted Rockets.

Full bore gun-boosted rockets theoretically possess excellent performance while retaining a portion of the gun's economy and low dispersion. Optimization of the gun-boosted system involves a trade-off between the amount of kinetic energy imparted by the launcher and the amount of chemical energy carried aboard, considering that as the total launch weight is increased, launch velocity decreases. As launch weight is decreased to obtain high muzzle velocity, the ballistic coefficient becomes the dominant factor just as with the ballistic glide missile. The optimum situation has been found to exist when relatively large rockets are matched with intermediate gun velocities; the gun performing as a reliable, retainable first stage for the system.

Initial development of a gun launched rocket was the Martlet 3A vehicle. A subcaliber projectile weighing 153-pounds, it contains a 57-pound case-bonded 6-inch nitrocellulose grain motor. Delay ignited a 14-seconds after launch, the motor burns for 7-seconds carrying a telemetry package weighing 50-pounds in a 46.8 cubic inch payload section. Many problems relating to the effects of highly accelerated motor propellants, telemetry packages and antenna designs were studied as well as various internal ballistic concepts. Additional types of vehicles were built for the 16-inch gun and one model was built for the 7-inch gun, the Martlet 3E.

Development of a full bore 16-inch Martlet 3D vehicle provide a first stage for the Martlet 4 orbital vehicle which consisted of three stages. Additional development of guidance control units and liquid upper stages have continued efforts along these lines.

A subcaliber vehicle was also developed for extreme high altitude performance or orbital potential with reduced complexity. This two stage Martlet 2G-1 vehicle is 169-inches long by 11.4 inches in diameter and has a total weight of 1,100 pounds.

All the gun-boosted rockets mentioned above are illustrated in Figure 7.5-1. Additional gun launched systems, such as a Scramjet first stage vehicle, have been proposed as further advancements of gun launch

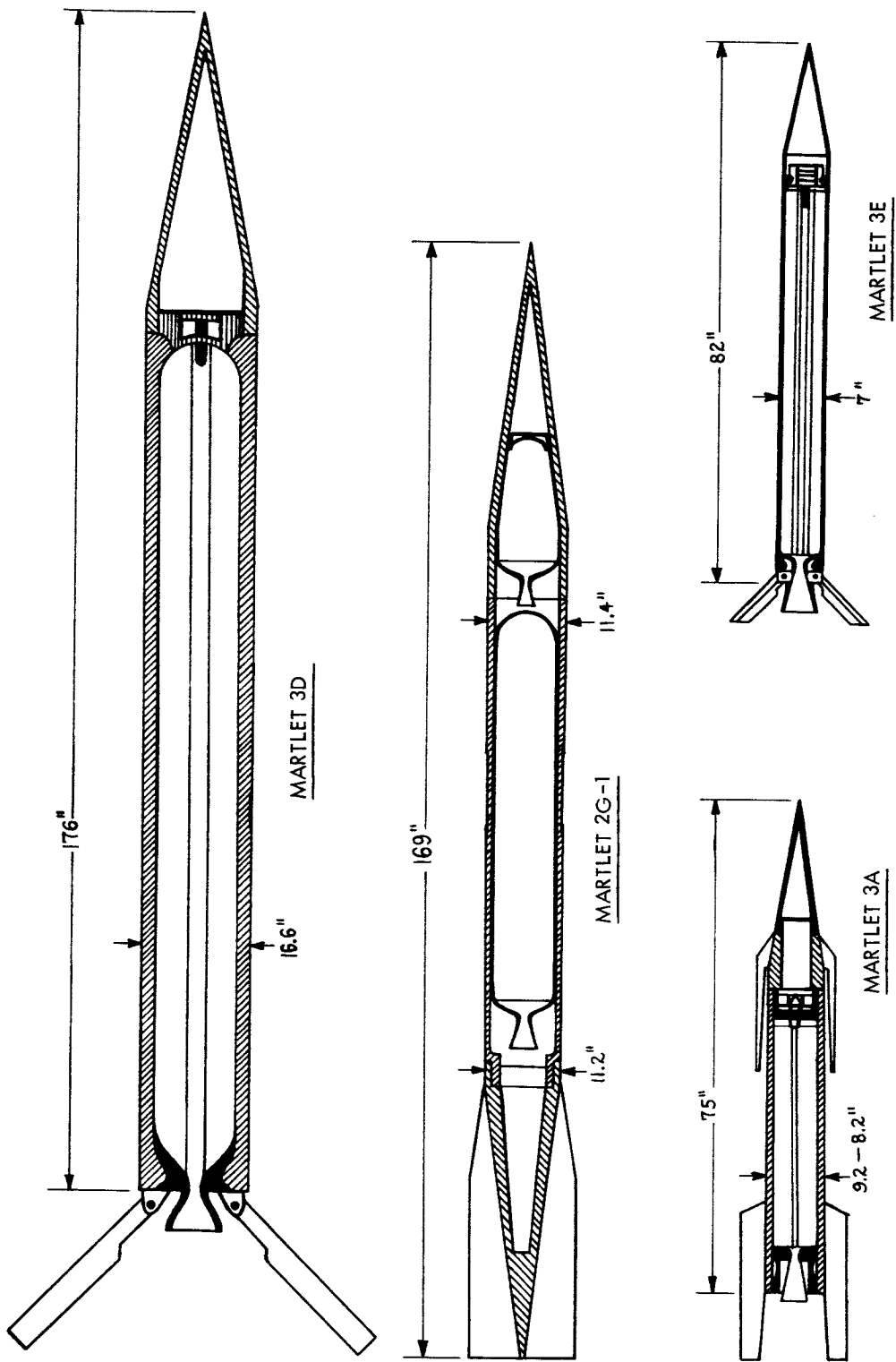


FIGURE 7.5-1 GUN-BOOSTED ROCKET CONFIGURATIONS

potentials. As further studies of high 'g' acceleration continue, utilization of the gun-boosted rocket for high altitude missions may become possible, although they may never become really practical in this application.

7.6 Meteorological Rocket vs Gun Probe Comparison.

Since the development of the gun launched projectiles has demonstrated an additional means of gathering high atmospheric data, comparison of this system with the meteorological rocket is necessary to evaluate its essential performance. Table 7-1 presents a comparison of gun-launched vehicles against operational meteorological rockets. Another effective means of comparison would be to consider the major aspects in categories of the advantages and disadvantages that gun probes have in relation to rockets.

Advantages.

1. Gun probes can achieve high accuracy in placing a package at a desired point in space. This performance can be achieved consistently without regard to changing weather conditions.
2. Minimal wind deviation and low dispersion provide decreased range limitations and restrictions. High velocities insure accuracy of the ballistic trajectory and decrease vehicle impact range.
3. The economy of the inert payload or the first stage substitution of the gun launched rocket is an important consideration. The cost of propelling a given weight to altitude is particularly interesting for orbital insertion vehicles, but is not really advantageous for meteorological applications. The economy in reduced range area is worth consideration.
4. Barrel confinement provides a reliable means of stabilization and guidance through high Mach numbers, insuring range safety at launch, and reducing complications which are inherent to rocket launched vehicles.

TABLE 7-1 METEOROLOGICAL ROCKET VS. GUN PROBE COMPARISON

		<u>Loki-Dart</u>	<u>Arcas</u>	<u>BRL-5</u>	<u>BRL-7</u>	<u>2G1</u>
Launcher or Gun	Diameter	5	13	5	7	16
Launcher or Gun	Length	10	21	34	55	119
Launcher or Gun	Weight	300	500	30,000	50,000	400,000
Projectile	Diameter	1.4	4.5	2.6	4	5.4
Projectile	Length	50	91	45	64	55
Projectile	Weight	10	75	22	60	185
Payload	Volume	40	310	15	45	
Maximum Altitude		200,000	200,000	200,000	330,000	500,000
Maximum Velocity	ft./sec.	5,000	3,800	5,500	5,800	7,100
Maximum Acceleration	g	150	100	45,000	35,000	15,000
Wind Sensitivity	deg/knt	0.067	0.525	0.007	0.010	0.012
Impact Dispersion, 3-sigma radius	nm	5.0	12.0	3.6	5.4	7.2
Launcher or Gun Cost, Total	\$	5,000	10,000	80,000	200,000	500,000
Per Firing	\$	10	20	230	500	1,000
Vehicle or Projectile Cost	\$	350	1,500	400	500	2,000
Powder Cost	\$			30	50	600
Instrumented Payload Cost*	\$	450	500	1,000	800	800
Total Cost per Firing	\$	800	2,020	1,660	1,850	4,400

Comments: Temperature and wind data being obtained operationally with rocketsonde payloads.

Need special loading fixture and hydraulic ram. Need rebaring after 200 rounds. Need new gun barrel after 350 rounds. Only meteorological payloads successfully flown have been chaff, parachutes and chemical releases.

*Payload cost is for wind and temperature measuring payload.

Disadvantages.

1. Only those measurements which involve apparatus that can be made resistant to high acceleration stresses are possible. The extreme acceleration loads produce an inflight elastic rebound phenomenon which restricts the structural fabrication of utilized hardware.
2. Payload volumes are restricted by the structural/weight ratio required of the high density projectiles. Additionally, high aerodynamic heating effects limit sensors, telemetry and antenna designs and create the greatest challenge in the development of instrumented payloads.
3. Since internal ballistics of the gun is a determining factor of flight trajectory, its performance should not vary from that computed for a particular launch. However, this has not always been the case, since variations have occurred from erratic internal propulsion. i.e. The powder bags used are highly sensitive to changes of temperature and humidity. Additionally, various disturbances at the gun, such as blast, muzzle whip and sabot separation, can impart linear and angular momentum to the missile, causing an oscillatory motion in the trajectory know as aerodynamic jump.
4. Muzzle emergence and transition to free flight have incurred further restrictions to vehicle design due to the high Reynolds number, heat and drag experienced at that time. The resultant noise intensity at firing creates a high nuisance value for this system.
5. Maintenance costs of the gun are high in comparison to rocket launchers. Although basic propellant costs per round are highly economical compared to rocket fuels, initial cost of the gun is high. Considering that the erosion life of a 5-inch tube alone is limited to 350 rounds with reboring necessary after 200 rounds, operating costs average high per vehicle launch compared with equivalent performance meteorological rocket systems.

Although there has been a great deal of discussion concerning the relative merits of gun probe systems for meteorological soundings, the gun probes appear to be more expensive and operationally more cumbersome than for the lower cost meteorological rocket systems. The gun probes are limited in payload diameter and volume. They currently offer state-of-the-art development problems for sensor instrumentation. The gun projectiles are fairly expensive, and the overall cost per launching does not compare favorably with the existing booster dart vehicles when account is made for the emplacement, reboring and launching costs. The gun probe systems may in the future be competitive with the booster dart systems for simple payloads such as the passive inflatable sphere if significant improvements are accomplished and a large number of launchings are to be made from a given site. There are no prevalent advantages for the gun-boosted rocket system in the meteorological rocket field since the added complexity of firing a rocket system from a gun is neither simple nor inexpensive.

SUMMARY

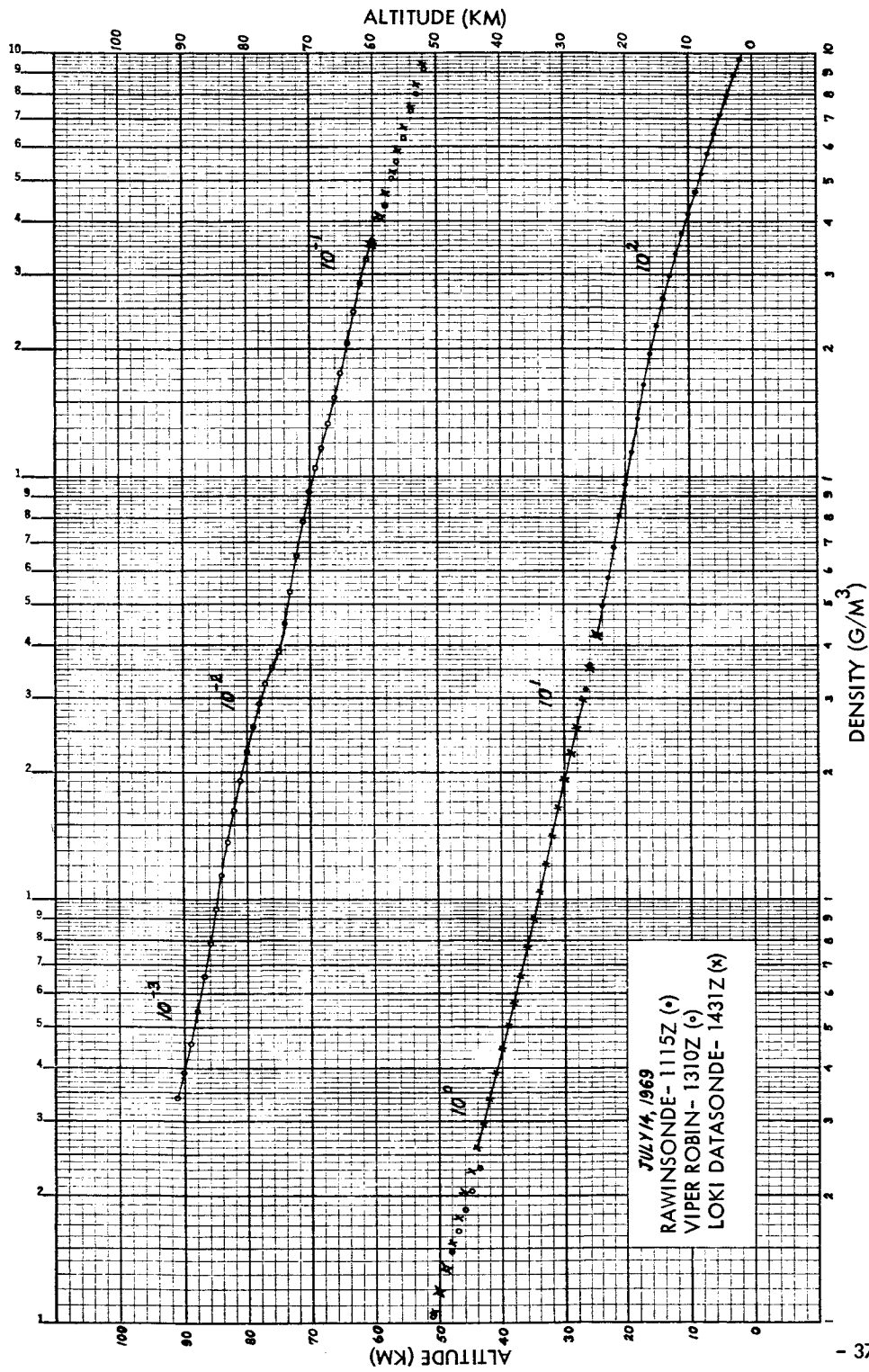
The strongest overall meteorological rocket requirements are for wind and temperature measurements throughout the rocketsonde region of 30 km to 60 km or slightly above. These measurements are currently being made on a routine basis with the Arcas and the lower cost Loki Dart rocketsonde systems. The bead thermistor measurements appear to be adequate to 60 km, and satisfactory soundings have been made to 68 km by applying aerodynamic heating and radiation correction factors to the raw temperature data. With a slower fall rate decelerator and advanced thermistor sensor techniques, it appears that the low cost rocketsonde technique with an immersion thermometry temperature measurement is possible up to an altitude of about 75 km. An additional improvement in the accuracy of the conversion of the measured temperature profiles into pressure and density profiles through the rocketsonde regions may be accomplished by the incorporation of a one-point pressure switch in the rocketsonde instrument package. If this switch can be made sufficiently accurate at a low cost to measure 28 mb (80,000 feet) within an rms error of 0.30 mb, this technique will be more accurate than using the hypsometer radiosonde data which may differ significantly in space and time from the rocketsonde run. A super Loki instrumented dart system with a large decelerator is being developed jointly by AFCRL and NASA/MSFC to accomplish the above extension of the current rocketsonde measurements. This appears to be the lowest cost approach for routine measurements in this altitude region.

The second most important requirement is for density and wind measurements from rocketsonde altitudes to 100 km. Currently the most promising system for this application is the Viper Dart vehicle with the Robin inflatable falling sphere. Development flight tests by AFCRL and the initial operational flight tests at Cape Kennedy and WSMR indicate that reasonable densities and winds can be obtained to about 90 km with this system. An AFCRL development program is underway to increase this altitude to 100 km in the near future. As the Viper Dart Robin system proves to be useful, costs can be significantly reduced by developing a lower cost booster than the Viper rocket motor or by developing a two-stage vehicle from two small low cost motors for this payload.

The Robin payload is quite suitable as a meteorological sensor because of its structural simplicity, low weight and volume characteristics, ease of deployment and compatibility with various vehicles and payloads, reliability and measurement accuracy, and its relative economy as compared with other more complex, sophisticated sensing systems.

A recent demonstration of the Robin sphere performance was in support of the Apollo II launch at Cape Kennedy, Florida. The support requirements of this particular mission necessitated a reliable measurement of atmospheric parameters from surface to 90 km. As part of this effort, the Viper Dart Robin vehicle was flown in conjunction with the Loki Datasonde and the respective Rawinsonde observations. The resulting data produced temperature, density, pressure and wind profiles from the surface to 90 km with excellent agreement in the overlap regions. These atmospheric parameters have an appreciable effect on the Saturn V vehicle guidance and control functions during its powered flight to 90 km. Figures 8.1-1 and 8.1-2 represent the density profiles derived from these data. Figures 8.1-3 and 8.1-4 present the wind profiles of these observations. It is interesting to note the overlapping of all three wind profiles in Figure 8.1-4 since the Rawinsonde utilized GMD-4 tracking and the others incorporated FPS-16 tracking. Temperature profiles are illustrated in Figures 8.1-5 and 8.1-6.

The main disadvantage of the Robin passive sphere technique is the requirement for a radar with the precision of the AN/FPS-16 or better. During the Sparrow-Arcas Denpro program, it was found that the tracking accuracy of the AN/GMD-2 compared favorably with the AN/FPS-16 radar data in the slant range parameters. No doubt this is due to the fact that the main tracking variable during vehicle ascent is slant range, and the GMD-2 is fairly accurate in slant range determination. Therefore, there may be a requirement for a low cost pitot probe system utilizing GMD-2 tracking and telemetry at sites where adequate radars are not available. The vehicle for such a system should consist of two low cost, relatively small rocket motors configured into a two-stage vehicle with a final stage diameter from 3.0" to 4.0". The vehicle apogee should be about 200 km in order to maintain sufficient velocity through 100 km to assure accurate density data to this altitude. Such a system should cost on the order of \$2,500 if the currently available vibrating diaphragm pressure gauge is found to be adequate. If wind data were desired from this system an inflatable sphere could be ejected near



ETR - APOLLO 11 LAUNCH SUPPORT DENSITY PROFILE - 14 July 1969 - CAPE KENNEDY, FLA.

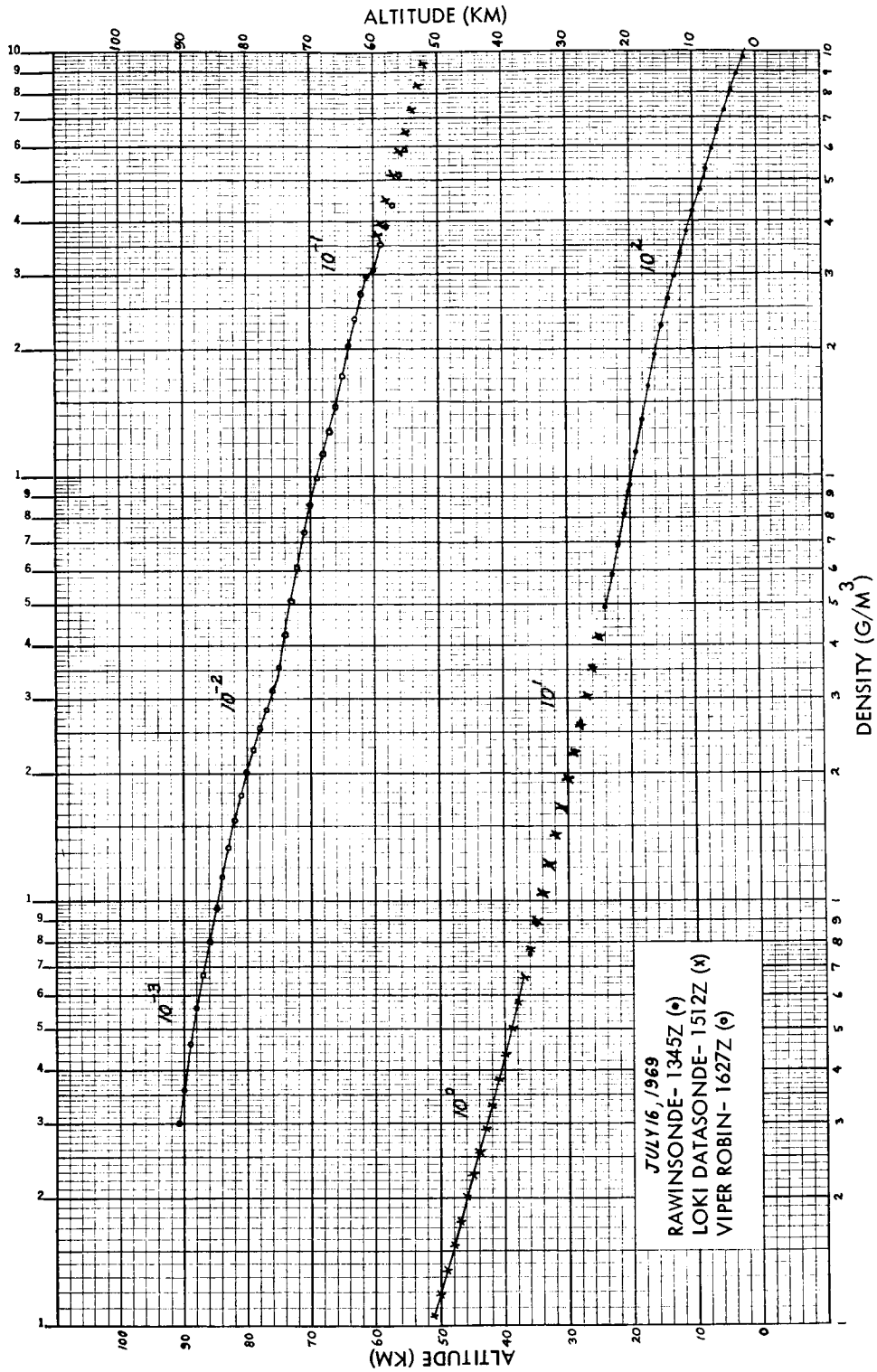
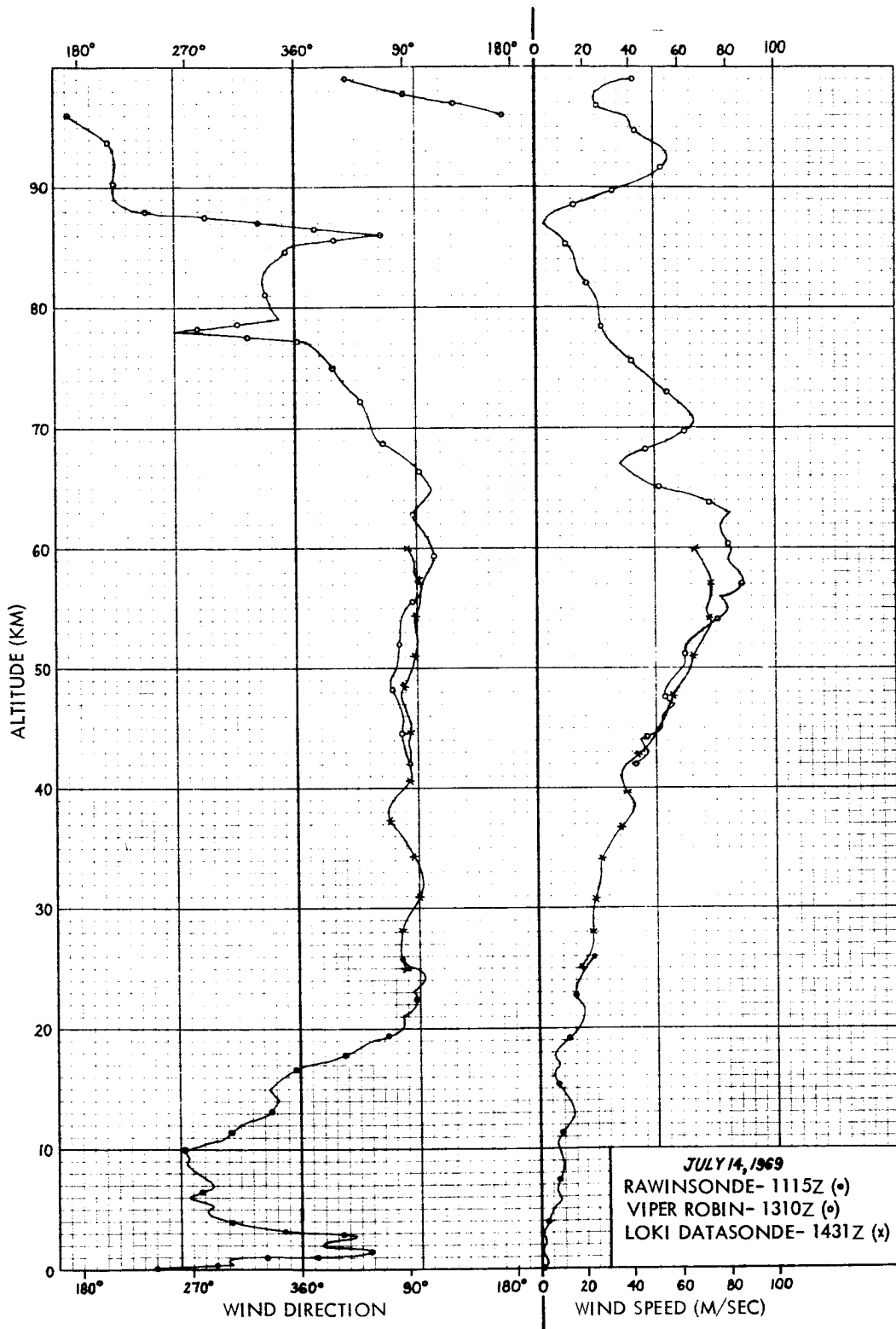
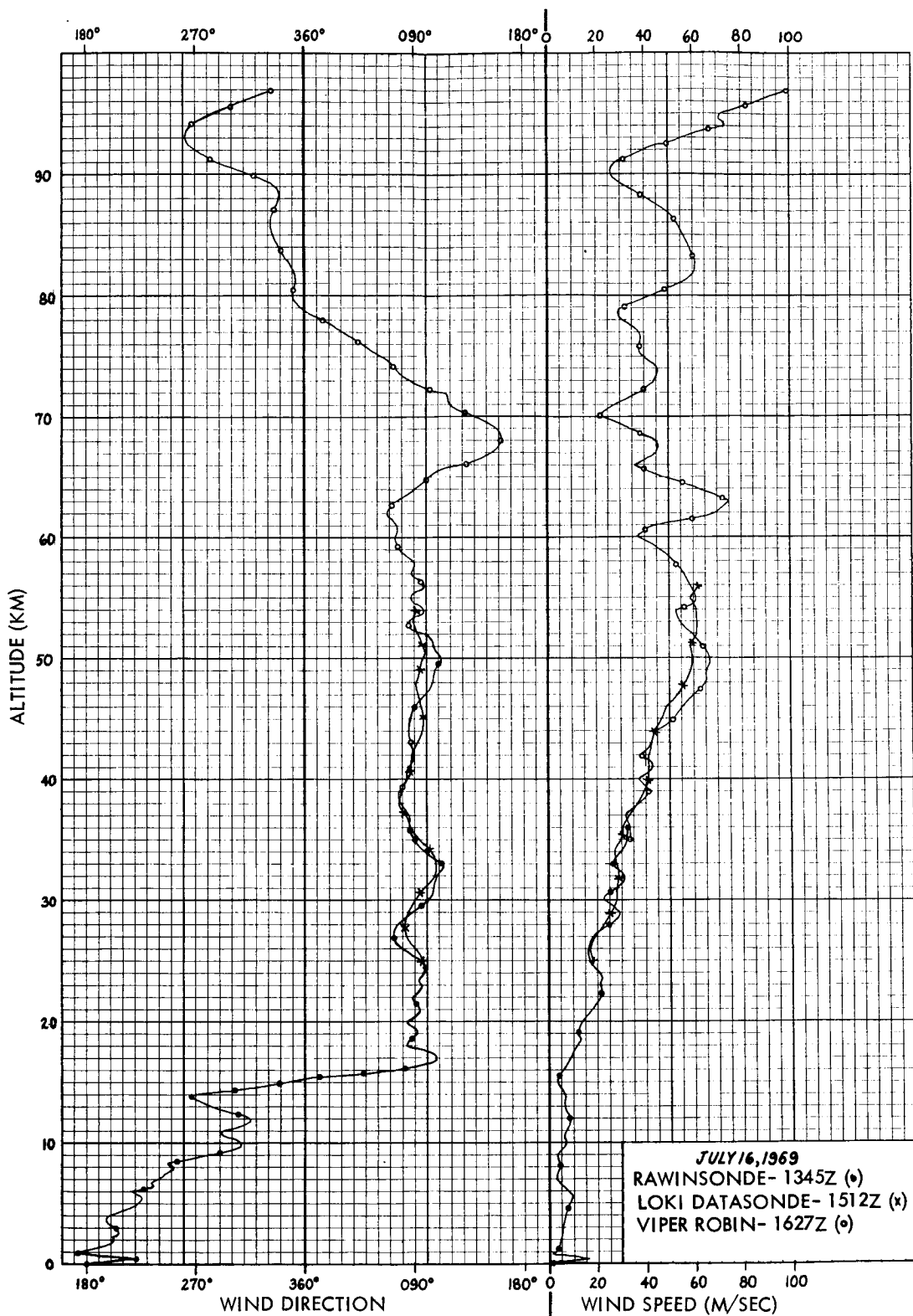


FIGURE 8.1-2 ETR - APOLLO 11 LAUNCH SUPPORT DENSITY PROFILE - 16 JULY 1969 - CAPE KENNEDY, FLA.



ETR - APOLLO 11 LAUNCH SUPPORT WIND PROFILE - 14 JULY 1969 - CAPE KENNEDY, FLA.

FIGURE 8.1-3



ETR - APOLLO 11 LAUNCH SUPPORT WIND PROFILE - 16 JULY 1969 - CAPE KENNEDY, FLA.

FIGURE 8.1-4

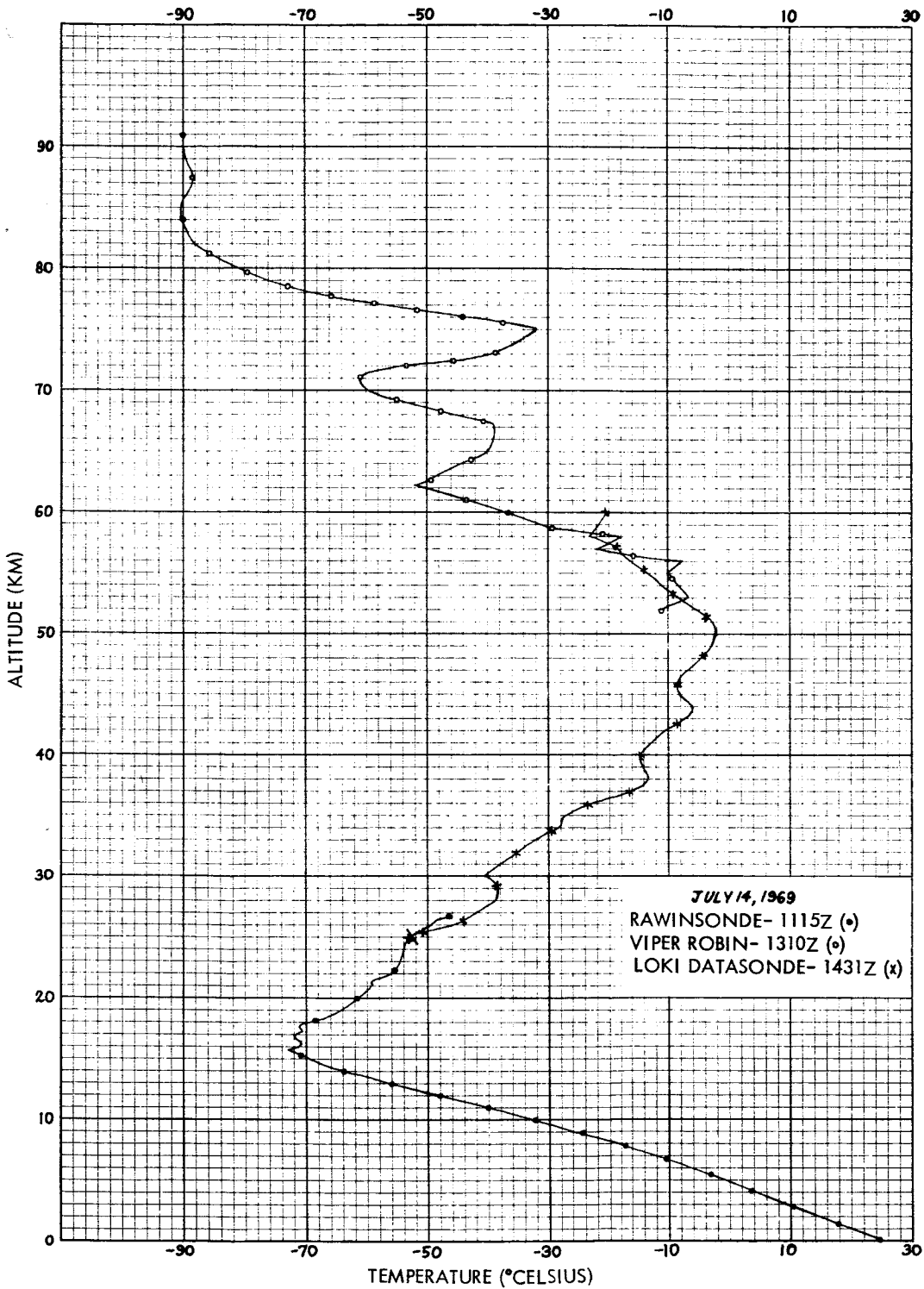
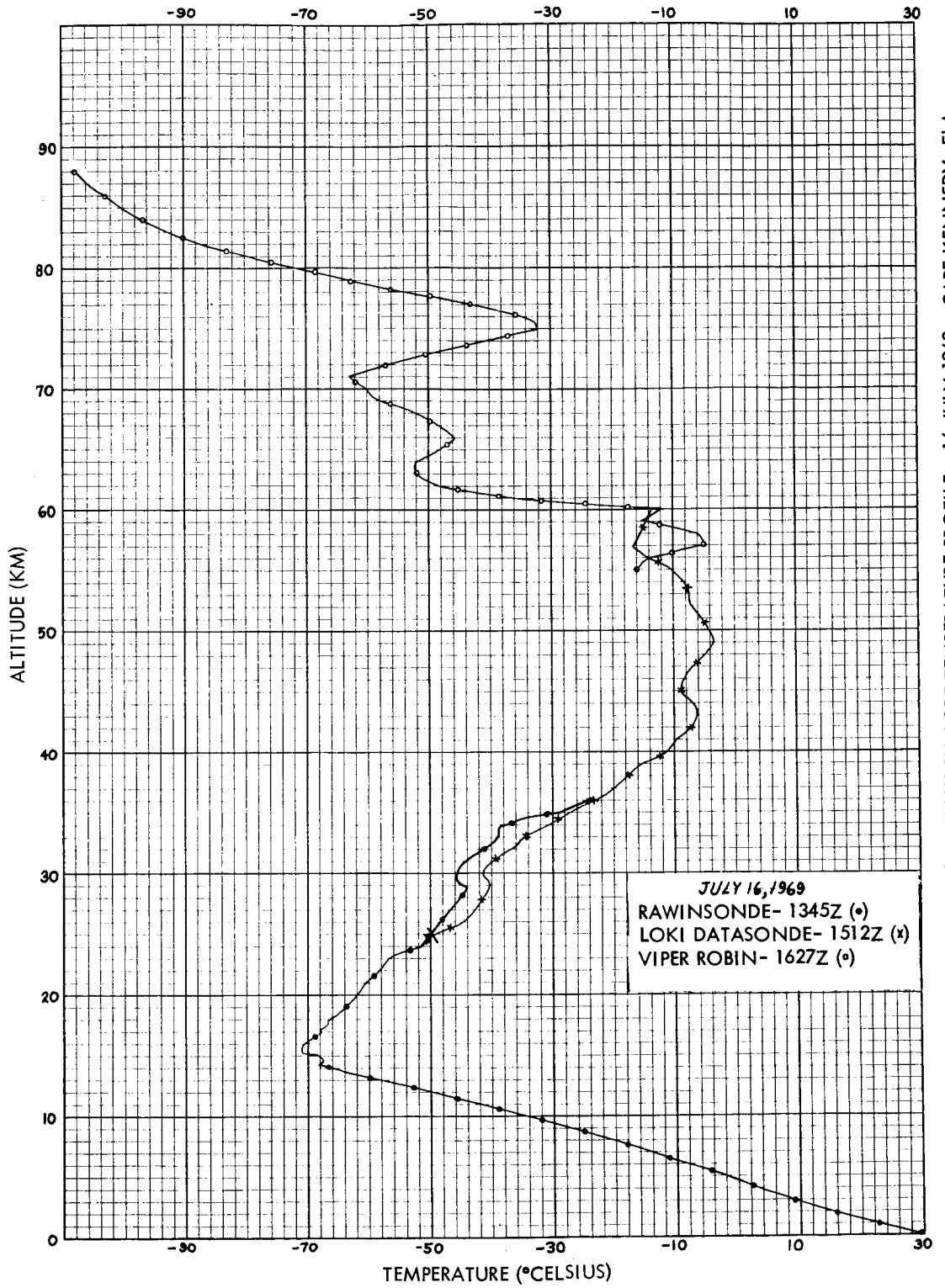


FIGURE 8.1-5 ETR - APOLLO 11 LAUNCH SUPPORT TEMPERATURE PROFILE - 14 JULY 1969 - CAPE KENNEDY, FLA.



ETR - APOLLO 11 LAUNCH SUPPORT TEMPERATURE PROFILE - 16 JULY 1969 - CAPE KENNEDY, FLA.

FIGURE 8.1-6

the vehicle apogee, and the wind data could be retrieved with a less precise radar than the FPS-16. If no radars were available at a particular site, an extra large inflatable sphere could be deployed with a relatively light-weight GMD-2 transponder. This system would be considerably more expensive than the simple inflatable falling sphere experiment, and this extra cost should be weighed against the necessity for obtaining 100 km wind and density data at sites without precision radar.

There appears to be an interest in a modest scale semi-synoptic ozone network to an altitude of about 75 km. Typical ozone payloads weigh about 35 pounds, and a reasonable diameter is about 5.5" to 6.5". Although fairly large signal-stage vehicle has been proposed for this application, a better choice might be a low cost two-stage vehicle. Currently such vehicles do not exist.

Electron density payloads are fairly small and lightweight. The same two-stage vehicle proposed for the pitot probe system would be most appropriate for electron density measurements to 200 km. Electron density measurement systems should be amenable to fairly low cost (\$2,000) production.

For large numbers of launchings per year at a given site, a sizeable investment in the ground-based facilities may be justified on the basis of reducing the expendable costs. For instance, if density is required to 100 km at a site where there is no radar, the choice may be to either construct an acceptable radar at the site, or to use a GMD-2 type system. With the radar, a low cost passive falling sphere system may be used, whereas with the GMD-2, a more expensive pitot probe type system may be required. The most economic choice would depend upon the number of firings anticipated during the useable life (estimating obsolescence) of the ground equipment. If the passive sphere system should cost \$1,300 and the pitot probe system cost \$2,300, then one thousand flights would be required from the given site to amortize the cost of a \$1 M radar. Thus, the establishment of a realistic requirement for the number of flights from a given launch site per year is quite important for future design efforts.

APPENDIX I

CORRECTIONS FOR METEOROLOGICAL ROCKET TEMPERATURE SOUNDINGS

ON AN INDIVIDUAL BASIS

By Robert M. Henry

NASA Langley Research Center
Langley Station, Hampton, Va.

Presented to the American Meteorological Society Conference
on High-Altitude Meteorology and Space Weather

Houston, Texas
March 29-31, 1967

CORRECTIONS FOR METEOROLOGICAL ROCKET TEMPERATURE SOUNDINGS

ON AN INDIVIDUAL BASIS

By Robert M. Henry

NASA Langley Research Center

ABSTRACT

Past studies have derived magnitudes of rocketsonde temperature errors from assumed atmospheric profiles and parachute trajectories; the present paper derives corrections using the actual trajectory and the measured temperature profile. Corrections are derived for aerodynamic heating, thermal lag, solar radiation, infrared radiation, electrical heating by the measuring current and by radio-frequency radiation, and for thermal emission by the thermistor and mount. Corrections are derived for a simple postmount and for a thin-film mount such as the Arcasonde IA sensor. It is shown that the thin-film mount produces large reductions in the magnitudes of the corrections required. A method of computing the ventilation velocity to improve the accuracy of the large aerodynamic heating correction is presented.

CORRECTIONS FOR METEOROLOGICAL ROCKET TEMPERATURE SOUNDINGS

ON AN INDIVIDUAL BASIS

By Robert M. Henry*

INTRODUCTION

With any measuring system, there is always concern as to the measurement errors of the system. These errors are of particular interest where meteorological rocket systems are concerned because the errors generally increase with altitude, and however much the systems are improved there is always a desire to utilize data from still higher altitudes where the errors become increasingly large.

A number of previous studies (for example, refs. 1 to 6) have considered the problem of measurement errors of bead thermistors primarily by assuming standard conditions and nominal trajectories and solving for the thermistor temperature from an assumed atmospheric temperature profile. The present study considers the inverse of this problem: given the time history of the thermistor temperature, to find the atmospheric temperature profile. This, of course, is the problem faced by the using meteorologist.

The purpose of this paper is to help extend the useful altitude range of meteorological rocket data by presenting a system of corrections based on the actual conditions and trajectory of the particular measuring system.

SYMBOLS

A	area
Alb.	albedo
C	heat capacity
C_D	drag coefficient
c_p	specific heat of air at constant pressure
G	geometric factor depending on shape and exposure
g	acceleration of gravity
h	coefficient of convective heat transfer for total area
J	solar constant

*Aerospace engineer.

k coefficient of thermal conductivity
 m mass of parachute plus payload
 r recovery coefficient
 S area of parachute
 T temperature
 T_{eff} effective radiation temperature of atmosphere
 V ventilation velocity
 \vec{V} vector velocity of parachute
 V_Z vertical component of parachute velocity
 \vec{W} three-dimensional vector wind velocity
 W_t electrical heating of thermistor due to measuring current and radio-frequency radiation
 W_Z vertical wind velocity
 w weighting factor
 X length of lead wire
 α absorptivity for radiation
 β cross-sectional area of lead wire
 ϵ thermal emissivity
 σ Stefan-Boltzmann constant
 ρ air density

Subscripts:

atm atmosphere
 f conductive thin film
 l long-wave (terrestrial) radiation
 m mount
 s short-wave (solar) radiation
 t thermistor

HEAT-TRANSFER EQUATIONS

To determine the corrections to be applied to the temperature measurements, it is necessary to evaluate the various heat-transfer mechanisms involved between the environment and the measuring system and between different parts of the measuring system.

The first relationship to be considered is the heat equation of the thermistor itself. This equation is a statement that the rate of increase in the heat content of the thermistor is equal to the sum of the heat inputs:

$$C_t \frac{dT_t}{dt} = h_t \left(T_{atm} + r_t \frac{V^2}{2c_p} - T_t \right) + \alpha_{st} G_{st} J(1 + Alb.) + \alpha_{zt} G_{zt} \sigma T_{eff}^4 - A_t \epsilon_t \sigma T_t^4 + W_t + \frac{2k\beta}{X} (T_m - T_t) \quad (1)$$

The term on the left of the equation represents the net rate of addition of heat. The first term on the right is the rate of heat transfer by conduction, and includes the aerodynamic heating $\left(r_t V^2 / 2c_p \right)$. The sum of $T_{atm} + r_t V^2 / 2c_p$ is called the recovery temperature, and represents the temperature of the atmosphere in actual contact with the surface of the thermistor.

The remaining terms represent, respectively, solar heating, infrared heating, thermal emission by the thermistor, electrical heating (by the measuring current and by the radio-frequency radiation from the transmitter antenna) and heat conduction through the lead wires from the mount.

The expression for heat conduction given here $(2k\beta/X)$ assumes a uniform gradient of temperature along the wire. This is appropriate if the heat transfer between wire and environment is small, the temperature lapse rate is not changing rapidly, and the system has recovered from any large initial temperature differences at deployment. It is not appropriate for systems having long lead wires, and may also be inappropriate for a short period of time immediately after deployment if the initial temperatures of the system components are greatly different from their respective recovery temperatures.

Heat-Transfer Equation for Thin Film

The widely used Arcasonde IA (ref. 5) and also a number of more recent designs developed by, for example, White Sands Missile Range, Metrophysics, Inc., and Thiokol's Astro-Met Division utilize a short lead wire plus a metallic thin film deposited on a plastic thin-film substrate in the electrical path of the measuring current. The original purpose of this arrangement was to achieve thermal isolation of the thermistor from the telemetry package. However, it is found that the large area of thin film in addition to providing

thermal isolation serves as a very effective heat exchanger with the atmosphere. In fact, the heat transfer from the film, conducted through the lead wires, dominates the transfer processes of the thermistor.

The heat-transfer equation of the thin film can be expressed by an equation similar to that for the thermistor:

$$C_f \frac{dT_f}{dt} = h_f \left(T_{atm} + r_f \frac{v^2}{2c_p} - T_f \right) + \alpha_{sf} G_{sf} J (1 + Alb.) + \alpha_{lf} G_{lf} \sigma T_{eff}^4 - A_f \epsilon_f \sigma T_f^4 + \frac{2k\beta}{X} (T_t - T_f) \quad (2)$$

which differs from equation (1) principally in the change of subscripts. The geometric factors in the radiation terms are different, and there is strong dependence on the solar angle. The electrical heating is expected to be negligible and is omitted. The conduction term is the negative of the conduction term in equation (1) with $T_m = T_f$.

CORRECTION EQUATIONS

Equations (1) and (2) provide a basis for not only evaluating the various errors in the film-wire-bead system, but also for correcting them using the conditions of the actual flight rather than nominal corrections.

Correction Equation for Bead

If the temperature of the bead thermistor T_t and, consequently, its derivative is a known function of time, equation (1) can be solved for the atmospheric temperature T_{atm} by simple algebraic manipulation. The resulting correction equation

$$T_{atm} = T_t - r_t \frac{v^2}{2c_p} + \frac{\epsilon_t}{h_t} \frac{dT_t}{dt} - \frac{G_{st} \alpha_{st} J (1 + Alb.)}{h_t} - \frac{G_{lt} \alpha_{lt} \sigma T_{eff}^4}{h_t} - \frac{W_t}{h_t} + \frac{A_t \epsilon_t \sigma T_t^4}{h_t} - \frac{2k\beta}{X h_t} (T_m - T_t) \quad (3)$$

gives the atmospheric temperature as the sum of the thermistor temperature plus a series of correction terms which may be called, respectively, the aerodynamic heating correction, lag correction, solar-radiation correction, long-wave-radiation correction, electrical heating correction, and conduction correction.

Actual evaluation of the corrections is complicated by difficulties and uncertainties in the determination of some of the correction parameters. In the altitude range of interest, the bead experiences transition from continuum flow to slip flow and from slip flow to free molecule flow. This affects the determination of both the convective heat-transfer coefficient h_t and the recovery coefficient r_t . The geometric factors G_{st} and G_{lt} are affected by deviations of the actual beads from the nominal diameters and from the nominal spherical shape. The solar and long-wave absorptivities and emissivities α_{st} and α_{lt} and the emissivity ϵ_t may vary with age and exposure to a contaminated atmosphere. While variations in the solar constant J may be neglected, the value of the albedo $Alb.$ will vary over a wide range depending on cloud cover, snow cover, vegetation, and at costal locations, on the solar angle. The effective radiating temperature of the atmosphere T_{eff} varies with latitude and season and also with cloud cover. As a result, it will be difficult to make radiation corrections with a high percentage of accuracy and reflective coatings or radiation shields are needed to keep the magnitude of these corrections small.

Finally, the conduction correction requires a knowledge of the mount temperature T_m which in the case of the thin-film mount is the film temperature T_f . This can be found from the heat equation of the film, equation (2). In order to obtain closed form solutions, it is necessary to make a suitable approximation for the quadratic term $A_t \epsilon_t \sigma T_f^4$. This may be done by using the first two terms of the Maclaurin series expansion of T_f^4

$$T_f^4 \approx T_t^4 + 4T_t^3(T_f - T_t) \quad (4)$$

This linear approximation will be very accurate at the temperature encountered by the meteorological rocket, producing an error of around 1.0 percent for a 30° difference between T_f and T_t .

With the substitution of equation (4) into equation (3), equation (3) can be solved for $(T_f - T_t)$. If the resulting value is substituted into equation (2) and the result solved for the atmospheric temperature, a system correction equation results:

$$T_{atm} = T_t + \frac{-h_t r_t \frac{v^2}{2c_p} + \epsilon_t \frac{dT_t}{dt} - G_{st} \alpha_{st} J(1 + Alb.) - G_{lt} \alpha_{lt} T_{eff}^4 - W_t + A_t \epsilon_t \sigma T_t^4}{h_t + \frac{h_f(2k\beta/X)}{h_f + 2k\beta/X + 4A_f \epsilon_f \sigma T_t^3}} + \frac{\frac{2k\beta/X}{h_f + 2k\beta/X + 4A_f \epsilon_f \sigma T_t^3} \left[-h_f r_f \frac{v^2}{2c_p} + C_f \frac{dT_f}{dt} - G_{sf} \alpha_{sf} J(1 + Alb.) - G_{lf} \alpha_{lf} \sigma T_{eff}^4 + A_f \epsilon_f \sigma T_t^4 \right]}{h_t + \frac{h_f(2k\beta/X)}{h_f + 2k\beta/X + 4A_f \epsilon_f \sigma T_t^3}} \quad (5)$$

in which the unknown film temperature T_f has been eliminated. The time derivative of the film temperature, which still appears, can be assumed to be approximately equal to the derivative of the thermistor temperature except for a brief period immediately after deployment where a step change in temperature may produce a temporarily large difference.

It can be seen from equation (5) that the expansion of the conduction term has also changed the aerodynamic, lag, radiation, and emission terms. In each case the denominator h_t has been replaced by the expression

$$h_t + \frac{h_f(2k\beta/X)}{h_f + 2k\beta/X + 4A_f\epsilon_f\sigma T_t^3}$$

which can be regarded as a system convective heat-transfer coefficient. The behavior of the system can be understood better by considering the corresponding terms in the first and second fractions. It can be seen that each term - aerodynamic heating, lag, radiation, etc. - is the sum of the term for the bead plus the corresponding term for the film multiplied by a weighting factor

$$w_f = \frac{2k\beta/X}{h_f + 2k\beta/X + 4A_f\epsilon_f\sigma T_t^3} \quad (6)$$

which is, approximately, the ratio of the conduction $2k\beta/X$ to the total thermal dissipation $h_f + 2k\beta/X + 4A_f\epsilon_f\sigma T_t^3$. The denominator - the system convective heat-transfer coefficient - is a similar weighted sum of the thermistor and film heat-transfer coefficient

$$h_{\text{system}} = h_t + w_f h_f \quad (7)$$

Thus, equation (5) can be rewritten

$$\begin{aligned} T_{\text{atm}} = T_t - \frac{h_t r_t + w_f h_f r_f}{h_t + w_f h_f} \frac{v^2}{2c_p} + \frac{Ct \frac{dT_t}{dt} + w_f C_f \frac{dT_f}{dt}}{h_t + w_f h_f} \\ + \frac{G_{st}\alpha_{st} + w_f G_{sf}\alpha_{sf}}{h_t + w_f h_f} J(1 + \text{Alb.}) - \frac{G_{lt}\alpha_{lt} + w_f G_{lf}\alpha_{lf}}{h_t + w_f h_f} T_{\text{eff}}^4 \\ - \frac{W_t}{h_t + w_f h_f} - \frac{A_t \epsilon_t + w_f A_f \epsilon_f}{h_t + w_f h_f} \sigma T_t^4 \end{aligned} \quad (8)$$

In equation (8) the aerodynamic, lag, radiation, electrical, and emission corrections appear as separate terms, defined for the total film-wire-bead system. There is no separate conduction term, since the length of the conductive film strip is great enough to effectively isolate the film-wire-bead system from the payload structure.

Equation (8) is completely general (except for omission of convection and radiation of the lead wires) and gives solutions for atmospheric temperature in terms of measurable values. Solutions can also be found when the radiation and convection terms for the wire are included (ref. 7). However, while these more complete equations are suitable for computer reduction of the sounding data, they are lengthy and cumbersome. The behavior of the sensor system is more clearly illustrated by the very close approximation of equation (8). Notice that the evaluation of equation (8) does not require knowledge of a "time constant," and there is no time dependence beyond the necessity for evaluating the thermistor temperature derivative. Thus, the correction equation can be applied to any portion of the temperature trace where the derivative can be evaluated.

The behavior of the sensor system over certain portions of the altitude range of interest can be illustrated even more clearly by considering some limiting cases of equation (8).

High-Altitude Case

One limiting case of interest is the case where the film convective transfer coefficient is very small compared to the conduction factor ($h_f \ll 2k\beta/X$). This condition is approached with increasing altitude and would be approximated at 100 km or above. In this case, equation (8) approaches

$$T_{atm} = T - r_f \frac{v^2}{2c_p} - \frac{G_{sf}\alpha_{ff}(1 + Alb.)}{h_f} + \frac{C_f \frac{dT_f}{dt}}{h_f} - \frac{G_{lf}\alpha_{lf}\sigma T_{eff}^4}{h_f} - \frac{W_t}{h_f A_f} + \frac{A_f \epsilon_f \sigma T_t^4}{h_f A_f} \quad (9)$$

Equation (9) shows that the bead-wire-film system approaches the behavior of a pure thin-film sensor at the higher altitudes. It should be noted that at the altitudes where this equation applies h_f will be sufficiently small that none of the indicated correction terms can be safely neglected, although with foreseeable parachute developments the aerodynamic heating correction is expected to be the term of greatest importance. Equation (9) indicates that thermistor temperatures can be readily corrected at higher altitudes and that the major obstacle to the use of present sensor systems at higher altitudes is the development of satisfactory parachutes or other decelerators for use at these altitudes.

Lower Altitude Case

Another limiting case of interest is the case where the conduction factor is very small compared with the film convective transfer coefficient ($2k\beta/X \ll h_f$). This condition is approximated at altitudes below about 70 km. In this lower altitude case equation (8) approaches:

$$T_{atm} = T_t - \frac{h_t r_t + (2k\beta/X) r_f v^2}{h_t + 2k\beta/X} + \frac{C_t \frac{dT_t}{dt}}{h_t + 2k\beta/X} - \frac{G_{st} \epsilon_{st} J (1 + Alb.)}{h_t + 2k\beta/X} - \frac{G_{lt} \alpha_{lt} \sigma T_{eff}^4}{h_t + 2k\beta/X} - \frac{W_t}{h_t + 2k\beta/X} + \frac{A_t \epsilon_t \sigma T_t^4}{h_t + 2k\beta/X} \quad (10)$$

In this case the system heat-transfer coefficient becomes $h_t + 2k\beta/X$. Notice that the numerators of the lag, radiation, electrical, and emission terms are the same as in the simple thermistor correction equation (3), that is, the same as for a simple thermally isolated thermistor. As a result, each of these terms is substantially reduced in magnitude by the increased denominator. In the 60- to 70-km range, h_t decreases with altitude to values an order of magnitude below $2k\beta/X$, with corresponding reduction in the lag, radiation, electrical heating, and emission corrections. The aerodynamic heating correction is reduced slightly, primarily because the film (whose recovery coefficient is heavily weighted) is in the continuum flow regime at these altitudes, with a recovery coefficient of about 0.9 compared to about 1.1 for the bead thermistor which is in the slip-flow regime. As a result, the radiation, electrical heating, and emission corrections are on the order of tenths of a degree, the lag correction is on the order of a degree, and the aerodynamic heating correction is on the order of tens of degrees. (It is about 10° K at 65 km for a nominal trajectory, but deviations from nominal always result in increases.)

Computation of Ventilation Velocity

Since it appears that the aerodynamic heating is the most important correction at all altitudes, it is important to determine this correction with the greatest accuracy which is feasible. In evaluating the aerodynamic heating it has frequently been assumed that the ventilation velocity V can be approximated by the magnitude of the vertical velocity V_z . However, this assumption is valid only if the vertical velocity approximates the terminal velocity, and previous study (ref. 8) shows that, for the range of ballistic coefficients of current parachutes, terminal velocity is not closely approached until below 60 km. It is thus desirable to obtain a better representation of the ventilation velocity.

The desired ventilation velocity V is the magnitude of the vector difference between the parachute velocity and the velocity of the atmosphere $|\vec{V} - \vec{W}|$. The equations of motion do not provide a unique solution for this

value from tracking data unless an assumption is made regarding one component of the velocity of the atmosphere. A very good approximation can be found, however, by neglecting the vertical wind velocity in comparison with the vertical component of parachute velocity. The equation of vertical motion for the parachute (the drag equation) is given by

$$-\frac{1}{2} C_D S \rho \left| \vec{V} - \vec{W} \right| (V_Z - W_Z) - m \frac{dV_Z}{dt} - mg = 0 \quad (11)$$

If the approximation that $V_Z \approx V_Z - W_Z$ is made, then equation (11) can be solved for the ventilation velocity:

$$v = \left| \vec{V} - \vec{W} \right| = \frac{-m \left(g + \frac{dV_Z}{dt} \right)}{\frac{1}{2} C_D S \rho V_Z} \quad (12)$$

which can be evaluated from known or measured quantities. Since the second derivative of the position must be determined, precise tracking is needed; radar tape data rather than plotboard data should be used.

The approximation in equation (12) will generally be very good throughout the region of the atmosphere of interest. It obviously will not apply for a short time after apogee when the parachute does not possess appreciable vertical velocity.

CONCLUDING REMARKS

Corrections to rocketsonde temperature profiles for aerodynamic heating, thermal lag, solar radiation, infrared radiation, electrical heating by the measuring current and by radio-frequency radiation, and for thermal emission can be made for current thin-film mount designs as well as for simple post mounting, and can be made for the actual conditions and parachute trajectory of the individual sounding.

The accuracy of the aerodynamic heating correction, which is the largest correction, can be improved by using the calculated ventilation velocity instead of the vertical velocity.

The use of a thin-film mount, which serves as a heat exchanger between atmosphere and thermistor results in great reduction of all the corrections except the aerodynamic heating correction.

The aerodynamic heating correction is reduced somewhat by the thin-film mount because transitions to slip flow and to free molecule flow occur at higher altitudes.

Because the corrections are substantial, especially at the higher altitudes, the accuracy of the sounding at the higher altitudes depends strongly on the accuracy of the corrections.

Additional research is needed to determine accurate values of the parameters used in the corrections, particularly the convective heat-transfer coefficients and recovery coefficients over the range of atmospheric conditions and flow regimes encountered.

REFERENCES

1. Barr, William C.: Theoretical Considerations in the Design of Atmospheric Temperature Sensing Elements. USASRD L Tech. Rept. 2195, April 1961. (Available from DDC as Document No. AD 255896.)
2. Ballard, Harold N.: Response Time of and Effects of Radiation on the VECO Bead Thermistor. Tech. Rept., Schellinger Research Lab., Texas Western College (Contract DA-29-040-ORD-2410), April 1961.
3. Wagner, N. K.: Theoretical Time Constant and Radiation Error of a Rocketsonde Thermistor. J. Meteorol., vol. 18, no. 5, Oct. 1961, pp. 606-614.
4. Wagner, N. K.: Theoretical Accuracy of a Meteorological Rocketsonde Thermistor. J. Appl. Meteorol., Vol. 3, No. 4, Aug. 1964, pp. 461-469.
5. Drews, William A.: A Thermistor Arrangement to Improve Temperature Measurements at High Altitudes. NASA CR-533, 1966.
6. Thompson, Donald C.: The Accuracy of Miniature Bead Thermistors in the Measurement of Upper Air Temperatures. Scientific Report No. 1 (Contract No. AF 19(628)-4165), Mass. Inst. Tech., Oct. 1966. (Also AFCRL-66-775.)
7. Staffanson, Forrest L.: Mathematical Model of the Film Mounted, Rocketsonde Thermistor. Paper presented at American Meteorology Society Conference on High Altitude Meteorology and Space Weather. Mar. 1967.
8. Murrow, Harold N.: Parachutes for Meteorological Applications. IRIG Doc. No. 111-64, Feb. 1965, pp. 237-245.

BIBLIOGRAPHY

BIBLIOGRAPHY

CHAPTER I - INTRODUCTION

1.1 GENERAL

Inter-Range Instrumentation Group, Meteorological Working Group, Meteorological Rocket Network Committee, (1960): Initiation of the Meteorological Rocket Network Report, AD 246 950.

Suomi, V. E.; Observing the Atmosphere - A Challenge: Proceedings of the IRE, Page 2192 - 2197 - November 1962.

1.2 ATMOSPHERIC PARAMETERS

Jehn, K. H., Wagner, N. K., Gerhardt, J. R., Haragan, D. R.; Wind and Temperature in the Atmosphere between 30 and 80 KM: 3rd Quarterly Technical Report - 1 Jan 1961 thru 31 March 1961, Contract A-23-072-ORD-1564.

Clark, G. Q., Webb, W. L., Jenkins, K. R.; (1960): High Atmosphere Meteorological Parameters, IRE Trans. Military Electronics, MIL-4, 238 - 243.

1.3 MEASUREMENT CONSIDERATIONS

Miers, B. T., Beyers, N. J.; Rocketsonde Wind and Temperature Measurements between 30 and 70 KM for selected Stations. ERDA-70, September 1963.

1.4 MEASUREMENT SYSTEMS

Joint Scientific Advisory Group to the Meteorological Rocket Network; An Analysis of the First Year in Operation: Journal of Geophysical Research, Vol 66, No. 9, Page 2821, September 1961.

CHAPTER 2 - SYSTEM REQUIREMENTS

2.1 GENERAL

2.2 MISSILE AND SPACE VEHICLE SUPPORT

Cook, G. E.; Comparison of Air Densities obtained from Orbital Decay and Instruments: Technical Report No. 66370, November 66.

Field, Jerome S. and Hargis, David E.; The Effects of the Accuracy of Atmospheric Data on the Structural Design Loads of a Typical Launch Vehicle: Aerospace, Mar. 1964.

Henry, Robert M. and Cochrane, James A.; Geographical Variations of Wind Loads on Vertically Rising Vehicles - NASA, 2-6 Mar. 64.

Moore, G. R. and Harmon, W. H.; Meteorological Data Required in Hypersonic Glide Research Flight Test Program - The Boeing Company, Seattle, Washington .

USAF; Some Effects of the Natural Environment on Aerospace Systems: 4 WGP 80-4-1, March 23, 1964.

Vaughan, William W.; Wind Profiles at Staging Altitudes (35 KM to 80 KM): NASA, 27 - 28 September 1961.

2.3 METEOROLOGICAL RESEARCH

Diamond, Marvin and Lee, Robert P.; Statistical Data on Atmospheric Design Properties above 30 KM: ERDA-75, October 1963.

Estes, Glen, D.; Meteorological Rocket Program, Vol. III, Rev. 1, Meteorological Research, Development, Test and Evaluation Rocket: USAMC - AD-804817, October 1966.

Friedman, H.; Sounding Rocket Research Techniques, IQSY Instruction Manual #9, IQSY Secretariat, London - 1964 - November.

2.3 Meteorological Research - (continued)

Howley, D.L.; A Study to Define a State-of-the-Art Rocket Vehicle Suitable for Synoptic Meteorological Soundings, Vol. I, NASA - CR-66002, (NAA) SID65-411, 1A, 16 June 1965 (Rev.)

Kellogg, Wm. W.; Rocket Research and the Upper Atmosphere: "The Earth", Page 157 - 168.

Rosenberg, Norman W.; Dynamic Model of Ionospheric Wind Profiles; Journal of Geophysical Research, Space Physics, Vol. 73, No. 15, Page 4965, August 1, 1968.

Smith, L. G., Weeks, L. H. and McKinnon, P. J.; Investigation of the D and E Regions of the Ionosphere during the International Quiet Sun Year. NASA CR-391 - March 1966.

Smith, W. S., Theon, J. S., Swartz, P. C. and Katchen, L. B.; Temperature, Pressure, Density and Wind Measurement in the Upper Stratosphere and Mesosphere, 1965 - NASA TR-R 263, September 67.

Webb, Willis, L.; The Dynamic Stratosphere - ERDA-62, August 63.

CHAPTER 3 - ATMOSPHERIC SENSORS

3.1 GENERAL

Radigan, J. (Director Internal Systems); High Altitude Sensing Techniques, Final Summary Report - NORT 65-11, January 1965.

Smith, W. S.; Temperature, Pressure, Density and Wind Measurements in the Upper Stratosphere and Mesosphere, NASA Technical Report, NASA TR R-263, 1965; TR R-245, 1964.

Smith, W., Theon, J., Katchen, L. and Swartz, P.; Temperature, Pressure, Density and Wind Measurements in the Upper Stratosphere and Mesosphere, 1964. NASA, TR R-245 - NASA 1966.

Smith, W. S., Theon, J. S., Swartz, P. C.; Katchen, L. B.; Temperature, Pressure, Density and Wind Measurements in the Stratosphere and Mesosphere, 1966 - NASA TR R-288, August 1968.

3.2 WIND MEASUREMENT TECHNIQUES

Avara, E. P. and Miers, B. T.; A Data Reduction Technique for Meteorological Wind Data above 30 Kilometers - ECOM-5168, December 67.

Barr, W. C.; Theoretical Evaluation of Cylindrical Chaff as a Wind Sensor at High Altitudes, USASRD, TR 2138, AD 241876, 36.

Battan, L. J.; (1959): Use of Chaff for Wind Measurements, Bull. AMS, Vol 39, 258 - 260.

Batten, E. S.; Wind Systems in the Mesosphere and Lower Ionosphere, P-2018, NSF, 13 June 1960. (Rand Corporation)

Beaudoin, P. E., Golomb, D., Noel, T. M., Rosenberg, N. W. and Vickery, W. K.; Observation of Mesosphere Winds and Turbulence with Smoke Trails: Journal of Geophysical Research, Vol 72, No. 14 15 July 1967.

3.2 Wind Measurement Techniques - (continued)

Beyers, N. J. and Miers, B. T.; A Summary of Studies of Diurnal Tidal Motions Near the Stratopause over White Sands Missile Range, New Mexico - June 1966.

Beyers, N. J. and Thiele, O. W. (1961): Meteorological Rocket Wind Sensors, (Unpublished).

Beyers, N. J. and Thiele, O. W. (1961): Performance Characteristics of Systems for High Altitude Wind and Temperature Observations, Instr. Soc. of Amer.-Amer. Meteor. Soc., 11-15, preprint 170 LA-61-1.

Beyers, N. J., Thiele, O. W., Wagner, N. K.; (1962): Performance Characteristics of Meteorological Rocket Wind and Temperature Sensors, Technical Report SELWS-M-4, U. S. Army Electronics Research and Development Activity, White Sands Missile Range, New Mexico.

Borden, T. R., Jr., Hering, W. S., Muench, H. S., Ohring, G. (1960): Contributions to Stratospheric Meteorology, GRD Notes, 2, Geophysics Research Directorate, AF Cambridge Research Laboratories, Bedford, Mass.

Bruch, A. and Morgan, G. M. Jr. (1961): Wind Variability in the Mesosphere as Determined by the Tracking of Falling Objects, AFCRL 660, Final Rep., Contract No. AF 19(604)-6193, New York University.

Eddy, Amos, Duchon, C. E., Hasse, F. M. and Haragan, D. R.; Determination of Winds from Meteorological Rocketsondes #2 - Nov. 65.

Finger, Frederick G., Teweles, Sidney; The Mid-Winter 1963 Stratospheric Warming and Circulation Change: Journal of Applied Meteorology Vol. 3, No. 1, PP - 1 - 15, February 1964.

Golomb, D., Harang, O. and DelGreco, F. P.; Upper Atmosphere Densities and Temperatures at 105-165 Kilometers from Diffusion and Spectral Intensity of AIO Trails: Journal of Geophysical Research, Vol. 72, No. 9, 1 May 1967.

Hoffman, J. M., Nelson, L. S. and Smith, L. B.; Yellow-Green Luminosity Accompanying the Injection of Triethylborane into the Upper Atmosphere: Nature, Vol. 214, #5094, pp 158 - 159, SC - R-67-1073, April 1967.

Jehn, K. H., Wagner, N. K., Gerhardt, J. R. and Haragan, D. R.; (1961): Wind and Temperature in the Atmosphere between 30 and 80 km, Second Quarterly Report, Contract DA-23-072-ORD-1564, University of Texas, Austin, Texas.

3.2 Wind Measurement Techniques - (continued)

Jenkins, K. R., Webb, W. L.; (1958): Rocket Wind Measurements, Bull. AMS, Vol. 39, 436.

Jenkins, K. R., Webb, W. L.; (1958): Rocket Wind Measurements, Tech Memo 531, USASMSA, White Sands Missile Range, New Mexico.

Jenkins, K. R., Webb, W. L. (1959): High Altitude Wind Measurements, J. Meteorological, Vol 16, 511-518.

Keegan, Thomas J.; Winds and Circulations in the Mesosphere: AFCRL-244, February 1961.

Lally, V. E. and Leviton, R.; (1958): Accuracy of Wind Determination from the Track of a Falling Object, AF Surveys in Geophysics, USAFCRL No. 93, AD 146858.

Peterson, Ray E., Schuetz, John, Shenk, Wm. E. and Lan, Wen.; Derivation of a Meteorological Body of Data Covering the Northern Hemisphere in the Longitude Region between 60°W and 160°W from March 1964 through February 1965: NASA CR-723, April 1967.

Ragsdale, George C. and Wasko, Peter E.; Wind Flow in the 80-400 km Altitude Region of the Atmosphere: MTP-AERO-62-49, 5 June 1962.

Rapp, R. R. (1969): The Accuracy of Winds derived by the Radar Tracking of Chaff at High Altitudes, J. Meteor., Vol 17, 507-514.

Smith, Lawrence B.; Use of Chaff Rockets for Measurement of High-Altitude Winds: Sandia Corporation, 5 - 8 December 1960.

Webb, Willis, L.; Stratospheric Tidal Circulations: Reviews of Geophysics, Vol. 4, No. 3, Page 363 - 375, August 1966.

Woodrum, Arthur and Justus, C. G.; Atmospheric Tides in the Heights Region 90 to 120 Kilometers: Journal of Geophysical Research, Vol. 73, No. 2, Page 467, 15 January 1968.

3.3 TEMPERATURE MEASUREMENT TECHNIQUES

Badgley, F. I.; (1957): Response of Radiosonde Thermistors, Rev. Sci. Inst., 28(12 1079 1084).

Ballard, H. N.; (1961): Response Time of and Effects of Radiation on the VECO Bead Thermistor, Inst. Soc. of Amer., Preprint No. 169-LA-61.

Ballard, J. C.; (1941): On the Interpretation of Temperature Measurements made at High Levels, Mon. Wea. Rev., Vol 69, 33-40.

Ballard, Harold N.; The Measurement of Temperature in the Stratosphere and Mesosphere, USAECOM Report #5056, May 1966.

Ballard, Harold N.; A Review of Seven Papers Concerning the Measurement of Temperature in the Stratosphere and Mesosphere: DA Task - IV650212A 27-03, ECOM-5125, May 1967.

Barr, W. C.; (1958): Heat Transfer Considerations in the Design of High Altitude Temperature Sensing Elements, Bull AMS, Vol 39, 435.

Barr, W. C.; (1961): Theoretical Considerations in the Design of Atmospheric Temperature Sensing Elements, USASRD, TR 2195.

Beyers, N. J., Thiele, O. W., Wagner, N. K.; (1961): "Performance Characteristic of Meteorological Rocket Wind and Temperature Sensors", Technical Report SELWS-M-4, Missile Meteorology Division, U. S. Army Electronics Research and Development Activity, White Sands Missile Range, New Mexico.

Cole, Allen E.; Temperature Variations in the Tropical Stratosphere and Mesosphere 25 to 80 Kilometers: AMS/AIAA Paper No. 66-344, 28 - 31 March 1966.

Daniels, Glenn E.; Errors of Radiosonde and Rocketsonde Temperature Sensors: Bulletin of the Amer. Meteorological Society, Vol. 49, No. 1, Page 16 - 18, January 1968.

3.3 Temperature Measurement Techniques - (continued)

Daniels, Glenn E.; Measurements of Gas Temperature and the Radiation Compensating Thermocouple:

Diedrick, James, H and Curtis, Henry B.; Experimental Investigation of Total Emittance and Solar Absorptance of Several Coatings between 300° and 575° K: NASA TND-3381, April 1966.

Drews, W. A.; An Improvement of Atmospheric Temperature Measurements above 30 km by Means of the Bead Thermistor Mounting Arrangement, NASA Contract NAS 1-1611, January 1966.

Drews, William A.; A Thermistor Arrangement to Improve Temperature Measurements of High Altitudes: NASA CR-533, August 1966.

Henry, Robert, M.; Corrections for Meteorological Rocket Temperature Soundings on an Individual Basis: NASA, 29 - 31 March 1967.

Hind, A. D.; Temperature Corrections to a Bead Thermistor in the Upper Atmosphere, Weapons Research Establishment, Australian Defense Scientific Service, Salisbury, South Australia, May 1966.

Newell, H. E.; (1959): Sounding Rockets, McGraw-Hill.

Ney, E. P.; (1961): The Measurement of Atmospheric Temperatures, J. Meteor., Vol. 18, 60 - 80.

Quinlan, F. T. and Crutcher, H. L.; The Comparison of Rocketsonde and Radiosonde Temperatures in the 25 - 32 KM Layer at Cape Canaveral, Florida between 20 May 60 and 25 April 62: NASA, MTP-AERO-63-35 15 May 1963.

Pearson, P. Q.; An Investigation into the Response and Corrections to a Thermistor and a Platinum Wire Resistance Thermometer, Weapons Research Establishment, Australian Defense Service, March 1964.

Rubio, Robert and Ballard, H. N.; Time Response and Aerodynamic Heating of Atmospheric Temperature Sensing Elements, AMS Conference on the Dynamic Structure of the Atmospheres, 8 - 10 November 1966.

3.3 Temperature Measurement Techniques - (continued)

Robinson, Elmer; New Meteorological Sensors to 150,000 feet, Phase I Survey and Bibliography of Current Techniques, USASRDL, Contract No. DA-26-039-SC-87296, SRI Project No. PAU-3692, 30 Apr. 1962.

Robinson, Elmer; New Meteorological Sensors to 150,000 feet, Phase II Contract No. DA-36-039-SC-87296, SRI Project No. PAU-3692, 14 September 1962.

Servomechanisms, Inc. Research and Development Center (1963); Study for improvements of Temperature Measurements with Thermistors in High Altitudes; Contract No. DA-29-040-ORD-2410, Santa Barbara Airport, Goleta, California

Thiele, Otto, W. and Beyers, Norman J.; Verification of Meteorological Rocket Temperature, Density and Pressure Measurements, AMS-ATAA, 28 - 31 March 1966.

Thiele, Otto, W. and Beyer, Norman J.; Comparison of Rocketsonde and Radiosonde Temperatures and an Evaluation of Computed Rocketsonde Pressure and Density: Journal of Geophysical Research, Vol. 72, No. 10, 15 May 1967.

Thompson, Donald, C.; The Accuracy of Miniature Bead Thermistor in the Measurement of Upper Air Temperatures; Contract No. 6670, Task #667001, AFCL-66-773 Scientific Report #1, 1 October 1966.

Thompson, Donald C. and Keily, D. P.; The Accuracy of Thermistors in the Measurement of Upper Air Temperatures: MIT, Revised form - 21 November 1966.

Wagner, Haragen, Gerhardt, (1962): Seventh Quart. Tech. Report, Contract DA-23-072-ORD-1564, University of Texas.

Wagner, N. K., (1963): Theoretical Accuracy of the Met. Rocketsonde Thermistor, Rep. 7-23, Contract DA-23-072-ORD-1564, Electrical Engineering Laboratories, University of Texas.

Wagner, N. K.; Theoretical Accuracy of a Meteorological Rocketsonde Thermistor; Journal of Applied Meteorology, Vol. 3, No. 4, Page 461-469, August 1964.

3.3 Temperature Measurement Techniques - (continued)

Wagner, N. K. (1961): Theoretical Time Constant and Radiation error of a Rocketsande Thermistor, J. Meteor., 606-614.

Webb, Willis, L.; Detailed Acoustic Structure above the Tropopause, USASMAS, 15 January 1962.

Wright, W. F.; (1961): "A Survey for Naval Ordnance Laboratory of High Altitude Atmospheric Temperature Sensors and Associated Problems: Final Report, Navy Contract N-60921-6136, Wright Instruments, Inc., Vestal, New York.

3.4 FALLING SPHERE DENSITY MEASUREMENT TECHNIQUES

Bartman, F. L.; Falling Sphere Meethod for Upper Air Density and Temperature, J. Atm. and Terr. Phys., Spec. Supply, Vol. 1, 1954.

Bartman, F. L., Chaney, L. W., Jones, L.M., and Liu, V. C.; Upper-Air Density and Temperature by the Falling-Sphere Meethod, Journal of Applied Physics, Vol. 27, No. 7, 1 July 1956.

Brockman, W. E., (1963): Computer Programs in Fortran and Balgol for Determining Winds, Density, Pressure and Temperature from the Robin Falling Balloon. University of Dayton Research Institute Report, Contract No. AF19 (604) 7450.

Champion, K. S. W. and Faire, A. C.; Falling Sphere Measurements of Atmospheric Density, Temperature and Pressure, Up to 115 km, Environmental Research Papers No. 34, 1964.

Engler, N. A.; Development of Methods to Determine Winds, Density, Pressure and Temperature from the Robin Falling Balloon. Contract AF 19(604) 7450, Met. Dev. Lab., AFCRL, Bedford, Massachusetts, 1961.

Faire, A. C.; AFCRL Rigid Falling Sphere Program, AFCRL, Hanscom Field, Massachusetts, June 1963.

Faire, A. C. and Champion, K. S. W.; Falling Sphere Measurements of Atmospheric Density, Temperature and Pressure, Up to 115 KM: AFCRL-64-554, July 1964.

Faucher, G. A., Procunier, R. W. and Stark, C. N.; Flight Information and Experimental Results of Inflatable Falling Sphere System for Measuring Upper Air Density: AFCRL-685, August 1961.

Faucher, G. A., Procunier, R. W. and Sherman, F. S.; Upper Atmosphere Density obtained from Falling Sphere Drag Measurements, Space Physics Lab., AFCRL, December 1962.

3.4 Falling Sphere Density Measurement Techniques - (continued)

Faucher, G. A., Morrissey, J. F. and Stark, C. N.; Falling Sphere Density Measurements: Journal of Geophysical Research, Vol. 72, No. 1, Page 299 - 305, 1 January 1967.

Heinrick, Helmut, G.; Aerodynamic Drag Characteristics of Spherical Balloons (Robin) Descending from 70 km Altitude - University of Minnesota , March 1964.

Heinrich, H. G., Haak, E. L. and Niccum, R. J. (1963): Research and Development of Robin Meteorological Rocket Balloons, University of Minnesota Report, Vol. II, Contract No. AF 19(604) 8034.

Jones, L. M.; Transit-time Accelerometer, Rev. Sci. Instr., 1956

Jones, L. M., Peterson, J. W., Schaeffer, E. J. and Schulte, H. F.; Upper-Air Densities and Temperatures from Eight IGY Rocket Flights by the Falling-Sphere Method: IGY Rocket Report Series #5, 1 Dec 1959.

Leviton, R. and Palmquist, W. E.; A Rocket Balloon Instrument, (Abstract) Bull. AMS, Vol. 40, Page 374, 1959.

Leviton, R. and Palmquist W., Robin, A Meteorological Sensor, ARS Meeting, Minneapolis, Minnesota, December 1960.

Leviton, R.; The Robin-Falling-Sphere, IGIG Docuemnt No. 105-60, GRD Research Note 73, AFCRL, August 1961.

Leviton, Robert and Wright, John B.; Accuracy of Density from the Robin Falling Sphere, AFCRL - 1095, December 1961.

Missile Meteorology Division; Density and Pressure Profiles Derived from Meteorological Rocket Measurements, TR-108, USASMSA, September 1961.

Pearson, P. H. O.; An Appraisal of the Falling Sphere Method of Density Measurements Using External Measuring Methods, Australian Defense Scientific Service, Weapons Research Establishment, Tech Note SAD82, October 1961.

3.4 Falling Sphere Density Measurement Techniques - (continued)

Peterson, J. W. and McWatters, K. D.; The Measurement of Upper-Air Density and Temperature by Two Radar - Tracked Falling Spheres, University of Michigan, Office of Research Administration, Tech Report No. 03598-13-T, March 1963.

Peterson, J. W., Hansen, W. H., McWatters, K. D. and Bonfante, G.; Atmospheric Measurements Over Kwajalein Using Falling Spheres; ORA - Project 05436, January 1965.

Schutte, H. F., Robinson, D. A. and Wagener, J. L.; Falling-Sphere Experiment for Upper-Air Density: Instrumentation Developments, The University of Michigan, Office of Res. Administration, Final Report 03558-6-F, April 1962.

Scoggins, James, R.; Sphere Behavior and the Measurement of Wind Profiles, NASA TND-3994, June 1967.

Welinski, B. R.; Robin, Meteorological Balloon Development, Final Report, AF 19(604) 6653, Page 31, 1960.

Welinski, B. R.; Research and Development of Robin Meteorological Rocket Balloons, G. T. Schjeldahl Company Report, Vol. I, Contract AF 19(604)8034, 1963.

Wright Instruments, Inc.; A survey of Pressure and Density Sensors and Associated Problems for the N.O.L. Hasp Program; NOL-N-60-21-5603, April 1959.

Wright, John B.; The Robin Falling Sphere, MRN, MWG, RCC Document 111-64.

3.5 PITOT PROBE DENSITY MEASUREMENTS

Ainsworth, J. E., Fox, D. F. and LaGow, H. E.; Measurement of Upper Atmosphere Structure by Means of the Pitot-Static Tube, NASA Technical Note D-670, 1961.

Ainsworth, J. E., Fox, D. G. and LaGow, H. E.; Upper-Atmosphere Structure Measurement made with the Pitot Static Tube; Journal of Geophysical Research, Vol. 66, No. 10, Page 3191, October 1961.

Arnold, J. W., Simmons, Harmon, L. and Miller, Wm. T.; An Investigation of the Aerodynamic Characteristics of a 25° Sphere-Cone Including a Pressure Distribution Analysis at Angles of Attack, and a Trajectory Analysis During a Typical Re-entry Trajectory, Ling-Temco-Vought, Inc., NASA, CR-66D37, August 1965.

Atlantic Research Corporation, Final Technical Report on the Denpro Program for the Design, Fabrication and Flight Testing of a Meteorological Rocket Probe: Contract N123(61756)32883A (PMR), April 1965.

Burcham, Frank W. Jr.; Calibration of a 40° Conical Pressure Probe at Mach Numbers from 3.5 to 7.4; NASA TN-D-4678, NASA, 1968.

Coates, Edward, M. Jr.; Stagnation and Static Pressures on a Nose-Mounted 15° Conical Probe with Various Forebody Configurations, NASA TN-D-3526, August 1966.

Horvath, J., Simmons, R., and Brace, L.; "Theory and Implementation of the Pitot-Static Technique for Upper Atmospheric Measurements, " Space Physics Research Lab, Report NS-1, University of Michigan, March 1962.

King, J. Derwin; Technology Utilization Report; Vibrating Diaphragm Pressure Transducer, NASA SP-5020, August 1966.

Norris, John D. and Pierpont, P. Kenneth; Experimental Performance of a Conical Pressure Probe at Mach Numbers of 3.0, 4.5 and 6.0; NASA TND-3719, December 1966.

Project Aries - Final Report, Science Communication, Contract No. 3071(00) 1 August 1960.

3.5 Pitot Probe Density Measurements (continued)

Quiroz, Roderick, S.; Seasonal and Latitudinal Variations of Air Density in the Mesosphere (30 to 80 Kilometers); Journal of Geophysical Research, Vol. 66, No. 7, July 1961.

Radigan, J. (Director, Inertial Systems Section); Ames Pressure Transducer Experimental Evaluation; NORT 64-355, December 1964.

Schaff, S. A.; The Pitot Probe in Low - Density Flow, Report #535, AD652-173, January 1966.

Smith, Lawrence B.; Measurement of Atmospheric Pressure Between 95 and 130 KM Using Cold-Cathode Ionization Gages; Southwest Research Institute; Vibrating Diaphragm Pressure Transducer; NASA SP-5020, August 1966.

Webb, Lannie, D.; Characteristics and Use of X-15 Air Data Sensors; NASATND-4597, June 1968.

3.6 SONIC GRENADES

Nordberg, W., Stroud, W.; "Results of IGY Rocket-Grenade Experiments to Measure Temperatures and Winds above the Island of Guam,"; J. Geophys. Res. 66(2):455-464, February 1961.

Nordberg, W., and Smith, W.; "The Rocket-Grenade Experiment," NASA Technical Note D-2107, March 1964.

Nordberg, W. and Smith, W.; "The Rocket Grenade Experiment," Sounding Rocket Research Techniques, IQSY, Instruction Manual, London, 1964.

Smith, W., Katchen, L., Sacher, P., Swartz, P., and Theon, J.; "Temperature, Pressure, Density and Wind Measurements with the Rocket Grenade Experiments, 1960-1963," NASA Technical Report R-211, October 1964.

Stroud, W., Nordberg, W., Bandeen, W. R., Bartman, F. L. and Titus, T.; "Rocket-Grenade Measurements of Temperatures and Winds in the Mesosphere over Churchill, Canada," J. Geophys. Res., 65 (8): 2307-2323, August 1960.

3.7 OZONE SENSORS AND TECHNIQUES

Craig, Richard, A.; DeLuisi, John, J., Stuetzer, Irmgard; Comparison of Chemiluminescent and Umkehr Observations of Ozone; Journal of Geophysical Research, Vol. 72, No. 6, March 15, 1967.

Randhawa, Jagir, S.; Mesospheric Ozone Measurements during a Solar Eclipse; Journal of Geophysical Research, Vol. 73, No. 2, January 15, 1968

Spurling, John F. (NASA) and Arizumi, Naosuke (JMA); The Japan-United States Meteorological Rocket Project, May 1967.

Reed, Edith I.; A Night Measurement of Mesospheric Ozone by Observations of Ultraviolet Airglow; Journal of Geophysical Research, Space Physics, Vol. 73, No. 9, May 1, 1968.

3.8 WATER VAPOR MEASUREMENT TECHNIQUES

3.9 ATMOSPHERIC COMPOSITION

Evans, W. F. J., Hunter, D. M., Llewellyn, E. J. and Jones, A. Vallance; Altitude Profile of the Infrared Atmospheric Systems of Oxygen in the Dayglow; Journal of Geophysical Research, Space Physics, Vol. 73, No. 9, May 1, 1968.

Hedin, A. E. and Nier, Alfred O.; A Determination of the Neutral Composition Number Density and Temperature of the Upper Atmosphere from 120 to 200 Kilometers with Rocket-Borne Mass Spectrometers; Journal of Geophysical Research, Vol. 71, No. 17, September 1966.

Smith, Leslie, G., Weeks, Lawrence; Molecular Oxygen Densities; NASA CR-392, March 1966.

Weeks, L. H. and Smith, L. G.; Molecular Oxygen Concentrations in the Upper Atmosphere by Absorption Spectroscopy; Journal of Geophysical Research, Space Physics, Vol. 73, No. 15, August 1, 1968.

3.10 ELECTRON DENSITY

Aiken, A. C. and Blumle, L. J.; Rocket Measurements of the E-Region Electron Concentration Distribution in the Vicinity of the Geomagnetic Equator; Journal of Geophysical Research, Space Physics, Vol. 73, No. 5, March 1, 1968.

Bettinger, Richard, T.; An In-Situ Probe System for the Measurement of Ionospheric Parameters, Vol. II, T.R. 277, Dept. of Physics and Astronomy, University of Maryland, June 1964.

Bettinger, Richard T.; Direct Probe Measurements in the Auroral Ionosphere; Contract AF 19(628) 2792, AFCRL 66-825, Sept. 1966.

Brooks, David R. and Hoell, James, M. Jr.; A Computerized Data-Reduction Technique for Langmuir Probe Analysis of Electron Temp. Variations in the Exhaust of a Magnetoplasmdynamic Arc; NASA TN-D-4220, November 1967.

Fejer, J. A., Heikkila, W. J., Holt, O.; (Principal Investigators): Comparison of Rocket-Borne Probes for Electron Density Measurement; Quarterly Status Report #5, Period 1 August 1965 through 31 October 1965; (NASA Contract NSR 44-004-017)

Heikkila, W. J., Eaker, N., Fejer, J. A., Tipple, K. R., Hugill, J., Schnerble, D. E. and Calvert, W.; Comparison of Several Probe Techniques for Ionospheric Electron Concentration Measurements, Journal of Geophysical Research, Space Physics, Vol. 73, No. 11, June 1, 1968.

Journal of Geophysical Research, Space Physics, Vol. 73, No. 11, June 1, 1968.

LeVier, R. E., Branscomb, L. M.; Ion Chemistry Governing Mesospheric Electron Concentrations; Journal of Geophysical Research, Vol. 73, No. 1, January 1, 1968.

Monro, P. E., Mechtly, E. A. and Sastry, Reginald E; Analysis of Ordinary Mode Standing Waves Observed by Rockets in the E. Region; Journal of Geophysical Research, Space Physics, Vol. 73, No. 13, July 1, 1968.

3.10 ELECTRON DENSITY - (continued)

Narcisi, R. S.; Ion Composition Measurements and Related Ionospheric Processes in the D and Lower E Regions; AFCRL-66-715, Environmental Research Papers, No. 230, October 1966.

Oster, A. L., Coroniti, S. C., A Method of Measuring Electron and Ion Densities in the Region of 4-80 Kilometers, Journal of Geophysical Research, Space Physics, the American Geographical Union, Vol. 73, No. 13, July 1, 1968.

Sonin, Ain, A.; Theory of Ion Collection by a Supersonic Atmospheric Sounding Rocket: Journal of Geophysical Research, Vol. 72, No. 17, September 1, 1967.

3.11 SOLAR AND TERRESTRIAL RADIATION FLUX SENSORS

Aagard, Robert L., Measurement of Infrared Radiation Divergence in the Atmosphere with the Double-Radiometer and the Black Ball,
J. Meteor. 1960.

3.12 MISCELLANEOUS DENSITY MEASUREMENT TECHNIQUES

Thiele, Otto W.; Feasibility Experiment for Measuring Atmospheric Density through the Altitude Range of 60 to 100 Kilometers over White Sands Missile Range; USAERDA, October 1964.

Weinstock, Jerome, Deducing of Magnitudes of Ionospheric, Irregularities from Backscatter Measurements; Journal of Geophysical Research Vol. 73, No. 1, January 1, 1968.

3.13 MISCELLANEOUS PRESSURE MEASUREMENT TECHNIQUES

Metro-Physics, Inc; Loki-Dart Transponder Rocketsonde Advanced Temperature Sensors and Thermoconductivity High Altitude Pressure Gages.

Thiele, Otto, W. and Beyers, Norman J.; Upper Atmosphere Pressure Measurements with Thermal Conductivity Gages; Journal of Atmospheric Science, Vol. 24, No. 5, September 1967.

CHAPTER 4 - ROCKETSONDE DESCENT SYSTEMS

4.1 GENERAL

Beyers, N. J. and Thiele, O. W.; Meteorological Rocket Wind Sensors, Special Rep. 21, USASMSA, White Sands Missile Range, New Mexico, 1960.

Heinrich, H. G.; Drag and Stability of Parachutes, Aero. Eng. Rev., Vol. 15, No. 6, 73-81, 1956.

Kay, Marvin and Olsen, R. O.; Improved Technique for Deriving Wind Profiles from Rocketsonde Parachutes. Journal of Geophysical Research, Vol. 72, Number 16, 15 August 1967.

Murrow, H. N. and Dozier, C. M.; Performance Studies and Requirements for Parachutes Utilized for Meteorological Data gathering at Altitudes between 200,000 and 100,000 feet, AMA/AIAA/Texas Western College Conference on the Structure of the Stratosphere-Mesosphere, El Paso, Texas (unpublished), 1963.

Olsen, R. O. and Kays, Marvin; Improved Rocketsonde Parachute - Derived Wind Profiles: ECOM-5086, October 1966.

4.2 CONVENTIONAL PARACHUTES

Eckstrom, C. V.; Flight Characteristics of a New Sounding Rocket Parachute, AMS Fifth Conference on Applied Meteorology, Atlantic City, New Jersey, (unpublished) 1964.

Heinrich, H. G.; The Effective Porosity of Parachute Cloth Flugwiss, II (Heft 10), 1963.

Jenkins, K. R.; Empirical Comparisons of Meteorological Rocket Wind Sensors, J. Appl. Meteor., Vol. 1, 1962.

Law, C. Herbert; A Study of Aerodynamic Deployable Decelerators at Hypersonic Velocities: AIAA Student Journal, Vol. 5, No. 1, February 1967.

Murrow, H. N. and Barker, L. E. Jr.; An Analytical Study of the Wind-Following Characteristics of a Parachute at High Altitudes, ARS Semi-Annual Meeting and Astronautical Exposition, El Cortez Hotel, San Diego, California (Unpublished) 1959.

Technical Documentary Report ASD-TDR-62-100; Stability and Drag of Parachutes with Varying Effective Porosity, Contract AF 33(616) 8310, 1962.

Whitlock, C. H. and Murrow, H. N.; Performance Characteristics of a Preformed Elliptical Parachute at Altitudes between 200,000 and 100,000 Feet obtained by In-Flight Photography, NASA TN D-2183, 1964.

4.3 PARACHUTES WITH GEOMETRY POROSITY

Eckstrom, Clinton V.; Development and Testing of the Disk-Gap-Band Parachute used for Low Dynamic Pressure Applications at Ejection Altitudes at or above 200,000 Feet: NASA - Contract NAS1-3372, August 10, 1965.

4.4 STOKES FLOW RIBBON MESH PARACHUTE

Astro Research Corporation, High Altitude Parachute System for Meteorological Research Sondes: ARC-P-233A, October 26, 1966.

Niederer, P. G.; Development of a High Altitude Stokes Flow Decelerator, Final Report; Astro-Research Corporation. Contract NAS5-10168, November 1966.

Rhyme, R. H., Erskin, C. W., Tolefson, H. B.; Experimental Investigation of the Drag Characteristics of Ribbon Mesh Decelerators at Low Reynolds Number. Langley Working Paper -443, Langley Research Center, NASA, 17 July 1967.

Santeler, D.; Holkeboer, H.; Jones, D; and Pagano, F.; Vacuum Technology and Space Simulation, NASA SP-105, NASA, 1966.

4.5 RAM-AIR DECELERATORS

Jaremenko, I. M.; Ballute Characteristics in 0.1 to 10 Mach Number Speed Regime: "J. Spacecraft, Vol. 4, No. 8, August 1967. "

Turk, Raymond, A.; Pressure Measurements on Rigid Model of Ballute Decelerator at Mach Numbers from 0.56 to 1.96. NASA TN-D 3545, August 1966.

CHAPTER 5 - TELEMETRY AND TRACKING

5.1 GENERAL

NASA - Wallops Station Handbook, 6 April 1964.

5.2 RADAR

Beyers, N. J.; Preliminary Radar Performance Data on Passive Rocketborne Wind Sensors, IRE-Trans-Actions on Military Electronics, MIL-4, No. 2-3, 1960.

Briggs, R. S. and Rotolante, R. A.; Installation of Radar Tracking Facilities at McMurdo Station, Antarctica, (Unpublished), 1963.

5.3 TELEMETRY

Atlantic Research Corporation, Flight Testing of the Arcasonde I Instrument Package Report, (Unpublished), 1960.

Clark, G. Q.; Development of a Rocket Telemetry Package for the Meteorological Rocket Network, Initiation of the Meteorological Rocket Network, IRIG Document No. 105-60; Revised August 1961, AD 246950, 1961

Clark, G. Q. and McCoy, J. G.; Meteorological Rocket Thermometry, Tech. Rep. MM-460, U. S. Army Signal Support Agency, White Sands Missile Range, New Mexico, 1962.

Cline, D. E.; Double-Direction Finding Rocket Meteorological Sensing System, USASRDL, TR 1981, AD 212-478, 1958.

Coppola, A.A.; Use of Rawin Set AN/GMD-2 with Radiosonde Set AN/DMQ-6, USASRDL, TR 2171, AD 251, 1961.

Coppola, A. A.; Radiosonde Set AN/DMQ-6, USA ELRDL Tech. Report 2354, 1963.

Grimesey, Robert P; Meteorological Sounding Rockets and Instrumentation, 6 December 1961.

Keegan, T. J.; Meteorological Rocketsonde Equipment and Techniques, Bull. AMS, Vol 42, 715-121, 1961.

Kendall, Bruce M.; Evaluation of the A-15497 1680 mHz Power Oscillator for Meteorological Sounding Rocket Application, NASA, 14 May 1965.

Kidd, K. W.; Further Development of the AN/DMQ-9 Rocketsonde (Bendix Corporation), Contract No. AF19(628) 4045, Project No. 6682, Task No. 668206, Final Report June 1965.

Krasin, Elvin, F. and Wood, Kenneth, J.; An Advanced Meteorological Sounding System (Design Plan), Contract #AF19(628) 4215, Project #6670, Task #667002, Scientific Report #1, AFCRL-66-256, 30 November 1965.

5.3 Telemetry - (continued)

Parker, M. J.; The Loki-Hasp Rocket Sonde Meteorological Equipment, (Unpublished) 1961.

Poppoff, I. G.; Low-Cost Meteorological Rocket Systems, Astronautics, 26 - 1958.

Poppoff, I. G.; Rocketsondes for High-Altitude Sounding; SRI Journal, Stanford Research Institute, Vol. 3, 56-60, 1959.

Radiosonde Recorders, AN/TMQ-5 and AN/TMQ-5A, Tech. Manual TM11-84-36, Dept. of the Army.

Rawin Set AN/GMD-1A, Tech. Manual, TM-11-27-1A; Department of the Army.

Roberts, W. C., Jr. and Webster, R. C.; Arcas Rocketsonde System Development, American Rocket Soc. National Conference on the High Atmosphere, Minneapolis, Minn., Atlantic Research Corporation, Alexandria, Virginia (Unpublished) 1959.

Turner, Robert E. and Jendrek, Richard A.; Radiosonde Automatic Data Processing System, NASA/MSFC, NASA TM-X-53186, December 1964.

Webb, W. L.; Dissipation of Power in the Sensor of the AN/AMT-4, USASMSA, 1960.

Wenzel, R. F.; Air-Launched Rocketsonde Study, General Dynamics, Contract #AF19(628) 3265, Project #6020, Task #602001, AFCRL-64-59, January 1964.

Wood, Kenneth; The Advanced Meteorological Sounding System; Motorola Report AFCRL Contract, 1969.

CHAPTER 6 - ROCKET VEHICLES

6.1 GENERAL

Atmore, Frank R. and Billings, Gail R.; A Study to Guide Research and Development Toward An Operational Meteorological Sounding Rocket System: Contract #NASW-1522, October 1966, April 1967.

6.2 HISTORICAL REVIEW

Jenkins, K. R.; Measurements of High Altitude Winds with Loki, USASMSA TM 544, AD 200 001, 1958.

Masterson, J. E.; The Loki Meteorological Rocket System, (Unpublished), 1961.

Smith, L. B.; The Measurement of Winds between 100,000 and 300,000 Feet by Use of Chaff-Rockets, J. Meteor., Vol. 17, 1960.

Smith, L. B.; Use of Chaff-Rockets for Measurement of High-Altitude Winds, Paper ARS, 15th Annual Meeting, Washington, 1960.

Tobin, J. E.; Flight Testing of the Rocketsonde 200-P and 200-1 Meteorological Sounding Rocket System, Marquardt Corporation, Rep. S-285, 1962.

Itokawa, Hideo; Development of Sounding Rockets in Japan (Tech. Translation F-87) NASA TT F-87, March 1963.

6.3 CURRENT VEHICLE SYSTEMS

Atlantic Research Corporation, Arcas Rocketsonde System; High Altitude and Meteorological Sounding Rocket, Atlantic Research Corporation, Alexandria, Virginia, 1960.

Bollermann, Bruce and Walker, Robert L.; Meteorological Probe PWN-8B, Qualification Program, Contract No. AF19(628) 5921, Project No. 6682, Task No. 668206, AFCRL-68-0132, 28 Feb 1968.

Bradford, W. C.; Theoretical and Experimental Dispersions for the Arcas-Robin Rocket, Tech. Doc. APGD-TDR-61-62, Air Proving Ground Center, Eglin Air Force Base, Florida, 1961.

Bradford, W. C. and Myers, P. W.; Dispersion Study for the Arcas-Robin with 230 Feet/Second Launch Velocity, APGC AIDR 62-2, Air Proving Ground Center, Eglin Air Force Base, Florida, 1962.

Brown, J. A.; Arcas High-Altitude Meteorological Rocketsonde System, Transactions, New York Academy of Science, Ser. II, Vol. 22, 175-183, 1960.

Clark, G. Q.; Arcas Nose Cone Alpha, Schellenger Res. Lab., Texas Western College, El Paso, Texas, 1959.

Cochran, V. C. and Hansen, J. K.; Theoretical Performance of the Arcas and Boosted Arcas, Tech. Rep. MM-432, U. S. Signal Missile Support Agency, White Sands Missile Range, New Mexico, 1963.

Development and Performance of the Sparrow-HV Arcas (DENPRO) Sounding Rocket Vehicle, Contract No. N123-(61756)32883A (PMR) August 30, 1963.

Griner, G. N. and Mahar, T. A.; Sparrow (c8)-HV Arcas Dispersion Analysis, Rep. No. ARC-FAI-2D1, Atlantic Research Corporation, Alexandria, Virginia, 1963.

Hansen, W. H. and Fischback, F. F.; The Nike-Cajun Sounding Rocket Project 2453, Contract No. AF 19(604)-1560, March 1967.

6.3 Current Vehicle Systems - (continued)

Hoidale, M. J.; Arcas Dispersion at White Sands Missile Range, New Mexico, 1961-1963, Internal Report, U. S. Army Electronics Research and Development Activity, White Sands Missile Range, New Mexico, 1964.

Kirchoff, G. F.; Reliability Report on the Arcas Sounding Rocket, Unnumbered Tech. Rep., Atlantic Research Corporation, Alexandria, Virginia, 1962.

Parker, M. J.; HASP, Instrumented, Status Report and Recommendation for Termination of Development of the Head, 1.625-Inch Rocket MK-2 Mod 2, NOLTR 64-17, 17 February 1964.

Space Data Corporation; Cajun-Dart Sounding Vehicle, Contract No. NAS8-11624, SDC TM-198, January 1967.

Thiele, O. W.; Boosted Arcas and Boosted Raven Systems for High Altitude Soundings, The Meteorological Rocket Network, IRIG MWG, 1965.

Turner, Robert E. and Gilchrist, Luke P.; Hopi-Dart and Cajun-Dart Rocket Wind Measuring Systems, NASA TM X-53303, 26 July 1965.

Ubico, R. E., Kirchoff, G. F. and Webster, R. C.; Fabrication and Delivery of Arcas Sounding Rocket Systems EX 6 Mod 0 and EX 6 Mod 1, Rep. ARC-PSR1-2B1, Atlantic Research Corporation, Alexandria, Va., 1963.

Walker, R. L., Zinsli, K. R. and Watson, C. W.; Judi-Robin Balloon Dart Sounding Vehicle, Rocket Power, Inc., Final Report, AFCRL 64-471, Contract AF 19(628) 2805, May 1964.

Webb, W. L., Jenkins, K. R. and Clark, G. Q.; Flight Testing of the Arcas USASMSA, White Sands Missile Range, New Mexico, 1959.

Webster, R. C. et al; Development of the Arcas Rocketsonde System, Final Report, NONR-2477-(00), Ad 235-345, 1960.

Webster, R. C., Roberts, W. C. Jr. and Donnell, W. P.; Development of the Arcas Rocketsonde System, Final Report, Atlantic Research Corp., Alexandria, Virginia, 1960.

6.3 Current Vehicle Systems - (continued)

Webster, R. C., and Roberts, W. C.; Arcas, All-Purpose Sounding Rocket, Paper, ARS, 15th Annual Meeting, Dec., Washington, D. C., 1960.

Webster, R.C., Dunfee, D. D. and Peterson, J. S.; A Closed Tube Launched Sounding Rocket, Atlantic Research Corporation, 14 July 1964.

6.4 DEVELOPMENT SYSTEMS

Bollermann, Bruce and Walker, Robert L.; Design, Development and Flight Test Viper Dart Robin Meteorological Rocket System; Contract No. AF 19(628) 5911, Project No. 6682, Task No. 668203, 30 June 1968.

Bollermann, Bruce and Walker, Robert L.; Super-Loki Dart Meteorological Rocket System; SDC TM-310, Contract No. NAS8-20797, 30 June 1968.

CHAPTER 7 - GUN PROBES

7.1 GENERAL

Allen, E. F.; Engineering Services to Optimize the 5-Inch Gun Probe, Space Data Corporation ASL Report Contract DO7-68-C-0071, November 1968.

Borwn, J. A. and Poughkeepsie, F. H (BRL), Sloan, G. J. (NOL); High Altitude Wind Measurements Using Radar-Tracked Parachutes Ejected from Gun Probes.

Glass, I. I.; Hypervelocity Launchers, Part I; Sample Launchers; University of Toronto, ARL-63-86, May 1963.

Harp Project, First Twelve Firings and Status as of July 30, 1963, Rep. No. 635, McGill University, 1963.

Harp Project, Description and Status, Rep. No. 625, McGill University, 1962.

MacAllister, L. C. and Bradley, J. W.; Comments on the Use of Guns to Launch High Altitude Probes, Memo Report #1252, March 1960.

Mermagen, W. H.; Telemetry Experiments Conducted on the Harp Project at Barbados, W. I. and Wallops Island, Va. During the Period - January - March 1964; BRL Memo. Report No. 1578, July 1964.

Mermagen, W. H.; "Harp 250 nc Telemetry Experiments, Jun-Oct 64", BRL Memo. Report No. 1614, November 1964.

Mermagen, W. H.; Cruickshank, W. K. and Vratavic, F.; "VHF and VHF High-G-Telemetry Instrumentation for HARP Vehicles, BRC Memo. Report No. 1768, May 1966.

Murphy, C. H. and Bull, G. V.; "Review of the High Altitude Research Program (HARP)" BRL Report No. 1327, July 1966.

Murphy, C. H. and Bull, G. V.; "HARP 5-Inch and 16-Inch Guns at Yuma Proving Ground, Arizona", BRL Memo. Report No. 1825, February 1967.

7.2 5-INCH GUN PROJECTILES

Boyer, E. D.; Five-Inch HARP Tests at Wallops Island, BRL Memo. Report No. 1532, 1963.

Boyer, E. D.; Five-Inch HARP Test at Barbados, West Indies; Jan - Feb 66; BRL Memo. Report No. 1771, July 66.

Cruickshank, W. J.; A Feasibility Test of a 1750 mc/s Telemetry and Tracking System for 5-Inch HARP Projectiles; BRL Memo. Report No. 1651, May 66.

Luckert, H. J.; Space Research Institute of McGill University; Report for March 65 Test Firing Series, Project Harp, AD No. 475146.

Marks, Spence T. and Boyer, Eugene D.; A Second Test of an Upper Atmosphere Gun Probe System; RD and E Projects #IA011001B021 and 1M010501A005, Memo Report #1464, April 1963.

Space Data Corporation, Program Plan for Engineering Services to Optimize the 5-Inch Gun Probe Vehicle; SDC TM-282, 5 Jan 1968.

Williamson, Edwin L.; Gun-Launcher Vertical Probes at White Sands Missile Range, ASL-ECOM Report No. 5030, Feb. 1966.

7.3 7-INCH GUN PROJECTILES

Boyer, E. D. and MacAllister, L. C.; Seven-Inch Harp Gun-Launched Verticle Probe System; Initial Development; BRL
Memo. Report No. 1770, July 1966.

7.4 16-INCH GUN PROJECTILES

Agard Conference Proceedings No. 10, "The Fluid Dynamic Aspects of Ballistics" September 1966.

Murphy, Charles H. (BRL), Bull, Gerald V. and Edwards, Howard, D.; Upper Atmosphere Winds Measured by Gun Launched Projectiles; BRL Memo. Report No. 1747, May 1966.

Murphy, Charles H. and Bull, Gerald V.; Ionospheric Winds over Yuma, Arizona, Measured by Gun-Launched Projectiles; Journal of Geophysical Research, Space Physics, Vol. 73, No. 9, Pg. 3005, May 1, 1968.

7.5 GUN-BOOSTED ROCKETS

Bull, G. V., Lyster, D. and Parkinson, G. V.; "Orbital and High Altitude Probing Potential of Gun Launched Rocket" Space Research Institute, McGill University Report, October 1966.

Bull, G. V and Murphy, C. H.; "Gun-Boosted Rockets for High Performance Sounding Missions: AIAA Technical Papers, Report No. A67-20550, 1967.